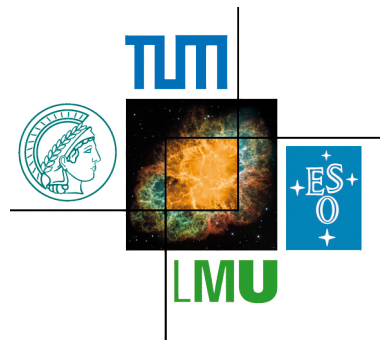


Impact of Flavor and Higgs Physics on Theories Beyond the Standard Model

Sandro Casagrande

Excellence Cluster Universe
Technische Universität München
D-85748 Garching
Email: sandro.casagrande@ph.tum.de



Supervised by
Dr. Martin Gorbahn

Garching
Jan 2013

TECHNISCHE UNIVERSITÄT MÜNCHEN
Exzellenzcluster “Origin and Structure of the Universe”

Impact of Flavor and Higgs Physics on Theories Beyond the Standard Model

Sandro Casagrande

Vollständiger Abdruck der von der Fakultät für Physik der Technischen Universität München zur Erlangung des akademischen Grades eines

Doktors der Naturwissenschaften (Dr. rer. nat.)

genehmigten Dissertation.

Vorsitzende:

Univ.-Prof. Dr. Laura Fabbietti

Prüfer der Dissertation: 1. TUM Junior Fellow Dr. Martin Gorbahn

2. Univ.-Prof. Dr. Alejandro Ibarra

Die Dissertation wurde am 23.01.2013 bei der Technischen Universität München eingereicht und durch die Fakultät für Physik am 13.02.2013 angenommen.

Abstract

Quantum effects of physics beyond the Standard Model receive strong indirect constraints from precisely measured collider observables. In the conceptual part of this thesis, we apply the generic relations between particle interactions in perturbatively unitary theories to calculate one-loop amplitudes for flavor physics. We provide template results applicable for any model of this class. We also investigate example models that are partly and such that are not perturbatively unitary: the Littlest Higgs model and Randall-Sundrum models. The latter have a unique coupling structure, which we cover exhaustively. We find strong constraints on the Randall-Sundrum models and numerically compare those from flavor, electroweak precision, and Higgs physics by performing detailed parameter scans. We observe interesting correlations between flavor observables, and we find that constraints from Higgs production and decays are already competitive.

Zusammenfassung

Quanteneffekte jenseits des Standardmodells sind indirekt, stark durch präzise gemessene Beschleunigerobservablen beschränkt. Im konzeptionellen Teil dieser Arbeit verwenden wir generische Relationen zwischen Teilchenwechselwirkungen perturbativ unitärer Theorien zur Berechnung von Einschleifenamplituden der Flavor-Physik. Wir geben allgemeine Resultate, anwendbar auf alle Modelle dieser Klasse. Wir untersuchen auch Beispielmole, welche teilweise, bzw. nicht perturbativ unitär sind: das Littlest Higgs Modell und Randall-Sundrum Modelle. Letztere haben eine besondere Kopplungsstruktur, welche wir eingehend besprechen. Wir finden starke Beschränkungen an Randall-Sundrum Modelle und vergleichen solche aus Flavor-, elektroschwacher Präzisions- und Higgs-Physik numerisch mittels detaillierter Parameterabtastung. Wir finden interessante Korrelationen zwischen Flavor-Observablen und dass Beschränkungen durch Higgs-Produktion und Zerfälle bereits kompetitiv sind.

Contents

1	Introduction	1
2	The Standard Model of Elementary Particle Physics	5
2.1	Preliminaries	5
2.1.1	First Principles	6
2.1.2	The SM as an Effective Field Theory	7
2.2	Nomenclature and the Symmetry Breaking Sector	9
2.3	Quantization and BRST Invariance	13
2.4	Reasons to Go Beyond	16
3	Theoretical Classification & Examples of New Physics	21
3.1	Relations for Perturbatively Unitary Theories	21
3.1.1	The Generic Lagrangian	21
3.1.2	Slavnov-Taylor Identities for Feynman Rules	23
3.2	A Little Higgs Model	31
3.2.1	Gauge Structure and T -Parity	31
3.2.2	Fermion Sector	35
3.3	Randall-Sundrum Models	40
3.3.1	Basic Geometry of the Setup	40
3.3.2	The Role of Compactification and Boundary Conditions	42
3.3.3	Fermions in a Curved Background	44
3.3.4	Minimal Randall-Sundrum Model	45
3.3.4.1	Gauge-Boson Sector	45
3.3.4.2	Fermion Sector	48
3.3.5	Custodial Randall-Sundrum Model	53
3.3.5.1	Gauge-Boson Sector	53
3.3.5.2	Fermion Sector	57
3.3.6	Bulk Profiles and Zero-Mode Spectrum	60
3.3.7	Two Paths to 5d Propagators	64
3.3.7.1	Summation over KK Modes	65
3.3.7.2	Solution to the 5d EOMs	68
3.3.8	Complete Coupling Structure	73
3.3.8.1	Higgs–Fermion Couplings	73
3.3.8.2	Gauge-Boson–Fermion Couplings	76
3.3.8.3	Purely Bosonic Couplings	78
3.3.8.4	Four Fermion Couplings	79
4	Aspects of Precision Physics	83

4.1	Flavor Physics	83
4.1.1	Structure of $\Delta F = 1$ Processes in Perturbative Models	84
4.1.1.1	Renormalization of the Generic Z Penguin	84
4.1.1.2	Result for the Generic Z Penguin and Box Diagrams	88
4.1.1.3	Results for the Littlest Higgs Model with T -parity	93
4.1.2	Constraints and Correlations in the Randall-Sundrum Model	94
4.1.2.1	A Comment on Bounds from Direct Collider Searches	95
4.1.2.2	Theoretical Framework and Relevant Formulas	95
4.1.2.3	Modifications of the CKM Matrix	106
4.1.2.4	Numerical Analysis of Flavor Observables	108
4.2	Electroweak Precision Measurements	124
4.2.1	Common Observables and Effective Parameters	124
4.2.1.1	General Discussion and Choice of Input Parameters	124
4.2.1.2	Effective Parameters for New Physics	127
4.2.1.3	Precision Observables from $Z \rightarrow b\bar{b}$	129
4.2.2	Constraints on the Randall-Sundrum Model	132
4.2.2.1	General Discussion and Input Parameters	132
4.2.2.2	Oblique and Universal Contributions	132
4.2.2.3	Bounds from the $Zb\bar{b}$ Vertex	135
4.3	Higgs Production and Decays at Hadron Colliders	140
4.3.1	Results in the SM and Measurements	140
4.3.2	Sensitivity of Higgs Production to New Fermions	148
4.3.3	Analytic Derivations in the Randall-Sundrum Model	151
4.3.3.1	General Strategy for Loop Mediated Processes	153
4.3.3.2	Evaluation of the Two Regulator Limits	156
4.3.3.3	UV Regulation as a Decision Criterion	163
4.3.4	Phenomenology of the Randall-Sundrum Model	166
4.3.4.1	Production Channels	166
4.3.4.2	Decays Channels: General Aspects, $ZZ, b\bar{b}$	173
4.3.4.3	The Decay into $\gamma\gamma$	177
4.3.4.4	The Decay into γZ	180
5	Conclusion	187
A	Collection of Formal Developments and Vertices	191
A.1	Collection of STIs for Feynman Rules	191
A.2	Formulas and Vertices of the Littlest Higgs Model	193
A.3	Analytic Solutions for the RS Model with One Generation	198
B	Collection of Numerical and Technical Details	203
B.1	Loop Functions	203
B.2	Numerical Input Parameters	204
B.3	Description of the Parameter Scans in RS Models	206
B.4	Numerical Scans of Higgs Processes in RS Models	210
	Bibliography	222
	Acknowledgments	235

Chapter 1

Introduction

We are to admit no more causes of natural things than such as are both true and sufficient to explain their appearances.

ISAAC NEWTON

For many decades now, research has been posing the question of truth and sufficiency of the Standard Model of elementary particle physics (SM). The answer to this questions depends on the very energy at which they are posed. The question of truth has been answered positively in collider experiments through the tremendous success of the virtual quantum corrections to precisely studied processes as they are predicted by the SM alone. Before the program at the CERN Large Hadron Collider (LHC), this applied to all scales relevant to the SM content except its symmetry breaking sector.

Here, we are concerned with theories beyond the SM. The quest for new physics approaches the question of sufficiency. It is in fact a joint program pursued at the intensity and energy frontier. The LHC program is now driving it up to unexplored energy scales with its recently finished run at 7 and 8 TeV center-of-mass energy, and hopefully soon even further. In the searches for direct productions the previously known resonances of the SM were rediscovered and it seems that the last missing piece at the heart of electroweak symmetry breaking was confirmed: a scalar resonance of about 126 GeV mass. Its interactions with other particles are roughly in agreement with the SM Higgs boson but not yet measured with an accuracy that would secure this identification. The mass, however, agrees with vacuum stability bounds and could leave the SM as the self-contained theory of non-gravitational forces almost up to the Planck scale.

We will start this thesis with introducing the SM as the basic low energy theory in chapter 2. Our later considerations can be considered as perturbations around this setup. We will also review the mechanism of electroweak symmetry breaking more closely for later purposes and point out the deficits of the SM, which still lead us to believe that the search for new physics is promising and ever more pressing.

Each confirmation of the SM as the correct background hypothesis at low — *i.e.* below electroweak — energies carries a potential rejection of the hypothesis of physics beyond the SM. Yet, this depends on the specific model in question, its resonances and the couplings amongst them. Importantly, most models of new physics carry an intrinsic energy scale (or a few scales), whose variation enhances or diminishes the non-SM effects induced by the model. Often, this scale is bounded from above by theoretical arguments such as unitar-

ity, vacuum-stability, triviality, or the more practical assumption of perturbativity. On the phenomenological side, it is important to identify physical observables that are precisely measured, as compared to the typical effects of new physics. Here we are concerned with indirect bounds on new physics, which restrict its virtual contributions through precise measurement of observables at lower energies. Several observables of three classes have been identified that typically lead to strong bounds. The classes are flavor physics, electroweak precision observables, and since recently also Higgs physics. Given that the constraints are strong, we call them precision constraints in reference to the specific new physics. This can be either due to indeed precisely measured observables, or due to large typical differences between the SM and new physics value of the observable, which may have its origin in a symmetry like in the case of flavor-changing neutral currents (FCNCs).

In order to systematize the study of precision physics for phenomenology beyond the SM, we divide all models of new physics into two classes: perturbatively unitary theories and theories that become strongly interacting at a high energy scale. The former theories are equivalent to the class of spontaneously broken gauge theories. Their perturbative high energy behavior implies generic relations among the interactions of particles. We review these generic relations in order to perform the general renormalization of flavor amplitudes in chapter 4. There, we also give template results that include the unphysical degrees of freedom that are necessary when working in a renormalizable gauge.

For theories with new strong interactions no such unifying approach exists, and we have to study the phenomenology model by model. To this end we present in chapter 3 two models that are not perturbatively unitary but partially composite. We review the Littlest Higgs model, which is in parts a spontaneously broken gauge theory but has also an explicitly broken sector. We use it to apply the template flavor results in chapter 4. We investigate why the result is feasible, even though the model is partly non-unitary. Later, we also use the model to exemplify the strength of Higgs production and decays in bounding new physics.

We finally present in chapter 3 one interesting model that we scrutinize in chapter 4 with observables from all three aforementioned sectors and compare the relative impact and quality of the resulting bounds. This is the Randall-Sundrum (RS) model, which features a compact extra-dimension with anti de-Sitter geometry. It gives a theoretically appealing explanation of the gauge-hierarchy problem and the hierarchies observed in the quark sector. The model is especially interesting from a precision physics perspective as it receives relevant constraints from electroweak precision physics, flavor-changing decays and most recently also from Higgs production and decays. In combination with the rather small number of free parameters this creates a good prospect for the falsifiability of the model.

We introduce the RS model in a minimal setup and a custodially protected version that lowers the strongest electroweak precision constraints by an enlarged gauge symmetry sector and a specific fermion embedding. We introduce this model in a very concise notation that summarizes the results of the minimal and custodial model and is also extensible to other enlarged fermion embeddings. This facilitates the comparison of the results in the different versions of the model. In contrast to most of the literature, the Kaluza-Klein decomposition of 5d fields into 4d states is then done directly in the mass basis. The technique is based on [1] and particularly useful for deriving analytic expressions for couplings between particles that allow for a clear understanding. It is also well suited for fast numerical evaluation in parameter scans. We give the full coupling structure and present also results for the 5d propagators of gauge bosons and fermions. For fermions we have to carefully treat the issue of the Higgs localization in the extra dimension. We derive the fermion propagator for the

regularized version of an infrared (IR)-brane Higgs boson based on our work in [2]. This is important for the discussion of Higgs physics in the Randall-Sundrum model, where we have to go into the conceptually demanding question of how to perform loop calculations in the given geometrical background.

Before doing so, we start the phenomenological discussion in chapter 4 with flavor constraints from kaon mixing and direct CP violation in $K \rightarrow \pi\pi$. We also study interesting correlations between different flavor observables in the kaon sector and present predictions for deviations in the Cabibbo-Kobayashi-Maskawa matrix and for the rare B_s decay into two muons, which was measured recently for the first time. The analyses are based on our work in [3]. We update all numerical input from experimental results and SM calculations to the recent values and improve the discussion of [3] by also taking into account subleading Higgs-induced FCNCs based on results we derived in [4]. It is important to identify the bounds that affect as few parameters as possible and therefore have good predictivity. We quantitatively assess the dependence of flavor bounds on all model parameters, most prominently the Yukawa sector. A parameter scan with high statistics allows us to find bounds that are more robust than the typical ones often quoted in the literature. This improves the comparability of the bounds to those inferred from electroweak precision observables. We review also the latter in general in section 4.2 and present updated bounds on the minimal and custodial RS model taking into account recent theoretical progress in the SM predictions of $Z \rightarrow b\bar{b}$. This section mainly assists to understand the incentive of the custodial RS setup and to benchmark the bounds from flavor physics and from Higgs processes.

Higgs physics is then discussed in the remainder of this thesis in section 4.3. There, we investigate how to obtain the correct one-loop result for the RS contribution to Higgs boson production via gluon-gluon fusion and also for subsequent decays to two photons. We carefully treat the interplay of the truncation of very heavy Kaluza-Klein modes, the necessary regularization of the IR-brane Higgs location in the extra dimension, and the UV-regularization of the theory. We give analytic and exact results for the processes. After that, we numerically investigate them together with all other relevant Higgs boson production and decay modes, starting from our work on gluon-gluon fusion in [4]. We find that already now interesting bounds on the scale of the custodial RS model can be derived from the Higgs boson decay into two photons.

The appendices finally contain technical summaries: detailed lists of further Slavnov-Taylor identities not used in the main text, Feynman rules for the Littlest Higgs model, an instructive analytic summation of Kaluza-Klein mode contributions to gluon-gluon fusion in a toy RS model, further definitions and numerical input, and a detailed description of the methods used for the RS parameter scans.

Chapter 2

The Standard Model of Elementary Particle Physics

We start with an obligatory and short presentation of the Standard Model of elementary particle physics (SM). In doing so, we will focus on the aspects that are necessary in the following work and set the relevant notation. We will present the reasons that lead us to trust in the SM as the correct theory of matter and fundamental forces up to the electroweak energy scale, and moreover, which of its shortcomings give us a strong incentive to study possible extensions at higher energies.

2.1 Preliminaries

The SM is formulated as a consistent quantum field theory, which has formed through a long history of interplay between experiment and theory. It unifies two theoretical branches, the Glashow-Weinberg-Salam theory of electroweak interactions [5–7] and Quantum Chromodynamics (QCD), the theory of strong asymptotically free interactions [8–10].

The theory, as it is formulated today, became widely accepted in the late seventies after the confirmation of the quark model [11, 12] by the deep inelastic scattering experiments at SLAC [13], the discovery of weak neutral currents in the Gargamelle experiment at CERN [14] and the observation of jets, particularly three-jets events [15] in the PETRA experiment at DESY. Since then, it has led to many successful predictions that were later confirmed by discoveries, *e.g.* the existence of the charm quark [16–18] and a third generation of quarks implied by CP violation in kaon decays [19–21] through the Glashow-Iliopoulos-Maiani (GIM) mechanism. The SM has also passed a multitude of experimental verifications at the level of testing higher order perturbation theory.

Before entering into theoretical details, we want to highlight one of the main features that the SM exhibits. A fact, most remarkable for the present experimental efforts at the Large Hadron Collider (LHC), is that the SM can be treated perturbatively beyond the scale of weak interactions ~ 100 GeV. This implies that the predictions obtained in perturbation theory can be reliably tested at the ongoing LHC experiments. Indeed, the latest results from ATLAS, CMS and LHCb rapidly close in on the SM. The great efforts taken by these experimental collaborations culminated in the announcement of the observation of a bosonic resonance of even spin by ATLAS [22] and CMS [29] in July 2012, which is by now established at a very high confidence level (CL). We expect that the boson is related to the mechanism of

electroweak symmetry breaking found in works by Brout, Englert, Higgs and independently by Guralnik, Hagen, and Kibble [37–40]¹. This mechanism is responsible for the masses of the W and Z bosons, the carriers of the weak force. In the pre-LHC era, the Higgs sector remained the only sector of the SM whose dynamics were untested. It was the designated main goal of the LHC program to investigate this topic. The mass and couplings of the found particle comply with the simplest incarnation of the mechanism of electroweak symmetry breaking and it is likely that what is found is indeed the Higgs particle. Further hints in this direction are given by complementary measurements in the final data set of CDF and D0 at Tevatron [41]. Increased statistics and more complementary measurements of the particle’s properties are necessary for a final answer. We will review Higgs physics and the results of the measurements in more detail in section 4.3.1.

2.1.1 First Principles

The SM and theories beyond it are based on a few, very general first principles. The formalism of fields, particles, and antiparticles is an inevitable consequence of Poincaré invariance, quantum mechanics, and the cluster decomposition principle [43]. The latter principle states that sufficiently distant experiments should yield uncorrelated results. It is guaranteed if all operators in the Hamiltonian are evaluated at the same point in space-time. Furthermore, physical observables must commute at space-like separations, what is referred to as locality. This does not necessarily apply to the correlator of the field operators themselves. Causality is then preserved by the existence of antiparticles. The conservation of probabilities of course requires a hermitian Hamiltonian and a unitary scattering matrix. This, in turn, guarantees real and finite eigenvalues of operators that define physical observables. Finally, stability of matter requires the vacuum state of the theory to be bounded from below.

The Poincaré group admits representations that can be classified according to their transformation property. Since the action itself must be invariant under such transformations, we require the Lagrangian to transform as a scalar. We know from the Clebsch-Gordan decomposition of coupled representations which couplings include a contribution that transforms as a scalar. Thus, we can use those bilinear, trilinear, etc. combinations of field operators and their derivatives that are found to transform as a scalar.

As we already mentioned, it turns out that the SM Lagrangian relies on additional internal symmetry principles. It is sufficient to consider such symmetries that are generated continuously out of the identity and can therefore be composed of infinitesimal transformations with parameters α^a as $g(\alpha) = 1 + i\alpha^a T^a + \mathcal{O}(\alpha^2)$. Those groups are called Lie groups and the space spanned by the generators T^a is the Lie algebra of this group. Only the latter is necessary for building the Lagrangian. Since we want the symmetries to act on a finite set of fields, we only need to consider finite dimensional representations of groups with a finite number of generators and exactly those algebras have been exhaustively classified. After splitting all contained $U(1)$ factors and dividing the group into its mutually commuting sets, the subsets are called simple. The classification of Élie Cartan [44] shows that only eight types of such groups exist. The SM is based on the direct product of the groups $SU(2)$, $SU(3)$ and an additional $U(1)$ factor

$$SU(3)_c \times SU(2)_L \times U(1)_Y \tag{2.1.1}$$

¹In this thesis, we abbreviate it simply as the Higgs mechanism without implying a value judgment.

symmetry, with the first group corresponding to strong interactions and the others to electroweak interactions.

Other global symmetries such as baryon number B , lepton number L , spatial parity P , charge conjugation C , and time reversal T may, or may not be conserved. We will discuss the origin of CP violation in the SM in section 2.2. However, the combined transformation CPT is conserved in any quantum field theory [45].

2.1.2 The SM as an Effective Field Theory

The aforementioned feature of perturbativity in the SM holds even up to the Planck scale, the scale where the gravitational coupling becomes strong. More generally, perturbative unitarity, which is the bounded high-energy growth of scattering amplitudes order by order in the loop expansion, has an intimate one-to-one correspondence with the fact that the theory is spontaneously broken and renormalizable. A theory is called renormalizable, if all formal divergences stemming from ultraviolet (UV) momenta that appear in intermediate calculations of correlation functions with virtual intermediate particles can be absorbed into a redefinition of the fundamental parameters of the bare Lagrangian. The latter is the most general Lagrangian one can conceive under certain space-time and internal symmetry assumptions and a few other consistency conditions, we mention below. Renormalizability of the SM was proven by t'Hooft and Veltman [46].

In the modern interpretation of the SM one does not see renormalizability as a necessary fundamental property, but one rather considers the SM as the effective field theory (EFT) relevant for energies at least up to the electroweak scale. The effects of the heavy particles ϕ_H in extensions of the SM $\mathcal{L}_{\text{NP}} = \mathcal{L}_{\text{SM}}(\phi_{\text{SM}}) + \mathcal{L}_{\text{H}}(\phi_H, \phi_{\text{SM}})$ can then be systematically incorporated in a matching calculation onto the relevant and marginal SM operators, supplemented with additional irrelevant operators $\mathcal{L}_{\text{eff}} = \mathcal{L}_{\text{SM}}(\phi_{\text{SM}}) + \mathcal{L}_{\text{irr}}(\phi_{\text{SM}})$. The latter encode the effects of the new physics (NP) beyond the SM at energies of physical processes below the matching scale μ_H , *i.e.* in the region where the new heavy particles are quasi non-dynamical. We already employed terminology from the classification of operators in the operator product expansion (OPE). In the OPE one uses the fact that the products of field operators A, B , entering Green's functions, can be expanded in terms of local operators and coefficient functions

$$\int dx e^{-ik \cdot x} A(x) B(0) \underset{k \rightarrow \infty}{\approx} \sum_j C_j(k) \mathcal{O}_j, \quad C_j(k) \sim k^{[A]+[B]-[\mathcal{O}_j]}, \quad (2.1.2)$$

where the Wilson coefficients C_j [47] encode the large momentum dependence according to the sum of mass dimensions of the operators in square brackets. This property holds under renormalization up to logarithmic corrections [48]. The effective operators need to comply with the global symmetry properties of the left-hand side. Using such expansions, one calculates a matching of all one light-particle irreducible Feynman diagrams with external light particles and requires them to be the same in the full and in the effective theory. This results in an effective Lagrangian where the operators \mathcal{O}_j depend only on light fields. The coefficient functions are analytic functions in k/μ_H in the region relevant for the low energy theory. They can therefore be cast into a series of terms with decreasing importance, where the matching procedure determines the constant coefficients

$$\mathcal{L}_{\text{eff}}(x) = \sum_j \frac{g_j}{\mu_H^{[Q_j]-4}} \mathcal{Q}_j(\phi_{\text{SM}}(x)). \quad (2.1.3)$$

The remaining momenta are combined with the fields ϕ_{SM} into gauge invariant operators \mathcal{Q}_j . From their mass dimension, one infers the relative importance due to the suppression with the high mass scale μ_H . Here, we have written it out explicitly. The expected scaling of the matrix elements is $\langle f|\mathcal{Q}_j|i\rangle \sim E^{[\mathcal{Q}_j]-4}$ with the typical energy E of the process $i \rightarrow f$. Once the matter content is defined, all possible operators compatible with the gauge symmetry group $SU(3)_c \times SU(2)_L \times U(1)_Y$ and $[\mathcal{Q}_j] \leq 4$ are indeed included in the SM. They are called marginal, or relevant depending on whether the equality is fulfilled or not. Integrating out new heavy degrees of freedom leads to a finite number of operators at any given value of $[\mathcal{Q}_j] > 4$, which are called irrelevant. Working at a given level of precision corresponds to neglecting operators in (2.1.3) with dimensionality higher than a fixed value. Supplemented with the prescription $\mathcal{Q}_j \equiv 0$, if $[\mathcal{Q}_j] > D_{\text{max}}$, an EFT is predictive, and in a sense trivially renormalizable by definition. On the other hand, increasing the required level of precision also requires increasing D_{max} , and thus further experimental input in the form of additional Wilson coefficients is necessary. In the use of EFTs for precision calculations in the SM, the renormalizability of the model allows higher order predictions based on a fixed set of input values, and is therefore an outstanding property in practical terms.

The general strength of EFTs lies in the possibility to connect physical phenomena at a high energy scale, *e.g.* a contribution to an amplitude at the electroweak scale, with the physics at a low scale, *e.g.* a meson oscillation, by use of renormalization group equations (RGE). In the matching of amplitudes from the full and effective theory, the coefficients and matrix elements of the operators in (2.1.3) in fact depend on the renormalization scale μ , which should be chosen close to the typical scale of the process, *e.g.* the mass of the particle that is integrated out, in order to avoid large logarithms from loop integrals.² If the process involves QCD at a low scale μ , one has to resort to a non-perturbative method, like lattice QCD, in order to calculate the matrix elements $\langle f|\mathcal{Q}_j(\mu)|i\rangle$. The connection between the scales makes use of the observation that matrix elements of observables ultimately do not depend on the artificial scale μ , *i.e.*

$$\frac{d}{d\ln(\mu)} \sum_j C_j(\mu) \langle f|\mathcal{Q}_j|i\rangle(\mu) = 0. \quad (2.1.4)$$

By expanding the derivatives of all matrix elements in the complete basis of operators one defines the anomalous dimension matrix γ , which is simply the negative of the corresponding coefficient matrix. Using (2.1.4) one obtains the RGE

$$\frac{d}{d\ln(\mu)} \vec{C}(\mu) = \gamma^T \vec{C}(\mu). \quad (2.1.5)$$

It is used to evolve the Wilson coefficients between a high matching scale μ_H and a lower scale μ , *e.g.* of a second matching step or the scale of an operator matrix element calculation. Thereby, it consistently sums powers of large logarithms to all orders in the expansion parameter, *e.g.* $(\alpha_s \ln(\mu/\mu_H))^n$, what is called the summation of leading logarithms (LL).

We remark that the set of operators at a fixed value of the mass dimension can be empty. This is the case for dimension 5 operators, if lepton number is also conserved by the new physics; otherwise only a single operator is allowed [51]. A full classification of all possible operators at mass dimension 6 and compatible with the SM gauge symmetry group has been carried out in [52, 53]. In total 59 operators arise, plus additional flavor structure for fermions.

²For regularization prescriptions and renormalization in general we refer to the excellent textbooks [48–50].

While model independent studies based on this set are an interesting possibility [54–60], the number of operators is very large. Furthermore, one cannot expect all coefficients g_i to be of the same order. In most models of new physics they strongly deviate from each other, depending on the precise dynamical assumptions, for instance if couplings are generated only at higher loop level, or if they are reduced or forbidden due to symmetries. The thesis at hand shows consequences of specific dynamical assumptions and ways to facilitate calculations for a generic set of dynamical assumptions.

We have seen how the SM forms the basis for all studies of models of new physics, which can be regarded as perturbations around the SM. In the following sections we lay out our standard nomenclature for the SM and briefly discuss some aspects relevant for this work.

2.2 Nomenclature and the Symmetry Breaking Sector

In the following, we set our nomenclature for the SM content. The formulation of massive gauge bosons of the electroweak interactions $SU(2)_L \times U(1)_Y$ requires the concept of spontaneous symmetry breaking, which we introduce subsequently. The issue of the quantization of such a theory is then reviewed in the next section. Our conventions agree mostly with [61]³.

The gauge fields of the local $SU(3)_c \times SU(2)_L \times U(1)_Y$ symmetry are represented by G_μ^a , $a = 1, \dots, 8$, W_μ^i , $i = 1, \dots, 3$, B_μ , with gauge couplings g_s , g , g' , generators T^a , τ^i , Y , and structure constants f^{abc} , e^{ijk} , 0, respectively. The gauge transformations act as

$$\delta W_\mu^i = \frac{1}{g} \partial_\mu \delta \theta^i + \epsilon^{ijk} W_\mu^j \delta \theta^k, \quad (2.2.1)$$

while the field strengths transform as a tensor of the adjoint

$$W_{\mu\nu}^i = \partial_\mu W_\nu^i - \partial_\nu W_\mu^i + g \epsilon^{ijk} W_\mu^j W_\nu^k, \quad \delta W_{\mu\nu}^i = \epsilon^{ijk} W_{\mu\nu}^j \delta \theta^k, \quad (2.2.2)$$

and analogous for $G_{\mu\nu}^a$ and $B_{\mu\nu}$. The field strengths are suitable to construct the kinetic terms for the gauge bosons

$$\mathcal{L}_V = -\frac{1}{4} G_{\mu\nu}^a G^{a,\mu\nu} - \frac{1}{4} W_{\mu\nu}^i W^{i,\mu\nu} - \frac{1}{4} B_{\mu\nu} B^{\mu\nu}. \quad (2.2.3)$$

The fermion sector consists of $n_f = 3$ generations of multiplets $\mathfrak{M} = (L_L, e_R, Q_L, u_R, d_R)$, where the left-handed fermions $L_L = (\nu_L, e_L)^T$, and $Q_L = (u_L, d_L)^T$ are eigenstates under the corresponding projectors $P_L = \frac{1}{2}(1 - \gamma_5)$, zero under the projection with $P_R = \frac{1}{2}(1 + \gamma_5)$, and vice versa for the right-handed fermions. The first two components of the multiplets, the leptons, are neutral under $SU(3)_c$ and the latter three, the quarks, each form a fundamental representation. For the $SU(2)_L$ transformation, we only need the two dimensional fundamental representation (chiral) for the left-handed fermions, while the right-handed fermions are singlets

$$\delta f_L = i(Y \delta \theta^Y + \tau^i \delta \theta^i) f_L, \quad \delta f_R = i Y \delta \theta^Y f_R. \quad (2.2.4)$$

The electroweak charges are summarized in table 2.1. Anomaly freedom of the SM is an important consistency condition, *i.e.* the gauge symmetries also hold at the loop-level [62–64]. It is remarkable that even though the SM employs a non-safe algebra [65], the specific charges of the multiplet \mathfrak{M} lead to a cancellation of the anomalies [66].

³We choose a reversed sign of the gauge coupling g' in contrast to [61] and $Q = Y + \tau^3$.

The fermionic kinetic terms are given by

$$\mathcal{L}_F = \sum_{i=1}^3 \sum_{f \in \mathfrak{M}} \bar{f}_i i \not{D} f_i, \quad \not{D} \equiv \gamma^\mu D_\mu, \quad (2.2.5)$$

$$D_\mu = \partial_\mu + ig_s T^a W_\mu^a + ig\tau^i W_\mu^i + ig' Y B_\mu.$$

Right-handed neutrinos would be neutral under all three gauge groups and are thus omitted in the minimal formulation of the SM. They might come useful in order to give sub-eV masses to left-handed neutrinos, and thus explain neutrino oscillations, via the see-saw mechanism. For a review see [67].

Except for the mentioned right-handed neutrino, explicit mass terms are forbidden for all fields introduced so far, due to the gauge symmetry and the choice of representations. They are instead generated in the SM by the simplest possible incarnation of the Higgs mechanism [37–40], which spontaneously breaks the gauge symmetry through a non-vanishing vacuum expectation value (VEV) of its neutral component. This is realized by a scalar doublet, which transforms under $SU(2)_L$ analogous to (2.2.4). We expand it into VEV and component fields as

$$\Phi(x) = \frac{1}{\sqrt{2}} \begin{pmatrix} -i\sqrt{2}\varphi^+(x) \\ v + h(x) + i\varphi^3(x) \end{pmatrix}, \quad (2.2.6)$$

and the complex charged scalar into components $\varphi^\pm = \frac{1}{\sqrt{2}}(\varphi^1 \mp i\varphi^2)$. The non-vanishing VEV is implied by the specific choice of signs for the general gauge-invariant self-interactions of the scalar doublet

$$\mathcal{L}_H = (D_\mu \Phi)^\dagger (D^\mu \Phi) - V(\Phi), \quad V(\Phi) = -\mu^2 \Phi^\dagger \Phi + \lambda (\Phi^\dagger \Phi)^2, \quad \mu^2, \lambda > 0. \quad (2.2.7)$$

The classical configuration $\langle \Phi \rangle = (0, v/\sqrt{2})^T$ that minimizes (2.2.7) is a uniform field with $v = \mu/\sqrt{\lambda}$. The Lagrangian (2.2.7) with fixed vacuum configuration (broken phase) is still invariant under $U(1)_{\text{em}}$ gauge transformations due to the annihilation of the vacuum by the charge $Q\langle \Phi \rangle = 0$. The charge operator is given by the Gell-Mann-Nishijima relation $Q = Y + \tau^3$. Only the neutral scalar obtains a mass $M_h = \sqrt{2}\mu$. The Goldstone theorem implies that the number of broken generators $N_{SU(2)} - N_{U(1)} = 3$ equals the number of massless scalar degrees of freedom. They are unphysical; this can be easily verified on the classical level in unitary gauge. More precisely, the would-be Goldstone bosons serve as longitudinal modes of the gauge bosons, which in turn become massive. Masses of the gauge bosons arise from the covariant derivatives $D_\mu \Phi$. One obtains the charge and mass eigenstates via

$$W_\mu^\pm = \frac{1}{\sqrt{2}}(W_\mu^1 \mp iW_\mu^2), \quad \begin{pmatrix} A_\mu \\ Z_\mu \end{pmatrix} = \begin{pmatrix} c_w & s_w \\ -s_w & c_w \end{pmatrix} \begin{pmatrix} B_\mu \\ W_\mu^3 \end{pmatrix}, \quad t_w \equiv \frac{g'}{g}, \quad (2.2.8)$$

	ν_L^c	e_L^-	e_R^-	u_L	d_L	u_R	d_R	Φ	
Q	0	-1	-1	$\frac{2}{3}$	$-\frac{1}{3}$	$\frac{2}{3}$	$-\frac{1}{3}$	1	0
T^3	$\frac{1}{2}$	$-\frac{1}{2}$	0	$\frac{1}{2}$	$-\frac{1}{2}$	0	0	$\frac{1}{2}$	$-\frac{1}{2}$
Y	$-\frac{1}{2}$	$-\frac{1}{2}$	-1	$\frac{1}{6}$	$\frac{1}{6}$	$\frac{2}{3}$	$-\frac{1}{3}$	$\frac{1}{2}$	$\frac{1}{2}$

Table 2.1: Electroweak quantum numbers of the SM matter content.

where here and in the rest of this thesis we abbreviate $s_w = \sin(\theta_w)$, $c_w = \cos(\theta_w)$, and $t_w = \tan(\theta_w)$ for the trigonometric values of the weak angle θ_w . The electric charge is given by $e = g s_w > 0$. After this redefinition one obtains

$$D_\mu \Phi = \frac{1}{\sqrt{2}} \left(\begin{array}{c} -i\sqrt{2}(\partial_\mu \varphi^+ + M_W W_\mu^+) \\ \partial_\mu h + i(\partial_\mu \varphi^3 + M_Z Z_\mu) \end{array} \right) + \text{field bilinears}, \quad (2.2.9)$$

where $M_W = gv/2 = c_w M_Z$ is the GWS relation. Remark that also a term linear in h is generated; the tadpole is proportional to $v(\mu^2 - \lambda v^2)$, *i.e.* zero at tree-level, but it reappears at higher loop-orders. Since it alters the VEV structure, it is convenient to set it to zero by a renormalization condition. This observation is interesting, as it allows to relate the VEV to the Fermi constant, defined below, by a simple relation.

The masses of the fermions are generated by the most general interactions one can write down thanks to the scalar being an $SU(2)_L$ doublet. Defining also the charge conjugated scalar doublet $\Phi^c \equiv 2i\tau^2 \Phi^*$, the Yukawa couplings read

$$\mathcal{L}_Y = -\bar{L}_L \mathbf{Y}_e \Phi e_R - \bar{Q}_L \mathbf{Y}_u \Phi^c u_R - \bar{Q}_L \mathbf{Y}_d \Phi d_R + \text{h.c.}, \quad (2.2.10)$$

where +h.c. denotes the addition of the hermitian conjugate of the preceding expression. The matrices \mathbf{Y}_f are general 3×3 matrices in flavor space, and thus break the global $SU(n_f)^5$ flavor symmetry present in the kinetic terms. The Yukawa matrices need to be diagonalized by biunitary transformations in order to obtain mass eigenstates

$$\begin{aligned} \mathbf{Y}_f &= \mathbf{U}_f \boldsymbol{\lambda}_f \mathbf{W}_f^\dagger, \quad \boldsymbol{\lambda}_f = \frac{\sqrt{2}}{v} \text{diag}(m_{f_i}), \\ f'_L &= \mathbf{U}_f f_L, \quad (f = u, d, L), \quad f'_R = \mathbf{W}_f f_R, \quad (f = u, d, e). \end{aligned} \quad (2.2.11)$$

Since only one Yukawa coupling is included for the lepton sector, the redefinition of left-handed charged leptons and neutrinos is the same. This results in the conservation of lepton generation number. Furthermore, the neutrinos remain massless. The singular value decomposition (2.2.11) is only unique up to an additional global $U(1)^3$ transformation, due to the identity

$$\mathbf{Y}_f = \mathbf{U}_f \boldsymbol{\lambda}_f \mathbf{W}_f^\dagger = \mathbf{U}_f \mathbf{P}_f \boldsymbol{\lambda}_f \mathbf{P}_f^* \mathbf{W}_f^\dagger, \quad \mathbf{P}_f = \text{diag}(e^{i\phi_{f_j}}). \quad (2.2.12)$$

The transformation of fermions with \mathbf{P}_f leaves all terms in the Lagrangian invariant, apart from the charged current interactions

$$\mathcal{L}_F|_{W^\pm} = -\frac{g}{\sqrt{2}} \bar{u}'_L \not{W}^+ \mathbf{V}_{\text{CKM}} d'_L + \text{h.c.}, \quad \mathbf{V}_{\text{CKM}} = \mathbf{U}_u \mathbf{U}_d^\dagger. \quad (2.2.13)$$

The Cabibbo-Kobayashi-Maskawa (CKM) matrix \mathbf{V}_{CKM} [19, 68] is a unitary matrix, so in general it is parametrized by 3 real parameters (moduli) and 6 phases. The redefinitions $\mathbf{V}_{\text{CKM}} \rightarrow \mathbf{P}_u \mathbf{V}_{\text{CKM}} \mathbf{P}_d^*$ then allow to absorb five of those phases in the phase differences of the matrices $\mathbf{P}_{u,d}$, such that a single phase δ remains. In the standard parametrization [69] one chooses four specific CKM entries to be real

$$\mathbf{V}_{\text{CKM}} = \begin{pmatrix} V_{ud} & V_{us} & V_{ub} \\ V_{cd} & V_{cs} & V_{cb} \\ V_{td} & V_{ts} & V_{tb} \end{pmatrix} = \begin{pmatrix} c_{12}c_{13} & s_{12}c_{13} & s_{13}e^{-i\delta} \\ -s_{12}c_{23} - c_{12}s_{23}s_{13}e^{i\delta} & c_{12}c_{23} - s_{12}s_{23}s_{13}e^{i\delta} & s_{23}c_{13} \\ s_{12}s_{23} - c_{12}c_{23}s_{13}e^{i\delta} & -s_{23}c_{12} - s_{12}c_{23}s_{13}e^{i\delta} & c_{23}c_{13} \end{pmatrix}, \quad (2.2.14)$$

where $c_{ij} \equiv \cos(\theta_{ij})$, and $s_{ij} \equiv \sin(\theta_{ij})$. In total we are now able to count 9 masses, 3 mixing angles, *i.e.* 12 moduli, and 1 phase in the Yukawa sector of the SM. This can also be elegantly inferred from a spurion analysis. Suppose the Yukawa matrix elements are replaced with flavon fields having $N_Y = 3 \times (n_f^2, n_f^2)$ flavon moduli and phases, which break the flavor symmetry $G = SU(n_f)^5$ to the remnant $H = U(1)_B \times U(1)_{L_i}^{n_f}$ baryon and lepton generation number factors⁴. Then, the Goldstone theorem directly tells us that

$$N_G - N_H = 5 \times \left(\frac{n_f(n_f - 1)}{2}, \frac{n_f(n_f + 1)}{2} \right) - (n_f + 1) \times (0, 1) \quad (2.2.15)$$

flavons remain massless. The Yukawa sector of the generalized SM with n_f generations thus has

$$N_Y - (N_G - N_H) = \left(\frac{n_f(n_f + 5)}{2}, \frac{n_f(n_f - 3)}{2} + 1 \right) \quad (2.2.16)$$

moduli and phases. For $n_f = 3$ we find as expected 12 moduli and 1 phase, and we see that at least three generations are necessary in order to obtain a phase at all. This phase is the only source of CP violation in the SM. We see from (2.2.14) that it is in fact always multiplied with the very small quantity $s_{13} = |V_{ub}|$. Even though this implies generally that physical observable in which CP violation is measurable must contain this small quantity, it does not necessarily imply a relative suppression compared to the leading contributions in a specific process. *E.g.* B -meson decays generally involve V_{ub} and V_{cb} , which are both similarly small.

The standard parametrization is recommended for numerical evaluations. When the CKM matrix is given in a general phase convention, we can transform to standard phase convention by fulfilling the requirement that the elements V_{ud}, V_{us}, V_{cb} and V_{tb} shall be real and the remaining two phase parameters correlated by

$$\text{Im}(V_{cs}) = \frac{V_{us}V_{cb}}{V_{ud}^2 + V_{us}^2} \text{Im}(V_{ub}). \quad (2.2.17)$$

Another common parametrization clearly reveals the structure of the CKM matrix. When we define

$$s_{12} \equiv \lambda, \quad s_{23} = A\lambda^2, \quad s_{13} = A\lambda^3(\rho - i\eta), \quad (2.2.18)$$

we can expand the CKM matrix in λ to arrive at

$$V_{\text{CKM}} = \begin{pmatrix} 1 - \frac{\lambda^2}{2} & \lambda & A\lambda^3(\rho - i\eta) \\ -\lambda & 1 - \frac{\lambda^2}{2} & A\lambda^2 \\ A\lambda^3(1 - \rho - i\eta) & -A\lambda^2 & 1 \end{pmatrix} + \mathcal{O}(\lambda^4). \quad (2.2.19)$$

This parametrization is named after Wolfenstein [73]. Since $\lambda = |V_{us}| + \mathcal{O}(\lambda^7) \approx 0.23$, equation (2.2.19) directly reveals the hierarchies of the CKM matrix. It is interesting to note that such a hierarchical pattern is not present in the lepton analogue of the CKM matrix, the Pontecorvo-Maki-Nakagawa-Sakata (PMNS) matrix [74–76]. Its elements can be measured

⁴Only the difference of total baryon and total lepton number, and the differences of two lepton generation numbers are exact conserved quantities. The single $U(1)$ factors of H are anomalous due to electroweak interactions. This is connected to instanton transitions between different vacuum configurations [70]. They lead to asymmetries at temperatures above the scale of electroweak symmetry breaking but are exponentially suppressed below [71, 72].

in neutrino oscillation experiments and are usually parametrized similar to the form (2.2.14). With an unspecified origin of neutrino masses, two additional CP phases are allowed in principle. In the PMNS matrix, the angles s_{12} and s_{23} are of similar size and only s_{13} is smaller by approximately a factor of 4. The small but non-zero (1, 3) element of the PMNS matrix has been established recently [77]. For a global analysis of the leptonic mixing angles and further references see [78].

2.3 Quantization and BRST Invariance

We will now discuss the quantization of a classical gauge theory, first in general terms, and then specify it to the SM in the remainder of this section. We will thereby introduce the generalized concept of gauge invariance at the quantum level. This concept forms the main ingredient of the discussion in section 3.1 and 4.1.1, where we find practical implications that are generically applicable to any renormalizable gauge theory beyond the SM.

The quantization can in principle be carried out in terms of canonical commutators of fields that are promoted to quantum field operators. Alternatively, we can consider the generating functional. For the relevant case of a spontaneously broken gauge symmetry with gauge fields A , and scalars Φ that may obtain VEVs, the generating functional is given by the path integral

$$\mathcal{Z}[J_A, J_\Phi] = \int \mathcal{D}A \mathcal{D}\Phi e^{i(S_V[A] + S_H[A, \Phi] + \int d^Dx [J_{A,\mu}(x)A^\mu(x) + J_\Phi(x)\Phi(x)])}. \quad (2.3.1)$$

Both quantization methods are equivalent in the sense that we can relate correlators, *i.e.* expectation values of a product of operators, to functional derivatives of \mathcal{Z} with respect to the sources $J_{A,\Phi}$. It is well known that a quantization by imposing canonical commutation relations of field operators leads to mathematical difficulties for local gauge theories, since the two degrees of freedom do not match the four entries of the usual spin-1 representation. In Lorentz gauge, the method of Gupta and Bleuler [79, 80] is applicable to abelian theories, but it does not generalize to the non-abelian case. Consequently, the canonical approach becomes impractical for explicit calculations, where the preservation of full gauge covariance is a useful property. A direct treatment of (2.3.1) runs into severe problems as well. By Fourier-transforming the space-time coordinates of the Lagrangian, one can easily show that the path integral is badly divergent on the subspace of modes that are gauge equivalent to $A_\mu = 0$. The Faddeev-Popov (FP) method for gauge fixing [81] resolves this issue, by removing the redundant integration over gauge equivalent subspaces and results in a rigorous and simple set of calculational rules. This makes functional quantization the standard method for the derivation of Feynman rules and ultimately to compute Green's functions and \mathcal{S} -matrix elements.

We shortly present the idea of the FP method. To simplify the notation, we skip the source terms $J_{A,\mu} = J_\Phi = 0$; the procedure works analogously in the general case. Let A^α and Φ^α denote the gauge transformed fields under some finite-dimensional representation of a compact Lie group

$$A_\mu^\alpha = U(\alpha) \left(\frac{i}{g} D_\mu \right) U(\alpha)^\dagger, \quad \Phi^\alpha = U(\alpha) \Phi. \quad (2.3.2)$$

A gauge fixing condition $\tilde{F}[A, \Phi] = 0$ is introduced by the insertion of the identity

$$1 = \int \mathcal{D}\alpha \delta(\tilde{F}[A^\alpha, \Phi^\alpha]) \det\left(\frac{\delta\tilde{F}[A^\alpha, \Phi^\alpha]}{\delta\alpha}\right). \quad (2.3.3)$$

Employing any choice of \tilde{F} that is linear in A and Φ implies that the functional derivative of \tilde{F} with respect to α will be independent of α . This allows to separate the integration over gauge equivalent subspaces into an infinite constant, which only affects the irrelevant overall normalization of \mathcal{Z} . The constant is proportional to the volume of the gauge group $\mathcal{V} = \int \mathcal{D}\alpha$ and the generating functional given by

$$\mathcal{Z}[0] = \mathcal{V} \int \mathcal{D}A \mathcal{D}\Phi e^{i(S_V + S_H)} \delta(\tilde{F}[A, \Phi]) \det\left(\frac{\delta\tilde{F}[A^\alpha, \Phi^\alpha]}{\delta\alpha}\right). \quad (2.3.4)$$

A convenient redefinition of \tilde{F} moves the functional determinant into a contribution to the action. Let $\tilde{F}[A, \Phi] \equiv F[A, \Phi] - \omega$ with a linear functional F and any function $\omega(x)$. Subsequently we integrate over ω with a Gaussian weight normalized by N_ξ

$$\tilde{\mathcal{Z}}[0] \equiv N_\xi \int \mathcal{D}\omega e^{-i \int d^4x \frac{\omega(x)^2}{2\xi}} \mathcal{Z}[0], \quad (2.3.5)$$

to obtain a new path integral

$$\tilde{\mathcal{Z}}[0] = (N_\xi \mathcal{V}) \int \mathcal{D}A \mathcal{D}\Phi e^{i(S_V + S_H + S_{GF})} \det\left(\frac{\delta F[A^\alpha, \Phi^\alpha]}{\delta\alpha}\right), \quad (2.3.6)$$

$$S_{GF} = \int d^4x \left(-\frac{1}{2\xi}\right) F[A, \Phi]^2. \quad (2.3.7)$$

The functional determinant determines the Faddeev-Popov ghost sector, which is an important ingredient for the definition of and calculations in renormalizable gauges. We use the formal identity for integration over a Grassmann valued complex field c and a hermitian operator \mathcal{O} , with

$$\det(\mathcal{O}) = \int \mathcal{D}c \mathcal{D}\bar{c} e^{i \int d^4x \bar{c} \mathcal{O} c}, \quad (2.3.8)$$

to rewrite the functional determinant as

$$\det\left(\frac{\delta F[A^\alpha, \Phi^\alpha]}{\delta\alpha}\right) = \int \mathcal{D}c \mathcal{D}\bar{c} e^{i \int d^4x \mathcal{L}_{FP}}, \quad \mathcal{L}_{FP} \propto \bar{c} \frac{\delta F[A^\alpha, \Phi^\alpha]}{\delta\alpha} c. \quad (2.3.9)$$

Constant factors can be included into the normalization of c . In general, c , F , and α are vectors with length equal to the dimension of the representation of the gauge group. We suppressed the corresponding indices above. c is called a ghost field for its counter-intuitive physical interpretation: The field is anti-commuting but a Lorentz scalar. Thus, it would violate the spin-statistics theorem. Just like the longitudinal light-like modes of the gauge field, or the would-be Goldstone bosons, the ghost field will also not appear in any final state. This can be formally proved by the introduction of a BRST symmetry, named after Becchi, Rouet, Stora and Tyutin [82–84]. After fixing the gauge, the usual gauge invariance of (2.2.1) and (2.2.4) is of course no longer manifest. Instead, the role of gauge transformations is precisely replaced by the BRST transformations. In order to obtain these non-linear

transformations, one has to replace the infinitesimal gauge parameter by the ghost field times an anti-commuting constant $\delta\lambda$, *i.e.* $\delta\theta^a \rightarrow \delta\lambda u^a$. The BRST operator s is then defined as the left derivative with respect to $\delta\lambda$. The BRST symmetry is therefore a supersymmetry, since it transforms fields with different spin-statistics properties into each other. It remains to specify the BRST transformation of the ghost fields. The BRST transformation of anti-ghost fields is determined by the gauge-fixing function F^a , while the transformation of ghost fields is determined by the structure constants f^{abc} (zero for abelian $U(1)$ factors):

$$su^a = -\frac{g}{2} f^{abc} u^b u^c, \quad s\bar{u}^a = -\frac{1}{\xi} F^a. \quad (2.3.10)$$

The BRST operator is nil-potent $s^2 = 0$ except for its action on anti-ghost fields. This can be enforced by the introduction of auxiliary non-dynamical fields, the Nakanishi-Lautrup fields [85, 86]. When doing so, the physical states, *i.e.* the two transverse degrees of freedom for massless gauge bosons, plus one longitudinal degree of freedom for massive gauge bosons, the Higgs boson, and the fermions, can be identified in terms of the kernel modulo the image of a conserved BRST charge defined through s . We do not need these formal aspect in the following. However, it is important to note that one can define physical components of asymptotic states, *i.e.* external states to the processes we want to compute, in such a way that their BRST transformation vanishes $s\psi_{\text{ph}} = 0$.

We did not yet specify an explicit form for the linear functional F . Most convenient are 't Hooft R_ξ -gauges, for which one usually introduces the gauge-fixing functions in terms of the mass eigenstates

$$\begin{aligned} F_{W^\pm} &= \partial_\mu W^{\pm\mu} \mp i\xi_W M_W \varphi^\pm, \\ F_Z &= \partial_\mu Z^\mu - \xi_Z M_Z \varphi^3, \\ F_A &= \partial_\mu A^\mu, \quad F_G = \partial_\mu G^\mu, \end{aligned} \quad (2.3.11)$$

allowing for a bare gauge parameter for each gauge field. The form is chosen such as to remove two-point mixing between each massive gauge boson and the corresponding Goldstone boson at tree level. Linearity of the gauge fixing assures that the gauge parameter does not appear in vertices.⁵

The 't Hooft-Feynman gauge sets $\xi_V = 1$ for all gauge parameters and is particularly convenient. In this gauge, the tree-level gauge field propagators obtain a simpler Lorentz structure and the poles of the Goldstone boson and ghost propagators coincide with the gauge boson masses

$$\begin{aligned} \mu \overset{V}{\text{---}} \nu \Big|_{k \rightarrow} &= \frac{-i}{k^2 - M_V^2} \left(g^{\mu\nu} - (1 - \xi_V) \frac{k^\mu k^\nu}{k^2 - \xi_V M_V^2} \right), \\ \text{---} \Big|_k \begin{matrix} \varphi, u \end{matrix} &= \frac{i}{k^2 - \xi_V M_V^2}, \end{aligned} \quad (2.3.12)$$

where u and φ are the ghost and Goldstone boson of the gauge boson V .

Taking instead the limit of $\xi_V \rightarrow \infty$, one can in fact decouple the unphysical degrees of freedom.⁶ We are then left with the non-renormalizable unitary gauge. Trouble arises in

⁵Scalar-ghost vertices are an exception.

⁶Nevertheless, one must take into account scalar-ghost, since they are linear in ξ [87].

this gauge if we encounter individual loop-diagrams that carry ξ -dependence and diverge in this limit. Yet, the gauge invariance of matrix elements of ξ -independent operators and the gauge invariance of the \mathcal{S} -matrix tell us that these divergences must cancel in the sum of all diagrams. Moreover, one cannot refer to power-counting arguments anymore, since the gauge-boson propagator does not fall off like k^{-2} in this limit. In total, the evaluation of loop-integrals in general becomes an involved and error prone task of rearrangements inside of loop-integrals and is an ill-advised strategy.

2.4 Reasons to Go Beyond

One of the most astonishing things about the world in which we live is that there seems to be interesting physics at all scales. Whenever we look in a previously unexplored regime of distance, time, or energy, we find new physical phenomena.

————— HOWARD GEORGI

Before entering the discussion of physics beyond the SM, we give a brief summary of the questions left open by the SM and indications of its incompleteness. We begin with the observational reasons and then turn to aspects of theoretical character.

The attempt to fill the whole gap between the SM and a quantum theory of gravity at once seems to be a daunting task, given that our observations cover only about half of the energy scales between van-der-Waals forces and the Planck scale — the scale where gravitational quantum effects are expected to become important. From the discussion of EFTs we learned that this is also not absolutely mandatory. For practical reasons, most of the model building effort may thus concentrate on new phenomena that could be observed at the LHC or a future linear collider. There are also tangible reasons to expect new physics between the electroweak and the Planck scale, and some of them indeed point towards new physics at the TeV scale. However, note that the present value of the top quark and Higgs mass put the SM Higgs potential in the region between metastability and absolute stability up to the Planck scale [88]. From a theoretical point of view, in principle this allows the SM to be the final theory of all non-gravitational forces.

One definite observational fact is already considered as physics beyond the SM: Non-zero neutrino masses can be inferred from measurements of neutrino oscillations. From the observed atmospheric neutrino mass squared difference, one derives that one of the neutrinos must have a mass of at least $4.6 \cdot 10^{-2}$ eV [69]. The masses could be accommodated by introducing right-handed Dirac neutrinos and a Yukawa coupling, either without explaining its smallness or by a type-I see-saw with a very large right-handed Majorana mass. An alternative is a non-vanishing Wilson coefficient λ_{ij} of the lepton-number violating $D = 5$ operator mentioned in section 2.1.2, the Weinberg operator $(L_i\Phi)^T(L_j\Phi)$ [51]. Gravitational effects in the Weinberg operator induce an insufficient value of only $m_{ij} = \lambda_{ij}v^2/(2M_{\text{Pl}}) \sim 10^{-5}$ eV for $\mathcal{O}(1)$ Wilson coefficients. Such a mechanism of neutrino mass generation would instead point towards a scale $\Lambda_{\text{GUT}} \sim 10^{15}$ GeV where the Weinberg operator could be sourced by a UV completion of the SM. This is referred to as the type-II see-saw. For a review of the see-saw variants, see [67]. The corresponding operators can also obtain contributions from scalar triplets instead of the doublets, see *e.g.* [89].

The most striking arguments for a richer structure of new physics actually stem from astrophysical and cosmological observations. The neutral non-baryonic relic matter component from the early universe makes up about 24% of the energy density of the universe. This can be inferred from measurements of the cosmic microwave background [90]. Dark matter is also found through many other astrophysical observations, *e.g.* the radial dependence of galaxy rotation curves. For recent reviews, we refer to [91, 92]. The only dark matter component of the SM are the light neutrinos. They cannot account for the necessary amount of relic density and are too relativistic to be responsible for structure formation in the early universe [93].

A common scenario for dark matter particles is the existence of weakly interacting massive particles (WIMPs) that are in thermal and chemical equilibrium with all other particles in the early universe, due to their self-annihilation into SM particles and vice versa. At some expansion state of the universe their density becomes too low and they freeze out of equilibrium. Their relic density can be approximated by $\Omega_X h^2 \approx 3 \cdot 10^{-27} \text{cm}^3 \text{s}^{-1} / \langle \sigma v \rangle \approx 0.1$ under some simplifying assumptions [91, 94]. This points towards a cross section that is typical of weak interactions in the SM. The annihilation cross sections depends on the dark matter particle's mass and constrains the values of the most common candidates to be in the range of $10 - 10^5$ GeV. The neutralino, as the lightest stable particle in many versions of the minimal supersymmetric extension of the SM (MSSM), is a prototypical WIMP candidate. Another widely studied candidate is the lightest Kaluza-Klein particle in theories of flat universal extra dimensions [95] with KK parity, a remnant of 5d momentum conservation.

Another unsolved aspect in the SM is the observed matter-antimatter asymmetry of the universe [90]. Even though the SM fulfills all three Sakharov conditions [96], with Baryon-number violation through anomalies at the non-perturbative level and a thermal non-equilibrium occurring in an early epoch of the expanding universe, *CP* violation from the CKM mechanism is known to be insufficient in order to obtain the necessary amount of asymmetry [97]. Note that a solution to this problem can also be found in baryogenesis through leptogenesis, *e.g.* by a heavy right-handed Majorana neutrino. See [98] for a review.

Besides observational, there exist also unanswered questions from the theoretical point of view. A suggestive property of the SM is that its running gauge couplings come very close but slightly miss each other at the aforementioned scale $\Lambda_{\text{GUT}} \sim 10^{15}$ GeV. This constitutes more an intriguing possibility than a shortcoming, as unification of running coupling constants could happen through modifications of the RGE below this scale. This explains also the name GUT, which stands for grand unified theory [99]. Simple non-supersymmetric $SU(5)$ is ruled out by the prediction of too rapid proton decay and an excluded value for weak mixing angle [100]. In supersymmetric GUTs the unification scale is usually more than an order of magnitude higher and the models can pass proton decay bounds [101]. In extra-dimensional extensions of the ADD type (see section 3.3.1), the unification scale can be lower [102]. The Randall-Sundrum models, which we extensively discuss in section 3.3, allow for gauge-coupling unification without supersymmetry [103].

The SM is free of relevant operators through the concept of electroweak symmetry breaking, which provides enough symmetry in order to forbid explicit mass terms but for a single exception: the parameter μ^2 of the Higgs boson is necessary for electroweak symmetry breaking. Radiative corrections to the Higgs two-point vertex function are easily seen to be quadratically sensitive to a cutoff scale Λ of high loop momenta. The one-loop correction from a fermion with Yukawa coupling y_f to the Higgs boson, mass m_f and a repetition factor

N_f , e.g. a possible color factor, is given by [104] (see also [105, 106])

$$\delta M_H^2 = \frac{N_f y_f^2}{8\pi^2} \left[-\Lambda^2 + 6m_f^2 \ln(\Lambda/m_f) - 2m_f^2 \right] + \mathcal{O}(\Lambda^{-2}). \quad (2.4.1)$$

Furthermore, there are also contributions from the SM gauge bosons and the Higgs boson itself. For a general scalar with mass m_S , trilinear and quadrilinear coupling to one and two Higgs bosons given by $v\lambda_S$ and λ_S , respectively, one finds

$$\delta M_H^2 = \frac{N_S \lambda_s}{16\pi^2} \left[-\Lambda^2 + 6M_S^2 \ln(\Lambda/M_S) \right] + \frac{N_S \lambda_s^2}{16\pi^2} v^2 \left[-1 + 2 \ln(\Lambda/M_S) \right] + \mathcal{O}(\Lambda^{-2}), \quad (2.4.2)$$

and a similar expression for gauge bosons. In total, the Λ^2 divergent term has a one-loop coefficient of $(M_H^2 + 2M_W^2 + M_Z^2 - 4m_t^2)/v^2$ in the SM. A cancellation between the masses, once proposed by Veltman [107], does not occur numerically with the recently found value of $M_h \approx 126$ GeV and would anyway not protect the quadratically divergent terms at two and higher loop levels. For values of the cutoff around the Planck or GUT scale, a very specific bare Higgs mass and a cancellation with the radiative corrections is required to achieve a physical Higgs mass near the electroweak scale. This is referred to as the naturalness or fine-tuning problem [108, 109]. In principle this is not a problem within the SM, since renormalizability assures that the cancellation occurs in a mathematically consistent way by choosing the appropriate counterterm that cancels the divergence. Nevertheless, a technical stability problem of the Higgs mass remains in the presence of a large mass gap to perturbative new physics far above the electroweak scale due to the explicit mass dependence contained in (2.4.1) and (2.4.2). To summarize, the natural value of the Higgs mass is driven to the highest resonance in the theory. This is called the gauge hierarchy problem. According to 't Hooft's naturalness criterion, this calls for a symmetry in a perturbative extension of the SM. A very elegant way that leads to a cancellation between contributions of the form (2.4.1) and (2.4.2) is given by supersymmetry: the left and right-handed squark account for $N_S = 2N_f$ and cancel the quadratic divergence of each quark respectively. The remaining contribution to the Higgs mass is then only sensitive to the splitting of m_f and M_S and can induce a little hierarchy, also called μ problem. In sections 3.2 and 3.3 we present the Little-Higgs and Randall-Sundrum models that are effective theories and impose a limited range of validity of $\Lambda \sim 10$ TeV, in order to explain the absence of the gauge hierarchy problem.

An open question also related to radiative corrections to the Higgs mass is the following. As we have seen, M_h^2 , or equivalently μ^2 in the phase of unbroken $SU(2)_L \times U(1)_Y$ symmetry, is additively renormalized. But for electroweak symmetry breaking necessarily $\mu^2|_{\text{TeV}} < 0$ holds, and there is no natural distinction between the two signs.

The SM shows further unexplained hierarchical values: The cosmological constant problem [110] refers to the $D = 0$ operator of the effective Lagrangian. It is already sourced by the bare Higgs potential $\varrho_h = M_h^2 v^2/8$, but unfortunately with a contribution that is 55 orders of magnitude above the experimental value $\varrho_{\text{vac}} \sim \text{meV}^4$ [90]. A very peculiar cancellation must also take place in the effective angle θ_{QCD} . The angle is restricted to be very tiny by the upper bound on the neutron electric dipole moment [111]. It obtains a priori unrelated contributions from the non-abelian gauge-group topology of the vacuum [71] and the chiral fermion transformations (2.2.11) [112]. The reason for the necessary cancellation of these contributions is unknown and called the strong CP problem.

Finally, the hierarchies of masses and mixing angles in the quark sector and the different pattern in the lepton sector are left unexplained. In contrast to the quark sector, where mass

and flavor eigenstates are similar, one of the neutrino mass eigenstates consists mainly of ν_e , one to nearly equal parts of ν_μ and ν_τ , and the third to similar parts of all three flavor eigenstates. Unlike for the Higgs mass, the fermion hierarchies do not imply a technical instability. But it is considered unsatisfying that the SM provides no explanation for the almost 6 orders of magnitude between the largest quark and lightest charged lepton masses and at least 6 additional orders of magnitude to the neutrino mass scale.

Apart from hierarchies, the particular structure of the SM is not inherently explained by the model itself, *i.e.* the number of fermion generations and why their charges are given as in the specific anomaly free assignment [64]. Thus, there are plenty of reasons to improve simplicity and elegance of the SM in a UV completion.

In our phenomenological discussion, we will also come across some experimental tensions from collider experiments, which are at the $2\text{--}3\sigma$ level. Here, we emphasize that they are all inconclusive and might be either due to experimental fluctuation or possible underestimated systematics from the experimental and/or theoretical side. Apparently it is an interesting fact that there exist more deviations at processes involving particles of higher mass. However, this should in fact be expected due to the unsettled experimental situation and the lower statistics. Yet, this drives model building of new physics into a specific direction, as the constraints related to quarks of the first two generations are stronger. We will discuss this in more detail below. We close with emphasizing that all models trying to solve some of the above issues are very likely to include the SM as the basic building block in the low energy limit.

Chapter 3

Theoretical Classification & Examples of New Physics

3.1 Relations for Perturbatively Unitary Theories

We start the discussion of models beyond the SM with a general summary of properties of perturbatively unitary theories. To this end, we consider a template Lagrangian, with an arbitrary number of massive degrees of freedom: gauge bosons, fermions, and scalars. Perturbative unitarity imposes important constraints on such generic extensions. The required cancellation of unbounded high-energy growth of scattering amplitudes leads to specific universal relations among the couplings, and it enables us to understand and perform the renormalization of the observables in a general way. The feasibility of this approach is expected on general grounds, since the equations implied by perturbative unitarity uniquely reflect the spontaneously broken gauge structure of renormalizable theories [113–115]. This property, which we have already discussed for the SM, in fact holds generically. Equalities from perturbative unitarity thus may as well be derived by means of Slavnov-Taylor identities (STIs). In section 4.1.1 we advocate the practical implementation of those simple relations in the calculation and renormalization of generic loop amplitudes. This goes beyond the typical application of perturbative unitarity in which one typically derives upper bounds on yet unobserved mass spectra [116–118] and combinations of masses and/or couplings [119–122].

3.1.1 The Generic Lagrangian

In the following, we consider an extension of the SM by an arbitrary number of heavy scalar, fermion, and vector fields, *i.e.* with masses above the electroweak scale. As our starting point, we define a generic template Lagrangian, whose interaction terms with massless SM vector fields – the photon and gluon – are fixed by QED and QCD gauge invariance. In particular, they are given in terms of the $SU(3)_c \times U(1)_{\text{em}}$ covariant derivative

$$(D_\mu)_{ij} = (\partial_\mu - ie Q_F A_\mu) \delta_{ij} - ig_s G_\mu^a T_{F,ij}^a, \quad (3.1.1)$$

by the usual kinetic terms of the massive fields F . Here, $T_{F,ij}^a$ and Q_F generate the action of the respective gauge group $SU(3)_c$ and $U(1)_{\text{em}}$ on the field F .

The interactions of massive fields up to mass-dimension four read

$$\begin{aligned}
 \mathcal{L}_{\text{int}} = & \sum_{s, \bar{f}_1, f_2, \sigma} y_{s, \bar{f}_1, f_2}^{\sigma, abc} h_s^a \bar{\psi}_{f_1}^b P_\sigma \psi_{f_2}^c + \sum_{v, \bar{f}_1, f_2, \sigma} g_{v, \bar{f}_1, f_2}^{\sigma, abc} V_{v, \mu}^a \bar{\psi}_{f_1}^b \gamma^\mu P_\sigma \psi_{f_2}^c \\
 & + \frac{i}{6} \sum_{v_1, v_2, v_3} g_{v_1, v_2, v_3}^{abc} \left(V_{v_1, \mu}^a V_{v_2, \nu}^b \partial^{[\mu} V_{v_3}^{c, \nu]} + V_{v_3, \mu}^c V_{v_1, \nu}^a \partial^{[\mu} V_{v_2}^{b, \nu]} + V_{v_2, \mu}^b V_{v_3, \nu}^c \partial^{[\mu} V_{v_1}^{a, \nu]} \right) \\
 & + \frac{1}{2} \sum_{v_1, v_2, s} g_{v_1, v_2, s}^{abc} V_{v_1, \mu}^a V_{v_2}^{b, \mu} h_s^c - \frac{i}{2} \sum_{v, s_1, s_2} g_{v, s_1, s_2}^{abc} V_v^{a, \mu} \left(h_{s_1}^b \partial_\mu h_{s_2}^c - (\partial_\mu h_{s_1}^b) h_{s_2}^c \right) \\
 & + \frac{1}{6} \sum_{s_1, s_2, s_3} g_{s_1, s_2, s_3}^{abc} h_{s_1}^a h_{s_2}^b h_{s_3}^c + \frac{1}{24} \sum_{s_1, s_2, s_3, s_4} g_{s_1, s_2, s_3, s_4}^{abcd} h_{s_1}^a h_{s_2}^b h_{s_3}^c h_{s_4}^d \\
 & - \frac{i}{2} \sum_{v_1, v_2} \left(e \omega_{A, v_1, v_2} F^{\mu\nu} V_{v_1, \mu}^a V_{v_2, \nu}^a + g_s \omega_{G, v_1, v_2}^{abc} G^{a, \mu\nu} V_{v_1, \mu}^b V_{v_2, \nu}^c \right). \tag{3.1.2}
 \end{aligned}$$

They involve physical scalars h_{s_i} , Dirac fermions¹ ψ_{f_i} , and vector fields V_{v_i} , with non-zero masses M_{s_i} , m_{f_i} , and M_{v_i} , respectively. These fields are enumerated by the corresponding indices s_i , f_i , v_i . The index σ denotes the two chiralities $\sigma = L, R$. Square brackets around Lorentz indices denote their anti-symmetrization. Furthermore, the kinetic term of V_i and the couplings to the field strength tensors ω contribute to triple gauge boson vertices with one photon or gluon. The standard Lorentz structure for these vertices is obtained if and only if we take

$$\omega_{A, v_1, v_2} = \delta_{\bar{v}_1, v_2} Q_{v_2}, \quad \omega_{G, v_1, v_2}^{abc} = \delta_{\bar{v}_1, v_2} T_{v_2, bc}^a. \tag{3.1.3}$$

We assume that all vector fields obtain their mass by a spontaneous breakdown of a local symmetry. The Lagrangian \mathcal{L}_{int} comprises only the model-dependent couplings: all remaining ‘‘unphysical’’ interactions, for instance of the would-be Goldstone bosons associated with the spontaneous symmetry breaking, can be inferred from the requirement of perturbative unitarity via the STIs, which we discuss below.

Through $SU(3)_c \times U(1)_{\text{em}}$ gauge invariance, non-vanishing couplings may only exist for index combinations that allow the fields to form an uncharged singlet. For instance, a non-vanishing coefficient $y_{s_1, \bar{f}_1, f_2}^{\sigma, abc}$ implies the charge relation $Q_{s_1} + Q_{f_2} = Q_{f_1}$, and²

$$y_{s, \bar{f}_1, f_2}^{\sigma, abc} T_{s, da}^e + y_{s, \bar{f}_1, f_2}^{\sigma, abd} T_{f_2, dc}^e = T_{f_1, bd}^e y_{s, \bar{f}_1, f_2}^{\sigma, adc}. \tag{3.1.4}$$

If one of the fermions – *e.g.* ψ_{f_2} – is uncharged, Schur’s lemma implies that $T_{s_1} = T_{f_1}$. Hermiticity puts further restrictions on the couplings. For instance, we can express the couplings of negatively charged Higgs and gauge bosons to fermions by the couplings of the corresponding positively charged particles. In general, we have

$$\begin{aligned}
 y_{s, \bar{f}_2, f_1}^\sigma &= (y_{\bar{s}, \bar{f}_1, f_2}^{\bar{\sigma}})^*, & g_{v, \bar{f}_2, f_1}^\sigma &= (g_{\bar{v}, \bar{f}_1, f_2}^{\bar{\sigma}})^*, & g_{v_1, v_2, s} &= (g_{\bar{v}_1, \bar{v}_2, \bar{s}})^*, \\
 g_{v, s_1, s_2} &= -(g_{\bar{v}, \bar{s}_1, \bar{s}_2})^*, & g_{v_1, v_2, v_3} &= -(g_{\bar{v}_1, \bar{v}_2, \bar{v}_3})^*.
 \end{aligned} \tag{3.1.5}$$

The bars over bosonic indices denote the exchange of indices within a pair of oppositely charged particles, as in $g_{\overline{W^+} \dots} = g_{W^- \dots}$. They have no effect for neutral particles. The bar over a σ denotes the opposite chirality.

¹For simplicity, we do not consider Majorana fermions here. A generalization is however straightforward.

²These properties allow for a systematic calculation of QCD corrections to our results in a similar way to the calculation of radiative decays in [123] and $\Delta F = 2$ processes in [124].

3.1.2 Slavnov-Taylor Identities for Feynman Rules

The constraints derived from perturbative unitarity reflect a spontaneously broken gauge symmetry. To exploit these constraints for our generic template Lagrangian, we use the STIs of an arbitrary spontaneously broken gauge theory. The massive vector fields of (3.1.2) are the gauge bosons of the fundamental theory, supplemented by a standard R_ξ gauge-fixing term. The outcome of this is twofold: the couplings of Goldstone bosons can be directly linked to the couplings of the corresponding vectors in the mass-eigenstate basis. This use of STIs is well known and summarized in the Goldstone-boson-equivalence theorem (GBET) [115, 116, 125, 126]. Moreover, we obtain certain sum rules, *i.e.* equations that impose non-trivial constraints on the couplings of physical fields and encode the full spontaneously broken gauge structure on the level of Feynman rules³. We will use the sum rules in section 4.1.1 to demonstrate the generic renormalization of the Z penguin.

From a technical point of view, it is easiest to derive the sum rules from the vanishing Becchi-Rouet-Stora-Tyutin (BRST) transformation [82–84] of suitable vertex functions. The derivation of the necessary relations between vertex functions is well summarized in [61]. Below, we also comment on how to obtain sum rules from a tree-level partial wave analysis. To start, we note that throughout this work the gauge freedom of (3.1.2) is fixed with a standard linear R_ξ Lagrangian [128]

$$\mathcal{L}_{\text{fix}} = - \sum_v (2\xi_v)^{-1} F_{\bar{v}} F_v, \quad F_v = \partial_\mu V_v^\mu - \sigma_v \xi_v M_v \varphi_v, \quad (3.1.6)$$

for every vector field V_v^μ of mass M_v and corresponding Goldstone boson φ_v , where σ_v can be $\pm i$ for complex fields and ± 1 for real fields. For the SM fields they are given by $\sigma_{W^\pm} = \pm i$ and $\sigma_Z = 1$, and we choose this convention in general for all charged and neutral vector fields.

By applying the BRST operator s to a Green's function

$$G^{\bar{u}_v (\dots)_{\text{ph}}}(x, \dots) \equiv \langle T \bar{u}_v(x) (\dots)_{\text{ph}} \rangle, \quad (3.1.7)$$

which involves an anti-ghost \bar{u}_v , and using the transformation property $s\bar{u}_v = -F_v/\xi_v$, we will obtain a linear relation between the connected and truncated Green's functions, schematically

$$sG^{\bar{u}_v (\dots)_{\text{ph}}} = 0 \quad \longrightarrow \quad \mathcal{F}_{\text{linear}} \left(G_{c,\mu}^{V_v (\dots)_{\text{ph}}}, G_c^{\varphi_v (\dots)_{\text{ph}}} \right) = 0. \quad (3.1.8)$$

Here, the dots $(\dots)_{\text{ph}}$ stand for any combination of physical asymptotic on-shell fields, whose BRST variations vanish. The underlining of a field indicates that the corresponding external leg has been amputated. In our convention, labels on vertex functions denote outgoing fields, whereas their momenta are incoming. The momentum of the first field shall be k_μ . The momentum configuration of the vectors and Goldstone bosons coming from the gauge-fixing function is not restricted any further.⁴

The STIs lead to the following relation in momentum space

$$\begin{pmatrix} k^\mu \\ i\sigma_{\bar{v}}\xi_v M_v \end{pmatrix}^T G_{(\mu\nu)}^{\bar{v}} \begin{pmatrix} \langle T \underline{V}_v^\nu (\dots)_{\text{ph}} \rangle_c \\ \langle T \underline{\varphi}_v (\dots)_{\text{ph}} \rangle_c \end{pmatrix} = 0. \quad (3.1.9)$$

³The couplings in (3.1.2) are defined such that the Feynman rules are given after multiplication by a factor of i and the usual Lorentz structures in the conventions of `FeynArts` [127].

⁴In the GBET, one projects on the longitudinal parts of the vector bosons and relates them to the corresponding amplitudes with Goldstone bosons. When doing so, one has to choose a certain momentum configuration in order to be able to neglect the transverse components [129]. Our arguments are based on the level of Green's functions for the total fields and independent of such considerations.

The truncation of the physical fields is straightforward and implicitly understood in the following. The first field is truncated by $G_{(\mu\nu)}^{\bar{v}}$, which denotes the matrix of two-point Green's functions for a vector boson (to which the Lorentz indices in brackets apply) and its Goldstone boson. It is given by the inverse of the two-point vertex function $\Gamma^{v(\mu\nu)}$. The explicit components of this function are given by

$$\Gamma_{(\mu\nu)}^v(k, -k) = \begin{pmatrix} \sum_{P=T,L} g_{\mu\nu}^P \Gamma_P^{V_v V_{\bar{v}}}(k^2) & k_\mu \Gamma_L^{V_v \varphi_{\bar{v}}}(k^2) \\ k_\nu \Gamma_L^{\varphi_v V_{\bar{v}}}(k^2) & \Gamma^{\varphi_v \varphi_{\bar{v}}}(k^2) \end{pmatrix}, \quad G_{(\mu\lambda)}^{\bar{v}} \Gamma^{v(\lambda\nu)} = i \begin{pmatrix} \delta_\mu^\nu & 0 \\ 0 & 1 \end{pmatrix}, \quad (3.1.10)$$

where $g_{\mu\nu}^T \equiv g_{\mu\nu} - \frac{k_\mu k_\nu}{k^2}$ and $g_{\mu\nu}^L \equiv g_{\mu\nu} - g_{\mu\nu}^T$. A short calculation [130] shows that the STIs are given by

$$\left\langle T \left(k_\mu \underline{V}_v^\mu - i\sigma_{\bar{v}} M_v A_v(k^2) \underline{\varphi}_v \right) (\dots)_{\text{ph}} \right\rangle_c = 0, \quad A_v(k^2) = \frac{\Gamma_L^{V_v V_{\bar{v}}} + \frac{k^2}{\xi_v}}{M_v (M_v - i\sigma_v \Gamma_L^{V_v \varphi_{\bar{v}}})}. \quad (3.1.11)$$

For our purposes, it is sufficient to know that $A_v(k^2) = 1$ at the tree-level. At loop-level, one would also have to take care of the mixing of different vector bosons.⁵ The derivation of (3.1.11) can be straightforwardly generalized to multiple insertions of the gauge fixing function. To this end, one starts from $\left\langle T \bar{u}_v(x) \prod_k F_{v_k}(x_k) (\dots)_{\text{ph}} \right\rangle_c$. Taking the BRST variation of this vertex function also leads to terms with derivatives of the gauge-fixing function $sF_{v_k} = s^2 \bar{u}_{v_k}$. Without introduction of Nakanishi-Lautrup fields, the BRST-operator is not exactly nil-potent; $sF_{v_k} = 0$ holds only on-shell. However, since the latter is exactly the equation of motion for the anti-ghost field, we can use the equation of motion inside the correlator to obtain for the additional part in coordinate space

$$\begin{aligned} & \left\langle T \bar{u}_v(x) (sF_{v_j})(x_j) \prod_{k \neq j} F_{v_k}(x_k) (\dots)_{\text{ph}} \right\rangle_c \\ &= -i \left\langle T \frac{\delta}{\delta \bar{u}_{v_j}(x_j)} \bar{u}_v(x) \prod_{k \neq j} F_{v_k}(x_k) (\dots)_{\text{ph}} \right\rangle_c = 0. \end{aligned} \quad (3.1.12)$$

The last equality holds, since the functional derivative only leads to a disconnected part proportional to $\delta(x - x_j)$ and consequently vanishes. Equation (3.1.11) thus generalizes to

$$\left\langle T \prod_i C_{v_i}(k_i) (\dots)_{\text{ph}} \right\rangle_c = 0, \quad C_v(k) \equiv k_\mu \underline{V}_v^\mu - i\sigma_{\bar{v}} M_v A_v(k^2) \underline{\varphi}_v. \quad (3.1.13)$$

We will now evaluate this identity at tree level for three- and four-point Green's functions, in order to find non-trivial renormalizability constraints between the generic couplings. We have checked explicitly that the STIs for five-point vertex functions do not imply additional constraints. The identity (3.1.13) is already sufficient to derive all couplings of Goldstone bosons from the physical couplings. The three-point couplings involving Goldstone bosons are related to the couplings of the corresponding gauge bosons via

$$\begin{aligned} g_{v_1 \varphi_2 \varphi_3} &= \sigma_{v_2} \sigma_{v_3} \frac{M_{v_2}^2 + M_{v_3}^2 - M_{v_1}^2}{2 M_{v_2} M_{v_3}} g_{v_1 v_2 v_3}, & g_{\varphi_1 \varphi_2 s} &= -\sigma_{v_1} \sigma_{v_2} \frac{M_s^2}{2 M_{v_1} M_{v_2}} g_{v_1 v_2 s}, \\ g_{v_1 v_2 \varphi_3} &= -i\sigma_{v_3} \frac{M_{v_1}^2 - M_{v_2}^2}{M_{v_3}} g_{v_1 v_2 v_3}, & g_{\varphi_1 s_1 s_2} &= i\sigma_v \frac{M_{s_1}^2 - M_{s_2}^2}{M_v} g_{v s_1 s_2}, \\ g_{v_1 \varphi_2 s} &= -i\sigma_{v_2} \frac{1}{2 M_{v_2}} g_{v_1 v_2 s}, & g_{\varphi_1 \varphi_2 \varphi_3} &= 0, \\ y_{\varphi_{\bar{f}_1} \bar{f}_2}^\sigma &= -i\sigma_v \frac{1}{M_v} (m_{f_1} g_{v \bar{f}_1 f_2}^\sigma - g_{v \bar{f}_1 f_2}^{\bar{\sigma}} m_{f_2}). \end{aligned} \quad (3.1.14)$$

⁵In the SM, (3.1.11) still holds at loop-level, since Z - A mixing drops out due to the photon's Ward identity.

Here, the subscripts φ_i on couplings correspond to Goldstone bosons as distinguished from the subscripts s_i , which correspond to physical scalars, *e.g.* Higgs bosons. The valid range for φ_i is the same as for the vector boson indices v_i , and we replace $\varphi_i \rightarrow v_i$ on the right-hand side of the equations for denoting indices of masses and couplings. Remark that in (3.1.13), we have to set only the additional fields $(\dots)_{\text{ph}}$ on-shell in order to derive the relations (3.1.14).

The STIs for four-point Green's functions have two consequences. If a four-point coupling contributes to the given vertex function, the resulting relation allows to express this coupling in terms of three-point couplings. In this way, the possible four-point couplings of physical fields with at least one vector boson are derived from $\langle C_{v_1}(V_{v_2}V_{v_3}V_{v_4})_{\text{ph}} \rangle_{\text{c}} = 0$ and $\langle C_{v_1}(V_{v_2}S_{s_1}S_{s_2})_{\text{ph}} \rangle_{\text{c}} = 0$. They read

$$g_{v_1v_2v_3v_4} = \sum_{v'} (g_{v_1v_4v'}g_{v_2v_3\bar{v}'} + g_{v_1v_3v'}g_{v_2v_4\bar{v}'}), \quad (3.1.15)$$

$$g_{v_1v_2s_1s_2} = \sum_{v'} g_{v_1v's_1}g_{v_2\bar{v}'s_2} \frac{1}{4m_{v'}^2} - \sum_{s'} g_{v_1s_1s'}g_{v_2s_2\bar{s}'} + \text{symm}(v_1, v_2), \quad (3.1.16)$$

where we have replaced three-point Goldstone-boson couplings by using (3.1.14). A symmetrization over the indices, indicated by $\text{symm}(v_1, v_2)$, means one has to sum the preceding terms over all cyclic permutations of the indices without multiplication by a symmetry factor. Analogously, all four point couplings with at least one Goldstone bosons can be derived. As an example, we obtain from $\langle C_{v_1}C_{v_2}C_{v_3}C_{v_4} \rangle_{\text{c}} = 0$ the relation

$$g_{\varphi_1\varphi_2\varphi_3\varphi_4} = \frac{-\sigma_{v_1}\sigma_{v_2}\sigma_{v_3}\sigma_{v_4}}{4m_{v_1}m_{v_2}m_{v_3}m_{v_4}} \sum_{s'} m_{s'}^2 (g_{v_1v_4s'}g_{v_2v_3\bar{s}'} + \text{symm}(v_2, v_3, v_4)). \quad (3.1.17)$$

All remaining four-point Goldstone-boson couplings are enlisted in appendix A.1. There, we also give the STIs for the special case when a gauge bosons is a gluon or photon, as this can be useful for the calculation of QCD and QED corrections to generic new physics amplitudes like in [123] and [124, 131], and we comment on ghost couplings, which are also simple to obtain [132, 133].

Some of the four-point STIs involve amplitudes in which no four-point coupling appears; in particular, this is the case if a fermion current is present. Alternatively, the STIs may involve additional Lorentz structures to which no four-point coupling is proportional. These cases lead to sum rules of physical couplings. The simplest variants are the sum rules stemming from $\langle C_{v_1}(V_{v_2}V_{v_3}V_{v_4})_{\text{ph}} \rangle_{\text{1PI}} = 0$ and $\langle C_{v_1}(V_{v_2}\psi_{f_1}\bar{\psi}_{f_2})_{\text{ph}} \rangle_{\text{c}} = 0$. They reflect the Lie-algebra structure of the vector and fermion couplings

$$\sum_{v'} (g_{v_1v_2v'}g_{v_3v_4\bar{v}'} + g_{v_2v_3v'}g_{v_1v_4\bar{v}'} + g_{v_3v_1v'}g_{v_2v_4\bar{v}'}) = 0, \quad (3.1.18)$$

$$\sum_{v'} g_{v'\bar{f}_1f_2}^\sigma g_{v_1v_2\bar{v}'} = \sum_{f'} (g_{v_1\bar{f}_1f'}^\sigma g_{v_2\bar{f}'f_2}^\sigma - g_{v_2\bar{f}_1f'}^\sigma g_{v_1\bar{f}'f_2}^\sigma). \quad (3.1.19)$$

Equation (3.1.18) is simply the Jacobi identity for the structure constants in the mass basis, and (3.1.19) relates the structure constants of fermion and vector representations.

The interpretation of (3.1.19) for external W -bosons and quarks it is particularly interesting. In the SM we obtain *e.g.*

$$(3.1.19) \quad \xrightarrow{\text{SM}} \quad g_{W^-W^+Z} g_{Z\bar{d}_i d_j} + g_{W^-W^+A} g_{A\bar{d}_i d_j} = g_{W^- \bar{d}_i u}^L g_{W^+ \bar{u} d_j}^L \\ \Leftrightarrow \quad -\frac{2c_w}{g} g_{Z\bar{d}_i d_j} = (V^\dagger V)_{ij} + 2s_w^2 Q_d \delta_{ij}, \quad (3.1.20)$$

and an analogous relation for external up-type quarks. In the second line, we inserted all SM couplings, except for Z -quark couplings. We observe that the unitarity of the CKM matrix and the universality and diagonality of the Z -quark couplings are mutually dependent. This extends trivially to leptons. The introduction of a single additional fermion, which mixes with any of the SM quarks, implies that the 3×3 CKM matrix automatically becomes non-unitary. On the other hand, fixing a unitary CKM structure, the introduction of a heavy Z' requires cancellations between modifications of the Z -fermion couplings and the Z' -fermion couplings, or the introduction of even more new particles.

Further sum rules provide non-trivial constraints on the unitarization properties of the given couplings. The remaining purely bosonic sum rules can be derived from

$$\langle C_{v_1} C_{v_2} C_{v_3} (V_{v_4})_{\text{ph}} \rangle_c = \langle C_{v_1} C_{v_2} (V_{v_3} S_s)_{\text{ph}} \rangle_c = \langle C_{v_1} (V_{v_2} S_{s_1} S_{s_2})_{\text{ph}} \rangle_c = 0. \quad (3.1.21)$$

In the given order, we obtain the sum rules

$$\begin{aligned} & \sum_{s'} \left(g_{v_1 v_2 s'} g_{v_3 v_4 \bar{s}'} - g_{v_1 v_4 s'} g_{v_2 v_3 \bar{s}'} \right) \\ &= \sum_{v'} \left(g_{v_1 v_3 v'} g_{v_2 v_4 \bar{v}'} (2m_{v'}^2 - m_{v_1}^2 - m_{v_2}^2 - m_{v_3}^2 - m_{v_4}^2) \right. \\ & \quad + g_{v_1 v_2 v'} g_{v_3 v_4 \bar{v}'} \left(m_{v'}^2 + \frac{(m_{v_1}^2 - m_{v_2}^2)(m_{v_3}^2 - m_{v_4}^2)}{m_{v'}^2} \right) \\ & \quad \left. + g_{v_1 v_4 v'} g_{v_2 v_3 \bar{v}'} \left(m_{v'}^2 - \frac{(m_{v_1}^2 - m_{v_4}^2)(m_{v_2}^2 - m_{v_3}^2)}{m_{v'}^2} \right) \right), \end{aligned} \quad (3.1.22)$$

$$\begin{aligned} & \sum_{s'} \left(g_{v_1 v_2 s'} g_{v_3 s \bar{s}'} - g_{v_2 v_3 s'} g_{v_1 s \bar{s}'} \right) \\ &= \sum_{v'} \left(g_{v_2 v' s} g_{v_1 v_3 \bar{v}'} + g_{v_3 v' s} g_{v_1 v_2 \bar{v}'} \frac{1}{2} \left(1 - \frac{m_{v_1}^2 - m_{v_2}^2}{m_{v'}^2} \right) \right. \\ & \quad \left. + g_{v_1 v' s} g_{v_2 v_3 \bar{v}'} \frac{1}{2} \left(1 + \frac{m_{v_2}^2 - m_{v_3}^2}{m_{v'}^2} \right) \right), \end{aligned} \quad (3.1.23)$$

$$\begin{aligned} \sum_{v'} g_{v_1 v_2 \bar{v}'} g_{v' s_1 s_2} &= \sum_{v'} \frac{1}{4m_{v'}^2} \left(g_{v_1 v' s_2} g_{v_2 \bar{v}' s_1} - g_{v_1 v' s_1} g_{v_2 \bar{v}' s_2} \right) \\ &+ \sum_{s'} \left(g_{v_1 s_1 s'} g_{v_2 s_2 \bar{s}'} - g_{v_2 s_1 s'} g_{v_1 s_2 \bar{s}'} \right). \end{aligned} \quad (3.1.24)$$

To obtain the last sum rule, one has to take the part of the amplitude that is proportional to $\epsilon_{v_2} \cdot (k_{s_1} - k_{s_2})$, such that the coupling $g_{v_1 v_2 s_1 s_2}$ drops out. Terms proportional to $1/m_{v'}^2$ are understood to be absent if v' is a massless gauge boson⁶.

Even though the three bosonic sum rules imply involved relations between many parameters in models of new physics with many new particles, they are in fact very short in the SM. Equation (3.1.22) describes the well known unitarization of longitudinal W - W scattering, which determines the Higgs-boson coupling. Using external states $v_1 = \bar{v}_2 = v_3 = \bar{v}_4 = W^+$ and $v_1 = v_2 = Z$, $v_3 = \bar{v}_4 = W^+$, we obtain the Higgs-boson couplings up to a sign convention

$$(3.1.22) \quad \xrightarrow{\text{SM}} \quad |g_{W^+W^-h}| = gM_W, \quad \frac{g_{W^+W^-h}}{g_{ZZh}} = c_w^2. \quad (3.1.25)$$

⁶The right-hand side of (3.1.23) has no contribution from massless gauge bosons at all, since the corresponding couplings vanish. See footnote in appendix A.1 for an explanation.

Given this knowledge, (3.1.23) simply encodes the GWS relation. In the absence of charged scalars the left-hand side is obviously zero for the choice $v_1 = \bar{v}_3 = W^+$, $v_2 = Z$, and $s = h$. Defining the ρ -parameter, we obtain

$$\rho_0 \equiv \frac{M_W^2}{c_w^2 M_Z^2} \xrightarrow{(3.1.23)} \rho_{0,\text{SM}} = \frac{g_{W^+W^-h}}{c_w^2 g_{ZZh}} \xrightarrow{(3.1.22)} \rho_{0,\text{SM}} = 1. \quad (3.1.26)$$

A very simple consequence of (3.1.24), which holds for any multi-Higgs extension of the SM, is that all couplings between a Z boson and two neutral Higgs bosons vanish, $g_{Zh_i^0 h_j^0} = 0$.

Finally, there exist two sum rules, which express further unitarization properties of amplitudes with a fermion current. From

$$\langle C_{v_1} C_{v_2} (\psi_{f_1} \bar{\psi}_{f_2})_{\text{ph}} \rangle_c = \langle C_{v_1} S_s (\psi_{f_1} \bar{\psi}_{f_2})_{\text{ph}} \rangle_c = 0, \quad (3.1.27)$$

we derive the identities

$$\begin{aligned} \sum_{s'} g_{v_1 v_2 \bar{s}'} y_{s' \bar{f}_1 f_2}^\sigma &= \sum_{v'} \frac{M_{v_1}^2 - M_{v_2}^2}{M_{v'}^2} g_{v_1 v_2 \bar{v}'} \left(m_{f_1} g_{v' \bar{f}_1 f_2}^\sigma - g_{v' \bar{f}_1 f_2}^{\bar{\sigma}} m_{f_2} \right) \\ &\quad + \sum_{f'} \left(-m_{f_1} (g_{v_2 \bar{f}_1 f'}^\sigma g_{v_1 \bar{f}' f_2}^\sigma + g_{v_1 \bar{f}_1 f'}^\sigma g_{v_2 \bar{f}' f_2}^\sigma) \right. \\ &\quad \quad \quad \left. - m_{f_2} (g_{v_2 \bar{f}_1 f'}^{\bar{\sigma}} g_{v_1 \bar{f}' f_2}^{\bar{\sigma}} + g_{v_1 \bar{f}_1 f'}^{\bar{\sigma}} g_{v_2 \bar{f}' f_2}^{\bar{\sigma}}) \right. \\ &\quad \quad \quad \left. + 2 m_{f'} (g_{v_2 \bar{f}_1 f'}^{\bar{\sigma}} g_{v_1 \bar{f}' f_2}^\sigma + g_{v_1 \bar{f}_1 f'}^{\bar{\sigma}} g_{v_2 \bar{f}' f_2}^\sigma) \right), \end{aligned} \quad (3.1.28)$$

$$\begin{aligned} \sum_{s'} g_{v s \bar{s}'} y_{s' \bar{f}_1 f_2}^\sigma &= -\sum_{v'} \frac{1}{2M_{v'}^2} g_{v \bar{v}'} \left(m_{f_1} g_{v' \bar{f}_1 f_2}^\sigma - g_{v' \bar{f}_1 f_2}^{\bar{\sigma}} m_{f_2} \right) \\ &\quad + \sum_{f'} \left(g_{v \bar{f}_1 f'}^{\bar{\sigma}} y_{s \bar{f}' f_2}^\sigma - y_{s \bar{f}_1 f'}^\sigma g_{v \bar{f}' f_2}^\sigma \right). \end{aligned} \quad (3.1.29)$$

Again, the specification to the SM provides an interesting insight. For external Z and Higgs bosons and given the diagonal Z -fermion couplings $g_{Z\bar{f}f}^\sigma = \frac{g}{c_w} (T_\sigma^{3f} - s_w^2 Q_f) \delta_{ff'}$, we obtain

$$(3.1.28) \quad \xrightarrow{\text{SM}} \quad g_{Zh h} y_{h \bar{f} f'}^\sigma = \frac{-2g^2}{c_w^2} m_f (T_\sigma^{3f} - T_\sigma^{3f})^2 \delta_{ff'}, \quad (3.1.30)$$

$$(3.1.29) \quad \xrightarrow{\text{SM}} \quad -\frac{m_f}{2M_Z^2} g_{ZZh} = y_{h \bar{f} f}^\sigma, \quad (3.1.31)$$

where the second equation is even linear in the couplings, since the expression factorizes. This implies that flavor-diagonal Higgs-fermion couplings are a consequence of flavor-diagonal Z -fermion couplings, and that the Yukawa couplings are fixed up to a sign convention as $|y_{h \bar{f} f}^\sigma| = \frac{m_f^2}{M_W^2} (T_L^{3f} - T_R^{3f})^2$. This relation is spoiled in the presence of multiple Higgs bosons; in particular, (3.1.29) does not factorize and one cannot solve for all Yukawa couplings. In the case of a CP -conserving multi-Higgs model, there still exists an interesting relation among the set of CP -even scalars Φ_e , which follows from the difference of (3.1.28) for $\sigma = L$ and $\sigma = R$

$$(3.1.29) \quad \xrightarrow{\text{SM} + CP\text{c scalars}} \quad \sum_{s \in \Phi_e} g_{v \bar{v} s} (y_{s \bar{f} f}^L - y_{s \bar{f} f}^R) = 0. \quad (3.1.32)$$

An explicit analysis of these sum rules for multi-Higgs models was given in [121]. One interesting fact is that in such a case, the non-trivial relations from the purely bosonic rules (3.1.22–3.1.24) always involve Higgs bosons of at least two different charges.

We re-emphasize that the results given above do not depend on the assumption of a specific degree of perturbativity of tree-level amplitudes. They were instead derived from the gauge structure of a general renormalizable theory. Indeed, this is equivalent to the fact that the theory has bounded high energy growth for amplitudes [113–115], viz. it will not inevitably violate probability conservation at some high energy. Hence, the same sum rules can be derived from the requirement of vanishing coefficients for all terms of tree-level $2 \rightarrow 2$ scattering amplitudes that have polynomial growth in the center-of-mass energy $\sqrt{S} \rightarrow \infty$. We checked this explicitly for all possible $2 \rightarrow 2$ scattering amplitudes, by generating the amplitudes for polarized particles with FeynArts [127] and FormCalc [134]. In table 3.1, we summarize how the use of sum rules and quartic couplings for physical particles imply vanishing coefficients for the terms with polynomial growth in \sqrt{S} . To this end, we expanded the amplitude in $S \gg M_{s_i}, m_{f_i}, M_{v_i}$. We already inserted the couplings with Goldstone bosons and denote the polarization of particles in the subscript, where \pm stands for helicity $\pm 1/2$ for fermions and ± 1 for vector bosons. We observe that some disentanglement between the

process	S growth	implications
$V_L V_L \rightarrow V_L V_L$	S^2	vanishes due to $g_{v_1 v_2 v_3 v_4}$ (3.1.15)
	S	vanishes due to $g_{v_1 v_2 v_3 v_4}$ (3.1.15) & Jacobi-Identity (3.1.18) & sum rule (3.1.22)
	\sqrt{S}	same coefficient as S^1 ($\times 2$)
$V_{\pm} V_{\mp} \rightarrow V_L V_L$	S, \sqrt{S}	vanish due to $g_{v_1 v_2 v_3 v_4}$ (3.1.15) & Jacobi-Identity (3.1.18)
$V_{\pm} V_{\pm} \rightarrow V_L V_L$	S, \sqrt{S}	
$V_{\pm} V_L \rightarrow V_L V_L$	\sqrt{S}	
...		
$V_L V_L \rightarrow V_L S$	S	vanishes due to sum rule (3.1.23)
$V_L V_L \rightarrow S S$	S	vanish due to $g_{v_1 v_2 s_1 s_2}$ (3.1.16) & sum rule (3.1.24)
$V_L S \rightarrow V_L S$	S	
$F_{\pm} F_{\mp} \rightarrow V_L V_L$	S^1	vanishes due to sum rule (3.1.19)
$F_{\pm} F_{\mp} \rightarrow V_{\pm} V_L$	S^1	
$F_{\pm} F_{\pm} \rightarrow V_L V_L$	\sqrt{S}	vanishes due to sum rule (3.1.19) & sum rule (3.1.28)
$F_{\pm} F_{\pm} \rightarrow V_L S$	\sqrt{S}	vanishes due to sum rule (3.1.29)

Table 3.1: Scheme of sum rules implying finiteness of amplitudes for $2 \rightarrow 2$ processes.

coefficients of the different processes and their angular dependence still has to be performed, in order to arrive at the simple and well interpretable form for the sum rules given above. This is even more so, if one aims to derive the Goldstone boson couplings, as well.

The direct calculation of polarized amplitudes for $2 \rightarrow 2$ processes, however, has another merit on which we shortly like to comment. The unitarity of the \mathcal{S} matrix, *i.e.* elementary conservation of total probability, also restricts the finite and non-divergent part of the amplitude after taking $S \rightarrow \infty$. We express the interacting part of the \mathcal{S} matrix as

$$\mathcal{S} = 1 + i\mathcal{T}, \quad \langle p'_a, \lambda'_a; p'_b, \lambda'_b | \mathcal{T} | p_a, \lambda_a; p_b, \lambda_b \rangle = (2\pi)^2 \delta(p_a + p_b - p'_a - p'_b) \mathcal{M}. \quad (3.1.33)$$

Here, $p_{a,b}$ and $\lambda_{a,b}$ are the initial state momenta and helicities and the primed quantities

apply to the final state. The best projections of the angular dependence are achieved by decomposing the amplitude \mathcal{M} in a basis of eigenstates of the total angular momentum with the helicity formalism of Jacob and Wick [135]. Using the Wigner d -functions $d_{\mu\mu'}^J$ [136] with total angular momentum J and the initial and final state helicity differences $\mu \equiv \lambda_a - \lambda_b$, $\mu' \equiv \lambda'_a - \lambda'_b$ and applying the Wigner-Eckart theorem on the scalar operator \mathcal{T} , one can cast the amplitude in the form

$$\mathcal{M}(s, \theta) = 32\pi \sum_J \left(J + \frac{1}{2}\right) d_{\mu\mu'}^J(\theta) \mathcal{M}^J, \quad (3.1.34)$$

where θ is the center-of-mass scattering angle and the summation over J runs over all integers starting from $\min(\mu, \mu')$. Unitarity of the \mathcal{S} matrix implies that eigenvalues of the \mathcal{T} operator have absolute value smaller than 2, *i.e.* for the amplitude in the center-of-mass frame

$$|\mathcal{M}^J| \leq \frac{\sqrt{S}}{2|\vec{p}_a|} \xrightarrow{S \rightarrow \infty} 1. \quad (3.1.35)$$

One can improve this bound in the case of elastic scattering starting from $\mathcal{T} - \mathcal{T}^\dagger = i\mathcal{T}^\dagger\mathcal{T}$, analogous to the derivation of the optical theorem (*e.g.* [137]). In the high energy limit it implies that real and imaginary part of the amplitude lie on a circle with radius $1/2$ shifted along the imaginary axis [138]

$$\left(\text{Im}(\mathcal{M}^J) - \frac{1}{2}\right)^2 + \text{Re}(\mathcal{M}^J)^2 \leq \left(\frac{1}{2}\right)^2. \quad (3.1.36)$$

We verified that, in general, interesting bounds can be derived from the s- and p-waves of the processes $V_L V_L \rightarrow V_L V_L$, $V_L V_L \rightarrow V_L S$, $V_L V_L \rightarrow SS$, $V_L S \rightarrow V_L S$, and the p-wave of $F_\pm F_\mp \rightarrow V_L V_L$. Higher partial waves carry decreasing prefactors and therefore become less restrictive. The inequalities restrict bilinear sums of couplings with additional factors up to $(m_{\text{int}}/m_{\text{ext}})^2$. They are of interest for light external particles of mass m_{ext} , if a very heavy exchanged particle contributes in the summation with a mass $m_{\text{int}} \gg m_{\text{ext}}$. Further inequalities that are linear in the masses are obtained from $V_\pm V_\pm \rightarrow V_L V_L$, $V_\pm V_\mp \rightarrow V_L V_L$, $F_\pm \bar{F}_\pm \rightarrow V_\pm V_L$, and $F_\pm \bar{F}_\mp \rightarrow V_L S$. Interesting inequalities may also be derived from $SS \rightarrow SS$ and $F_\pm \bar{F}_\mp \rightarrow F_\mp \bar{F}_\pm$, since they contain a quartic Higgs couplings and scalar-fermion couplings, respectively.

Classically the inequalities have been used to derive upper bounds on the Higgs mass of the SM. The most stringent bound follows from the s-wave of $W_L W_L \rightarrow W_L W_L$, where one obtains $\mathcal{M}^0 = (G_F M_h)/(4\sqrt{2}\pi)$ for $S \gg M_h$ [116]. One can extend this beyond a single channel and bound the largest eigenvalue of the coupled channel matrix for the in- and outgoing states $(W_L W_L, \frac{1}{\sqrt{2}} Z_L Z_L, \frac{1}{\sqrt{2}} hh, Z_L h, W_L h, W_L Z_L)$ [139]. Using the improved bound (3.1.36) leads to $M_h < 710 \text{ GeV}$.⁷ On the other hand $\mathcal{M}^0 = (G_F S)/(16\sqrt{2}\pi)$ follows for the limit $S \ll M_h$. This implies that some new physics had to occur in the TeV range, in order to restore unitarity, if the Higgs boson would not exist below this scale. Another classical application was to bound the masses of chiral fermions in the SM [117, 118].

Note that these classical applications of tree-level perturbative unitarity assumed perturbativity of the Higgs self-coupling $\lambda = M_h^2/(2v^2)$. However, since it grows with the Higgs

⁷This tree-level estimate for the breakdown of perturbation theory is indeed close to values found by calculating two-loop corrections [140, 141], and to non-perturbative lattice calculations [138]

mass, unitarity might also be restored by large loop corrections, signaling the failure of perturbation theory and the loss of predictivity of the SM [142]. At least, this shows that bounds derived from tree-level perturbative unitarity can have loopholes. An alternative and presently more relevant criterion of theoretical bounds on the Higgs mass is precisely derived from the Higgs self-coupling. Finiteness of the running self-coupling up to the Planck scale leads to $M_h \lesssim 175$ GeV, called the perturbativity bound [138, 143], while positivity implies $M_h > 129.4 \pm 1.8$ GeV [88], called the stability bound. The present experimental value of the Higgs mass is marginally compatible with the latter bound.

In a similar approach to generic new physics that we take here, the sum rules and inequalities from the s- and p-wave of $F_{\pm} F_{\mp} \rightarrow V_L V_L$ have also been derived recently in [122]. The authors apply the inequality to interpret unitarization properties in simple W' models. They find that an accompanying Z' is constrained to have mass below 7–8 TeV if no further scalars contribute.

We summarize that also the inequalities following from tree-level perturbative unitarity are in general interesting in order to constrain the spectrum of new physics. Our emphasis in this thesis is different, however. We will only resort to the sum rule equations, which we derived in this section. They hold exactly due to gauge invariance. In this way, we will be able to renormalize and simplify the Z -penguin at a generic level in section 4.1.1.

3.2 A Little Higgs Model

The main motivation of little Higgs theories [144, 145] is to cure the hierarchy problem of SM. A common assumption of these models is the existence of an approximate global symmetry G_f , which is broken into a subgroup H at a scale $f \sim \text{TeV}$ due to new resonances, which strongly interact at a higher scale $\Lambda_S \sim 10 \text{TeV}$. Hence, the theory has only a perturbative window. It may still be interesting from the point of view of the renormalizability constraints discussed above, due to the mechanism with which the Higgs boson is naturally kept light; a subgroup G_w of G_f is weakly gauged and spontaneously broken in a second stage by the Higgs mechanism. One includes the Higgs boson of the second stage breaking in the coordinates of the coset space G_f/H of the explicit first stage breaking. This provides a realization of the long existing idea of the Higgs being a pseudo-Nambu-Goldstone boson [146, 147]. The precise way in which the high scale symmetry breaking is achieved remains unspecified. The EFT of the resulting Goldstone bosons is described as a non-linear σ -model (NL σ M) [145]. A subset of the Goldstone bosons is “eaten” by the Higgs mechanism, but the remaining ones generically obtain bare masses of the order Λ_s times a weak gauge coupling, *i.e.* masses of $\mathcal{O}(f)$. In addition, the idea of collective symmetry breaking [144] is used to further suppress the bare mass of the Higgs boson by a second power of the weak gauge coupling. In this way one can keep the onset of strong interactions well separated from the weak scale, without reintroducing a fine-tuning in the Higgs mass. In contrast to supersymmetric theories, particles of the same spin cancel quadratically divergent contributions to the Higgs mass among themselves. Therefore, yet another ingredient of the model consists in an extended quark sector.

In the following discussion, we adopt the most commonly studied realization, called littlest Higgs (LH) model. It is based on the coset $G_f/H = SU(5)/SO(5)$. This serves as a good test-bed for studying the coupling structure that enters loop amplitudes, in particular for flavor-changing transitions. We present the model with an emphasis on this conceptual aspect. Other realizations of the little Higgs idea that have been studied in the literature include the simplest little Higgs using $(SU(3) \times U(1))^2/(SU(2) \times U(1))^2$ [148], a model based on $SO(9)/(SO(5) \times SO(4))$ [149], and the minimal composite Higgs model (MCHM) $SO(5)/SO(4)$ [150].

3.2.1 Gauge Structure and T -Parity

We start to establish our notation by reviewing the full model Lagrangian. The vacuum coordinates of G_f/H are parametrized by a symmetric tensor Σ , which transforms under the **15** representation of $SU(5)$. For the covariant kinetic term of the effective low energy theory of Goldstone bosons, we can use the leading order dimension two term of the NL σ M [145]

$$\mathcal{L}_\Sigma = \frac{f^2}{8} \text{Tr} \left[D_\mu \Sigma (D^\mu \Sigma)^\dagger \right]. \quad (3.2.1)$$

Remark that a tree-level potential for Σ is forbidden by the global symmetry. Thus, electroweak symmetry breaking is triggered by quadratically divergent contributions to the Coleman-Weinberg potential, which occur first at one-loop [145]. We use the following parametrization

of the matrix Π of the 14 Goldstone bosons

$$\Sigma = e^{i\Pi/f} \Sigma_0 e^{i\Pi^T/f} = e^{2i\Pi/f} \Sigma_0, \quad \Sigma_0 = \begin{pmatrix} 0 & 0 & 1_2 \\ 0 & 1 & 0 \\ 1_2 & 0 & 0 \end{pmatrix},$$

$$\Pi = \chi^a X^a = \begin{pmatrix} \Gamma + \eta \frac{1}{\sqrt{20}} & \Phi & -i\Delta \\ \Phi^\dagger & -\eta \sqrt{\frac{4}{5}} & \Phi^T \\ i\Delta^* & \Phi^* & \Gamma^* + \eta \frac{1}{\sqrt{20}} \end{pmatrix}, \quad (3.2.2)$$

and denote the possible VEVs of the neutral scalars h and ϕ^0 as v and v' . The components of the doublet Φ , triplet Δ , and Γ are given by⁸

$$\Gamma = -\omega^0 \frac{\sigma^3}{2} - i\omega^+ \frac{\sigma^+}{\sqrt{2}} + i\omega^- \frac{\sigma^-}{\sqrt{2}}, \quad \Delta = \begin{pmatrix} \phi^{++} & \frac{1}{\sqrt{2}} \phi^+ \\ \frac{1}{\sqrt{2}} \phi^+ & \frac{1}{\sqrt{2}} (v' + \phi^0 + i\phi^P) \end{pmatrix}.$$

$$\Phi = \left(\frac{1}{\sqrt{2}} \pi^+, \frac{1}{2} (v + h + i\pi^0) \right)^T, \quad (3.2.3)$$

The broken generators $\tau^a \in SU(5)$ can be identified as being odd under the automorphism

$$\tau^a \xrightarrow{T} -\Sigma_0 (\tau^a)^T \Sigma_0, \quad (3.2.4)$$

while the unbroken generators are even. The image of the Goldstone boson matrix under this automorphism is given by

$$\Sigma \xrightarrow{T} \tilde{\Sigma} = \Sigma_0 \Omega \Sigma^\dagger \Omega \Sigma_0, \quad \Omega \equiv \text{diag}(1, 1, -1, 1, 1). \quad (3.2.5)$$

Remark that the VEV of Σ can be expressed in short and exact form as

$$\langle \Sigma \rangle = \begin{pmatrix} 0 & 0 & 0 & 1 & 0 \\ 0 & \frac{1}{2} \alpha + \frac{v'}{v} \beta & \frac{i}{\sqrt{2}} (\beta - \frac{v'}{v} \alpha) & 0 & 1 + \alpha \left(\frac{1}{2} + \left(\frac{v'}{v} \right)^2 \right) \\ 0 & \frac{i}{\sqrt{2}} (\beta - \frac{v'}{v} \alpha) & 1 + \alpha & 0 & \frac{i}{\sqrt{2}} (\beta + \frac{v'}{v} \alpha) \\ 1 & 0 & 0 & 0 & 0 \\ 0 & 1 + \alpha \left(\frac{1}{2} + \left(\frac{v'}{v} \right)^2 \right) & \frac{i}{\sqrt{2}} (\beta + \frac{v'}{v} \alpha) & 0 & \frac{1}{2} \alpha - \frac{v'}{v} \beta \end{pmatrix}, \quad (3.2.6)$$

with $\alpha \equiv \frac{\cos(\frac{v}{\sqrt{2}f}) - 1}{1 + (\frac{v'}{v})^2}, \quad \beta \equiv \frac{\sin(\frac{v}{\sqrt{2}f})}{\sqrt{1 + (\frac{v'}{v})^2}}.$

It is suitable to choose $G_w = (SU(2) \times U(1))_1 \times (SU(2) \times U(1))_2$ as the weakly gauged subgroup. Since it does not entirely lie in the remnant $SO(5)$, the high scale breaking $G \rightarrow H$ also breaks G_w and the additional gauge bosons obtain TeV-scale masses.

$$\begin{array}{ccc} \text{global:} & SU(5) & \xrightarrow{\langle \Sigma \rangle} & SO(5) \\ & \cup (g_{1,2}) & & \cup (g = sg_1 = cg_2) \\ \text{local:} & [SU(2) \times U(1)]^2 & \xrightarrow{\langle \Sigma \rangle} & [SU(2) \times U(1)]_{\text{diag}} \end{array}$$

⁸Conventionally, the Goldstone bosons in Φ are denoted by the symbols π , to express the analogy to the pions from the chiral symmetry of QCD. In this context, they correspond to the usual Goldstone bosons of the SM Higgs doublet, which we called φ in (2.2.6). In particular, they do not obtain mass by symmetry breaking; instead h becomes the pseudo Goldstone-boson.

The interesting aspect of this symmetry breaking pattern is that each $SU(2) \times U(1) \subset SU(5)$ has a full global $SU(3)$ symmetry in its coset. Each of the two $SU(3)$ symmetries protects the one-loop scalar potential, which we discuss below, from developing a coefficient for the Higgs mass M_h . Thus, both couplings g_1 and g_2 have to be present in a diagram in order to generate a Higgs mass term, which is then naturally light compared to the cutoff scale Λ_s . This is referred to as collective symmetry breaking [144]. The charges and the covariant derivative of Σ in G_w are given by

$$Q_1^i = \begin{pmatrix} \frac{\sigma^i}{2} & 0 \\ 0 & 0_3 \end{pmatrix}, \quad Q_2^i = \begin{pmatrix} 0_3 & 0 \\ 0 & -\frac{\sigma^{i*}}{2} \end{pmatrix}, \quad (3.2.7)$$

$$Y_1 = \frac{1}{10} \text{diag}(3, 3, -2, -2, -2), \quad Y_2 = \frac{1}{10} \text{diag}(2, 2, 2, -3, -3),$$

$$D_\mu \Sigma = \partial_\mu \Sigma - i\mathcal{V}(\Sigma), \quad \mathcal{V}(\Sigma) = g_j W_j^a (Q_j^a \Sigma + \Sigma (Q_j^a)^T) - g'_j B_j (Y_j \Sigma + \Sigma Y_j). \quad (3.2.8)$$

The given direction⁹ of G_w in G_f ensures that the diagonal subgroup of G_w is unbroken by Σ_0 and can therefore represent the SM-like $SU(2)_L \times U(1)_Y$. The appropriate rotation fulfills $g_j W_j Q_j = g(WQ + W'Q')$ and reads¹⁰

$$\begin{aligned} W' &= cW_1 - sW_2, & W &= sW_1 + cW_2, \\ Q &= Q_1 + Q_2, & Q' &= \frac{c}{s}Q_1 - \frac{s}{c}Q_2, & g &= sg_1 = cg_2 \end{aligned} \quad (3.2.9)$$

An analogous rotation is applied for B_j , $g'_j Y_j$, and angles θ' instead of W_j , $g_j Q_j$, and θ . The trigonometric functions are denoted by $c^{(\prime)} = \cos(\theta^{(\prime)})$, $s^{(\prime)} = \sin(\theta^{(\prime)})$, and $t^{(\prime)} = \tan(\theta^{(\prime)})$, and analogous for further angles, which are defined below.

In the general setup discussed above, the scale f has been found to be pushed to values beyond 4 TeV, because of large contributions to electroweak precision observables [153–155]. The fact that the corresponding dimension six operators are sourced by tree-level exchanges of new particles, suggests an obvious way to alleviate the bounds. A simple Z_2 symmetry called T -parity [156], under which only SM-like fields are even, can circumvent the bounds. This is simply done by promoting the automorphism (3.2.4) to a fundamental symmetry, which interchanges the two $SU(2) \times U(1)$ gauge groups. Thus, it acts on gauge fields as $T : A_1 \leftrightarrow A_2$ where $A_i = W_i^a Q^a$ or $B_i Y$. We furthermore define the action on scalars as $T : \Pi \rightarrow -\Omega \Pi \Omega$. This obviously renders all scalars T -odd except those contained in the doublet Φ . Remark that the invariance of the Lagrangian together with T -parity implies equal gauge couplings $g_1^{(\prime)} = g_2^{(\prime)} = \sqrt{2} g^{(\prime)}$. We continue to present the general setup for gauge bosons and comment on an issue concerning the gauge fixing procedure, necessary for the quantization of the theory. The T -parity symmetric case (LHT model) can be obtained by the specific choice of some of the parameters. We will only refer to the latter for the calculation of the flavor-changing Z -transitions in chapter 3.1, since the T -symmetric case turns out to be phenomenological more interesting, and has a richer fermion sector.

As stated above, the Coleman-Weinberg-potential triggers electroweak symmetry breaking at one-loop order. It was recognized in [151] that we obtain essentially three new parameters. Two of them are the mass M_h for the Higgs boson h and the degenerate masses $M_\phi^2 = 2 \frac{f^2}{v^2} M_h^2$

⁹One assumes the dynamics of the unknown UV completion to choose this direction of G_w relative to Σ_0 .

¹⁰We define W' and B' with an additional sign compared to most of the literature on the LH without T -Parity [151, 152]. This sign convention is compatible with all the literature on the LH with T -Parity. In order to agree with most of the literature, we also use a reversed sign for the coupling g' compared to section 2.2.

3. THEORETICAL CLASSIFICATION & EXAMPLES OF NEW PHYSICS

for all scalars contained in the triplet Δ . Furthermore, remark that a positive spectrum requires

$$x_\lambda = \frac{\lambda_{\Phi\Delta\Phi}}{2\lambda_{\Phi^4}} = \frac{2\sqrt{2}v'f}{v^2} < 1, \quad (3.2.10)$$

where $(if\lambda_{\Phi\Delta\Phi})$ and λ_{Φ^4} are the coefficients of the corresponding neutral fields in the subscripts, as being part of the one loop Coleman-Weinberg Higgs potential. The relation (3.2.10) induces a hierarchy of the VEVs $v' \ll v$, similar to the case of triplet VEVs in the left-right symmetric model presented in the last section. Requiring T -parity as a symmetry of the theory completely forbids the triplet VEV $v' = 0$.

To obtain the gauge boson mass eigenstates, we simply insert $\Sigma \rightarrow \langle \Sigma \rangle$ into (3.2.1) and expand to $\mathcal{O}(v/f)^2$ and $\mathcal{O}(v'/v)^2$. Using $m_w = c_w m_z = \frac{gv}{2}$ the mass eigenstates are

$$\begin{aligned} \begin{pmatrix} W_L^\pm \\ W_H^\pm \end{pmatrix} &= \begin{pmatrix} 1 & -\frac{1}{2}\frac{v^2}{f^2}cs\delta_g \\ \frac{1}{2}\frac{v^2}{f^2}cs\delta_g & 1 \end{pmatrix} \begin{pmatrix} W^\pm \\ W'^\pm \end{pmatrix}, & M_{W_L}^2 &= m_w^2 \left(1 - \frac{v^2}{f^2} \left(\frac{1}{6} + \frac{\delta_g - x_\lambda^2}{4}\right)\right), \\ & & M_{W_H}^2 &= \frac{f^2}{v^2} \frac{m_w^2}{c^2 s^2} \left(1 - \frac{v^2}{f^2} c^2 s^2\right), \end{aligned} \quad (3.2.11)$$

$$\begin{pmatrix} A \\ Z_L \\ A_H \\ Z_H \end{pmatrix} = \begin{pmatrix} c_w & -s_w & 0 & 0 \\ s_w & c_w & -\frac{v^2}{f^2}x_Z^{B'} & -\frac{v^2}{f^2}x_Z^{W'} \\ \frac{v^2}{f^2}s_w x_Z^{B'} & \frac{v^2}{f^2}c_w x_Z^{B'} & 1 & \frac{v^2}{f^2}x_H \\ \frac{v^2}{f^2}s_w x_Z^{W'} & \frac{v^2}{f^2}c_w x_Z^{W'} & -\frac{v^2}{f^2}x_H & 1 \end{pmatrix} \begin{pmatrix} B \\ W^3 \\ B' \\ W'^3 \end{pmatrix}, \quad \begin{aligned} M_{Z_L}^2 &= m_z^2 \left(1 - \frac{v^2}{f^2} \left(\frac{1}{6} + \frac{\delta_g + 5\delta_{g'} - 2x_\lambda^2}{4}\right)\right), \\ M_{A_H}^2 &= \frac{f^2}{v^2} \frac{m_w^2 t_w^2}{5c'^2 s'^2} \left(1 - \frac{v^2}{f^2} 5c'^2 s'^2\right), \\ M_{Z_H}^2 &= m_{W_H}^2, \end{aligned}$$

where we parametrized the mixing of B' and W'^3 into the mass eigenstate Z_L and the heavy mass eigenstates with the quantities $x_Z^{B'}$, $x_Z^{W'}$ and x_H . They are given by

$$x_H = \frac{1}{4} \left(\frac{1}{t_w} \frac{c's'}{cs} - \frac{t_w}{5} \frac{cs}{c's'} \right)^{-1} (1 + \delta_g \delta_{g'}), \quad (3.2.12)$$

$$x_Z^{W'} = \frac{\delta_g sc}{2c_w}, \quad x_Z^{B'} = \frac{5\delta_{g'} s' c'}{2s_w}, \quad \delta_{g^{(\prime)}} = c^{(\prime)2} - s^{(\prime)2}. \quad (3.2.13)$$

Requiring T -parity sets all quantities in (3.2.13) identically to 0 and forbids mixing of the gauge eigenstates B' , and W'_3 into Z_L with the consequence that the ρ -parameter, as defined in (3.1.26), is set to 1. However, the W and Z mass still obtain a universal contribution, altering the standard relation between v and G_F . We summarize for further reference

$$\begin{aligned} T\text{-parity: } \begin{pmatrix} A_H \\ Z_H \end{pmatrix} &= \begin{pmatrix} 1 & \frac{v^2}{f^2}x_H \\ -\frac{v^2}{f^2}x_H & 1 \end{pmatrix} \begin{pmatrix} B' \\ W'^3 \end{pmatrix}, & M_{W_L}^2 &= c_w^2 m_{Z_L}^2 = m_w^2 \left(1 - \frac{v^2}{6f^2}\right), \\ & & M_{A_H}^2 &= \frac{f^2}{v^2} m_w^2 t_w^2 \left(\frac{4}{5} - \frac{v^2}{f^2}\right), \\ x_H &= \frac{1}{4} \left(\frac{1}{t_w} - \frac{t_w}{5} \right)^{-1}, & M_{Z_H}^2 &= m_{W_H}^2 = \frac{f^2}{v^2} m_w^2 \left(4 - \frac{v^2}{f^2}\right). \end{aligned} \quad (3.2.14)$$

Observe that to leading order in $\frac{v^2}{f^2}$ the mass of the heavy neutral gauge boson A_H is approximately one fourth of the Z_H mass and close to twice the W mass

$$M_{A_H} \approx 2M_{W_L} \frac{f}{\text{TeV}} \left(1 - 0.13 \frac{f}{\text{TeV}}\right)^2. \quad (3.2.15)$$

If T -parity is also a symmetry of the ultraviolet completion of the LH model, it has been recognized that A_H can be a potential weak scale dark matter candidate and account for the observed relic density of dark matter in the universe [157].

Up to now, we brought the bosonic mass terms into canonical form. We also need to account for standard kinetic terms of the scalars, which are a priori spoiled in the basis of (3.2.2) because of the NL σ M, and consider the mixing terms of scalars with gauge bosons arising from \mathcal{L}_Σ of (3.2.1). The former is achieved by a hermitian redefinition of the scalars. This is due to the fact that, *e.g.* in the neutral sector, the kinetic terms can be cast into the form

$$\mathcal{L}_\Sigma \supset \frac{1}{2} \sum_{\phi^a} \partial_\mu \phi^a \left(\delta_{ab} + \frac{v^2}{f^2} H_{ab} \right) \partial^\mu \phi^b, \quad (\phi^a = h, \phi^0, \phi^P, \pi^0, \eta, \omega^0), \quad (3.2.16)$$

with H_{ab} forming a hermitian matrix. Therefore, we simply redefine $\phi'^a = (\delta_{ab} + \frac{v^2}{2f^2} H_{ab}) \phi^b$. Thereafter, we are still allowed to make a unitary redefinition of the scalar fields without spoiling the canonical kinetic terms. We can finally render the terms

$$\mathcal{L}_\Sigma \supset -\frac{f^2}{4} \text{Im Tr} \left[(\partial_\mu \Sigma) \mathcal{V}(\Sigma)^\dagger \right] \quad (3.2.17)$$

canonical in the mass basis, *i.e.* of the form $-\sigma_a M_{V^a} (\partial^\mu V_{m\mu}^{\bar{a}}) \phi_m^a$, where the subscript m denotes fields in the mass basis. A treatment of the charged scalar sector is analogous. The necessary redefinition is unitary at $\mathcal{O}(v^2/f^2, v'^2/v^2, v'/f)$ and included in appendix A.2. We remark, that we found the redefinition to be non-unitary starting at $\mathcal{O}(vv'/f^2) = \mathcal{O}(v^3/f^3)$. This indicates the necessity of a non-linear gauge fixing procedure at subleading order in the expansion in v/f . However, considering the divergence structure of $\Delta F = 1$ amplitudes discussed in chapter 3.1, it is important to see that the leading contributions can be calculated reliably in the standard quantization approach.

The bosonic Lagrangian is completed by standard covariant kinetic terms \mathcal{L}_V of the linearly realized gauge bosons of G_w . We give \mathcal{L}_V for completeness in (A.2.1).

3.2.2 Fermion Sector

Since little Higgs models are constructed as a solution to the hierarchy problem, one also addresses the one-loop contributions to the Higgs boson mass from the top-Yukawa coupling. This is done via a contribution of the same order $y_t^2 \Lambda_S^2 / (16\pi^2) \sim f^2$ originating from an additional vector-like heavy fermion. We will discuss the LHT model in the following. It turns out that the setup without T -parity requires only one new fermion, which also appears in the model with T -parity and has similar couplings.

As an additional obstacle in the LHT model, one has to assure that the SM fermions are introduced as T -even states. This is achieved by introducing two doublets $\psi_{1,2}$ that each transform linearly under one of the $SU(2)$ groups in G_w . Only the remaining T -odd linear combination shall get a mass of order f , which is achieved by introducing a full $SO(5)$ multiplet of T -odd mirror fermions Ψ' [158]. To this end, a non-linear realization of $SU(5)$ avoids the introduction of yet another copy of mirror fermions, and completeness of the multiplet again protects the Higgs mass from a potential two-loop quartic divergence [159].

We first summarize the relevant fermion content of the model. It has been realized in [160] that in order to accommodate the hypercharge of the Standard Model fermions, one has to add two $U(1)$ factors to the original setup. For each of these $U(1)$ factors only the diagonal subgroup with one of the $U(1)$ factors contained in G_w is gauged. Here we summarize only the resulting charges for the gauged groups in table 3.2.

	$q_{1,i}$	u_i^c	d_i^c	$q_{HR,i}$	t'_1	t_1^c	$l_{1,i}$	e_i^c	$l_{HR,i}$
$SU(2)_{1 \times 2}$	(2, 1)	(1, 1)	(1, 1)		(1, 1)	(1, 1)	(2, 1)	(1, 1)	
Y_1	1/30	1/3	-1/6	1/3	8/15	8/15	-3/10	-1/2	0
Y_2	2/15	1/3	-1/6	1/3	2/15	2/15	-1/5	-1/2	0
T	$-q_{2,i}$	+	+	-	$-t'_2$	$-t_2^c$	$-l_{2,i}$	+	-

Table 3.2: Charges for the full fermion sector of the LHT model. In the last line, we give either T eigenvalues or the definition for the fields $q_{2,i}, t'_2, t_2^c, l_{2,i}$ as the T -parity image of the corresponding fields.

T -parity eigenstates for the fermions are given by

$$q_{L,i} = \frac{1}{\sqrt{2}}(q_{1,i} - q_{2,i}), \quad q_{HL,i} = \frac{1}{\sqrt{2}}(q_{1,i} + q_{2,i}), \quad t'_\pm = \frac{1}{\sqrt{2}}(t'_1 \mp t'_2) \quad (3.2.18)$$

and analogous linear combinations for leptons $l_{n,i}$ and the right-handed top partner fermions t_n^c . Here $q_{n,i} = (u_{n,i}, d_{n,i})^T$ denotes two fundamental quark doublets. The T -even top partner t'_+ now has the same quantum numbers like the SM-like up-type quarks $u_{L,i}$ and may mix with them. To write down the Lagrangian, we embed the fermion content into incomplete representations of $SU(5)$

$$\Psi_{1,i} = \begin{pmatrix} \psi_{1,i} \\ 0 \\ 0 \end{pmatrix}, \quad \Psi_{2,i} = \begin{pmatrix} 0 \\ 0 \\ \psi_{2,i} \end{pmatrix}, \quad \Psi'_i = \begin{pmatrix} \tilde{\psi}'_i \\ \chi'_i \\ \psi'_i \end{pmatrix}, \quad (3.2.19)$$

where $\psi_{n,i} = -i\sigma_2 q_{n,i}$ and $\psi'_i = -i\sigma_2 q_{HR,i}$. $\tilde{\psi}'$ and χ' are assumed to obtain very large Dirac masses from couplings to additional fermions and can be safely decoupled from the theory [157]. Using $\xi = e^{i\Pi/f}$ the mirror mass terms are given by

$$\mathcal{L}_{\text{mirror}} = f \kappa_{ij} (\Psi_{2,i} \xi + \Psi_{1,i} \Sigma_0 \Omega \xi^\dagger \Omega) \Psi'_j. \quad (3.2.20)$$

After a singular value decomposition of κ and rotation of the mirror fermions $f = u, d$

$$\kappa = \mathbf{V}_H \text{diag} \left(\frac{m_{H,i}^q}{\sqrt{2}f} \right) \mathbf{U}_H^\dagger, \quad f_{HL,i} = (V_H)_{ij} f_{HL,j}^{(m)}, \quad f_{HR,i} = (U_H)_{ij} f_{HR,j}^{(m)}, \quad (3.2.21)$$

we obtain masses $m_{H,i}^d = m_{H,i}^q$ and $m_{H,i}^u = m_{H,i}^q (1 - \frac{v^2}{8f^2})$. The upper index (m) in (3.2.21) stands for mass eigenstates. We will skip the index in the following and work with mass eigenstates only. Mirror masses for leptons can be written down in full analogy.

For the Yukawa interactions of the T -even fermions, it is convenient to define

$$Q_{n,i} \equiv \Psi_{n,i} + \delta_{n,3} (0, i t'_n, 0)^T, \quad \Psi'_{n,i} \equiv (q_{n,i}, 0, 0)^T, \quad X = (\Sigma_{33})^{-1/4}. \quad (3.2.22)$$

Gauge invariant Yukawa interactions and a T -even Dirac mass term for t'_n are given by

$$\begin{aligned} \mathcal{L}_{Y,u} &= \frac{i}{2\sqrt{2}} f (\lambda_U)_{ij} \sum_{i,j,k=1}^3 \sum_{x,y=4}^5 \epsilon_{abc} \epsilon_{xy} \left[(\bar{Q}_{2,i} \Sigma_0)_a \tilde{\Sigma}_{bx} \tilde{\Sigma}_{cy} - (\bar{Q}_{1,i})_a \Sigma_{bx} \Sigma_{cy} \right] u_j^c \\ &\quad - f \lambda_+ (\bar{t}'_1 t_1^c + \bar{t}'_2 t_2^c) + \text{h.c.}, \quad (3.2.23) \\ \mathcal{L}_{Y,d} &= \frac{i}{2\sqrt{2}} f (\lambda_D)_{ij} \sum_{a,b=1}^2 \sum_{x,y,z=3}^5 \epsilon_{ab} \epsilon_{xyz} \left[(\bar{\Psi}'_{2,i})_x \Sigma_{ay} \Sigma_{bz} X - (\bar{\Psi}'_{1,i} \Sigma_0)_x \tilde{\Sigma}_{ay} \tilde{\Sigma}_{bz} \tilde{X} \right] d_j^c + \text{h.c.} \end{aligned}$$

The Lagrangian implements the idea of collective symmetry breaking. This is due to the fact that $Q_{n,i}$ is an incomplete representation of the subgroup $SU(3)_i$ in $SU(5)$, which is left invariant when $g_i = 0$, for $i = 1$ and 2 respectively.¹¹ Remark that for this reason t_- does not couple to the Higgs boson directly and does not participate in the processes discussed in section 4.3.

We start the diagonalization of the mass terms by going into a basis where λ_D is diagonal via two unitary redefinitions in the down sector. t'_- does not mix with other fermions. We denote its mass eigenstate with $T_- = t'_-$. Its mass is given by $m_{T_-} = f\lambda_+$. The remaining mass matrix for the up-quarks $U = (u, c, t, t'_+)$ is given by

$$\mathcal{L}_{Y,u} \supset -\bar{U}_L \mathcal{M}_U U_R + \text{h.c.}, \quad \mathcal{M}_U = v \begin{pmatrix} \lambda_U(1 - \frac{v^2}{3f^2}) & 0 \\ (\lambda_U)_{3n}(1 - \frac{v^2}{2f^2}) & \lambda_+ \frac{f}{v} \end{pmatrix}, \quad (3.2.24)$$

where the third row elements of the 3×3 matrix λ_U are repeated in the fourth row of \mathcal{M}_U . In all of the existing literature we are aware of, the diagonalization of this matrix assumes vanishing $\lambda_{31}, \lambda_{32}$ and only applies rotations in the $t - t'_+$ sub-block. Explicit treatments are given *e.g.* in [151, 163–168]. The first assumption is justified, since we know the general solution can be written as

$$\mathbf{v}_u^\dagger \mathcal{M}_U \mathbf{u}_u = \begin{pmatrix} \hat{\mathbf{V}}^\dagger & 0 \\ 0 & 1 \end{pmatrix} \text{diag}(m_u, m_c, m_t, m_{T_+}), \quad (3.2.25)$$

where $\hat{\mathbf{V}}$ is a CKM-like unitary 3×3 matrix, and $\mathbf{v}_u, \mathbf{u}_u$ are perturbations around the unit matrix. Consequently, $(\lambda_U)_{31}, (\lambda_U)_{32}$ are chirally suppressed. However, the $t - t'_+$ rotation produces off-diagonal terms in the $(1, 4)$ and $(2, 4)$ entries on the right-hand side of (3.2.25), which are only suppressed by the square of the Cabibbo-angle, λ^2 , and are not chirally suppressed. While it is still reasonable from a phenomenological point of view to neglect those terms, this assumption is usually not stated explicitly. We take $u, c - T_+$ mixings into account, in order to keep the coupling structure most general. This is useful for testing the generic result on flavor-changing Z transitions in chapter 3.1. We will see below that terms implied by these new rotations can be summarized in a sensible vertex definition of the CKM matrix. To this end, we derived the exact decomposition of (3.2.25) and neglected chirally suppressed $m_{u,c}/m_t$ only afterwards. The intermediate step of this calculation are cumbersome but result only in two simple, additional, elementary rotations for the left-handed up-quarks. The mass eigenstates of the up-quarks are finally given by

$$U_R = \mathbf{u}_u (u^{(m)}, c^{(m)}, t^{(m)}, T_+)_R^T, \quad U_L = \mathbf{v}_u \begin{pmatrix} \hat{\mathbf{V}}^\dagger & 0 \\ 0 & 1 \end{pmatrix} (u^{(m)}, c^{(m)}, t^{(m)}, T_+)_L^T, \quad (3.2.26)$$

with the unitary matrices

$$\mathbf{u}_u = \begin{pmatrix} \mathbf{1}_2 & & 0 \\ & c_R & s_R \\ 0 & -s_R & c_R \end{pmatrix}, \quad \mathbf{v}_u = \begin{pmatrix} \mathbf{1}_2 & & 0 \\ & c_L & s_L \\ 0 & -s_L & c_L \end{pmatrix} \begin{pmatrix} 1 & 0 & 0 & 0 \\ 0 & c_L^c & 0 & s_L^c \\ 0 & 0 & 1 & 0 \\ 0 & -s_L^c & 0 & c_L^c \end{pmatrix} \begin{pmatrix} c_L^u & 0 & s_L^u \\ 0 & \mathbf{1}_2 & 0 \\ -s_L^u & 0 & c_L^u \end{pmatrix}.$$

¹¹For the LH model without T -parity, the authors of [161, 162] showed that the assumption of a common $SU(3)$ symmetric Yukawa coupling y_1 for the components in Q_n is unstable against radiative corrections. This implies a two-loop quadratic divergence to the Higgs mass, which is estimated to be of the same order as the logarithmically divergent one-loop contribution, and requires a certain amount of hidden fine-tuning or an intricate UV completion.

We choose phases for the entries of $\hat{\mathbf{V}}$ in a non-standard convention, with positive entries in the third row. This renders the given angles $c_{L,R}^{(u,c)}$ free of phases and particularly simple

$$\begin{aligned}
 s_R &= \sqrt{x_L} \left(1 - \frac{v^2}{f^2} \left(\frac{1}{2} - \frac{x_L}{\hat{V}_{33}^2} \right) (1 - x_L) \right), & c_R &= \sqrt{1 - x_L} \left(1 + \frac{v^2}{f^2} \left(\frac{1}{2} - \frac{x_L}{\hat{V}_{33}^2} \right) x_L \right), \\
 s_L &= \frac{v}{f} x_L \left(1 + d_2 \frac{v^2}{f^2} \right), & c_L &= 1 - \frac{v^2}{f^2} \frac{x_L^2}{2}, \\
 s_L^c &= \frac{v}{f} x_L \left(1 + \frac{v^2}{f^2} \left(d_2 + \frac{x_L^2}{2} \right) \right) \frac{\hat{V}_{32}}{\hat{V}_{33}}, & c_L^c &= 1 - \frac{v^2}{f^2} \frac{x_L^2}{2} \frac{\hat{V}_{32}^2}{\hat{V}_{33}^2}, \\
 s_L^u &= \frac{v}{f} x_L \left(1 + \frac{v^2}{f^2} \left(d_2 + \frac{x_L^2}{2} \frac{1 - \hat{V}_{31}^2}{\hat{V}_{33}^2} \right) \right) \frac{\hat{V}_{31}}{\hat{V}_{33}}, & c_L^u &= 1 - \frac{v^2}{f^2} \frac{x_L^2}{2} \frac{\hat{V}_{31}^2}{\hat{V}_{33}^2},
 \end{aligned} \tag{3.2.27}$$

$$d_2 = -\frac{5}{6} + x_L - \frac{x_L^2}{2} + \frac{x_L(1-x_L)}{\hat{V}_{33}^2}, \tag{3.2.28}$$

where $x_L = \lambda_{U,33}^2 / (\lambda_{U,33}^2 + \lambda_+^2)$, the unitary CKM entries \hat{V}_{ij} , and the SM quark masses are now used as the model input parameters. The value of x_L is constrained by electroweak precision data [169], but the exact constraint strongly depends on the realization and parameters of the T -odd sector and possible UV dependent terms. Remark that our definition of $\hat{\mathbf{V}}$ is different from the usual definition in the literature in two ways. There, higher orders in the Cabibbo angle are implicitly neglected, which amounts to setting $s_L^u = s_L^c = 0$. Furthermore, \mathbf{V}_u is effectively defined as being commuted with the unitary CKM when compared to our definition. We checked that the redefinition $\hat{V}_{ij} \rightarrow c_L (\hat{V}_{\text{literature}})_{ij}$ for $(i=3) \neq (j=3)$ reproduces the results for charged currents at $\mathcal{O}(v^2/f^2 \cdot \lambda^0)$. As anticipated above, we define the CKM matrix via the W -vertex to light fermions

$$W^+ \text{ vertex} = i \frac{g}{\sqrt{2}} V_{ij}, \quad V_{ij} \equiv \hat{V}_{ij} - \frac{v^2}{f^2} \frac{x_L^2}{2 \hat{V}_{33}^2} \left(\hat{V}_{ij} \hat{V}_{3j} + 2 \sum_{k=1}^{j-1} \hat{V}_{ik} \hat{V}_{3k} \right) \hat{V}_{3j}. \tag{3.2.29}$$

The usage of \mathbf{V} , instead of $\hat{\mathbf{V}}$, in the Feynman rules, which we enlist in appendix A.2, encodes all higher order corrections in the Cabibbo angle as compared to the literature. Furthermore, it simplifies the expressions derived in section 3.1 significantly. We note in passing, that the 3×3 CKM matrix \mathbf{V} is non-unitary. This is expected if the sum-rule (3.1.19) holds, like we discussed it in the text below this equation. The only additional contribution to this sum rule is given by a T_+ quark exchange, using the Feynman rules of appendix A.2 we expect

$$(\mathbf{V}^\dagger \mathbf{V})_{ij} - \delta_{ij} = \frac{v^2}{f^2} \frac{g^2 x_L^2}{2 \hat{V}_{33}^2} V_{3i} V_{3j}, \tag{3.2.30}$$

if the sum rule holds. Indeed, this is the case as we can easily check from the definition (3.2.29) and the unitarity of $\hat{\mathbf{V}}$. From the $\mathcal{O}(v^2/f^2 \cdot \lambda^6)$ suppression in (3.2.30), it is already clear that non-unitarity of the first column, $\Delta_{\text{col1}}^{\text{non}} \equiv 1 - \sum_i |V_{1i}|^2 < 0$, is tiny and way below the observable limits, which are of the order of 10^{-2} [170]. Non-unitarity of the first row is better constrained by approximately one order of magnitude. However, in the LHT model, the sum rules imply that in a unitarized version of the model $(\mathbf{V} \mathbf{V}^\dagger)_{ij} - \delta_{ij} \propto \delta_{i3} \delta_{j3}$, *i.e.* no first row non-unitarity would be present at all, while the definition (3.2.29) again gives a result $\Delta_{\text{row1}}^{\text{non}} = \mathcal{O}(v^2/f^2 \cdot \lambda^6)$. Consequently, non-unitarity is unobservable in all cases. However, a full analysis of non-unitarity aspects would furthermore require the calculation of corrections

to charged current mediated processes that enter the extraction of the CKM matrix elements from experiment and appear at one loop in the model at hand. The mass eigenvalues of the heavy top-quark partners $m_{T_{\pm}}$ are fixed by the relations

$$\frac{m_t^2}{m_{T_{-}}^2} = \frac{v^2}{f^2} \frac{x_L}{V_{33}^2}, \quad \frac{m_{T_{+}}^2}{m_{T_{-}}^2} (1 - x_L) = 1 + \frac{v^2}{f^2} x_L \left(\frac{x_L}{V_{33}^2} - 1 \right). \quad (3.2.31)$$

Since $0 < x_L \leq 1$, we see that the minimal mass for the T -even top partner is given by

$$m_{T_{+}} \geq \frac{4f}{v} m_t V_{33} \approx 2.8 f. \quad (3.2.32)$$

Yukawa interactions for leptons can be written down analogously to $\mathcal{L}_{Y,d}$. We refrain from introducing right-handed neutrinos.

Kinetic terms for the linearly transforming fermion multiplets are straightforward to write down [157, 171]. Remark that Ψ'_2 transforms as a $\bar{\mathbf{5}}$ and $g_1^{(\prime)} = g_2^{(\prime)} = \sqrt{2} g^{(\prime)}$, such that we obtain

$$\mathcal{L}_{F,\text{lin}} = \sum_{i=1,2} \bar{\Psi}'_i i \not{D}^{(i)} \Psi'_i + \sum_{\substack{f=u^c, d^c, \\ t'_i, t'_i c}} \bar{f} i \not{D} f, \quad \begin{aligned} D_{\mu}^{(1)} &= D_{\mu} - i\sqrt{2}g(Q_1^a W_{1\mu}^a + Q_2^a W_{2\mu}^a), \\ D_{\mu}^{(2)} &= D_{\mu} + i\sqrt{2}g((Q_1^a)^T W_{1\mu}^a + (Q_2^a)^T W_{2\mu}^a), \\ D_{\mu} &= \partial_{\mu} + i\sqrt{2}g'(Y_1 B_{1\mu} + Y_2 B_{2\mu}). \end{aligned} \quad (3.2.33)$$

Furthermore, we also need a kinetic term for the right-handed mirror fermions. It is constructed by following the approach of Callan, Coleman, Wess and Zumino [172, 173]. An explicit construction of the necessary Maurer-Cartan one form was first given in [158, 159]

$$\mathcal{L}_{F,\text{mir}} = \frac{1}{2} \bar{\Psi}' [\xi^{\dagger} i \not{D}^{(1)} \xi + \xi \Sigma_0 i \not{D}^{(1)*} \Sigma_0 \xi^{\dagger}] \Psi'. \quad (3.2.34)$$

The hypercharge in $\not{D}^{(1)}$ must be adapted to account for the insertion of ξ , *i.e.* explicitly $Y = Y_i^{(\xi\Psi')} = Y_i^{(\Sigma)} + Y_i^{(\Psi')}$. It is useful to note that in terms of T -parity eigenstates

$$\Sigma_0 \not{D}^{(1)*} \Sigma_0 = \partial_{\mu} - ig(Q^a W_{\mu}^a - Q'^a W_{\mu}'^a) + ig'(Y B_{\mu} - Y' B'_{\mu}) \quad (3.2.35)$$

Remark that one has to take special care when deriving the interactions of mirror fermions from (3.2.34), since their couplings to Z_L and W_L are not vector-like at $\mathcal{O}(v^2/f^2)$ after electroweak symmetry breaking [160]. This has implications on perturbativity of the theory and the calculations performed in chapter 3.1. Furthermore, heavy gauge bosons mediate currents between a SM fermion and a mirror fermion. Those interaction are all proportional to a combination of heavy and light mixing matrices, for which it is useful to introduce abbreviations

$$\mathbf{V}_{Hd} \equiv \mathbf{V}_H^{\dagger}, \quad \mathbf{V}_{Hu} \equiv \mathbf{V}_{Hd} \mathbf{V}^{\dagger}. \quad (3.2.36)$$

The matrix \mathbf{V}_H was defined in (3.2.21). It introduces three new mixing angles and three CP -violating phases [174]. In the context of flavor observables they allow for interesting departures from the minimally flavor violating patterns. Since we are only interested in the coupling structure of the model and do not study the precise numerical consequences of the model, we end the discussion at this point and refer to the given references for further details.

3.3 Randall-Sundrum Models

As a last example of physics beyond the SM we present models with a warped extra dimension. They belong to the class of theories for which non-perturbativity at a given new energy scale, is directly implied by construction. The models become strongly interacting due to lowering the effective scale of gravity for heavy fermions and, most prominently, for the Higgs boson. However, they do not aim to reduce the little hierarchy problem in contrast to the little Higgs models presented in the last section.

The first scenario of this type was first proposed by Randall and Sundrum [175]. It provides a natural explanation for the absence of the gauge-hierarchy problem, and also a very compelling theory of the hierarchies in the flavor sector. Therefore, such models are especially interesting from a precision physics perspective as they receive relevant constraints from electroweak precision physics, flavor-changing decays and most recently also from Higgs production and decays. In combination with the rather small number of free parameters this creates a good prospect for their falsifiability.

We give a short introduction into the necessary geometric structure of the extra dimension and discuss a minimal realization of the Randall-Sundrum (RS) model. As for the theories discussed in the previous section, we also present an extension of the RS model that accounts for the strongest electroweak precision constraints by implementing an enlarged gauge symmetry sector and a specific fermion embedding, the custodial RS model.

3.3.1 Basic Geometry of the Setup

Quantum field theories with extra dimensions offer an interesting candidate as a fundamental theory since they provide a framework that naturally connects the electroweak scale with a higher fundamental scale. The geometry of the extra dimension is explicitly adapted to serve this purpose. Length scales r_c orthogonal to our usual 3+1 space-time are usually compactified and resolvable with energies not too far above the electroweak scale $1/r_c \sim \Lambda_{\text{IR}} \gtrsim M_{\text{weak}}$. The higher scale Λ_{UV} can be implemented in various ways and is mostly used to establish a geometric connection to gravity. The first viable scenarios with large and flat extra dimensions were proposed in the late '90s by Arkani-Hamed, Dimopoulos and Dvali (ADD) [176] which can be regarded as the root of this branch of model building. In these theories it is illustrative to compare Newton's law at distances much smaller than r_c which has a fundamental Planck scale $M_{\text{Pl}}^{(4+n)}$, with Newton's law relevant to a macroscopic observer at distances much larger than r_c . The latter shows an effective Planck scale $(M_{\text{Pl}}^{(4,\text{eff})})^2 \approx (M_{\text{Pl}}^{(4+n)})^{2+n} r_c^n$, when using n extra dimensions of equal size. For large enough r_c or n we obtain a potentially large separation between the fundamental and the effective scale. Colloquially one says that the propagation of gravity in the bulk of the extra dimensions dilutes its force compared to other forces whose quantum fluctuations can be localized to a specific position in the extra dimension. As in every model, the fundamental Planck scale also serves as the UV cutoff of the theory, since one expects the onset of a quantum theory of gravity at this scale. Choosing a low scale $M_{\text{Pl}}^{(4+n)} = \Lambda_{\text{IR}} \sim 1 \text{ TeV}$ and the effective scale $M_{\text{Pl}}^{(4,\text{eff})} = M_{\text{Pl}} \sim 10^{16} \text{ TeV}$ gives a natural explanation for the absence of the gauge-hierarchy problem in this effective theory due to gravity. This is analogous to the onset of QCD-like strong interaction in composite Higgs models. However, to obtain the numerical values given above, $n < 3$ dimensions are excluded by direct measurements of the inverse square law [177] and astrophysical measurements of the release of gravitational binding energy in type-II supernovae [178]. The latter takes place

through nucleon-nucleon scattering processes, where the light Kaluza Klein (KK)-graviton states are produced in the final state. KK states are the Fourier-modes of a quantum field that extends into a compactified extra dimension, like the graviton does in the ADD model. Besides the strong direct bounds, the ADD model has the theoretical drawback that the separation of Planck and electroweak scale is achieved only by the introduction of yet another scale parameter r_c without explaining its size. One way to overcome this was proposed by Randall and Sundrum [175] through the use of a non-trivial geometry in a 5d anti-de Sitter space AdS_5 . For their setup a single extra dimension is sufficient, given the non-factorizable metric

$$ds^2 = e^{-2\sigma(\phi)} \eta_{\mu\nu} dx^\mu dx^\nu - r^2 d\phi^2; \quad \sigma(\phi) = kr|\phi|. \quad (3.3.1)$$

Here, x^μ denote the coordinates on the 4d hyper-surfaces of constant ϕ with metric $\eta_{\mu\nu} = \text{diag}(1, -1, -1, -1)$. Length and energy scales are modified by the exponential warp factor $\sigma(\phi)$ depending on the extra coordinate $\phi \in [-\pi, \pi]$. For the localization of fields and to make the geometry a solution to 5d Einstein equations, is reasonable to introduce topological defects, so-called branes, in the form of an orbifold.¹² Here, the S^1/Z_2 orbifold compactification leaves two 3-branes that are located at the orbifold fixed points at $\phi = 0$ (UV brane) and $\phi = \pi$ (IR brane). The curvature parameter k and the inverse radius r^{-1} of the extra dimension are assumed to be of the size of the only fundamental mass parameter M_{Pl} . As mentioned above the fundamental energy scale is position-dependent and in fact $M_{\text{Pl}} e^{-\sigma(\phi)}$ sets the effective Planck scale at a given point along the extra dimension. It serves as a natural UV cutoff, since quantum gravity becomes relevant above this scale. Higher-dimensional spaces with warp factors arise naturally in flux compactifications of string theory [181–184], which could provide a UV completion of this effective model. Like in the ADD model, one assumes that the effective cutoff scale on the IR brane $\Lambda_{\text{TeV}} = M_{\text{Pl}} e^{-\sigma(\pi)} \equiv M_{\text{Pl}} \epsilon$ is in roughly around 20 TeV in order to solve the (big) hierarchy problem. In contrast to the ADD model the exponential hierarchy of energy scales is generated by the AdS_5 background itself. This requires $L \equiv kr\pi = -\ln \epsilon \approx 34$ to be only moderately large, leaving a little hierarchy problem: The fact that the Higgs mass is two orders of magnitude smaller than the cutoff scale, is not addressed in the minimal RS framework. The warped curvature scale, $M_{\text{KK}} \equiv ke^{-\sigma(\pi)} = k\epsilon$, is assumed to lie somewhat lower, in the range of a few TeV. This allows for predictive phenomenology since M_{KK} sets the mass scale for the low-lying KK excitations of the SM fields. The first KK photon and gluon states in fact obtain masses of $2.45 M_{\text{KK}}$, the first KK graviton a mass of $3.83 M_{\text{KK}}$, and fermion masses are in a similar range [185]. Another conceptual difference to the ADD model is that the effective Planck scale $(M_{\text{Pl}}^{(4,\text{eff})})^2 = (M_{\text{Pl}}^{(5)})^3 (1 - e^{-2\pi kr})/k \sim M_{\text{Pl}}^2$ is of the same size as all the introduced fundamental mass parameters [175].

It will be convenient to introduce a conformal coordinate for the extra dimension. Here, we use it in the way of reference [186] with mass dimension zero as $t = \epsilon e^{\sigma(\phi)}$ as this renders the results especially compact: t equals ϵ on the UV brane and 1 on the IR brane. Integrals over the orbifold are obtained using

$$\int_{-\pi}^{\pi} d\phi \rightarrow \frac{2\pi}{L} \int_{\epsilon}^1 \frac{dt}{t}, \quad \int_{-\pi}^{\pi} d\phi e^{\sigma(\phi)} \rightarrow \frac{2\pi}{L\epsilon} \int_{\epsilon}^1 dt. \quad (3.3.2)$$

¹²Another possibility of confining fields to regions of finite width (“fat branes”) uses domain wall solutions of additional scalar fields [179] and has been used *e.g.* in [180] to separate the positions of fermions in large extra dimensions. The branes in the RS model are not of this kind, so we will not further elaborate on this.

The form $z = t/M_{\text{KK}}$ includes the appropriate mass scale to write the metric conformally [187]

$$ds^2 = \left(\frac{R}{z}\right)^2 (\eta_{\mu\nu} dx^\mu dx^\nu - dz^2), \quad (3.3.3)$$

and is also often used in the literature. To facilitate comparison we note that $z \in [R, R']$, where $R = 1/k$ and $R' = 1/M_{\text{KK}}$ denote the positions of the UV and IR branes, and $L = \ln(R'/R)$.

It has been noted by Goldberger and Wise [188] that the geometric setup of the given distance between the two branes described above can be stabilized. The radion is the scalar quantum fluctuation along the coordinate ϕ . Its potential has to be modeled such that the radion VEV determines the size of the extra dimension L . Additionally, the radion must be massive, which is necessary because of the equivalence principle [175]. All this can be achieved with the introduction of an additional scalar field and only moderate fine-tuning in its corresponding coupling parameters. Remark that in principle one may introduce a mixing parameter for the Higgs boson with the radion. For definiteness we will assume it to be negligible, or equivalently assume a large mass of the radion. We refer to [189–191] for a closer discussion.

We close the discussion of the geometry with a short comment on the actual size of L . From a purely phenomenological point of view, it is possible to lower the UV cutoff from the Planck scale to a value only few orders of magnitude above the TeV scale. This less ambitious bottom-up approach is akin to the Little Higgs models discussed in 3.2 and called little Randall-Sundrum model (LRS) [192]. The possibility of lowering L leads to interesting phenomenological consequences since many contributions to observables are proportional to L . We keep this possibility in mind and apply it in our analysis.

3.3.2 The Role of Compactification and Boundary Conditions

In the last section, we already anticipated that the RS model is based on an orbifold background which introduces lower dimensional branes that are distinguished hypersurfaces. They are topologically disconnected from the surrounding bulk of the extra dimension and allow to write down part of the fundamental fields localized to the brane as 4 instead of 5 dimensional. In the original formulation of the RS model, this simple possibility was used for all SM fields, which were located at the IR brane. Though not necessary, it is still a reasonable choice for Higgs boson in order to eliminate the gauge-hierarchy problem. To the remaining fields this reasoning does not apply and it was soon realized that allowing gauge [185, 193, 194] and matter fields [186, 195] to spread in the AdS_5 bulk does indeed have certain advantages. Importantly, bulk fermions significantly lower the RS corrections to the Peskin-Takeuchi S parameter, which arise through delocalized W^\pm and Z bosons [195–198]. The remaining corrections to the T parameter will be reviewed in section 4.2.2. Furthermore, it also lowers constraints from dimension-six four-fermion operators, like those mediating proton decay or flavor-changing neutral currents (FCNCs), which are otherwise suppressed only by powers of Λ_{IR} . Those operators will receive a larger suppression scale for bulk fermions. Moreover, the variation of the localization of the fermion zero modes, which are the 4d SM-fields, accounts for additional suppression factors whose size are intimately connected to one of the main theoretical advantages of bulk fermions: The different localization automatically arises in the model without further assumptions and can explain the flavor structure and hierarchies of

fermions masses and mixings [199, 200] by order one parameters¹³, which we will define and examine below. In other words, the assumption of the warp factor as the solution of the gauge-hierarchy problem implies split fermions and realizes the idea of geometrical sequestering [180]. The entanglement of hierarchies in the fermion spectrum and the additional suppression of dangerous FCNCs [195], is referred to as the RS-GIM mechanism [201, 202].

After this short digression into the necessity of bulk fields we shall review the possible boundary conditions (BCs) for bulk fields. To this end it is necessary to understand the compactification and orbifolding procedure. In principle, there exist ordinary and Scherk-Schwarz compactifications [203] and to furthermore introduce topological defects also the orbifold compactification. In the case relevant for us the compactification is done by a discrete group of translations acting on a real line $G \ni \tau_n : \mathbb{R} \rightarrow \mathbb{R} : \phi \rightarrow \phi + n2\pi$. The quotient space $S^1 = \mathbb{R}/G$ built by using all operators τ_n as projections is compact and obtains the topological defect only after acting non-freely with another discrete group on S^1 . Here, they are given by the reflections at $\phi = \pi$ given by $\mathbb{Z}_2 \ni \zeta : S^1 \rightarrow S^1 : \phi \rightarrow 2\pi - \phi$, which have a fixed point precisely at 0 and π . After the projection we obtain the orbifold $\mathcal{O} = S^1/\mathbb{Z}_2$, which looks mainly like an interval and is the only one-dimensional orbifold [204]. It is important to realize that, while G and \mathbb{Z}_2 must be symmetries of the 5d Lagrangian, the fields, collectively denoted by Φ , can have additional transformation behavior

$$\Phi(x^\mu, \tau_k(\phi)) = T^k \Phi(x^\mu, \phi), \quad \Phi(x^\mu, \zeta_k(\phi)) = Z \Phi(x^\mu, \phi), \quad (3.3.4)$$

with the consistency condition $Z^2 = 1$ and $TZT = Z$. In principle, the reflection behavior Z at the origin can be a matrix with eigenvalues ± 1 for fields of higher spin, but we will only need the simple case where $Z = \pm 1$. It implies Dirichlet boundary conditions for even fields $\Phi(x^\mu, \pi) = 0$ and Neumann boundary conditions for odd fields $\partial_\phi \Phi(x^\mu, \pi) = 0$. This transformation behavior is mostly referred to as *the* parity, while parity under translations T is called (anti-)periodicity or Scherk-Schwarz twist for $T = -1$. Using $T = -1$ fields is sometimes also expressed as working on the manifold $S^1/(\mathbb{Z}_2 \times \mathbb{Z}'_2)$. In the KK decomposition of 5d fields, we will denote (anti-)periodicity by a superscript, *e.g.*

$$\Phi(x^\mu, \phi) = N \sum_{n=0}^{\infty} \Phi^{(n)}(x^\mu) \chi_n^{(\pm)}(\phi). \quad (3.3.5)$$

Usually N is a universal normalization factor, $\Phi^{(n)}$ are 4d fields called KK modes and $\chi_n^{(\pm)}$ form the corresponding basis of Fourier modes called profile functions. We indicate the parity at the origin by using different symbols for χ . *E.g.*, for fermions we use C for even and S for odd modes. For comparison with the literature, we remark that another common nomenclature carries the boundary conditions at UV and IR brane as upper indices. An odd twisted function, in our nomenclature *e.g.* $S_n^{(-)}$, would correspond to the notation $f_n^{[+,-]}$.

The role of parity will become clear in the explicit decompositions of KK fermions and gauge bosons. As a general principle only the 5d fields with periodic, even modes will obtain so-called zero modes that remain massless in the gauge-symmetric phase. The counting for odd KK modes starts accordingly at one. Those higher KK modes will obtain an explicit mass of order M_{KK} in the 4d picture. For gauge fields there is a Stückelberg-like mechanism

¹³In fact from a probabilistic point of view the converse is true as well. The fermion hierarchies imply peaked distributions of all but one localization parameters [3] when assuming a flat prior *e.g.* the left-handed top quark.

[205] at work that involves the fifth component of the gauge fields as the corresponding scalar mode. The zero modes in turn obtain mass only after electroweak symmetry breaking through insertions of the Higgs VEV and further mixings with other KK modes that are also generated by electroweak symmetry breaking. This resolves a great obstacle in the implementation of chiral low-mass 4d fermions. In principle, chirality projections do not exist for fields in odd space-time dimensions, the reason being that the Clifford algebra relation $\{\gamma_M, \gamma_N\} = 2\eta_{MN}\mathbf{1}$ in $n = 2\nu$ and $n = 2\nu + 1$ dimensions can be fulfilled by n matrices of size $2^\nu \times 2^\nu$ [206]. The graduating automorphism γ_5 that distinguishes the two chiral representations in 4d is part of the Clifford algebra in 5d and part of the 5d representation of the Lorentz-group for Dirac fermions to generate translations in ϕ -direction. However, we can resemble chiral fermions by assigning an odd parity to the wrong chirality of fermions, *i.e.* to right-handed doublets and left-handed singlets. Remark that the spectrum of heavy fermion modes will thus contain at least twice as many degrees of freedom per KK modes compared to the SM-fermion spectrum.

Much like periodic, odd modes, also anti-periodic modes of both parity do not possess a zero mode and all modes obtain mass of order M_{KK} . This combination of boundary conditions turns out to be useful to give exotic fermions a heavy KK spectrum and to break additional gauge symmetries by a combination of periodic and anti-periodic boundary conditions as we will discuss in section 3.3.5.

We shortly come back to the remaining Higgs sector, which is confined to the IR brane with a function $\delta(\phi - \pi)$ in the setup we consider below. The 5d Yukawa coupling of the Higgs boson presents a localized source in the 5d equations of motion (EOMs) for fermions and distorts the fermion profiles. The presence of a δ -function seemingly leads to jump conditions well known from simple quantum mechanics problems. This is referred to as modified boundary conditions for the fermions. To clarify this terminology a comment is in order. We will show in section 3.3.8.1 that a proper regularization of the δ -function used to regularize the Higgs boson, is essential to obtain correct 4d Yukawa couplings [4, 207]. This is done with the usual weak limit of smooth kernel functions, extending infinitesimally into the bulk, which define the δ -distribution in the limit of a regularization parameter η approaching 0. In the regularized theory, only smooth functions are involved and thus the boundary conditions remain exactly Neumann or Dirichlet. Only in the limit of $\eta \rightarrow 0$, odd profile functions may develop a value $\lim_{\epsilon \rightarrow 0} S(\pi - \epsilon) \neq 0$ whilst $S(\pi) = 0$ remains true. We denote the limiting value also with $S(\pi^-)$, as it enters many relevant quantities.

3.3.3 Fermions in a Curved Background

In order to treat fermions in a curved background we give a short digression into the formal treatment of their general action. Spinor formalism in a general curved background can be conveniently expressed in the vielbein formalism. Roughly spoken, the inverse vielbein $e_a^A = \text{diag}(e^{\sigma(\phi)}, \dots, e^{\sigma(\phi)}, 1)$ represents the local coordinate system. Analogous to the Levi-Civita-connection Γ_{MP}^N for the treatment of gravity in the framework of general relativity, we also need its generalization, the so-called spin connection ω_{bcA} . Geometrically it is a mixed object from $\text{Lie}(SO(1,4)) \otimes \Lambda^1 M$, where M is our 5d manifold. It represents the induced unique, metric, and torsion-free Levi-Civita-connection of M inside the spinor bundle. That said the action of a single Dirac spinor ψ is given by

$$S_{\text{F}} = \int d\Omega \left[e_a^A \left(\frac{i}{2} \bar{\psi} \gamma^a \overleftrightarrow{\partial}_A \psi + \frac{1}{8} \omega_{bcA} \bar{\psi} \{ \gamma^a, \sigma^{bc} \} \psi \right) - m \text{sgn}(\phi) \bar{\psi} \psi \right]. \quad (3.3.6)$$

We have used the general measure of a curved space $d\Omega = d^4x r d\phi \sqrt{G}$, where in the RS background $G = e^{-8\sigma}$ is the determinant of the metric. Observe that for the mass term to be non-vanishing, we have to assign an odd parity to it, so an additional sign function was included. A thorough discussion of the action can be found in [208]. We indicate that the spin connection can easily be calculated with the non-zero Christoffel symbols

$$\Gamma_{5\nu}^\mu = \Gamma_{\nu 5}^\mu = -\sigma'(\phi)\delta_\nu^\mu, \quad \Gamma_{\mu\nu}^5 = -e^{-2\sigma(\phi)}\sigma'(\phi)\eta_{\mu\nu} \quad (3.3.7)$$

as

$$\begin{aligned} \omega_M &= \frac{1}{4}\omega^{ab}{}_M \gamma_a \gamma_b = \frac{1}{4}\eta^{bc} \left\{ (\partial_M e_c^N) e_N^a + e_N^a \Gamma_{MP}^N e_c^P \right\} \gamma_a \gamma_b \\ &= (1 - \delta_{M5}) \frac{\sigma'(\phi) e^{-\sigma(\phi)}}{2} \delta_M^a \gamma_a \gamma_5 \end{aligned} \quad (3.3.8)$$

It gives in fact no contribution to the action [186] since

$$e_a^A \{ \gamma^a, \omega_A \} \propto \delta_a^A \{ \gamma^a, \delta_A^b \gamma_b \gamma_5 \} = 0. \quad (3.3.9)$$

We postpone the further treatment of (3.3.6) to the discussion of the model-specific implementations given below.

3.3.4 Minimal Randall-Sundrum Model

In the following, we consider the gauge and fermion sector of the minimal realization of a RS model that reproduces the SM field content as zero modes. We will discuss the KK decomposition for the electroweak and fermion sector. The extension to the QCD sector is straightforward.

3.3.4.1 Gauge-Boson Sector

In the simplest version, we consider a $SU(2)_L \times U(1)_Y$ gauge theory, coupled to a scalar sector on the IR brane. As explained in the last section, the vector components W_μ^a and B_μ have to be even under the \mathbb{Z}_2 orbifold symmetry and in order to remove the scalar components W_ϕ^a and B_ϕ from the low energy spectrum they are chosen to be odd. The action can be split up as

$$S_G = \int d^4x r \int_{-\pi}^{\pi} d\phi \left(\mathcal{L}_V + \mathcal{L}_H + \mathcal{L}_{GF} + \mathcal{L}_{FP} \right), \quad (3.3.10)$$

where

$$\mathcal{L}_V = \frac{\sqrt{G}}{r} G^{KM} G^{LN} \left(-\frac{1}{4} W_{KL}^a W_{MN}^a - \frac{1}{4} B_{KL} B_{MN} \right), \quad (3.3.11)$$

$$\mathcal{L}_H = \frac{\delta(|\phi| - \pi)}{r} \left[(D_\mu \Phi)^\dagger (D^\mu \Phi) - V(\Phi) \right], \quad V(\Phi) = -\mu^2 \Phi^\dagger \Phi + \lambda (\Phi^\dagger \Phi)^2 \quad (3.3.12)$$

are the Lagrangian for the 5d gauge theory and brane-localized Higgs sector. We replace four-component indices with five-component capital indices and denote the 5d metric as G_{MN} . We use the same notation as in the SM (2.2.6) for the components of the Higgs doublet after electroweak symmetry breaking and we apply the usual rotation with a weak mixing angle,

defined here via the 5d gauge couplings as $\tan(\theta_w) \equiv g'_5/g_5$, to arrive at the fields A_M and Z_M . The kinetic terms for the Higgs field give rise to 5d mass terms $M_{W_5} = vg_5/2 = M_{Z_5}c_w$ of mass dimension 1/2, and bilinear terms involving the gauge and would-be Goldstone bosons. Moreover, the kinetic terms for the gauge fields in (3.3.11) also contain bilinear terms of the gauge bosons and their scalar components W_ϕ^\pm , Z_ϕ , and A_ϕ . All of these mixed terms can be removed with a suitable choice of the gauge-fixing Lagrangian [1]

$$\begin{aligned}
 \mathcal{L}_{\text{GF}} = & -\frac{1}{2\xi} \left(\partial^\mu A_\mu - \xi \left[\frac{\partial_\phi e^{-2\sigma(\phi)} A_\phi}{r^2} \right] \right)^2 \\
 & - \frac{1}{2\xi} \left(\partial^\mu Z_\mu - \xi \left[\frac{\delta(|\phi| - \pi)}{r} M_{Z_5} \varphi^3 + \frac{\partial_\phi e^{-2\sigma(\phi)} Z_\phi}{r^2} \right] \right)^2 \\
 & - \frac{1}{\xi} \left(\partial^\mu W_\mu^+ - \xi \left[\frac{\delta(|\phi| - \pi)}{r} M_{W_5} \varphi^+ + \frac{\partial_\phi e^{-2\sigma(\phi)} W_\phi^+}{r^2} \right] \right) \\
 & \times \left(\partial^\mu W_\mu^- - \xi \left[\frac{\delta(|\phi| - \pi)}{r} M_{W_5} \varphi^- + \frac{\partial_\phi e^{-2\sigma(\phi)} W_\phi^-}{r^2} \right] \right).
 \end{aligned} \tag{3.3.13}$$

Note that there is no problem in squaring the δ -functions. We will see below that the derivatives of the scalar components of the gauge fields W_ϕ^\pm and Z_ϕ also contain a δ -function contribution, which precisely cancels the δ -functions from the Higgs sector. As a result, contrary to the treatment in [209], we do not need to introduce separate gauge-fixing Lagrangians in the bulk and on the IR brane. Such a separate treatment is useful when considering the 5d propagator of gauge bosons as discussed in section 3.3.7 in general R_ξ gauge [210]. The bilinear terms in the action now read

$$\begin{aligned}
 S_{G,2} = & \int d^4x r \int_{-\pi}^{\pi} d\phi \left\{ -\frac{1}{4} F_{\mu\nu} F^{\mu\nu} - \frac{1}{2\xi} (\partial^\mu A_\mu)^2 \right. \\
 & + \frac{e^{-2\sigma(\phi)}}{2r^2} [\partial_\mu A_\phi \partial^\mu A_\phi + \partial_\phi A_\mu \partial_\phi A^\mu] - \frac{\xi}{2} \left[\frac{\partial_\phi e^{-2\sigma(\phi)} A_\phi}{r^2} \right]^2 \\
 & - \frac{1}{4} Z_{\mu\nu} Z^{\mu\nu} - \frac{1}{2\xi} (\partial^\mu Z_\mu)^2 + \frac{e^{-2\sigma(\phi)}}{2r^2} [\partial_\mu Z_\phi \partial^\mu Z_\phi + \partial_\phi Z_\mu \partial_\phi Z^\mu] \\
 & - \frac{1}{2} W_{\mu\nu}^+ W^{-\mu\nu} - \frac{1}{\xi} \partial^\mu W_\mu^+ \partial^\mu W_\mu^- + \frac{e^{-2\sigma(\phi)}}{r^2} [\partial_\mu W_\phi^+ \partial^\mu W_\phi^- + \partial_\phi W_\mu^+ \partial_\phi W^{-\mu}] \\
 & + \frac{\delta(|\phi| - \pi)}{r} \left[\frac{1}{2} \partial_\mu h \partial^\mu h - \lambda v^2 h^2 + \partial_\mu \varphi^+ \partial^\mu \varphi^- + \frac{1}{2} \partial_\mu \varphi^3 \partial^\mu \varphi^3 + \frac{M_{Z_5}^2}{2} Z_\mu Z^\mu + M_{W_5}^2 W_\mu^+ W^{-\mu} \right] \\
 & - \frac{\xi}{2} \left[\frac{\delta(|\phi| - \pi)}{r} M_{Z_5} \varphi^3 + \frac{\partial_\phi e^{-2\sigma(\phi)} Z_\phi}{r^2} \right]^2 \\
 & \left. - \xi \left[\frac{\delta(|\phi| - \pi)}{r} M_{W_5} \varphi^+ + \frac{\partial_\phi e^{-2\sigma(\phi)} W_\phi^+}{r^2} \right] \left[\frac{\delta(|\phi| - \pi)}{r} M_{W_5} \varphi^- + \frac{\partial_\phi e^{-2\sigma(\phi)} W_\phi^-}{r^2} \right] + \mathcal{L}_{\text{FP}} \right\}.
 \end{aligned} \tag{3.3.14}$$

The form of the Faddeev-Popov ghost Lagrangian is analogous to that of the SM, with the only generalization that a ghost field is required for every KK mode.

The KK decompositions of the 5d fields has the general form

$$V_\mu(x, \phi) = \frac{1}{\sqrt{r}} \sum_n V_\mu^{(n)}(x) \chi_{V,n}^{(+)}(\phi), \quad V_\phi(x, \phi) = \frac{1}{\sqrt{r}} \sum_n a_n^V \varphi_V^{(n)}(x) \partial_\phi \chi_{V,n}^{(+)}(\phi), \quad (3.3.15)$$

where $V = A, Z, W^\pm$. $V_\mu^{(n)}$ are the 4d mass eigenstates, the various $\chi_{V,n}^{(+)}$ profiles form complete sets of even functions on the orbifold, which obey orthonormality conditions on S^1 with respect to the measure $d\phi$. The superscript (+) indicates untwisted, *i.e.* periodic modes, and a_n^V are coefficients, which we determine below. The choice of $\partial_\phi \chi_n^V$ as modes for the scalar fifth components is a viable ansatz since it automatically reverses the BCs. It is in fact also necessary as one can easily show. The 5d scalar fields also have to be expanded in the basis of 4d mass eigenstates. To associate a scalar Goldstone mode with each KK level we write

$$\varphi^\pm(x) = \sum_n b_n^W \varphi_W^{\pm(n)}(x), \quad \varphi^3(x) = \sum_n b_n^Z \varphi_Z^{(n)}(x), \quad (3.3.16)$$

and determine the coefficients b_n^V below. We will denote the masses of 4d vector fields by $m_n^V \geq 0$. As usual the masses of scalar fields $\varphi_V^{(n)}$ will be related to these by gauge invariance.

Inserting these decompositions into the action, one finds that the profiles χ_n^a obey the 5d equation of motion [185, 193]

$$-\frac{1}{r^2} \partial_\phi e^{-2\sigma(\phi)} \partial_\phi \chi_{V,n}^{(+)}(\phi) = (m_n^V)^2 \chi_{V,n}^{(+)}(\phi) - \frac{\delta(|\phi| - \pi)}{r} M_{V5}^2 \chi_{V,n}^{(+)}(\phi). \quad (3.3.17)$$

In summary we have to find the spectrum of the differential operator $-\frac{1}{r^2} \partial_\phi e^{-2\sigma(\phi)} \partial_\phi$ on $[0, \pi]$ subject to the boundary conditions

$$\partial_\phi \chi_{V,n}^{(+)}(0) = 0, \quad \partial_\phi \chi_{V,n}^{(+)}(\pi^-) = -\frac{r M_{V5}^2}{2\epsilon^2} \chi_{V,n}^{(+)}(\pi). \quad (3.3.18)$$

The superscript notation π^- signifies the left limiting value of the function at the IR brane. Note that the derivative of $\chi_{V,n}^{(+)}$ becomes discontinuous at π due to (3.3.17). The appropriate IR BCs for the profiles have been obtained by integrating the EOM (3.3.17) over an infinitesimal interval around $|\phi| = \pi$ and carrying out the regulating limit involved in the definition of the δ -function. Remark that the IR BCs force the profile to be $\chi_{V,n}^{(+)}$ to be non-smooth at $\phi = \pi$. Since the profiles of the scalar components are taken to be proportional the ϕ -derivative of the vector profiles, they develop discontinuities at the IR brane.

We find that the action takes the desired form

$$\begin{aligned} S_{G,2} = \sum_n \int d^4x \left\{ & -\frac{1}{4} F_{\mu\nu}^{(n)} F^{\mu\nu(n)} - \frac{1}{2\xi} \left(\partial^\mu A_\mu^{(n)} \right)^2 + \frac{(m_n^A)^2}{2} A_\mu^{(n)} A^{\mu(n)} \right. \\ & - \frac{1}{4} Z_{\mu\nu}^{(n)} Z^{\mu\nu(n)} - \frac{1}{2\xi} \left(\partial^\mu Z_\mu^{(n)} \right)^2 + \frac{(m_n^Z)^2}{2} Z_\mu^{(n)} Z^{\mu(n)} \\ & - \frac{1}{2} W_{\mu\nu}^{+(n)} W^{-\mu\nu(n)} - \frac{1}{\xi} \partial^\mu W_\mu^{+(n)} \partial^\mu W_\mu^{-(n)} + (m_n^W)^2 W_\mu^{+(n)} W^{-\mu(n)} \\ & + \frac{1}{2} \partial_\mu \varphi_A^{(n)} \partial^\mu \varphi_A^{(n)} - \frac{\xi (m_n^A)^2}{2} \varphi_A^{(n)} \varphi_A^{(n)} + \frac{1}{2} \partial_\mu \varphi_Z^{(n)} \partial^\mu \varphi_Z^{(n)} - \frac{\xi (m_n^Z)^2}{2} \varphi_Z^{(n)} \varphi_Z^{(n)} \\ & \left. + \partial_\mu \varphi_W^{+(n)} \partial^\mu \varphi_W^{-(n)} - \xi (m_n^W)^2 \varphi_W^{+(n)} \varphi_W^{-(n)} \right\} \\ & + \int d^4x \left(\frac{1}{2} \partial_\mu h \partial^\mu h - \lambda v^2 h^2 \right) + \sum_n \int d^4x \mathcal{L}_{\text{FP}}^{(n)}, \end{aligned} \quad (3.3.19)$$

if and only if

$$a_n^V = -\frac{1}{m_n^V}, \quad b_n^V = \frac{M_{V5}}{\sqrt{r}} \frac{\chi_{V,n}^{(+)}(\pi^-)}{m_n^V}. \quad (3.3.20)$$

The resulting theory contains a tower of massive gauge bosons with masses m_n^V , accompanied by a tower of massive scalars with masses $\sqrt{\xi} m_n^V$, as well as the Higgs field h with mass $\sqrt{2\lambda}v$. Note that with (3.3.20) the 4d gauge-fixing Lagrangian derived from (3.3.13) takes the simple form

$$r \int_{-\pi}^{\pi} d\phi \mathcal{L}_{\text{GF}} = \sum_n \mathcal{L}_{\text{GF}}^{(n)}, \quad (3.3.21)$$

with

$$\begin{aligned} \mathcal{L}_{\text{GF}}^{(n)} = & -\frac{1}{2\xi} \left(\partial^\mu A_\mu^{(n)} - \xi m_n^A \varphi_A^{(n)} \right)^2 - \frac{1}{2\xi} \left(\partial^\mu Z_\mu^{(n)} - \xi m_n^Z \varphi_Z^{(n)} \right)^2 \\ & - \frac{1}{\xi} \left(\partial^\mu W_\mu^{+(n)} - \xi m_n^W \varphi_W^{+(n)} \right) \left(\partial^\mu W_\mu^{-(n)} - \xi m_n^W \varphi_W^{-(n)} \right). \end{aligned} \quad (3.3.22)$$

For each KK mode these expressions are identical to those of the SM. It follows that the form of the Faddeev-Popov ghost Lagrangians $\mathcal{L}_{\text{FP}}^{(n)}$ in (3.3.19) is analogous to that of the SM, with the only generalization that a ghost field is required for every KK mode.

3.3.4.2 Fermion Sector

For the minimal embedding of fermions we consider the SM gauge-representations and quantum numbers, however using Dirac fermions because of the absence of the chiral representation of the Lorentz group in 5d as discussed in section 3.3.2. Instead we give appropriate \mathbb{Z}_2 -parities to the formally defined chiral projections $P_{L,R} = (1 - \gamma_5)/2$ of the vector-like Dirac fermions, *i.e.* for the $SU(2)_L$ doublets we give even parity to the left-handed and odd parity to the right-handed chirality and vice versa for the fermion singlets.

We denote the components of $SU(2)_L$ doublets by u, d and singlets by u^c, d^c and consider only quarks for the moment. We generalize the fermion action (3.3.6) and add Yukawa interactions with the IR-brane Higgs boson that have the same form like in the SM. The bilinear part of the fermion action can then be written as [186, 195]

$$\begin{aligned} S_{\text{F},2} = & \int d^4x r \int_{-\pi}^{\pi} d\phi \left\{ \sum_{q=U,u,D,d} \left(e^{-3\sigma(\phi)} \bar{q} i \not{\partial} q - e^{-4\sigma(\phi)} \text{sgn}(\phi) \bar{q} \mathbf{M}_{\bar{q}} q \right. \right. \\ & \left. \left. - \frac{1}{2r} \left[\bar{q}_L e^{-2\sigma(\phi)} \overleftrightarrow{\partial}_\phi e^{-2\sigma(\phi)} q_R + \text{h.c.} \right] \right) \right. \\ & \left. - \delta(|\phi| - \pi) e^{-3\sigma(\phi)} \frac{v}{\sqrt{2}r} \sum_{\substack{(Q,q)= \\ (U,u),(D,d)}} \left[\bar{Q}_L \mathbf{Y}_{\bar{q}}^{(5d)} q_R + \bar{Q}_R \mathbf{Y}_{o\bar{q}}^{(5d)} q_L + \text{h.c.} \right] \right\}, \end{aligned} \quad (3.3.23)$$

with $\overleftrightarrow{\partial}_\phi \equiv \overrightarrow{\partial}_\phi - \overleftarrow{\partial}_\phi$ and we used a generalized notation that will facilitate the transition to more complicated fermion embeddings. For the minimal model the notation reduces trivially to

$$\begin{aligned} \vec{U} & \equiv u, \quad \vec{D} \equiv d, \quad \mathbf{M}_{\vec{U}} = \mathbf{M}_{\vec{D}} \equiv \mathbf{M}_Q, \\ \vec{q} & \equiv q^c, \quad \mathbf{M}_{\vec{q}} = \mathbf{M}_q, \quad \mathbf{Y}_{(o)\vec{q}}^{(5d)} \equiv \mathbf{Y}_{(o)q}^{(5d)}, \quad (q = u, d). \end{aligned} \quad (3.3.24)$$

Canonical kinetic terms and flavor-diagonal and real masses in (3.3.23) have been achieved by appropriate unitary transformations of the quark fields, so the given form stands without loss of generality. In contrast to the SM where fermion masses solely come from the Yukawa interactions, we cannot exclude negative diagonal entries in the mass matrices. Indeed, phenomenologically it turns out that the definitions

$$\mathbf{c}_Q \equiv \frac{1}{k} \mathbf{M}_Q, \quad \mathbf{c}_q \equiv -\frac{1}{k} \mathbf{M}_q \quad (3.3.25)$$

are useful, since all quarks except the top quark will be clustered around $c_{Q,q} \approx 1/2$.

In principle, there are two different types of Yukawa matrices either for two \mathbb{Z}_2 -even or \mathbb{Z}_2 -odd fermions. The latter has been neglected in [1] and all the literature before since it does naively not contribute because of the Dirichlet BCs at the IR brane. Indeed, the correct spectrum can be inferred by neglecting this type of Yukawa matrices. However, in [207] it was recognized that they are essential to derive the correct Higgs–fermion couplings. Considering the brane-localized Higgs sector as the limit of a bulk Higgs boson, 5d Lorentz invariance renders both types of Yukawa matrices identical $\mathbf{Y}_{(o)\bar{q}}^{(5d)} = \mathbf{Y}_{\bar{q}}^{(5d)}$. We will adopt this choice in the following. In the decomposition it will be useful to furthermore define dimensionless Yukawa matrices

$$\mathbf{Y}_{\bar{q}} \equiv \frac{k}{2} \mathbf{Y}_{\bar{q}}^{(5d)}, \quad (q = u, d). \quad (3.3.26)$$

The entries of this matrix shall take naturally non-hierarchical, complex values of $\mathcal{O}(1)$. The hierarchies of the Yukawa matrices of the SM quarks in the effective 4d theory are explained in terms of a geometrical realization of the Froggatt-Nielsen mechanism in RS models [1, 200, 211, 212].

Of course, we can also shed light on the remaining leptons by localization in the bulk. For instance one of the first ideas in considering fermionic fields in the RS bulk was how to obtain small and phenomenologically viable neutrino masses. This can be done by introducing two right-handed sterile neutrinos that live in the bulk [186] and additionally suppressing contributions from higher dimensional operators, by very small brane values of the modes [195].

For the KK decomposition we use a compact notation [2], in which the profile functions of the left-handed (right-handed) interaction eigenstates that can mix into the left-handed (right-handed) components of the 4d mass eigenstates are collected in vectors $\mathcal{Q}_A^{(n)}(t)$. They are defined in terms of the KK decompositions

$$\begin{aligned} \sqrt{r} \left(\frac{\epsilon}{t} \right)^2 \begin{pmatrix} \vec{Q}_L(x, t) \\ \vec{q}_L(x, t) \end{pmatrix} &= \sum_n \begin{pmatrix} \mathbf{C}_n^Q(t) \vec{a}_n^Q \\ \mathbf{S}_n^q(t) \vec{a}_n^q \end{pmatrix} q_L^{(n)}(x) \equiv \sqrt{\frac{L\epsilon}{2\pi}} \sum_n \mathcal{Q}_L^{(n)}(t) q_L^{(n)}(x), \\ \sqrt{r} \left(\frac{\epsilon}{t} \right)^2 \begin{pmatrix} \vec{Q}_R(x, t) \\ \vec{q}_R(x, t) \end{pmatrix} &= \sum_n \begin{pmatrix} \mathbf{S}_n^Q(t) \vec{a}_n^Q \\ \mathbf{C}_n^q(t) \vec{a}_n^q \end{pmatrix} q_R^{(n)}(x) \equiv \sqrt{\frac{L\epsilon}{2\pi}} \sum_n \mathcal{Q}_R^{(n)}(t) q_R^{(n)}(x). \end{aligned} \quad (3.3.27)$$

In this formula Q , q , and \mathcal{Q} are assumed to take the values U , u , and \mathcal{U} for the up-sector, or D , d , and \mathcal{D} for the down sector, *etc.*. In the minimal model, the generalized vectors with capital letters contain $SU(2)_L$ -doublet components and those with small letters the singlets. Thus, the combined notation expresses mixing between KK modes and singlet–doublet mixing due to electroweak symmetry breaking, both in the same compact form. We anticipate that the vectors will be extended even further in the custodial model, where additional 5d quarks with

twisted BCs are introduced, yet, the notation of (3.3.27) is general enough to accommodate also this extended case. In (3.3.27), we directly switched to t -coordinate notation (see (3.3.2) and text before) and extracted normalization factors that simplify the following expressions. $\mathbf{C}_n^{Q,q}(t)$ and $\mathbf{S}_n^{Q,q}(t)$ are diagonal matrices of even and odd profile functions and $\vec{a}_n^{Q,q}$ are decomposition vectors that parametrize the full mixing implied by electroweak symmetry breaking. The symbols Q, q are understood to take either the values U, u or D, d here. In the minimal RS model, this general notation again breaks down to equivalent values for the 3×3 matrices of the profile functions of the doublet fermions

$$\mathbf{C}_n^U(t) = \mathbf{C}_n^D(t) \equiv \mathbf{C}_n^{Q(+)}(t), \quad \mathbf{S}_n^U(t) = \mathbf{S}_n^D(t) \equiv \mathbf{S}_n^{Q(+)}(t), \quad (3.3.28)$$

where the superscript (+) indicates untwisted profiles. There are three zero modes in the up and down sector that represent the SM-like fermions. Each higher KK level contains six modes with $\mathcal{O}(v)$ mass splittings, while the different levels are split by an amount of $\mathcal{O}(M_{\text{KK}})$. We choose the index n to enumerate all these modes subsequently, *i.e.* 1 – 3 for the zero modes 4 – 9 for the KK modes of the first level, etc. Remark that $\vec{Q}_{L,R}(x, \phi)$ can be expanded in terms of the same vector \vec{a}_n^Q . With this choice, the even and odd profiles $\mathbf{C}_n^Q(\phi)$ and $\mathbf{S}_n^Q(\phi)$ will be normalized in the same way. The same holds for $Q \rightarrow q$. The orthonormality conditions for the new vectors read

$$\int_{\epsilon}^1 dt \mathcal{Q}_\sigma^{(m)\dagger}(t) \mathcal{Q}_\sigma^{(n)}(t) = \delta_{mn}, \quad (3.3.29)$$

$$\sum_n \mathcal{Q}_\sigma^{(n)}(t) \mathcal{Q}_\sigma^{(n)\dagger}(t') = \delta(t - t'), \quad (3.3.30)$$

where $\sigma = L, R$. A thorough discussion of the individual normalization of the profiles $\mathbf{C}_n^Q(\phi)$ and $\mathbf{S}_n^Q(\phi)$ can be found in [4], but we refrain from repeating it here. However, note that it is important to realize that the individual profiles $\mathbf{C}_n^{Q,q} \vec{a}_n^{Q,q}$ do not satisfy relations analogous to (3.3.29) and (3.3.30). This non-orthogonality is intuitive since the modes of different chiralities are mixed in the mass eigenstate basis, however it is not uniquely distributed on the profiles $\mathbf{C}_n^{Q,q}$ and eigenvectors $\vec{a}_n^{Q,q}$. The split into these two quantities is in fact only necessary in order to derive analytic expressions for the profiles and to clearly separate the mixing into $\vec{a}_n^{Q,q} = \vec{e}_n/\sqrt{2} + \mathcal{O}(v^2/M_{\text{KK}}^2)$, with unit vectors \vec{e}_n . The choice to normalize the mixing vectors as

$$(\vec{a}_n^Q)^\dagger \vec{a}_n^Q + (\vec{a}_n^q)^\dagger \vec{a}_n^q = 1, \quad (3.3.31)$$

fixes the analytic form of the profiles, which we give below in section 3.3.6.

The 5d variational principle requires all the variations of the action (3.3.23) to vanish for arbitrary infinitesimal changes of the fermionic fields. It is straightforward to see that the EOMs for 5d Dirac fermions lead to the following EOMs for the profiles after the KK decomposition [4]

$$\frac{\delta S_f}{\delta(\vec{Q}_\sigma, \vec{q}_\sigma)^T} : \quad \left((-1)^{\delta_{\sigma R}} \partial_t + \mathcal{M}_q(t) \right) \mathcal{Q}_{\bar{\sigma}}^{(n)}(t) = x_n \mathcal{Q}_\sigma^{(n)}(t), \quad (\sigma = L, R). \quad (3.3.32)$$

Here, $x_n = m_{q_n}/M_{\text{KK}}$ are the mass eigenvalues, $\bar{\sigma}$ denotes the opposite chirality and

$$\mathcal{M}_q(t) = \frac{1}{t} \begin{pmatrix} \mathbf{c}_{\vec{Q}} & \mathbf{0} \\ \mathbf{0} & -\mathbf{c}_{\vec{q}} \end{pmatrix} + \delta^\eta(t-1) \frac{v}{\sqrt{2}M_{\text{KK}}} \begin{pmatrix} \mathbf{0} & \mathbf{Y}_{\vec{q}} \\ \mathbf{Y}_{\vec{q}}^\dagger & \mathbf{0} \end{pmatrix}, \quad (3.3.33)$$

is the generalized mass matrix. Remark that we have added the regularization parameter η to the notation of the δ -function. It has been emphasized in [207] that in order to properly evaluate the Yukawa couplings this careful treatment is essential. The reason is that with a brane-localized Higgs sector the odd fermion profiles $\mathcal{S}_n^{Q,q}(t)$ are discontinuous at $t = 1$ [213], and hence the overlap integral of a product of two such functions with the naive Higgs profile $\delta(t - 1)$ is in fact ill defined. In the following, we will therefore consider the δ -function as the weak limit of a sequence of normalized, regularized functions δ^η with support on the interval $x \in [-\eta, 0]$ as

$$\lim_{\eta \rightarrow 0^+} \int_{-\infty}^{+\infty} dx \delta^\eta(x) f(x) = f(0), \quad (3.3.34)$$

for all test functions $f(x)$, *i.e.* smooth functions of compact support. The precise shape of this function will be irrelevant.

Due to the regularization of the Higgs profile the simple Dirichlet boundary conditions hold like in the case of a bulk Higgs boson

$$\begin{pmatrix} \mathbf{0} & \mathbf{1} \end{pmatrix} \mathcal{Q}_L^{(n)}(t) = \mathbf{0} = \begin{pmatrix} \mathbf{1} & \mathbf{0} \end{pmatrix} \mathcal{Q}_R^{(n)}(t) \quad \text{for } t = \{\epsilon, 1\}. \quad (3.3.35)$$

Within the bulk and away from the support of the Higgs profile, *i.e.*, for $t < 1 - \eta$, the general solutions [186, 195] to the EOMs (3.3.32) can be written as linear combinations of Bessel functions, which we discuss below in section 3.3.6. The appearance of the regularized Higgs profile $\delta^\eta(t - 1)$ as a source in (3.3.32) however renders the solutions for $t > 1 - \eta$, *i.e.* close to the brane, completely different. In the following we derive the solution for $\eta \ll 1$. In this case the Higgs profile source terms in the EOM (3.3.32) are dominant $\delta^\eta \sim 1/\eta$ and as a result the behavior of the profiles $\mathcal{C}_n^{Q,q}(\phi)$ and $\mathcal{S}_n^{Q,q}(\phi)$ become independent of the mass terms. Then, the integral version of the $1/\eta$ components of the EOM reads

$$\mathcal{Q}_\sigma^{(n)}(t) - \mathcal{Q}_\sigma^{(n)}(1) = (-1)^{\delta_{\sigma L}} \frac{v}{\sqrt{2}M_{\text{KK}}} \begin{pmatrix} \mathbf{0} & \mathbf{Y}_{\bar{q}} \\ \mathbf{Y}_q^\dagger & \mathbf{0} \end{pmatrix} \int_t^1 dt' \delta^\eta(t' - 1) \mathcal{Q}_\sigma^{(n)}(t'). \quad (3.3.36)$$

In order to solve (3.3.36), we first introduce the regularized Heaviside function

$$\bar{\theta}^\eta(x) \equiv 1 - \int_{-\infty}^x dy \delta^\eta(y), \quad (3.3.37)$$

which obeys $\partial_x \bar{\theta}^\eta(x) = -\delta^\eta(x)$ and has the values $\bar{\theta}^\eta(0) = 0$, and $\bar{\theta}^\eta(-\eta) = 1$. Using the latter properties it is readily shown that

$$\int_t^1 dt' \delta^\eta(t' - 1) \bar{\theta}^\eta(t' - 1)^n = \frac{1}{n+1} \bar{\theta}^\eta(t - 1)^{n+1}. \quad (3.3.38)$$

Thus for any arbitrary invertible matrix \mathbf{A} one has

$$\begin{aligned} \int_t^1 dt' \delta^\eta(t' - 1) \sinh(\bar{\theta}^\eta(t' - 1) \mathbf{A}) &= \left(\cosh(\bar{\theta}^\eta(t - 1) \mathbf{A}) - \mathbf{1} \right) \mathbf{A}^{-1}, \\ \int_t^1 dt' \delta^\eta(t' - 1) \cosh(\bar{\theta}^\eta(t' - 1) \mathbf{A}) &= \sinh(\bar{\theta}^\eta(t - 1) \mathbf{A}) \mathbf{A}^{-1}, \end{aligned} \quad (3.3.39)$$

where the hyperbolic sine and cosine are defined via their power expansions. These relations directly show the solution to the Peano-iteration of (3.3.36)

$$\begin{aligned} \mathcal{Q}_L^{(n)}(t) &= \sqrt{\frac{2\pi}{L\epsilon}} \begin{pmatrix} \cosh\left(\bar{\theta}^\eta(t-1) \frac{v}{\sqrt{2M_{\text{KK}}}} \sqrt{\mathbf{Y}_{\bar{q}}\mathbf{Y}_{\bar{q}}^\dagger}\right) \mathbf{C}_n^Q(1) \vec{a}_n^Q \\ -\mathbf{Y}_{\bar{q}}^\dagger \left(\sqrt{\mathbf{Y}_{\bar{q}}\mathbf{Y}_{\bar{q}}^\dagger}\right)^{-1} \sinh\left(\bar{\theta}^\eta(t-1) \frac{v}{\sqrt{2M_{\text{KK}}}} \sqrt{\mathbf{Y}_{\bar{q}}\mathbf{Y}_{\bar{q}}^\dagger}\right) \mathbf{C}_n^Q(1) \vec{a}_n^Q \end{pmatrix}, \\ \mathcal{Q}_R^{(n)}(t) &= \sqrt{\frac{2\pi}{L\epsilon}} \begin{pmatrix} \mathbf{Y}_{\bar{q}}^\dagger \left(\sqrt{\mathbf{Y}_{\bar{q}}\mathbf{Y}_{\bar{q}}^\dagger}\right)^{-1} \sinh\left(\bar{\theta}^\eta(t-1) \frac{v}{\sqrt{2M_{\text{KK}}}} \sqrt{\mathbf{Y}_{\bar{q}}\mathbf{Y}_{\bar{q}}^\dagger}\right) \mathbf{C}_n^q(1) \vec{a}_n^q \\ \cosh\left(\bar{\theta}^\eta(t-1) \frac{v}{\sqrt{2M_{\text{KK}}}} \sqrt{\mathbf{Y}_{\bar{q}}\mathbf{Y}_{\bar{q}}^\dagger}\right) \mathbf{C}_n^q(1) \vec{a}_n^q \end{pmatrix}. \end{aligned} \quad (3.3.40)$$

The six components of $\mathcal{Q}_L^{(n)}$ are both determined by the three boundary values $\mathbf{C}_n^Q(1) \vec{a}_n^Q$. This implies a relation between the components. In this sense (3.3.40) represents the regularized analoga to the IR BC for gauge bosons (3.3.18). In the latter case, we were able to directly work with the naive description of the δ -function. Here, we will see effectively a similar result. The correct treatment of the δ -function finally only amounts to a redefinition of the Yukawa matrix as far as the KK spectrum is concerned. This is seen as follows. The non-trivial connecting condition between the usual form of the solution and the one derived here is now located at $t = 1 - \eta$. At this point we evaluate (3.3.40) and eliminate the on-brane values $\mathbf{C}_n^{Q,q}(1)$. Introducing the rescaled Yukawa matrices

$$\tilde{\mathbf{Y}}_{\bar{q}} \equiv \tilde{\mathbf{X}}_{\bar{q}} \mathbf{X}_{\bar{q}}^{-1} \mathbf{Y}_{\bar{q}}, \quad \mathbf{X}_{\bar{q}} \equiv \frac{v}{\sqrt{2M_{\text{KK}}}} \sqrt{\mathbf{Y}_{\bar{q}}\mathbf{Y}_{\bar{q}}^\dagger}, \quad \tilde{\mathbf{X}}_{\bar{q}} = \tanh(\mathbf{X}_{\bar{q}}), \quad (3.3.41)$$

which coincide at leading order with the original ones, *i.e.* $\tilde{\mathbf{Y}}_{\bar{q}} = \mathbf{Y}_{\bar{q}} + \mathcal{O}(v^2/M_{\text{KK}}^2)$, we obtain the IR BCs

$$\left(\frac{v}{\sqrt{2M_{\text{KK}}}} \tilde{\mathbf{Y}}_{\bar{q}}^\dagger \quad \mathbf{1} \right) \mathcal{Q}_L^{(n)}(1 - \eta) = 0, \quad \left(\mathbf{1} \quad -\frac{v}{\sqrt{2M_{\text{KK}}}} \tilde{\mathbf{Y}}_{\bar{q}} \right) \mathcal{Q}_R^{(n)}(1 - \eta) = 0, \quad (3.3.42)$$

Hence, they take precisely the same form as in [1], with the original Yukawa couplings replaced by the rescaled ones as defined in (3.3.41). Since in practice the Yukawa matrices (together with the quark profiles) are chosen such that the zero-mode masses as well as the quark mixing angles match the ones determined by experiment, such a rescaling has no observable effect on the mass spectrum and the mixing pattern. However, as we will explain in more detail below, the inclusion of the Yukawa coupling involving Z_2 -odd fermions alters the form of the tree-level interactions of the Higgs boson with fermions.

Finally, the mass eigenvalues m_n follow from the solutions to the equation

$$\det \left(\mathbf{1} + \frac{v^2}{2M_{\text{KK}}^2} \tilde{\mathbf{Y}}_{\bar{q}} \mathbf{C}_n^q(\pi^-) [\mathbf{S}_n^q(\pi^-)]^{-1} \tilde{\mathbf{Y}}_{\bar{q}}^\dagger \mathbf{C}_n^Q(\pi^-) [\mathbf{S}_n^Q(\pi^-)]^{-1} \right) = 0. \quad (3.3.43)$$

Once they are known, the eigenvectors $\vec{a}_n^{Q,q}$ can be determined from (3.3.42). Note that, while it is always possible to work with real and diagonal profiles $\mathbf{C}_n^{Q,q}(\phi)$ and $\mathbf{S}_n^{Q,q}(\phi)$, the vectors $\vec{a}_n^{Q,q}$ are, in general, complex-valued objects.

3.3.5 Custodial Randall-Sundrum Model

3.3.5.1 Gauge-Boson Sector

As an extension to the discussion in 3.3.4.1, we also consider the RS model as proposed in [214, 215] with the custodial symmetry of the SM Higgs sector as a full bulk gauge symmetry $O(4) \times U(1)_X \sim SU(2)_L \times SU(2)_R \times U(1)_X \times P_{LR}$. The rationale for the left-right parity P_{LR} will be explained below when discussing fermions. However, we will allow for explicit sources of P_{LR} violation in the following and comment on them. The action reads

$$S_G = \int d^4x r \int_{-\pi}^{\pi} d\phi \left(\mathcal{L}_{L,R,X} + \mathcal{L}_H + \mathcal{L}_{GF} \right), \quad (3.3.44)$$

with the gauge-kinetic terms

$$\mathcal{L}_{L,R,X} = \frac{\sqrt{G}}{r} G^{KM} G^{LN} \left(-\frac{1}{4} L_{KL}^a L_{MN}^a - \frac{1}{4} R_{KL}^a R_{MN}^a - \frac{1}{4} X_{KL} X_{MN} \right). \quad (3.3.45)$$

The 5d gauge couplings are denoted by g_{L,R,X_5} . We furthermore define the dimensionless 4d gauge couplings as $g_a = g_{a5}/\sqrt{2\pi r}$. The choice of \mathbb{Z}_2 -parity, for vector and scalar fifth component are again even and odd respectively. The Higgs Lagrangian is given by

$$\mathcal{L}_H = \frac{\delta(|\phi| - \pi)}{r} \left(\frac{1}{2} \text{Tr} |(D_\mu \Phi^b)|^2 - V(\Phi^b) \right) \quad (3.3.46)$$

We employ the symmetry-breaking pattern $SU(2)_L \times SU(2)_R \rightarrow SU(2)_V$ to the diagonal subgroup by using a Higgs bidoublet in the real representation $(2, 2)_0$. This scheme provides a custodial symmetry, which protects the T parameter. Additionally P_{LR} symmetry prevents the left-handed $Zb\bar{b}$ coupling from receiving excessively large corrections [216]. On the UV brane, the symmetry breaking $SU(2)_R \times U(1)_X \rightarrow U(1)_Y$ is achieved by a mixture of UV and IR BCs. Remark that in contrast to left-right symmetric models that employ a breaking pattern to a diagonal $SU(2)$ subgroup [217–221], where this step is taken at a scale $u \gg v$ in addition to the usual Higgs mechanism, the breaking pattern here is fundamentally different. It rather resembles the pattern of composite Higgs models [222], *e.g.* the Little Higgs models discussed in section 3.2, where the Higgs sector \mathcal{L}_H is SM-like, the only difference being the gauged custodial symmetry. In particular the same number of degrees of freedom are used by rewriting the complex representation $\Phi \sim (1, 2)_{Y=1/2}$, used by the SM Higgs mechanism, to a real bifundamental $\Phi^b = (\Phi^c, \Phi) \sim (2, 2)_0$ with approximately¹⁴ the same diagonal VEV $\langle \Phi^b \rangle = v/\sqrt{2} \mathbf{1}$. Accordingly, $SU(2)_L$ transformations act from the left on the bidoublet, while the $SU(2)_R$ transformations act from the right. Using $T_{L,R}^i = \sigma^i/2$, the covariant derivative in the Higgs sector reads

$$\begin{aligned} D_\mu \Phi^b &= \partial_\mu \Phi^b - ig_{L5} L_\mu^i T_L^i \Phi^b + ig_{R5} \Phi^b R_\mu^i T_R^i \\ &= \frac{1}{\sqrt{2}} \begin{pmatrix} \partial_\mu (h - i\varphi^3) - i\frac{v}{2}(g_{L5} L_\mu^3 - g_{R5} R_\mu^3) & -\partial_\mu i\sqrt{2}\varphi^+ - i\frac{v}{2}(g_{L5} L_\mu^+ - g_{R5} R_\mu^+) \\ -\partial_\mu i\sqrt{2}\varphi^- - i\frac{v}{2}(g_{L5} L_\mu^- - g_{R5} R_\mu^-) & \partial_\mu (h + i\varphi^3) + i\frac{v}{2}(g_{L5} L_\mu^3 - g_{R5} R_\mu^3) \end{pmatrix} \\ &\quad + \text{terms bilinear in fields,} \end{aligned} \quad (3.3.47)$$

¹⁴We will see below that a tree-level contribution to the W -mass slightly shifts the VEV.

The structure of (3.3.47) shows that the mass matrix is diagonalized by defining the new fields [223]

$$\begin{pmatrix} \tilde{A}_M^i \\ V_M^i \end{pmatrix} = \begin{pmatrix} c_W & -s_W \\ s_W & c_W \end{pmatrix} \begin{pmatrix} R_M^i \\ L_M^i \end{pmatrix} \equiv \mathbf{R}_W \begin{pmatrix} R_M^i \\ L_M^i \end{pmatrix}, \quad t_W = \frac{g_R}{g_L}. \quad (3.3.48)$$

Afterwards, the 5d mass term adopts the form

$$\mathcal{L}_{G,\text{mass}} = \frac{\delta(|\phi| - \pi)}{r} \frac{(g_{L5}^2 + g_{R5}^2) v^2}{8} \tilde{A}_\mu^i \tilde{A}^{\mu i} \equiv \frac{\delta(|\phi| - \pi)}{r} \frac{1}{2} M_{A5}^2 \tilde{A}_\mu^i \tilde{A}^{\mu i}. \quad (3.3.49)$$

This explicitly shows the IR brane induced breaking pattern $SU(2)_L \times SU(2)_R \rightarrow SU(2)_V$. The mixing angle θ_W introduced in (3.3.48) is the only rotation we need in the 5d charged sector. The zero mode of the coupled system $\vec{W}_M^\pm = (\tilde{A}_M^\pm, V_M^\pm)^T$ will resemble the SM-like W^\pm . The rotations in the neutral sector are more intricate as we discuss in the following.

We mentioned above that appropriate BCs on the UV brane break the extended electroweak gauge group down to the SM gauge group $SU(2)_R \times U(1)_X \rightarrow U(1)_Y$. Explicitly, this is done as follows. We introduce the new fields

$$\begin{pmatrix} B_M \\ Z'_M \end{pmatrix} = \frac{1}{\sqrt{g_R^2 + g_X^2}} \begin{pmatrix} g_R & g_X \\ -g_X & g_R \end{pmatrix} \begin{pmatrix} X_M \\ R_M^3 \end{pmatrix}, \quad (3.3.50)$$

and give Dirichlet BCs to Z'_μ and $R_\mu^{1,2}$ on the UV brane. The SM-like neutral electroweak gauge bosons are defined in the standard way with the $U(1)_Y$ hypercharge coupling given by $g_Y^{-2} = g_R^{-2} + g_X^{-2}$, such that

$$\begin{pmatrix} A_M \\ Z_M \end{pmatrix} = \begin{pmatrix} c_w & s_w \\ -s_w & c_w \end{pmatrix} \begin{pmatrix} B_M \\ L_M^3 \end{pmatrix}, \quad t_w = \frac{g_Y}{g_L}, \quad (3.3.51)$$

and we give Neumann BCs to Z_μ , A_μ and $L_\mu^{1,2}$ on the UV brane. The different choice of BCs explicitly breaks the mentioned symmetry and makes the necessity of Scherk-Schwarz twisted KK modes apparent.

Finally, the fields V_M^3 and X_M can be rotated to the photon field A_M and a state Z_M^H via

$$\begin{pmatrix} A_M \\ Z_M^H \end{pmatrix} = \frac{1}{g_{LRX}^2} \begin{pmatrix} g_L g_R & g_X \sqrt{g_L^2 + g_R^2} \\ -g_X \sqrt{g_L^2 + g_R^2} & g_L g_R \end{pmatrix} \begin{pmatrix} X_M \\ V_M^3 \end{pmatrix}, \quad (3.3.52)$$

where $g_{LRX}^4 = g_L^2 g_R^2 + g_L^2 g_X^2 + g_R^2 g_X^2$. We also write $\tilde{Z}_M \equiv \tilde{A}_M^3$, as it is already the correct linear combination of Z_M and Z'_M , which is orthogonal to Z_M^H . The necessary rotation in the 5d neutral sector for the Z boson is in summary given by

$$\begin{pmatrix} \tilde{Z}_M \\ Z_M^H \end{pmatrix} = \begin{pmatrix} c_Z & -s_Z \\ s_Z & c_Z \end{pmatrix} \begin{pmatrix} Z_M \\ Z'_M \end{pmatrix} \equiv \mathbf{R}_Z \begin{pmatrix} Z_M \\ Z'_M \end{pmatrix}, \quad t_Z = \frac{g_R^2}{g_{LRX}^2}. \quad (3.3.53)$$

The zero mode of the coupled system $\vec{Z}_M = (\tilde{Z}_M, Z_M^H)^T$ will resemble the SM-like Z . Remark that the three introduced angles c_w, c_W, c_Z parametrize the weak mixing angle defined by the usual rotation of the $U(1)_Y$ in the $U(1)_{\text{em}}$ boson, the relative size of the two $SU(2)$ gauge couplings comparable to what is usually called c_β in multi-Higgs doublet models and *e.g.* the left-right-symmetric model, and the third angle is dependent, $c_Z^2 = c_W^2/c_w^2$.

$SU(2)_R \times U(1)_X \rightarrow U(1)_Y$	$SU(2)_L \times SU(2)_R \rightarrow SU(2)_V$
$\partial_\phi L_\mu^\pm(x, 0) = 0$	$\partial_\phi \tilde{A}_\mu^\pm(x, \pi^-) = -\frac{r}{2\epsilon^2} M_{\tilde{A}5}^2 \tilde{A}_\mu^\pm(x, \pi)$
$R_\mu^\pm(x, 0) = 0$	$\partial_\phi V_\mu^\pm(x, \pi) = 0$
$\partial_\phi Z_\mu(x, 0) = 0$	$\partial_\phi \tilde{Z}_\mu(x, \pi^-) = -\frac{r}{2\epsilon^2} M_{\tilde{A}5}^2 \tilde{Z}_\mu(x, \pi)$
$Z'_\mu(x, 0) = 0$	$\partial_\phi Z_\mu^H(x, \pi) = 0$
$\partial_\phi A_\mu(x, 0) = 0$	$\partial_\phi A_\mu(x, \pi) = 0$

Table 3.3: UV and IR BCs in the gauge sector of the custodial RS model.

In table 3.3 we summarize the BCs at the two different branes that we choose for the fields in order to obtain the correct mass spectrum for the SM gauge bosons. We refer to these sets of fields as the UV and IR basis, respectively. The BCs can easily be transformed between these two bases with the matrices $\mathbf{R}_{W,Z}$ at the expense of obtaining expressions that mix different fields. Remark that enforcing the P_{LR} symmetry uniquely determines these rotations with $c_W = 1/\sqrt{2}$ and $c_Z = 1/(\sqrt{2}c_w)$. The photon A_μ has individual and source-free Neumann BCs at both branes, and therefore its zero mode remains massless. Note that there is just one mass parameter $M_{\tilde{A}}$ entering the IR BCs, in contrast to the two parameters M_Z and M_W appearing in the minimal model. This is crucial for the custodial protection of the T parameter. The different masses for the lightest electroweak gauge bosons are here accomplished through the mixed UV BCs of the gauge fields in the IR basis. As the Higgs sector is localized on the IR brane, it is natural to work in the IR basis for that purpose.

The action of the theory still contains mixing terms between gauge fields and scalars, which can be removed by an appropriate gauge-fixing Lagrangian. It turns out that

$$\begin{aligned}
 \mathcal{L}_{\text{GF}} = & -\frac{1}{2\xi} \left(\partial^\mu A_\mu - \xi \left[\frac{\partial_\phi e^{-2\sigma(\phi)}}{r^2} A_\phi \right] \right)^2 \\
 & - \frac{1}{2\xi} \left(\partial^\mu \tilde{Z}_\mu - \xi \left[\frac{\delta(|\phi| - \pi)}{r} M_{\tilde{A}5} \tilde{\varphi}^3 + \frac{\partial_\phi e^{-2\sigma(\phi)}}{r^2} \tilde{Z}_\phi \right] \right)^2 \\
 & - \frac{1}{\xi} \left(\partial^\mu \vec{W}_\mu^+ - \xi \left[\frac{\delta(|\phi| - \pi)}{r} M_{\tilde{A}5} \tilde{\varphi}^+ + \frac{\partial_\phi e^{-2\sigma(\phi)}}{r^2} \vec{W}_\phi^+ \right] \right)^T \\
 & \times \left(\partial^\mu \vec{W}_\mu^- - \xi \left[\frac{\delta(|\phi| - \pi)}{r} M_{\tilde{A}5} \tilde{\varphi}^- + \frac{\partial_\phi e^{-2\sigma(\phi)}}{r^2} \vec{W}_\phi^- \right] \right), \tag{3.3.54}
 \end{aligned}$$

is an appropriate choice.

To perform the KK decomposition of the 5d fields, it is convenient to work with profiles that obey definite Neumann (+) or Dirichlet (-) BCs at the UV brane, and parametrize the mixing between the components of $\vec{W}_M^\pm(x, \phi)$ and $\vec{Z}_M(x, \phi)$ that is induced by the IR BCs. Both advantages are elegantly combined by writing the KK decomposition as

$$\vec{V}_\mu(x, \phi) = \frac{\mathbf{R}_V}{\sqrt{r}} \sum_n \chi_{V,n}^+(x) \vec{A}_n^V V_\mu^{(n)}(x), \quad \vec{V}_\phi(x, \phi) = \frac{\mathbf{R}_V}{\sqrt{r}} \sum_n \partial_\phi \chi_{V,n}^+(x) \vec{A}_n^V a_n^V \varphi_V^{(n)}(x), \tag{3.3.55}$$

where $V = Z, W^\pm, A$. In fact, the decomposition of the photon A is the same as in (3.3.15) and we account for this by setting $\mathbf{R}_A = \mathbf{1}$ and $\vec{A}_n^A = (1, 0)^T$. Note that $V_\mu^{(n)}(x)$ are 4d mass

eigenstates and the lightest, zero modes are identified with the SM gauge bosons just like in the structurally simpler decomposition of the minimal model (3.3.15). Mixing between the KK modes of $V = W^\pm, Z$ is encoded in the two-component vectors \vec{A}_n^V , which are normalized according to $(\vec{A}_n^a)^T \vec{A}_n^a = 1$. Furthermore, we have introduced the diagonal matrix

$$\chi_{V,n}^+(\phi) = \begin{pmatrix} \chi_{V,n}^{(+)}(\phi) & 0 \\ 0 & \chi_{V,n}^{(-)}(\phi) \end{pmatrix}, \quad (3.3.56)$$

The superscripts (+) and (−) label the type of BC we impose on the profiles at the UV brane. Remind from table 3.3 that both profiles satisfy an even BC at the IR brane, which we do not indicate explicitly to simplify the notation. The superscript therefore also indicates Scherk-Schwarz untwisted and twisted even functions. We also introduce the shorthand notations

$$\vec{\chi}_n^V(\phi) = (\chi_{V,n}^L(\phi), \chi_{V,n}^R(\phi))^T = \chi_{V,n}^+(\phi) \vec{A}_n^V, \quad (3.3.57)$$

The profiles $\chi_{V,n}^+(\phi)$ do not separately obey orthonormality conditions. This fact is related to the decomposition of fields with Neumann and Dirichlet BCs into the same 4d gauge-boson basis and the implied mixing. This is analogous to the fermion decomposition of the minimal model discussed above. It is only the complete vectors $\vec{\chi}_n^V(\phi)$ that are orthonormal and complete,

$$\int_{-\pi}^{\pi} d\phi \vec{\chi}_m^V(\phi)^T \vec{\chi}_n^V(\phi) = \delta_{mn}, \quad (3.3.58)$$

$$\sum_n \vec{\chi}_n^V(\phi) \vec{\chi}_n^V(\phi')^T = \frac{1}{2} \left(\delta(\phi - \phi') + \delta(\phi + \phi') \right) \mathbf{1}. \quad (3.3.59)$$

Note that the photon still obeys a standard orthonormality condition. To associate a scalar Goldstone mode with each KK level, again we expand the 5d Goldstone bosons in the basis of 4d mass eigenstates $\varphi_V^{(n)}(x)$ by [4]

$$\vec{\varphi}^3(x) = \sum_n \vec{b}_n^Z \varphi_Z^{(n)}(x), \quad \vec{\varphi}^\pm(x) = \sum_n \vec{b}_n^W \varphi_W^{\pm(n)}(x). \quad (3.3.60)$$

We insert the decomposition (3.3.55) into the action (3.3.44) and derive the following EOMs [1, 185, 193] for the two component vectors of (3.3.57)

$$-\frac{1}{r^2} \partial_\phi e^{-2\sigma(\phi)} \mathbf{R}_V \partial_\phi \vec{\chi}_n^V(\phi) = (m_n^V)^2 \mathbf{R}_V \vec{\chi}_n^V(\phi) - \frac{\delta(|\phi| - \pi)}{r} M_{V5}^2 \mathbf{P}_{(+)} \mathbf{R}_V \vec{\chi}_n^V(\phi), \quad (3.3.61)$$

where $V = Z, W, A$ the 5d masses are $M_{Z5} = M_{W5} = M_{A5}$, $M_{A5} = 0$, and we defined the projectors $\mathbf{P}_{(+)} = \text{diag}(1, 0)$ and $\mathbf{P}_{(-)} = \text{diag}(0, 1)$. After an integration of (3.3.61) an infinitesimal region around the IR brane we obtain as the generalization of (3.3.18) the condition

$$\frac{m_n^V}{M_{\text{KK}}} \mathbf{R}_V \chi_{V,n}^-(\pi^-) \vec{A}_n^V = -X^2 L \mathbf{P}_{(+)} \mathbf{R}_V \chi_{V,n}^+(\pi) \vec{A}_n^V, \quad (3.3.62)$$

where

$$\chi_{V,n}^-(\phi) \equiv \frac{1}{m_n^V r} e^{-\sigma(\phi)} \partial_\phi \chi_{V,n}^+(\phi), \quad X^2 \equiv \frac{(g_L^2 + g_R^2) v^2}{4M_{\text{KK}}^2}. \quad (3.3.63)$$

Notice that for the photon the right-hand side in (3.3.62) is equal to zero.

After applying the EOMs and the orthonormality condition, we observe that the 4d action takes the desired canonical form, if and only if

$$a_n^V = -\frac{1}{m_n^V}, \quad \vec{b}_n^V = \frac{M_{V5}}{\sqrt{r} m_n^V} \mathbf{P}_{(+)} \mathbf{R}_V \vec{\chi}_n^V(\pi^-). \quad (3.3.64)$$

The spectrum of the theory is determined by the IR BCs (3.3.62). Therefore, the numerical determination of the eigenvalues $x_n^V \equiv m_n^V/M_{\text{KK}}$ is done by finding the solutions to the characteristic equation

$$\det \left[x_n^V \chi_{V,n}^-(\pi^-) + L X^2 \mathbf{D}_V \chi_{V,n}^+(\pi) \right] = 0, \quad (3.3.65)$$

$$\mathbf{D}_V \equiv \mathbf{R}_V^{-1} \mathbf{P}_{(+)} \mathbf{R}_V = \begin{pmatrix} c_V^2 & -s_V c_V \\ -s_V c_V & s_V^2 \end{pmatrix}.$$

Once the eigenvalues are known, the eigenvectors \vec{A}_n^V are determined by (3.3.62).

3.3.5.2 Fermion Sector

The extended RS model shall also implement a custodial protection of the $Z b_L \bar{b}_L$ vertex [216] to comply with precision constraints from Z -pole observables in addition to the constraints from the oblique T -parameter (see section 4.2.2). The fermion embedding shall therefore adhere to a discrete P_{LR} symmetry that interchanges the two $SU(2)$ groups and the left-handed bottom quark has to be part of a $SU(2)_L \times SU(2)_R$ bidoublet with isospin quantum numbers¹⁵ $T_L^3 = -T_R^3 = -1/2$. This fixes the quantum numbers of the other fields and implies the following, most economical multiplet structure for the quark fields with even \mathbb{Z}_2 -parity:

$$Q_L \equiv \begin{pmatrix} u_L^{(+)\frac{2}{3}} & \lambda_L^{(-)\frac{5}{3}} \\ d_L^{(+)\frac{2}{3}} & u_L'^{-}\frac{2}{3} \end{pmatrix}_{\frac{2}{3}}, \quad u_R^c \equiv \left(u_R^{c(+)\frac{2}{3}} \right)_{\frac{2}{3}},$$

$$\mathcal{T}_R \equiv \mathcal{T}_{1R} \oplus \mathcal{T}_{2R} \equiv \begin{pmatrix} \Lambda_R'^{-}\frac{5}{3} \\ U_R'^{-}\frac{2}{3} \\ D_R'^{-}\frac{2}{3} \end{pmatrix}_{\frac{2}{3}} \oplus \left(D_R^{(+)\frac{2}{3}} U_R^{(-)\frac{2}{3}} \Lambda_R^{(-)\frac{5}{3}} \right)_{\frac{2}{3}}. \quad (3.3.66)$$

Again the superscript $(-)$ denotes a Scherk-Schwarz twist. The inner and outer subscripts correspond to the electromagnetic and $U(1)_X$ charges, respectively, which are connected through the relations $Y = -T_R^3 + Q_X$ and $Q = T_L^3 + Y$. In addition to (3.3.66), we have a second set of multiplets, belonging to the components of opposite chirality. The corresponding states have opposite BCs. In particular, they all obey Dirichlet BCs at the IR brane. The $SU(2)_{L,R}$ transformations act vertically and horizontally on the multiplets. We summarize the quantum numbers of the quark fields in table 3.4. Note that we have chosen the same $SU(2)_L \times SU(2)_R$ representations for all three generations, which is necessary if one wants to consistently incorporate quark mixing in the fully anarchic approach to flavor in warped extra dimensions. The

¹⁵Remark that we have adapted the sign convention of [4] for T_R^3 . Compared with typical conventions in the LR symmetric model the sign is reversed.

3. THEORETICAL CLASSIFICATION & EXAMPLES OF NEW PHYSICS

	$u_L^{(+)}$	$d_L^{(+)}$	$\lambda_L^{(-)}$	$u_L'^{-}$	$u_R^c^{(+)}$	$\Lambda_R'^{-}$	$U_R'^{-}$	$D_R'^{-}$	$D_R^{(+)}$	U_R^{-}	$\Lambda_R^{(-)}$
Q	2/3	-1/3	5/3	2/3	2/3	5/3	2/3	-1/3	-1/3	2/3	5/3
Q_X	2/3	2/3	2/3	2/3	2/3	2/3	2/3	2/3	2/3	2/3	2/3
Y	1/6	1/6	7/6	7/6	2/3	2/3	2/3	2/3	-1/3	2/3	5/3
T_L^3	1/2	-1/2	1/2	-1/2	0	1	0	-1	0	0	0
T_R^3	1/2	1/2	-1/2	-1/2	0	0	0	0	1	0	-1

Table 3.4: Charge assignments of the quark fields in the custodial RS model.

chosen representations also play a crucial role in the suppression of flavor-changing left-handed Z -boson couplings which we discuss in section 4.1.2.

Altogether we obtain 15 different quark fields in the up-type and nine in the down-type sector. Due to the BCs, there will be three light modes in each sector to be identified with the SM quarks. These are accompanied by KK towers which consist of groups of 15 and nine modes of similar masses in the up- and down-type quark sector, respectively. Moreover the embedding implies interesting exotic fermion fields of electric charge $5/3$, which exhibits nine excitations with small mass splitting in each level.

A comment on the uniqueness of the given embedding is in order. The right-handed quarks have to be embedded in $SU(2)_R$ triplets or singlets in order to arrive at a $U(1)_X$ -invariant Yukawa coupling. The $U(1)_X$ -charge of the bidoublet implies the triplet for the down-type quarks, whereas up-type quarks can be embedded in a singlet or triplet. Since the latter choice implies also another $SU(2)_L$ triplet like in the down sector we restrict our discussion to the more economical choice of a singlet.

The given setup of fermions can be embedded into $SO(5) \times U(1)_X$ multiplets if P_{LR} is exact in the gauge sector, too. The given representation can arise from a $5 \sim (2, 2) \oplus (1, 1)$ and from a $10 \sim (2, 2) \oplus (3, 1) \oplus (1, 3)$ of $SO(5) \otimes U(1)_X$ in various possible combinations [224]. Therefore, the given representation is suitable for comparison with models of gauge-Higgs unification, where a bulk Higgs boson can arise from the scalar fifth component of gauge fields in $SO(5)/(SU(2)_L \times SU(2)_R)$.

The only structurally new ingredient of the fermionic action, compared to the minimal RS Lagrangian, are the Yukawa couplings between the bidoublet and the singlet or triplet, respectively. To denote the Lagrangian, it is most convenient to write the $SU(2)_L$ triplet components in the basis of Pauli-matrices

$$\mathcal{T}_1 = \begin{pmatrix} \frac{1}{\sqrt{2}} U'^{-} \frac{2}{3} & \Lambda'^{-} \frac{5}{3} \\ D'^{-} \frac{-1}{3} & \frac{1}{\sqrt{2}} U'^{-} \frac{2}{3} \end{pmatrix} = \frac{\sigma_3}{\sqrt{2}} U'^{-} \frac{2}{3} + \sigma_- D'^{-} \frac{-1}{3} + \sigma_+ \Lambda'^{-} \frac{5}{3}, \quad (3.3.67)$$

and analogous for the $SU(2)_R$ triplet \mathcal{T}_2 with the unprimed component fields $\Lambda^{(-)} \frac{5}{3}$, $U^{(-)} \frac{2}{3}$, and $D^{(+)} \frac{-1}{3}$. The possible gauge-invariant Yukawa couplings are found to be [225].

$$S_{\text{yuk}} = - \int d^4x r \int_{-\pi}^{\pi} d\phi \delta(|\phi| - \pi) \frac{e^{-3\sigma(\phi)}}{r} \text{Tr} \left[\Phi^b (\bar{Q}_L \mathbf{Y}_u^{(5d)} u_R^c + \bar{Q}_R \mathbf{Y}_{ou}^{(5d)} u_L^{cj})^T \right. \\ \left. + \frac{1}{\sqrt{2}} (\bar{Q}_L^i)^T \mathbf{Y}_d^{(5d)} (\mathcal{T}_{1R} \Phi^b + \Phi^b \mathcal{T}_{2R}) + \frac{1}{\sqrt{2}} (\bar{Q}_R^i)^T \mathbf{Y}_{od}^{(5d)} (\mathcal{T}_{1L} \Phi^b + \Phi^b \mathcal{T}_{2L}) \right]. \quad (3.3.68)$$

Like for the minimal RS model, we will choose the brane-localized Higgs sector as the limit of a bulk Higgs boson, which forces the Yukawa matrix for the coupling of both chirality structures to be equal $\mathbf{Y}_{oq}^{(5d)} = \mathbf{Y}_q^{(5d)}$. A generalization to different Yukawa matrices, which would in general be allowed for a perfectly brane-localized Higgs boson, is straightforward.

Like for gauge bosons, we will later directly decompose into the KK basis of 4d mass eigenstates for the quark fields. After electroweak symmetry breaking, the Yukawa couplings (3.3.68) give rise to mass terms which mix different 5d fields with the same electromagnetic charge. Therefore, it is possible and reasonable to cast the bilinear part of the fermion action in the generic form introduced already for the minimal RS model (3.3.23). The vectors of fermions, which were trivial in the latter case, now contain fields of same charge and chirality for even parity, and the sums over quark fields in (3.3.23) now also extend over the exotic fermions Λ, λ . The corresponding vectors, mass, and Yukawa matrices are given by

$$\begin{aligned} \vec{U} &\equiv \begin{pmatrix} u \\ u' \end{pmatrix}, & \vec{D} &\equiv d, & \vec{\Lambda} &\equiv \lambda, & \mathbf{M}_{\vec{U}} &\equiv \begin{pmatrix} \mathbf{M}_Q & 0 \\ 0 & \mathbf{M}_Q \end{pmatrix}, & \mathbf{M}_{\vec{D}} &= \mathbf{M}_{\vec{\Lambda}} \equiv \mathbf{M}_Q, \\ \vec{u} &\equiv \begin{pmatrix} u^c \\ U' \\ U \end{pmatrix}, & \vec{d} &\equiv \begin{pmatrix} D \\ D' \end{pmatrix}, & \vec{\lambda} &\equiv \begin{pmatrix} \Lambda' \\ \Lambda \end{pmatrix}, & \mathbf{M}_{\vec{u}} &\equiv \begin{pmatrix} \mathbf{M}_{u^c} & 0 & 0 \\ 0 & \mathbf{M}_{\mathcal{T}_1} & 0 \\ 0 & 0 & \mathbf{M}_{\mathcal{T}_2} \end{pmatrix}, \\ & & & & & & \mathbf{M}_{\vec{d}} &\equiv \begin{pmatrix} \mathbf{M}_{\mathcal{T}_2} & 0 \\ 0 & \mathbf{M}_{\mathcal{T}_1} \end{pmatrix}, & \mathbf{M}_{\vec{\lambda}} &\equiv \begin{pmatrix} \mathbf{M}_{\mathcal{T}_1} & 0 \\ 0 & \mathbf{M}_{\mathcal{T}_2} \end{pmatrix}, \\ \mathbf{Y}_{\vec{u}} &\equiv \begin{pmatrix} \mathbf{Y}_u & \frac{1}{\sqrt{2}}\mathbf{Y}_d & \frac{1}{\sqrt{2}}\mathbf{Y}_d \\ \mathbf{Y}_u & -\frac{1}{\sqrt{2}}\mathbf{Y}_d & -\frac{1}{\sqrt{2}}\mathbf{Y}_d \end{pmatrix}, & \mathbf{Y}_{\vec{d}} &= \mathbf{Y}_{\vec{\lambda}} \equiv (\mathbf{Y}_d \quad \mathbf{Y}_d). \end{aligned} \quad (3.3.69)$$

where \mathbf{M}_A are the 3×3 bulk-mass matrices of the corresponding multiplets $A = Q, u^c, \mathcal{T}_1, \mathcal{T}_2$ and we have defined the dimensionless order one Yukawa matrices like in section 3.3.4.2.

Also the KK decomposition works with the generic formulas presented in section 3.3.4.2. The derivation of the form of profiles close to the IR brane (3.3.40), and consequently the IR BCs (3.3.42), did not rely on the UV BC and thus holds for both types. The vectors $\mathcal{Q}_{L,R}^{(n)}(t)$ have to be built by using the following form of the generalized profile matrices

$$\begin{aligned} \mathbf{C}_n^U &\equiv \text{diag}(\mathbf{C}_n^{Q(+)}, \mathbf{C}_n^{Q(-)}), & \mathbf{C}_n^u &\equiv \text{diag}(\mathbf{C}_n^{u^c(+)}, \mathbf{C}_n^{\mathcal{T}_1(-)}, \mathbf{C}_n^{\mathcal{T}_2(-)}), \\ \mathbf{C}_n^D &\equiv \mathbf{C}_n^{Q(+)}, & \mathbf{C}_n^d &\equiv \text{diag}(\mathbf{C}_n^{\mathcal{T}_2(+)}, \mathbf{C}_n^{\mathcal{T}_1(-)}), \\ \mathbf{C}_n^\Lambda &\equiv \mathbf{C}_n^{Q(-)}, & \mathbf{C}_n^\lambda &\equiv \text{diag}(\mathbf{C}_n^{\mathcal{T}_1(-)}, \mathbf{C}_n^{\mathcal{T}_2(-)}), \end{aligned} \quad (3.3.70)$$

the same relation for $\mathbf{C} \rightarrow \mathbf{S}$, and the decomposition vectors

$$\vec{a}_n^U \equiv \begin{pmatrix} a_n^u \\ a_n^{u'} \\ a_n^U \end{pmatrix}, \quad \vec{a}_n^u \equiv \begin{pmatrix} a_n^{u^c} \\ a_n^{U'} \\ a_n^U \end{pmatrix}, \quad \vec{a}_n^D \equiv a_n^d, \quad \vec{a}_n^d \equiv \begin{pmatrix} a_n^D \\ a_n^{D'} \end{pmatrix}, \quad \vec{a}_n^\Lambda \equiv a_n^\lambda, \quad \vec{a}_n^\lambda \equiv \begin{pmatrix} a_n^{\Lambda'} \\ a_n^\Lambda \end{pmatrix}. \quad (3.3.71)$$

In order to derive the fermion couplings to gauge bosons below, we need the form of the covariant derivative determined by the fermionic representations. While this is a straightforward generalization of the SM in the case of the minimal model, the custodial embedding

might be unfamiliar to the reader. In the UV basis of gauge bosons, we have

$$D_\mu = \partial_\mu - i \sum_{V=L,R; s=\pm} \frac{g_{V5}}{\sqrt{2}} V_\mu^s T_V^s - i \sum_{V=Z,Z'} g_{V5} Q_V V_\mu - i e_5 Q A_\mu. \quad (3.3.72)$$

With Z couplings and charges defined by

$$\begin{aligned} g_Z &= \sqrt{g_L^2 + g_Y^2}, & g_{Z'} &= \sqrt{g_R^2 + g_X^2}, \\ Q_Z &= T_L^3 - \frac{g_Y}{g_Z} Q, & Q_{Z'} &= -T_R^3 - \frac{g_X}{g_{Z'}} Y. \end{aligned} \quad (3.3.73)$$

As usual, we define the generators $T_{L,R}^\pm = T_{L,R}^1 \pm i T_{L,R}^2$ and $T_{L,R}^i$ are given by the 1/2 times Pauli matrices in standard convention times when acting on bidoublets

$$T_{L,R}^+ = \begin{pmatrix} 0 & \sqrt{2} & 0 \\ 0 & 0 & \sqrt{2} \\ 0 & 0 & 0 \end{pmatrix}, \quad T_{L,R}^- = (T_{L,R}^+)^\dagger, \quad T_{L,R}^3 = \text{diag}(1, 0, -1) \quad (3.3.74)$$

The traces over gauge group indices in the fermion kinetic term *e.g.* lead to the following charged currents coupling to (L_μ^\pm, R_μ^\pm)

$$\vec{J}_{W_Q}^{\mu\pm} = \frac{1}{\sqrt{2}} \begin{pmatrix} g_L \text{Tr} [\bar{Q} \gamma^\mu T^\pm Q] \\ g_R \text{Tr} [\bar{Q} \gamma^\mu Q T^\pm] \end{pmatrix}, \quad \vec{J}_{W_\tau}^{\mu\pm} = \frac{1}{\sqrt{2}} \begin{pmatrix} g_L \bar{\mathcal{T}}_1 \gamma^\mu T^\pm \mathcal{T}_1 \\ g_R \text{Tr} [\bar{\mathcal{T}}_2 \gamma^\mu \mathcal{T}_2 T^\pm] \end{pmatrix}. \quad (3.3.75)$$

3.3.6 Bulk Profiles and Zero-Mode Spectrum

We start with the explicit form of the bulk gauge profiles $\chi_{V,n}^{(+)}(t)$. Here, we use the dimensionless parameter $t = \epsilon e^{-kr\phi}$ as introduced at the end of section 3.3.2. The explicit form of the profiles χ_n was first obtained in [185, 193] for the case of an unbroken gauge symmetry. Rewriting the profile functions that fulfill Neumann (+) and Dirichlet (-) IR BCs in the form

$$\chi_{V,n}^{(\pm)}(t) = N_n^{(\pm)} \sqrt{\frac{L}{\pi}} t c_n^{(\pm)+}(t), \quad (3.3.76)$$

it is directly seen that the EOMs (3.3.17) and (3.3.61) have the form of ordinary Bessel differential equations of order 1 inside the bulk $t \in (\epsilon, 1)$. For brevity, we skip the index V in the following expressions. The UV boundary conditions dictate the form of $c_n^{(\pm)+}(t)$ as

$$\begin{aligned} c_n^{(+)+}(t) &= Y_0(x_n \epsilon) J_1(x_n t) - J_0(x_n \epsilon) Y_1(x_n t), \\ c_n^{(-)+}(t) &= Y_1(x_n \epsilon) J_1(x_n t) - J_1(x_n \epsilon) Y_1(x_n t). \end{aligned} \quad (3.3.77)$$

We furthermore define the following derivatives

$$\begin{aligned} c_n^{(+)-}(t) &= \frac{1}{x_n t} \frac{d}{dt} (t c_n^{(+)+}(t)) = Y_0(x_n \epsilon) J_0(x_n t) - J_0(x_n \epsilon) Y_0(x_n t), \\ c_n^{(-)-}(t) &= \frac{1}{x_n t} \frac{d}{dt} (t c_n^{(-)+}(t)) = Y_1(x_n \epsilon) J_0(x_n t) - J_1(x_n \epsilon) Y_0(x_n t). \end{aligned} \quad (3.3.78)$$

The masses of the KK states normalized to the KK scale x_n are determined by the IR BCs as explained above. The normalization constants $N_n^{(\pm)}$ are determined from the orthonormality condition

$$(N_n^{(\pm)})^{-2} = c_n^{(\pm)+}(1)^2 + c_n^{(\pm)-}(1^-)^2 - \frac{2}{x_n} \left(c_n^{(\pm)+}(1) c_n^{(\pm)-}(1^-) - \epsilon c_n^{(\pm)+}(\epsilon) c_n^{(\pm)-}(\epsilon^+) \right) - \epsilon^2 \left(c_n^{(\pm)+}(\epsilon)^2 + c_n^{(\pm)-}(\epsilon^+)^2 \right). \quad (3.3.79)$$

This formula contains terms due to the different UV BCs. Depending on the type of the UV BCs, some of the terms in (3.3.79) vanish identically since $c_n^{(+)-}(\epsilon) = c_n^{(-)+}(\epsilon) = 0$.

Remark that for the photon and gluon that do not participate in electroweak symmetry breaking the EOM is remarkably simpler and reads $N_n^{(+)} c_n^{(+)-}(1) = 0$. In this case the spectrum contains a massless zero mode, which has a flat profile $\chi_0^{(+)}(t) = 1/\sqrt{2\pi}$. Since $Y_0(x_n\epsilon) \gg J_0(x_n\epsilon)$ the higher KK modes correspond to a good approximation to zeros of the Bessel function J_0 . This implies $x_1 \approx 2.45$ and subsequent modes in approximately equidistant spacings of π . The latter is in fact also true for all other bosons and fermions in the limit of large n .

The flatness of the profile of the photon and gluon have to be kept in mind for the calculation of couplings to bulk fermions. Using an orthonormality condition for the fermions, we will see that this implies exactly the form of couplings as in the SM.

It is useful for the following discussion to have expressions for the massive zero-modes profiles of the W and Z expanded in $x_0^2 \sim v^2/M_{\text{KK}}^2$

$$\begin{aligned} \chi_0^{(+)}(t) &= \frac{1}{\sqrt{2\pi}} \left[1 + \frac{x_0^2}{4} \left(1 - \frac{1}{L} + t^2 (1 - 2L - 2 \ln t) \right) + \mathcal{O}(x_0^4) \right], \\ \chi_0^{(-)}(t) &= \sqrt{\frac{L}{2\pi}} t^2 \left[-2 + \frac{x_0^2}{4} \left(t^2 - \frac{2}{3} \right) + \mathcal{O}(x_0^4) \right], \end{aligned} \quad (3.3.80)$$

The corresponding decomposition vector and mass-eigenvalues follow from an expansion of the characteristic equation (3.3.65). They read

$$\begin{aligned} M_W^2 &\equiv (m_0^W)^2 = \frac{g^2 v^2}{4} \left[1 - \frac{g^2 v^2}{4} \frac{1}{2M_{\text{KK}}^2} \left(\frac{L}{c_W^2} - 1 + \frac{1}{2L} \right) + \mathcal{O}\left(\frac{v^4}{M_{\text{KK}}^4}\right) \right], \\ M_Z^2 &\equiv (m_0^Z)^2 = \frac{g^2 v^2}{4c_w^2} \left[1 - \frac{g^2 v^2}{4c_w^2} \frac{1}{2M_{\text{KK}}^2} \left(\frac{L}{c_Z^2} - 1 + \frac{1}{2L} \right) + \mathcal{O}\left(\frac{v^4}{M_{\text{KK}}^4}\right) \right]. \end{aligned} \quad (3.3.81)$$

For the minimal RS model one has to set the additional mixing angles $c_W = s_W = 1$. For the custodial RS model we make the identification $g \equiv g_L$, and $g' \equiv g_Y$. We discuss in section 4.2.2 how the specific values of the additional mixing angles c_W , and s_W , given in (3.3.48), and (3.3.53), protect the oblique T -parameter. However, notice that (3.3.80) contains also t -dependent contributions that will in general lead to flavor non-universal corrections of the vertices with SM fermions with the W and Z bosons. This non-universality turns out to be negligibly small for light fermions, *i.e.* the first two generations. Therefore, additionally to the oblique corrections we also have to consider corrections to the vertex $Zb\bar{b}$. In this discussion, it is illuminating to have the analytic expression for the decomposition vector in the custodial RS model

$$\vec{A}_0^V = \begin{pmatrix} 1 \\ -s_V c_V X^2 \sqrt{L}/4 \end{pmatrix}. \quad (3.3.82)$$

The second component parametrizes the admixture of $\chi_0^{(-)}(t)$ in the zero mode, which is responsible for the custodial protection mechanism of the $Zb_L\bar{b}_L$ vertex and also its flavor-changing counterparts. The second component is simply zero in the minimal RS model.

Next, we give the explicit form of the solutions of the fermion profiles [186, 195] in the bulk and outside of the support of the Higgs profile. There is an implicit bulk -mass dependence encoded in the position of the profile on the diagonal matrix, *e.g.* $C_n^{Q(\pm)}(t) = \text{diag}(C_n^{Q(\pm)}(t, c_{Q_i}))$ and analogous for $Q \rightarrow q$ and $C \rightarrow S$. We will drop the label Q and the index i for the purposes of most of the discussion, since they should be clear from the context. One finds for $t \in [\epsilon, 1 - \eta]$

$$\begin{aligned} C_n^{(\pm)}(t, c) &= \mathcal{N}_n^{(\pm)}(c) \sqrt{\frac{L\epsilon t}{\pi}} f_n^{(\pm)+}(t, c), \\ S_n^{(\pm)}(t, c) &= \pm \mathcal{N}_n^{(\pm)}(c) \text{sgn}(\phi) \sqrt{\frac{L\epsilon t}{\pi}} f_n^{(\pm)-}(t, c), \end{aligned} \quad (3.3.83)$$

where the overall “+” sign entering the Z_2 -odd profiles holds if $c = c_Q \equiv +M_Q/k$ refers to the bidoublet, while the “-” sign applies in the case of $c = c_q \equiv -M_q/k$, with $q = u^c, d^c, \mathcal{T}_1, \mathcal{T}_2$. The functions $f_n^{(\pm)\pm}(t, c)$ are given by

$$\begin{aligned} f_n^{(+)\pm}(t, c) &= J_{-\frac{1}{2}-c}(x_n\epsilon) J_{\mp\frac{1}{2}+c}(x_nt) \pm J_{+\frac{1}{2}+c}(x_n\epsilon) J_{\pm\frac{1}{2}-c}(x_nt), \\ f_n^{(-)\pm}(t, c) &= J_{+\frac{1}{2}-c}(x_n\epsilon) J_{\mp\frac{1}{2}+c}(x_nt) \mp J_{-\frac{1}{2}+c}(x_n\epsilon) J_{\pm\frac{1}{2}-c}(x_nt). \end{aligned} \quad (3.3.84)$$

They satisfy the equalities

$$f_n^{(+)+}(t, c) = f_n^{(-)-}(t, -c), \quad f_n^{(+)-}(t, c) = -f_n^{(-)+}(t, -c). \quad (3.3.85)$$

The orthonormality relations (3.3.29) imply the normalization conditions

$$2 \int_{\epsilon}^1 dt t \left[f_n^{(a)\pm}(t, c) \right]^2 = \frac{1}{[\mathcal{N}_n^{(a)}(c)]^2} \pm \frac{f_n^{(a)+}(1, c) f_n^{(a)-}(1^-, c)}{x_n}, \quad (3.3.86)$$

where $a = \pm$. From these relations, we derive the following expressions for the normalization

$$\begin{aligned} [\mathcal{N}_n^{(a)}(c)]^{-2} &= \left[f_n^{(a)+}(1, c) \right]^2 + \left[f_n^{(a)-}(1^-, c) \right]^2 \\ &\quad - \frac{2c}{x_n} f_n^{(a)+}(1, c) f_n^{(a)-}(1^-, c) - \epsilon^2 \left(\left[f_n^{(a)+}(\epsilon, c) \right]^2 + \left[f_n^{(a)-}(\epsilon^+, c) \right]^2 \right). \end{aligned} \quad (3.3.87)$$

For the special cases where $c + 1/2$ is an integer, the profiles must be obtained from the above relations by a limiting procedure, where the definition of the Bessel Y -function can be used.

For the SM fermions, it is a very good approximation to expand the profiles in the limit $x_n \ll 1$, since even the top-quark mass is much lighter than the KK scale. We will refer to such an expansion as the zero-mode approximation (ZMA). A detailed derivation of this approximation starting from the full expressions (3.3.84) and (3.3.87) can be found in [226].

We obtain

$$\begin{aligned}
 C_n^{(+)}(\phi) &\approx \sqrt{\frac{L\epsilon}{\pi}} F(c) t^c, & S_n^{(+)}(\phi) &\approx \pm \operatorname{sgn}(\phi) \sqrt{\frac{L\epsilon}{\pi}} x_n F(c) \frac{t^{1+c} - \epsilon^{1+2c} t^{-c}}{1+2c}, \\
 C_n^{(-)}(\phi) &\approx -\sqrt{\frac{L\epsilon}{\pi}} x_n F(-c) \frac{t^{1-c} - \epsilon^{1-2c} t^c}{1-2c}, & S_n^{(-)}(\phi) &\approx \pm \operatorname{sgn}(\phi) \sqrt{\frac{L\epsilon}{\pi}} F(-c) t^{-c},
 \end{aligned}
 \tag{3.3.88}$$

where we have introduced the zero-mode profile [186, 195]

$$F(c) \equiv \operatorname{sgn} [\cos(\pi c)] \sqrt{\frac{1+2c}{1-\epsilon^{1+2c}}}.
 \tag{3.3.89}$$

The sign factor in (3.3.89) is chosen such that the signs in (3.3.88) agree with those derived from the exact profiles (3.3.76). The quantity $F(c)$ depends strongly on the value of c . One obtains

$$F(c) \approx \begin{cases} -\sqrt{-1-2c} \epsilon^{-c-\frac{1}{2}}, & -3/2 < c < -1/2, \\ \sqrt{1+2c}, & -1/2 < c < 1/2, \end{cases}
 \tag{3.3.90}$$

which implies that for UV-localized fermions the corresponding zero-mode profile is exponentially small, while it is of $\mathcal{O}(1)$ for IR-localized fields. The hierarchy in the values of $F(c)$ is central for the approach to hierarchical fermion masses and mixing in the RS model.

This is seen by the fermion mass matrix for the three lightest quarks in the ZMA, which can be written with the effective Yukawa matrix

$$\mathbf{Y}_q^{\text{eff}} = F(\mathbf{c}_Q) \mathbf{Y}_q F(\mathbf{c}_q)
 \tag{3.3.91}$$

In the custodial model, the bulk mass matrix $\mathbf{c}_{\mathcal{T}_2}$ takes the role of \mathbf{c}_q . The matrix (3.3.91) is diagonalized in RS similar to the SM with a singular value decomposition with two unitary matrices $\mathbf{U}_q^\dagger \mathbf{Y}_q^{\text{eff}} \mathbf{W}_q = \sqrt{2} \operatorname{diag}(m_{q_i}/v)$, where the first three components of the decomposition vectors $(\vec{a}^Q)_{1-3}/\sqrt{2}$ form the columns of \mathbf{U}_q and $(\vec{a}^q)_{1-3}/\sqrt{2}$ of \mathbf{W}_q . The hierarchical structure of quark masses and mixing angles can be explained by the hierarchy in the profile values. It is determined by the Cabibbo angle $\lambda = \sin(\theta_c)$, since $\mathbf{V}_{\text{CKM}} = \mathbf{U}_u^\dagger \mathbf{U}_d$ in the given approximation. This fixes the ratios

$$\left| \frac{F(c_{Q_1})}{F(c_{Q_2})} \right| \sim \lambda, \quad \left| \frac{F(c_{Q_2})}{F(c_{Q_3})} \right| \sim \lambda^2, \quad \left| \frac{F(c_{Q_1})}{F(c_{Q_3})} \right| \sim \lambda^3,
 \tag{3.3.92}$$

while the ratios of the singlet profiles involve chiral suppression factors $\sim m_{q_i}/m_t$ and inverse factors of λ . We refer to [1, 212, 226], where this has been formally derived in a Froggatt-Nielsen [227] like analysis¹⁶ and very useful approximation formulas for the quark masses, mixing, and phases of the CKM in terms of ratios of fundamental Yukawa matrices and the profiles $F(c)$ were given. The case of aligned singlet down-quark bulk masses, where all down-quark hierarchies are generated in the doublet sector, has been worked out in [226]. Even though the combinations are involved and lengthy, they have a very practical value: they are still much more efficient to evaluate, compared to the eigenvalue problem (3.3.43)

¹⁶The Froggatt-Nielsen factors $\epsilon^{a_i+a_j}$ with $\epsilon \ll 1$ and group-structure motivated charges a_i are replaced by powers of λ in the given context.

that determines the exact spectrum and compared to the numerical integrations necessary to obtain the exact CKM matrix. The approximate and the exact method allow for a two step procedure to realize efficient, yet precise numerical scans over the parameter space, which we describe closer below. Let us emphasize here that the RS model does not explain the size of the CKM phase δ .

Finally, we remark that in the custodial model the profiles $C_n^{(+)}(\phi)$ and $S_n^{(-)}(\phi)$ are of $\mathcal{O}(1)$, while $C_n^{(-)}(\phi)$ and $S_n^{(+)}(\phi)$ are of $\mathcal{O}(v/M_{\text{KK}})$ for zero modes. The fact that the twisted profiles are non-vanishing parametrizes the admixture from fermions of twisted BCs due to electroweak symmetry breaking. This implies an extra contribution, not present in the minimal model, which allows to partially shield the $Zb_L\bar{b}_L$ and $Zd_L^i\bar{d}_L^j$ vertices from corrections due to mixing of zero-mode quarks with their KK excitations. This setup does not influence fermion masses and mixing angles at the level of the Froggatt-Nielsen analysis we described above, but it has relevant effects in all corrections to gauge boson–fermion and Higgs boson–fermion couplings.

3.3.7 Two Paths to 5d Propagators

The benefit of 5d propagators for the calculation of tree and loop amplitudes is twofold, so we start in summarizing the main motivation and techniques for calculations in the 5d picture.

First of all, it turns out that the multiplicity of heavy KK particles from the infinite tower of states can lead to tedious summations when working in the 4d decomposed version of the theory. This is not a conceptual problem for tree-level processes. When we work in a scheme, or a specific amplitude where the decoupling theorem [228] holds, the separation of KK levels by mass spacings of order πM_{KK} tells us that we can truncate the evaluation above a KK level that fits our required precision. However, the use of a 5d propagator leads to compact, and easily interpretable results [1] and can be just more convenient. Moreover, in the LRS model we found that a high multiplicity of KK modes of the gluon gives a relevant contribution to FCNC processes [229]. It arises from the UV region of the extra dimension and is therefore strong for light fermions that need to be localized the stronger in the UV, the lower the volume L is. The contributions to FCNCs can become very large for $L \lesssim 10$ for order anarchic, order one Yukawa matrices. This effect is missed in the decomposed calculation with only a first few gluon KK modes.

A consistent 5d framework becomes of even greater importance for the calculation of processes that arise only at loop-level. Since the given framework is non-renormalizable, naive sums over 4d convergent diagrams can in fact circumvent the decoupling theorem due to their multiplicity and diverge or give UV dominated finite contributions as the superficial degree of divergence increases in going from a 4d to a 5d theory. We will show an example for of this effect in a process that involves an IR-brane Higgs boson in section 4.3.3. The correct regularization of the Higgs localization and the properties of a sensible regularization scheme will be important in this discussion. At this point, we have to comment on the current status of topic. Large efforts have been taken to carry out the first full fledged 5d calculation by two independent groups [230, 231] only very recently. These works are aimed at the contribution of dipole operators to the anomalous magnetic moment of the muon $a_\mu = (g - 2)/2$ and the flavor changing processes $\mu \rightarrow e\gamma$ [230] and have also been applied to the process $b \rightarrow s\gamma$ [232]. The processes all turn out to be finite in the RS model, despite the fact that a naive logarithmic divergence would occur for a non-compact fifth dimension, so the calculations are carried out without a 5d specific regularization of large 4d momenta. Unfortunately, as

also recognized in [231], a precise regularization scheme, required to be able to calculate finite renormalizations in the warped 5d background, has not yet been developed. In [103] a general outline has been given on how to implement the 5d position dependent range of validity of the EFT in terms of a cutoff of 4d momenta. As a general rule, the cut-off $\Lambda(t)$ should be close to the corresponding warped Planck scale so $\Lambda(t=1) = \Lambda_{\text{IR}} \gtrsim \text{TeV}$.¹⁷

In the following, we derive certain limits of the 5d propagators in the mixed representation using 4d momenta and bulk position coordinates. For the purpose of this work we only need the limits of these propagators for zero momentum. This drastically simplifies the calculations. We use these expressions in the presence of electroweak symmetry breaking. This resums mass insertions, which would otherwise have to be treated as perturbation in the sense that the effective action in the gauge symmetric phase Γ_Φ and the broken phase Γ_h are schematically related via

$$\Gamma_h^{f_1, \dots, f_n}(p_1, \dots, p_n) = \sum_k \frac{v^k}{(\sqrt{2})^k k!} \Gamma_\Phi^{f_1, \dots, f_n, \Phi^k}(p_1, \dots, p_n, 0, \dots, 0). \quad (3.3.93)$$

where the sum on the right-hand side goes over all configurations corresponding to gauge invariant combinations of the external fields f_j and Φ [52] and has to be approximated in the ratio of v over a mass scale of the heavy particles. Since the Higgs profile needs to be properly regularized in order to study tree-level Higgs-boson-exchange interactions and the loop processes for Higgs production and decay, it is more convenient to calculate in the broken phase. This also allows us to relate a 4d decomposed calculation of the latter processes in a simple manner to the 5d propagator and study general properties of the UV, and brane Higgs regularization.

Expressions for 5d propagators with the full momentum dependence and arbitrary spin, but in the absence of electroweak symmetry breaking were first derived in [103]. These expressions were extended including brane kinetic terms of fermions in [233], and explicit expressions have also been summarized in [230, 231], again for the case without electroweak symmetry breaking. In [210] the author derived the involved expression for 5d fermion and gauge boson propagators with electroweak symmetry breaking in the minimal RS model but without finite brane Higgs regularization. We derived the 5d fermion propagator for the minimal RS model including a finite brane Higgs regularization $\eta > 0$ and zero momentum in [2]. In the thesis at hand, we go further and extend the latter result to arbitrary fermion embeddings.

3.3.7.1 Summation over KK Modes

In this section we consider the 5d propagator for gauge bosons in the generalized notation of the custodial RS model

$$\begin{aligned} D_{\mu\nu}^V(q, \xi; t, t') &= \int d^4x e^{ip \cdot x} \langle 0 | T \vec{V}_\mu(x, t) \vec{V}_\nu^T(0, t') | 0 \rangle \\ &= D_{\mu\nu}^{V\perp}(q; t, t') \left(\eta^{\mu\nu} - \frac{p^\mu p^\nu}{p^2} \right) + D_{\mu\nu}^{V\parallel}(q, \xi; t, t') \frac{p^\mu p^\nu}{p^2}. \end{aligned} \quad (3.3.94)$$

¹⁷ The authors of [103] suggest a modification of the bulk length, which is implemented by a momentum dependent position of the IR brane, *i.e.* $t < \Lambda_{\text{IR}}/q$ with 4d momentum q . They achieved to show logarithmic running of non-abelian gauge coupling constants using this prescription. Another possibility would be the removal of high momenta in the dual conformal field theory, which would cut off IR distances in the extra-dimensional direction, *i.e.* $q < \Lambda_{\text{IR}}/|t - t'|$, or $q < \Lambda_{\text{IR}} \min(t, t') / \max(t, t')$.

Remark that the gauge fixing condition as given by the Lagrangian (3.3.54) complicates the approach via 5d EOMs. Even though the form of \mathcal{L}_{GF} is especially simple, it relies on the possibility to decompose the scalar fifth components of the gauge bosons and the Goldstone bosons in the same basis of KK modes. We refer to [210], where separate gauge fixing terms on the IR brane and in the bulk are used, as it was suggested in [209]. Here, we only need the propagator for tree-level diagrams, thus it is sufficient to go to unitary gauge. We demonstrate the technique developed in [234] and used in [229] and [4], which relies on an expansion in q^2

$$r\mathbf{D}_{\mu\nu}^{V,\perp}(q; t, t') = \sum_n (-i) \frac{\vec{\chi}_n^V(t) \vec{\chi}_n^V(t')^T}{q^2 - (m_n^V)^2} = \sum_{k=1}^{\infty} \frac{i q^{2(k-1)}}{M_{\text{KK}}^{2k}} \boldsymbol{\Sigma}_V^{(k)}(t, t'), \quad (3.3.95)$$

$$\boldsymbol{\Sigma}_V^{(k)}(t, t') \equiv \sum_n \frac{\vec{\chi}_n^V(t) \vec{\chi}_n^V(t')^T}{(x_n^V)^{2k}}.$$

We obtain sums over gauge-boson profiles $\vec{\chi}_n^V(t)$ weighted by inverse powers of the normalized KK mode masses $(x_n^a)^2$. The infinite sums can be calculated by first integrating the EOMs (3.3.61) twice, accounting for the BCs on both the UV and IR brane. This yields

$$\frac{\vec{\chi}_n^V(t)}{(x_n^V)^2} = \vec{\mathcal{I}}_n^V(t) - (t^2 - \epsilon^2) \mathbf{X}_V \vec{\mathcal{I}}_n^V(1) + [\mathbf{1} - (t^2 - \epsilon^2) \mathbf{X}_V] \mathbf{P}_{(+)} \frac{\vec{\chi}_n^V(\epsilon)}{(x_n^V)^2}, \quad (3.3.96)$$

where we have defined

$$\vec{\mathcal{I}}_n^V(t) \equiv \int_{\epsilon}^t dt' t' \int_{t'}^{1^-} \frac{dt''}{t''} \vec{\chi}_n^V(t''), \quad \mathbf{X}_V \equiv \tilde{X}^2 \mathbf{D}_V \equiv \frac{LX^2}{2 + LX^2(1 - \epsilon^2)} \mathbf{D}_V. \quad (3.3.97)$$

Using the completeness relation (3.3.59), in t -notation

$$\sum_n \frac{1}{t} \vec{\chi}_n^V(t) \vec{\chi}_n^V(t')^T = \frac{L}{2\pi} \delta(t - t') \mathbf{1}, \quad (3.3.98)$$

for the gauge-boson profiles, it is then easy to prove that

$$\sum_n \vec{\mathcal{I}}_n^V(t) \vec{\chi}_n^V(t')^T = \frac{L}{4\pi} (t_{<}^2 - \epsilon^2) \mathbf{1}, \quad (3.3.99)$$

where $t_{<} \equiv \min(t, t')$. We insert (3.3.96) twice into (3.3.95) and use (3.3.99) several times to arrive at

$$\begin{aligned} \boldsymbol{\Sigma}_V^{(1)}(t, t') &= \frac{L}{4\pi} \left[(t_{<}^2 - \epsilon^2) \mathbf{1} + (t^2 - \epsilon^2)(t'^2 - \epsilon^2) \mathbf{X}_V \right] \\ &\quad + \left[\mathbf{1} - (t^2 - \epsilon^2) \mathbf{X}_V \right] \mathbf{P}_{(+)} \boldsymbol{\Sigma}_V^{(1)}(\epsilon, \epsilon) \mathbf{P}_{(+)} \left[\mathbf{1} - (t'^2 - \epsilon^2) \mathbf{X}_V \right]^T. \end{aligned} \quad (3.3.100)$$

This relation is exact to all orders in v^2/M_{KK}^2 . With the help of the orthonormality relation (3.3.58), the remaining sum over gauge profiles evaluated at the UV brane can be brought

into the form

$$\begin{aligned} \mathbf{P}_{(+)} \boldsymbol{\Sigma}_V^{(1)}(\epsilon, \epsilon) \mathbf{P}_{(+)} &= \frac{L}{2\pi(x_0^V)^2} (\vec{\chi}_0^V(\epsilon))_1 \left(\int_{\epsilon}^1 \frac{dt}{t} \left[(1 - c_V^2 \tilde{X}^2(t^2 - \epsilon^2)) (\vec{\chi}_0^V(t))_1 \right. \right. \\ &\quad \left. \left. + s_V c_V \tilde{X}^2(t^2 - \epsilon^2) (\vec{\chi}_0^V(t))_2 \right] \right)^{-1} \mathbf{P}_{(+)}, \\ &= \left(\frac{1}{2\pi(x_0^V)^2} + \frac{1}{4\pi} \left[1 - \frac{1}{2L} - \epsilon^2 \left(L - \frac{1}{2L} \right) \right] + \mathcal{O}(x_0^V)^2 \right) \mathbf{P}_{(+)}. \end{aligned} \quad (3.3.101)$$

where $(\vec{\chi}_0^a(t))_i$ denotes the i^{th} component of the corresponding zero-mode vector. In the last line, we expanded in powers of v^2/M_{KK}^2 by using (3.3.80) and (3.3.82). Keeping in mind that $X^2 = (x_0^V/c_v)^2 + \mathcal{O}(x_0^V)^4$ and dropping phenomenologically irrelevant terms of second order in $\epsilon \approx 10^{-15}$, we finally arrive at

$$\boldsymbol{\Sigma}_V^{(1)}(t, t') = \frac{L}{4\pi} \left[t_{<}^2 \mathbf{1} - t^2 \mathbf{P}_V - t'^2 \mathbf{P}_V^T \right] + \left[\frac{1}{2\pi(x_0^V)^2} + \frac{1}{4\pi} \left(1 - \frac{1}{2L} \right) \right] \mathbf{P}_{(+)} + \mathcal{O}(x_0^V)^2, \quad (3.3.102)$$

where we defined additionally

$$\mathbf{P}_V = \begin{pmatrix} 1 & 0 \\ -\frac{s_V}{c_V} & 0 \end{pmatrix}. \quad (3.3.103)$$

The method presented here can be iterated to derive the higher coefficients $\boldsymbol{\Sigma}_V^{(k>1)}$. In [229] we presented the sum for $k = 2$ in the minimal RS model.

It is also useful to have the corresponding analytic expression for the zero-mode contribution alone at hand. A straightforward application of (3.3.80) and (3.3.82) leads to

$$\begin{aligned} \boldsymbol{\Pi}_V^{(1)}(t, t') &\equiv \frac{\vec{\chi}_0^V(t) \vec{\chi}_0^{VT}(t')}{(x_0^V)^2} = -\frac{L}{4\pi} \left[\mathbf{P}_V t^2 + \mathbf{P}_V^T t'^2 \right] \\ &\quad + \left[\frac{1}{2\pi(x_0^V)^2} + \frac{1}{4\pi} \left(1 - \frac{1}{L} + t^2 \left(\frac{1}{2} - \ln(t) \right) + t'^2 \left(\frac{1}{2} - \ln(t') \right) \right) \right] \mathbf{P}_{(+)} + \mathcal{O}(x_0^V)^2. \end{aligned} \quad (3.3.104)$$

Comparing (3.3.102) to (3.3.104) we see that all terms enhanced by the factor $L \approx 34$ in $\boldsymbol{\Sigma}_V^{(1)}(t, t')$, apart from the non-factorizable term proportional to $t_{<}^2$, arise from the zero-mode contribution $\boldsymbol{\Pi}_V(t, t')$. Factorizable contributions due to the SM-like ground-state W and Z bosons are therefore enhanced by the logarithm of the warp factor with respect to contributions from the tower of KK excitations [1]. We recall that the $t_{<}^2$ dependence reflects the full 5d structure of the RS model, which is lost when one considers only a few low-lying KK modes. Then, the term indeed factorizes but the approximation can break down for very low values of L used in LRS models [229].

The analytic results presented here allow for a clear understanding of the cancellation of certain terms in FCNC interactions. In particular, the exact form of the matrix \mathbf{P}_V and its interplay with the terms proportional to the 2×2 unit matrix are key ingredients for the custodial protection of the flavor-conserving $Z b_L \bar{b}_L$ coupling as well as of the flavor-violating $Z d_L^i \bar{d}_L^j$ vertices. We will return to this aspect in section 3.3.8.2.

The results for the minimal model are already contained in the upper left entries of (3.3.102) and (3.3.104). The same applies to the KK sums of massless gauge bosons, *i.e.* the photon and gluon, since they do not participate in electroweak symmetry breaking. For that

case we should consider only the sums over higher KK modes. They can be readily extracted from the following difference

$$(\boldsymbol{\Sigma}_V^{(1)}(t, t'))_{11} - (\boldsymbol{\Pi}_V^{(1)}(t, t'))_{11} = \frac{1}{4\pi} \left[L t_{<}^2 - t^2 \left(\frac{1}{2} - \ln t \right) - t'^2 \left(\frac{1}{2} - \ln t' \right) + \frac{1}{2L} \right]. \quad (3.3.105)$$

Remark that in this expressions the terms proportional to t^2 and t'^2 are not enhanced by L like it is the case for $\boldsymbol{\Sigma}_V^{(1)}(t, t')$. We anticipate that couplings of the 5d propagator to external fermion currents are both additionally suppressed by the RS-GIM mechanism and potentially flavor violating exactly for the terms that show non-trivial t -dependence. The $t_{<}^2$ term is therefore responsible for $\Delta F = 2$ FCNC processes whereas the t^2 and t'^2 terms generate contributions to $\Delta F = 1$ FCNCs.

3.3.7.2 Solution to the 5d EOMs

We study the propagator functions of fermions built by using spinors in the compact notation defined in (3.3.27)

$$\mathcal{Q}_\sigma(t, x) = \sum_n \mathcal{Q}_\sigma^{(n)}(t) q_\sigma^{(n)}(x) = \sqrt{\frac{2\pi r}{L\epsilon}} \left(\frac{\epsilon}{t} \right)^2 \begin{pmatrix} \bar{Q}_\sigma(x, t) \\ \bar{q}_\sigma(x, t) \end{pmatrix}. \quad (3.3.106)$$

The grand propagator in the mixed momentum/position representation [233, 235] is given by

$$\begin{aligned} i\mathcal{S}^q(t, t'; p) &= \int d^4x e^{ip \cdot x} \langle 0 | T(\mathcal{Q}_L(t, x) + \mathcal{Q}_R(t, x)) (\bar{\mathcal{Q}}_L(t', 0) + \bar{\mathcal{Q}}_R(t', 0)) | 0 \rangle \quad (3.3.107) \\ &= \sum_n \left[\mathcal{Q}_L^{(n)}(t) \frac{1 - \gamma_5}{2} + \mathcal{Q}_R^{(n)}(t) \frac{1 + \gamma_5}{2} \right] \frac{i}{\not{p} - m_n^q} \left[\mathcal{Q}_L^{(n)\dagger}(t') \frac{1 + \gamma_5}{2} + \mathcal{Q}_R^{(n)\dagger}(t') \frac{1 - \gamma_5}{2} \right], \end{aligned}$$

where we wrote the propagator in the second line in terms of the KK modes and canonical 4d propagators. The matrix $\mathcal{S}^q(t, t'; p)$ describes mixing of chiralities and singlet doublet mixing during propagation. Using the generalized mass matrix defined in (3.3.33) the Dirac operator and equation take the form

$$\mathcal{D} = \not{p} - M_{\text{KK}} (\gamma_5 \partial_t - \mathcal{M}_q(t)), \quad \mathcal{D} \mathcal{S}^q(t, t'; p) = \delta(t - t'). \quad (3.3.108)$$

Remark that we will use matrix notation to indicate the doublet and singlet components and denote chiralities via projectors separately. This is in contrast to most of the literature where propagators are derived in the absence of electroweak symmetry breaking, and where the EOM of doublet and singlet components can be treated separately. Like in the case of gauge bosons, equations (3.3.107) and (3.3.108) suggest two ways to derive the full expression. We can either resum the second line of (3.3.107) using the completeness relations (3.3.30), EOMs (3.3.32) and derived result (3.3.84) for the decomposed fermion profiles, or we can directly solve the 5d EOM (3.3.108). While both methods are applicable for gauge boson propagators at low momenta, the direct solution turns out to be much more feasible in the case of fermions. The usefulness of (3.3.107) is therefore not in the retrieval of a direct solution but rather in the derivation of a sum-rule for 4d fermion triangle diagrams [236] that relates them to a part of the 5d propagator. We will present and examine the validity of this method in section 4.3.3.

With our exact treatment of Yukawa interactions, there are no massless zero modes of the fermion fields and the propagator does not exhibit a singularity at $p^2 = 0$. We can therefore study the limit $p^\mu \rightarrow 0$ without complications. We obtain

$$\mathbf{S}^q(t, t'; 0) = - \left[\Delta_{RL}^q(t, t') \frac{1 + \gamma_5}{2} + \Delta_{LR}^q(t, t') \frac{1 - \gamma_5}{2} \right], \quad (3.3.109)$$

where

$$\Delta_{RL}^q(t, t') = \sum_n \frac{1}{m_{q_n}} \mathcal{Q}_R^{(n)}(t) \mathcal{Q}_L^{\dagger(n)}(t'), \quad \Delta_{LR}^q(t, t') = \Delta_{RL}^{q\dagger}(t', t). \quad (3.3.110)$$

The Dirac equation (3.3.108) for the 5d propagator implies the differential equation

$$\left[\partial_t + \mathcal{M}_q(t) \right] \Delta_{RL}^q(t, t') = \frac{1}{M_{\text{KK}}} \delta(t - t'), \quad (3.3.111)$$

We will construct solutions to this equation assuming first that $t \neq t'$, distinguishing the cases where $t > t'$ and $t < t'$. In general, for $t \neq t'$ a solution is given by the t -ordered exponential.

$$\Delta_{RL}^q(t, t')|_{t>t'} = T \exp \left[- \int_1^t ds \mathcal{M}_q(s) \right] \Delta_{RL}^q(1, t'), \quad (3.3.112)$$

The time ordering symbol is required since the matrices

$$\int_1^t ds \mathcal{M}_q(s) = \ln(t) \begin{pmatrix} \mathbf{c}_{\bar{q}} & \mathbf{0} \\ \mathbf{0} & -\mathbf{c}_{\bar{q}} \end{pmatrix} - \frac{v}{\sqrt{2}M_{\text{KK}}} \bar{\theta}^\eta(t-1) \begin{pmatrix} \mathbf{0} & \mathbf{Y}_{\bar{q}} \\ \mathbf{Y}_{\bar{q}}^\dagger & \mathbf{0} \end{pmatrix}, \quad (3.3.113)$$

do not commute at different t values. To solve the equation, we split into the regions $t > 1 - \eta$ or $t < 1 - \eta$, and analogous for t' , such that either the Yukawa interactions are absent or dominant, respectively. The most general solution to (3.3.111) is then given by

$$\begin{aligned} \Delta_{RL}^q(t, t') &= \begin{cases} t^{-\text{diag}(\mathbf{c}_{\bar{q}}, -\mathbf{c}_{\bar{q}})} [\theta(t-t')\mathbf{A}(t') + \theta(t'-t)\mathbf{B}(t')] & , t < 1 - \eta \\ \begin{pmatrix} \mathbf{C}_q(t) & \mathbf{y}_{\bar{q}} \bar{\mathbf{S}}_{\bar{q}}(t) \\ \mathbf{y}_{\bar{q}}^\dagger \mathbf{S}_{\bar{q}}(t) & \bar{\mathbf{C}}_{\bar{q}}(t) \end{pmatrix} [\theta(t-t')\boldsymbol{\alpha}(t') + \theta(t'-t)\boldsymbol{\beta}(t')] & , t > 1 - \eta \end{cases} \quad (3.3.114) \\ &= \begin{cases} [\theta(t-t')\tilde{\mathbf{A}}(t') + \theta(t'-t)\tilde{\mathbf{B}}(t')] t'^{\text{diag}(\mathbf{c}_{\bar{q}}, -\mathbf{c}_{\bar{q}})} & , t' < 1 - \eta \\ \begin{pmatrix} \mathbf{C}_{\bar{q}}(t') & -\mathbf{y}_{\bar{q}} \bar{\mathbf{S}}_{\bar{q}}(t') \\ -\mathbf{y}_{\bar{q}}^\dagger \mathbf{S}_{\bar{q}}(t') & \bar{\mathbf{C}}_{\bar{q}}(t') \end{pmatrix} [\theta(t-t')\tilde{\boldsymbol{\alpha}}(t') + \theta(t'-t)\tilde{\boldsymbol{\beta}}(t')] & , t' > 1 - \eta \end{cases} \end{aligned}$$

where used abbreviations for the hyperbolic functions, and the combination of Yukawa matrices known from (3.3.40) and (3.3.41), as

$$\begin{aligned} \mathbf{C}_{\bar{q}}(t) &= \cosh \left(\bar{\theta}^\eta(t-1) \mathbf{X}_{\bar{q}} \right), \quad \bar{\mathbf{C}}_{\bar{q}}(t) = \mathbf{C}_{\bar{q}}(t)|_{\mathbf{y}_{\bar{q}} \leftrightarrow \mathbf{y}_{\bar{q}}^\dagger} \\ \mathbf{S}_{\bar{q}}(t) &= \mathbf{X}_{\bar{q}}^{-1} \sinh \left(\bar{\theta}^\eta(t-1) \mathbf{X}_{\bar{q}} \right), \quad \bar{\mathbf{S}}_{\bar{q}}(t) = \mathbf{S}_{\bar{q}}(t)|_{\mathbf{y}_{\bar{q}} \leftrightarrow \mathbf{y}_{\bar{q}}^\dagger} \\ \mathbf{y}_{\bar{q}} &= \frac{v}{\sqrt{2}M_{\text{KK}}} \mathbf{Y}_{\bar{q}}, \quad \mathbf{X}_{\bar{q}} = \sqrt{\mathbf{y}_{\bar{q}} \mathbf{y}_{\bar{q}}^\dagger}. \end{aligned} \quad (3.3.115)$$

Note that the following identities hold:

$$\mathbf{y}_{\bar{q}} \bar{\mathbf{C}}_q(t) = \mathbf{C}_q(t) \mathbf{y}_{\bar{q}}, \quad \mathbf{y}_{\bar{q}}^\dagger \mathbf{C}_q(t) = \bar{\mathbf{C}}_q(t) \mathbf{y}_{\bar{q}}^\dagger. \quad (3.3.116)$$

Up to this point the discussion is valid for any fermion embedding. We illustrate the general procedure to arrive at a solution first for the minimal RS model where the BCs are simpler and generalize the result subsequently.

In the following, we determine the coefficient functions in (3.3.114). First, we use the cusp condition that follows from the integration of (3.3.111)

$$\lim_{\delta \rightarrow 0} \left[\Delta_{RL}^q(t + \delta, t') - \Delta_{RL}^q(t - \delta, t') \right] = \frac{1}{M_{KK}}. \quad (3.3.117)$$

Furthermore, we apply the BCs on the UV and IR branes. Since we have regularized the Higgs profile, they take the simple form

$$(\mathbf{1}_3 \quad \mathbf{0}_3) \Delta_{RL}^q(t, t') = (\mathbf{0}_3 \quad \mathbf{0}_3), \quad \text{if } t \in \{\epsilon, 1\}. \quad (3.3.118)$$

This follows, since the Z_2 -odd profile functions $\mathbf{S}_n^{(Q,q)}(t)$, which sit in the upper components of the right-handed spinors in (3.3.27), vanish on the branes. For a general fermion embedding, which we discussed below, the projection matrix in (3.3.118) has to be generalized. In total, we have three equations, and analogous equations with reversed arguments t and t' . They determine the matrix function $\Delta_{RL}^q(t, t')$ to be of the form

$$\Delta_{RL}^q(t, t') = \frac{1}{M_{KK}} \begin{cases} \begin{pmatrix} \left(\begin{array}{cc} (t'/t)^{c_Q} \theta(t-t') & \mathbf{0} \\ t^{c_q} \mathbf{a}_q t'^{c_Q} & -(t/t')^{c_q} \theta(t'-t) \end{array} \right) & , \\ \left(\begin{array}{cc} \mathbf{S}_q(t) \mathbf{y}_q \mathbf{b}_q t'^{c_Q} & \mathbf{0} \\ \bar{\mathbf{C}}_q(t) \mathbf{b}_q t'^{c_Q} & \mathbf{0} \end{array} \right) & , \end{pmatrix} & t, t' < 1 - \eta \\ & t > 1 - \eta > t' \\ \begin{pmatrix} t^{c_q} \mathbf{d}_q \mathbf{C}_q(t') & -t^{c_q} \mathbf{d}_q \mathbf{S}_q(t') \mathbf{y}_q \\ \left(\begin{array}{cc} -\kappa_q(t, t') + \mathbf{S}_q(t) \mathbf{y}_q \mathbf{e}_q \mathbf{C}_q(t') & \mathbf{S}_q(t) \mathbf{C}_q(t) \mathbf{y}_q - \mathbf{y}_q \bar{\mathbf{S}}_q(t) \mathbf{e}_q \mathbf{S}_q(t') \mathbf{y}_q \\ -\mathbf{y}_q^\dagger \mathbf{C}_q(t) \mathbf{S}_q(t') + \bar{\mathbf{C}}_q(t) \mathbf{e}_q \mathbf{C}_q(t') & \bar{\kappa}_q(t', t) - \bar{\mathbf{C}}_q(t) \mathbf{e}_q \mathbf{y}_q \bar{\mathbf{S}}_q(t') \end{array} \right) & , \end{pmatrix} & t < 1 - \eta < t' \\ & \text{else} \end{cases}$$

$$\kappa_q(t, t') = \mathbf{C}_q(t) \mathbf{C}_q(t') \theta(t' - t) - \mathbf{y}_q \mathbf{y}_q^\dagger \mathbf{S}_q(t) \mathbf{S}_q(t') \theta(t - t'). \quad (3.3.119)$$

The coefficients \mathbf{a}_q , \mathbf{b}_q , \mathbf{d}_q , \mathbf{e}_q are still general 3×3 matrices in generation space, to be determined by continuity at $t = 1 - \eta$ or $t' = 1 - \eta$. In the minimal RS model, it is easy to see that

$$\begin{aligned} \mathbf{a}_q &= \mathbf{e}_q = \mathbf{b}_q \mathbf{C}(1 - \eta) = \mathbf{b}_q \cosh(\mathbf{X}_q), \\ \mathbf{b}_q &= \mathbf{d}_q = \mathbf{y}_q^{-1} \mathbf{S}(1 - \eta)^{-1} = \mathbf{y}_q^{-1} \mathbf{X}_q \sinh^{-1}(\mathbf{X}_q). \end{aligned} \quad (3.3.120)$$

For the analysis of Higgs boson production and decays, we will see in section 4.3.3 that the off-diagonal blocks of the propagator at $p = 0$ and $t, t' > 1 - \eta$ are important. Therefore, we summarize their final form again explicitly

$$\Delta_{RL}^q(t > 1 - \eta, t' > 1 - \eta) \quad (3.3.121)$$

$$= \begin{pmatrix} \ddots & \begin{bmatrix} \sinh(\bar{\theta}^\eta(t_{>} - 1) \mathbf{X}_q) \cosh(\bar{\theta}^\eta(t_{<} - 1) \mathbf{X}_q) \\ -\sinh(\bar{\theta}^\eta(t_{>} - 1) \mathbf{X}_q) \sinh(\bar{\theta}^\eta(t_{<} - 1) \mathbf{X}_q) \coth(\mathbf{X}_q) \end{bmatrix} \mathbf{X}_q \left(\frac{v}{\sqrt{2}} \mathbf{Y}_q^\dagger \right)^{-1} \\ \left(\frac{v}{\sqrt{2}} \mathbf{Y}_q \right)^{-1} \mathbf{X}_q \begin{bmatrix} -\cosh(\bar{\theta}^\eta(t_{>} - 1) \mathbf{X}_q) \sinh(\bar{\theta}^\eta(t_{<} - 1) \mathbf{X}_q) \\ +\cosh(\bar{\theta}^\eta(t_{>} - 1) \mathbf{X}_q) \cosh(\bar{\theta}^\eta(t_{<} - 1) \mathbf{X}_q) \coth(\mathbf{X}_q) \end{bmatrix} & \ddots \end{pmatrix}.$$

In the following, we generalize the last result by including general 5d fermions with mixed BCs. As explained in section 3.3.5.2, superscripts (+) and (−) indicate Neumann or Dirichlet BC on the UV brane respectively and even and odd parity is assigned to the two different chirality projections. We parametrize the number of light fermion generations that emerge of type $Q_L^{(+)}$ and $q_R^{(+)}$ with $n_Q^+ = n_q^+ = n_f$, and the number of additional partner fermions $Q_L'^{(-)}$ and $q_R'^{(-)}$ as n_Q^- and n_q^- respectively. We also set $n_{Q,q} = n_f + n_{Q,q}^-$ and the number of KK modes per KK level $n_F = n_Q + n_q$. The additional bulk-mass parameters compared to the minimal model are called $\mathbf{c}_{\bar{Q},q}$. Remark that $\mathbf{Y}_{\bar{q}}$ is a complex $n_Q \times n_q$ matrix which we decompose into its sub-matrices according to the BCs of the fermions, *i.e.*

$$\mathbf{y}_{\bar{q}} = \frac{x_v}{\sqrt{2}} \mathbf{Y}_{\bar{q}} = \begin{pmatrix} \mathbf{y}_q^{(++)} & \mathbf{y}_q^{(+-)} \\ \mathbf{y}_q^{(-+)} & \mathbf{y}_q^{(--)} \end{pmatrix} \in \mathbb{C}_{n_Q \times n_q}. \quad (3.3.122)$$

The (+, +) sub-block is always of size $n_f \times n_f$. We start with the general form (3.3.114), use the cusp condition (3.3.117) and implement the generalized BCs

$$\begin{aligned} (\mathbf{1}_{n_Q} \quad \mathbf{0}_{n_Q \times n_q}) \Delta_{RL}(1, t') &= \mathbf{0}_{n_Q \times n_F}, \quad \Delta_{RL}(t, 1) \begin{pmatrix} \mathbf{0}_{n_Q \times n_q} \\ \mathbf{1}_{n_q} \end{pmatrix} = \mathbf{0}_{n_F \times n_q}, \quad (3.3.123) \\ \begin{pmatrix} \mathbf{1}_{n_f} & \mathbf{0} & \mathbf{0}_{n_f} & \mathbf{0} \\ \mathbf{0} & \mathbf{0}_{n_q^- \times n_Q^-} & \mathbf{0} & \mathbf{1}_{n_q^-} \end{pmatrix} \Delta_{RL}(\epsilon, t') &= \mathbf{0}_{n_q \times n_F}, \quad \Delta_{RL}(t, \epsilon) \begin{pmatrix} \mathbf{0}_{n_f} & \mathbf{0} \\ \mathbf{0} & \mathbf{1}_{n_Q^-} \\ \mathbf{1}_{n_f} & \mathbf{0} \\ \mathbf{0} & \mathbf{0}_{n_q^- \times n_Q^-} \end{pmatrix} = \mathbf{0}_{n_F \times n_Q}. \end{aligned}$$

The general solution reads

$$\begin{aligned} \Delta_{RL}^q(t, t') &= \frac{1}{M_{\text{KK}}} \times \quad (3.3.124) \\ &\begin{cases} \begin{pmatrix} \left(\frac{t'}{t}\right)^{c_Q} \theta(t-t') & \mathbf{0} & \mathbf{0} & \mathbf{0} \\ t^{-c_{\bar{Q}}} \mathbf{a}_{q11} t'^{c_Q} & -\left(\frac{t'}{t}\right)^{c_{\bar{Q}}} \theta(t'-t) & \mathbf{0} & t^{-c_{\bar{Q}}} \mathbf{a}_{q12} t'^{-c_q^-} \\ t^{c_q} \mathbf{a}_{q21} t'^{c_Q} & \mathbf{0} & -\left(\frac{t'}{t'}\right)^{c_q} \theta(t'-t) & t^{c_q} \mathbf{a}_{q22} t'^{-c_q^-} \\ \mathbf{0} & \mathbf{0} & \mathbf{0} & \left(\frac{t'}{t}\right)^{c_q^-} \theta(t-t') \end{pmatrix}, & t, t' < 1 - \eta \\ \begin{pmatrix} \mathcal{S}_q(t) \mathbf{y}_{\bar{q}} \mathbf{b}_{q1} t'^{c_Q} & \mathbf{0}_{n_Q \times n_Q} & \mathcal{S}_q(t) \mathbf{y}_{\bar{q}} \mathbf{b}_{q2} t'^{-c_q^-} \\ \bar{\mathcal{C}}_q(t) \mathbf{b}_{q1} t'^{c_Q} & \mathbf{0}_{n_q \times n_Q} & \bar{\mathcal{C}}_q(t) \mathbf{b}_{q2} t'^{-c_q^-} \end{pmatrix}, & t > 1 - \eta > t' \\ \begin{pmatrix} \mathbf{0}_{n_f \times n_Q} & \mathbf{0}_{n_f \times n_q} \\ t^{-c_{\bar{Q}}} \mathbf{d}_{q1} \mathcal{C}_q(t') & -t'^{-c_{\bar{Q}}} \mathbf{d}_{q1} \mathcal{S}_q(t') \mathbf{y}_q \\ t^{c_q} \mathbf{d}_{q2} \mathcal{C}_q(t') & -t^{c_q} \mathbf{d}_{q2} \mathcal{S}_q(t') \mathbf{y}_q \\ \mathbf{0}_{n_q^- \times n_Q} & \mathbf{0}_{n_q^- \times n_q} \end{pmatrix}, & t < 1 - \eta < t' \\ \begin{pmatrix} -\kappa_q(t, t') & \mathcal{S}_q(t_{>}) \mathcal{C}_q(t_{<}) \mathbf{y}_{\bar{q}} \\ -\mathbf{y}_{\bar{q}}^\dagger \mathcal{C}_q(t_{>}) \mathcal{S}_q(t_{<}) & \bar{\kappa}_q(t', t) \end{pmatrix} + \begin{pmatrix} \mathbf{y}_{\bar{q}} \bar{\mathcal{S}}_q(t) \\ \bar{\mathcal{C}}_q(t) \end{pmatrix} e_q \left(\mathcal{C}_q(t') - \mathcal{S}_q(t') \mathbf{y}_{\bar{q}} \right), & \text{else} \end{cases} \end{aligned}$$

Again we derive the coefficient matrices by continuity at $1 - \eta$ and obtain

$$\begin{aligned}
 \mathbf{a}_q &= \begin{pmatrix} \mathbf{a}_{q11} & \mathbf{a}_{q12} \\ \mathbf{a}_{q21} & \mathbf{a}_{q22} \end{pmatrix} = \begin{pmatrix} -\mathbf{C}_q^{(+)} & \mathbf{y}_q^{s(++)} \\ -\mathbf{C}_q^{(-)} & \mathbf{y}_q^{s(+)} \end{pmatrix}^{-1} \begin{pmatrix} \mathbf{C}_q^{(+)} & -\mathbf{y}_q^{s(+)} \\ \mathbf{C}_q^{(+)\dagger} & -\mathbf{y}_q^{s(-)} \end{pmatrix}, \\
 \mathbf{b}_q &= (\mathbf{b}_{q1} \quad \mathbf{b}_{q2}) = \begin{pmatrix} \mathbf{y}_q^{s(++)} & \mathbf{y}_q^{s(+)} \\ \mathbf{C}_q^{(+)\dagger} & \mathbf{C}_q^{(+)} \end{pmatrix}^{-1}, \\
 \mathbf{d}_q &= \begin{pmatrix} \mathbf{d}_{q1} \\ \mathbf{d}_{q2} \end{pmatrix} = \begin{pmatrix} -\mathbf{C}_q^{(+)\dagger} & \mathbf{y}_q^{s(++)} \\ -\mathbf{C}_q^{(-)} & \mathbf{y}_q^{s(+)} \end{pmatrix}^{-1}, \\
 \mathbf{e}_q &= \begin{pmatrix} \mathbf{y}_q^{s(++)} & \mathbf{y}_q^{s(+)} \\ \mathbf{C}_q^{(+)\dagger} & \mathbf{C}_q^{(-)} \end{pmatrix}^{-1} \begin{pmatrix} \mathbf{C}_q^{(+)} & \mathbf{C}_q^{(+)} \\ \mathbf{y}_q^{s(+)\dagger} & \mathbf{y}_q^{s(-)\dagger} \end{pmatrix},
 \end{aligned} \tag{3.3.125}$$

where we set

$$\mathbf{S}_q(1 - \eta) \mathbf{y}_{\bar{q}} = \begin{pmatrix} \mathbf{y}_q^{s(++)} & \mathbf{y}_q^{s(+)} \\ \mathbf{y}_q^{s(-)} & \mathbf{y}_q^{s(-)} \end{pmatrix}, \quad \mathbf{C}_q(1 - \eta) = \begin{pmatrix} \mathbf{C}_q^{(+)} & \mathbf{C}_q^{(+)} \\ \mathbf{C}_q^{(+)\dagger} & \mathbf{C}_q^{(-)} \end{pmatrix}. \tag{3.3.126}$$

The result (3.3.125) with the submatrices inserted is very lengthy, even when expanded to second order in v/M_{KK} using the sub-block notation of (3.3.122). We will see in the analysis of Higgs boson production and decays in section 4.3.3 that the matrix \mathbf{e}_q is of special interest. We will only give the expansion in v/M_{KK} for the specific result in that analysis, as it turns out to be simple and illuminating.

The structure of the Yukawa matrices for the given custodial embedding of section 3.3.5.2, which involves only two 3×3 matrices $\mathbf{Y}_{u,d}$, results in simple expressions for the propagator. By working out the matrix exponentials of $\mathbf{y}_{\bar{q}} \mathbf{y}_q^\dagger$ and $\mathbf{y}_q^\dagger \mathbf{y}_{\bar{q}}$ for the Yukawa matrices (3.3.69) of the three sectors of equal charge, we obtain

$$\begin{aligned}
 \mathbf{e}_u &= \begin{pmatrix} \frac{1}{2} \mathbf{y}_u^{-1} \mathbf{s}_{2u}^{-1} (\mathbf{c}_{2u} + \mathbf{c}_{2d}^{-1}) & \frac{1}{2} \mathbf{y}_u^{-1} \mathbf{s}_{2u}^{-1} (\mathbf{c}_{2u} - \mathbf{c}_{2d}^{-1}) \\ \frac{1}{\sqrt{2}} \mathbf{y}_d^\dagger \mathbf{s}_{2d} \mathbf{c}_{2d}^{-1} & -\frac{1}{\sqrt{2}} \mathbf{y}_d^\dagger \mathbf{s}_{2d} \mathbf{c}_{2d}^{-1} \\ \frac{1}{\sqrt{2}} \mathbf{y}_d^\dagger \mathbf{s}_{2d} \mathbf{c}_{2d}^{-1} & -\frac{1}{\sqrt{2}} \mathbf{y}_d^\dagger \mathbf{s}_{2d} \mathbf{c}_{2d}^{-1} \end{pmatrix}, \\
 \mathbf{e}_d &= \begin{pmatrix} \mathbf{y}_d^{-1} \mathbf{s}_{2d}^{-1} (\frac{1}{2} \mathbf{c}_{2d} + \mathbf{1}) \\ \mathbf{y}_d^{-1} \mathbf{s}_{2d}^{-1} (\frac{1}{2} \mathbf{c}_{2d} - \mathbf{1}) \end{pmatrix}, \quad \mathbf{e}_\lambda = \begin{pmatrix} \mathbf{y}_d^\dagger \mathbf{s}_{2d} \mathbf{c}_{2d}^{-1} \\ \mathbf{y}_d^\dagger \mathbf{s}_{2d} \mathbf{c}_{2d}^{-1} \end{pmatrix}.
 \end{aligned} \tag{3.3.127}$$

Here, we observe that the larger representations of the custodial compared to the minimal fermion embedding imply the general feature that the arguments in the involved trigonometric functions are rescaled by a factor of $\sqrt{2}$. We included this in the abbreviations

$$\mathbf{c}_{2q} = \cosh(\sqrt{2} \mathbf{X}_q), \quad \mathbf{s}_{2q} = \sinh(\sqrt{2} \mathbf{X}_q) (\sqrt{2} \mathbf{X}_q)^{-1}. \tag{3.3.128}$$

The remaining coefficients are now straightforward to work out explicitly. We end the discussion of propagators and move on to examine the relevant coupling structure of the model.

3.3.8 Complete Coupling Structure

In contrast to the discussion of renormalizable, or partly renormalizable models presented above, RS models have a conceptually different coupling structure. First of all, the models are of course non-renormalizable and therefore loop-order calculations are not expected to be constrained in their general coupling structure. One has to check process by process if non-UV sensitive statements can be made. Below, we will show the fortunate example of loop processes for Higgs physics where this is the case. For this purpose, we need a good understanding of Higgs–fermion couplings, for which we give the relevant results here. Concerning electroweak precision tests and constraints from FCNC, statements can be made due to the fact that the most relevant processes are influenced already at tree-level. In the following, we will give all relevant couplings for the case of a minimal as well as the custodial RS model and use a notation that facilitates comparison between them.

3.3.8.1 Higgs–Fermion Couplings

For the derivation of Higgs-boson couplings to fermion currents, we have to compute overlap integrals of fermion profiles with the δ -profile function of the IR localized Higgs boson. The coupling is therefore given by

$$g_{h\bar{q}_m q_n}^R = \frac{1}{\sqrt{2}} \int_{\epsilon}^1 dt \delta^\eta(t-1) \mathcal{Q}_L^{\dagger(m)}(t) \begin{pmatrix} \mathbf{0} & \mathbf{Y}_{\bar{q}} \\ \mathbf{Y}_{\bar{q}}^\dagger & \mathbf{0} \end{pmatrix} \mathcal{Q}_R^{(n)}(t). \quad (3.3.129)$$

The correct procedure is to start from a regularized Higgs profile, insert the profile form (3.3.40), compute the relevant overlap integrals, and then take η to zero [207].

$$\begin{aligned} \lim_{\eta \rightarrow 0} g_{h\bar{q}_m q_n}^R &= \frac{\sqrt{2}\pi}{L\epsilon} \int_{\epsilon}^1 dt \delta^\eta(t-1) \bar{a}_m^{Q\dagger} C_m^Q(1-\eta) \frac{1}{\cosh^2 \mathbf{X}_{\bar{q}}} \\ &\times \left[\cosh^2(\bar{\theta}^\eta(t-1) \mathbf{X}_{\bar{q}}) - \sinh^2(\bar{\theta}^\eta(t-1) \mathbf{X}_{\bar{q}}) \right] \mathbf{Y}_{\bar{q}} C_n^q(1-\eta) \bar{a}_n^q \quad (3.3.130) \\ &= \frac{\sqrt{2}\pi}{L\epsilon} \bar{a}_m^{Q\dagger} C_m^Q(1^-) \frac{1}{\cosh^2 \mathbf{X}_{\bar{q}}} \mathbf{Y}_{\bar{q}} C_n^q(1^-) \bar{a}_n^q. \end{aligned}$$

In this equation there is of course the implicit assumption that the fermion mass x_n^q is fixed, while the limit on η is performed. It is useful to consider the expression also for finite η and very large KK masses. One can derive that the form of the couplings changes drastically in the region $x_n^q \approx M_{\text{weak}}/\eta$. We illustrate this behavior in a simple toy model with one fermion generation and vanishing bulk masses in appendix A.3. Here, we only summarize that the qualitative difference in the case of one generation is that inside a given KK level the two KK fermions of that level show a diagonal Higgs-boson coupling of opposite sign if $x_n^q \ll M_{\text{weak}}/\eta$. Close to the threshold M_{weak}/η , one of the couplings vanishes approximately, while the other stays finite.

Remark that (3.3.130) involves a combination of Yukawa matrices that is different from $\tilde{\mathbf{Y}}_{\bar{q}}$ defined in (3.3.41), which determines the spectrum. This has relevant consequences for the flavor off-diagonal transitions, which receive a contribution that is not chirally suppressed, *i.e.* not proportional to one of the external quark masses.

For a clear separation of effects, it is also useful to rewrite the Higgs–fermion couplings (3.3.130) in the form of a leading SM-like contribution and correction terms

$$\begin{aligned} \lim_{\eta \rightarrow 0} g_{h\bar{q}_m q_n}^R &\equiv \delta_{mn} \frac{m_m^q}{v} - (\Delta g_h^q)_{mn}, \\ (\Delta g_h^q)_{mn} &= \frac{m_m^q}{v} (\Phi_q)_{mn} + (\Phi_Q)_{mn} \frac{m_n^q}{v} + (\Delta \tilde{g}_h^q)_{mn}. \end{aligned} \quad (3.3.131)$$

We split the correction terms into the chirally suppressed terms, whose coefficients $\Phi_{q,Q}$ are given by

$$(\Phi_{q,Q})_{mn} = \frac{2\pi}{L\epsilon} \int_{\epsilon}^1 dt \bar{a}_m^{Q,q\dagger} \mathbf{S}_m^{Q,q}(t) \mathbf{S}_n^{Q,q}(t) \bar{a}_n^{Q,q} \quad (3.3.132)$$

In [1], we have shown that these quantities, which parametrize the non-orthogonality of fermion modes, are given by

$$(\Phi_{q,Q})_{mn} = \delta_{mn} \mp \frac{2}{r} \frac{m_m^q \mathbf{C}_m^{(Q,q)}(\pi) \mathbf{S}_n^{(Q,q)}(\pi^-) - m_n^q \mathbf{C}_n^{(Q,q)}(\pi) \mathbf{S}_m^{(Q,q)}(\pi^-)}{(m_m^q)^2 - (m_n^q)^2}. \quad (3.3.133)$$

The additional chiral suppression for light quarks, which we mentioned above, becomes obvious in the ZMA. We will give the expression for both the minimal and the custodial model in a common notation that facilitates the comparison. For the custodial model, we make use of $\mathcal{O}(v^2/M_{\text{KK}}^2)$ expressions for the eigenvectors of the twisted fermions $\bar{a}_n^{D',u',U',U}$. First note that these eigenvectors contribute to the normalization of the combined vectors $\bar{a}_n^{Q,q}$ as explained in (3.3.31), so it is expected that there are relations between the three-block sub-components of the combined vectors. We find that in the ZMA

$$\begin{aligned} a_n^{D'} &= x_n^q F^{-1}(\mathbf{c}_{\mathcal{T}_2}) F^{-1}(-\mathbf{c}_{\mathcal{T}_1}) a_n^D, & a_n^{u'} &= x_n^q F^{-1}(-\mathbf{c}_Q) F^{-1}(\mathbf{c}_Q) a_n^u, \\ a_n^{U'} &= F(-\mathbf{c}_{\mathcal{T}_2}) F^{-1}(-\mathbf{c}_{\mathcal{T}_1}) a_n^U, & a_n^U &= \frac{x_n^q}{\sqrt{2}} F^{-1}(-\mathbf{c}_{\mathcal{T}_2}) \mathbf{Y}_d^\dagger (\mathbf{Y}_u^\dagger)^{-1} F^{-1}(\mathbf{c}_{u^c}) a_n^{u^c}. \end{aligned} \quad (3.3.134)$$

With these relation it is straightforward to show that

$$\begin{aligned} \Phi_q &= \mathbf{x}_q \mathbf{U}_q^\dagger \text{diag} \left[\frac{1}{1-2c_{Q_i}} \left(\frac{1}{F^2(c_{Q_i})} [1 + \omega_h^{q_i}] - 1 + \frac{F^2(c_{Q_i})}{3+2c_{Q_i}} \right) \right] \mathbf{U}_q \mathbf{x}_q, \\ \Phi_Q &= \mathbf{x}_q \mathbf{W}_q^\dagger \left(\text{diag} \left[\frac{1}{1-2c_{q_i}} \left(\frac{1}{F^2(c_{q_i})} [1 + \omega_h^{Q_i}] - 1 + \frac{F^2(c_{q_i})}{3+2c_{q_i}} \right) \right] + \tilde{\omega}_h^{Q_i} \right) \mathbf{W}_q \mathbf{x}_q, \end{aligned} \quad (3.3.135)$$

with $\mathbf{x}_u = \text{diag}(m_u, m_c, m_t)/M_{\text{KK}}$. \mathbf{U}_q and \mathbf{W}_q are the left- and right-handed rotation matrices diagonalizing the effective Yukawa couplings. As described in section 3.3.6 the vectors $a_n^Q/\sqrt{2}$ and $a_n^q/\sqrt{2}$ form the columns of these matrices. The correction terms $\omega_h^{Q_i, q_i}$ are all zero in the minimal model. Their purpose is to summarize the non-universal changes in going to the custodial embedding, which are given by

$$\begin{aligned} c_{d_i} &\rightarrow c_{\mathcal{T}_{2i}}, & \omega_h^{d_i} &= \omega_h^{U_i} = \tilde{\omega}_h^{D_i} = 0, & \omega_h^{u_i} &= \frac{1-2c_{Q_i}}{F^2(-c_{Q_i})}, & \omega_h^{D_i} &= \frac{1-2c_{\mathcal{T}_{2i}}}{F^2(-c_{\mathcal{T}_{1i}})}, \\ \tilde{\omega}_h^{U_i} &= \frac{1}{2} F^{-1}(\mathbf{c}_{u_i^c}) \mathbf{Y}_u^{-1} \mathbf{Y}_d \left(F^{-2}(-c_{\mathcal{T}_{2i}}) + F^{-2}(-c_{\mathcal{T}_{1i}}) \right) \mathbf{Y}_d^\dagger [\mathbf{Y}_u^\dagger]^{-1} F^{-1}(\mathbf{c}_{u_i^c}). \end{aligned} \quad (3.3.136)$$

The correction terms involve the zero-mode profiles $F(-c_{\mathcal{T}_{1i}})$, $F(-c_{\mathcal{T}_{2i}})$, and $F(-c_{Q_i})$, which arise from the admixture of the $\mathbf{S}_n^{\mathcal{T}_{1i}(-)}(t)$, $\mathbf{S}_n^{\mathcal{T}_{2i}(-)}(t)$, and $\mathbf{S}_n^{Q(-)}(t)$ profiles in the corresponding zero-mode profile. In each case, the suppression by v/M_{KK} due to the admixture is offset by the $\mathcal{O}(M_{\text{KK}}/v)$ enhancement of the Z_2 -odd ($-$) profile relative to its ($+$) counterpart. For $c_{Q_i} < 1/2$, the leading contribution in Φ_u is thus numerically enhanced by a factor of approximately 2 with respect to the minimal model. If the $Z d_L^i \bar{d}_L^j$ vertices are protected from fermion mixing by $c_{\mathcal{T}_1} = c_{\mathcal{T}_2}$ and $c_{\mathcal{T}_{2i}} < 1/2$, then the same holds true for Φ_D . Depending on the structure of the Yukawa matrices and bulk masses, also an enhancement in Φ_U is possible.

The second type of corrections to the Higgs–fermion couplings (3.3.131) is given by

$$\begin{aligned} \Delta \tilde{g}_h^q &= -\sqrt{2} \frac{2\pi}{L\epsilon} \int_{\epsilon}^1 dt \delta(t-1) \left(\bar{a}_m^{q\dagger} \mathbf{S}_m^q(t) \mathbf{Y}_q^\dagger \mathbf{S}_n^Q(t) \bar{a}_n^Q \right)_{mn} \\ &= \frac{\sqrt{2}v^2}{3M_{\text{KK}}^2} \frac{\pi}{L\epsilon} \left(\bar{a}_m^{Q\dagger} \mathbf{C}_m^Q(1^-) \tilde{\mathbf{Y}}_q \tilde{\mathbf{Y}}_q^\dagger \tilde{\mathbf{Y}}_q \mathbf{C}_n^q(1^-) \bar{a}_n^q \right)_{mn}, \end{aligned} \quad (3.3.137)$$

with

$$\tilde{\mathbf{Y}}_q^\dagger \equiv \tilde{\mathbf{Y}}_q^\dagger \frac{3}{2} \left[\tilde{\mathbf{X}}_q^{-2} + \text{atanh}(\tilde{\mathbf{X}}_q) \tilde{\mathbf{X}}_q^{-1} (\mathbf{1} - \tilde{\mathbf{X}}_q^{-2}) \right]. \quad (3.3.138)$$

The result in the ZMA becomes simply

$$\Delta \tilde{g}_h^q = \frac{v^2}{3\sqrt{2}M_{\text{KK}}^2} \mathbf{U}_q^\dagger F(c_{Q_i}) \mathbf{Y}_q \mathbf{Y}_q^\dagger \mathbf{Y}_q F(c_{q_i}) \mathbf{W}_q \cdot \begin{cases} 1, & \text{minimal RS,} \\ 2, & \text{custodial RS.} \end{cases} \quad (3.3.139)$$

Notice that this kind of correction is not parametrically suppressed by light quark masses for the first two up and all down type generations. The chirally unsuppressed contributions $\Delta \tilde{g}_h^{d,u}$ arise from the Z_2 -odd Yukawa couplings, and present the dominant sources of flavor violation in the Higgs sector [207]. They are potentially comparable to Z boson mediated FCNCs. Compared to the minimal RS model, the corrections $\Delta \tilde{g}_h^{d,u}$ are again bigger by a factor of 2 in the extended scenario.

Note that for the diagonal entries we can write the ZMA result (3.3.139) also as

$$(\Delta \tilde{g}_h^q)_{nn} = \frac{4m_t^2}{3vM_{\text{KK}}^2} \sum_{j=1}^3 m_j^q \left(\mathbf{U}_q^\dagger F^{-2}(c_Q) \mathbf{U}_u \right)_{jn} \left(\mathbf{W}_u^\dagger F^{-2}(c_q) \mathbf{W}_u \right)_{nj} \cdot \begin{cases} 1 \\ 2 \end{cases}. \quad (3.3.140)$$

The term with $j = n$ is obviously positive semi-definite. Since terms with $j = 1, 2$ have a chiral suppression compared to the term with $j = 3$, we find that $(\Delta \tilde{g}_h^u)_{33}$ is real and positive to a good approximation, while the phase of all other entries of $(\Delta \tilde{g}_h^u)_{nm}$ can take in principle any value. Since also $(\Delta \Phi_{Q,q})_{nn}$ are absolute squares, we conclude with the important result that $ht\bar{t}$ and $hb\bar{b}$ couplings are predicted to be suppressed relative to their SM values in all RS models discussed here. A similar conclusion has been drawn in the context of models where the Higgs arises as a pseudo Nambu-Goldstone boson [236, 237].

Let us finally mention that a model-independent analysis of the flavor misalignment of the SM fermion masses and the Yukawa couplings has been presented in [238]. There, it has been shown that at the level of dimension six, chirally unsuppressed contributions to flavor-changing Higgs boson vertices will generically arise from dimension 6 operators like $\bar{q}_L^i \Phi q_R^j (\Phi^\dagger \Phi)$ in models where the Higgs boson is a bound state of a new strongly interacting theory. If

present, the latter terms will dominate over the chirally suppressed contributions originating from operators of the form $\bar{q}_L^i \not{D} q_L^j (\Phi^\dagger \Phi)$. This is due to the possibly large couplings y_{q^*} of the composite Higgs boson to the other strongly interacting states, which results in $y_{q^*}^2/(16\pi^2) \gg m_q/v$. Considering all relevant dimension-six operators in the given RS models to lowest order of the mass insertion approximation, allows to recover the ZMA results (3.3.135) and (3.3.139) quantifying the misalignment between the Yukawa couplings and the zero-mode masses (see [207] for an illuminating discussion). We emphasize that our exact solution given above resums all new-physics effects induced by the mass insertions, corresponding to both the non-derivative and derivative dimension-six operators. The interplay of both in fact leads to the chirally unsuppressed terms in (3.3.131).

3.3.8.2 Gauge-Boson–Fermion Couplings

We turn to the phenomenologically relevant expressions for weak gauge interactions of quark currents and identify the RS contribution at order v^2/M_{KK}^2 . For the Z -boson couplings to quarks, we extract a universal prefactor and write the couplings in (infinite-dimensional) matrix form as

$$g_{Z\bar{q}_m q_n}^\sigma = \frac{g}{c_w} \left[1 + \frac{M_Z^2}{4M_{\text{KK}}^2} \left(1 - \frac{1}{L} \right) \right] (g_{Z,\sigma}^q)_{mn}, \quad (3.3.141)$$

with

$$\begin{aligned} g_{Z,L}^q &= (T_L^{3qL} - s_w^2 Q_q) \left[\mathbf{1} - \frac{M_Z^2}{2M_{\text{KK}}^2} (\omega_Z^{qL} L \Delta_Q - \Delta'_Q) \right] - \delta_Q + \frac{M_Z^2}{2M_{\text{KK}}^2} (L \varepsilon_Q - \varepsilon'_Q), \\ g_{Z,R}^q &= -s_w^2 Q_q \left[\mathbf{1} - \frac{M_Z^2}{2M_{\text{KK}}^2} (\omega_Z^{qR} L \Delta_q - \Delta'_q) \right] + \delta_q - \frac{M_Z^2}{2M_{\text{KK}}^2} (L \varepsilon_q - \varepsilon'_q). \end{aligned} \quad (3.3.142)$$

The charges are either SM-like for the minimal RS model, or as summarized in table 3.4 for the custodial RS model. For the latter, we define T_σ^{3qL} for $\sigma = L, R$ as the quantum numbers of the quark in the uppermost component of \vec{Q} and T_σ^{3qR} via the uppermost component of \vec{q} in the notation of (3.3.23). Like in the case of Higgs-fermion couplings there is an embedding dependent factor in the leading contribution, which comes linear in $L \approx 34$. Analogous to before, we encode this in a factor ω_Z^q . However, here the factor is universal for all generations. It is given by ω_Z^q in the minimal RS model and for a general LR -symmetric embedding as

$$\omega_Z^q = 1 - \frac{s_Z}{c_Z} \frac{g_{Z'} Q_{Z'}}{g_Z Q_Z^q} = \frac{c_w^2}{2g_L^2} \frac{(g_L^2 + g_R^2)(T_L^{3q} + T_R^{3q}) + (g_L^2 - g_R^2)(T_L^{3q} - T_R^{3q})}{T_L^{3q} - s_w^2 Q_q}. \quad (3.3.143)$$

This allows one to read off that the two possible choices

$$\begin{aligned} P_C \text{ symmetry: } & T_L^{3q} = T_R^{3q} = 0, \\ P_{LR} \text{ symmetry: } & g_L = g_R, \quad T_L^{3q} = -T_R^{3q}, \end{aligned} \quad (3.3.144)$$

are suitable to protect the Z -boson vertices from receiving L -enhanced corrections. Since the custodial representation (3.3.66) features $T_L^{3dL} = -T_R^{3dL}$, $T_L^{3\lambda L} = -T_R^{3\lambda L}$ and $T_{L,R}^{3uR} = 0$, we observe that the $Z d_L^i \bar{d}_L^j$, $Z \lambda_L^i \bar{\lambda}_L^j$, and $Z u_R^i \bar{u}_R^j$ vertices are protected to leading order in L by the P_{LR} and P_C symmetries, respectively. On the other hand, the L -enhanced corrections

of the vertices with opposite fermion chiralities are raised by $\omega_Z^{dR} \approx 10.0$, $\omega_Z^{\lambda R} \approx 2.0$, and $\omega_Z^{uL} \approx 2.2$.

In (3.3.142), we have furthermore split the corrections to the Z -boson couplings into leading contributions, denoted by $\Delta_{Q,q}^{(\prime)}$, and subleading ones, parametrized by $\varepsilon_{Q,q}^{(\prime)}$. The elements of the leading contributions are defined as

$$\begin{cases} (\Delta_Q)_{mn} \\ (\Delta'_Q)_{mn} \end{cases} = \frac{2\pi}{L\epsilon} \int_{\epsilon}^1 dt \left\{ t^2 \left(\frac{1}{2} - \ln(t) \right) \right\} \left[\vec{a}_m^{Q\dagger} \mathbf{C}_m^Q(t) \mathbf{C}_n^Q(t) \vec{a}_n^Q + \vec{a}_m^{q\dagger} \mathbf{S}_m^q(t) \mathbf{S}_n^q(t) \vec{a}_n^q \right], \quad (3.3.145)$$

and the same formulas with $Q \leftrightarrow q$. In the minimal model, the subleading contributions $\varepsilon_{Q,q}^{(\prime)}$ are obtained from the same equations without the contribution from the even profiles $\mathbf{C}_m^{Q,q}$. Furthermore, the matrices $\delta_{Q,q}$, which arise from the non-orthonormality of the quark profiles and describe mixings between the different multiplets, are given by the same expressions $\Phi_{Q,q}$ that were defined in (3.3.132). They inherently contain a $\mathcal{O}(v^2/M_{\text{KK}}^2)$ suppression and are formally of the same order as the $\Delta_{Q,q}$, for which this suppression is factored out in (3.3.142). Employing the ZMA and neglecting $\mathcal{O}(1)$ factors, one can show that all the leading quantities $(\Delta_{Q,q}^{(\prime)})_{ij}$ and $(\delta_{Q,q})_{ij}$ have an inherent suppression with two factors of the profile brane values $F(c_{Q_i,q_i})F(c_{Q_j,q_j})$ of the corresponding fermions [1]. Light mass values and the smallness of non-standard contributions to gauge-boson couplings are therefore correlated. This is the RS-GIM mechanism [201, 202]. In the custodial model, the general order of magnitude of the expressions is unchanged, however the expression become more involved. We summarize

- minimal :

$$\epsilon_{Q,q}^{(\prime)} = T_L^{3q} \Delta_{Q,q}^{(\prime)}|_{\mathbf{C}_n^{Q,q} \rightarrow 0}, \quad \delta_{Q,q} = T_L^{3q} \Phi_{Q,q}. \quad (3.3.146)$$

- custodial :

$$\begin{aligned} \begin{cases} (\varepsilon_Q)_{mn} \\ (\varepsilon'_Q)_{mn} \end{cases} &= \frac{2\pi}{L\epsilon} \int_{\epsilon}^1 dt \left\{ t^2 \left(\frac{1}{2} - \ln(t) \right) \right\} \times \\ &\times \left[\vec{a}_m^{Q\dagger} \mathbf{C}_m^Q(t) \left(T_L^{3qL} \mathbf{1} - \mathbf{T}_L^{3Q} + \left\{ \frac{t_W^2}{0} \right\} \left(T_R^{3qL} \mathbf{1} - \mathbf{T}_R^{3Q} \right) \right) \mathbf{C}_n^Q(t) \vec{a}_n^Q \right. \\ &\quad \left. + \vec{a}_m^{q\dagger} \mathbf{S}_m^q(t) \left(T_L^{3qL} \mathbf{1} - \mathbf{T}_L^{3q} + \left\{ \frac{t_W^2}{0} \right\} \left(T_R^{3qL} \mathbf{1} - \mathbf{T}_R^{3q} \right) \right) \mathbf{S}_n^q(t) \vec{a}_n^q \right], \end{aligned} \quad (3.3.147)$$

$$\begin{aligned} \begin{cases} (\varepsilon_q)_{mn} \\ (\varepsilon'_q)_{mn} \end{cases} &= \frac{2\pi}{L\epsilon} \int_{\epsilon}^1 dt \left\{ t^2 \left(\frac{1}{2} - \ln(t) \right) \right\} \times \\ &\times \left[\vec{a}_m^{q\dagger} \mathbf{C}_m^q(t) \left(\mathbf{T}_L^{3q} - \left\{ \frac{t_W^2}{0} \right\} \left(T_R^{3qR} \mathbf{1} - \mathbf{T}_R^{3q} \right) \right) \mathbf{C}_n^q(t) \vec{a}_n^q \right. \\ &\quad \left. + \vec{a}_m^{Q\dagger} \mathbf{S}_m^Q(t) \left(\mathbf{T}_L^{3Q} - \left\{ \frac{t_W^2}{0} \right\} \left(T_R^{3qR} \mathbf{1} - \mathbf{T}_R^{3Q} \right) \right) \mathbf{S}_n^Q(t) \vec{a}_n^Q \right], \\ (\delta_Q)_{mn} &= \frac{2\pi}{L\epsilon} \int_{\epsilon}^1 dt \left[\vec{a}_m^{Q\dagger} \mathbf{C}_m^Q(t) \left(T_L^{3qL} \mathbf{1} - \mathbf{T}_L^{3Q} \right) \mathbf{C}_n^Q(t) \vec{a}_n^Q \right. \\ &\quad \left. + \vec{a}_m^{q\dagger} \mathbf{S}_m^q(t) \left(T_L^{3qL} \mathbf{1} - \mathbf{T}_L^{3q} \right) \mathbf{S}_n^q(t) \vec{a}_n^q \right], \end{aligned} \quad (3.3.148)$$

$$(\delta_q)_{mn} = \frac{2\pi}{L\epsilon} \int_{\epsilon}^1 dt \left[\vec{a}_m^{q\dagger} \mathbf{C}_m^q(t) \mathbf{T}_L^{3q} \mathbf{C}_n^q(t) \vec{a}_n^q + \vec{a}_m^{Q\dagger} \mathbf{S}_m^Q(t) \mathbf{T}_L^{3Q} \mathbf{S}_n^Q(t) \vec{a}_n^Q \right].$$

In the expressions above, we abbreviated the diagonal charge matrices as $\mathbf{T}_{\sigma=L,R}^{3Q,q}$:

$$\begin{aligned} \mathbf{T}_{\sigma}^{3U} &= \text{diag} (T_{\sigma}^{3u} \mathbf{1}_{n_f}, T_{\sigma}^{3u'} \mathbf{1}_{n_f}), & \mathbf{T}_{\sigma}^{3u} &= \text{diag} (T_{\sigma}^{3uc} \mathbf{1}_{n_f}, T_{\sigma}^{3U'} \mathbf{1}_{n_f}, T_{\sigma}^{3U} \mathbf{1}_{n_f}), \\ \mathbf{T}_{\sigma}^{3D} &= T_{\sigma}^{3d} \mathbf{1}_{n_f}, & \mathbf{T}_{\sigma}^{3d} &= \text{diag} (T_{\sigma}^{3D} \mathbf{1}_{n_f}, T_{\sigma}^{3D'} \mathbf{1}_{n_f}), \\ \mathbf{T}_{\sigma}^{3\Lambda} &= T_{\sigma}^{3\lambda} \mathbf{1}_{n_f}, & \mathbf{T}_{\sigma}^{3\lambda} &= \text{diag} (T_{\sigma}^{3\Lambda'} \mathbf{1}_{n_f}, T_{\sigma}^{3\Lambda} \mathbf{1}_{n_f}). \end{aligned} \quad (3.3.149)$$

Note that with the embedding (3.3.66), the matrices \mathbf{T}_{σ}^{3u} vanish identically. ZMA results have been given in [1] and [4] and we do not repeat them here, except for one case below.

The second ingredient for the protection of the $Zb_L^i \bar{b}_L^j$ vertex in the custodial model can now be derived from (3.3.148). Inserting quantum numbers we see that¹⁸

$$\begin{aligned} \delta_D &= -\frac{1}{2} \frac{2\pi}{L\epsilon} \int_{\epsilon}^1 dt \left(a_m^{D\dagger} \mathbf{S}_m^{\mathcal{T}_2(+)}(t) \mathbf{S}_n^{\mathcal{T}_2(+)}(t) a_n^D - a_m^{D'\dagger} \mathbf{S}_m^{\mathcal{T}_1(-)}(t) \mathbf{S}_n^{\mathcal{T}_1(-)}(t) a_n^{D'} \right)_{mn} \\ &= -\frac{1}{2} \mathbf{x}_d \mathbf{W}_d^{\dagger} \text{diag} \left[\frac{1}{1 - 2c_{\mathcal{T}_{2i}}} \left(\frac{1}{F^2(c_{\mathcal{T}_{2i}})} [1 - \omega_h^{q_i}] - 1 + \frac{F^2(c_{\mathcal{T}_{2i}})}{3 + 2c_{\mathcal{T}_{2i}}} \right) \right] \mathbf{W}_d \mathbf{x}_d, \end{aligned} \quad (3.3.150)$$

where the second line in the approximation in the ZMA. The quantity $\omega_h^{q_i}$ has been defined in (3.3.136). In fact it enters Φ_D in (3.3.135) with the opposite sign. The rest of the expression is unchanged compared to (3.3.150). We have seen there that $\omega_h^{q_i}$ is one to a very good approximation if $c_{\mathcal{T}_{1i}} = c_{\mathcal{T}_{2i}} < 1/2$. The equality of bulk masses is of course enforced by the P_{LR} symmetry acting on the down-type quarks as $P_{LR}(D') = D$. In consequence, effects due to quark mixing entering the Z -boson couplings are generically suppressed in the custodial RS model relative to the minimal scenario as long as the Z_2 -odd quark fields are not too far localized in the UV. It remains a viable option to break this symmetry softly by choosing different bulk masses, since the zero mode masses are not affected by $c_{\mathcal{T}_{1i}}$ in an appreciable way, as long as they stay UV localized. The protection mechanism discussed here has also been studied in [239] employing a perturbative approach to electroweak symmetry breaking. Compared to the perturbative approach, the exact treatment of the EOMs used here has the salient advantage that the dependence of the $Zd_L^i \bar{d}_L^j$ vertices on quark mixing, *i.e.* on the bulk masses $\mathbf{M}_{\mathcal{T}_{1,2}}$ in (3.3.150), can be clearly deciphered.

It is interesting to observe that only the leading terms in L and $F^{-2}(c_{\mathcal{T}_2})$ of the $Zd_L^i \bar{d}_L^j$ vertex can be protected. There is no such mechanism available for the subleading terms, since they arise from the fact that the twisted and untwisted orbifold representations obey different UV BCs. These effects hence represent an irreducible source of P_{LR} symmetry breaking.

3.3.8.3 Purely Bosonic Couplings

Finally, we will also evaluate the RS corrections to the W^+W^-h , ZZh , and W^+W^-Z tree-level vertices, where the gauge bosons are the SM-like zero-modes. They will be important for our discussion of Higgs processes. Due to the unbroken $U(1)_{\text{EM}}$ gauge group, the $W^+W^- \gamma$

¹⁸The second line of (3.3.150) also holds in the minimal model with $c_{\mathcal{T}_{2i}} \rightarrow c_{d_i}$ and $\omega_h^{q_i} = 0$.

coupling is unchanged with respect to the SM to all orders in v^2/M_{KK}^2 . Furthermore, the calculation of the W^+W^-Z vertex is greatly simplified by the following two observations. First, one has

$$\frac{2\pi}{L} \int_{\epsilon}^1 \frac{dt}{t} \chi_0^{(+)}(t) = \sqrt{2\pi} + \mathcal{O}\left(\frac{v^4}{M_{\text{KK}}^4}\right), \quad (3.3.151)$$

and second $((\vec{A}_0^a)_2 \chi_0^{(-)}(t))^2 = \mathcal{O}(v^4/M_{\text{KK}}^4)$. In combination, these two relations imply that the W^+W^-Z vertex does not receive corrections at $\mathcal{O}(v^2/M_{\text{KK}}^2)$ in the RS model, regardless of the specific gauge group. By the same line of reasoning, it is also readily seen that all quartic gauge-boson vertices first differ at order v^4/M_{KK}^4 from the corresponding SM expressions.

We express the W^+W^-h , ZZh vertices relative to their SM expressions. To expand the zero-mode profiles in M_V^2/M_{KK}^2 we use (3.3.80) evaluated at the IR brane and (3.3.82). We obtain

$$\kappa_V = \frac{g_{VV^*h}|_{\text{RS}}}{g_{VV^*h}|_{\text{SM}}} = 1 - \frac{M_V^2}{M_{\text{KK}}^2} \left(\frac{L}{c_V^2} - 1 + \frac{1}{2L} \right) + \mathcal{O}\left(\frac{v^4}{M_{\text{KK}}^4}\right). \quad (3.3.152)$$

In the case of the P_{LR} symmetry in the custodial model, one has $c_W^{-2} = 2$ and $c_Z^{-2} = 2c_w^2$, which implies that the leading absolute correction to $g_{W^+W^-h}$ and $g_{W^+W^-h}$ takes the form $-2M_V^2/M_{\text{KK}}^2 L$. For $M_{\text{KK}} = 2 \text{ TeV}$ ($M_{\text{KK}} = 3 \text{ TeV}$) these terms lead to a suppression of the WW^+h and ZZh couplings by about -10% (-5%) compared to the SM. In the minimal RS model, expression (3.3.152) holds with $c_V \rightarrow 1$, and consequently the corrections to the couplings of the Higgs boson to massive gauge bosons are smaller by about a factor of 2. Our finding that the couplings WW^+h and ZZh experience a reduction from their SM expectations confirms the model-independent statements made in [237].

3.3.8.4 Four Fermion Couplings

In this final section on the fundamentals of the RS coupling structure, we discuss four-fermion interactions induced by the exchange of the 5d propagator at low momentum using the results of section 3.3.7. The resulting effective Hamiltonian encodes the effects obtained by integrating out all new physics and is valid below the matching scale $\mu_{\text{KK}} = \mathcal{O}(M_{\text{KK}})$. We start with the case of charged currents with leptons and quarks. They are relevant for the extraction of the CKM matrix. Again, we extract a universal prefactor of the Wilson coefficients

$$\mathcal{H}_{\text{eff}}^{(W)} = \frac{2\pi\alpha}{s_w^2 M_W^2} \left[1 + \frac{M_W^2}{4M_{\text{KK}}^2} \left(1 - \frac{1}{L} \right) \right] \sum_l [\bar{u}_L \gamma^\mu \mathbf{V}_L d_L + \bar{u}_R \gamma^\mu \mathbf{V}_R d_R] (\bar{l}_L \gamma_\mu \nu_{lL}) + \text{h.c.} \quad (3.3.153)$$

The total prefactor defines the modified expression of G_F , as we discuss in section 4.2.2. The CKM matrices as extracted from experiment are given by

$$\begin{aligned} \mathbf{V}_L &= \mathbf{\Delta}^{+Q} + \sqrt{2} \boldsymbol{\varepsilon}^{+q} - \frac{M_W^2}{2M_{\text{KK}}^2} L \left(\bar{\mathbf{\Delta}}^{+Q} + \sqrt{2} \bar{\boldsymbol{\varepsilon}}^{+q} \right), \\ \mathbf{V}_R &= \sqrt{2} \mathbf{\Delta}^{+q} + \boldsymbol{\varepsilon}^{+Q} - \frac{M_W^2}{2M_{\text{KK}}^2} L \left(\sqrt{2} \bar{\mathbf{\Delta}}^{+q} + \bar{\boldsymbol{\varepsilon}}^{+Q} \right), \end{aligned} \quad (3.3.154)$$

with

$$\left\{ \begin{array}{l} \mathbf{\Delta}_{mn}^{+Q,q} \\ \bar{\mathbf{\Delta}}_{mn}^{+Q,q} \end{array} \right\} = \frac{2\pi}{L\epsilon} \int_{\epsilon}^1 dt \bar{a}_m^{U,u\dagger} C_m^{U,u}(t) \left\{ \begin{array}{l} \boldsymbol{\Omega}^{Q,q} \\ t^2 \bar{\boldsymbol{\Omega}}^{Q,q} \end{array} \right\} C_n^{D,d}(t) \bar{a}_n^{D,d}, \quad (3.3.155)$$

3. THEORETICAL CLASSIFICATION & EXAMPLES OF NEW PHYSICS

and $\epsilon_{mn}^{+Q,q}$, $\bar{\epsilon}_{mn}^{+Q,q}$ defined by analogous formulas with the even profiles $C_i^{Q,q}$ replaced by odd profiles $S_i^{Q,q}$. The involved kernel-matrices are given by $\Omega^Q = \bar{\Omega}^Q = \mathbf{1}$ and $\Omega^q = \bar{\Omega}^q = \mathbf{0}$ in the minimal RS model, and

$$\Omega^Q = \begin{pmatrix} \mathbf{1} \\ \mathbf{0} \end{pmatrix}, \quad \Omega^q = \begin{pmatrix} \mathbf{0} & \mathbf{0} \\ \mathbf{0} & \mathbf{1} \\ \mathbf{0} & \mathbf{0} \end{pmatrix}, \quad \bar{\Omega}^Q = \begin{pmatrix} \mathbf{1} \\ -\frac{g_R^2}{g_L^2} \mathbf{1} \end{pmatrix}, \quad \bar{\Omega}^q = \begin{pmatrix} \mathbf{0} & \mathbf{0} \\ \mathbf{0} & \mathbf{1} \\ -\frac{g_R^2}{g_L^2} \mathbf{1} & \mathbf{0} \end{pmatrix}, \quad (3.3.156)$$

in the model with custodial protection.

Notice that this definition of $\mathbf{V}_{L,R}$ includes the exchange of the entire tower of W bosons and their KK excitations and therefore differs from the definition of the CKM matrix employed in [1, 239], which is based on the $Wu_L^i d_L^j$ and $Wu_R^i d_R^j$ vertices.

Of particular interest for the discussion of constraints from FCNCs in section 4.1.2 are the effective dimension six operators arising from the tree-level exchange of KK photons and gluons and of Z bosons. Again, the relevant sums over KK modes are evaluated with the techniques presented in section 3.3.7. In the case of KK-photon exchange, we find that the effective Hamiltonian is given by

$$\mathcal{H}_{\text{eff}}^{(\gamma)} = \frac{2\pi\alpha}{M_{\text{KK}}^2} \sum_{f,f'} Q_f Q_{f'} \left\{ \frac{1}{2L} (\bar{f}\gamma^\mu f) (\bar{f}'\gamma_\mu f') - 2(\bar{f}_L\gamma^\mu \Delta'_F f_L + \bar{f}_R\gamma^\mu \Delta'_f f_R) (\bar{f}'\gamma_\mu f') \right. \\ \left. + 2L(\bar{f}_L\gamma^\mu \tilde{\Delta}'_F f_L + \bar{f}_R\gamma^\mu \tilde{\Delta}'_f f_R) \otimes (\bar{f}'_L\gamma_\mu \tilde{\Delta}'_{F'} f'_L + \bar{f}'_R\gamma_\mu \tilde{\Delta}'_{f'}) \right\}. \quad (3.3.157)$$

The matrices Δ'_A have been defined in (3.3.145). In addition, we encounter non-factorizable overlap integrals that are the relevant sources of $\Delta F = 2$ transitions

$$(\tilde{\Delta}'_F)_{mn} \otimes (\tilde{\Delta}'_{f'})_{m'n'} = \frac{2\pi^2}{L^2 \epsilon^2} \int_{\epsilon}^1 dt \int_{\epsilon}^1 dt' t_{<}^2 \\ \times \left[\bar{a}_m^{(F)\dagger} C_m^{(Q)}(\phi) C_n^{(Q)}(\phi) \bar{a}_n^{(F)} + \bar{a}_m^{(f)\dagger} S_m^{(f)}(\phi) S_n^{(f)}(\phi) \bar{a}_n^{(f)} \right] \\ \times \left[\bar{a}_{m'}^{(f')\dagger} C_{m'}^{(f')}(\phi') C_{n'}^{(f')}(\phi') \bar{a}_{n'}^{(f')} + \bar{a}_{m'}^{(F)\dagger} S_{m'}^{(Q)}(\phi') S_{n'}^{(Q)}(\phi') \bar{a}_{n'}^{(F')} \right]. \quad (3.3.158)$$

The result (3.3.157) is exact, *i.e.* no expansion in powers of v^2/M_{KK}^2 has been performed. The effective interactions arising from KK-gluon exchange have an analogous structure. We only need to restrict the sum over fermions in (3.3.157) to quarks and replace $\alpha Q_f Q_{f'}$ by $\alpha_s T^a \otimes T^a$, where the color matrices t^a must be inserted inside the quark bilinears. The expressions for the flavor matrices defined in (3.3.158) are tensor products, which a priori do not factorize in the form of simple matrix products. In the ZMA, we obtain [229]

$$(\tilde{\Delta}'_F)_{mn} \otimes (\tilde{\Delta}'_{f'})_{m'n'} \approx \sum_{i,j} (U_f^\dagger)_{mi} (U_f)_{in} (\tilde{\Delta}'_{Ff})_{ij} (W_f^\dagger)_{m'j} (W_f)_{j'n'}, \quad (3.3.159) \\ (\tilde{\Delta}'_{Ff})_{ij} = \frac{F^2(c_{F_i})}{3 + 2c_{F_i}} \frac{3 + c_{F_i} + c_{f_j}}{2(2 + c_{F_i} + c_{f_j})} \frac{F^2(c_{f_j})}{3 + 2c_{f_j}}.$$

Analogous expressions hold for the remaining combinations of indices F and f . Using the fact that all c_i parameters except c_{u_3} are very close to $-1/2$, it is a reasonable approximation

to replace $(3 + c_{F_i} + c_{f_j})/(2 + c_{F_i} + c_{f_j})$ by 2, in which case we obtain rough approximation

$$\tilde{\Delta}_A \otimes \tilde{\Delta}_B \approx \Delta_A \Delta_B, \quad (3.3.160)$$

In the same approximation, there is no need to distinguish between the Δ'_A and Δ_A matrices. We found that this approximate factorization receives significant corrections in setups where the volume of the extra dimension is reduced to $L \lesssim 10$ [229], and (3.3.159) obtains relevant subleading contributions if the down-type singlet bulk masses c_{d_i} are aligned [3]. We discuss these cases closer in section 4.1.2.

The interactions arising from the exchange of the Z boson and its KK excitations have a richer structure. We have given the full and exact effective Hamiltonian in [1]. Here, we only repeat the contributions at $\mathcal{O}(v^2/M_{\text{KK}}^2)$ which renders the result compact

$$\begin{aligned} \mathcal{H}_{\text{eff}}^{(Z)} = & \frac{4\pi\alpha}{s_w^2 c_w^2 m_Z^2} \left[1 + \frac{m_Z^2}{2M_{\text{KK}}^2} \left(1 - \frac{1}{2L} \right) \right] J_Z^\mu J_{Z\mu} \\ & - \frac{8\pi\alpha}{s_w^2 c_w^2 m_Z^2} \sum_f \left[\bar{f}_L \gamma^\mu T_3^f \delta_F f_L - \bar{f}_R \gamma^\mu T_3^f \delta_f f_R \right] J_{Z\mu} \\ & - \frac{4\pi\alpha L}{s_w^2 c_w^2 M_{\text{KK}}^2} \sum_f \omega_Z^f \left[\left(T_3^f - s_w^2 Q_f \right) \bar{f}_L \gamma^\mu \Delta_F f_L - s_w^2 Q_f \bar{f}_R \gamma^\mu \Delta_f f_R \right] J_{Z\mu} \\ & + \frac{4\pi\alpha L}{s_w^2 c_w^2 M_{\text{KK}}^2} \sum_{f,f'} \Omega_Z^{ff'} \left[\left(T_3^f - s_w^2 Q_f \right) \bar{f}_L \gamma^\mu \tilde{\Delta}_F f_L - s_w^2 Q_f \bar{f}_R \gamma^\mu \tilde{\Delta}_f f_R \right] \\ & \quad \otimes \left[\left(T_3^{f'} - s_w^2 Q_{f'} \right) \bar{f}'_L \gamma^\mu \tilde{\Delta}_{F'} f'_L - s_w^2 Q_{f'} \bar{f}'_R \gamma^\mu \tilde{\Delta}_{f'} f'_R \right]. \end{aligned} \quad (3.3.161)$$

Here, J_Z^μ is the familiar SM expression for the neutral current

$$J_Z^\mu \equiv \sum_f \left[\left(T_3^f - s_w^2 Q_f \right) \bar{f}_L \gamma^\mu f_L - s_w^2 Q_f \bar{f}_R \gamma^\mu f_R \right]. \quad (3.3.162)$$

The differences between the minimal and custodial RS model are again encoded in the factors ω_Z^f as defined in (3.3.143) and another universal factor for the non-factorizable overlap integrals given by

$$\Omega_Z^{ff'} = 1 + \frac{g_{Z'}^2 Q_{Z'}^f Q_{Z'}^{f'}}{g_Z^2 Q_Z^f Q_Z^{f'}} = 1 + \frac{c_w^2 (1 - \omega_Z^f) (1 - \omega_Z^{f'})}{1 - \left(1 + \frac{g_L^2}{g_R^2} \right) s_w^2}. \quad (3.3.163)$$

In order to abbreviate the notation in (3.3.161), the factors ω_Z^f and $\Omega_Z^{ff'}$ are meant to act as operators on the fermion bilinears in the sense that f and f' depend on the chiralities of the corresponding fermions. Remark the reversed sign in (3.3.163) and the absent factor of s_Z/c_Z compared to (3.3.143), which directly come from the corresponding factors of the $t_{<}^2$ and t^2 terms in (3.3.102). The numerical values

$$\Omega_Z^{d_L d_L} = 2.5, \quad \Omega_Z^{d_L d_R} = -10.9, \quad \Omega_Z^{d_R d_R} = 94.6, \quad (3.3.164)$$

are necessary to explain differences in down type $\Delta F = 2$ FCNCs in the different fermion embeddings. To this end, one needs of course to compare the overall size of the Z -boson and KK-gluon contributions to the latter processes. We will review this more closely in section 4.1.2.

Chapter 4

Aspects of Precision Physics

4.1 Flavor Physics

It is well known that precision flavor observables put strong constraints on generic new physics. In most models, the constraints are complementary to bounds derived from collider searches for direct production of resonances and to astrophysical bounds. This is due to the inherent dependence of flavor off-diagonal observables on the Yukawa sector and its deviations from the SM prediction. Hence, while models of new physics typically predict new particles, whose existence will be scrutinized by LHC experiments, it is important to examine their effects on precision flavor observables as well, in order to check the consistency of the models.

The objective of our discussion is twofold. First, we shall study amplitudes necessary for flavor physics on a conceptual level for any theory with perturbatively unitary high energy behavior. Secondly, we shall also present a numerical analysis of bounds and correlations from flavor observables in a specific example that does not fall into the latter class, the RS model.

In the conceptual part, our intention can be summarized as follows: A repeatedly emerging task is the calculation of amplitudes for fermion transitions between different generations, induced by a massive neutral gauge boson at one-loop — the so-called penguin amplitude. An example is the FCNC $s \rightarrow d$ transition with the emission of a virtual Z boson, leading to processes like the rare $K \rightarrow \pi\nu\bar{\nu}$ decays. Just like the SM, many models of new physics generate this transition first at the one-loop level. This property drastically improves the potential agreement of a model with experimental flavor constraints, especially from $\Delta S = 2$ observables. In the absence of a tree-level coupling for this process, we expect UV-finiteness of the penguin amplitude. However, the practical verification in models with many new gauge and Goldstone bosons in a renormalizable gauge can be tedious. We perform this calculation for any spontaneously broken gauge theory, using the generic Lagrangian supplemented with the implied STIs as presented in section 3.1. We demonstrate and advocate the practical use of the STIs to perform renormalization and simplifications of this generic process. We give the full template result for the finite Z penguin and also for box-type diagrams, thereby specializing to down-type quarks for notational convenience. Yet, the result can also be applied to up-type and lepton-flavor-violating processes. The generic result is useful, since the flavor amplitudes for any model of new physics can now be quickly implemented by

the simple specification of its couplings of physical particles.¹ We check that the full result indeed reproduces the well known SM-result and the result of the LHT model introduced in section 3.2. For the latter model we provide a deeper understanding why the Z penguin turns out to be free of UV-sensitivity and investigate whether this is due to the partly gauged structure of the model. As a byproduct, we also simplify the result for the Z penguin and boxes considerably as compared to the literature.

In the numerical analysis, we study the bounds and correlations in the RS model. We focus on kaon mixing and direct CP violation in $K \rightarrow \pi\pi$, since measurements of these processes provide the strongest bounds on the scale of the model. The RS model possesses tree-level FCNCs but explains the smallness of the corresponding observables by the RS-GIM mechanism (see section 3.3.8.2). It is well known that this suppression is typically insufficient to explain the smallness of observed FCNCs. We find that the dependence on the Yukawa sector introduces a significant spread in the distribution of the RS predictions. We quantitatively assess the implications on the scale bounds and find a strong dependence, even in the case of non-fine-tuned RS scenarios. The bounds inferred from flavor processes thus depend strongly on the required amount of viable parameter space. We derive new bounds from the lower edge of these distributions, which are more robust than the typical bounds often quoted in the literature. This makes the scale bounds more comparable to bounds from electroweak precision observables. We also discuss two scenarios that are specifically designed to alleviate the flavor bounds, a model with active flavor-symmetry $SU(3)_d$ for singlet down-type quarks and a model with a reduced volume of the extra dimension.

Beyond the scale bounds, we find that the restriction of the Yukawa structure also leads to complementary predictions, *i.e.* correlations between different flavor observables. To this end, we study leptonic and semileptonic kaon decays. The phenomenological discussion is rounded off with a discussion of CKM non-unitarity and predictions for the rare B decays into two muons, where measurements recently start to probe the RS parameter space.

4.1.1 Structure of $\Delta F = 1$ Processes in Perturbative Models

4.1.1.1 Renormalization of the Generic Z Penguin

In the following we present the derivation of the generic result for the Z penguin. To this end the renormalization by using the STIs of section 3.1.2 is described in some detail. We give the results in (4.1.9) – (4.1.10). It is self-contained and can be used as it stands. The reader who is interested in the result only might skip this discussion, which serves to clarify the structure of the result and shows how our method can be extended to include tree-level $d_j \rightarrow d_i$ transitions.

Generally, in order to determine the Wilson coefficients of an effective theory, it is sufficient to match the effective actions in both the full and the effective theory. This entails that we have to compute one-light-particle irreducible diagrams only. In particular, diagrams with self-energy insertions on external light particle legs should not be included. However, in certain models containing tree-level transitions between down-type quarks of the same generation, diagrams with a heavy particle reducible line exist on the full theory side of the matching. Typically, this reducible line might be due to a down-type vector-like fermion.

¹ A potential application is to link the template to the output of a computer algebra package such as FeynRules [240], creating an automated yet simple tool for the generation of analytic flavor results without the need to invoke a full amplitude generator.

An example of this is found in models where the flavor symmetry $SU(3)^3$ is considered non-accidental and gauged [241, 242], thereby extending the idea of minimal flavor violation (MFV) and explaining quark-hierarchies with a see-saw mechanism. This concept received renewed interest in the last years as a consequence of the persistent failure to find new physics in flavor violating transitions. Since the flavor group is anomalous, new heavy fermions have to be added to the theory. Another example are effective models that extend the SM by a vector-like fermionic sector in order to explain the hierarchy of SM Yukawa couplings through small mixing angles between the SM and heavy fermions [56, 243, 244]. Such a setup can be used to effectively parametrize the fermionic contributions that arise in the RS model of section 3.3, where these effects are, however, subleading in all relevant cases. Furthermore, such models generically induce flavor-violating Z couplings to light quarks, which we exclude from the discussion here.

The fermion one-loop self-energies in the full theory lead to mixing among the fermions beyond tree level. We perform an off-diagonal field renormalization for both heavy and light fermions, with finite terms chosen to restore diagonal and canonically normalized kinetic and mass terms [245]. In consequence, diagrams of the form shown in figure 4.1 are exactly canceled by corresponding counterterm diagrams. However, we have to carefully treat the

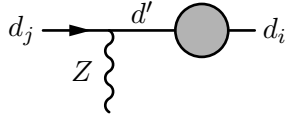


Figure 4.1: One-heavy-particle reducible contribution to the Z penguin.

renormalization constants that the self-energy sub-diagram in figure 4.1 induces in the vertex renormalization.

We first calculate the one-loop corrections to the renormalized fermion two-point function. They can be written as

$$\delta\Gamma_{\sigma}^{f_j f_i} = \left[\left(\Sigma_{V, \bar{f}_i f_j}^{\psi, \sigma} + \delta Z_{H, \bar{f}_i f_j}^{\psi, \sigma} \right) \not{p} + \Sigma_{S, \bar{f}_i f_j}^{\psi, \sigma} - \frac{1}{2} \left(m_{f_i} \delta Z_{\bar{f}_i f_j}^{\psi, \sigma} + \delta Z_{\bar{f}_i f_j}^{\psi, \bar{\sigma} \dagger} m_{f_j} \right) - \delta_{ij} \delta m_{f_i} \right] P_{\sigma}, \quad (4.1.1)$$

where the fermion-field-renormalization constant is written as a sum of a Hermitian and an anti-Hermitian part. δm_{f_i} is an additive mass renormalization. The divergent parts of the Hermitian field-renormalization constants have the simple structure

$$\begin{aligned} \delta Z_{H, \bar{f}_i f_j}^{\psi, \sigma} \Big|_{\text{div}} &\equiv \frac{1}{2} \left(\delta Z_{\bar{f}_i f_j}^{\psi, \sigma} + \delta Z_{\bar{f}_i f_j}^{\psi, \sigma \dagger} \right) \Big|_{\text{div}} = -\Sigma_{V, \bar{f}_i f_j}^{\psi, \sigma} \Big|_{\text{div}} = -\frac{\Delta}{16\pi^2} \left[\frac{1}{2} \sum_{s', f'} y_{s' \bar{f}_i f'}^{\bar{\sigma}} y_{\bar{s}' f' f_j}^{\sigma} \right. \\ &\quad \left. + \sum_{v', f'} \left\{ g_{v' \bar{f}_i f'}^{\sigma} g_{\bar{v}' f' f_j}^{\sigma} + \frac{m_{f'}^2}{2m_{v'}^2} \left(g_{v' \bar{f}_i f'}^{\sigma} - \frac{m_{f_i}}{m_{f'}} g_{v' \bar{f}_i f'}^{\bar{\sigma}} \right) \left(g_{\bar{v}' f' f_j}^{\sigma} - \frac{m_{f_j}}{m_{f'}} g_{\bar{v}' f' f_j}^{\bar{\sigma}} \right) \right\} \right]. \end{aligned} \quad (4.1.2)$$

Here $\Delta = 1/\varepsilon - \gamma_E + \ln(4\pi)$ includes also the finite $\overline{\text{MS}}$ subtractions, $d = 4 - 2\varepsilon$ is the space-time dimension in dimensional regularization, and γ_E is Euler's constant. The finite parts of the field-renormalization constants for $i \neq j$ are given by

$$\begin{aligned} \delta Z_{\bar{f}_i f_j}^{\psi, \sigma} \Big|_{\text{fin}} &= \frac{1}{m_{f_i}^2 - m_{f_j}^2} \left(m_{f_j}^2 \Sigma_{V, \bar{f}_i f_j}^{\psi, \sigma} + m_{f_i} m_{f_j} \Sigma_{V, \bar{f}_i f_j}^{\psi, \bar{\sigma}} + m_{f_i} \Sigma_{S, \bar{f}_i f_j}^{\psi, \sigma} + m_{f_j} \Sigma_{S, \bar{f}_i f_j}^{\psi, \bar{\sigma}} \right) \Big|_{\text{fin}}, \quad (4.1.3) \\ \delta Z_{\bar{f}_i f_j}^{\psi, \sigma \dagger} \Big|_{\text{fin}} &= -\frac{1}{m_{f_i}^2 - m_{f_j}^2} \left(m_{f_i}^2 \Sigma_{V, \bar{f}_i f_j}^{\psi, \sigma} + m_{f_i} m_{f_j} \Sigma_{V, \bar{f}_i f_j}^{\psi, \bar{\sigma}} + m_{f_i} \Sigma_{S, \bar{f}_i f_j}^{\psi, \sigma} + m_{f_j} \Sigma_{S, \bar{f}_i f_j}^{\psi, \bar{\sigma}} \right) \Big|_{\text{fin}}. \end{aligned}$$

They enter our generic result after having been expanded in small mass ratios. The diagonal field-renormalization constants are not necessary in our case. For a full generalization to tree-level $d_j \rightarrow d_i$ transitions, or an analogous treatment of charged current couplings, one would have to fix these constants by renormalization conditions. The best practice here depends on the context and we will not go into further details. As a non-trivial example we mention the renormalization of the SM CKM matrix in non-minimal schemes that preserve decoupling, where it turns out that STIs allow to renormalize the CKM-matrix gauge-independently but restrict the diagonal field renormalization constants [246].

In the following section we present the general result for models (or parts thereof) where tree-level FCNCs for the $d_j \rightarrow d_i$ transition are absent; in this case the contributions of the vertex and gauge-boson field-renormalization constants vanish. Here, we will show that all divergences in our generic result completely cancel against the divergent terms in the field rotation, without the necessity of additional counterterms. This is due to the absence of tree-level contributions to the Z penguin, to which these counterterms would be proportional. In order to make this cancellation manifest, it is necessary to use the consequences of tree-level perturbative unitarity derived in section 3.1.1 in form of the STIs. They yield relations between various couplings, and allow for the automatic inclusion of the effects of the would-be Goldstone bosons. This step is independent of the specification of a model and can be applied without detailed knowledge about the sector responsible for the spontaneous symmetry breaking. Note that the following treatment is valid also in the general case of non-flavor-diagonal tree-level couplings.

We are now ready to study the general expression for the one-loop contributions to the renormalized $V_{v_a} \bar{\psi}_{f_j} \psi_{f_k}$ three-point function. They are given by

$$\begin{aligned} \delta\Gamma_{\mu\sigma}^{f_j f_i v_a} = & \Gamma_{\mu\sigma}^{f_j f_i v_a, (1)} + \left[\delta Z_{v_a \bar{f}_i f_j}^{g, \sigma} + \frac{1}{2} \sum_{f'} \left(g_{v_a \bar{f}_i f'}^{\sigma} \delta Z_{\bar{f}' f_j}^{\psi, \sigma} + \delta Z_{\bar{f}_i f'}^{\psi, \sigma \dagger} g_{v_a \bar{f}' f_j}^{\sigma} \right) \right. \\ & \left. + \frac{1}{2} \sum_{v'} \delta Z_{v_a v'}^V g_{v' \bar{f}_i f_j}^{\sigma} \right] P_{\sigma}. \end{aligned} \quad (4.1.4)$$

Here, $\Gamma_{\mu\sigma}^{v_a f_j f_i, (1)}$ denotes the sum of all contributing one-loop diagrams, and the rest are the vertex, fermion field, and gauge-boson field-renormalization constants, respectively. We use the STIs (3.1.19), (3.1.28) and (3.1.29) to show that the fermion-field-renormalization constants are sufficient to cancel all divergences in (4.1.4). In principle, the procedure is straightforward. It is instructive to start with considering the divergence of the diagram that contains three internal particles of different spin, one scalar s' , one fermion f' , and one vector v' , and is thus proportional to the couplings $g_{v_a v' s'}^{\sigma} g_{v' \bar{f}_j f'}^{\sigma} g_{s' \bar{f}' f_i}^{\sigma}$. It turns out that the sum over all such possible diagrams can be rewritten by using (3.1.28) and (3.1.29). In figure 4.2 we illustrate how the sum rules have to be combined with couplings, which are separated by the dotted cut line, in order to match the divergence of one of the mixed diagrams. After subtracting the sum of these two contributions from the total divergence and inserting the explicit expressions of the fermion-field-renormalization constants (4.1.2), the reformulated expression can be grouped into parts that involve either internal scalars or internal vectors. In fact, the contributions with two internal scalars are already finite now. The remaining contributions are treated analogously. *E.g.* from the diagram with two internal vectors, we infer that (3.1.19) must be combined with $g_{v_a v' v''}$ and summed over v' and v'' in order to reformulate the remaining part of the divergence with two internal vectors. Finally, the

parts of which read explicitly

$$\begin{aligned}
 \delta Z_{A,\bar{f}_i f_j}^{\psi,\sigma} &= \begin{cases} \frac{1}{2m_{f_i}} \left[\Sigma_{S,\bar{f}_i f_i}^{\psi,\sigma} - \Sigma_{S,\bar{f}_i f_i}^{\psi,\bar{\sigma}} \right]_{\text{div}} & , j = k \\ \frac{2}{m_{f_i}^2 - m_{f_j}^2} \left[\frac{m_{f_i}^2 + m_{f_j}^2}{2} \Sigma_{V,\bar{f}_i f_j}^{\psi,\sigma} + m_{f_i} m_{f_j} \Sigma_{V,\bar{f}_i f_j}^{\psi,\bar{\sigma}} + m_{f_i} \Sigma_{S,\bar{f}_i f_j}^{\psi,\sigma} + \Sigma_{S,\bar{f}_i f_j}^{\psi,\bar{\sigma}} m_{f_j} \right]_{\text{div}} & , j \neq k \end{cases} \\
 &= \frac{\Delta}{16\pi^2} \left(\sum_{s',f'} \left\{ \frac{1-\delta_{ij}}{m_{f_i}^2 - m_{f_j}^2} \left(\frac{m_{f_i}^2 + m_{f_j}^2}{2} y_{s'\bar{f}_i f'}^{\bar{\sigma}} y_{s'\bar{f}' f_j}^{\sigma} + m_{f_i} m_{f_j} y_{s'\bar{f}_i f'}^{\sigma} y_{s'\bar{f}' f_j}^{\bar{\sigma}} \right) \right. \right. \\
 &\quad \left. \left. + 2m_{f'} \left(m_{f_i} y_{s'\bar{f}_i f'}^{\sigma} y_{s'\bar{f}' f_j}^{\bar{\sigma}} + m_{f_j} y_{s'\bar{f}_i f'}^{\bar{\sigma}} y_{s'\bar{f}' f_j}^{\sigma} \right) \right. \right. \\
 &\quad \left. \left. + \delta_{ij} \frac{m_{f'}}{2m_{f_i}} \left(y_{s'\bar{f}_i f'}^{\sigma} y_{s'\bar{f}' f_i}^{\bar{\sigma}} - y_{s'\bar{f}_i f'}^{\bar{\sigma}} y_{s'\bar{f}' f_i}^{\sigma} \right) \right\} \right. \\
 &\quad \left. + \sum_{v',f'} \left\{ \frac{1-\delta_{ij}}{m_{f_i}^2 - m_{f_j}^2} \left(g_{v'\bar{f}_i f'}^{\sigma} g_{v'\bar{f}' f_j}^{\bar{\sigma}} \left((m_{f_i}^2 + m_{f_j}^2) \left(1 - \frac{3m_{f'}^2}{2m_{v'}^2} \right) + \frac{m_{f_i}^2 m_{f_j}^2}{m_{v'}^2} \right) \right. \right. \right. \\
 &\quad \left. \left. + g_{v'\bar{f}_i f'}^{\bar{\sigma}} g_{v'\bar{f}' f_j}^{\sigma} m_{f_i} m_{f_j} \left(2 + \frac{m_{f_i}^2 + m_{f_j}^2 - 6m_{f'}^2}{2m_{v'}^2} \right) \right. \right. \\
 &\quad \left. \left. + g_{v'\bar{f}_i f'}^{\sigma} g_{v'\bar{f}' f_j}^{\bar{\sigma}} m_{f'} m_{f_j} \left(-8 + \frac{m_{f_i}^2 - m_{f_j}^2 + 4m_{f'}^2}{2m_{v'}^2} \right) \right. \right. \\
 &\quad \left. \left. + g_{v'\bar{f}_i f'}^{\bar{\sigma}} g_{v'\bar{f}' f_j}^{\sigma} m_{f_i} m_{f'} \left(-8 + \frac{m_{f_j}^2 - m_{f_i}^2 + 4m_{f'}^2}{2m_{v'}^2} \right) \right. \right. \\
 &\quad \left. \left. + \delta_{ij} \frac{m_{f'}}{m_{f_i}} \left(2 + \frac{m_{f_i}^2 - m_{f'}^2}{2m_{v'}^2} \right) \left(g_{v'\bar{f}_i f'}^{\sigma} g_{v'\bar{f}' f_i}^{\bar{\sigma}} - g_{v'\bar{f}_i f'}^{\bar{\sigma}} g_{v'\bar{f}' f_i}^{\sigma} \right) \right\} \right). \tag{4.1.7}
 \end{aligned}$$

The terms in the second line of (4.1.6) vanish after an explicit Z -boson field renormalization. To see this, one would have to use the STIs for ghost couplings and additional sum rules which we included in the appendix (see (A.1.2)). In fact, one can read off the result for the Z -boson field renormalization from the fact that the second line in (4.1.6) has to vanish. The finite part of the renormalization will lead to a shift which is universal for all flavors and can be absorbed in the corresponding gauge-coupling constant.

4.1.1.2 Result for the Generic Z Penguin and Box Diagrams

We present our result for the renormalized Z penguin in the form of an effective vertex, in the spirit of [248]. The penguin function $C_{d_j d_i Z}^{\sigma}$ is defined in terms of the amputated vertex function as

$$\Gamma_{\mu\sigma}^{d_j d_i Z} = \gamma_{\mu} P_{\sigma} \frac{G_F}{\sqrt{2}} \frac{e}{\pi^2} M_Z^2 \frac{c_w}{s_w} C_{d_j d_i Z}^{\sigma}, \tag{4.1.8}$$

and depends on all masses which appear. $\sigma = L, R$ stands for the chiral projection. Setting the external momenta and light fermion masses to zero in our results, we obtain in the

't Hooft-Feynman gauge

$$\begin{aligned}
 \Gamma_{\mu\sigma}^{d_j d_i Z} = & \frac{\gamma_\mu P_\sigma}{(4\pi)^2} \left\{ \right. \\
 & \sum_{f_1 v_1} \sum_{f_2 \notin \text{SM}} \left[\kappa_{f_1 f_2 v_1}^\sigma B_0(m_{f_1}, m_{v_1}) + \kappa'_{f_1 f_2 v_1}{}^\sigma \right] + \sum_{f_1 s_1} \sum_{f_2 \notin \text{SM}} \kappa_{f_1 f_2 s_1}^\sigma B_0(m_{f_1}, m_{s_1}) \\
 & + \sum_{f_1 f_2 v_1} \left[\tilde{k}_{f_1 f_2 v_1}^\sigma \left(\tilde{C}_0(m_{f_1}, m_{f_2}, M_{v_1}) - \frac{1}{2} \right) + k_{f_1 f_2 v_1}^\sigma C_0(m_{f_1}, m_{f_2}, M_{v_1}) + k'_{f_1 f_2 v_1}{}^\sigma \right] \\
 & + \sum_{f_1 v_1 v_2} \left[\tilde{k}_{f_1 v_1 v_2}^\sigma \left(\tilde{C}_0(m_{f_1}, M_{v_1}, M_{v_2}) + \frac{1}{2} \right) + k_{f_1 v_1 v_2}^\sigma C_0(m_{f_1}, M_{v_1}, M_{v_2}) + k'_{f_1 v_1 v_2}{}^\sigma \right] \quad (4.1.9) \\
 & + \sum_{f_1 v_1 s_1} \left[\tilde{k}_{f_1 v_1 s_1}^\sigma \left(\tilde{C}_0(M_{s_1}, m_{f_1}, M_{v_1}) + \frac{1}{2} \right) + k_{f_1 v_1 s_1}^\sigma C_0(M_{s_1}, m_{f_1}, M_{v_1}) \right] \\
 & + \sum_{f_1 f_2 s_1} \left[\tilde{k}_{f_1 f_2 s_1}^\sigma \left(\tilde{C}_0(M_{s_1}, m_{f_1}, m_{f_2}) - \frac{1}{2} \right) + k_{f_1 f_2 s_1}^\sigma C_0(M_{s_1}, m_{f_1}, m_{f_2}) \right] \\
 & \left. + \sum_{f_1 s_1 s_2} \tilde{k}_{f_1 s_1 s_2}^\sigma \left(\tilde{C}_0(M_{s_1}, M_{s_2}, m_{f_1}) + \frac{1}{2} \right) \right\},
 \end{aligned}$$

where all indices run over all particles contained in the theory, with the exception of f_2 in the second line. This index only runs over heavy, *i.e.* non-SM, fermions. The corresponding contributions originate in the finite wave-function renormalizations of heavy fermions, which are necessary to achieve a canonical mass term at one loop. They are only present if Z couplings between light and heavy fermions exist at tree-level. The loop functions used in (4.1.9) and below are summarized in appendix B.1. There, one can skip the divergence in the expressions for the loop functions, since we have explicitly shown in the last chapter that they vanish due to the STIs. We find for the coefficients of (4.1.9)

$$\begin{aligned}
 \kappa_{f_1 f_2 v_1}^\sigma &= -\frac{m_{f_1}}{m_{f_2}} \left(g_{Z\bar{d}_i f_2}^\sigma \left[\left(4 - \frac{m_{f_1}^2}{M_{v_1}^2} \right) g_{v_1 \bar{f}_2 f_1}^\sigma + \frac{m_{f_1} m_{f_2}}{M_{v_1}^2} g_{v_1 \bar{f}_2 f_1}^\sigma \right] g_{v_1 \bar{f}_1 d_j}^\sigma \right. \\
 & \quad \left. + g_{\bar{v}_1 \bar{d}_i f_1}^\sigma \left[\left(4 - \frac{m_{f_1}^2}{M_{v_1}^2} \right) g_{v_1 \bar{f}_1 f_2}^\sigma + \frac{m_{f_1} m_{f_2}}{M_{v_1}^2} g_{v_1 \bar{f}_1 f_2}^\sigma \right] g_{Z \bar{f}_2 d_j}^\sigma \right), \quad (4.1.10) \\
 \kappa'_{f_1 f_2 v_1}{}^\sigma &= \frac{2m_{f_1}}{m_{f_2}} \left(g_{Z\bar{d}_i f_2}^\sigma g_{v_1 \bar{f}_2 f_1}^\sigma g_{\bar{v}_1 \bar{f}_1 d_j}^\sigma + g_{v_1 \bar{d}_i f_1}^\sigma g_{\bar{v}_1 \bar{f}_1 f_2}^\sigma g_{Z \bar{f}_2 d_j}^\sigma \right), \\
 \kappa_{f_1 f_2 s_1}^\sigma &= \frac{m_{f_1}}{m_{f_2}} \left(g_{Z\bar{d}_i f_2}^\sigma y_{s_1 \bar{f}_2 f_1}^\sigma y_{\bar{s}_1 \bar{f}_1 d_j}^\sigma + y_{\bar{s}_1 \bar{d}_i f_1}^\sigma y_{\bar{s}_1 \bar{f}_1 f_2}^\sigma g_{Z \bar{f}_2 d_j}^\sigma \right), \\
 \tilde{k}_{f_1 f_2 v_1}^\sigma &= \left(g_{Z \bar{f}_2 f_1}^\sigma + \frac{m_{f_1} m_{f_2}}{2M_{v_1}^2} g_{Z \bar{f}_2 f_1}^\sigma \right) g_{v_1 \bar{d}_i f_2}^\sigma g_{v_1 \bar{f}_1 d_j}^\sigma, \\
 k_{f_1 f_2 v_1}^\sigma &= -\frac{m_{f_1} m_{f_2}}{M_{v_1}^2} \left(m_{f_1} m_{f_2} g_{Z \bar{f}_2 f_1}^\sigma + 2M_{v_1}^2 g_{Z \bar{f}_2 f_1}^\sigma \right) g_{v_1 \bar{d}_i f_2}^\sigma g_{v_1 \bar{f}_1 d_j}^\sigma, \\
 k'_{f_1 f_2 v_1}{}^\sigma &= -g_{Z \bar{f}_2 f_1}^\sigma g_{\bar{v}_1 \bar{d}_i f_2}^\sigma g_{v_1 \bar{f}_1 d_j}^\sigma + \frac{1}{2} \left(g_{Z \bar{d}_i d_i}^\sigma g_{v_1 \bar{d}_i f_1}^\sigma g_{\bar{v}_1 \bar{f}_1 d_j}^\sigma + g_{\bar{v}_1 \bar{d}_i f_1}^\sigma g_{v_1 \bar{f}_1 d_j}^\sigma g_{Z \bar{d}_j d_j}^\sigma \right) \delta_{f_1 f_2},
 \end{aligned}$$

$$\begin{aligned}
 \tilde{k}_{f_1 v_1 v_2}^\sigma &= -\frac{m_{f_1}^2 (M_{v_1}^2 + M_{v_2}^2 - M_Z^2) + 12M_{v_1}^2 M_{v_2}^2}{4M_{v_1}^2 M_{v_2}^2} g_{Z v_1 \bar{v}_2} g_{\bar{v}_1 \bar{d}_i f_1}^\sigma g_{v_2 \bar{f}_1 d_j}^\sigma \\
 &\quad - \frac{1}{2} \left(1 + \frac{m_{f_1}^2}{2M_{v_1}^2} \right) \left(g_{Z \bar{d}_i d_i}^\sigma g_{v_1 \bar{d}_i f_1}^\sigma g_{\bar{v}_1 \bar{f}_1 d_j}^\sigma + g_{\bar{v}_1 \bar{d}_i f_1}^\sigma g_{v_1 \bar{f}_1 d_j}^\sigma g_{Z \bar{d}_j d_j}^\sigma \right) \delta_{v_1 v_2}, \\
 k_{f_1 v_1 v_2}^\sigma &= \frac{m_{f_1}^2 (M_{v_1}^4 + M_{v_2}^4 - M_Z^2 (M_{v_1}^2 + M_{v_2}^2))}{M_{v_1}^2 M_{v_2}^2} g_{Z v_1 \bar{v}_2} g_{\bar{v}_1 \bar{d}_i f_1}^\sigma g_{v_2 \bar{f}_1 d_j}^\sigma, \\
 k'_{f_1 v_1 v_2} &= 2 g_{Z v_1 \bar{v}_2} g_{\bar{v}_1 \bar{d}_i f_1}^\sigma g_{v_2 \bar{f}_1 d_j}^\sigma, \\
 \tilde{k}_{f_1 v_1 s_1}^\sigma &= -\frac{k_{f_1 v_1 s_1}^\sigma}{4M_{v_1}^2}, \quad k_{f_1 v_1 s_1}^\sigma = m_{f_1} \left(g_{Z \bar{v}_1 s_1} y_{\bar{s}_1 \bar{d}_i f_1}^\sigma g_{v_1 \bar{f}_1 d_j}^\sigma + g_{Z v_1 \bar{s}_1} y_{s_1 \bar{f}_1 d_j}^\sigma g_{\bar{v}_1 \bar{d}_i f_1}^\sigma \right), \\
 \tilde{k}_{f_1 f_2 s_1}^\sigma &= \frac{1}{2} g_{Z \bar{f}_2 f_1}^\sigma y_{\bar{s}_1 \bar{d}_i f_2}^\sigma y_{s_1 \bar{f}_1 d_j}^\sigma, \quad k_{f_1 f_2 s_1}^\sigma = -m_{f_1} m_{f_2} g_{Z \bar{f}_2 f_1}^\sigma y_{\bar{s}_1 \bar{d}_i f_2}^\sigma y_{s_1 \bar{f}_1 d_j}^\sigma, \\
 \tilde{k}_{f_1 s_1 s_2}^\sigma &= \frac{1}{2} g_{Z \bar{s}_1 s_2} y_{\bar{s}_2 \bar{d}_i f_1}^\sigma y_{s_1 \bar{f}_1 d_j}^\sigma - \frac{1}{4} \left(g_{Z \bar{d}_i d_i}^\sigma y_{s_1 \bar{d}_i f_1}^\sigma y_{\bar{s}_1 \bar{f}_1 d_j}^\sigma + y_{s_1 \bar{d}_i f_1}^\sigma y_{\bar{s}_1 \bar{f}_1 d_j}^\sigma g_{Z \bar{d}_j d_j}^\sigma \right) \delta_{s_1 s_2}.
 \end{aligned}$$

We have suppressed the color indices. Recall that the scalar-index sums in (4.1.9) run only over physical fields; contributions of would-be Goldstone bosons have already been taken into account implicitly in these equations. The dependence on the external light-fermion masses has been neglected in (4.1.10). For the coefficients \tilde{k} , k , and k' , it can easily be reconstructed by replacing all instances of $g_{v \bar{f} d_j}^\sigma m_f/M_v$ by $(m_f g_{v \bar{f} d_j}^\sigma - m_{d_j} g_{v \bar{f} d_j}^\sigma)/M_v$ and similarly $g_{v \bar{d}_i f}^\sigma m_f/M_v$ by $(m_f g_{v \bar{d}_i f}^\sigma - m_{d_i} g_{v \bar{d}_i f}^\sigma)/M_v$. Neglecting light-fermion masses also implies that the off-diagonal field renormalizations (4.1.3) entering (4.1.10) proportional to the flavor-universal $Z d_i \bar{d}_i$ couplings are determined by the vectorial part of the self-energies. non-universal couplings would induce further contributions.

Note that the contribution of the Z penguin to processes like rare K and B decays is not separately gauge-invariant without including the contributions from box diagrams. The box-diagram contribution to the effective Hamiltonian for $d_j \rightarrow d_i l_k \bar{l}_l$ transitions reads

$$\begin{aligned}
 \mathcal{H}_{\text{eff}}^{\Delta F=1 \text{ Box}} &= \frac{4G_F}{\sqrt{2}} \frac{\alpha}{2\pi s_w^2} \left\{ \sum_{\sigma_1 \sigma_2} \left(B_{d_j d_i l_l l_k}^{S \sigma_1 \sigma_2} (\bar{d}_i P_{\sigma_1} d_j) (\bar{l}_k P_{\sigma_2} l_l) + B_{d_j d_i l_l l_k}^{V \sigma_1 \sigma_2} (\bar{d}_i \gamma^\mu P_{\sigma_1} d_j) (\bar{l}_k \gamma_\mu P_{\sigma_2} l_l) \right) \right. \\
 &\quad \left. + \sum_{\sigma} B_{d_j d_i l_l l_k}^{T \sigma} (\bar{d}_i \sigma^{\mu\nu} P_{\sigma} d_j) (\bar{l}_k \sigma_{\mu\nu} P_{\sigma} l_l) \right\}, \quad (4.1.11)
 \end{aligned}$$

with $\sigma_{\mu\nu} = i[\gamma^\mu, \gamma^\nu]/2$. The use of chiral Fierz identities (see *e.g.* [249]) shows that the tensor structures with mixed chirality $(\bar{d}_i \sigma^{\mu\nu} P_{\sigma} d_j) (\bar{l}_k \sigma_{\mu\nu} P_{\sigma} l_l)$ vanish identically. Hence, they are omitted from (4.1.11). We decompose the box functions $B_{d_j d_i l_l l_k}^{M \sigma_1 \sigma_2}$ as

$$\begin{aligned}
 B_{d_j d_i l_l l_k}^{M \sigma_1 \sigma_2} &= \frac{\sqrt{2} s_w^2}{G_F \alpha} \frac{1}{32\pi} \times \left\{ \right. \\
 &\quad \sum_{f_1 f_2 v_1 v_2} \left(\tilde{c}_{f_1 f_2 v_1 v_2}^{M \sigma_1 \sigma_2} \tilde{D}_0(m_{f_1}, m_{f_2}, M_{v_1}, M_{v_2}) + c_{f_1 f_2 v_1 v_2}^{M \sigma_1 \sigma_2} D_0(m_{f_1}, m_{f_2}, M_{v_1}, M_{v_2}) \right) \\
 &\quad + \sum_{f_1 f_2 v_1 s_1} \left(\tilde{c}_{f_1 f_2 v_1 s_1}^{M \sigma_1 \sigma_2} \tilde{D}_0(M_{s_1}, m_{f_1}, m_{f_2}, M_{v_1}) + c_{f_1 f_2 v_1 s_1}^{M \sigma_1 \sigma_2} D_0(M_{s_1}, m_{f_1}, m_{f_2}, M_{v_1}) \right) \\
 &\quad \left. + \sum_{f_1 f_2 s_1 s_2} \left(\tilde{c}_{f_1 f_2 s_1 s_2}^{M \sigma_1 \sigma_2} \tilde{D}_0(M_{s_1}, M_{s_2}, m_{f_1}, m_{f_2}) + c_{f_1 f_2 s_1 s_2}^{M \sigma_1 \sigma_2} D_0(M_{s_1}, M_{s_2}, m_{f_1}, m_{f_2}) \right) \right\}, \quad (4.1.12)
 \end{aligned}$$

where the superscript takes the values $M = S, V, T$. The coefficients for the vector projection are given by

$$\begin{aligned}
 c_{f_1 f_2 v_1 v_2}^{V \sigma_1 \sigma_2} &= m_{f_1}^2 m_{f_2}^2 \left(\frac{1}{M_{v_1}^2} + \frac{1}{M_{v_2}^2} \right) g_{\bar{v}_2 \bar{d}_i f_1}^{\sigma_1} g_{v_1 \bar{f}_1 d_j}^{\sigma_1} \left(g_{\bar{v}_1 \bar{l}_k f_2}^{\sigma_2} g_{v_2 \bar{f}_2 l_i}^{\sigma_2} - \text{flip}_{f_2}^V \right), \\
 \tilde{c}_{f_1 f_2 v_1 v_2}^{V \sigma_1 \sigma_2} &= -\frac{1}{4(M_{v_1}^2 + M_{v_2}^2)} c_{f_1 f_2 v_1 v_2}^{V \sigma_1 \sigma_2} + \left(g_{\bar{v}_1 \bar{l}_k f_2}^{\sigma_2} g_{v_2 \bar{f}_2 l_i}^{\sigma_2} - 4 \text{flip}_{f_2}^V \right) \times \begin{cases} -g_{\bar{v}_2 \bar{d}_i f_1}^{\sigma_1} g_{v_1 \bar{f}_1 d_j}^{\sigma_1}, & \sigma_1 = \sigma_2 \\ g_{\bar{v}_1 \bar{d}_i f_1}^{\sigma_1} g_{v_2 \bar{f}_1 d_j}^{\sigma_1}, & \sigma_1 \neq \sigma_2 \end{cases}, \\
 c_{f_1 f_2 v_1 s_1}^{V \sigma_1 \sigma_2} &= m_{f_1} m_{f_2} \left(g_{\bar{v}_1 \bar{d}_i f_1}^{\sigma_1} y_{s_1 \bar{f}_1 d_j}^{\sigma_1} + \text{flip}_{f_1}^V \right) \left(y_{\bar{s}_1 \bar{l}_k f_2}^{\sigma_2} g_{v_1 \bar{f}_2 l_i}^{\sigma_2} + \text{flip}_{f_2}^V \right), \\
 \tilde{c}_{f_1 f_2 v_1 s_1}^{V \sigma_1 \sigma_2} &= -\frac{1}{4M_{v_1}^2} c_{f_1 f_2 v_1 s_1}^{V \sigma_1 \sigma_2}, \quad c_{f_1 f_2 s_1 s_2}^{V \sigma_1 \sigma_2} = 0, \\
 \tilde{c}_{f_1 f_2 s_1 s_2}^{V \sigma_1 \sigma_2} &= -\frac{1}{4} y_{\bar{s}_2 \bar{d}_i f_1}^{\sigma_1} y_{s_1 \bar{f}_1 d_j}^{\sigma_1} \left(y_{\bar{s}_1 \bar{l}_k f_2}^{\sigma_2} y_{s_2 \bar{f}_2 l_i}^{\sigma_2} - \text{flip}_{f_2}^V \right).
 \end{aligned} \tag{4.1.13}$$

Here, $\text{flip}_{f_1}^V$ represents contributions for which we interchange the coupling constants via $g_{\dots \bar{d}_i f_1}^\sigma \leftrightarrow g_{\dots \bar{f}_1 d_j}^\sigma$ and $y_{\dots \bar{d}_i f_1}^\sigma \leftrightarrow y_{\dots \bar{f}_1 d_j}^\sigma$, and $\text{flip}_{f_2}^V$ acts analogously on $l_{i,k}$ and f_2 . For the scalar projections we obtain the coefficients

$$\begin{aligned}
 \tilde{c}_{f_1 f_2 v_1 v_2}^{S \sigma_1 \sigma_2} &= m_{f_1} m_{f_2} \left(\frac{1}{M_{v_1}^2} + \frac{1}{M_{v_2}^2} \right) g_{\bar{v}_2 \bar{d}_i f_1}^{\sigma_1} g_{v_1 \bar{f}_1 d_j}^{\sigma_1} \left\{ g_{\bar{v}_1 \bar{l}_k f_2}^{\sigma_2} g_{v_2 \bar{f}_2 l_i}^{\sigma_2} + \text{flip}_{f_2}^S \right\}, \\
 c_{f_1 f_2 v_1 v_2}^{S \sigma_1 \sigma_2} &= -\frac{4M_{v_1}^2 M_{v_2}^2 + m_{f_1}^2 m_{f_2}^2}{M_{v_1}^2 + M_{v_2}^2} \tilde{c}_{f_1 f_2 v_1 v_2}^{S \sigma_1 \sigma_2}, \\
 \tilde{c}_{f_1 f_2 v_1 s_1}^{S \sigma_1 \sigma_2} &= \left(y_{\bar{s}_1 \bar{d}_i f_1}^{\sigma_1} g_{v_1 \bar{f}_1 d_j}^{\sigma_1} - \text{flip}_{f_1}^S \right) \left(g_{\bar{v}_1 \bar{l}_k f_2}^{\sigma_2} y_{s_1 \bar{f}_2 l_i}^{\sigma_2} - \text{flip}_{f_2}^S \right), \\
 c_{f_1 f_2 v_1 s_1}^{S \sigma_1 \sigma_2} &= -\frac{m_{f_1}^2 m_{f_2}^2}{M_{v_1}^2} \tilde{c}_{f_1 f_2 v_1 s_1}^{S \sigma_1 \sigma_2}, \quad \tilde{c}_{f_1 f_2 s_1 s_2}^{S \sigma_1 \sigma_2} = 0, \\
 c_{f_1 f_2 s_1 s_2}^{S \sigma_1 \sigma_2} &= -m_{f_1} m_{f_2} y_{\bar{s}_2 \bar{d}_i f_1}^{\sigma_1} y_{s_1 \bar{f}_1 d_j}^{\sigma_1} \left(y_{\bar{s}_1 \bar{l}_k f_2}^{\sigma_2} y_{s_2 \bar{f}_2 l_i}^{\sigma_2} + \text{flip}_{f_2}^S \right),
 \end{aligned} \tag{4.1.14}$$

and finally the tensor coefficients read

$$\begin{aligned}
 c_{f_1 f_2 v_1 v_2}^{T \sigma} &= -m_{f_1} m_{f_2} g_{\bar{v}_2 \bar{d}_i f_1}^{\bar{\sigma}} g_{v_1 \bar{f}_1 d_j}^{\sigma} \left(g_{\bar{v}_1 \bar{l}_k f_2}^{\sigma} g_{v_2 \bar{f}_2 l_i}^{\sigma} - \text{flip}_{f_2}^S \right), \\
 \tilde{c}_{f_1 f_2 v_1 v_2}^{T \sigma} &= -\frac{1}{4} \left(\frac{1}{M_{v_1}^2} + \frac{1}{M_{v_2}^2} \right) c_{f_1 f_2 v_1 v_2}^{T \sigma}, \\
 \tilde{c}_{f_1 f_2 v_1 s_1}^{T \sigma} &= \frac{1}{4} \left(y_{\bar{s}_1 \bar{d}_i f_1}^{\sigma} g_{v_1 \bar{f}_1 d_j}^{\sigma} + \text{flip}_{f_1}^S \right) \left(g_{\bar{v}_1 \bar{l}_k f_2}^{\sigma} y_{s_1 \bar{f}_2 l_i}^{\sigma} + \text{flip}_{f_2}^S \right), \\
 c_{f_1 f_2 v_1 s_1}^{T \sigma} &= c_{f_1 f_2 s_1 s_2}^{T \sigma} = \tilde{c}_{f_1 f_2 s_1 s_2}^{T \sigma} = 0.
 \end{aligned} \tag{4.1.15}$$

Similar to above $\text{flip}_{f_1}^S$ stands for additional contributions, here with the coupling constants $y_{\dots \bar{d}_i f_1}^\sigma \leftrightarrow y_{\dots \bar{f}_1 d_j}^\sigma$ and $g_{\dots \bar{d}_i f_1}^\sigma \leftrightarrow g_{\dots \bar{f}_1 d_j}^\sigma$ interchanged, and $\text{flip}_{f_2}^S$ acts analogously on $l_{i,k}$ and f_2 .

It is possible to extract the generic effective Hamiltonian for the $|\Delta F| = 2$ boxes from the above results, if one keeps in mind that the external particle – antiparticle pairs allow for additional Wick contractions of the transition amplitude and that the conventional normalization of the effective Hamiltonian is different. We use Fierz identities to cast the result in

the operator basis of [250] where

$$\begin{aligned} \mathcal{H}_{\text{eff}}^{\Delta F=2 \text{ Box}} &= \frac{G_F^2}{4\pi^2} M_W^2 \left(\sum_{\sigma} S_{1,d_j d_i}^{V\sigma\sigma} Q_{1,d_i d_j}^{V\sigma\sigma} + \sum_{n=1,2} \left(S_{n,d_j d_i}^{LR} Q_{n,d_i d_j}^{LR} + \sum_{\sigma} S_{n,d_j d_i}^{S\sigma\sigma} Q_{n,d_i d_j}^{S\sigma\sigma} \right) \right), \\ Q_1^{V\sigma\sigma} &= (\bar{d}_j \gamma_{\mu} P_{\sigma} d_i) (\bar{d}_j \gamma^{\mu} P_{\sigma} d_i), \\ Q_1^{LR} &= (\bar{d}_j \gamma_{\mu} P_L d_i) (\bar{d}_j \gamma^{\mu} P_R d_i), \quad Q_2^{LR} = (\bar{d}_j P_L d_i) (\bar{d}_j P_R d_i), \\ Q_1^{S\sigma\sigma} &= (\bar{d}_j P_{\sigma} d_i) (\bar{d}_j P_{\sigma} d_i), \quad Q_2^{S\sigma\sigma} = (\bar{d}_j^{\alpha} P_{\sigma} d_i^{\beta}) (\bar{d}_j^{\beta} P_{\sigma} d_i^{\alpha}). \end{aligned} \quad (4.1.16)$$

A summation over color indices α, β is understood. In order to obtain the coefficients S from (4.1.13)–(4.1.15), the following prescription holds:

$$\begin{aligned} S_{1,d_j d_i}^{V\sigma\sigma} &= 4 B_{d_j d_i l_l l_k}^{V\sigma\sigma} |_{l_{k,l} \rightarrow d_{i,j}}, \\ S_{1,d_j d_i}^{LR} &= 8 B_{d_j d_i l_l l_k}^{VLR} |_{l_{k,l} \rightarrow d_{i,j}}, \quad S_{1,d_j d_i}^{RL} = 8 B_{d_j d_i l_l l_k}^{SLR} |_{l_{k,l} \rightarrow d_{i,j}}, \\ S_{1,d_j d_i}^{S\sigma\sigma} &= (4 B_{d_j d_i l_l l_k}^{S\sigma\sigma} - 16 B_{d_j d_i l_l l_k}^{T\sigma\sigma}) |_{l_{k,l} \rightarrow d_{i,j}}, \quad S_{1,d_j d_i}^{S\sigma\sigma} = -32 B_{d_j d_i l_l l_k}^{T\sigma\sigma} |_{l_{k,l} \rightarrow d_{i,j}}. \end{aligned} \quad (4.1.17)$$

As a check of the normalization and general structure of the result, we insert the SM couplings in (4.1.9) and (4.1.10). All necessary couplings were already mentioned in section 3.1.2. As usual, we set $x_q \equiv m_q^2/M_W^2$ and rewrite the loop-functions in terms of x_{u_k} and M_W^2 . Terms independent of x_{u_k} drop in the result due to the CKM unitarity. This is the well known GIM mechanism [16]. We recover the result of Inami and Lim [251]

$$C_{d_j d_i Z}^{L(\text{SM})} = \lambda_t^{(d_j d_i)} C(x_t), \quad C(x) = \frac{x}{8} \left(\frac{x-6}{x-1} + \frac{3x+2}{(x-1)^2} \ln(x) \right), \quad (4.1.18)$$

for the top-quark contribution to the $d_j \rightarrow d_i Z$ vertex. The relevant CKM-factors are abbreviated as $\lambda_q^{(d_j d_i)} = V_{qd_j} V_{qd_i}^*$. Similarly we recover from (4.1.12) the result of the box diagrams for the vertices $d_j \rightarrow d_i e^+ e^-$ and $d_j \rightarrow d_i \bar{\nu} \nu$

$$B_{d_j d_i e e}^{VLL(\text{SM})} = -\frac{1}{4} B_{d_j d_i \nu \nu}^{VLL(\text{SM})} = \lambda_t^{(d' d)} B(x_t), \quad B(x) = \frac{x}{4} \left(\frac{1}{1-x} + \frac{\ln(x)}{(x-1)^2} \right), \quad (4.1.19)$$

and for the $\Delta F = 2$ transition $d_j \rightarrow d_i \bar{d}_j d_i$

$$S_{d_j d_i d_j d_i}^{VLL(\text{SM})} = (\lambda_t^{(d_j d_i)})^2 S(x_t) + (\lambda_c^{(d_j d_i)})^2 S(x_c) + 2 \lambda_t^{(d_j d_i)} \lambda_c^{(d_j d_i)} S(x_c, x_t), \quad (4.1.20)$$

$$\begin{aligned} S(x) &= S(x, x), \quad S(x, y) = \frac{xS'(y) - yS'(x)}{x-y}, \\ S'(x) &= -\frac{x}{4} \left(\frac{3}{x-1} + \frac{4-8x+x^2}{(x-1)^2} \ln(x) \right). \end{aligned}$$

Here we kept the finite contribution from the charm-quark mass m_c , which is important due to the CKM factor $\text{Re}(\lambda_c) = \mathcal{O}(\lambda)$, whereas $\lambda_t = \mathcal{O}(\lambda^5) = \text{Im}(\lambda_c)$. The unusual definition of S in terms of S' turns out to be useful for the result in the LHT model, which we give in the following section.

4.1.1.3 Results for the Littlest Higgs Model with T -parity

In the following we apply our results to the partly renormalizable LHT model of section 3.2. This provides the insight why the Z penguin is UV finite in the given model. As a byproduct, we reproduce the result in the literature and simplify it considerably.

We obtain the analytic expressions for quark-flavor violating Z penguin and box diagrams, by inserting the couplings of appendix A.2 into the generic results (4.1.9), (4.1.12), and (4.1.17). Using this specified expression, we can check if the divergence of the penguin diagram vanishes. We find that this is indeed the case. It is only expected on general grounds, if the sum rules (3.1.19), (3.1.28), and (3.1.29) hold in all possible combinations of external particles that can appear in the penguin diagram after applying the cuts demonstrated in section 4.1.1.1. In other words, if we can verify that the relevant parts entering the process in question all fulfill the constraints from tree-level perturbativity, we are allowed to safely use (4.1.9) also for models with sectors of explicitly broken symmetry. This is the case for the partly gauged LHT model. We created all possible combinations of tree-subdiagrams for the off-diagonal down-type Z penguin and found that the STIs (3.1.19) are indeed fulfilled. The STIs (3.1.28) and (3.1.29) are not exactly fulfilled for subdiagrams with an external down-type mirror-quark. However, the difference of left- and right-hand side of these STIs is always suppressed with a light quark mass m_{d_i} or $m_{d_j}^2$. Furthermore, the differences are proportional to the mirror-mixing matrix \mathbf{V}_{H_d} (or $\mathbf{V}_{H_d}^\dagger$). The remaining coupling, necessary to form the penguin diagram always contributes another factor of $\mathbf{V}_{H_d}^\dagger$ (or \mathbf{V}_{H_d}). After a summation over the ‘‘cut’’ particle line, the unitarity of \mathbf{V}_{H_d} implies that even the differences proportional to the light quark masses $m_{d_{i,j}}$ vanish in the penguin diagram³. It is interesting to note that even though the complete divergence in the down-type Z penguin vanishes identically, there are parts of the divergence (proportional to light quark masses), which do not vanish due perturbative unitarity, but only accidentally. This provides a deeper understanding why the Z penguin turns out to be free of UV-sensitivity in the LHT model.

We also reproduce the finite part for the Z penguin and box diagrams as known in the literature [160, 163, 165, 253]. We summarize it here in a shorter form. To this end we define

$$\begin{aligned} x_T &= m_{T^+}^2/m_W^2, \quad z_k = m_{H,k}^2/m_{W_H}^2, \quad y_n = m_{H,n}^2/m_{W_H}^2, \\ \lambda_q &= (V)_{qd_j}(V)_{qd_i}^*, \quad \xi_k = (V_{Hd})_{kd_j}(V_{Hd})_{kd_i}^*, \quad \lambda_n^{Hl} = (V_{Hl})_{nl_i}(V_{Hl})_{nl_k}^*, \end{aligned} \quad (4.1.21)$$

and arrive at the result

$$\begin{aligned} C_{d_j d_i Z}^{L(\text{LHT})} &= \frac{v^2}{4f^2} \left\{ \lambda_t \frac{x_L^2}{2V_{tb}^2} \left(-5 - x_t \left[\frac{1-2x_L}{1-x_L} + 2\ln(x_t) \right] + (3+2x_t)\ln(x_T) \right) \right. \\ &\quad \left. + \sum_{k=2,3} \xi_k [C(z_k) - C(z_1)] \right\}, \end{aligned} \quad (4.1.22)$$

²The quark-mass suppression comes in addition to the v^2/f^2 suppression of the new physics contribution to the penguin diagram. Hence, the terms are only conceptually interesting.

³There are similar m_b terms in the relevant subdiagrams for the calculation of $Z \rightarrow b\bar{b}$. Only a full calculation can show if these contributions also vanish accidentally. Neglecting the m_b terms, the finiteness of the $Z \rightarrow b\bar{b}$ amplitude has been explicitly confirmed in [252]

$$\begin{aligned}
 B_{d_j d_i l l_k}^{VLL(\text{LHT})} &= \frac{v^2}{4f^2} \left\{ \frac{3 \pm 5}{2} \lambda_t \frac{x_L^2}{V_{tb}^2} \delta_{l\nu} \right. \\
 &\quad \left. \pm \frac{1}{16} \sum_{n=1}^3 \sum_{k=2,3} \lambda_n^{Hl} \xi_k \left[B'_{\pm}(z_k, y_n) - B'_{\pm}(z_1, y_n) + B'_{\pm}(z_k) - B'_{\pm}(z_1) \right] \right\}, \quad (4.1.23)
 \end{aligned}$$

$$\begin{aligned}
 S_{1, d_j d_i}^{VLL(\text{LHT})} &= \frac{v^2}{4f^2} \left\{ \lambda_t \frac{x_L^2}{V_{tb}^2} \left(\lambda_t \frac{x_t x_L}{1 - x_L} + \sum_{q=c,t} \lambda_q \left[8 S'(x_q) + 2 x_q \ln(x_T) \right] \right) \right. \\
 &\quad \left. - \frac{1}{4} \sum_{j,k=2,3} \xi_j \xi_k \left[B'_-(z_j, z_k) - B'_-(z_j, z_1) - B'_-(z_1, z_k) + B'_-(z_1, z_1) \right] \right\}. \quad (4.1.24)
 \end{aligned}$$

In (4.1.23) the upper (lower) sign is valid for $l = \nu$ ($l = e$). The second row of each equation contains the contribution originating from T -odd particles. There, we also used the GIM mechanism for the matrix V_{Hd} , which generates the subtracted terms with z_1 . For the T -odd box contributions we introduced the following additional loop functions

$$\begin{aligned}
 B'_{\pm}(z, y) &= \frac{-(3 \pm 9)zy}{(z-1)(y-1)} + \left\{ \frac{z(z^3 - 8z^2 + (10 \pm 9)z - \frac{6t_w^2}{25}(z-1))}{(z-1)^2(z-y)} \ln(z) + \dots \Big|_{z \rightarrow y} \right\}, \\
 B'_{\pm}(z) &= z \left(\frac{10 \pm 9}{z-1} + (z-8) \frac{z \ln(z)}{(z-1)^2} \right). \quad (4.1.25)
 \end{aligned}$$

Remark that the results given here completely reproduce the full results of [160, 253], but we summarized it in a much shorter form. This is achieved by using the vertex definition of the CKM-matrix \mathbf{V} given in (3.2.29). This renders the input parameters also closer to physical observables. Furthermore, we have expanded in the mass ratio $m_{A_H}^2/m_{Z_H}^2 = t_w^2(1 - v^2/f^2)/5$. In the latter ratio we neglect higher order terms; they are of the same numerical size that one expects from the likewise neglected contribution at order v^4/f^4 .

4.1.2 Constraints and Correlations in the Randall-Sundrum Model

In the following, we discuss numerical results for potentially restrictive FCNC processes in the RS model. In doing so, we focus on kaon mixing, direct CP violation in $K \rightarrow \pi\pi$, $B_s \rightarrow \mu\mu$, and CKM non-unitarity. Very strong bounds on the RS scale have been inferred from CP violation in kaon mixing in the past [211, 212, 229, 254, 255]. We emphasize the well known complementarity of those constraints to direct searches and assess the influence of the Yukawa sector. Instead of calculating bounds from “typical” predictions of the RS model, whose interpretation remains ambiguous, we scan the full parameter space in a detailed numerical analysis. Having access to the full distributions allows us to investigate two directions. On the one hand, we can attach a pseudo-statistical significance to the notion of a bound on the RS scale. We will see that bounds derived in a rigorous sense are much weaker than what could be expected generically and that they are at most of similar importance compared to electroweak precision constraints. On the other hand, we find that the restriction of the Yukawa structure can in fact lead to more interesting and complementary predictions, namely the correlation between different flavor observables. We study leptonic and semileptonic kaon decays and find that relevant restrictions on the potential deviations in these processes can be inferred from the aforementioned bounds.

A generalization of this discussion to B -physics and the lepton sector is conceptually trivial (apart from the issue of Neutrino mass terms [256–259]). As mentioned, we also present the results for $B_s \rightarrow \mu\mu$, since it has been measured recently for the first time by LHCb [260]. We refer the reader to our extensive analysis [3], where we also presented results for $B_{d,s}-\bar{B}_{d,s}$ mixing, semileptonic B decays, the hadronic decays $B \rightarrow \pi\pi$, and $B \rightarrow K\pi$ in the minimal RS model. In [212, 261] extensive corresponding analyses were presented for the custodial RS model. For relevant constraints on the Yukawa structure of the lepton sector that arise from lepton flavor violating processes such as $\mu \rightarrow e\gamma$, $\mu \rightarrow 3e$, and μ - e conversion in nuclei we refer to [230, 262–265].

4.1.2.1 A Comment on Bounds from Direct Collider Searches

In order to have a reference value for direct bounds on the KK scale M_{KK} , we refer to the most recent search for resonances in the $t\bar{t}$ mass spectrum⁴. This final state is suitable to search for the first KK gluon excitation, whose mass $M_{G^{(1)}} \approx 2.45 M_{\text{KK}}$ is a robust prediction of the RS model with bulk gauge bosons. The top quark and $G^{(1)}$ are IR localized, thus their coupling is enhanced compared to g_s . The precise value depends on the bulk-masses. For UV-localized light fermions, the couplings to $G^{(1)}$ have a suppression of approximately $1/\sqrt{L}$ compared to the SM coupling. This explains why $G^{(1)} \rightarrow t\bar{t}$ is the main decay channel for the first KK gluon excitation. The typical branching ratio of this decay was estimated to be 92.5% in [266] and 95% in [267]. Using the former and the latter value, respectively, a bound of $M_{G^{(1)}} > 1.5$ TeV was found by ATLAS [268] and $M_{G^{(1)}} > 1.8$ TeV by CMS [269], both at 95% CL.

4.1.2.2 Theoretical Framework and Relevant Formulas

Kaon Mixing

Here we adopt the effective Hamiltonian for $K-\bar{K}$ mixing [270–272]

$$\mathcal{H}_{\text{eff}}^{\Delta S=2} = \sum_{i=1}^5 C_i Q_i^{sd} + \sum_{i=1}^3 \tilde{C}_i \tilde{Q}_i^{sd}, \quad (4.1.26)$$

in the basis where

$$\begin{aligned} Q_1^{sd} &= (\bar{d}_L \gamma^\mu s_L) (\bar{d}_L \gamma_\mu s_L), & \tilde{Q}_1^{sd} &= (\bar{d}_R \gamma^\mu s_R) (\bar{d}_R \gamma_\mu s_R), \\ Q_2^{sd} &= (\bar{d}_R s_L) (\bar{d}_R s_L), & \tilde{Q}_2^{sd} &= (\bar{d}_L s_R) (\bar{d}_L s_R), \\ Q_3^{sd} &= (\bar{d}_R^\alpha s_L^\beta) (\bar{d}_R^\beta s_L^\alpha), & \tilde{Q}_3^{sd} &= (\bar{d}_L^\alpha s_R^\beta) (\bar{d}_L^\beta s_R^\alpha), \\ Q_4^{sd} &= (\bar{d}_R s_L) (\bar{d}_L s_R), \\ Q_5^{sd} &= (\bar{d}_R^\alpha s_L^\beta) (\bar{d}_L^\beta s_R^\alpha). \end{aligned} \quad (4.1.27)$$

This corresponds to the basis (4.1.16) after a single Fierz transformation $Q_1^{LR} = -2Q_3^{sd}$ and renaming the operators in order to agree with literature that we use below. We write the Wilson coefficients as a sum of a SM and a new-physics contribution, $C_i \equiv C_i^{\text{SM}} + C_i^{\text{RS}}$, where

⁴Bounds on the first KK Graviton from $\gamma\gamma$ and lepton mass spectra are only relevant for the RS model with IR-brane matter, which we do not consider for reasons explained in section 3.3.1.

in the SM only C_1^{SM} is non-zero. Using the general results from section 3.3.8 along with standard Fierz identities, we obtain for the contributions in the RS model⁵

$$\begin{aligned}
 C_1^{\text{RS,V}} &= \frac{2\pi L}{M_{\text{KK}}^2} (\tilde{\Delta}_D)_{12} \otimes (\tilde{\Delta}_D)_{12} \left[\frac{\alpha_s}{2} \left(1 - \frac{1}{N_c} \right) + Q_d^2 \alpha + \Omega_Z^{d_L d_L} \frac{(T_3^d - s_w^2 Q_d)^2 \alpha}{s_w^2 c_w^2} \right], \\
 \tilde{C}_1^{\text{RS,V}} &= \frac{2\pi L}{M_{\text{KK}}^2} (\tilde{\Delta}_d)_{12} \otimes (\tilde{\Delta}_d)_{12} \left[\frac{\alpha_s}{2} \left(1 - \frac{1}{N_c} \right) + Q_d^2 \alpha + \Omega_Z^{d_R d_R} \frac{(s_w^2 Q_d)^2 \alpha}{s_w^2 c_w^2} \right], \\
 C_4^{\text{RS,V}} &= \frac{2\pi L}{M_{\text{KK}}^2} (\tilde{\Delta}_D)_{12} \otimes (\tilde{\Delta}_d)_{12} [-2\alpha_s], \\
 C_5^{\text{RS,V}} &= \frac{2\pi L}{M_{\text{KK}}^2} (\tilde{\Delta}_D)_{12} \otimes (\tilde{\Delta}_d)_{12} \left[\frac{2\alpha_s}{N_c} - 4Q_d^2 \alpha + \Omega_Z^{d_L d_R} \frac{4s_w^2 Q_d (T_3^d - s_w^2 Q_d) \alpha}{s_w^2 c_w^2} \right], \\
 C_2^{\text{RS,h}} &= \frac{1}{2M_h^2} (g_h^d)_{12}^2, \quad \tilde{C}_2^{\text{RS,h}} = \frac{1}{2M_h^2} (g_h^d)_{21}^{*2}, \quad C_4^{\text{RS,h}} = \frac{1}{2M_h^2} (g_h^d)_{12} (g_h^d)_{21}^*,
 \end{aligned} \tag{4.1.28}$$

where the factors $\Omega_Z^{dd'}$ are equal to one in the minimal RS model and were given for the custodial model in (3.3.163). The expressions in square brackets in $C_i^{\text{RS,V}}$ refer, in an obvious way, to the contributions from KK gluons, KK photons, and from the Z boson and its KK excitations. It was recognized in [273] that the chirally unsuppressed Higgs FCNCs, as discussed in section 3.3.8.1, are mostly subleading, even for a Higgs mass as low as 126 GeV. We take them nevertheless into account here as $C_i^{\text{RS,h}}$, since they can be relevant when compared with the small allowed range for contributions of new physics. The Wilson coefficients C_3 and \tilde{C}_3 do not receive tree-level contributions in the RS model, as they can arise from charged scalar or tensor exchange only. Notice that in the minimal RS model, the QCD contributions are in all cases larger by more than a factor of 3 than the combined QED and electroweak effects, and that the numerically largest contribution proportional to $C_4^{\text{RS,V}}$ is solely a QCD effect. For the relevant observables we quantify this more precisely below. KK-gluon exchange thus dominates all mixing amplitudes in the original RS scenario with SM bulk gauge symmetry. Due to the large coefficients $\Omega_Z^{d_L d_R}$ and $\Omega_Z^{d_R d_R}$, this can be different in the custodial RS model. Indeed, the contributions from KK-gluon and KK- Z exchange become indeed of comparable size and the coefficients of C_1 , \tilde{C}_1 , and C_5 are enhanced by factors of approximately 1.3, 1.8, and 2.4. For $K-\bar{K}$ mixing, which we discuss below, the pure QCD operator C_4 is by far dominant. This observation is important, as it implies that these mixing phenomena mainly probe the extra-dimensional aspects of the strong interactions, but they are to first approximation insensitive to the precise embedding of the electroweak gauge symmetry in the higher-dimensional geometry. Thus, we will only show results for the minimal model below. However, for $B_d-\bar{B}_d$ and $B_s-\bar{B}_s$ mixing the KK- Z exchanges becomes important, too, as recognized in [212].

The tree-level expressions for the Wilson coefficients $C_i^{\text{RS,V}}$ given above refer to a renormalization scale $\mu_{\text{KK}} = \mathcal{O}(M_{\text{KK}})$ and $C_i^{\text{RS,h}}$ to the scale $\mu_h = M_h$. They must be evolved down to a scale $\mu \approx 2 \text{ GeV}$, where the hadronic matrix elements of the four-quark operators can be evaluated using lattice QCD. The evolution is accomplished with the help of formulas compiled in [271]. The hadronic matrix elements of the various operators are customarily

⁵We correct our result in [3] by a symmetry factor 1/2, which was missed in this work.

expressed in terms of parameters B_i . For the operators relevant to our analysis, one defines

$$\begin{aligned}\langle K^0|Q_1(\mu)|\bar{K}^0\rangle &= \langle K^0|\tilde{Q}_1(\mu)|\bar{K}^0\rangle = \left(1 + \frac{1}{N_c}\right) \frac{M_K f_K^2}{4} B_1(\mu), \\ \langle K^0|Q_4(\mu)|\bar{K}^0\rangle &= \left[\frac{M_K}{m_s(\mu) + m_d(\mu)}\right]^2 \frac{M_K f_K^2}{4} B_4(\mu), \\ \langle K^0|Q_5(\mu)|\bar{K}^0\rangle &= \frac{1}{N_c} \left[\frac{M_K}{m_s(\mu) + m_d(\mu)}\right]^2 \frac{M_K f_K^2}{4} B_5(\mu),\end{aligned}\tag{4.1.29}$$

where the meson states are normalized to one, $\langle K^0|K^0\rangle = \langle \bar{K}^0|\bar{K}^0\rangle = 1$. These definitions are such that in the vacuum-insertion approximation (VIA)

$$\begin{aligned}[B_1(\mu)]_{\text{VIA}} &= 1, \\ [B_4(\mu)]_{\text{VIA}} &= 1 + \frac{1}{2N_c} \left[\frac{m_s(\mu) + m_d(\mu)}{M_K}\right]^2, \\ [B_5(\mu)]_{\text{VIA}} &= 1 + \frac{N_c}{2} \left[\frac{m_s(\mu) + m_d(\mu)}{M_K}\right]^2.\end{aligned}\tag{4.1.30}$$

In our numerical analysis we employ the B_i parameters from [274]. We collect the set of input values entering our calculations in appendix B.2.

The K_L - K_S mass difference ΔM_K and the CP -violating quantity ϵ_K are given by

$$\Delta M_K = 2 \operatorname{Re} \langle K^0|\mathcal{H}_{\text{eff,full}}^{\Delta S=2}|\bar{K}^0\rangle, \quad \epsilon_K = \frac{\kappa_\epsilon e^{i\varphi_\epsilon}}{\sqrt{2}(\Delta M_K)_{\text{exp}}} \operatorname{Im} \langle K^0|\mathcal{H}_{\text{eff,full}}^{\Delta S=2}|\bar{K}^0\rangle,\tag{4.1.31}$$

where $\varphi_\epsilon = (43.52 \pm 0.05)^\circ$ [69] and $\kappa_\epsilon = 0.94 \pm 0.02$ [275]. The suppression factor κ_ϵ parametrizes the effects due to the imaginary part of the isospin-zero amplitude in $K \rightarrow \pi\pi$ decays [276–278]. The best prediction of the SM including NNLO charm quark contributions [279] reads

$$|\epsilon_K|_{\text{SM}} = (1.81 \pm 0.28) \cdot 10^{-3}.\tag{4.1.32}$$

The dominant theoretical uncertainties arise from η_{cc} , η_{ct} , the lattice QCD prediction of B_1 and the error on κ_ϵ . The largest parametric uncertainty stems from the value of $|V_{cb}|$. Within errors the SM prediction agrees fairly well with the experimental value $|\epsilon_K|_{\text{exp}} = (2.228 \pm 0.011) \cdot 10^{-3}$ [69]. We do not consider ΔM_K numerically, as is plagued by very large hadronic uncertainties.

In order to understand quantitatively which Wilson coefficient generically gives the dominant contribution in the presence of new physics, we derive the approximate relation

$$\langle K^0|\mathcal{H}_{\text{eff,RS}}^{\Delta S=2}|\bar{K}^0\rangle \propto C_1^{\text{RS}} + \tilde{C}_1^{\text{RS}} + 114.8 \left(1 + 0.14 \ln\left(\frac{\mu_{\text{KK}}}{3 \text{ TeV}}\right)\right) \left(C_4^{\text{RS}} + \frac{C_5^{\text{RS}}}{3.1}\right),\tag{4.1.33}$$

where the large scale-independent coefficient consists of a factor of about 15 arising from the chiral enhancement of the hadronic matrix elements [280, 281], and a factor of about 8 due to the RG evolution [270, 271] from 3 TeV down to 2 GeV. We neglected the different evolution for the Higgs boson contributions for the illustration here. Assuming that all Wilson

coefficients are of similar size, this relation implies that C_4^{RS} gives the dominant new physics contribution to both ΔM_K and $|\epsilon_K|$ in the RS framework.⁶

Direct CP Violation in $K \rightarrow \pi\pi$

We write the new-physics contributions to these decays using the usual operator basis Q_{1-10} augmented with chirality-flipped operators \tilde{Q}_{1-10} that are obtained from the original ones by exchanging left- by right-handed fields. Explicitly, we use

$$\begin{aligned} \mathcal{H}_{\text{eff}}^{\Delta S=1} = & \frac{G_F}{\sqrt{2}} \sum_{q=u,c} \lambda_q^{(sb)} \left(C_1 Q_1^q + C_2 Q_2^q + \sum_{i=3}^{10} C_i Q_i + C_7^\gamma Q_7^\gamma + C_8^g Q_8^g \right) \\ & + \sum_{i=3}^{10} \left(C_i^{\text{RS}} Q_i + \tilde{C}_i^{\text{RS}} \tilde{Q}_i \right), \end{aligned} \quad (4.1.34)$$

where $\lambda_q^{(pr)} \equiv V_{qp}^* V_{qr}$ and $Q_{1,2}^q$ are the left-handed current-current operators arising from W^\pm -boson exchange, Q_{3-6} and Q_{7-10} are QCD and electroweak penguin operators, and Q_7^γ and Q_8^g are the electromagnetic and chromomagnetic dipole operators. The operators relevant to our discussion are defined as

$$\begin{aligned} Q_3 &= 4 (\bar{d}_L \gamma^\mu s_L) \sum_q (\bar{q}_L \gamma_\mu q_L), & Q_4 &= 4 (\bar{d}_L^\alpha \gamma^\mu s_L^\beta) \sum_q (\bar{q}_L^\beta \gamma_\mu q_L^\alpha), \\ Q_5 &= 4 (\bar{d}_L \gamma^\mu s_L) \sum_q (\bar{q}_R \gamma_\mu q_R), & Q_6 &= 4 (\bar{d}_L^\alpha \gamma^\mu s_L^\beta) \sum_q (\bar{q}_R^\beta \gamma_\mu q_R^\alpha), \\ Q_7 &= 6 (\bar{d}_L \gamma^\mu s_L) \sum_q Q_q (\bar{q}_R \gamma_\mu q_R), & Q_8 &= 6 (\bar{d}_L^\alpha \gamma^\mu s_L^\beta) \sum_q Q_q (\bar{q}_R^\beta \gamma_\mu q_R^\alpha), \\ Q_9 &= 6 (\bar{d}_L \gamma^\mu s_L) \sum_q Q_q (\bar{q}_L \gamma_\mu q_L), & Q_{10} &= 6 (\bar{d}_L^\alpha \gamma^\mu s_L^\beta) \sum_q Q_q (\bar{q}_L^\beta \gamma_\mu q_L^\alpha). \end{aligned} \quad (4.1.35)$$

A summation over color indices α, β and flavors $q = u, d, s, c, b$ is implied. To leading order in small parameters, we obtain

$$\begin{aligned} C_3^{\text{RS}} &= \frac{\pi \alpha_s}{M_{\text{KK}}^2} \frac{(\Delta'_D)_{12}}{2N_c} - \frac{\pi \alpha}{6s_w^2 c_w^2 M_{\text{KK}}^2} (\Sigma_D)_{12}, & \tilde{C}_3^{\text{RS}} &= \frac{\pi \alpha_s}{M_{\text{KK}}^2} \frac{(\Delta'_d)_{12}}{2N_c}, \\ C_4^{\text{RS}} &= C_6^{\text{RS}} = -\frac{\pi \alpha_s}{2M_{\text{KK}}^2} (\Delta'_D)_{12}, & \tilde{C}_4^{\text{RS}} &= \tilde{C}_6^{\text{RS}} = -\frac{\pi \alpha_s}{2M_{\text{KK}}^2} (\Delta'_d)_{12}, \\ C_5^{\text{RS}} &= \frac{\pi \alpha_s}{M_{\text{KK}}^2} \frac{(\Delta'_D)_{12}}{2N_c}, & \tilde{C}_5^{\text{RS}} &= \frac{\pi \alpha_s}{M_{\text{KK}}^2} \frac{(\Delta'_d)_{12}}{2N_c} + \frac{\pi \alpha}{6s_w^2 c_w^2 M_{\text{KK}}^2} (\Sigma'_d)_{12}, \\ C_7^{\text{RS}} &= \frac{2\pi \alpha}{9M_{\text{KK}}^2} (\Delta'_D)_{12} - \frac{2\pi \alpha}{3c_w^2 M_{\text{KK}}^2} (\Sigma_D)_{12}, & \tilde{C}_7^{\text{RS}} &= \frac{2\pi \alpha}{9M_{\text{KK}}^2} (\Delta'_d)_{12} - \frac{2\pi \alpha}{3s_w^2 M_{\text{KK}}^2} (\Sigma'_d)_{12}, \\ C_8^{\text{RS}} &= C_{10}^{\text{RS}} = 0, & \tilde{C}_8^{\text{RS}} &= \tilde{C}_{10}^{\text{RS}} = 0, \\ C_9^{\text{RS}} &= \frac{2\pi \alpha}{9M_{\text{KK}}^2} (\Delta'_D)_{12} + \frac{2\pi \alpha}{3s_w^2 M_{\text{KK}}^2} (\Sigma_D)_{12}, & \tilde{C}_9^{\text{RS}} &= \frac{2\pi \alpha}{9M_{\text{KK}}^2} (\Delta'_d)_{12} + \frac{2\pi \alpha}{3c_w^2 M_{\text{KK}}^2} (\Sigma'_d)_{12}, \end{aligned} \quad (4.1.36)$$

⁶The chiral enhancement of the mixed-chirality matrix elements is much less pronounced for $B_{d,s} - \bar{B}_{d,s}$ and $D - \bar{D}$ mixing and amounts to at most a factor of two. Furthermore, the Wilson coefficients are only evolved down to the mass scale of bottom and charm mesons. We gave the resulting factors in [3], and we confirmed that in this case the contribution from C_1^{RS} and \tilde{C}_1^{RS} can compete with the one arising from C_4^{RS} and C_5^{RS} .

where

$$\Sigma_A \equiv L \left(\frac{1}{2} - \frac{s_w^2}{3} \right) \omega_Z^{d_L} \Delta_A + \frac{M_{\text{KK}}^2}{M_Z^2} \delta_A, \quad \Sigma'_A \equiv L \frac{s_w^2}{3} \omega_Z^{d_R} \Delta_A + \frac{M_{\text{KK}}^2}{M_Z^2} \delta_A. \quad (4.1.37)$$

It is an interesting fact that, for $\Delta F = 1$ transitions in general, the QCD contributions from KK-gluon exchange no longer give the dominant contributions to the Wilson coefficients. The effects due to Z -boson exchange are enhanced by an extra factor of L in (4.1.37), which compensates for the smaller gauge couplings. Numerically, one finds in the minimal RS model that, relative to $C_{4,6}^{\text{RS}}$, the Wilson coefficients C_3^{RS} , C_5^{RS} , C_7^{RS} , and C_9^{RS} are typically a factor of about 2, 1/3, 3, and 9 different in magnitude. The chirality-flipped coefficients \tilde{C}_{3-10} are generically very small in the model at hand, since they involve right-handed fermion profiles that are naturally more UV-localized than their left-handed counterparts. The factors $\omega_Z^{d_{L,R}}$ in (4.1.37) were defined in (3.3.143). They switch off the main left-handed contribution and enhance the right-handed contribution by a factor of 10 in the custodial model, while they both equal one in the minimal model.

The Wilson coefficients (4.1.36) enter the prediction for ϵ'_K/ϵ_K , which measures the ratio of the direct and indirect CP -violating contributions to $K \rightarrow \pi\pi$. One extracts it from

$$\left| \frac{\eta_{00}}{\eta_{+-}} \right|^2 \approx 1 - 6 \operatorname{Re} \left(\frac{\epsilon'_K}{\epsilon_K} \right) \approx 1 - 6 \frac{\epsilon'_K}{\epsilon_K}, \quad \eta_{ij} \equiv \frac{A(K_L \rightarrow \pi^i \pi^j)}{A(K_S \rightarrow \pi^i \pi^j)}, \quad (4.1.38)$$

where the first approximation holds, since direct CP violation is very small. The second approximation neglects the tiny phase difference of a few tenths of a degree, which can be inferred from a chiral perturbation theory analysis [282]. Experimental evidence shows that the parameter ϵ'_K/ϵ_K is non-vanishing. The current average is given by $(\epsilon'_K/\epsilon_K)_{\text{exp}} = (16.6 \pm 2.3) \cdot 10^{-4}$ [69].

Unfortunately, unlike the rare K decays with leptons in the final state, the observable ϵ'_K/ϵ_K is affected by large hadronic uncertainties. In spite of the large theory errors, a study of ϵ'_K/ϵ_K can provide useful information on the flavor structure of the underlying theory, since this ratio depends very sensitively on the relative size of contributions from the QCD penguin Q_6 and electroweak penguin Q_8 , which cancel to a large extent in the SM. The strong sensitivity of ϵ'_K/ϵ_K to the electroweak penguin sector can lead to interesting correlations with the rare $K \rightarrow \pi\nu\bar{\nu}$ and $K_L \rightarrow \pi^0 l^+ l^-$ decays. We investigate below to which extent such correlations exist in the RS scenario.

In the presence of new-physics contributions to the Wilson coefficients of the operators Q_{3-10} and their chirality-flipped partners \tilde{Q}_{3-10} , the ratio ϵ'_K/ϵ_K can be approximated by

$$\frac{\epsilon'_K}{\epsilon_K} = -\operatorname{Im} \left(\lambda_t^{(ds)} F_{\text{SM}} + F_{\text{RS}} \right) \frac{|\epsilon_K|_{\text{exp}}}{|\epsilon_K|}, \quad (4.1.39)$$

where

$$\begin{aligned} F_{\text{SM}} &= -1.4 + 13.6 R_6 - 6.4 R_8, \\ F_{\text{RS}} &= 27.1 K_3 - 56.1 K_4 + 8.7 K_5 + 36.0 K_6 - 544.4 K_7 - 1663.5 K_8 \\ &\quad + 141.0 K_9 + 56.1 K_{10} - (11.4 K_3 + 61.5 K_4 - 177.1 K_5 - 479.1 K_6 \\ &\quad + 6.0 K_7 + 27.5 K_8 - 18.7 K_9 + 16.4 K_{10}) R_6 - (17.6 K_3 - 45.0 K_4 \\ &\quad + 90.8 K_5 + 218.6 K_6 - 8976.4 K_7 - 28190.5 K_8 + 102.4 K_9 + 23.8 K_{10}) R_8. \end{aligned} \quad (4.1.40)$$

We derived this formula in [3] following the approach outlined in detail in [283, 284]. The function F_{SM} comprises the information on the SM contributions to the Wilson coefficients of the $\Delta S = 1$ weak effective Hamiltonian at the next-to-leading order [285–290]. The given expression corresponds to a charm-quark renormalization scale of $\mu_c = 1.3 \text{ GeV}$, and we have employed two-loop formulas to calculate $\alpha_s(\mu)$ from $\alpha_s(M_Z)$ and to convert the top-quark mass from the pole into the $\overline{\text{MS}}$ scheme. For the coefficients K_i entering the new-physics contribution F_{RS} , we obtain

$$K_i = \frac{2 s_w^2 c_w^2 M_Z^2}{\pi \alpha} \left(C_i^{\text{RS}} - \tilde{C}_i^{\text{RS}} \right), \quad i = 3, \dots, 10. \quad (4.1.41)$$

The minus sign is a consequence of the odd parity $\langle \pi\pi | \tilde{Q}_i | K \rangle = -\langle \pi\pi | Q_i | K \rangle$. The electromagnetic coupling constant α as well as the Wilson coefficients C_i^{RS} and \tilde{C}_i^{RS} are taken to be renormalized at the scale M_W . In our numerical analysis, we determine C_i^{RS} and \tilde{C}_i^{RS} from the initial conditions in (4.1.36) using the leading order RG equations for the evolution from M_{KK} down to M_W . Notice that the inclusion of running effects is necessary to obtain the correct result in this case, because a non-zero value of K_8 , having the largest numerical coefficient in (4.1.40), is only generated through operator mixing. We find to excellent approximation

$$\begin{aligned} C_3(M_W) &= (0.416 \eta^2 - 0.962 \eta + 1.570) C_3(M_{\text{KK}}) - (0.002 \eta^2 - 0.242 \eta + 0.263) C_6(M_{\text{KK}}), \\ C_4(M_W) &= -(0.505 \eta^2 - 1.465 \eta + 1.017) C_3(M_{\text{KK}}) - (0.416 \eta^2 - 1.190 \eta - 0.189) C_6(M_{\text{KK}}), \\ C_5(M_W) &= -(0.034 \eta^2 - 0.036 \eta - 0.001) C_3(M_{\text{KK}}) + (0.192 \eta^2 - 0.592 \eta + 0.090) C_6(M_{\text{KK}}), \\ C_6(M_W) &= (0.002 \eta^2 + 0.093 \eta - 0.102) C_3(M_{\text{KK}}) + (1.376 \eta^2 - 3.005 \eta + 2.703) C_6(M_{\text{KK}}), \\ C_7(M_W) &= 0.987 \eta^{0.143} C_7(M_{\text{KK}}), \\ C_8(M_W) &= (0.371 \eta^{-1.143} - 0.329 \eta^{0.143}) C_7(M_{\text{KK}}), \\ C_9(M_W) &= (0.528 \eta^{-0.571} + 0.487 \eta^{0.286}) C_9(M_{\text{KK}}), \\ C_{10}(M_W) &= (-0.528 \eta^{-0.571} + 0.487 \eta^{0.286}) C_9(M_{\text{KK}}), \end{aligned} \quad (4.1.42)$$

where $\eta \equiv \alpha_s(M_{\text{KK}})/\alpha_s(m_t)$. Here, we have omitted the suppressed contributions of $C_{7,9}(M_{\text{KK}})$ to the QCD penguin coefficients $C_{3-6}(M_W)$ for simplicity. We stress that the coefficients K_{3-10} , which contain the (1,2) elements of the mixing matrices, have to be calculated in the standard phase convention for the CKM matrix (2.2.14) in order to obtain correct results. The same applies to all Wilson coefficients appearing hereafter.

The non-perturbative parameters R_6 and R_8 are given in terms of the hadronic parameters $B_6^{(1/2)} \equiv B_6^{(1/2)}(m_c)$ and $B_8^{(3/2)} \equiv B_8^{(3/2)}(m_c)$ and the strange- and down-quark masses⁷ as

$$R_i \equiv B_i^{(j)} \left[\frac{112.3 \text{ MeV}}{m_s(m_c) + m_d(m_c)} \right]^2. \quad (4.1.43)$$

The hadronic parameters present the dominant source of theoretical uncertainty in the prediction of the ratio ϵ'_K/ϵ_K . The status of the calculation of the $\langle \pi\pi | Q_{6,8} | K \rangle$ matrix elements is reviewed in [291]. While $B_8^{(3/2)} = 1.0 \pm 0.2$ is obtained in various approaches, the situation with $B_6^{(1/2)}$ is far less clear. For instance, in the framework of the $1/N_c$ expansion, values for

⁷The normalization is adapted to our updated values of m_d and m_s compared to *e.g.* [291].

$B_6^{(1/2)}$ notably above unity are obtained [292–295]. For example, the authors of [292, 293] find $B_6^{(1/2)} = 2.5 \pm 0.4$ and $B_8^{(3/2)} = 1.1 \pm 0.3$. On the other hand, while the quenched calculations of the values of $B_8^{(3/2)}$ are compatible with unity [296, 297], they are lower than 1 for $B_6^{(1/2)}$ [298, 299]. First unquenched determinations of the parameters $B_6^{(1/2)}$ and $B_8^{(3/2)}$ are becoming possible very recently. A qualitative understanding of the $\Delta I = 1/2$ rule — the fact that the final two pion state is about 450 times more likely to have isospin $I = 0$ than $I = 2$ — was given in [300]. They find that the two dominant non-perturbative matrix elements entering the isospin 2 and 0 amplitudes cancel in the former, while they add constructively in the latter. However, a final result for the isospin 0 amplitude at physical meson masses is not yet available.

In view of the rather uncertain value of $B_6^{(1/2)}$, we adopt a very conservative point of view and scan the hadronic parameters and light masses in our SM analysis of ϵ'_K/ϵ_K over the ranges

$$B_6^{(1/2)} \in [0.8, 2.0], \quad B_8^{(3/2)} \in [0.8, 1.2], \quad m_s(m_c) + m_d(m_c) \in [107.8, 117.0] \text{ MeV}, \quad (4.1.44)$$

requiring in addition $B_6^{(1/2)} > B_8^{(3/2)}$, as suggested by studies of the $\langle \pi\pi | Q_{6,8} | K \rangle$ matrix elements in the framework of the $1/N_c$ expansion [292–295]. The quoted ranges of the light quark masses at the scale m_c correspond to the 2σ ranges of the values given in appendix B.2 for the scale 2 GeV, when including all relevant errors in the renormalization-group evolution.

Our SM prediction reads

$$\left(\frac{\epsilon'_K}{\epsilon_K} \right)_{\text{SM}} = \left(11.3_{-3.6}^{+31.5} \right) \cdot 10^{-4}, \quad (4.1.45)$$

where the quoted central value has been obtained from (4.1.39) by setting $F_{\text{RS}} = 0$ and $R_{6,8} = 1$. In particular, it includes the normalization factor $|\epsilon_K|_{\text{exp}}/|\epsilon_K|_{\text{SM}}$ with $|\epsilon_K|_{\text{SM}}$ taken from (4.1.32). Rather than corresponding to a 68% CL, the given uncertainties represent the ranges in which we believe that the true value of $(\epsilon'_K/\epsilon_K)_{\text{SM}}$ lies with a high probability. Note that within errors the SM prediction is in agreement with the experimental value given above, as well as other SM predictions [284, 291, 301]. In our numerical analysis of ϵ'_K/ϵ_K in the RS scenario, we scan independently over the ranges given in (4.1.44) requiring $B_6^{(1/2)} > B_8^{(3/2)}$, and check whether it is possible to achieve agreement with the measured value. We will see below that, even with such a conservative treatment of errors, the constraint from ϵ'_K/ϵ_K has a non-negligible effect on the possible new-physics effects in rare K decays within the RS model.

Rare K and B Decays

In the following, we gather the formulas for the numerical analysis of rare kaon decays. We begin with the “golden modes” $K \rightarrow \pi\nu\bar{\nu}$ and then discuss the theoretically less clean $K_L \rightarrow \mu^+\mu^-$ and $K_L \rightarrow \pi^0 l^+ l^-$ channels. We emphasize that the latter modes can add useful information on the chiral nature of the flavor structure of possible non-standard interactions. Finally, we summarize also the necessary formulas for an evaluation of $B_{d,s} \rightarrow \mu\mu$.

The effective Hamiltonian describing $s \rightarrow d\nu\bar{\nu}$ transitions reads

$$\mathcal{H}_{\text{eff}}^{s \rightarrow d\nu\bar{\nu}} = C_\nu (\bar{d}_L \gamma^\mu s_L) \sum_l (\bar{\nu}_{lL} \gamma_\mu \nu_{lL}) + \tilde{C}_\nu (\bar{d}_R \gamma^\mu s_R) \sum_l (\bar{\nu}_{lL} \gamma_\mu \nu_{lL}), \quad (4.1.46)$$

where the new-physics contributions arising in the RS model are given by

$$C_\nu^{\text{RS}} = \frac{2\pi\alpha}{s_w^2 c_w^2 M_{\text{KK}}^2} (\Sigma_D)_{12}, \quad \tilde{C}_\nu^{\text{RS}} = -\frac{2\pi\alpha}{s_w^2 c_w^2 M_{\text{KK}}^2} (\Sigma'_d)_{12}. \quad (4.1.47)$$

Higgs exchange gives no contribution due to the smallness of neutrino masses.

After summation over the three neutrino flavors, the branching ratios for the $K \rightarrow \pi\nu\bar{\nu}$ modes can be written as

$$\begin{aligned} \text{Br}(K_L \rightarrow \pi^0 \nu\bar{\nu}) &= \kappa_L (\text{Im } X)^2, \\ \text{Br}(K^+ \rightarrow \pi^+ \nu\bar{\nu}(\gamma)) &= \kappa_+ (1 + \Delta_{\text{EM}}) |X|^2, \end{aligned} \quad (4.1.48)$$

where $\kappa_L = (2.231 \pm 0.013) \cdot 10^{-10} (\lambda/0.225)^8$ and $\kappa_+ = (0.5173 \pm 0.0025) \cdot 10^{-10} (\lambda/0.225)^8$ capture isospin-breaking corrections in relating $K \rightarrow \pi\nu\bar{\nu}$ to $K \rightarrow \pi e\nu$, while the factor $\Delta_{\text{EM}} = -0.003$ encodes long-distance QED corrections affecting the charged mode [302]. The SM and RS contributions entering the coefficient $X \equiv X_{\text{SM}} + X_{\text{RS}}$ take the form

$$X_{\text{SM}} = \frac{\lambda_t^{(ds)}}{\lambda^5} X_t + \frac{\text{Re } \lambda_c^{(ds)}}{\lambda} P_{c,u}, \quad X_{\text{RS}} = \frac{s_w^4 c_w^2 M_Z^2}{\alpha^2 \lambda^5} (C_\nu^{\text{RS}} + \tilde{C}_\nu^{\text{RS}}). \quad (4.1.49)$$

The top-quark contribution is $X_t = 1.469 \pm 0.017$ [303–305], and the parameter $P_{c,u} = (0.41 \pm 0.04) (0.225/\lambda)^4$ includes dimension-six and -eight charm-quark effects and genuine long-distance contributions due to up-quark loops [306–309].⁸

Adding individual errors in quadrature, we find the following SM predictions for the two $K \rightarrow \pi\nu\bar{\nu}$ branching fractions:

$$\begin{aligned} \text{Br}(K_L \rightarrow \pi^0 \nu\bar{\nu})_{\text{SM}} &= (2.5 \pm 0.4) \cdot 10^{-11}, \\ \text{Br}(K^+ \rightarrow \pi^+ \nu\bar{\nu}(\gamma))_{\text{SM}} &= (8.0 \pm 0.9) \cdot 10^{-11}. \end{aligned} \quad (4.1.50)$$

The quoted errors are dominated by the uncertainties due to the CKM input. For a more precise break-up into the various sources of uncertainty, we refer to [305]. In view of the expected improvement in the extraction of the mixing angles, precise measurements of the $K \rightarrow \pi\nu\bar{\nu}$ branching ratios will provide a unique test of the flavor sector of a variety of models of new physics, in particular of those where the strong Cabibbo suppression of the SM amplitude is not present.

The effective Hamiltonian for $s \rightarrow dl^+l^-$ transitions contains the following operators in addition to those entering $\mathcal{H}_{\text{eff}}^{\Delta S=1}$ as given in (4.1.34):

$$\begin{aligned} \mathcal{H}_{\text{eff}}^{s \rightarrow dl^+l^-} &= C_{l1} (\bar{d}_L \gamma^\mu s_L) \sum_l (\bar{l}_L \gamma_\mu l_L) + C_{l2} (\bar{d}_L \gamma^\mu s_L) \sum_l (\bar{l}_R \gamma_\mu l_R) \\ &+ \tilde{C}_{l1} (\bar{d}_R \gamma^\mu s_R) \sum_l (\bar{l}_R \gamma_\mu l_R) + \tilde{C}_{l2} (\bar{d}_R \gamma^\mu s_R) \sum_l (\bar{l}_L \gamma_\mu l_L) \\ &+ C_{l3} (\bar{d}_L s_R) \sum_l (\bar{l}l) + \tilde{C}_{l3} (\bar{d}_R s_L) \sum_l (\bar{l}l), \end{aligned} \quad (4.1.51)$$

⁸The parameter $P_{c,u}$ is affected by new-physics contributions of order $m_{Z,W}^2/M_{\text{KK}}^2$ to the neutral- and charged-current interactions present in the RS scenario. Compared to the SM contribution these corrections are negligible. The same applies to the charm-quark effects appearing in $K_L \rightarrow \mu^+\mu^-$.

where in the RS model

$$\begin{aligned}
 C_{l1}^{\text{RS}} &= -\frac{4\pi\alpha}{3M_{\text{KK}}^2} (\Delta'_D)_{12} - \frac{2\pi\alpha(1-2s_w^2)}{s_w^2 c_w^2 M_{\text{KK}}^2} (\Sigma_D)_{12}, \\
 C_{l2}^{\text{RS}} &= -\frac{4\pi\alpha}{3M_{\text{KK}}^2} (\Delta'_D)_{12} + \frac{4\pi\alpha}{c_w^2 M_{\text{KK}}^2} (\Sigma_D)_{12}, \\
 \tilde{C}_{l1}^{\text{RS}} &= -\frac{4\pi\alpha}{3M_{\text{KK}}^2} (\Delta'_d)_{12} - \frac{4\pi\alpha}{c_w^2 M_{\text{KK}}^2} (\Sigma'_d)_{12}, \\
 \tilde{C}_{l2}^{\text{RS}} &= -\frac{4\pi\alpha}{3M_{\text{KK}}^2} (\Delta'_d)_{12} + \frac{2\pi\alpha(1-2s_w^2)}{s_w^2 c_w^2 M_{\text{KK}}^2} (\Sigma'_d)_{12}, \\
 C_{l3}^{\text{RS}} &= -\frac{2m_l}{M_h^2 v} (\Delta g_h^d)_{12}, \quad \tilde{C}_{l3}^{\text{RS}} = -\frac{2m_l}{M_h^2 v} (\Delta g_h^d)_{21}^*. \tag{4.1.52}
 \end{aligned}$$

Similar to the case of Higgs contributions to ϵ_K , the corrections to $s \rightarrow dl^+l^-$ arising from C_{l3}^{RS} and $\tilde{C}_{l3}^{\text{RS}}$ turn out to be mostly subleading. We take them into account, in order to reproduce the correct distribution also for the region with small effects of new physics.

Notice that electromagnetic dipole operators enter the effective Hamiltonian for $s \rightarrow dl^+l^-$ first at the one-loop level and thus are formally subleading with respect to the contributions from semileptonic operators. Whether this formal suppression translates into a numerical one can only be seen by calculating the complete one-loop matching corrections to the Wilson coefficients of the electromagnetic dipole operators in the RS model. Such a computation seems worthwhile but is beyond the scope of this thesis. The possibility that the inclusion of such one-loop effects could have a non-negligible impact on our results should however be kept in mind.

The branching ratio of the $K_L \rightarrow \mu^+\mu^-$ decay can be expressed as [310]

$$\text{Br}(K_L \rightarrow \mu^+\mu^-) = \left(6.7 + [1.1 \text{Re}(Y'_A) + y_c \pm y_{\gamma\gamma}]^2 + [0.08 \text{Im}(Y'_S)]^2 \right) \cdot 10^{-9}, \tag{4.1.53}$$

where $y_c = (-0.20 \pm 0.03)$ and $y_{\gamma\gamma} = 0.4 \pm 0.5$ encode the charm-quark contribution [311] and two-photon correction [312], respectively. The sign of the latter contribution depends on the sign of the $K_L \rightarrow \gamma\gamma$ amplitude, which in turn depends on the sign of an unknown low-energy constant. Theoretical arguments suggest that the sign of the $K_L \rightarrow \gamma\gamma$ amplitude is positive [313]. Better measurements of $K_S \rightarrow \pi^0\gamma\gamma$ and $K^+ \rightarrow \pi^+\gamma\gamma$ could settle this issue. The error on $y_{\gamma\gamma}$ reflects only the uncertainty on the dispersive part of the two-photon amplitude, which at present is the dominant individual source of error.

The coefficients $Y'_{A,S}$ are given by

$$Y'_A = y_A + \frac{s_w^2 c_w^2 M_Z^2}{2\pi\alpha^2 \lambda_t^{(ds)}} \left(C_{l1}^{\text{RS}} - C_{l2}^{\text{RS}} + \tilde{C}_{l1}^{\text{RS}} - \tilde{C}_{l2}^{\text{RS}} \right), \quad Y'_S = \frac{s_w^4 c_w^4 M_Z^4}{\alpha^2 m_l m_s} \left(C_{l3}^{\text{RS}} - \tilde{C}_{l3}^{\text{RS}} \right), \tag{4.1.54}$$

where $y_A = (-0.68 \pm 0.03)$ is the SM contribution to the Wilson coefficient of the semileptonic axial-vector operator [314], and the coefficients C_{l1-3}^{RS} . The coefficient Y'_S describes the correction due to tree-level Higgs exchange. This correction is scale dependent but numerically insignificant, so that in practice one can neglect its RG evolution.

In the SM, one finds for the $K_L \rightarrow \mu^+\mu^-$ branching ratio

$$\text{Br}(K_L \rightarrow \mu^+\mu^-)_{\text{SM}} = \{7.0 \pm 0.6, 8.5 \pm 1.4\} \cdot 10^{-9}, \tag{4.1.55}$$

in the case of positive/negative sign of the two-photon amplitude. The shown uncertainties have been obtained by adding the individual errors in quadrature. The world average of the measured value is dominated by the B871 experiment at BNL. It reads $\text{Br}(K_L \rightarrow \mu^+ \mu^-)_{\text{exp}} = (6.84 \pm 0.11) \cdot 10^{-9}$ [69]. We will see below that the $K_L \rightarrow \mu^+ \mu^-$ decay can lead to interesting constraints in the RS model, once they are measured precisely.

The branching ratios of the decays $K_L \rightarrow \pi^0 l^+ l^-$ are obtained from

$$\text{Br}(K_L \rightarrow \pi^0 l^+ l^-) = \left(C_{\text{dir}}^l \pm C_{\text{int}}^l |a_S| + C_{\text{mix}}^l |a_S|^2 + C_{\gamma\gamma}^l + C_S^l \right) \cdot 10^{-12}, \quad (4.1.56)$$

where the chiral-perturbation-theory counterterm $|a_S| = 1.20 \pm 0.20$ has been extracted from the measurements of the $K_S \rightarrow \pi^0 l^+ l^-$ branching fraction [315, 316]. The coefficients $C_{\text{dir,int,mix},\gamma\gamma,S}^l$ read [310]

$$\begin{aligned} C_{\text{dir}}^e &= (4.62 \pm 0.24) [(\text{Im } Y_A)^2 + (\text{Im } Y_V)^2], \\ C_{\text{int}}^e &= (11.3 \pm 0.3) \text{Im } Y_V, \quad C_{\text{mix}}^e = 14.5 \pm 0.5, \quad C_{\gamma\gamma}^e \approx C_S^e \approx 0, \\ C_{\text{dir}}^\mu &= (1.09 \pm 0.05) [2.32 (\text{Im } Y_A)^2 + (\text{Im } Y_V)^2], \\ C_{\text{int}}^\mu &= (2.63 \pm 0.06) \text{Im } Y_V, \quad C_{\text{mix}}^\mu = 3.36 \pm 0.20, \quad C_{\gamma\gamma}^\mu = 5.2 \pm 1.6, \\ C_S^\mu &= (0.04 \pm 0.01) \text{Re } Y_S + 0.0041 (\text{Re } Y_S)^2. \end{aligned} \quad (4.1.57)$$

They describe short-distance direct CP violation C_{dir}^l , long-distance indirect CP violation C_{mix}^l , which can be determined from the experimental data on $K_S \rightarrow \pi^0 l^+ l^-$, and a long-distance CP -conserving correction $C_{\gamma\gamma}^l$, which can be extracted from a measurement of $K_L \rightarrow \pi^0 \gamma\gamma$. The direct and indirect CP -violating amplitudes interfere, leading to the term C_{int}^l . The analyses in [317, 318] point towards a constructive interference, *i.e.* the plus sign in (4.1.56). Correction due to scalar operators are encoded in C_S^l . Both $C_{\gamma\gamma}^l$ is helicity suppressed and is therefore negligible.

The coefficients $Y_{A,V,S}$ take the form

$$\begin{aligned} Y_A &= y_A + \frac{s_w^2 c_w^2 M_Z^2}{2\pi\alpha^2 \lambda_t^{(ds)}} \left(C_{l1}^{\text{RS}} - C_{l2}^{\text{RS}} - \tilde{C}_{l1}^{\text{RS}} + \tilde{C}_{l2}^{\text{RS}} \right), \\ Y_V &= y_V - \frac{s_w^2 c_w^2 M_Z^2}{2\pi\alpha^2 \lambda_t^{(ds)}} \left(C_{l1}^{\text{RS}} + C_{l2}^{\text{RS}} + \tilde{C}_{l1}^{\text{RS}} + \tilde{C}_{l2}^{\text{RS}} \right), \\ Y_S &= \frac{s_w^4 c_w^4 M_Z^4}{\alpha^2 m_l m_s} \left(C_{l3}^{\text{RS}} + \tilde{C}_{l3}^{\text{RS}} \right), \end{aligned} \quad (4.1.58)$$

where $y_V = 0.73 \pm 0.04$ represents the SM contribution to the Wilson coefficient of the semileptonic vector operator [314]. The coefficients C_{l1-3}^{RS} and $\tilde{C}_{l1-3}^{\text{RS}}$ entering Y_V are understood to be evaluated at a low-energy scale $\mu \approx 1$ GeV. In the numerical analysis we use leading order RG running to determine these coefficients from the initial conditions of $C_{3-6,l1-3}^{\text{RS}}$ and $\tilde{C}_{3-6,l1-3}^{\text{RS}}$ as given in (4.1.36) and (4.1.52). The new-physics contributions affect mainly Y_A , as the corresponding contributions in Y_V cancel each other to a large extent and Y_S is suppressed. In consequence, RG effects influence the obtained results only in a minor way.

The SM predictions for the branching ratios of $K_L \rightarrow \pi^0 l^+ l^-$ are given by

$$\begin{aligned} \text{Br}(K_L \rightarrow \pi^0 e^+ e^-)_{\text{SM}} &= \{3.5 \pm 0.9, 1.6 \pm 0.6\} \cdot 10^{-11}, \\ \text{Br}(K_L \rightarrow \pi^0 \mu^+ \mu^-)_{\text{SM}} &= \{1.4 \pm 0.3, 0.9 \pm 0.2\} \cdot 10^{-11}, \end{aligned} \quad (4.1.59)$$

for constructive/destructive interference. Better measurements of the $K_S \rightarrow \pi^0 l^+ l^-$ decay rate would allow to improve the quoted errors, which are currently dominated by the uncertainty due to the chiral-perturbation-theory parameter $|a_S|$.

The integrated forward-backward CP asymmetry for $K_L \rightarrow \pi^0 \mu^+ \mu^-$ is given by [310]

$$A_{\text{FB}}(K_L \rightarrow \pi^0 \mu^+ \mu^-) = \frac{(1.3 \pm 0.1) \text{Im} Y_V \mp 0.057 |a_S| \text{Re} Y_S \pm (1.7 \pm 0.2) |a_S|}{\text{Br}(K_L \rightarrow \pi^0 \mu^+ \mu^-)} \cdot 10^{-12}, \quad (4.1.60)$$

and the corresponding SM predictions read

$$A_{\text{FB}}(K_L \rightarrow \pi^0 \mu^+ \mu^-)_{\text{SM}} = \{21 \pm 4, -12 \pm 4\} \%, \quad (4.1.61)$$

with the upper and lower sign in the case of constructive and destructive interference, respectively. Despite the fact that the predictions of the decays $K_L \rightarrow \pi^0 l^+ l^-$ are not fully under theoretical control, the latter transitions represent promising channels to study new physics. In particular, the different impact of helicity-suppressed contributions to the muon and electron modes makes the comparison of $K_L \rightarrow \pi^0 \mu^+ \mu^-$ and $K_L \rightarrow \pi^0 e^+ e^-$ a powerful tool for analyzing the chiral properties of non-standard flavor interactions.

Finally, we also consider the decay channel of B_q mesons to two muons. The branching ratios for $q = d, s$ can be expressed as

$$\begin{aligned} \langle \text{Br}(B_q \rightarrow \mu^+ \mu^-) \rangle &= \frac{1}{1 - y_q} \frac{G_F^2 \alpha^2 m_{B_q}^3 f_{B_q}^2 \tau_{B_q}}{64 \pi^3 s_w^4} |\lambda_t^{(qb)}|^2 \sqrt{1 - \frac{4m_\mu^2}{m_{B_q}^2}} \\ &\times \left(\frac{4m_\mu^2}{m_{B_q}^2} |C_A - C'_A|^2 + m_{B_q}^2 \left[1 - \frac{4m_\mu^2}{m_{B_q}^2} \right] \left| \frac{m_b C_S - m_q C'_S}{m_b + m_q} \right|^2 \right), \end{aligned} \quad (4.1.62)$$

where m_{B_q} , f_{B_q} , and τ_{B_q} are the mass, decay constant, and lifetime of the B_q meson. The electromagnetic coupling α entering the branching ratios is to be evaluated at M_Z . Here we consider the time-averaged values over $t \gg \tau_{B_q}$. This is indicated by the angle brackets in (4.1.62). It was found in [319] that the finite lifetime difference of the two B_q mass eigenstates gives a relevant shift between the experimentally accessible time-averaged value and the theoretically calculated value at decay time $t = 0$ in the case of $q = s$. This is encoded in the relative deviation of the two B_s mass eigenstates $y_s = (\Gamma_s^L - \Gamma_s^H)/(\Gamma_s^L + \Gamma_s^H) = 0.088 \pm 0.014$, whereas the effect is negligible for $q = d$. This result holds for new physics only if (pseudo-)scalar contributions are small, which is true in the case at hand.

The coefficients $C_{A,S}$ and $C'_{A,S}$ read

$$\begin{aligned} C_A &= c_A - \frac{s_w^4 c_w^2 M_Z^2}{\alpha^2 \lambda_t^{(qb)}} \left(C_{l1}^{\text{RS}} - C_{l2}^{\text{RS}} \right), & C'_A &= \frac{s_w^4 c_w^2 M_Z^2}{\alpha^2 \lambda_t^{(qb)}} \left(\tilde{C}_{l1}^{\text{RS}} - \tilde{C}_{l2}^{\text{RS}} \right), \\ C_S &= \frac{2s_w^4 c_w^2 M_Z^2}{\alpha^2 m_b \lambda_t^{(qb)}} C_{l3}^{\text{RS}}, & C'_S &= \frac{2s_w^4 c_w^2 M_Z^2}{\alpha^2 m_q \lambda_t^{(qb)}} \tilde{C}_{l3}^{\text{RS}}, \end{aligned} \quad (4.1.63)$$

where $c_A = 0.96 \pm 0.02$ denotes the SM contribution to the Wilson coefficient of the axial-vector current [303, 304], and the coefficients C_{l1-3}^{RS} and $\tilde{C}_{l1-3}^{\text{RS}}$ now contain the (1,3) or (2,3) elements of the mixing matrices for $q = d, s$. Note that C_A and C'_A are scale independent.

The SM branching ratios of the $B_q \rightarrow \mu^+ \mu^-$ decay channels evaluate to

$$\begin{aligned} \langle \text{Br}(B_d \rightarrow \mu^+ \mu^-)_{\text{SM}} \rangle &= (1.05 \pm 0.11) \cdot 10^{-10}, \\ \langle \text{Br}(B_s \rightarrow \mu^+ \mu^-)_{\text{SM}} \rangle &= (3.48 \pm 0.32) \cdot 10^{-9}, \end{aligned} \quad (4.1.64)$$

with our choice of input parameters. This agrees well with values given in [319–321]. Leptonic B -meson decays belong to the channels that are studied by three out of the four major LHC experiments, namely ATLAS, CMS, and LHCb. A very recent analysis of LHCb has indeed found evidence at 3.5σ CL for a branching ratio that is compatible with the SM prediction $\langle \text{Br}(B_s \rightarrow \mu^+ \mu^-)_{\text{exp}} \rangle = (3.2_{-1.2}^{+1.5}) \cdot 10^{-9}$ [260] with an error that is to 95% of statistical origin, so the measurement is expected to improve significantly in the near future. The latter reference also includes an upper limit of $\langle \text{Br}(B_d \rightarrow \mu^+ \mu^-)_{\text{exp}} \rangle < 9.4 \cdot 10^{-10}$ at 95% CL. This result strongly constrains new physics contributions, particularly through the scalar semileptonic operators, which occur *e.g.* in the MSSM at large $\tan(\beta)$. We will see below that the constraint also starts to cut into the RS parameter space.

4.1.2.3 Modifications of the CKM Matrix

A physically meaningful definition of the CKM matrix, which can be compared to experimental results, is based on effective four-fermion interactions. In the RS model, it is induced by the exchange of the entire tower of W bosons and their KK excitations. In the custodial model this includes the modes of the charged gauge bosons from the additional $SU(2)_R$. Furthermore, an extraction of a CKM element generally involves a normalization of the semileptonic amplitude relative to the Fermi constant G_F . We accounted for this, such that the individual factors in the combination $G_F \mathbf{V}_{L,R}$ are physically observable, and we have given the result for the corresponding CKM matrices in (3.3.154).

The dominant contribution to the right-handed mixing matrix \mathbf{V}_R is suppressed both by a factor v^2/M_{KK}^2 and a chiral factor $m_u m_d/v^2$. The latter reflects the fact that \mathbf{V}_R purely originates from quark mixing. In consequence, right-handed charged-current interactions are too small to give rise to any observable effect.

Unlike the CKM matrix in the SM, the left-handed quark mixing matrix \mathbf{V}_L is not unitary [1, 200, 239, 322]. However, we found in an explicit numerical analysis of the minimal RS model [3] that the effect is unobservable. Here, we summarize the general argument why this is to be expected.

The leading contribution to \mathbf{V}_L in (3.3.154) stems from Δ_{mn}^{+Q} , which is unitary to a very good approximation. Corrections of order v^2/M_{KK}^2 arise from the non-universality of KK-gauge bosons encoded in $\bar{\Delta}_{mn}^{+Q}$. In the custodial RS model also the admixtures from U' and D' quarks described by ϵ_{mn}^{+q} are relevant, whereas the admixtures of U , D , and u' quarks are of order v^4/M_{KK}^4 and will be neglected in the following. From (3.3.154), it is also evident that no custodial protection mechanism is at work in the charged-current sector [216].

The most precise measure of CKM unitarity violation is given by the combination of the first row elements

$$\Delta_{\text{row}1}^{\text{non}} \equiv (\mathbf{1} - \mathbf{V}_L \mathbf{V}_L^\dagger)_{11} = 1 - (|V_{ud}|^2 + |V_{us}|^2 + |V_{ub}|^2), \quad (4.1.65)$$

and determined to be $\Delta_{\text{row}1}^{\text{non}} = (1 \pm 6) \cdot 10^{-4}$ [69]. We obtain an approximate expression for the first row non-unitarity using a Froggatt-Nielsen analysis, *i.e.* we obtain the leading contribution in an expansion in the Cabibbo angle λ (see (3.3.92)). Normalizing the result to the typical value of the bulk-mass parameter c_{Q_1} as given in table B.1, we obtain in the

custodial RS model

$$\begin{aligned} \Delta_{\text{row1}}^{\text{non}} &\approx 2 \cdot 10^{-6} \left(\frac{F(c_{Q_1})}{F(-0.63)} \frac{\text{TeV}}{M_{\text{KK}}} \right)^2 \\ &\times \left[\left| \text{diag} \left(\sqrt{\frac{2}{3+2c_{Q_i}}} \right) \vec{u} \right|^2 - \frac{v^2}{M_W^2 L} \left| \text{diag} \left(\sqrt{\frac{2}{1-2c_{\mathcal{T}_i}}} \right) \mathbf{Y}_d^T \vec{u} \right|^2 \right]. \end{aligned} \quad (4.1.66)$$

The vector \vec{u} is given by

$$\vec{u} = \left(1, -\frac{(M_u)_{21}}{(M_u)_{11}}, \frac{(M_u)_{31}}{(M_u)_{11}} \right), \quad (4.1.67)$$

where M_u denotes the matrix of minors of \mathbf{Y}_u . In the minimal RS model, only the first contribution in the square brackets in (4.1.66) is present. It gives a strictly positive contribution to Δ_1^{non} , which is typically of $\mathcal{O}(1)$ but may vary with the up Yukawa matrix elements in \vec{u} . The resulting non-unitarity however stays well below the observable limit due to the very small prefactor in (4.1.66). The contributions from the admixture of U' and D' quarks feed into second term in the square brackets in (4.1.66). They are typically of $\mathcal{O}(y_d^2/4)$ and have negative sign. This can in principle lead to negative values of Δ_1^{non} , but is again below observable limits.

A detailed discussion of the breakdown of CKM non-unitarity in the custodial RS model has also been presented in [239]. Unfortunately, in that work the CKM matrix is defined via the $W u_L^i d_L^j$ vertex and not the effective four-fermion interactions induced by the exchange of the W boson and its KK excitations. Also the modification of G_F is not considered there. These differences prevent us from a straightforward comparison of the results in [239] with ours.

In [3], we also considered direct extractions of the CKM matrix elements $|V_{ub}|$, $|V_{cb}|$, and $|V_{tb}|$. The value of $|V_{ub}/V_{cb}|$ can be determined from the relative ratio of charmless over charmed semileptonic B decays. It enters the expression $R_u \equiv |(V_{ud}V_{ub}^*)/(V_{cd}V_{cb}^*)|$, *i.e.* the length of the side of the rescaled unitarity triangle opposite to the angle β . We found that also the RS contributions to R_u and contributions to the $B \rightarrow \tau \nu_\tau$ branching ratio from the modification of $|V_{ub}|$ alone stay below the observable level. Particularly it is not possible to explain the 3σ tension between the inclusive and exclusive determination of V_{ub} [323]. A direct determination of $|V_{tb}|$ without assuming unitarity is possible from measurements of the single top-quark production cross section. This could become interesting at the high energy LHC run. Simulation studies by ATLAS [324] and CMS [325] suggest that the cross section of the most promising single-top-production channel, namely $pp \rightarrow tqb + X$, will be measurable with a total error of 10%, which implies that $|V_{tb}|$ could be determined with 5% accuracy. It is straightforward to find an approximation for V_{tb} in the RS model in the same way as we arrived at (4.1.66). We obtain in the custodial RS model

$$V_{tb} \approx 1 - 3 \cdot 10^{-2} \left(\frac{F(c_{Q_3})}{F(-0.34)} \frac{\text{TeV}}{M_{\text{KK}}} \right)^2 \left[\frac{2}{3+2c_{Q_3}} - \frac{v^2}{M_W^2 L} \sum_i \frac{2|Y_d)_{3i}|^2}{1-2c_{\mathcal{T}_i}} \right], \quad (4.1.68)$$

where the second term in square brackets is again absent in the minimal RS model. Remark that no further Yukawa entries are present in the strictly negative contribution of the minimal RS model. This modification cannot be enhanced much further — it leads to a minimal 4% reduction at $c_{Q_3} = 0.5$ instead of the typical 3% — such that the modification of V_{tb} remains

close to, but below the potentially observable level, even for a KK scale as low as 1 TeV. The positive contribution in the custodial model typically even cancels this modification.

We conclude that the split fermion structure and the necessarily high scale of the RS model effectively prevents modifications of the CKM matrix from potential observation, and that a cancellation of contributions in the custodial model countervails the possible effect of a lower accessible scale.

4.1.2.4 Numerical Analysis of Flavor Observables

In the following part, we describe our numerical analysis of the flavor processes we introduced above, based on the minimal RS model of section 3.3.4.2.

We scan the parameter space of the RS model, taking into account also the constraints from precision measurements of $Z \rightarrow b\bar{b}$ decays. A discussion of these constraints follows in section 4.2.2. Details of the employed algorithm and statistical quality of the parameter space sample we use here are summarized in appendix B.3. We remark that it is not possible to associate a rigorous statistical meaning to the calculated fractions of such a frequentistic Monte-Carlo probe of the parameter space, as it always depends on how the parameters are generated and fits are performed. Therefore, we lay out the details of our technique in the appendix.

We introduce a standard scenario, which corresponds to the usual setup of the RS model, with natural Yukawa matrices that are restricted by the perturbativity bound of [211], and full warping that connects UV-brane energy scales with the Planck scale. We will quantify constraints and correlations within this standard scenario (labeled “std” below). We will also investigate to which extent a scenario with an $SU(3)_{d_i}$ flavor symmetry in the right-handed down-quark bulk masses $c_{d_i} = c_d$ [254] (labeled “SU3d” and abbreviated as aligned scenario) and a scenario with warping of only three orders of magnitude $\epsilon = 10^{-3}$, the LRS model [192], allows us to relax the constraints arising and quark-flavor physics.

Kaon Mixing

The predictions for $|\epsilon_K|$ in the minimal RS model with standard parameter choices is displayed in the upper left panel of figure 4.3. The lower two panels shows the predictions for the two modified scenarios introduced above. All shown points reproduce the correct quark masses and CKM parameters within errors and are fine-tuned not stronger than one per-mil. These requirements are imposed on all the numerical data used below and understood implicitly in the following. We define the fine-tuning measure following Barbieri and Giudice [326] and describe our Monte-Carlo procedure in detail in appendix B.3. Points marked in blue are consistent with the bounds from electroweak precision observables (EWPOs) of the $Zb\bar{b}$ observables at the 3σ CL. The bound corresponds to (4.2.17), and we discuss it in detail in section 4.2.2. Points marked orange are furthermore consistent with the measurement of ϵ_K at 99% CL after combining theoretical and experimental errors. We observe a slow decoupling behavior with M_{KK} and a large spread of the RS corrections, which is illustrated by the middle cyan line, which represents the fit to the median value of $|\epsilon_K|$, as obtained after a fine grained binning in M_{KK} of the data set of gray points. We verified that the fit to the data set that fulfills the $Zb\bar{b}$ constraint is essentially unchanged, *i.e.* there is no correlation between this constraint and the distribution of $|\epsilon_K|$. While the median value of $|\epsilon_K|$ becomes consistent with the measurement for $M_{KK} \gtrsim 8$ TeV only, the 5% quantile crosses the experimentally allowed range already at 1.8 TeV. For such low values of M_{KK} one observes

from all three panels that the values of $|\epsilon_K|$ are on average a factor of about 100 larger than the SM prediction [211, 212, 229, 254, 255]. The order-of-magnitude enhancement of $|\epsilon_K|$ is explained by the following observations. First, it turns out that even for low KK scales the magnitude of the RS contribution to ΔM_K typically does not exceed the SM contribution by an unacceptably large amount given the huge SM uncertainties. Second, the ratio of imaginary to real part of the $K-\bar{K}$ mixing amplitude is strongly suppressed in the SM due

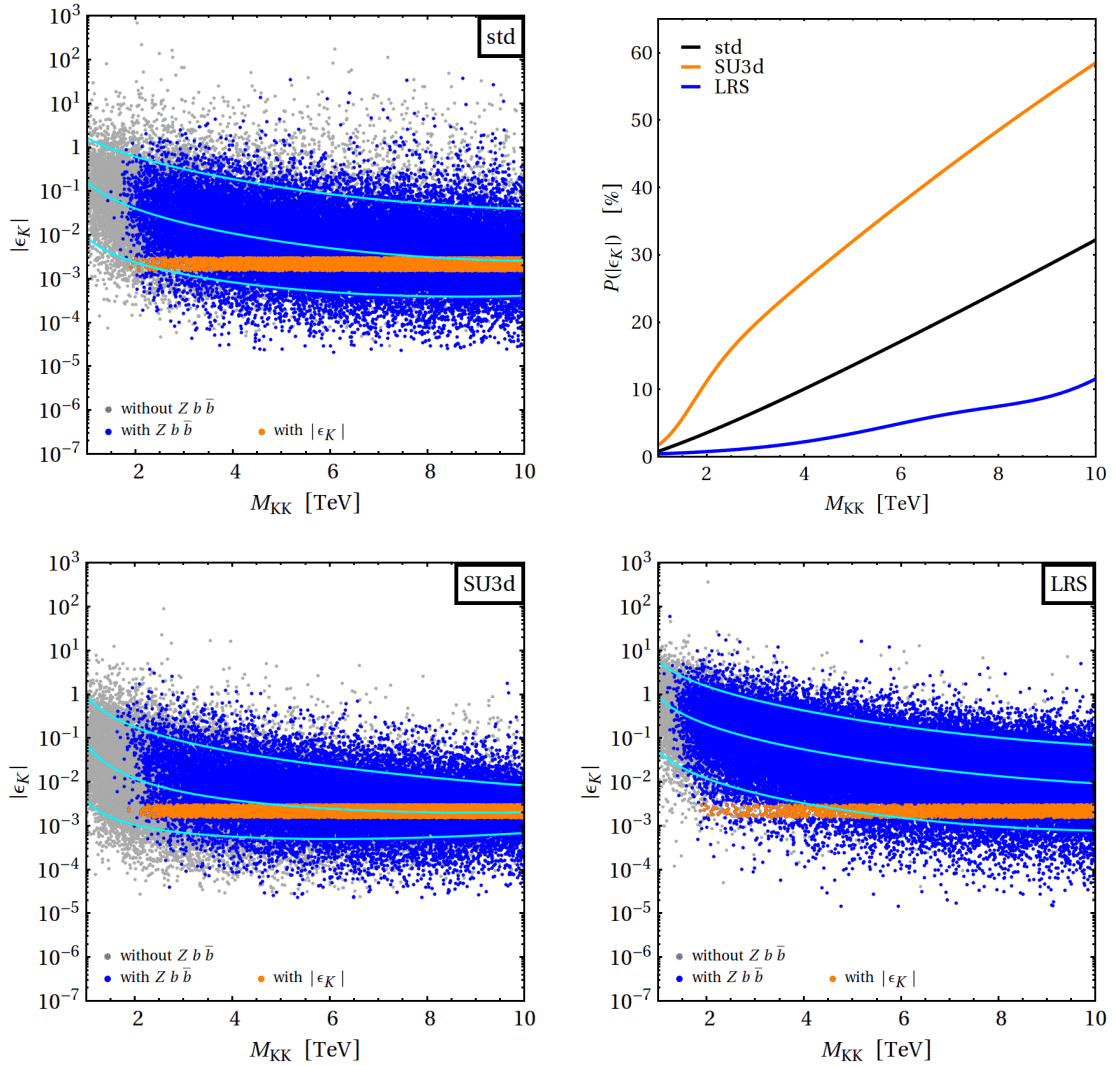


Figure 4.3: Predictions for $|\epsilon_K|$ as a function of M_{KK} in the three benchmark scenarios of the minimal RS model. Blue points fulfill the EWPO bounds of the $Zb\bar{b}$ vertex at the 3σ CL. Points that are additionally in agreement with the experimental value of $|\epsilon_K|$ at 99% CL (including the theory uncertainty) are colored orange. The three cyan lines illustrate the decoupling behavior with M_{KK} , as obtained from a fit to the 5%, 50%, and 95% quantile of the distribution of gray points. The upper right panel shows the percentage of gray scatter points that are consistent with the experimental values of $|\epsilon_K|$ as a function of M_{KK} .

to the smallness of $\text{Im}(V_{ts}^* V_{td})$. Numerically, one finds

$$\left[\frac{\text{Im} M_{12}^{K*}}{\text{Re} M_{12}^{K*}} \right]_{\text{SM}} \approx -2A^4 \lambda^{10} (1 - \bar{\rho}) \bar{\eta} \eta_{tt} S_0(x_t) / (\lambda^2 \eta_{cc} x_c) \approx -1/150, \quad (4.1.69)$$

where $S_0(x_t)$ originates from the one-loop box diagrams containing a top quark, while η_{tt} and η_{cc} summarize higher-order QCD corrections in the top- and charm-quark sectors [279, 327]. Under the natural assumption that the phase in $(M_{12}^{K*})_{\text{RS}}$ is of $\mathcal{O}(1)$, it follows that $|\epsilon_K|_{\text{RS}}/|\epsilon_K|_{\text{SM}} \sim 100$. Large deviations of $|\epsilon_K|_{\text{RS}}$ from this generic value require a certain, but mild tuning of parameters, for example an adjustment of the phase of the associated combination of Yukawa couplings, so that $\text{Im} M_{12}^{K*}$ becomes comparable to the SM value. We verified that this tuning is mild by producing the diagrams of figure 4.3 also for fine-tuning of less than one percent and find that relevant changes in the distribution appear only for values of $|\epsilon_K|$ far below the allowed region; in particular, there would be a hard cutoff of values $|\epsilon_K| \lesssim 0.1 |\epsilon_K|_{\text{exp}}$, which is irrelevant for the discussion at hand.

One method to protect specifically $|\epsilon_K|$ is to arrange for common bulk-mass parameters $c_d \equiv c_{d_i}$ in the sector of the right-handed down-type quarks [254], *e.g.* coming from a flavor symmetry $SU(3)_{dc}$ (labeled ‘‘SU3d’’ here). In this case, certain mixing matrices differ from the ones present in the RS model with hierarchical values of $F(c_{d_i})$. The phenomenologically most important change occurs in the case of $(\tilde{\Delta}_D)_{mn} \otimes (\tilde{\Delta}_d)_{mn}$, which becomes quasi-diagonal. To derive an expression for the off-diagonal elements, one has to expand the flavor matrices defined in (3.3.158) up to $\mathcal{O}(v^2/M_{\text{KK}}^2)$. Employing (3.3.88), we find that the relation (3.3.159) receives the correction

$$\begin{aligned} (\tilde{\delta}_D)_{mn} \otimes (\tilde{\delta}_d)_{mn} = \frac{m_{d_m} m_{d_n}}{M_{\text{KK}}^2} \sum_{i,j} & \left[(U_d^\dagger)_{mi} (U_d)_{in} (\tilde{\delta}_D)_{ij} (U_d^\dagger)_{mj} (U_d)_{jn} \right. \\ & \left. + (W_d^\dagger)_{mi} (W_d)_{in} (\tilde{\delta}_d)_{ij} (W_d^\dagger)_{mj} (W_d)_{jn} \right] \end{aligned} \quad (4.1.70)$$

from the terms in (3.3.158) involving both even $\mathbf{C}_m^{(A)}(\phi)$ and odd $\mathbf{S}_m^{(A)}(\phi)$ fermion profiles. Neglecting terms suppressed by $F^2(c_{Q_i})$ and $F^2(c_{Q_i})F^2(c_{Q_j})$, the elements of $(\tilde{\delta}_D)_{ij}$ take the form

$$(\tilde{\delta}_D)_{ij} = \frac{2(3 + c_{Q_i} - c_{Q_j})}{(3 + 2c_{Q_i})(3 - 2c_{Q_j})(2 + c_{Q_i} - c_{Q_j})} \frac{F^2(c_{Q_i})}{F^2(c_{Q_j})}. \quad (4.1.71)$$

An analogous expression holds in the case of $(\tilde{\delta}_d)_{ij}$ with c_{Q_i} replaced by c_{d_i} . Using a Froggatt-Nielsen like analysis, as discussed in section 3.3.6, we find that to leading order in hierarchies

$$(\tilde{\Delta}_D)_{mn} \otimes (\tilde{\Delta}_d)_{mn} \sim \begin{cases} F(c_{Q_m})F(c_{Q_n})F(c_{d_m})F(c_{d_n}), & \text{‘‘standard’’}, \\ F(c_{Q_m})F(c_{Q_n})F^2(c_d) \left(\delta_{mn} + \frac{Y_d^2 v^2}{2M_{\text{KK}}^2} \right), & \text{‘‘aligned’’}. \end{cases} \quad (4.1.72)$$

We have only shown the leading order flavor-off-diagonal contribution. Notice that the $\mathcal{O}(v^2/M_{\text{KK}}^2)$ correction arising in the aligned case is solely due to the first line in (4.1.70) involving left-handed rotations U_d . The contribution from the second line in (4.1.70) is further suppressed, since the universality of $(\tilde{\delta}_d)_{ij} \sim 1$ in combination with the unitarity of the W_d matrices renders it negligibly small.

The relation (4.1.72) implies that there is a suppression of the Wilson coefficient C_4^{RS} in the aligned relative to the standard hierarchical case. We find the following approximate scaling

$$\frac{(C_4^{\text{RS}})^{\text{“aligned”}}}{(C_4^{\text{RS}})^{\text{“standard”}}} \sim \frac{y_d^2 v^2}{2M_{\text{KK}}^2} \frac{m_d}{m_s} \frac{1}{\lambda} \approx 8 \cdot 10^{-3} \left(\frac{\text{TeV}}{M_{\text{KK}}} \right)^2 y_d^2, \quad (4.1.73)$$

where y_d is the typical absolute value of entries of the 5d down-type Yukawa matrix. Our results (4.1.72) and (4.1.73) agree with the findings in [254] derived by means of the mass-insertion approximation. The equivalence of our exact approach and the mass-insertion approximation follows from the “IR dominance” of the overlap integrals (3.3.158) and the boundary conditions in (3.3.42), which connect the odd $\mathcal{S}_n^{(A)}(\pi^-)$ with the even $\mathcal{C}_n^{(A)}(\pi)$ fermion profiles. While the suppression factor of $\mathcal{O}(100)$ in (4.1.73) appears promising, only a rigorous numerical analysis including all contributions can tell us to which extent the aligned scenario allows to relax the stringent constraint from $|\epsilon_K|$. The results of such an analysis are depicted in the lower left panel of figure 4.3, which shows a visible improvement relative to the standard benchmark scenario.

To quantify the improvement, we calculate the fraction $P(|\epsilon_K|)$ of points fulfilling the $|\epsilon_K|$ constraint by binning the data in M_{KK} in steps of 100 GeV and fitting the binned data to an appropriate function. In the case at hand, we find that the combination of a Fermi function and a second-order polynomial is perfectly suited to reproduced the observed behavior. From the upper right panel in figure 4.3, it is apparent that a significantly larger fraction of parameter space leads to a consistent description of the experimental data on $|\epsilon_K|$ compared to the standard scenario. Numerically, we find that $P(|\epsilon_K|) > 3\%$ is fulfilled for $M_{\text{KK}} > 1.8$ TeV ($M_{G(1)} > 4.4$ TeV) in the standard case and already for $M_{\text{KK}} > 1.2$ TeV ($M_{G(1)} > 3.0$ TeV) in the aligned case. We have also studied the effect of a slight misalignment of the bulk-mass parameters c_d , which effectively simulates the presence of flavor non-universal brane kinetic terms. In agreement with [254], we find that the obtained results depend very sensitively on the exact amount of non-universality and that already small deviations from $c_{d_i} = c_d$ can spoil the $\mathcal{O}(v^2/M_{\text{KK}}^2)$ suppression in (4.1.73). A drawback of the aligned RS framework is the impaired consistency with the EWPOs from $Z \rightarrow b\bar{b}$. This comes from the fact that the singlet b_R has to be localized further away from the IR brane compared to the original hierarchical case. Typically one has $c_{b_R} = c_d \approx -0.60$ instead of $c_{b_R} \approx -0.58$ (c.f. table B.1). In order to obtain the correct value of the bottom-quark mass, the doublet (t_L, b_L) thus needs to be localized more closely to the IR brane, which is disfavored by the resulting contributions to the $Zb_L\bar{b}_L$ coupling in the minimal RS model. Hence, it is even more favorable to combine the aligned scenario with the custodial bulk symmetry, where the $Zb_L\bar{b}_L$ corrections are essentially absent.

The presence of the “volume factor” L in (4.1.28) suggests another cure for the “flavor problem” in the $\Delta S = 2$ sector by reducing the UV cutoff sufficiently below the Planck scale. Indeed, the alleviation of the $|\epsilon_K|$ constraint has been mentioned as one of the attractive features of the LRS scenario [192]. However, a careful analysis reveals that the naive conjecture of a reduction of terms proportional to L is flawed in the case of $|\epsilon_K|$ [229]. This feature is illustrated in the lower right panel and the blue (lower) curve in the upper right panel of figure 4.3. We see that in the LRS scenario with $L = \ln(10^3)$, the value of $P(|\epsilon_K|)$ is strictly smaller than in the standard scenario for all values of M_{KK} . Comparing to the values given above, we find $P(|\epsilon_K|) > 3\%$ for $M_{\text{KK}} > 4.7$ TeV ($M_{G(1)} > 11.4$ TeV) only. The origin of the enhancement of flavor-changing $\Delta S = 2$ effects is the phenomenon of “UV dominance”,

which arises whenever the bulk-mass parameters determining the strange-quark mass satisfy the critical condition $c_{Q_2} + c_{d_2} < -2$ [229]. The relevant overlap integrals (3.3.158) are then dominated by the region near the UV brane, thereby partially evading the RS-GIM mechanism. New physics contributions to $|\epsilon_K|$ are then exponentially enhanced with respect to the standard scenario with $L = \ln(10^{16})$. While in the LRS scenarios thus no improvement concerning $|\epsilon_K|$ is achieved unless the UV cutoff is raised above several 10^3 TeV, this class of models still helps to relax the constraint from $Z \rightarrow b\bar{b}$. We discuss this in more detail in section 4.2.2. Further details on variants of the RS model with volume-truncated background can be found in [229].

It should have become clear from the above discussion and explanations that the “flavor problem” in the $\Delta S = 2$ sector in the framework of warped extra dimensions [211, 212, 229, 254, 255] depends highly on the required amount of allowed parameter space, even for natural parameters. We showed that the huge spread caused by the RS parameter space combined with the slow decoupling creates difficulties on what is to be considered as a bound on the scale of the RS model. For this reason, we warn the reader that simple statements on strong bounds from $|\epsilon_K|$ found in the literature can be misleading. Instead, we quantified the decoupling behavior, which allows for a detailed comparison of the standard minimal RS model to modified versions of the model with an $SU(3)_{d^c}$ flavor-symmetry or with volume-truncated background. Being very conservative, we find in the standard scenario of the minimal RS model

$$M_{\text{KK}} \gtrsim 0.7 \text{ TeV}, \quad M_{G^{(1)}} \gtrsim 1.7 \text{ TeV}, \quad (4.1.74)$$

from the total closure of the viable parameter space, *i.e.* $P(|\epsilon_K|) = 0$, in our parameter set with less than one per mil fine-tuning. This bound is similar to the one inferred from direct searches for resonances in the $t\bar{t}$ channel, which we discussed in section 4.1.2.1. A very natural solution with only one percent fine-tuning and $P(|\epsilon_K|) = 1\%$ is obtained for

$$M_{\text{KK}} \gtrsim 1.5 \text{ TeV}, \quad M_{G^{(1)}} \gtrsim 3.6 \text{ TeV}. \quad (4.1.75)$$

Deriving bounds from stricter requirements on the tuning are unsubstantiated in the light of the unsolved little hierarchy problem of the Higgs-mass value.

Rare Kaon Decays

We continue our numerical investigations with the rare decays $K \rightarrow \pi\nu\bar{\nu}$, $K_L \rightarrow \pi^0 l^+ l^-$, and $K_L \rightarrow \mu^+ \mu^-$. In the former case, the special role of the $K \rightarrow \pi\nu\bar{\nu}$ and $K_L \rightarrow \pi^0 l^+ l^-$ modes is emphasized, which is due to their theoretical cleanliness and their enhanced sensitivity to non-standard flavor and CP violation. They are unique tools to potentially set severe constraints on the RS parameter space, or find clean deviations, once they are measured.

In the lower left panel of figure 4.4, we display the predictions for the branching ratio of the neutral mode versus that of the charged one for the standard scenario of the minimal RS model. The blue points correspond to parameter values that satisfy the constraints from $Z \rightarrow b\bar{b}$ and $|\epsilon_K|$ as discussed in the last section. For comparison, the central value and the 68% CL range $\text{Br}(K^+ \rightarrow \pi^+ \nu\bar{\nu}(\gamma))_{\text{exp}} = (1.73_{-1.05}^{+1.15}) \cdot 10^{-10}$ based on seven events in the E949 experiment [328] is indicated by the vertical dashed black line and the yellow band. The experimental 90% CL upper limit $\text{Br}(K_L \rightarrow \pi^0 \nu\bar{\nu})_{\text{exp}} < 2.6 \cdot 10^{-8}$ [329] is not displayed in the figure. The central values of the SM predictions (4.1.50) are indicated by the green cross. The branching fractions of both $K \rightarrow \pi\nu\bar{\nu}$ channels can be significantly enhanced compared

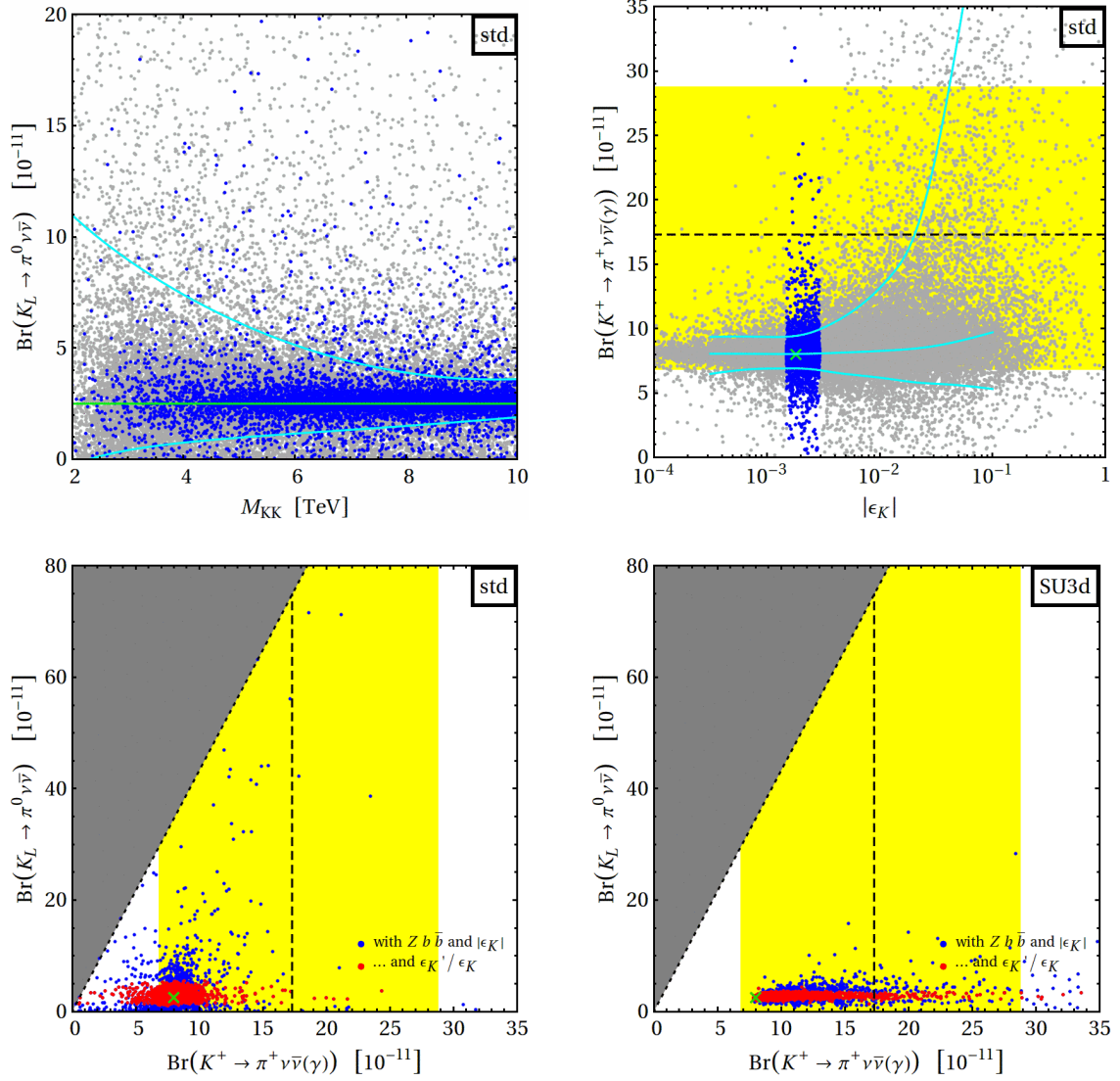


Figure 4.4: *upper left panel:* Predictions for $\text{Br}(K_L \rightarrow \pi^0 \nu \bar{\nu})$ as a function of M_{KK} . The solid green line represents the SM prediction. Grey points fulfill the constraint from $Z \rightarrow b \bar{b}$ at the 3σ CL. Blue points additionally reproduce the value of $|\epsilon_K|$ at 99% CL. The two cyan lines are obtained from a fit to the 5% and 95% quantile of the distribution of gray points. *upper right panel:* Predictions for $\text{Br}(K^+ \rightarrow \pi^+ \nu \bar{\nu}(\gamma))$ versus ϵ_K . Color coding and constraints are the same as in the upper left panel. Additionally the median curve is displayed. *lower panels:* Results for $\text{Br}(K^+ \rightarrow \pi^+ \nu \bar{\nu}(\gamma))$ versus $\text{Br}(K_L \rightarrow \pi^0 \nu \bar{\nu})$ in the standard benchmark scenario (left) and the aligned scenario (right). Color coding and constraints are the same as in the upper panels. The gray shaded area shows the GN bound. The vertical dashed black line and the yellow band display the experimental central value and 68% CL range. Points marked red are compatible with ϵ'_{K}/ϵ_K as discussed below.

to the SM prediction. For a very small fraction of parameter space, it is even possible to saturate the model-independent Grossman-Nir (GN) bound [330]

$$\text{Br}(K_L \rightarrow \pi^0 \nu \bar{\nu}) \leq \frac{\kappa_L}{\kappa_+(1 + \Delta_{\text{EM}})} \text{Br}(K^+ \rightarrow \pi^+ \nu \bar{\nu}(\gamma)) \approx 4.3 \text{Br}(K^+ \rightarrow \pi^+ \nu \bar{\nu}(\gamma)), \quad (4.1.76)$$

The inequality (4.1.76) is indicated by the straight dotted black line in the figure, and the inaccessible area is colored gray. Because the weak phase entering the $s \rightarrow d\nu\bar{\nu}$ transition can take essentially any value in the standard scenario, the predictions for the charged and neutral mode are mostly uncorrelated.

From the plots in the upper two panels of figure 4.4, we observe that very large deviations of more than a factor of two are yet disfavored by the bound on $|\epsilon_K|$, due to a weak correlation of $|\epsilon_K|$ to both decay modes. This is displayed by the gray points, which only fulfill the $Z \rightarrow b\bar{b}$ constraint and populate a much larger region for both decay modes. We illustrate the decoupling behavior of the neutral decay mode by fits to the 5% and 95% quantile, obtained after a fine grained binning in M_{KK} . In principle, the result indicates a strong sensitivity of the neutral mode to RS corrections even at high KK scales. However, as we will show below, the possible deviations are very restricted by the constraint following from ϵ'_K/ϵ_K . Large shifts in the CP -violating neutral decay mode typically appear together with an unacceptable amount of direct CP violation in $K \rightarrow \pi\pi$. The correlation is more pronounced than the one with ϵ_K , as shown by the red points in the lower panels of figure 4.4. We discuss this in more detail below. Concerning the charged mode, the correlation with $|\epsilon_K|$ imposes in fact the most relevant constraint on possible deviations. We illustrate in the upper right panel of figure 4.4 how this constraint excludes a large fraction of the parameter space, where otherwise order-of-magnitude deviations would be possible. As can be seen from the cyan lines, which are spline interpolations of the 5%, 50%, and 95% quantiles after binning in $|\epsilon_K|$, very large values of $|\epsilon_K|$ would allow for a large fraction of parameter space that has large deviations in the charged decay mode. On the other hand, one should keep in mind that the correlation disfavors, but does not exclude certainly, large deviations in the charged mode.

While the pattern of deviations found in the LRS scenario follows that observed in the standard case, a considerably different picture emerges in the aligned scenario, with common bulk-mass parameters $c_{d_i} = c_d$. This is illustrated in the lower right panel of figure 4.4. To understand the observed pattern, we recall that in the aligned scenario right-handed currents entering $|\epsilon_K|$ in form of the Wilson coefficients \tilde{C}_1^{RS} , C_4^{RS} , and C_5^{RS} (see (4.1.72)) as well as $K \rightarrow \pi\nu\bar{\nu}$ in form of $\tilde{C}_\nu^{\text{RS}}$ are parametrically suppressed by factors of v^2/M_{KK}^2 and thus numerically subleading compared to the left-handed corrections C_1^{RS} and C_ν^{RS} . The latter are to leading order in L proportional to $(\Delta_D)_{12} \otimes (\Delta_D)_{12}$ and $(\Delta_D)_{12}$. Furthermore, the fact that the left-handed contribution $(\Delta_D)_{12} \otimes (\Delta_D)_{12}$ factorizes as $(\Delta_D)_{12} \otimes (\Delta_D)_{12} \approx (\Delta_D)_{12}^2 = |(\Delta_D)_{12}|^2 e^{2i\varphi_{12}}$ implies that $|\epsilon_K|$ as well as $K \rightarrow \pi\nu\bar{\nu}$ are governed by the same weak phase φ_{12} . The requirement $|\epsilon_K|_{\text{RS}} \propto \text{Im}((\Delta_D)_{12} \otimes (\Delta_D)_{12}) \approx 0$ then forces φ_{12} in the standard CKM phase convention (2.2.14) to be a multiple of $\pi/2$. One can show model-independently that in such a situation only two branches of solutions in the $\text{Br}(K^+ \rightarrow \pi^+ \nu \bar{\nu}(\gamma)) - \text{Br}(K_L \rightarrow \pi^0 \nu \bar{\nu})$ plane are allowed [331]. The first branch features $\text{Br}(K_L \rightarrow \pi^0 \nu \bar{\nu}) \approx \text{Br}(K_L \rightarrow \pi^0 \nu \bar{\nu})_{\text{SM}}$, while the second runs through the SM point (4.1.50) with a slope approximately equal to the slope of the GN bound (4.1.76). The second branch of solutions is absent in the case at hand, as we show now. To leading order in CKM hierarchies, the (1,2) elements of the charged-current matrix \mathbf{V}_L and the mixing matrix $\mathbf{\Delta}_D$ take the following form in the case

of alignment

$$(V_L)_{12} = \left[\frac{(\mathbf{M}_d \mathbf{M}_d^\dagger)_{21}}{(\mathbf{M}_d \mathbf{M}_d^\dagger)_{11}} - \frac{(M_u)_{21}}{(M_u)_{11}} \right] \frac{F(c_{Q_1})}{F(c_{Q_2})},$$

$$(\Delta_D)_{12} = -\frac{1}{2} \left[\frac{(\mathbf{M}_d \mathbf{M}_d^\dagger)_{21}}{(\mathbf{M}_d \mathbf{M}_d^\dagger)_{11}} + \frac{(\mathbf{Y}_d \mathbf{Y}_d^\dagger)_{23}^*}{(\mathbf{Y}_d \mathbf{Y}_d^\dagger)_{33}} \frac{(\mathbf{M}_d \mathbf{M}_d^\dagger)_{31}}{(\mathbf{M}_d \mathbf{M}_d^\dagger)_{11}} \right] F(c_{Q_1}) F(c_{Q_2}),$$
(4.1.77)

where \mathbf{M}_d denotes the matrix of minors of \mathbf{Y}_d . This result is derived from a Froggatt-Nielsen analysis for the $SU(3)_{dc}$ symmetric case.

Sizable corrections in $K \rightarrow \pi \nu \bar{\nu}$ necessarily correspond to large values of $|(\Delta_D)_{12}|$. $|(\Delta_D)_{12}|$ grows with decreasing $(\mathbf{Y}_d \mathbf{Y}_d^\dagger)_{33}$ and decreasing $(\mathbf{M}_d \mathbf{M}_d^\dagger)_{11}$. Furthermore, in the anarchic setup $(\mathbf{Y}_d \mathbf{Y}_d^\dagger)_{33}$ has a natural size close to the square of the maximally allowed Yukawa entry, *i.e.* $\mathcal{O}(y_{\max}^2)$. Barring accidental cancellations, we need to consider the conditions for a vanishing product of minors. In the limit $(\mathbf{M}_d \mathbf{M}_d^\dagger)_{11} \rightarrow 0$, the expressions (4.1.77) are approximated by

$$(V_L)_{12} \approx \frac{(\mathbf{M}_d \mathbf{M}_d^\dagger)_{21}}{(\mathbf{M}_d \mathbf{M}_d^\dagger)_{11}} \frac{F(c_{Q_1})}{F(c_{Q_2})},$$

$$(\Delta_D)_{12} \approx -\frac{1}{2} \left[1 + \frac{(\mathbf{Y}_d \mathbf{Y}_d^\dagger)_{22}}{(\mathbf{Y}_d \mathbf{Y}_d^\dagger)_{33}} \right] \frac{(\mathbf{M}_d \mathbf{M}_d^\dagger)_{21}}{(\mathbf{M}_d \mathbf{M}_d^\dagger)_{11}} F(c_{Q_1}) F(c_{Q_2}),$$

so that in the standard CKM phase convention (2.2.14), *i.e.* after rotating away the phase of $(V_L)_{12}$, one ends up with

$$(\Delta_D)_{12} e^{-i \arg(V_L)_{12}} \approx -\frac{1}{2} \left[1 + \frac{(\mathbf{Y}_d \mathbf{Y}_d^\dagger)_{22}}{(\mathbf{Y}_d \mathbf{Y}_d^\dagger)_{33}} \right] \frac{|(\mathbf{M}_d \mathbf{M}_d^\dagger)_{21}|}{(\mathbf{M}_d \mathbf{M}_d^\dagger)_{11}} F(c_{Q_1}) F(c_{Q_2}) < 0.$$
(4.1.78)

Using (4.1.37) and (4.1.47), we find that this inequality implies that $\text{Re}(X_{\text{RS}}) < 0$ and $\text{Im}(X_{\text{RS}}) \approx 0$ for the quantity X_{RS} defined in (4.1.49). Recalling that in the SM one has $\text{Re}(X_{\text{SM}}) \approx -1.2$ and $\text{Im}(X_{\text{SM}}) \approx 0.3$, we then deduce from (4.1.48) that in the limit (4.1.78) the aligned scenario predicts constructive interference in the branching ratio of $K^+ \rightarrow \pi^+ \nu \bar{\nu}$, while the $K_L \rightarrow \pi^0 \nu \bar{\nu}$ rate is expected to take approximately its SM value. Invoking the $|\epsilon_K|$ constraint further drives the solutions toward (4.1.78), as it singles out solutions with $\varphi_{12} \approx \pi$, so that $\text{Re}(X_{\text{RS}}) < 0$ and $\text{Im}(X_{\text{RS}}) \approx 0$ turn out to hold in the aligned case even when $|(\Delta_D)_{12}|$ is small. We conclude that in the aligned scenario, the allowed points in the $\text{Br}(K^+ \rightarrow \pi^+ \nu \bar{\nu}(\gamma)) - \text{Br}(K_L \rightarrow \pi^0 \nu \bar{\nu})$ all lie close to a horizontal line to the right of the SM point (4.1.50), what is clearly observed in the lower right panel of figure 4.4.

The discussion above highlights that the $K \rightarrow \pi \nu \bar{\nu}$ decays offer a unique tool to study the fermion geography in the down-type quark sector of models with warped extra dimensions, since they provide, in combination with $|\epsilon_K|$, a powerful way to test the universality of new-physics contributions in $\Delta S = 1$ and $\Delta S = 2$ transitions. Precision measurements of the $K_L \rightarrow \pi^0 \nu \bar{\nu}$ and $K^+ \rightarrow \pi^+ \nu \bar{\nu}$ branching fractions feasible at high-intensity proton-beam facilities such as NA62, J-PARC, and Project X should therefore be primary goals of the future flavor-physics program.

While theoretically not as clean as $K \rightarrow \pi \nu \bar{\nu}$, the $K_L \rightarrow \pi^0 l^+ l^-$ channels offer the opportunity to constraint additional $\Delta S = 1$ effective operators that are inaccessible to

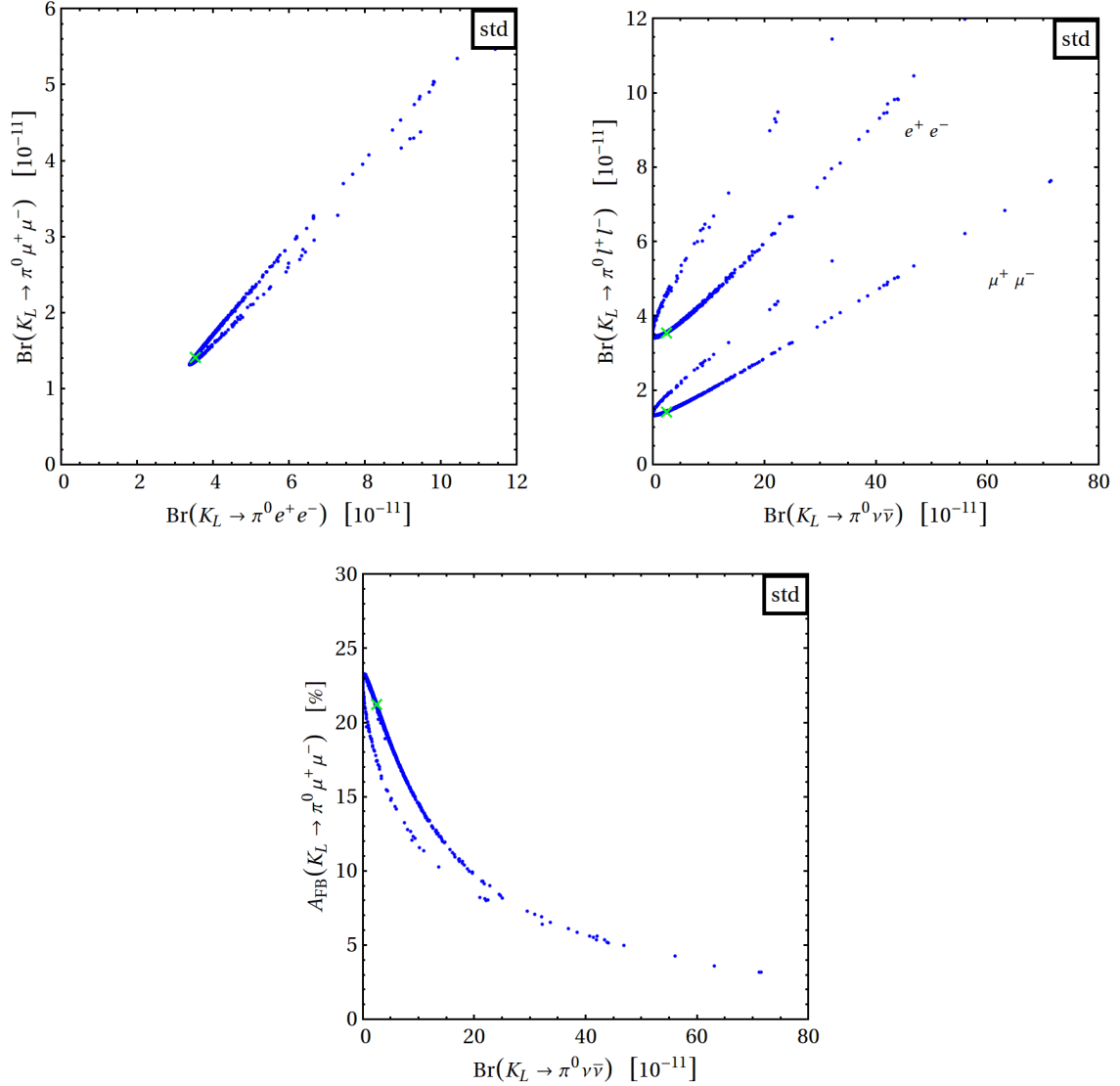


Figure 4.5: Prediction for $\text{Br}(K_L \rightarrow \pi^0 l^+ l^-)$, $l = e, \mu$ (upper left), $\text{Br}(K_L \rightarrow \pi^0 \nu \bar{\nu}) - \text{Br}(K_L \rightarrow \pi^0 l^+ l^-)$ (upper right), and $\text{Br}(K_L \rightarrow \pi^0 \nu \bar{\nu}) - A_{\text{FB}}(K_L \rightarrow \pi^0 \mu^+ \mu^-)$ (lower panel). The green crosses indicate the SM point, while the blue scatter points fulfill the constraint for $Z \rightarrow b\bar{b}$ and $|\epsilon_K|$ as discussed in the text.

the neutrino modes. In figure 4.5, we show predictions for $K_L \rightarrow \pi^0 l^+ l^-$ with $l = e, \mu$ and their correlation with the $K_L \rightarrow \pi^0 \nu \bar{\nu}$ mode. All plots correspond to our standard scenario including the constraint from $Z \rightarrow b\bar{b}$ and $|\epsilon_K|$. The predictions in the remaining benchmark scenarios are essentially indistinguishable from the ones displayed. In the case of the $K_L \rightarrow \pi^0 l^+ l^-$ observables we have assumed constructive interference between the direct and indirect CP -violating amplitudes as favored by the analyses [317, 318]. We observe that enhancements of the branching ratio of both $K_L \rightarrow \pi^0 l^+ l^-$ modes by a factor of about 5 are possible without violating any constraints. On the other hand, the RS predictions for $A_{\text{FB}}(K_L \rightarrow \pi^0 \mu^+ \mu^-)$ can be smaller than the SM value by almost a factor of 10. Notice that modifications in $\text{Br}(K_L \rightarrow \pi^0 \mu^+ \mu^-)$ and $A_{\text{FB}}(K_L \rightarrow \pi^0 l^+ l^-)$ are anti-correlated, since

the branching ratio enters (4.1.60) in the denominator. The pattern of the correlations seen in the upper left panel of figure 4.5 arises because the coefficient Y_V of the semileptonic vector operator is suppressed with respect to the coefficient Y_A of the axial-vector operator by a factor of about $(1 - 4s_w^2) \approx 0.08$, and scalar interactions play essentially no role. The suppression factor stems from the coupling of the Z boson and its KK excitations to the charged lepton pair. The ratio Y_V/Y_A determines the angle between the two possible branches in the $\text{Br}(K_L \rightarrow \pi^0 \mu^+ \mu^-) - \text{Br}(K_L \rightarrow \pi^0 e^+ e^-)$ plane. Since Y_V/Y_A is generically small in the RS model, the two branches are very close to each other. The correlations observed in the upper right and lower panel of figure 4.5 have a similar origin. In this case, they are a result of the interplay of the coupling of the Z boson and its KK excitations to a pair of charged and neutral leptons. While the former is mostly axial-vector like, the latter is purely left-handed. The observed correlations between $K_L \rightarrow \pi^0 \nu \bar{\nu}$ and $K_L \rightarrow \pi^0 l^+ l^-$ should therefore be considered a generic feature of models where the couplings of heavy neutral gauge bosons to leptons are SM-like, rather than a specific characteristic of the RS framework.

Interesting complementary information can be obtained from the $K_L \rightarrow \mu^+ \mu^-$ decay mode, which has been measured precisely. The predictions for $\text{Br}(K_L \rightarrow \mu^+ \mu^-)$ as a function of $\text{Br}(K^+ \rightarrow \pi^+ \nu \bar{\nu}(\gamma))$ in the parameter standard hierarchical and the aligned scenario are displayed in figure 4.6 including the constraint from $Z \rightarrow b\bar{b}$ and $|\epsilon_K|$. We have assumed that

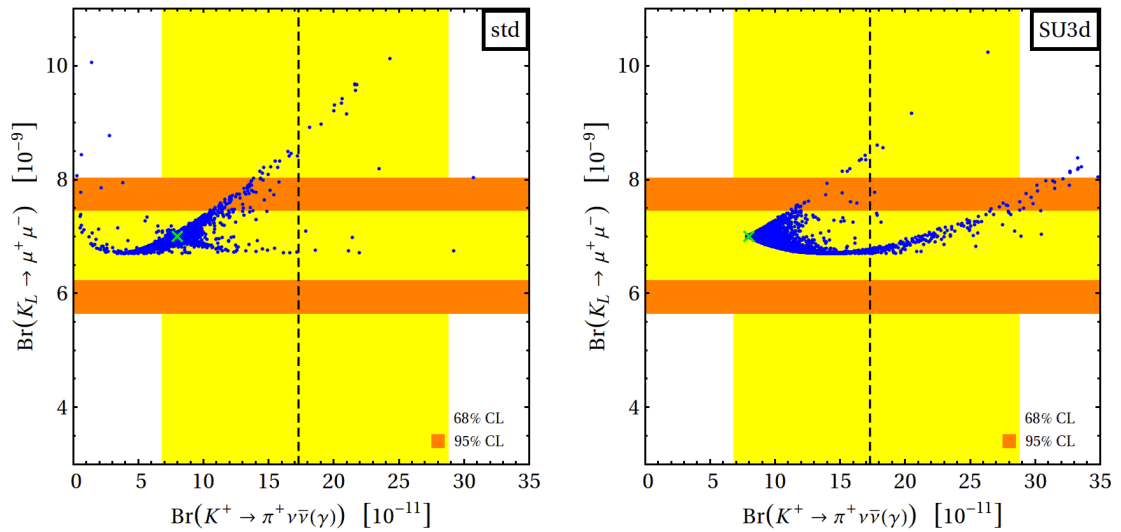


Figure 4.6: Prediction for $\text{Br}(K^+ \rightarrow \pi^+ \nu \bar{\nu}(\gamma))$ versus $\text{Br}(K_L \rightarrow \mu^+ \mu^-)$ in the standard and aligned scenario. The green crosses indicate the SM point, while the blue scatter points fulfill the constraint for $Z \rightarrow b\bar{b}$ and $|\epsilon_K|$ as discussed in the text. The experimental central value and 68% CL range for $\text{Br}(K^+ \rightarrow \pi^+ \nu \bar{\nu}(\gamma))$ (vertical dashed line and yellow vertical band) as well as the 68% and 95% CL regions for $\text{Br}(K_L \rightarrow \mu^+ \mu^-)$ (yellow and orange horizontal band) including both experimental and theoretical errors are shown.

the two-photon amplitude in $K_L \rightarrow \mu^+ \mu^-$ has positive sign, which is supported by theoretical arguments [313]. In the case of the $K_L \rightarrow \mu^+ \mu^-$ branching ratio the error band includes the theory error, which by far dominates the total uncertainty. We observe that the branching ratio of $K_L \rightarrow \mu^+ \mu^-$ can reach experimentally disfavored values with an enhancement of about 20% relative to both the SM prediction and the measured value. A mostly positive linear correlation between $K^+ \rightarrow \pi^+ \nu \bar{\nu}$ and $K_L \rightarrow \mu^+ \mu^-$ is visible. This correlation originates

from the fact that $K^+ \rightarrow \pi^+ \nu \bar{\nu}$ measures the vector, while $K_L \rightarrow \mu^+ \mu^-$ measures the axial-vector component of the $Z d \bar{s}$ vertex. Since the SM flavor-changing Z penguin is purely left-handed and the RS contribution is dominated in our case by the very same component, the SM and new-physics contributions enter both decay modes with the same sign. Notice that the correlation is more pronounced in the aligned scenario, because the right-handed contributions to the $Z d \bar{s}$ vertex are further suppressed in this benchmark scenario. In a RS variant with custodial protection, the correlation between $K^+ \rightarrow \pi^+ \nu \bar{\nu}$ and $K_L \rightarrow \mu^+ \mu^-$ has expected to be inverse to the minimal model shown here, since the given quark embedding (3.3.66) implies a simultaneous protection of all $Z d_i \bar{d}_j$ couplings. This has been confirmed in [261]. Hence, precision measurements of $K^+ \rightarrow \pi^+ \nu \bar{\nu}$ accompanied by theoretical progress in the prediction of $K_L \rightarrow \mu^+ \mu^-$ would allow one to identify the chiral structure of the $Z d \bar{s}$ vertex and in this way could select between different models of non-standard interactions.

We close this section with a comparison to the expected results in the RS model with custodial protection. Employing the quark embedding (3.3.66), we found in (3.3.142) that the ratios of the corrections to the flavor-changing Z -boson couplings in the minimal and custodial model are given by

$$\begin{aligned} \frac{(\delta g_L^d)_{ij}^{\text{custo}}}{(\delta g_L^d)_{ij}^{\text{minimal}}} &= -\frac{(1/2 - s_w^2/3) (\Delta'_D)_{ij}}{(1/2 - s_w^2/3) (L (\Delta_D)_{ij} - (\Delta'_D)_{ij})} \approx -\frac{1}{L}, \\ \frac{(\delta g_R^d)_{ij}^{\text{custo}}}{(\delta g_R^d)_{ij}^{\text{minimal}}} &= -\frac{c_w^2 L (\Delta_d)_{ij} - s_w^2/3 (\Delta'_d)_{ij}}{s_w^2/3 (L (\Delta_d)_{ij} - (\Delta'_d)_{ij})} \approx -\frac{3c_w^2}{s_w^2}, \end{aligned} \quad (4.1.79)$$

where we use $(\Delta_{D,d})_{ij} \approx (\Delta'_{D,d})_{ij}$. A suppression factor for the left-handed couplings of roughly 100 has been claimed in [212, 261] using the diagonalization of large mass matrices. We observe that the origin of this suppression is very clear in our analytic approach. On the other hand, we find that the $Z^0 d_i R \bar{d}_j R$ vertices in the model with custodial protection are enhanced in magnitude by a factor of about 10 relative to the original RS formulation, which is in accordance with [212, 261]. From (4.1.79), we also observe that

$$\frac{(g_R^d)_{ij}^{\text{custo}}}{(g_L^d)_{ij}^{\text{minimal}}} \approx -\frac{c_w^2}{1/2 - s_w^2/3} \frac{(\Delta_d)_{ij}}{(\Delta_D)_{ij}} \approx -2 \frac{(\Delta_d)_{ij}}{(\Delta_D)_{ij}} \approx -2 \frac{F(c_{d_i}) F(c_{d_j})}{F(c_{Q_i}) F(c_{Q_j})}. \quad (4.1.80)$$

To arrive at this relation, we used that the bulk masses do not depend on whether one considers the custodially protected or the original RS model, since the c_{A_i} parameters are determined by the quark masses and mixings. In order to have effects in rare kaon decays of similar magnitude in the custodially protected and the original RS model requires the products $F(c_{d_1}) F(c_{d_2})$ and $F(c_{Q_1}) F(c_{Q_2})$ to be of similar size. Yet the locations of the zero-modes are not unique solutions [200], a feature that manifests itself in the invariance under a set of reparametrization transformations [1]. In particular, a simultaneous rescaling of the fermion profiles for $SU(2)_L$ doublet and singlet fields by opposite factors, while leaving the 5D Yukawa couplings invariant, allows one to redistribute effects between the left- and right-handed sectors. This freedom can be used to express $(F(c_{d_1}) F(c_{d_2})) / (F(c_{Q_1}) F(c_{Q_2}))$ through the quark masses, Wolfenstein parameters, and $F(c_{u_3})$. To leading power in hierarchies we find the scaling relations

$$\left| \frac{(g_R^d)_{12}^{\text{custo}}}{(g_L^d)_{12}^{\text{minimal}}} \right| \sim \frac{m_d m_s y_u^4 v^2}{2A^4 \lambda^{10} m_t^4 y_d^2} F(c_{u_3})^4 \approx 0.08 \frac{y_u^4}{y_d^2} F(c_{u_3})^4, \quad (4.1.81)$$

which implies that the ratio of right- to left-handed $Zd\bar{s}$ couplings can be enhanced by localizing the right-handed top quark closer to the IR brane. We observe that the degree of compositeness of the top quark thus plays a crucial role in this context. For comparison we give the numerical values $0.08 F(1)^4 = 0.7$ and $0.08 F(2)^4 = 2.0$. Analogous formulas hold in the case of the $Z \rightarrow b\bar{d}$ and $b\bar{s}$ transitions with $(m_d m_s)/(A^4 \lambda^{10})$ replaced by $(m_d m_b)/(A^2 \lambda^6)$ ($(m_s m_b)/(A^2 \lambda^4)$). The corresponding numerical factors (4.1.81) are 0.006 and 0.005 instead of 0.08. Hence, barring accidental cancellations and given bulk that do not exceed the curvature scale by far, we expect a relative suppression in the custodial setup as compared to the minimal setup of at least an order of magnitude for rare B decays.

Analysis of $B_q \rightarrow \mu^+ \mu^-$

The predictions for $\text{Br}(B_s \rightarrow \mu^+ \mu^-)$ versus $\text{Br}(B_d \rightarrow \mu^+ \mu^-)$ as obtained from a parameter scan in the standard scenario are displayed in figure 4.7. The two other benchmark scenarios show a similar distribution. We observe that even after imposing of the $Z \rightarrow b\bar{b}$ constraints

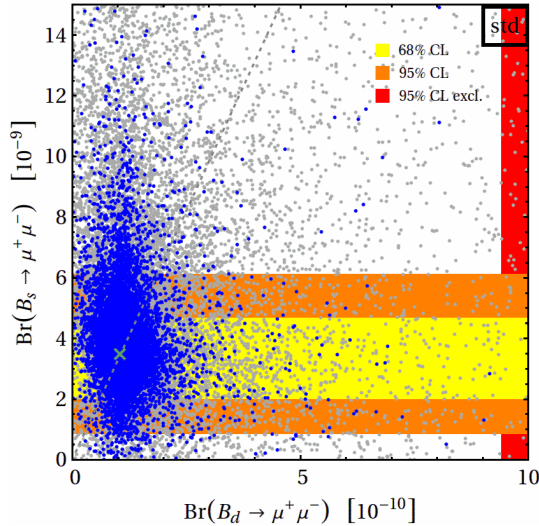


Figure 4.7: Prediction for $\text{Br}(B_q \rightarrow \mu^+ \mu^-)$, $q = d, s$ in the standard scenario of the minimal RS model. The green crosses indicates the SM point. The blue scatter points fulfill the $Z \rightarrow b\bar{b}$ constraints as discussed in the text. The experimental and 95% CL exclusion region for the B_d and the 68% and 95% CL for the B_s mode from LHCb are marked with red, yellow, and orange, respectively. The gray dashed line represents the correlation found in CMFV models.

large uncorrelated enhancements by a factor of 3–4 are possible in both the B_d and B_s decay modes without violating existing constraints. The uncorrelated distribution implies that large deviations from the relation [332]

$$\frac{\text{Br}(B_s \rightarrow \mu^+ \mu^-)}{\text{Br}(B_d \rightarrow \mu^+ \mu^-)} = \frac{f_{B_s}^2 m_{B_s} \tau_{B_s} |V_{ts}|^2}{f_{B_d}^2 m_{B_d} \tau_{B_d} |V_{td}|^2} \approx 32.8, \quad (4.1.82)$$

which is valid in models with constrained MFV (CMFV) [333], are possible in the RS model. The measurement of the B_s mode by LHCb [260] already constrains a small part of the RS parameter space in the minimal model. We have mentioned in section 4.1.2.2 that the error of

the measurement has small systematic errors and still exceeds the uncertainty of the theory prediction by a factor of 5, such that this mode will unfold a strong constraining power in the near future, given the central value remains compatible with the SM. The existing limit in the case of $B_d \rightarrow \mu^+ \mu^-$ is much weaker and not expected to become very relevant soon, and has to await further investigations at a super flavor factory.

We refer to the previous paragraph for a comparison of the expected changes in going to the custodial setup presented in section 3.3.5.2, where we found a suppression of at least one order of magnitude for the RS contributions. A similar result was found in [261].

Analysis of ϵ'_K/ϵ_K and its Effect on Rare Kaon Decays

Within the SM the smallness of direct CP violation in $K \rightarrow \pi\pi$ is the result of a destructive interference between the positive contribution due to QCD penguins and the negative contribution arising from electroweak penguin diagrams. In new-physics models in which the $\Delta I = 1/2$ and $\Delta I = 3/2$ contributions to $s \rightarrow dq\bar{q}$ processes are affected differently from each other, this partial cancellation is usually much less pronounced or even absent. A qualitative understanding of the situation in the minimal RS model can be obtained from the approximate relation

$$\left(\frac{\epsilon'_K}{\epsilon_K}\right)_{\text{RS}} \propto 1 + [-0.1, 0.1] B_6^{(1/2)} - 12 B_8^{(3/2)}, \quad (4.1.83)$$

which has been obtained from the second expression in (4.1.40) by inserting typical values of the Wilson coefficients C_{3-10}^{RS} and $\tilde{C}_{3-10}^{\text{RS}}$. The smallness of the coefficient multiplying the hadronic parameter $B_6^{(1/2)}$ compared to the coefficient of $B_8^{(3/2)}$ is easily explained by the structure of ϵ'_K/ϵ_K within the SM. While both the QCD and electroweak penguin contributions are strongly enhanced by RG effects, the QCD correction results mainly from the mixing of Q_6 with $Q_{1,2}$. Thus, it is essentially unaffected by new physics. On the other hand, mixing with the current-current operators plays only a minor role in the case of the electroweak penguins, so that any new-physics contribution to the initial conditions in this sector directly feeds through into ϵ'_K/ϵ_K . This implies that electroweak penguin operators give the dominant RS correction to direct CP violation in the kaon sector. Our numerical analysis confirms this model-independent conclusion. Notice that the sign of $(\epsilon'_K/\epsilon_K)_{\text{RS}}$ in (4.1.83) is not fixed, so the prediction for the total ratio ϵ'_K/ϵ_K can be both positive or negative. An enhancement occurs in the case of an electroweak penguin contribution that has opposite sign with respect to the SM Z -penguin amplitude, and vice versa.

The observables ϵ'_K/ϵ_K and $|\epsilon_K|$ are not independent from each other, if ϵ'_K/ϵ_K is calculated fully in theory. Since the central value of the theory prediction for ϵ'_K/ϵ_K (4.1.45) is below the experimental world average, models with new positive contributions to $|\epsilon_K|$ and negative contributions to ϵ'_K are disfavored. The correlation between ϵ'_K/ϵ_K and $|\epsilon_K|$ in the standard scenario is shown in the left panel of figure 4.8. Like before, points that are consistent with the constraints from $Z \rightarrow b\bar{b}$ at the 3σ CL are colored blue. Points marked orange are furthermore compatible with $|\epsilon_K|$ at the 99% CL after combining theory and experimental uncertainty, and they can be brought into agreement with the experimental 95% CL of ϵ'_K/ϵ_K when scanning over the conservative ranges in (4.1.44) for the non-perturbative input parameters $R_{6,8}$ and light masses. The abscissa value of each point is obtained by setting the non-perturbative parameters $R_{6,8}$ equal to 1 and light quark masses to their central values. It is evident from the distribution of points that solutions featuring excluded values of $|\epsilon_K|$

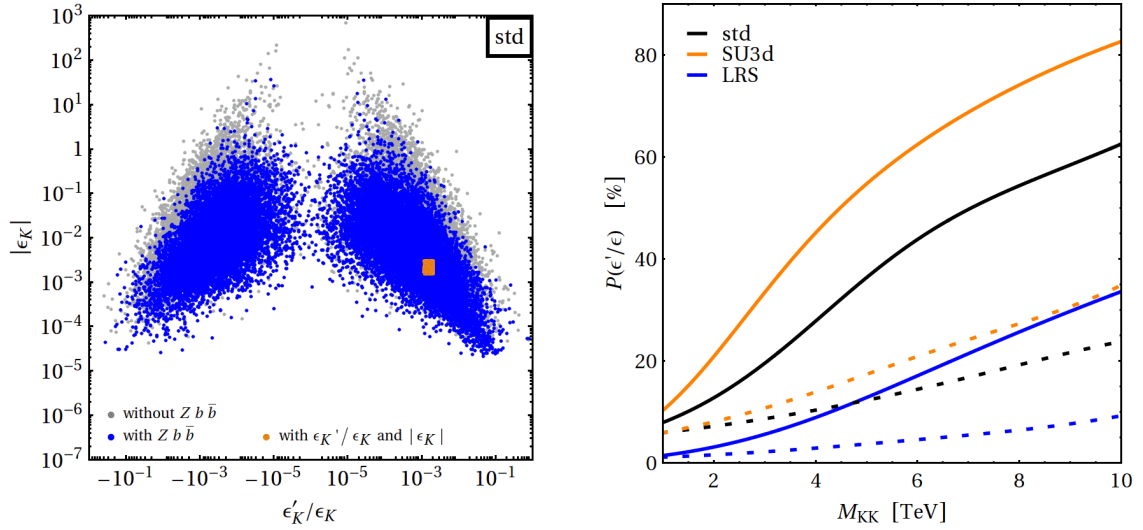


Figure 4.8: *left panel*: Correlation between ϵ'_K/ϵ_K and $|\epsilon_K|$ in the standard scenario of the minimal RS model. The blue points fulfill the constraints from $Z \rightarrow b\bar{b}$ as discussed in the text. Points in agreement with the experimental values of both ϵ'_K/ϵ_K and $|\epsilon_K|$, after accounting for theoretical errors as described in the text, are marked orange.

right panel: Percentage of points that are consistent with ϵ'_K/ϵ_K as a function of M_{KK} in the three benchmark scenarios. The underlying data fulfill the $Z \rightarrow b\bar{b}$ constraint. The solid lines include the experimental and theory uncertainties as described in the text, whereas the dashed lines are obtained by setting the SM and experimental central value equal to each other and considering the experimental uncertainty only.

are typically also in conflict with ϵ'_K/ϵ_K , since they predict too low values for the latter observable. For points in line with $|\epsilon_K|$, it is however still possible to obtain values for ϵ'_K/ϵ_K in the range $[-1, 1] \cdot 10^{-1}$. The wide spread of viable results suggests that the data on ϵ'_K/ϵ_K impose non-trivial constraints on the allowed model parameters even if the $|\epsilon_K|$ constraint is satisfied.

The right plot in figure 4.8 illustrates the severity of the ϵ'_K/ϵ_K constraint in each of the three benchmark scenarios. The shown curves for $P(\epsilon'_K/\epsilon_K)$ are obtained in the same way as described for $P(\epsilon_K)$ in figure 4.3. For a qualitative explanation of the curves, we recall the pattern of enhancements and depletions of $\Delta F = 2$ and $\Delta F = 1$ contributions in the different benchmark scenarios. Compared to the default scenario, corrections to $|\epsilon_K|$ are typically less pronounced in the aligned scenario, because this scenario is specifically designed to suppress $|\epsilon_K|$ by eliminating flavor mixing that arises from the non-universality of the right-handed down-type quark profiles. On the other hand the corrections to $Zd\bar{s}$ entering ϵ'_K/ϵ_K are only indirectly affected. They tend to be smaller as well, since the aligned scenario shows a preference for a stronger localization of the first two SM-like doublets towards the UV, which is necessary in order to obtain the correct values of the quark masses. In the LRS scenario the situation is reversed. Numerically, we find that for $M_{KK} = 1$ TeV still $P(\epsilon'_K/\epsilon_K) = 7.9\%$ of the parameter space fulfills the constraint on ϵ'_K/ϵ_K after imposing the $Z \rightarrow b\bar{b}$, but without the $|\epsilon_K|$ constraint. In the aligned and LRS scenario the corresponding values are $P(\epsilon'_K/\epsilon_K) = 10.3\%$ and $P(\epsilon'_K/\epsilon_K) = 1.4\%$

The given numbers imply that — at least with our conservative treatment of errors —

we are not able to derive a precision constraint from ϵ'_K/ϵ_K . This is in contrast to the situation for $|\epsilon_K|$, due to the very precise measurement of the latter parameter and a much better control over theory uncertainties. We also show by the dashed lines in the plot for $P(|\epsilon_K|)$ in figure 4.8 that even a major improvement in the theoretical understanding of the non-perturbative input will not render ϵ'_K/ϵ_K a precision test of the RS scale M_{KK} . These lines are obtained for the hypothetical scenario that the SM and experimental central values are equal and assuming a 20% theory uncertainty, which we combine quadratically with the experimental error. Instead, the bound from ϵ'_K/ϵ_K is very interesting and relevant because of its impact on the Yukawa structure and the restrictions it imposes on other flavor observables, namely CP -violating rare K decays, as we will see below.

Before that, we must mention that potentially large corrections to ϵ'_K/ϵ_K could arise from the presence of the chromomagnetic dipole operator Q_8^g and its chirality-flipped partner \tilde{Q}_8^g . In the context of scenarios with hierarchical fermion profiles, this issue has been analyzed in a model-independent way in [334]. Interestingly, the contributions to ϵ'_K/ϵ_K from C_8^g and \tilde{C}_8^g and to ϵ_K from C_4^{RS} depend in an opposite way on the absolute size of the Yukawa couplings. This makes it difficult to decouple flavor-violating effects in ϵ_K by using large Yukawa couplings, and it will lead to a tension between tree- and loop-level effects, similar to what happens in the case of $B \rightarrow X_s \gamma$ and ϵ_K [255]. A study of this anti-correlation including the first KK level of the quarks and the zero-mode of a bulk Higgs field has been presented recently in [335]. There, it has been pointed out that the NDA estimate for the typical size of the the chromomagnetic dipole-operator contribution leads to a value of ϵ'_K/ϵ_K that, when combined with the NDA estimate for $|\epsilon_K|$, becomes compatible with the measured value only for $M_{G^{(1)}} > 5.5$ TeV, if the Higgs boson is maximally spread into the bulk. This value is raised to 7.5 TeV if one considers the case of the two-site model [255]. It is important to realize that the quoted numbers are no “bounds” in the strict terminology we use here. They neglect the full parameter distribution, which is found to be widely spread. Moreover, the numbers are obtained for typical values of the down-type quark Yukawa couplings ($y_d = 4.6$ and $y_d = 5.9$) that are larger than the value $y_{\text{max}} = 3$ allowed by perturbativity in our benchmark scenarios. We estimate the chromomagnetic dipole contribution to ϵ'_K/ϵ_K , utilizing the formulas presented in [335]. We find that the chromomagnetic contribution to ϵ'_K/ϵ_K is smaller than the electroweak penguin contribution for perturbative Yukawa matrices; to this end, we express the additional contribution to ϵ'_K/ϵ_K arising from Q_8^g and \tilde{Q}_8^g as F_{RS}^g , which has to be added to F_{RS} in (4.1.40). Using the central values for $c_{Q_{1,2}}$ quoted in table B.1, we compare F_{RS}^g to the largest contribution of in F_{RS} , which arises from the Wilson coefficient C_7^{RS} . Applying furthermore a Froggatt-Nielsen analysis to leading order in the Cabibbo angle, we find approximate typical values of

$$|F_{\text{RS}}^g| \approx 2.5 \cdot 10^{-3} B_g^{(1/2)} f_g \left(\frac{1 \text{ TeV}}{M_{\text{KK}}} \right)^2, \quad |F_{\text{RS}}| \approx 1.0 \cdot 10^{-2} B_8^{(3/2)} f_8 \left(\frac{1 \text{ TeV}}{M_{\text{KK}}} \right)^2, \quad (4.1.84)$$

where $B_g^{(1/2)} \approx 1$ denotes the hadronic parameter related to the matrix element of Q_8^g , while f_g , and f_8 are functions of ratios of Yukawa couplings and thus naturally of $\mathcal{O}(1)$. It follows that after requiring the correct quark hierarchies, the corrections due to the chromomagnetic dipole operators are typically an order of magnitude smaller than those arising from the electroweak penguin sector. This justifies to ignore effective couplings in ϵ'_K/ϵ_K generated first at the one-loop level in the discussion at hand.

The marked sensitivity of ϵ'_K/ϵ_K to modifications of the electroweak penguin sector leads to stringent correlations between ϵ'_K/ϵ_K and the $s \rightarrow d\nu\bar{\nu}$, $s \rightarrow dl^+l^-$ observables. This

feature is illustrated in Figure 4.9, where the left panel shows the predictions for ϵ'_K/ϵ_K as a function of the branching fraction of $K_L \rightarrow \pi^0 \nu \bar{\nu}$ in the standard scenario. There, we

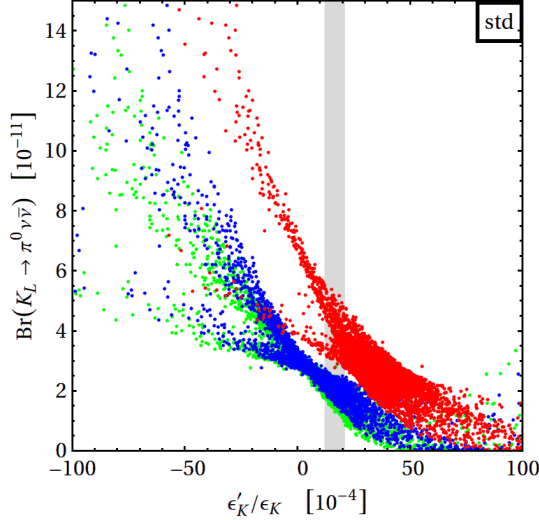


Figure 4.9: Correlation between $\text{Br}(K_L \rightarrow \pi^0 \nu \bar{\nu})$ and ϵ'_K/ϵ_K in the standard scenario of the minimal RS model. All points fulfill constraints from $Z \rightarrow b\bar{b}$ and $|\epsilon_K|$ as described in the text. The blue points correspond to the central value for ϵ'_K/ϵ_K obtained for $R_{6,8} = 1$. The red/green points illustrate the maximal/minimal achievable values of ϵ'_K/ϵ_K for the same set of points, as obtained by varying the hadronic parameters in the ranges (4.1.44). For comparison, the experimental 95% CL on ϵ'_K/ϵ_K is displayed.

show three vertically displaced distributions. They are based on the same set of parameter points as used above imposing both the constraint from $Z \rightarrow b\bar{b}$ and ϵ_K . For each point we plot three values of ϵ'_K/ϵ_K , one in blue corresponding to fixed central values of the hadronic parameters $R_{6,8} = 1$ and light quark masses, one in red obtained by maximizing ϵ'_K/ϵ_K from using the range of hadronic parameters and light quark masses given in (4.1.44), and one in green for the minimal possible value. This is analogous to the scan used in figure 4.8. The light gray band represents the experimental 95% CL. We observe that an enhancement of the CP -violating $\text{Br}(K_L \rightarrow \pi^0 \nu \bar{\nu})$ tends to be accompanied by a suppression of ϵ'_K/ϵ_K , and vice versa. This implies that large enhancements of the former decay mode are disfavored by the measured amount of direct CP violation in $K \rightarrow \pi\pi$. Notice that values of $B_8^{(3/2)}$ near the upper end of the range shown in (4.1.44) are particularly problematic in this respect, since they amplify the electroweak penguin contributions to ϵ'_K/ϵ_K . Since enhancements of the branching fractions $K_L \rightarrow \pi^0 \nu \bar{\nu}$ and $K_L \rightarrow \pi^0 l^+ l^-$ are strongly correlated with each other, similar statements apply to the rare kaon decay modes with charged leptons in the final state. The same strong anti-correlation between $\text{Br}(K_L \rightarrow \pi^0 \nu \bar{\nu})$ and ϵ'_K/ϵ_K is also present in the LRS parameter scenario and it even effectively constrains the correlated distribution between $\text{Br}(K_L \rightarrow \pi^0 \nu \bar{\nu})$ and $\text{Br}(K^+ \rightarrow \pi^+ \nu \bar{\nu})$ found in the aligned model. It arises since both observables receive the dominant correction from the imaginary part of the left-handed $Zd\bar{s}$ amplitude, which enters linearly and with opposite sign relative to the SM contribution in ϵ'_K/ϵ_K , whereas it appears quadratically and with the same sign in $\text{Br}(K_L \rightarrow \pi^0 \nu \bar{\nu})$. We conclude that even with a conservative treatment of errors, ϵ'_K/ϵ_K has a very relevant impact on the possible new-physics effects in rare K decays within the RS model.

4.2 Electroweak Precision Measurements

In this section we introduce some of the most important electroweak precision observables (EWPOs) and discuss the strong constraint they put on deviations from the SM. We review up-to-date analyses that significantly impact the constraints on models of new physics. Finally, we present detailed numerical consequences in the RS model. There, an analysis with a few effective parameters leads to a good understanding of the qualitatively different bounds on the parameter space and the efficacy of model-building solutions that are used in order to relax the bounds.

As an outlook, we remark that the observables discussed here are an excellent field of application for the sum rules presented in section 3.1.2. They can assist in identifying the constraining properties on different sectors in perturbatively unitary theories and distinguish them against more general contributions. Such an analysis, analogous to the one for FCNCs presented in section 4.1, is left for future work.

4.2.1 Common Observables and Effective Parameters

4.2.1.1 General Discussion and Choice of Input Parameters

The most constraining observables in the class of EWPOs are related to properties of the electroweak gauge bosons, which were precisely measured in large data sets of e^+e^- collisions at LEP and SLC in the early 90s. Later, LEP 2 extended the knowledge of the W boson's properties, and the Tevatron experiments improved W and top mass measurements. Very recently the LHC Higgs-mass measurement added valuable information to the overall picture.

In general, an EWPO can be categorized into one of the three classes: low energy observables, measurements at the Z pole, and direct mass measurements. The most important low energy observables stem from results on elastic neutrino–electron scattering, deep-inelastic neutrino–nucleon scattering, the τ lifetime, atomic parity violation (*e.g.* in Caesium), and the anomalous magnetic moment of the muon⁹. The latter shows a long-standing 3.0σ deviation from the SM theory calculation, which could be due to statistical fluctuations, underestimation of theory uncertainties, or indeed new physics; but the situation is inconclusive. We will not go into further detail on the low-energy observables and refer to [337] for a comprehensive review. Flavor-violating observables are usually not considered in this context. We considered constraints from off-diagonal flavor transitions separately in section 4.1.

Precision observables at the Z pole can either be constructed from the total and partial widths Γ_Z and $\Gamma_{ff} \equiv \Gamma(Z \rightarrow ff)$, or from asymmetries. From the former, one obtains the total resonant cross section with hadronic final states $\sigma_{\text{had}} = 12\pi \Gamma_{ee} \Gamma_{\text{had}} / (M_Z^2 \Gamma_Z)$, defines the width ratios $R_q \equiv \Gamma_{qq} / \Gamma_{\text{had}}$ for identifiable primary quarks in the hadronic final state ($q = c, b$), and $R_l \equiv \Gamma_{\text{had}} / \Gamma_{ll}$ for $l = e, \mu, \tau$. Here, $\Gamma_{\text{had}} \equiv \sum_{q=u,d,s,c,b} \Gamma_{qq}$ is the partial width for decay into hadrons. The three measured values Γ_{ll} are consistent with lepton universality. Additionally one uses the invisible-decay width $\Gamma_{\text{inv}} \equiv \Gamma_Z - \sum_l \Gamma_{ll} - \Gamma_{\text{had}}$ to determine that the number of neutrino flavors with mass much less than $M_Z/2$ is 2.984(9) [338].

The standard formulas¹⁰ for the asymmetries at the Z pole use the definition of the

⁹The anomalous magnetic moment of the electron is measured even more precisely, but effects of new physics are suppressed generically by $\mathcal{O}(m_e/m_\mu)$ in comparison to the muon anomalous magnetic moment. It is instead currently used to determine the fine structure constant α [336].

¹⁰This discussion hides certain radiative corrections that we take into account below, see *e.g.* (4.2.14).

asymmetry parameter

$$A_f = \frac{(g_{Z\bar{f}f}^L)^2 - (g_{Z\bar{f}f}^R)^2}{(g_{Z\bar{f}f}^L)^2 + (g_{Z\bar{f}f}^R)^2}. \quad (4.2.1)$$

Using a fully polarized initial e^- beam, SLD (at SLC) [339] measured the left–right asymmetries which are asymmetries between cross sections for left- and right-handed incident electrons. They are directly equal to A_e . The forward–backward asymmetries for other fermions are given by

$$A_{\text{FB}}^{(P_e, f)} = \frac{3}{4} A_f \frac{A_e + P_e}{1 + P_e A_e}, \quad (4.2.2)$$

and were extracted in experiments at LEP ($P_e = 0$) and SLC ($P_e = 1$).¹¹ In the SLD experiment this was extracted from double left–right forward–backward asymmetries

$$A_{\text{FB}}^{(1, f)} = \frac{\sigma_{LF}^f - \sigma_{LB}^f - \sigma_{RF}^f + \sigma_{RB}^f}{\sigma_{LF}^f + \sigma_{LB}^f + \sigma_{RF}^f + \sigma_{RB}^f} = \frac{3}{4} A_f, \quad (4.2.3)$$

for final states with $f = b, c, s, \tau, \mu$. Very precise information was added at LEP by measurements of $A_{\text{FB}}^{(0, f)}$ for the same final states and also for $f = e$. The multiplicity of asymmetry parameters advantageously cancels systematic uncertainties to a large extent in the difference (*e.g.* detector asymmetries) and quotient (*e.g.* overall normalizations). The lepton asymmetries are very sensitive to s_w^2 because of the proximity of s_w^2 to $1/4$. We illustrate this by inserting the SM $SU(2)_L$ charges of the tree-level couplings and expanding

$$\begin{aligned} A_f &= \frac{(T_L^{3f} - s_w^2 Q_f)^2 - (s_w^2 Q_f)^2}{(T_L^{3f} - s_w^2 Q_f)^2 + (s_w^2 Q_f)^2} \\ &= \frac{1 - |Q_f|}{1 - |Q_f|(1 - |Q_f|/2)} + \frac{|Q_f|^2(1 - |Q_f|/2)}{(1 - |Q_f|(1 - |Q_f|/2))^2} (1 - 4s_w^2) + \mathcal{O}(1 - 4s_w^2)^2. \end{aligned} \quad (4.2.4)$$

The constant term vanishes precisely for $|Q_f| = 1$. $A_{e, \mu, \tau}$ thus allow us to determine the weak angle. The measurement of A_f then defines the effective angle $\sin^2(\theta_{\text{eff}}^l)$, as opposed to s_w^2 , which was defined by the ratio of bare gauge couplings and not directly expressed by observable quantities. Alternative definitions of the weak mixing angle using input data induce *e.g.* the on-shell angle $s_{\text{os}}^2 = 1 - M_W^2/M_Z^2$ or the weak angle given in terms of very precise electroweak input $\sin^2(2\theta_0) = (4\pi\alpha(M_Z)/(\sqrt{2}G_F M_Z^2))^{1/2}$. The best definition of the weak mixing angle in the presence of new physics is often a question of convenience. Using s_{eff}^{l2} or s_0^2 is favorable, since they present very precise input. Equation (4.2.4) holds true in models of new physics where the corrections to Z –lepton couplings are at least universal for both chiralities, and to a large extent also lepton-flavor universal. Then the effective weak angle is an obvious choice of input. The asymmetries of the down quarks are in comparison rather insensitive to s_w^2 , by a factor of almost 100, and provide a good precision constraint in many models of new physics.

The maximal set of EWPOs considered in standard global fits of the SM parameters contains approximately 40 observables. To constrain models of new physics, model-adapted techniques or effective parameters usually reduce the relevant set to a few observables. Before we discuss this approach in more detail we summarize the fit in the SM.

¹¹Similar measurements were also carried out at Tevatron for e^+e^- final states [340], however with less precision due to the difficulty to disentangle $q\bar{q}$ in the underlying initial $p\bar{p}$ Drell–Yan process.

Tools for sophisticated, statistically rigorous analyses are available, like ZFITTER [341], GAPP [342], and the recently developed modular toolkit GFITTER [343]. GFITTER only uses the 14 most important observables but is actively developed and updated with state of the art theoretical input. A recent evaluation from this group [344] takes into account the Higgs-mass value $M_h = 125.7 \pm 0.4 \text{ GeV}$ reported by ATLAS and CMS in July 2012 (average of [22, 29]). They find a p -value of 0.07 for the SM to describe the 14 observables, corresponding to 1.8σ . The compatibility of the fit result with the measurements is displayed in the left panel of figure 4.10 as a pull for each observable. No single observable shows a deviation of more than 3σ . However, one aspect of the updated analysis attracts interest. While overall the SM is still fully compatible with experimental data, the inclusion of a recent calculation of two-loop electroweak corrections to R_b [345] has impaired the fit. It presents the second largest deviation, close to the tension in $A_{\text{FB}}^{(0,b)}$. Deviations of this kind are not unusual in a large set of observables; however it is remarkable that they are both related to the couplings of the Z boson to b quarks. We take this as a phenomenological motivation to discuss b -related EWPOs in more detail below.

The global SM fit also confirms the spectrum of the bosons related to electroweak symmetry breaking. Leaving the direct Higgs-mass measurement aside, [344] obtains a fit result of $M_h = 94_{-22}^{+25} \text{ GeV}$ consistent with the direct measurement. Similarly, one can also indirectly determine the W -boson mass. At first sight, obvious input for that purpose is the weak mixing angle in order to use the relation $M_W^2 = e^2/(4\sqrt{2}s_w^2 G_F)$. The weak mixing angle has been measured over a wide range of energy scales. The most precise direct determination is obtained from polarization asymmetries measured at Z -pole energies, as discussed above, $s_{\text{eff}}^{l2} = 0.23153 \pm 0.00016$ [338]. Remarkably, this angle can be extracted indirectly from the fit with a precision that supersedes the direct measurements. Moreover, the indirect determination of the W -boson mass with the full set of EWPOs, $M_W = 80.359 \pm 0.011 \text{ GeV}$, is at the same level of precision as the SM prediction with the minimal set of input parameters that we describe below. The strong effect of the direct Higgs-mass measurement in over-constraining the SM is illustrated in the right panel of figure 4.10. We observe a shrinkage by a factor of approximately 3 in the CL ranges of the W -boson mass, when including the direct Higgs-mass measurement (blue) compared to ignoring it (gray).

As already mentioned, we must choose a set of input parameters in order to predict the EWPOs in the model under consideration. Besides the Higgs mass M_h , the fermion masses m_c , m_b , m_t , and the strong coupling constant α_s , a particularly useful choice is given by the set of Z -boson mass M_Z , the fine structure constant $\alpha(M_Z^2)$, and the Fermi constant G_F . The Fermi constant is measured with a high precision from the muon decay constant $G_F = 1.1663787(6) \times 10^{-5} \text{ GeV}^{-2}$ [69]. We summarize the input values used in the following in appendix B.2. The SM relation $G_F = 1/(\sqrt{2}v_{\text{SM}}^2)$ fixes the value of the SM VEV v_{SM} . However, in models of new physics, this relation is not necessarily fulfilled. After having worked out a theory and its symmetry breaking in terms of fundamental VEVs, one must carefully relate those VEVs to the muon decay and properly derive the relation to v_{SM} . In most models of new physics, a SM-like Higgs doublet (or an appropriate linear combination from a bidoublet in left–right symmetric models) is included and carries a VEV v , such that it is useful to define the ratio $\kappa_v \equiv v/v_{\text{SM}}$.

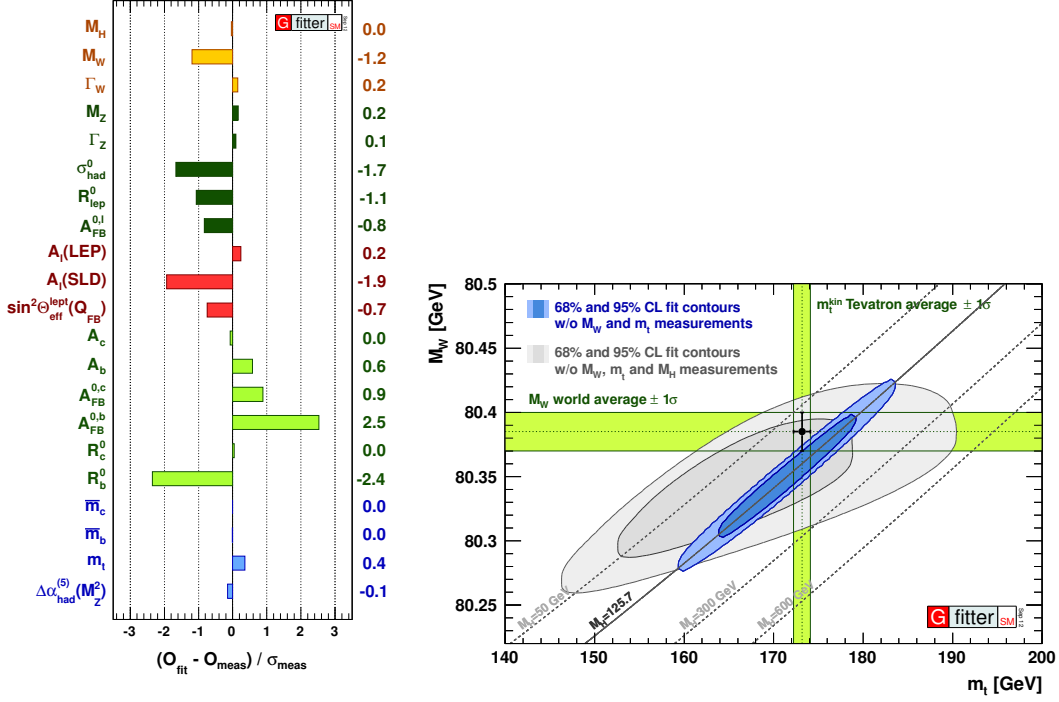


Figure 4.10: Results of the global fit including the Higgs-mass measurement taken from [344]. The left panel shows pull values for all used observables in units of the experimental uncertainty. The right panel shows contours of the 68% and 95% CLs of indirectly determined M_W and m_t . The contours with lighter colors result from the exclusion of the direct measurement of M_h . The vertical bands indicate the 1σ uncertainty of the directly measured values.

4.2.1.2 Effective Parameters for New Physics

For some models of new physics an adapted strategy — using additional input parameters wisely — is the preferable approach to EWPOs. However, in most cases a large fraction of the constraints follows from oblique corrections, *i.e.* gauge-boson-self-energy corrections. Under the assumption of heavy new physics, one integrates out any additional particles that lead to universal corrections, *i.e.* corrections that can be absorbed into the correlators of SM gauge bosons. In this approach one constrains the effective parameters in a model-independent way through their impact on the full set of EWPOs. The effective parameters then provide a convenient restricted interface of constraints on universal new physics. This comes at the price of neglecting some of the constraints (*e.g.* the anomalous magnetic moment of the muon [346]). One usually extends this strategy by additionally considering important non-universal contributions, in many cases and most importantly from corrections to the $Zb\bar{b}$ vertex that we discuss below. To define the effective parameters, one expands the two point correlators in the momentum as

$$\begin{aligned} \langle J_V^\mu(q) J_V^\nu(-q) \rangle &= ig^{\mu\nu} \Pi_{VV}(q^2) + q^\mu q^\nu \dots, \\ \Pi_{VV}(q^2) &= \Pi_{VV}(0) + q^2 \Pi'_{VV}(q^2) + \frac{q^4}{2} \Pi''_{VV}(q^2) + \dots, \end{aligned} \quad (4.2.5)$$

where J_V^μ is the current that couples to V_μ in the Lagrangian. We employ the classical parametrization by Peskin and Takeuchi¹² for the terms up to q^2 in the basis of mass eigenstates [348, 349]:

$$\begin{aligned} S &= \frac{16\pi s_w^2 c_w^2}{e^2} \left[\Pi'_{ZZ}(0) + \frac{s_w^2 - c_w^2}{s_w c_w} \Pi'_{ZA}(0) - \Pi'_{AA}(0) \right], \\ T &= \frac{4\pi}{e^2 c_w^2 M_Z^2} \left[\Pi_{WW}(0) - c_w^2 \Pi_{ZZ}(0) - 2s_w c_w \Pi_{ZA}(0) - s_w^2 \Pi_{AA}(0) \right], \\ U &= \frac{16\pi s_w^2}{e^2} \left[\Pi'_{WW}(0) - c_w^2 \Pi'_{ZZ}(0) - 2s_w c_w \Pi'_{ZA}(0) - s_w^2 \Pi'_{AA}(0) \right]. \end{aligned} \quad (4.2.6)$$

These parameters are defined relative to a fixed set of SM values, where they are usually set to zero. Gauge invariance guarantees that $\Pi_{AA}(0) = 0$ to all orders in perturbation theory, and one furthermore has $\Pi_{ZA}(0) = \Pi'_{ZA}(0) = 0$ when working at tree level. The parameter T thus is sensitive to the difference between the corrections to the W - and Z -boson vacuum-polarization functions and measures isospin violation. Usually, T expresses isospin breaking in the quotient of W and Z masses via the relation $\rho_0 \equiv \frac{M_W^2}{c_w^2 M_Z^2 \rho_{\text{SM}}} = (1 - \alpha T)^{-1} \approx 1 + \alpha T$. This relation holds for instance for the case of an extra, heavy, non-degenerate multiplet of chiral fermions or scalars. However, universal factors in the fermion couplings are also absorbed into the definitions (4.2.5) and (4.2.6). In that sense, T is more general and suitable as an effective parameter. S is related to the difference of contributions to the Z -boson self energy at $p^2 = M_Z^2$ and $p^2 = 0$; the sum $S + U$ is related to the analogous difference in the W -boson self energies. All three parameters are defined with a factor of α removed from the self energies such that they are expected to be of order unity in the presence of new physics.

The parameter U is only marginally affected in most models of new physics. This is expected due to the dimensionality of the corresponding effective operator in the operator product expansion in v/M_{NP} , where M_{NP} is the scale of new resonances. In the $SU(2)_L \times U(1)_Y$ symmetric phase, S and T are proportional to the coefficients of the dimension-6 operators $(\Phi^\dagger T^a \Phi) W_{\mu\nu}^a B^{\mu\nu}$ and $|\Phi^\dagger D_\mu^a \Phi|^2$, whereas U is proportional to the coefficient of the dimension-8 operator $|\Phi^\dagger W_{\mu\nu}^a \Phi|^2$.

There exist four further parameters necessary to describe the modifications in (4.2.5) at fourth order in the momentum. Only two of them receive contributions from dimension-6 operators, namely $(\partial_\rho B_{\mu\nu})^2$ and $(D_\rho^a W_{\mu\nu})^2$. In [350], the coefficients are defined in the electroweak eigenbasis as

$$\begin{aligned} Y &= \frac{g' M_W^2}{2} (s_w^2 \Pi''_{ZZ}(0) - 2c_w s_w \Pi''_{ZA}(0) + c_w^2 \Pi''_{AA}(0)), \\ W &= \frac{g M_W^2}{2} (c_w^2 \Pi''_{ZZ}(0) + 2c_w s_w \Pi''_{ZA}(0) + s_w^2 \Pi''_{AA}(0)). \end{aligned} \quad (4.2.7)$$

Those two parameters are useful in order to disentangle the information provided by LEP 2 experiments on e^+e^- cross sections at center-of-mass energies 189–207 GeV, above the Z pole [351]. However, the resulting constraints are small in most models of new physics, due to small contributions to Y and W . In [352], it was recognized that the original S , T , and U parameters are affected in the presence of W and Y , leading to the effective parameters

$$S_{\text{eff}} = S - \frac{4s_w^2}{\alpha} (W + Y), \quad T_{\text{eff}} = T - \frac{s_w^2}{\alpha c_w^2} Y, \quad (4.2.8)$$

¹²An alternative parametrization by Altarelli and Barbieri [347] can be translated into the one given here.

which enter the calculations of EWPOs in the same way as S and T do when $Y = W = 0$.

The experimental 68% CL bounds on the S , T , and U parameters and their correlation matrix are given in [344]

$$\begin{aligned} S &= 0.03 \pm 0.10, \\ T &= 0.05 \pm 0.12, \\ U &= 0.03 \pm 0.10, \end{aligned} \quad \rho = \begin{pmatrix} 1.00 & 0.89 & -0.54 \\ 0.89 & 1.00 & -0.83 \\ -0.54 & -0.83 & 1.00 \end{pmatrix}, \quad (4.2.9)$$

and with the constraint $U = 0$ imposed, as

$$\begin{aligned} S|_{U=0} &= 0.05 \pm 0.09, \\ T|_{U=0} &= 0.08 \pm 0.07, \end{aligned} \quad \rho|_{U=0} = \begin{pmatrix} 1.00 & 0.91 \\ 0.91 & 1.00 \end{pmatrix}. \quad (4.2.10)$$

The log likelihood for model testing, given the above values, is constructed by

$$\chi^2 = \sum_{i,j} (X_{i,\text{NP}} - X_{i,\text{obs-ref}})(\sigma^2)_{ij}^{-1} (X_{j,\text{NP}} - X_{j,\text{obs-ref}}), \quad (4.2.11)$$

where $\sigma_{ij}^2 = \sigma(X_{i,\text{obs-ref}}) \rho_{ij} \sigma(X_{j,\text{obs-ref}})$ is the covariance matrix. The $X_{i,\text{obs-ref}}$ are the values given in (4.2.9) or (4.2.10) with the subtraction of the fixed SM reference point, which correspond to the input values compiled in appendix B.2. Remark that conventionally one neglects the top mass uncertainty and considers it separately. The approximate one-loop contribution is given by [348]

$$\Delta S = -\frac{1}{6\pi} \ln \left(\frac{m_t^2}{m_{t,\text{ref}}^2} \right), \quad \Delta T = \frac{3}{16\pi s_w^2 c_w^2} \frac{m_t^2 - m_{t,\text{ref}}^2}{m_Z^2}, \quad \Delta U = \frac{1}{2\pi} \ln \left(\frac{m_t^2}{m_{t,\text{ref}}^2} \right). \quad (4.2.12)$$

This does also apply to the numerical values given above. The shift $\Delta T = \pm 0.013$, obtained for the 1σ CL of the top mass, is numerically relevant.

It is interesting to evaluate the shifts of the oblique parameters due to a Higgs mass different from the one measured. Keeping only the leading logarithmic loop effects in the SM, they are [349]

$$\Delta S = \frac{1}{12\pi} \ln \left(\frac{M_h^2}{M_{h,\text{ref}}^2} \right), \quad \Delta T = -\frac{3}{16\pi c_w^2} \ln \left(\frac{M_h^2}{M_{h,\text{ref}}^2} \right), \quad \Delta U = 0. \quad (4.2.13)$$

while U remains unchanged. Before the direct Higgs-mass measurement, in many models of new physics it turned out to be an interesting option to cancel contributions to the S parameter with a larger Higgs mass. E.g. in [1] we speculated that high values of M_h were possible and natural in the context of the minimal RS model. Similar options were present in the context of the two-Higgs-doublet model and models with a fourth chiral fermion generation [353]. This underlines the strong qualitative impact that the discovery of the Higgs boson has already had on the search for new physics.

4.2.1.3 Precision Observables from $Z \rightarrow b\bar{b}$

We often have to consider additional non-universal EWPOs, as mentioned above. Most importantly $Zb\bar{b}$ couplings are severely constrained but often affected in models of new physics. Here, we use the width of the Z -boson decay into bottom quarks and the total hadronic width,

R_b^0 , A_b , and $A_{\text{FB}}^{0,b}$ as introduced above. The general dependencies on the left- and right-handed $Zb\bar{b}$ couplings are given by [354]

$$R_b^0 = \left[1 + \frac{4 \sum_{q=u,d} [(g_{Z\bar{q}q}^L)^2 + (g_{Z\bar{q}q}^R)^2]}{\eta_{\text{QCD}} \eta_{\text{QED}} \eta' [(1 - 6z_b)(g_{Z\bar{b}b}^L - g_{Z\bar{b}b}^R)^2 + (g_{Z\bar{b}b}^L + g_{Z\bar{b}b}^R)^2]} \right]^{-1}, \quad (4.2.14)$$

$$A_b = \frac{2\sqrt{1 - 4z_b} \frac{g_{Z\bar{b}b}^L + g_{Z\bar{b}b}^R}{g_{Z\bar{b}b}^L - g_{Z\bar{b}b}^R}}{1 - 4z_b + (1 + 2z_b) \left(\frac{g_{Z\bar{b}b}^L + g_{Z\bar{b}b}^R}{g_{Z\bar{b}b}^L - g_{Z\bar{b}b}^R} \right)^2}, \quad A_{\text{FB}}^{0,b} = \frac{3}{4} A_e A_b.$$

The radiative QCD corrections given in [354] are summarized in the factors $\eta_{\text{QCD}} = 0.9954$ and $\eta_{\text{QED}} = 0.9997$. The most recent and precise evaluation [345] takes into account fermionic electroweak two-loop corrections, which are relatively large, by using numerical Mellin-Barnes integrals. In comparison to [354], higher-order corrections to the final state and gauge-boson propagators were taken into account. The authors of [345] provide a convenient fit formula from which we extract the numerical value corresponding to the input of appendix B.2 and adapt the general functional form (4.2.14) with a correction factor $\eta' = 0.9939$. The asymmetry parameter A_b is corrected for a non-zero bottom-quark mass via $z_b \equiv m_b^2(M_Z)/M_Z^2 = 0.997 \cdot 10^{-3}$. We assume that one can neglect new physics contributions to the left- and right-handed couplings of the light quarks $g_{Z\bar{q}q}^{L,R}$, and to the asymmetry parameter of the electron A_e . We fix these quantities to their SM values

$$\begin{aligned} (g_{Z\bar{u}u}^L)_{\text{SM}} &= 0.34674, & (g_{Z\bar{u}u}^R)_{\text{SM}} &= -0.15470 \quad [338], \\ (g_{Z\bar{d}d}^L)_{\text{SM}} &= -0.42434, & (g_{Z\bar{d}d}^R)_{\text{SM}} &= 0.077345 \quad [338], \\ (A_e)_{\text{SM}} &= 0.1462 \quad [341]. \end{aligned} \quad (4.2.15)$$

This assumption is well motivated by the very precise determination of these parameters, and also by the fact that in many models of new physics the magnitude of deviations is controlled by the fermion masses. We have seen in section 3.3.8.2 that this is the case for tree-level couplings in the RS-Models due to the RS-GIM mechanism.

We evaluate the relations (4.2.14) using $(g_{Z\bar{b}b}^L)_{\text{SM}} = -0.42114$ and $(g_{Z\bar{b}b}^R)_{\text{SM}} = 0.077420$ [338], to obtain for the central SM values of the bottom-quark pseudo observables¹³

$$(R_b^0)_{\text{SM}} = 0.21475, \quad (A_b)_{\text{SM}} = 0.935, \quad (A_{\text{FB}}^{0,b})_{\text{SM}} = 0.1033. \quad (4.2.16)$$

Comparing these numbers with the experimental results [338]

$$\begin{aligned} (R_b^0)_{\text{exp}} &= 0.21629 \pm 0.00066, \\ (A_b)_{\text{exp}} &= 0.923 \pm 0.020, \\ (A_{\text{FB}}^{0,b})_{\text{exp}} &= 0.0992 \pm 0.0016, \end{aligned} \quad \rho = \begin{pmatrix} 1.00 & -0.08 & -0.10 \\ -0.08 & 1.00 & 0.06 \\ -0.10 & 0.06 & 1.00 \end{pmatrix}, \quad (4.2.17)$$

we find a p -value of only 1.3% for the set of the three b -quark related EWPOs considered here. The experimental 1, 2 and 3σ CL are shown in figure 4.11 where the SM point is found at 2.5σ . We also reproduce the pull of A_{FB} obtained in [344] and shown in figure 4.10, where

¹³Errors of the SM predictions are negligible compared to the experimental values and therefore omitted.

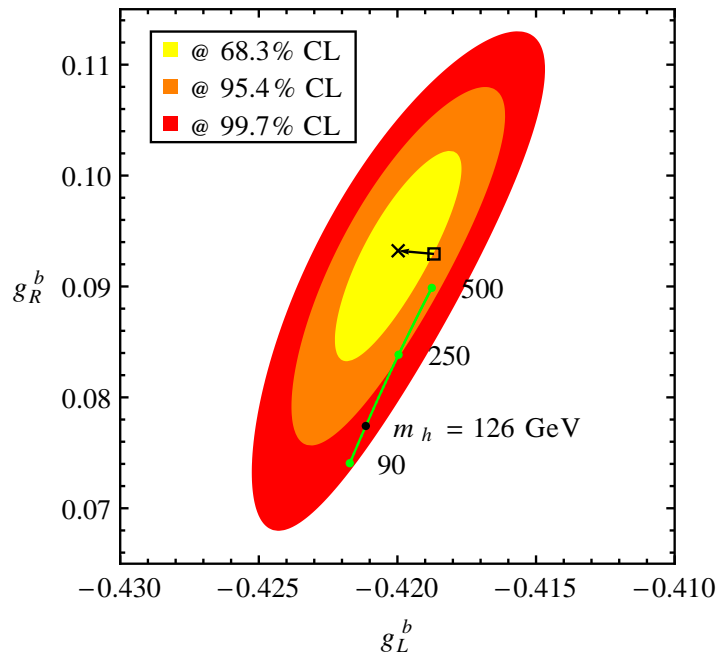


Figure 4.11: Fit to b -quark related EWPOs. The ellipses show the various confidence levels of the experimental value. The black dot marks the SM value. The green line illustrates variations of the Higgs mass, which are now fixed by the direct measurement. The black box shows the shift of the ellipsis with the state-of-the-art calculation compared to the result in [354], *i.e.* the shift induced by including η' .

the central SM value is 2.5σ away from the experimental value. The improved SM calculation of R_b now yields a value also -2.3σ off the measured value. When considering a large set of observables in a global fit, such deviations are not very unusual, thus we are far from stating an inconsistency. At this point, we also have to warn the reader that part of the tension might be due to an unfortunate statistical fluctuation or experimental systematics, since the values of A_b extracted at SLD and the experiments at LEP are only compatible at 1.6σ . Note that considering only the three b -related observables is also no unsubstantiated selection: It has the physical motivation that deviations from the SM Z -fermion couplings could be suppressed with an additional mechanism that depends on the mass of the fermion, *e.g.* the RS-GIM mechanism or general compositeness of couplings. Yet, we will see below that contributions in the RS model are rather harmful and cannot alleviate the existing deviations of the SM. In general, b -related EWPOs tell us at least in which direction of parameter space new physics is not allowed to move, and beyond, to speculations how it might improve the fit. The best fit values are given by $g_{Z\bar{b}b}^L = -0.41997$ and $g_{Z\bar{b}b}^R = 0.093220$. A shift of order $+15\%$ in the right-handed bottom-quark couplings relative to the SM could reach this value. On the other hand, with constant right-handed coupling, negative shifts in the left-handed coupling of only less than approximately -0.5% are allowed, but they do not improve the fit significantly. Similar conclusions have been reached in [355], where also a toy model of mirror fermions is presented that can reach the minimum χ^2 of the fit.

4.2.2 Constraints on the Randall-Sundrum Model

The leading effects on EWPOs in RS models arise already at tree-level and therefore have the potential to be highly constraining. Thanks to the RS-GIM mechanism, we have seen in section 3.3.8.2 that the contributions for light fermions localized near the UV brane are universal to a large extent. In the following, we quantify the universal and the b -quark related constraints in turn. We will discuss in detail how the custodial fermion embedding permits to alleviate the bounds from EWPOs.

4.2.2.1 General Discussion and Input Parameters

We start with reviewing the input parameters. In the last section we have seen that universal modifications of the couplings of the light fermions cancel in the asymmetries — as defined in (4.2.4) — making the effective weak angle s_{eff}^{l2} a natural choice. At tree-level we can therefore simply work with the value given in the last section for s_{eff}^{l2} and s_w^2 . The shift in the on-shell definition s_{os}^2 and s_0^2 are simple to work out, but we remark that their expressions are modified by a term $\sim LM_W^2/M_{\text{KK}}^2$ compared to the usual SM expression. The Fermi-constant is affected by the universal shift. Extracting it from the charged-current four-fermion coupling given in (3.3.153) we obtain at $\mathcal{O}(v^2/M_{\text{KK}}^2)$

$$\frac{G_F}{\sqrt{2}} = \frac{g^2}{8M_W^2} \left[1 + \frac{M_W^2}{2M_{\text{KK}}^2} \left(1 - \frac{1}{2L} \right) \right]. \quad (4.2.18)$$

It is useful to maintain the definition of v_{SM} in terms of G_F and relate it to the Higgs VEV v that is necessary in the RS model to obtain the correct W -boson mass from (3.3.81). We express this as [356]

$$\kappa_v \equiv \frac{v}{v_{\text{SM}}} = 1 + \frac{M_W^2}{4M_{\text{KK}}^2} \left(\frac{L}{c_V^2} - 1 + \frac{1}{2L} \right), \quad (4.2.19)$$

which holds for the custodial RS model and for the minimal model with $c_V \rightarrow 1$.

Concerning low energy EWPOs, it is interesting to note that a full 5d one-loop calculation of the anomalous magnetic moment of the muon [231] finds a very small contribution, well below the current uncertainty, even for M_{KK} as low as 500 GeV.

4.2.2.2 Oblique and Universal Contributions

We summarize the oblique and universal contributions to the EWPOs with light fermions with the S , T , and U parameters introduced in section 4.2.1.2. Following [187], we write these in standard self-energy notation, despite the fact that the 5d contributions arise in fact at tree level.

We calculated the non-zero tree-level correlators $\Pi_{VV}(0)$ and $\Pi'_{VV}(0)$ with $V = W, Z$ in two ways. The simplest method is to use the zero-mode masses (3.3.81) and profiles (3.3.80) in order to calculate the modifications to the pure zero mode exchange. This corresponds to the original on-shell definition of Peskin and Takeuchi. We obtain at $\mathcal{O}(v^2/M_{\text{KK}}^2)$

$$S_{\text{eff}} = \frac{2\pi v^2}{M_{\text{KK}}^2} \left(1 - \frac{1}{L} \right), \quad T_{\text{eff}} = \frac{\pi v^2}{2c_w^2 M_{\text{KK}}^2} \left(\left[\frac{1}{c_Z^2} - \frac{c_w^2}{c_W^2} \right] \frac{L}{s_w^2} - \frac{1}{2L} \right), \quad U_{\text{eff}} = 0. \quad (4.2.20)$$

As an alternative, yet more lengthy, check of the result we used the full 5d bosonic propagator to derive S , T , and U in the definition of Barbieri et. al. [350]. This summarizes the full

contribution from all KK bosons, according to the approach of [350] to summarize all universal corrections. To this end one can use $\Sigma_V^{(k)}(t, t')$ for $k = 1$ given in (3.3.102), in order to derive $\Pi_{VV}(0)$, and generalize the method to $k = 2, 3$ to obtain the derivatives of the vacuum polarization. Here, we used instead the full gauge boson propagator for the minimal model from [210]. Taking the version for euclidean momentum $p_E^0 = -ip^0$ we obtain the vacuum polarization and its derivatives as

$$\Pi_{VV}(p_E) = -\left(\frac{L}{k} D_{\mu\nu}^{V\perp}(q; \epsilon, \epsilon)\right)^{-1} - p_E^2 - M_V^2 = \Pi_{VV}(0) - p_E^2 \Pi'_{VV}(0) + \frac{p_E^4}{2} \Pi''_{VV}(0). \quad (4.2.21)$$

A straightforward calculation leads to

$$S = \frac{2\pi v^2}{M_{\text{KK}}^2}, \quad T = \frac{\pi v^2}{2c_w^2 M_{\text{KK}}^2} L, \quad W = Y = \frac{g^2 v^2}{16 M_{\text{KK}}^2 L}, \quad (4.2.22)$$

in agreement with [214, 357–359]. Relating this to the effective parameters via (4.2.8) we obtain the same result as before in (4.2.20) with $c_V = 1$.

The result (4.2.20) clearly shows that custodial protection is automatically at work in the breaking scheme where $SU(2)_L \times SU(2)_R$ is broken to the diagonal subgroup. We have seen in section 3.3.5.1 that this leads to the relation $c_Z^2 = c_W^2/c_w^2$, canceling the L -enhanced term in T_{eff} . This holds irrespective of further details of the model, like *e.g.* the P_{LR} symmetry. The minimal model holds with $c_{W,Z} \rightarrow 1$ such that T_{eff} is larger by a factor of approximately $2L^2 \sim 10^3$ in the minimal model compared to the custodial model. We derive the following numerical constraints on the KK scale and first KK gluon excitation at 99.73% (3σ) CL

$$\begin{aligned} \text{minimal RS:} & \quad \epsilon = 10^{-15}, & M_{\text{KK}} > 4.6 \text{ TeV}, & M_{G(1)} > 11.3 \text{ TeV}, \\ \text{custodial RS:} & \quad \epsilon = 10^{-15}, & M_{\text{KK}} > 1.7 \text{ TeV}, & M_{G(1)} > 4.1 \text{ TeV}, \\ \text{little RS:} & \quad \epsilon = 10^{-3}, & M_{\text{KK}} > 1.8 \text{ TeV}, & M_{G(1)} > 4.7 \text{ TeV}. \end{aligned} \quad (4.2.23)$$

The full dependence of the lower bound on the KK scale on the volume of the extra dimension is shown in figure 4.12. There, and in the bounds given in (4.2.23), we take the uncertainty on m_t and M_h into account, allowing it to vary at the same CL like the S and T parameters. Almost all of the variation stems from the top-mass uncertainty. The full variation of the lower limit with the uncertainties is shown in the shaded bands in figure 4.12. Using the mean values for m_t and M_h , one would overestimate the bound on the minimal RS model in (4.2.23) by 13%. We observe that the LRS model [192] with small warp factor poses a viable alternative to the custodial protection in order to protect the T parameter. Of course one gives up the idea of connecting the weak scale with the scale of gravity but rather assumes new phenomena to set in at an intermediate scale.

The limits on the custodial RS model stem almost entirely from the bound on S and are essentially independent of L . We see that the 68% CL limit on M_{KK} is relatively high due to the measurement being only compatible with the reference SM point at approximately this CL. The small negative shift in T from the custodial RS model cannot improve the fit. Rather on the contrary, there might be harmful negative contributions to the T -parameter at loop-level for relatively light KK fermions. In [224, 360] the fermion contribution to the T parameter is found to be finite at one-loop level for a related fermion embedding in the context of an $SO(5)$ gauge–Higgs–unification model. The presence of bidoublets — as introduced in section 3.3.5.2 to embed the left-handed quark doublet in the extended $SU(2)_L \times SU(2)_R \times U(1)_X$

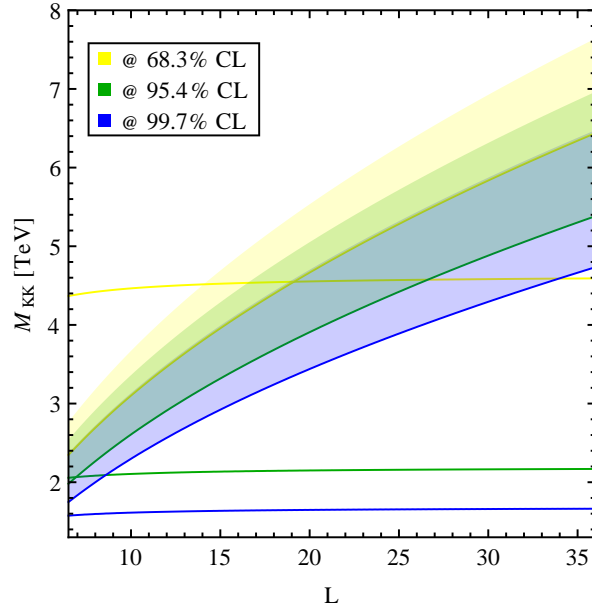


Figure 4.12: Constraints on the KK scale from S and T . The solid lines show the lower limit on the KK scale in dependence on the volume of the extra dimension L . The shaded bands indicate the uncertainty from m_t and M_h . We include the uncertainty on m_t and M_h at the same CL like the constraint on S and T . The steep/flat lines are valid for the minimal/custodial model.

gauge group — is found to typically induce a negative shift in the T parameter. Obtaining very light KK fermions (called custodians) is impossible with our fermion embedding, since the necessary bulk mass configuration requires strong P_{LR} breaking. This leads to mixing into the left-handed b quark, whose couplings to the Z boson are modified, but they are strongly restricted as we discuss below. Furthermore, the one-loop Higgs-sector contribution to the T -parameter has been found to be finite as well, but logarithmically UV divergent for the S parameter [223]. The authors of the latter reference find this result independently of the model details. This could result in a large and positive S parameter. The numerical details of the one-loop corrections to S and T remain unquantified and are beyond the scope of this thesis. Qualitatively, the discussion given here tells us that the bounds in (4.2.23) could be raised.

When one allows for more elaborate extra-dimensional model building and departures from the minimal setups we consider here, then there exist of course methods to protect the T -parameter. One possibility uses large brane-localized kinetic terms for the gauge fields [357, 361, 362]. Since such terms are needed as counterterms to cancel divergences appearing at the loop level [363, 364], they are expected on general grounds to be present in an orbifold theory. The bare contributions to the brane-localized kinetic terms encode the unknown UV physics at or above the cutoff scale. To retain the predictivity of the model, we assume that these bare contributions are small. As we concentrate on the leading contributions to the electroweak precision observables, we furthermore ignore possible effects of brane-localized kinetic terms appearing at the loop level. Even if these assumptions would be relaxed, the bound on the KK-gauge-boson masses that derives from the constraints on the S and T parameters would remain anti-correlated with the mass of the Higgs boson. For example, the

authors of [362] found that having a light KK spectrum would require a value of the Higgs mass in the range of several hundred GeV. Another alternative direction of model building, which we did not discuss here, allows for variations of the 5d metric in the IR region. For the required model building and details we refer to [365, 366].

4.2.2.3 Bounds from the $Zb\bar{b}$ Vertex

We continue with an analysis of the most important non-oblique correction, given by the precision measurements of the $Zb\bar{b}$ vertex. To this end we derive approximate expressions for $g_{Z\bar{b}b}^L$ and $g_{Z\bar{b}b}^R$ in the ZMA (see section 3.3.6) and furthermore use relations following from a Froggatt-Nielsen analysis, *i.e.* corresponding to an expansion in the Cabibbo angle. Starting from the general expression for the couplings (3.3.142) we find to the order considered

$$\begin{aligned}
 g_{Z,L}^b = & \left(-\frac{1}{2} + \frac{s_w^2}{3} \right) \left[1 - \frac{M_Z^2}{2M_{\text{KK}}^2} \frac{F^2(c_{b_L})}{3 + 2c_{b_L}} \left(\omega_Z^{b_L} L - \frac{5 + 2c_{b_L}}{2(3 + 2c_{b_L})} \right) \right] \\
 & + \frac{m_b^2}{2M_{\text{KK}}^2} \left\{ \frac{1}{1 - 2c_{b_R}} \left(\frac{1}{F^2(c_{b_R})} \left[1 - \delta_c \frac{1 - 2c_{b_R}}{1 - 2c_{b'_R}} \right] - 1 + \frac{F^2(c_{b_R})}{3 + 2c_{b_R}} \right) \right. \\
 & \left. + \sum_{i=1}^2 \frac{|(Y_d)_{3i}|^2}{|(Y_d)_{33}|^2} \frac{1}{1 - 2c_{d_i}} \frac{1}{F^2(c_{b_R})} \left[1 - \delta_c \frac{1 - 2c_{d_i}}{1 - 2c_{d'_i}} \right] \right\}, \quad (4.2.24)
 \end{aligned}$$

$$\begin{aligned}
 g_{Z,R}^b = & \frac{s_w^2}{3} \left[1 - \frac{M_Z^2}{2M_{\text{KK}}^2} \frac{F^2(c_{b_R})}{3 + 2c_{b_R}} \left(\omega_Z^{b_R} L - \frac{5 + 2c_{b_R}}{2(3 + 2c_{b_R})} \right) \right] \\
 & - \frac{m_b^2}{2M_{\text{KK}}^2} \left\{ \frac{1}{1 - 2c_{b_L}} \left(\frac{1}{F^2(c_{b_L})} - 1 + \frac{F^2(c_{b_L})}{3 + 2c_{b_L}} \right) + \sum_{i=1}^2 \frac{|(Y_d)_{i3}|^2}{|(Y_d)_{33}|^2} \frac{1}{1 - 2c_{Q_i}} \frac{1}{F^2(c_{b_L})} \right\},
 \end{aligned}$$

where $c_{b_L} \equiv c_{Q_3}$. In order to unify the notation of the custodial with the minimal model, we also write $c_{d_i} \equiv c_{\mathcal{T}_{2,i}}$ and $c_{d'_i} \equiv c_{\mathcal{T}_{1,i}}$. The coefficient $\delta_c \in \{0, 1\}$ multiplies terms that are only present in the custodial model. In these terms we assumed $c_{d'_i} < 1/2$, what is also required for obtaining a sensible quark spectrum. Note that we use the bottom-quark $\overline{\text{MS}}$ mass $m_b \equiv m_b(M_{\text{KK}})$ evaluated at the KK scale. On the other hand, the electromagnetic coupling and the weak mixing angle are running parameters in the low-energy EFT, which is obtained after decoupling the RS contributions at the scale M_{KK} . We effectively include the associated large logarithms by replacing $s_w^2(M_{\text{KK}})$ with $s_w^2(m_Z)$ in (4.2.24). We still allow for $c_{\mathcal{T}_{1,i}} \neq c_{\mathcal{T}_{2,i}}$, *i.e.* P_{LR} symmetry breaking by the triplet bulk masses, and retain the parameters $\omega_Z^{b_L}$ and $\omega_Z^{b_R}$. Remind that in the custodial embedding of section 3.3.5.2, we found $\omega_Z^{b_L} = 0$ and $\omega_Z^{b_R} \approx 10$, while both factors are set to one in the minimal model.

From (4.2.24), we observe that the non-universal reduction of $g_{Z,R}^b$ is in any case negative and approximately 10 times more so in the custodial model. This direction of contributions to $g_{Z,R}^b$ is strongly constrained by the bottom-quark pseudo observables, as we have seen in section 4.2.1. We will see below, that this puts a mild upper bound on the size of c_{b_R} in the custodial model, while the contributions are irrelevant in minimal model. The shift in g_L^b is positive in the minimal model and almost absent in the model with custodial protection with a small negative contribution remaining. If one allows the P_{LR} symmetry to be broken by $c_{d_i} \neq c_{d'_i}$, then the shift in g_L^b can also be positive in the custodial model as a result of fermion

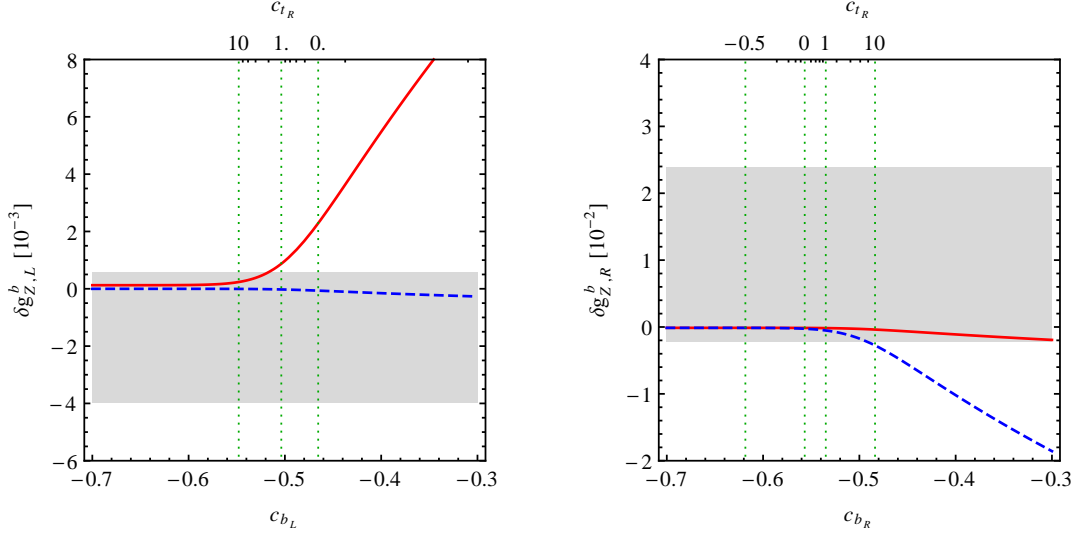


Figure 4.13: Anomalous couplings δg_L^b (left) and δg_R^b (right) as functions of c_{b_L} and c_{b_R} . The red solid and blue dashed lines correspond to the predictions obtained in the minimal model and custodial RS model. The b -bulk-mass parameters not explicitly shown is set to $-1/2$. The elements of the down-type Yukawa matrix are set to equal magnitude. The scale of c_{t_R} on the upper frame axis corresponds to $(Y_u)_{33} = 3$ and $(Y_d)_{33} = 1$. The light gray bands indicate the experimentally allowed 3σ CL ranges.

mixing. Positive contributions to $g_{Z,L}^b$ are strongly constrained by the bottom-quark pseudo observables and imply relevant restrictions on the parameter space of the minimal model.

In order to obtain a quantitative impression of the anomalous couplings, we show in figure 4.13 our predictions for $\delta g_{Z,\sigma}^b \equiv g_{Z,\sigma}^b - (g_{Z,\sigma}^b)_{\text{SM}}$ as functions of the bulk-mass parameters c_{b_σ} for $M_{\text{KK}} = 1$ TeV. Similar plots have been presented in [224]. The shown curves correspond to median bulk-mass parameters for the first two generations, which we obtained in a parameter scan $c_{Q_1} = -0.63$, $c_{Q_2} = -0.57$, $c_{d_1} = -0.65$, and $c_{d_2} = -0.62$. Variations of this choice in the allowed ranges have little impact on the results. We furthermore fix the ratios of Yukawa entries $|(Y_d)_{3i}|/|(Y_d)_{33}|$ and $|(Y_u)_{i3}|/|(Y_u)_{33}|$ with $i = 1, 2$ to be equal to one. Compared to the minimal case (red solid line) the prediction for $\delta g_{Z,L}^b$ in the RS model with extended P_{LR} symmetry (blue dashed line) is, essentially independent of c_{b_L} . The predictions for the anomalous coupling $\delta g_{Z,L}^b$ are thus easily within the experimental 99.73% CL (3σ) bound shown as the light gray band, which gives a strong motivation to protect the $Zb_L\bar{b}_L$ vertex through the mechanism employed here. In the case of the minimal RS model, δg_L^b can be suppressed by localizing the right-handed top quark very close to the IR brane. This feature is illustrated by the ticks on the upper border of the frame in the left panel. The given values of $c_{t_R} \equiv c_{u_3^c}$ have been obtained by solving the Froggatt-Nielsen relation $m_t = v/\sqrt{2}|(Y_u)_{33}|F(c_{b_L})F(c_{t_R})|$ for the bulk-mass parameter c_{t_R} , evaluating the top-quark $\overline{\text{MS}}$ mass at $M_{\text{KK}} = 1$ TeV and setting $|(Y_u)_{33}| = 3$. For smaller values of $|(Y_u)_{33}|$ the ticks are shifted even further to the right.

As anticipated above, the corrections δg_R^b are negative and always larger in the custodial RS model than in the minimal formulation. In principle, this puts an upper bound on the size of c_{b_R} in the former case, as we see from the experimental bound indicated again by the light

gray band. Still, the $Zb_R\bar{b}_R$ coupling is predicted to be SM-like if we require to reproduce the large top-quark mass with Yukawa couplings of $\mathcal{O}(1)$. This can be inferred from the ticks on the upper border of the frame in the right panel. They have been obtained by combining the Froggatt-Nielsen approximation $m_b = v/\sqrt{2}|(Y_d)_{33}|F(c_{b_L})F(c_{b_R})|$ with the one for m_t given earlier, solving again for c_{t_R} . The Yukawa parameters have been fixed to $|(Y_d)_{33}| = 1$ and $|(Y_u)_{33}| = 3$. For smaller values of $|(Y_d)_{33}|$ the ticks move to the right and vice versa for larger values. Rescaling $|(Y_u)_{33}|$ has the opposite effect. With the choice of a bulk-mass parameter not exceeding the curvature scale¹⁴ $c_{t_R} < 1$, we observe that the bound is only relevant for very low values of $|(Y_d)_{33}|$. This observation leads us to the conclusion that, irrespectively of the bulk gauge group, naturalness in combination with the requirement to reproduce the observed top- and bottom-quark masses excludes large corrections to δg_R^b in models of warped extra dimensions in which the left-handed bottom and top quark reside in the same multiplet. This model-independent conclusion should be contrasted with the analysis [367], which finds sizable corrections in δg_R^b . The values of the bulk-mass parameters $c_{b_{L,R}}$ and c_{t_R} considered in the latter article lead to bottom- and top-quark masses of $m_b \approx 40$ GeV and $m_t \approx 75$ GeV, which are in conflict with observation. We finally remark that if the left-handed bottom and top quarks arise as an admixture of the zero-mode fields of two $SU(2)_L$ doublets, then the bottom- and top-quark masses are determined by two independent sets of bulk-mass parameters, so that it is possible to account simultaneously for the quark masses and mixings as well as the $A_{\text{FB}}^{0,b}$ anomaly [368].

The full impact of the constraints on the anomalous $Zb\bar{b}$ couplings on the relevant model parameters are shown in figure 4.14 for the minimal, and figure 4.15 for the custodial RS model. The colored contours indicate the magnitude $|(Y_d)_{33}|$ necessary to achieve the observed value of the bottom-quark mass. Requiring in addition a consistent value of the top quark mass restricts the parameter space further. This is indicated by the cyan, dashed regions, which enclose the allowed range for allowed hierarchies in the Yukawa matrices between one for the innermost and four for the outermost region.

In the case of the minimal model we illustrate with bright colors the importance of including the m_b^2/M_{KK}^2 corrections as opposed to the region with faint colors, where they are set to zero. They originate from the term $(\delta_{Q,q})_{33}$ in (3.3.142) that parametrizes singlet–doublet fermion mixing and contribute with a term that is proportional to $F(c_{b_{L,R}})^{-2}$. This term is relevant for $\delta g_{Z,b}^L$, in which c_{b_R} enters. Consequently, the b -related EWPOs, pose a tight constraint on the amount of UV localization of the right-handed b -quark. A similar constraint is also active in the custodial model when we break the P_{LR} symmetry by the bulk-mass parameters $c_{b'_R} \neq c_{b_R}$. In the case of full P_{LR} symmetry the whole faintly colored region of figure 4.15 is accessible. We demonstrate by the brightly colored region that the choice $c_{b'_R} = 0$ cuts away a relevant part of the parameter space for low values of M_{KK} . Notice that the main P_{LR} breaking correction to g_{b_L} in (4.2.24) scales like $-v^2/M_{\text{KK}}^2|(Y_d)_{33}|^2F^2(c_{b_L})$ as seen from the aforementioned Froggatt-Nielsen approximation. This explains why values $|(Y_d)_{33}| \gtrsim 1$ are not compatible with the $Z \rightarrow b\bar{b}$ data in the case $c_{b'_R} = 0$.

Taking a completely random approach to the fundamental Yukawa and bulk-mass parameters, we also did a numerical scan over the parameter space. We generated a large sample of parameter points with viable quark spectrum and calculated the $Zb\bar{b}$ -couplings without resorting to the approximations used above. Further details on this parameter scan are described in appendix B.3. With the parameter scan, we can quantify the constraining power

¹⁴Remark that one also has to require $c_{t_R} > -1/2$ in order to reproduce the large top mass.

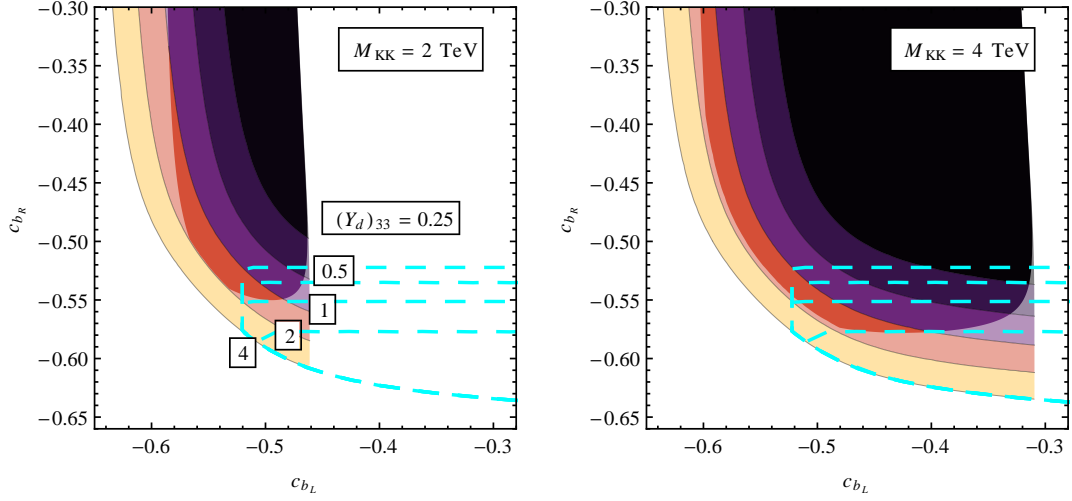


Figure 4.14: 3σ CL in the c_{b_L} - c_{b_R} plane for the minimal RS model and $M_{\text{KK}} = 2 \text{ TeV}$ and $M_{\text{KK}} = 4 \text{ TeV}$. The colored contours indicate the value of $|(Y_d)_{33}|$ necessary to reproduce the value of the bottom-quark mass. The same color code is used in all plots. The bright colors show the numerical result of the full expressions for $g_{Z,\sigma}^b$ (4.2.24), while faint colors indicate the result without terms proportional m_b^2/M_{KK}^2 . The dashed cyan lines enclose the regions where top and bottom-quark mass can be reproduced with $|c_{t_R}| < 1$, and all Yukawa elements and ratios of Yukawa elements in the range $[1/n, n]$, with $n = 1, 2, 3, 4$ for the four successively larger regions.

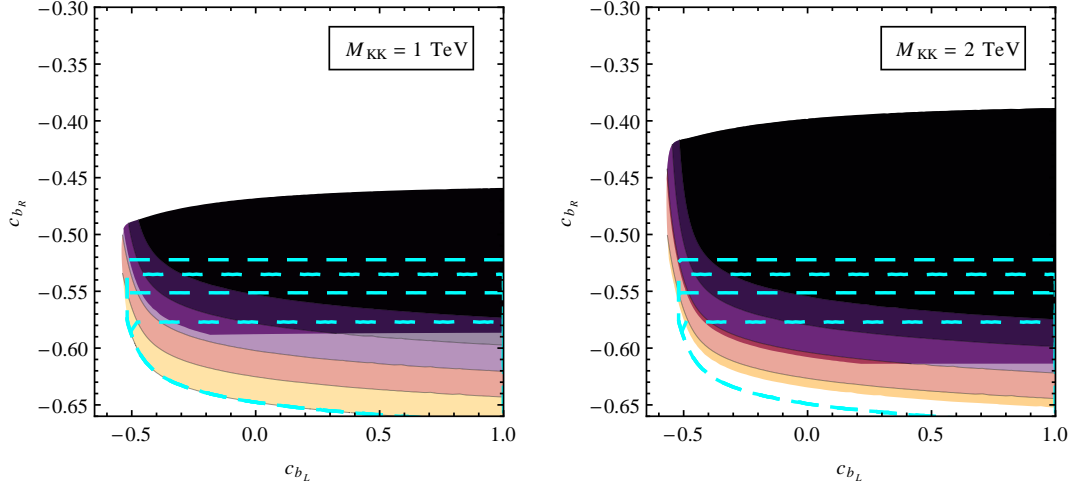


Figure 4.15: 3σ CL in the c_{b_L} - c_{b_R} plane for the custodial RS model for $M_{\text{KK}} = 1 \text{ TeV}$ and $M_{\text{KK}} = 2 \text{ TeV}$. Here the faint colors correspond to the full result (including m_b^2/M_{KK}^2 terms) and active P_{LR} symmetry $c_{b'_R} = c_{b_R}$. Only the brightly colored region is accessible for broken P_{LR} symmetry with a fixed value of $c_{b'_R} = 0$. The remaining properties of the plot agree with figure 4.14

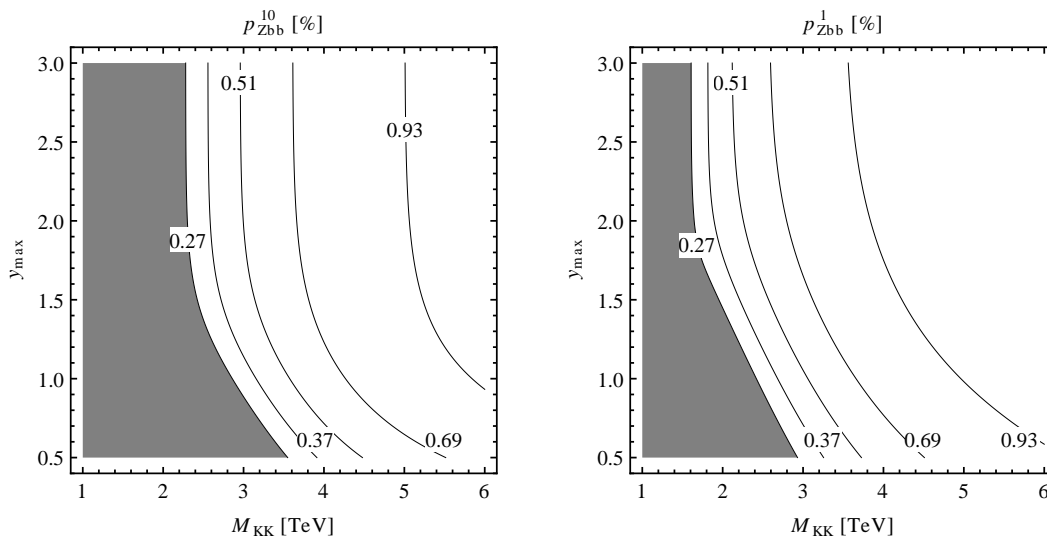


Figure 4.16: Contours for p -values of the three b -related EWPOs in the minimal RS model, obtained from a numerical scan of the RS parameters. p_{Zbb}^q is the q %-quantile for the p -value, *i.e.* a fraction of q % of the parameter space (10% and 1% in the left and right panel) have a probability that is equal or higher than p_{Zbb}^q . The values are given in percent and correspond to the 3...2.6 σ level in steps of 0.1 from left to right. The SM value is at approximately 2.5 σ .

of the b -related EWPO under a given assumption of allowed tuning. We illustrate this in figure 4.16, where we show contours for the minimal probability of the best 10% (left panel), or 1% (right panel) of the total parameter space of the minimal RS model. The grayed region in those plots corresponds to the excluded white region of figure 4.14, with the additional requirement of 10%, or 1% available parameter space. We observe a peculiar dependence on the size of the maximally allowed values of the fundamental Yukawa matrix elements y_{\max} . Starting from $y_{\max} \approx 1.5$, the required KK scale necessary to suppress the contribution to the $Zb\bar{b}$ -couplings sharply rises for lower values of y_{\max} . On the other hand, allowing for maximal perturbatively safe values of $y_{\max} = 3$, still more than 1% of the parameter space is open for a KK scale of 1.6 TeV, which is considerably below the bounds imposed on the minimal RS model by oblique correction.

We conclude that the b -related EWPOs impose tight constraints on the parameter space of the minimal RS model, whereas they are only relevant in the custodial model with large P_{LR} -breaking from bulk masses. In contrast to the oblique and universal corrections, the constraints are weaker in the sense that they do not only affect the KK scale. They rather constrain the localization of the left and right-handed b -quark beyond the requirement of reproducing a sensible quark spectrum and can impose a certain amount of hierarchy between $(Y_u)_{33}$ and $(Y_d)_{33}$ for low values of M_{KK} .

4.3 Higgs Production and Decays at Hadron Colliders

The remainder of this thesis is devoted to the topic of Higgs production and decays. Since such processes were only very recently measured for the first time, the subject is in a major upheaval period from the experimental point of view. This implies that Higgs processes will soon constitute a third pillar of precision constraints on models beyond the SM. On the theoretical and phenomenological side, the physics behind these processes is well understood and precise predictions can be made for the SM. Also beyond the SM, the effects of additional particles are well understood for perturbatively unitary theories like the minimal supersymmetric SM, general two-Higgs-doublet models, and left–right symmetric models. For reviews on Higgs phenomenology in these models see [106, 369, 370] and the references therein. Here, we investigate the effect of specific composite models. First, we review the SM results, the experimental status, and contributions from partner fermions in the simple example of the LHT model. Our main focus is then to determine the analytical and numerical structure of the effects in the RS model, discuss the subtle issue of convergence of loop integrals, and the potential to constrain the parameter space.

4.3.1 Results in the SM and Measurements

With the recent discovery of a bosonic resonance [22, 29, 41] that is presumably due to the Higgs boson¹⁵, we entered a new era of particle physics. Since apart from the resonance mass $M_h \approx 126$ GeV also the first bounds on its couplings were obtained, Higgs physics has reached a turning point in making the transition from discovery to precision physics.

The couplings of the Higgs boson to fermions and gauge bosons have a peculiar structure in the SM. This originates in the simple mechanism of electroweak symmetry breaking. The couplings of the Higgs boson to gauge bosons are obtained from covariant derivatives, whilst fermions couple to the Higgs boson via Yukawa couplings. Since these terms are the only sources of all particle masses and there is only a single scalar direction that takes a VEV, the corresponding couplings of the physical Higgs boson are directly proportional the same mass. Decay widths to heavy particles are consequently enhanced compared to those into light particles. The same is true for the production of the Higgs boson: Direct Higgs-boson couplings of the light quarks contained in protons, or of electrons in the initial state contribute to production to a negligible extent. Thus, the main production channels we must consider either involve heavy quarks, most importantly the top quark, or heavy gauge bosons.

For hadron colliders, such as the Tevatron and the LHC, the main production process is due to fusion of two gluons. The leading order (LO) Feynman diagram is depicted in the upper left panel of figure 4.17. Since this process is particularly interesting in the models of new physics we discuss below, we will review it in some detail before commenting on the other production modes.

We take a closer look at the on-shell amplitude for the diagram depicted in the upper left

¹⁵Since the discovered particle decays also into two photons it must be a boson. The Landau-Yang theorem [371, 372] implies that it cannot be of spin 1. Evidence for the decay into Z bosons suggests that it participates in electroweak symmetry breaking. Recent measurements of ATLAS [27] and CMS [36] already disfavor the pseudo-scalar and spin two hypothesis roughly at the level of one percent. For simplicity we call the observed resonance the Higgs boson.

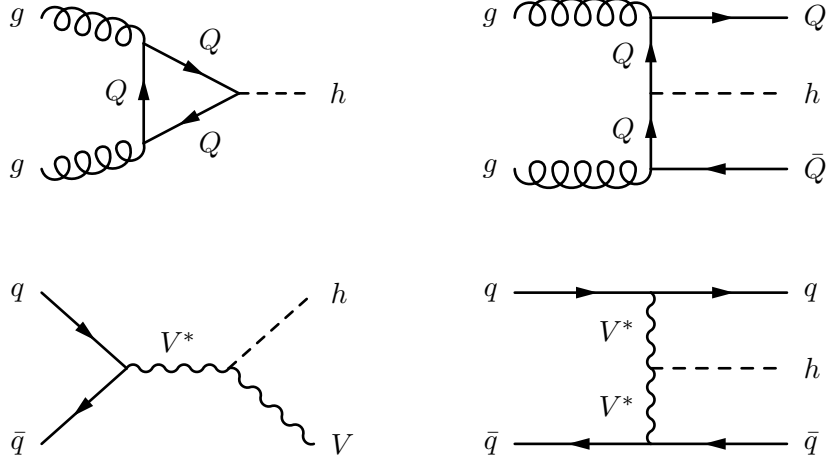


Figure 4.17: Feynman diagrams for the leading order contributions to the dominant Higgs production mechanisms in the SM at hadron colliders. For the subleading production with heavy quarks in the upper right panel there are additional tree-level diagrams with the Higgs boson attached to other lines, with a trilinear gluon coupling, and with $q\bar{q}$ initial state.

panel of figure 4.17. After evaluating the fermionic trace it is given by

$$\begin{aligned} \mathcal{M}(gg \rightarrow h) &= 2i \frac{g_s^2 m_q^2}{v} \delta^{ab} \epsilon_\mu(p) \epsilon_\nu(q) \\ &\times \mu^{2\epsilon} \int \frac{d^D k}{(2\pi)^D} \frac{g^{\mu\nu} \left(m_q^2 - M_h^2/2 - k^2 \right) + 4k^\mu k^\nu + q^\mu p^\nu}{(k^2 - m_q^2) [(k+p)^2 - m_q^2] [(k-q)^2 - m_q^2]}, \end{aligned} \quad (4.3.1)$$

where m_q is the mass of the internal fermion. The momentum p , Lorentz-index μ , and color-index a belong to one gluon and q , ν , b to the other. We have already written the expression using dimensional regularization in $D = 4 - 2\epsilon$ dimensions, even though we know the loop-integral must be finite because of renormalizability of the SM. However, a gauge invariant regulator is necessary to obtain the correct finite result, which fulfills the Ward identities. They require the amplitude to be proportional to $q^\mu p^\nu - g^{\mu\nu} M_h^2/2$. One can indeed observe a curious cancellation of two specific finite terms. We rewrite the loop-integral in the second line of (4.3.1) with the conventional three-point functions, defined *e.g.* in [373], to obtain

$$\begin{aligned} &\frac{i}{(4\pi)^2} \left(C_{\rho\sigma}(p^2, q^2; m_q, m_q, m_q) (4g^{\mu\rho} g^{\nu\sigma} - g^{\mu\nu} g^{\rho\sigma}) \right. \\ &\quad \left. + C_0(p^2, q^2; m_q, m_q, m_q) (g^{\mu\nu} [m_q^2 - M_h^2/2] + q^\mu p^\nu) \right). \end{aligned} \quad (4.3.2)$$

Reducing the tensor function $C_{\rho\sigma}$ with the Passarino-Veltman method [374] one sees that it contains a contributions from a scalar two point functions $g_{\rho\sigma} B_0(p; m_q, m_q)$. The $1/\epsilon$ divergence in B_0 is however multiplied with a Lorentz structure from the fermion trace that would vanish in $D = 4$ given by $(4g^{\mu\rho} g^{\nu\sigma} - g^{\mu\nu} g^{\rho\sigma}) g_{\rho\sigma} = 2\epsilon g^{\mu\nu}$. This leads to a finite, non-gauge invariant term which cancels against the non-gauge invariant terms in the second line of (4.3.2). The necessity of a proper regularization is a crucial observation that we also encounter in the 5-dimensional calculation in the RS model in section 4.3.3. However, the argument is of different nature in that model. Instead of the breakdown of gauge invariance

we observe a resonance phenomenon at an artificial physical scale that is inexistent when the theory is properly UV-regularized.

The amplitude for $gg \rightarrow h$ can finally be written as [375]

$$\begin{aligned} \mathcal{M}(gg \rightarrow h) &= \frac{\alpha_s}{3\pi v} \delta^{ab} \epsilon_\mu(p) \epsilon_\nu(q) \left(g^{\mu\nu} \frac{M_h^2}{2} - q^\mu p^\nu \right) A_q^h(\tau_q), \\ A_q^h(\tau) &= 3 \int_0^1 dx \int_0^{1-x} dy \left(\frac{1-4xy}{1-4xy/\tau} \right), \quad \tau_q = \frac{4m_q^2}{M_h^2} - i\varepsilon, \end{aligned} \quad (4.3.3)$$

where we included a factor 2 to account for the diagram with crossed gluon lines. Up to prefactors, the result is encoded in the function $A_q^h(\tau_q)$ and often called form factor in this context. The form factors of all processes relevant for our discussion are compiled in appendix B.1. We observe that in the limit $\tau_q \ll 1$ we obtain $A_q^h(\tau_q) = -3/8\tau_q(\ln(4\tau_q) + i\pi)^2$. This directly shows the marginal relevance of light quarks. The final partonic cross section is given by

$$\hat{\sigma}(gg \rightarrow h) = \frac{\alpha_s^2 M_h^2}{576\pi v^2} \left| \sum_q A_q^h(\tau_q) \right|^2 \delta(\hat{s} - M_h^2), \quad (4.3.4)$$

with the partonic center of mass energy \hat{s} . To obtain the hadronic cross section it has to be folded with the gluon luminosity involving appropriate parton distribution functions (PDF). In the narrow-width approximation, one considers the Higgs boson as a stable particle and neglects interference effects with background and other channels by employing the δ -function in (4.3.4). This treatment is appropriate for a light Higgs mass as shown below in figure 4.19. The luminosity integral thus becomes a simple multiplication at leading order and for all virtual corrections at higher orders. Consequently, the involved uncertainties drop out to a large extent, if we consider ratios of processes with different final states [376]. This is important, for accessing the coupling structure of the Higgs boson. We discuss this in more detail below.

The largest contribution to the amplitude comes from the triangle diagram with internal top quarks. It can be described by an effective operator of mass dimension 5 that arises from integrating out the top quark¹⁶. The most general effective Lagrangian, on which this contribution is to be matched, reads

$$\mathcal{L}_{ggh}^{\text{eff}} = C_1(\mu) \frac{\alpha_s(\mu)}{12\pi} \frac{h}{v} G_{\mu\nu}^a G^{\mu\nu,a} - C_5(\mu) \frac{\alpha_s(\mu)}{8\pi} \frac{h}{v} G_{\mu\nu}^a \tilde{G}^{\mu\nu,a}, \quad (4.3.5)$$

where $G_{\mu\nu}^a$ is the gluon field strength tensor and $\mu \leq m_t$ is the scale at which the effective operators are renormalized. We also included a CP -violating operator that involves the dual field strength tensor $\tilde{G}^{\mu\nu,a} = -\frac{1}{2}\epsilon^{\mu\nu\rho\sigma} G_{\rho\sigma}^a$ (with $\epsilon^{0123} = -1$). It could be generated by pseudo-scalar couplings from new physics but is zero in the SM. The Wilson coefficients are thus given by $C_1(\mu) = A_q^h(m_t)$ and $C_5(\mu) = 0$. We discuss the evolution of the Wilson coefficients in the next section.

We can furthermore approximate the result using the limit of a heavy top mass. With our normalization $A_q^h(\tau) \rightarrow 1$ for $\tau \rightarrow \infty$. The resulting effective ggh coupling stays finite even after decoupling the top quark. This behavior stems from the top Yukawa coupling that is included in the form factor $A_q^h \sim y_t/v$. In fact, there exists no physical decoupling limit which

¹⁶Interestingly this description is even valid for $M_h > m_t$. See [377] for a didactic explanation.

takes only the quark masses to infinity. The limit $v \rightarrow \infty$ would uniformly rescale the whole spectrum, thereby violating the low energy constraint $v = (\sqrt{2} G_F^\mu)^{-1/2} \approx 246 \text{ GeV}$.¹⁷ This justifies the non-decoupling of heavy chiral fermions, and the same reasoning also applies to any possible fermions of new physics that receive their masses purely from electroweak symmetry breaking.

The large m_t approximation is very useful for the derivation of a specific low-energy theorem [378–380]. This theorem relates the given amplitude with one external Higgs boson to such amplitudes with no, or more than one Higgs boson in the heavy m_t limit. For amplitudes with more than one Higgs boson this is easily seen by inserting an additional top propagator and a Yukawa coupling in the diagram, what leads to the replacement

$$\frac{1}{\not{k} - m_t} \longrightarrow \frac{1}{\not{k} - m_t} \frac{m_t}{v} \frac{1}{\not{k} - m_t} = \frac{m_t}{v} \frac{\partial}{\partial m_t} \frac{1}{\not{k} - m_t}. \quad (4.3.6)$$

The general low-energy theorem is the intuitive generalization of this recipe

$$\lim_{p_h \rightarrow 0} \mathcal{M}(\mathcal{I} \rightarrow \mathcal{F} + h) = \sum_q \lambda_q^h \frac{m_q}{v} \frac{\partial}{\partial m_q} \mathcal{M}(\mathcal{I} \rightarrow \mathcal{F}). \quad (4.3.7)$$

\mathcal{M} is the matrix element for any initial state \mathcal{I} , a final state \mathcal{F} that may already contain Higgs bosons, and a generalized sum over fermions of bare mass m_q in the loop. The vanishing Higgs momentum on the left-hand side is equivalent to taking the large m_q limit, since the mass inside the loop cannot be resolved by the external momentum. The sum (4.3.7) is already suitable for more general chiral quarks by including the factor λ_q^h that is equal to one only in the SM. Already for a Higgs sector with more than one doublet those factors are given in terms of mixing angles of the extended scalar sector [380]. Apart from the possibility to calculate multi-Higgs production with (4.3.7), the relation also directly relates the large m_t limit of the ggh amplitude to the QCD β -function. This provides the possibility to calculate the ggh amplitude at all orders from gluon self energies. On the right-hand side of equation (4.3.7), one only has to account for the renormalization of the bare masses by dividing by a factor $1 + \gamma_{m_q}$, with the mass anomalous dimension γ_{m_q} . This results in the approximate next-to-leading order (NLO) result of the SM

$$\begin{aligned} \mathcal{L}_{ggh}^{\text{eff}} &= \frac{\alpha_s(\mu)}{12\pi} \frac{\beta_s^t}{4\alpha_s(1 + \gamma_m)} \frac{h}{v} G_{\mu\nu}^a G^{\mu\nu,a} \\ &= \frac{\alpha_s(\mu)}{12\pi} \left(1 + \frac{\alpha_s(\mu)}{4\pi} (5N_c - 3C_F) + \mathcal{O}(\alpha_s^2) \right) \frac{h}{v} G_{\mu\nu}^a G^{\mu\nu,a}. \end{aligned} \quad (4.3.8)$$

where β_s^t is the top-quark contribution to the QCD β -function, $N_c = 3$ the number of colors, and $C_F = (N_c^2 - 1)/(2N_c)$ the quadratic Casimir operator. Remarkably, the accuracy of the large m_t approximation is very high for $M_h < 300 \text{ GeV}$, better than 1% compared to the full m_t dependence even at next-to-next-to-leading order (NNLO) [381]. In [237] the authors have used (4.3.7) to derive a very general expression for C_1 in models of new physics and relate the sign of the shift in C_1 to the cancellation of the quadratic divergence in the Higgs mass in various scenarios of new physics.

¹⁷Infinite quark masses at fixed v require Yukawa couplings to enter the strong coupling regime, in which perturbative arguments fail to apply.

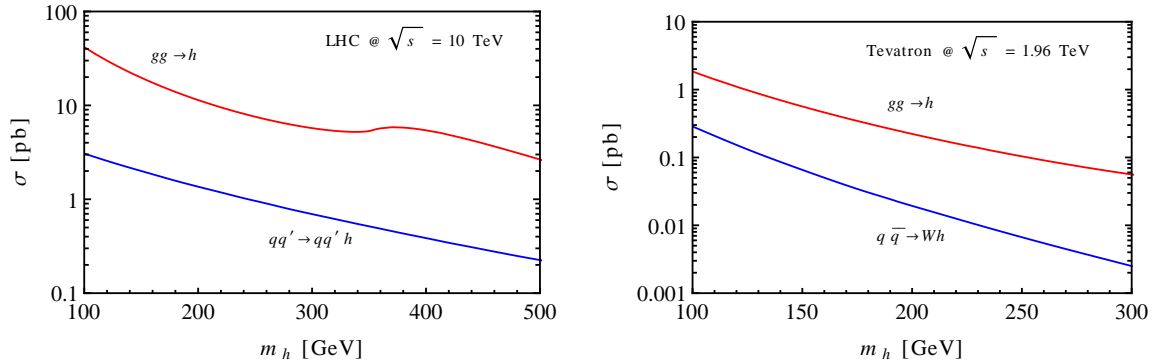


Figure 4.18: The two dominant production cross sections at center of mass energies relevant for the LHC at 10 TeV (left) and the Tevatron at 1.96 TeV (right). The upper red line shows the gluon–gluon fusion mode. The lower blue line shows weak gauge boson boson fusion for the LHC and associated production with W for the Tevatron. For uncertainties see comments in the main text.

Beyond the top quark, also the bottom-quark contribution has to be taken into account. Numerically, it suffices to very good accuracy to multiply the final cross section $\sigma(gg \rightarrow h)$ without the bottom-quark corrections by a factor $(1 + 2 \operatorname{Re} A_b^h)$. This approximate treatment decreases the cross section by about 9%, 2%, and less than 1% for $M_h = 100$ GeV, 300 GeV, and 600 GeV, in good agreement with the NLO calculation including the exact mass dependence [382–384].

Note that higher-order QCD corrections to the gluon–gluon fusion process are very important. At the LHC they increase the LO cross section by about 80-100% at NLO, by about 25% at NNLO [385–387], and another 6-9% stem from the resummation of soft gluons at NNLL. The current state of the art, including electroweak corrections, detector acceptances, and cuts on differential distributions is compiled by the LHC Higgs Cross Section Working Group Collaboration in [388, 389]. We should also account for QCD corrections when integrating out heavy colored particles in models of new physics in the following sections. For extra quarks, which have the same $SU(3)_c$ quantum number as the SM quarks, the QCD corrections are very similar to those from integrating out the SM top quark. Like for the top quark, the generalization of (4.3.8) involves only the QCD β -function and mass anomalous dimension, which solely depend on the $SU(3)_c$ representation in a mass independent renormalization scheme.

We show numerical values for the Higgs-production cross sections at the LHC and Tevatron for center-of-mass energies $\sqrt{s} = 10$ TeV and $\sqrt{s} = 1.96$ TeV in figure 4.18. There we employ the calculation of $\sigma(gg \rightarrow h)$ given in [390], which combines the next-to-next-to-leading fixed-order corrections [385–387] with resummation of both threshold logarithms from soft-gluon emission [391–395] and terms of the form $(N_c \pi \alpha_s)^n$, which have been identified as part of the source of large perturbative corrections [396]. The result is depicted in the red curves of figure 4.18, where the MRST2006NNLO PDFs [397] and the associated normalization $\alpha_s(m_Z) = 0.1191$ for the strong coupling constant are used. The choice of low-energy input in the form of different sets of PDFs introduces a major theoretical uncertainty. Furthermore, there is the issue how renormalization and factorization scale choices reflect the uncertainty related to the truncation of the perturbative series. The total theoretical accuracy [388] is at the level of 20%, on which the recent experimental precision is already closing in [22, 29].

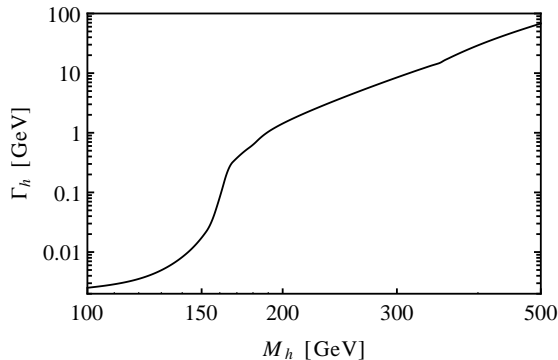


Figure 4.19: Total width of the SM-Higgs boson. Both axes have a logarithmic scale.

Besides gluon–gluon fusion there are two main production processes mediated by weak gauge bosons, whose LO diagrams are depicted in the bottom row of figure 4.17. This is the associated production with W/Z bosons [116, 398], which is the relevant production channel for the $p\bar{p}$ collisions at Tevatron, and the weak vector boson fusion processes [399, 400], which is a subleading contribution at the LHC. Their total cross sections in hadronic collisions is approximately 10 times lower than the gluon fusion cross section in the relevant Higgs-mass range, as depicted by the blue curves [401] in figure 4.18. Nevertheless, they provide an additional hadronic probe that allows to distinguish them from the overall hadronic background. For weak vector boson fusion the probes can be enhanced collinear forward jets in a back-to-back geometry [402], which provide a very efficient cut against QCD backgrounds. Moreover, the QCD uncertainty of the theory prediction is much lower than in gluon–gluon fusion and the dominant, remnant PDF uncertainty stays below 3% in the relevant Higgs-mass range [388].

An additional, subleading, but experimentally important production mode is the associated Higgs production with two heavy top [403, 404] or bottom [405, 406] quarks. Considered with a subsequent decay $h \rightarrow b\bar{b}$ it will play an important role in later stages of the LHC program as it allows to directly measure the top–Higgs coupling and constrain the bottom–Higgs coupling in supersymmetric models with large $\tan(\beta)$. For the plethora of other suppressed production processes, *e.g.* with one or more hard jets in the final state, double-Higgs production, diffractive production, *etc.*, we refer to [142] and references therein.

After production of the Higgs particle we can separately consider its subsequent decay widths. As mentioned above, it couples to all particles, including itself, proportional to the particles masses. The total width of the SM-Higgs boson shown in figure 4.19 is therefore dominated by the decay into the heaviest states allowed by phase space, which is either $b\bar{b}$ below, or W^+W^- above the W^+W^- threshold. The width increases drastically at this transition. For the relevant low Higgs mass range we have already discussed that the narrow width approximation is suitable.

The past successive reduction of the allowed mass region [407–410] shows that a detection of the Higgs boson at a mass of $M_h \approx 126$ GeV has been difficult, particularly compared to higher values of the Higgs mass, where the golden channel $h \rightarrow Z^{(*)}Z^{(*)} \rightarrow 2l^+2l^-$ with the experimentally clear leptonic final state would have allowed for real intermediate configurations of the two Z bosons. The dominant decay into bottom-quark pairs is difficult to access if originating from gluon–gluon fusion, since the QCD background of $b\bar{b}$ production is

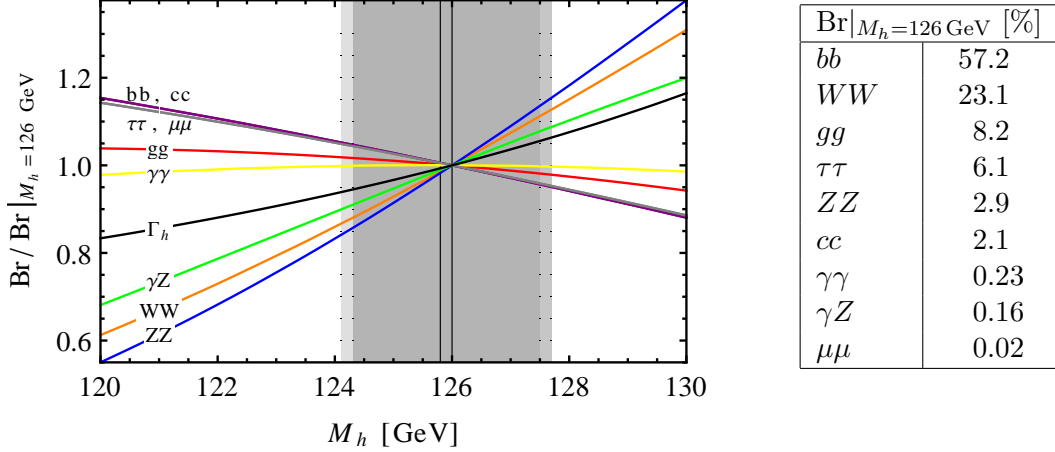


Figure 4.20: Variation of the SM branching ratios of the Higgs decay normalized at $M_h = 126$ GeV and absolute values at the normalization point. The values are obtained using HDECAY version 5.00 [412] with the standard input parameter set. The total Higgs width Γ_h is also normalized at the same Higgs mass. The dark gray band indicates the 3σ CL of the measured Higgs mass at ATLAS and the faint gray band at CMS. Statistical and systematical uncertainties are added in quadrature.

at the level of μb compared to the Higgs-production rate, which is at the level of $\sim 10\text{pb}$ for $M_h \approx 126$ GeV.¹⁸

Still, as the Higgs boson is detected at the given light mass, nature now turns out to leave us in a fortunate position with the possibility to reconstruct the Higgs particle in a large number of decay modes. The variation of the branching ratios over the now relevant Higgs-mass range and absolute values are given in figure 4.20. In fact all the given final states except $c\bar{c}$ and gg should be accessible during the LHC program. Most remarkably, for the given light Higgs mass, the loop-induced decay to $\gamma\gamma$ has a branching fraction that is sizable enough to render it even the main discovery channel. This process receives contributions from diagrams analogous to those we discussed for gluon-gluon fusion, but also from a W -triangle diagram that interferes destructively with the top-triangle diagram. At LO the partial width is [378, 379]

$$\Gamma(h \rightarrow \gamma\gamma) = \frac{\alpha^2 M_h^3}{144\pi^3 v^2} \left| \sum_f Q_f N_c A_q^h(\tau_f) + A_W^h(\tau_W) \right|^2, \quad (4.3.9)$$

where the sum now extends over all fermions, $\tau_W = 4M_W^2/M_h^2 - i\varepsilon$, and the explicit form of A_W^h is again given in appendix B.1. The W contribution is always dominant, starting from light Higgs masses, where $A_W^h(\infty) = -21/3$, up to relatively heavy Higgs masses. Only above the $t\bar{t}$ threshold $M_h > 2m_t$, the partial decay width starts to deviate significantly from the M_h^3 behavior and drops to almost full cancellation at $M_h \approx 650$ GeV. In the relevant mass region $M_h \approx 126$ GeV we have a ratio of $A_W^h(\tau_W)/(2A_q^h(\tau_t)) \approx 3.0$. The decay $h \rightarrow Z\gamma \rightarrow l^+l^-\gamma$ will also become accessible at the LHC at higher luminosity. Much like the decay into two Z bosons, this channel has little background and the kinematics of the decay can be cleanly reconstructed. However, it is more rare and suffers the penalty of low branching fraction for the decay $Z \rightarrow l^+l^-$. The LO decay is calculated from the same diagrams as $h \rightarrow \gamma\gamma$ with

¹⁸The $b\bar{b}$ final state is accessible in associated W production in a specific, highly transversally boosted kinematic region [411], and, more difficult, in weak gauge boson fusion [388].

one photon replaced by a Z boson. Thus, it is given by

$$\Gamma(h \rightarrow Z\gamma) = \frac{\alpha^2 M_h^3}{72\pi^2 v^2 s_w^2} \left(1 - \frac{M_Z^2}{M_h^2}\right)^3 \left| \sum_f \frac{2Q_f \hat{v}_f}{c_w} N_c A_q^h(\tau_f, \lambda_f) + A_W^h(\tau_W, \lambda_W) \right|^2, \quad (4.3.10)$$

where $\lambda_i = 4M_i^2/M_Z^2 - i\epsilon$, the charges of the vectorial Z -fermion couplings are $\hat{v}_f = T_f^3 - 2s_w^2 Q_f$, and the explicit form factors again given in appendix B.1. The size of the W -boson form factor is similar to the one for the decay into $\gamma\gamma$, but the top contribution is reduced by more than 50%, due to \hat{v}_f . The QCD corrections to both processes are purely virtual because of color conservation and have the expected size: The correction factor to the top-quark-form factor is given by $1 + \alpha_s/\pi$ in the heavy m_t limit [413]. Also NLO electroweak corrections have been calculated [414] reducing the remnant uncertainty from higher order corrections to less than 1%. The remaining relevant decays widths are known to a comparable accuracy of $\approx 1\%$ [388], except for $h \rightarrow gg$. There are relevant parametric uncertainties, which have been conservatively estimated in [415]. At the given Higgs mass they are driven by bottom-quark mass uncertainties in the $h \rightarrow b\bar{b}$ decay width. It enters the branching ratios of all relevant final states via the total width and amounts to approximately 5% uncertainty.

Summary of Recent Higgs Measurements

In this paragraph, we shortly repeat the recent results of the LHC Higgs searches. In total, ATLAS [22] (updates in [23–28]) and CMS [29] (updates in [30–36]) have observed the Higgs boson with maximal combined local significances of 7.0σ and 6.9σ at the mass 125.2 ± 0.3 (stat) ± 0.6 (sys) GeV and $125.8 \pm 0.4 \pm 0.4$ GeV, respectively. While both mass measurements are well consistent with each other, their precision should be taken with a grain of salt; the latest ATLAS analysis [28] found a difference between the mass measurements in $H \rightarrow \gamma\gamma$ and $H \rightarrow ZZ^* \rightarrow 4l$ with a significance of 2.7σ . The mass splitting is lower and of reversed order in the CMS result [36]. A fact, most interesting for the derivation of constraints on new physics, is that the experimental collaborations also gave results for the relative signal strengths $\mu_f = \sigma_{\text{total}} \text{Br}(h \rightarrow f) / [\sigma_{\text{total}} \text{Br}(h \rightarrow f)]_{\text{SM}}$ in the various channels. The results are summarized in table 4.1. The measurements of the two boson final states

	μ_{WW}	μ_{ZZ}	$\mu_{\gamma\gamma}$	μ_{bb}	$\mu_{\tau\tau}$	$M_h _{\text{fix}} [\text{GeV}]$
ATLAS [28]	1.5(6)	1.0(4)	1.8(4)	-0.4(10)	0.8(7)	125.0
CMS [36]	0.7(2)	0.8(3)	1.6(4)	1.1(6)	0.9(5)	125.8

Table 4.1: Measured relative signal strengths μ_f for the decays into the various final states f measured by ATLAS and CMS. The last column contains the fixed Higgs mass hypothesis for which the values were obtained.

are in principle all in agreement with the SM. A slight upward fluctuation in the $\gamma\gamma$ channel exists, but is below the 2σ level. Evidence for the decay $h \rightarrow b\bar{b}$ at the LHC has to await increased statistics; the CMS result has a maximum local significance of 1.8σ in this channel. The CDF and D0 experiments have reported a broad excess in this channel in their final, combined data set, seemingly with an upward fluctuation of $\mu_{bb} = 2.0 \pm 0.7$ [41, 42] in the mass range measured by the LHC experiments.

The production cross section σ in the results for μ_f will in general be a combination of production processes resulting from the particular set of cuts used in the measurement. For

the comparison with theories of new physics an unfolding of the different production channels is necessary. The experimental collaborations have partially provided the result for specific tags of the final state. Interestingly, in the CMS result, the enhanced central value of $\mu_{\gamma\gamma}$ is only present in the channel where a tag for vector boson related production was applied, while the central value for the combination of gluon–gluon fusion and associated top production was found to be marginally below one. On the other hand, no enhancement was found for the the WW and ZZ final state with a vector boson related tag. A precise unfolding procedure for the production modes is beyond the scope of this thesis. Below we will comment if our conclusions are limited by this partial knowledge. At present this restriction is not yet very relevant, but will become so in the future. We refer to the very recent analyses [416, 417] where the unfolding based on simplifying assumptions was attempted in order to improve limits on deviations from the SM.

4.3.2 Sensitivity of Higgs Production to New Fermions

In the last section we discussed the effective Lagrangian obtained by integrating out the top quark (4.3.5). Analogously, also contributions to the amplitude from heavy chiral fermions beyond the SM have the same non-decoupling behavior. In fact, the constant form factor in the limit of large fermion masses implies a counting of heavy chiral fermions. This is very relevant for the model with a simple sequential fourth fermion generation (SM4). This model was already cornered from bounds of several sources. On the one hand, unitarity of the partial S -wave amplitude for color-singlet, elastic, same-helicity $t't'$ scattering at tree level leads to a bound of $m_{t'} \lesssim 500$ GeV [139]. On the other hand, direct searches for decays of heavy quarks at LHC lead to the bounds $m_{b'} > 495$ GeV [418] and $m_{t'} > 656$ GeV [419] at 95% CL, and EWPOs also strongly restrict the up–down and lepton–neutrino mass splittings [420, 421] and further mixing parameters of this simple extension of the SM. The recent measurements of Higgs decays at the LHC have led to the final exclusion of the SM4 (without modified Higgs sector) at the level of approximately 5σ [422]. Two main effects in the Higgs processes can be identified. The Higgs-production cross section via gluon–gluon fusion is simply enhanced by a factor of approximately 9 due to the additional t' and b' -quarks in the loop [420]. Thus, a strong enhancement of $\tau^+\tau^-$ events is also expected. On the contrary, extra loop-contributions of chiral fermions add constructively to the top-contribution in the amplitude of the decay $h \rightarrow \gamma\gamma$ and thus increase the cancellation of the W -boson loop [423], which leads to an overcompensation of the enhanced production.

The sensitivity of Higgs processes is of course less dramatic, or even inexistent, in models where new fermions enter in vector-like form, *i.e.* with the same gauge-group representations for both chiralities, as they may obtain a TeV scale mass mainly from an explicit mass term. This is the case in the LHT model of section 3.2, where one parametrizes the strong dynamics that leads to the explicit mass by an additional input parameter λ_+ (3.2.23). In the RS model, which we presented in section 3.3, mass terms arise in the form of eigenvalues for the momenta in the direction of a compact extra dimension.

Before entering the conceptually demanding calculation of loop processes for Higgs physics in the RS model, it is instructive to reconsider the main aspects in the LHT model. A useful parametrization became widely used recently. It is particularly suitable to categorize the typical contributions of models in which the Higgs arises as a pseudo Nambu-Goldstone boson in the framework of an EFT. The low-energy effective Lagrangian of the leading dimension-six operators [424] has been used as a basis for a matching of typical little Higgs models in [166].

They find that in the LHT model, the coefficient of the effective operator $|\partial_\mu(\Phi^\dagger\Phi)|^2/(2f^2)$ is given by $c_H = 1/6$. Its only source is the non-linearity of the NL σ M, which changes the standard relation between the W -boson mass and the Higgs VEV and can be read off (3.2.11).¹⁹ For the RS model we expressed the analogous shift with definition of a modified Higgs VEV (4.2.19).

As we have seen in section 3.2, the vector-like state t'_+ then mixes under electroweak symmetry breaking with the SM-like up-quarks and thus obtains also couplings to the Higgs boson, while the T -parity odd combination t'_- remains unmixed. The effect of the modified top-coupling and the heavy mass eigenstate T_+ can be elegantly calculated from the low-energy theorem that lead to (4.3.8). This was observed in [237] and the argument goes as follows. The leading logarithmic contribution to the QCD β -function that stems from integrating out a heavy particle at the scale μ can in general be written as

$$\frac{1}{g_{s,\text{eff}}^2(\mu, H)} = \frac{1}{g_s(\mu)^2} - b \frac{t_r}{4\pi^2} \ln\left(\frac{m(H)}{\mu}\right), \quad (4.3.11)$$

where $m(H)$ is the coupling that determines the particles mass once $H = v + h$ is inserted, t_r is the Dynkin index of the representation and $b = 2/3$ for Dirac fermions and $1/6$ for scalars. Here we only discuss the example of an additional fermion in the fundamental representation, $t_r = 1/2$, but the applicability of the strategy is more general. The linearization in v and application of the low-energy theorem leads to the modified one-loop Wilson coefficient [166]

$$\begin{aligned} C_1 &= \sum_i \frac{\partial \ln(m_i(v))}{\partial \ln(v)} \Big|_{v=v_{\text{SM}}} - \frac{c_H}{2} \frac{v_{\text{SM}}^2}{f^2} \\ &= \frac{v}{2} \frac{\partial}{\partial v} \ln \det(\mathcal{M}^\dagger(v)\mathcal{M}(v)) \Big|_{v=v_{\text{SM}}} - \frac{c_H}{2} \frac{v_{\text{SM}}^2}{f^2}, \end{aligned} \quad (4.3.12)$$

where $m_i(v)$ summarizes the masses of the top quark and heavy top partners, like the T_+ . Furthermore, all form factors have been set to one, and all particles are integrated out at the same scale. In this approximation we see that there is no need to diagonalize the mass matrix, and one only needs the determinant of the squared mass matrix $\mathcal{M}(v)$ of the top quark and top partners in the gauge eigenstate basis. Using the lower-right 2×2 sub-block of the mass matrix (3.2.24) one directly finds to $\mathcal{O}(v^2/f^2)$

$$\frac{v}{2} \frac{\partial}{\partial v} \ln \det(\mathcal{M}^\dagger\mathcal{M}) \Big|_{v=v_{\text{SM}}} = 1 - \frac{2}{3} \frac{v_{\text{SM}}^2}{f^2} \quad \longrightarrow \quad C_1^{\text{LHT, even}} = 1 - \frac{3}{4} \frac{v_{\text{SM}}^2}{f^2}, \quad (4.3.13)$$

in agreement with [166]. With $f \gtrsim 500$ GeV being allowed from limits on $\Delta F = 2$ FCNCs [163], the reduction could reach approximately -35% in the ratio of cross sections; 11% of this are due to the modified VEV.

In [166], mirror masses have been realized with a coupling to additional scalar fields X . In this way the mirror fermions do not couple directly to the Higgs boson and do not contribute to the Higgs processes at leading order. We abbreviate this model as LHTX. The contributions from the traditional mirror mass terms, which we presented in (3.2.20), were calculated in [425]. We find from the couplings in (A.2.8) that

$$\frac{v g_h \bar{f}_{H,i} f_{H,i}}{m_{H,i}^f} = -\frac{v_{\text{SM}}^2}{4f^2} \frac{v g_h \bar{t} t}{m_t}, \quad (f = u, \nu), \quad (4.3.14)$$

¹⁹The additional effects from gauge-boson mixing for $g \neq g'$ and a non-vanishing triplet VEV in the LHT model can be read off the same mass formula (3.2.11).

and vanishing Higgs coupling to down-type and lepton mirror quarks. For production via gluon–gluon fusion this implies a total modification from the T -odd sector, of the same size like from the T -even sector

$$C_1^{\text{LHT,odd}} = -\frac{3}{4} \frac{v_{\text{SM}}^2}{f^2}. \quad (4.3.15)$$

This agrees with the result in [425]. Within the used approximations, there exists no dependence on the mirror mass values. In particular, the mirror-fermion contribution cannot be separately decoupled due to (4.3.14). Interestingly, precisely the same reductions were found in minimal composite Higgs models (MCHM), which are similar models based on $SO(5)/SO(4)$ [426]. With both, the top being part of a full representation **5** or **10** of $SO(5)$, one obtains the same result $C_1^{\text{MCHM}_5} = C_1^{\text{MCHM}_{10}} = C_1^{\text{LHT,even}} + C_1^{\text{LHT,odd}}$ [166]. We summarize that

$$R_h \equiv \frac{\hat{\sigma}(gg \rightarrow h)_{\text{LHT}}}{\hat{\sigma}(gg \rightarrow h)_{\text{SM}}} \approx 1 - \frac{v_{\text{SM}}^2}{f^2} \cdot \begin{cases} 3, & \text{LHT, MCHM}_{5,10}, \\ \frac{3}{2}, & \text{LHTX}. \end{cases} \quad (4.3.16)$$

We emphasize that for low values of f the correction is very large and one should in fact compute higher terms in the expansion in v/f , in order to set precise bounds on the scale f .

It is straightforward to continue along the same lines for the Higgs decays. The couplings of $h\tau^+\tau^-$ and $hb\bar{b}$ are reduced by $1 - v_{\text{SM}}^2/(6f^2)$, while $g_{WW}h = -g_{W_H}h$ are both reduced by $1 - v_{\text{SM}}^2/(3f^2)$ compared to the SM coupling. This is already everything one needs in order to find a reduction of the total width

$$\begin{aligned} R_\Gamma \equiv \frac{\Gamma(h)_{\text{LHT}}}{\Gamma(h)_{\text{SM}}} &= 1 + \sum_{f=b\bar{b}, WW, ZZ} \text{BR}(h \rightarrow f) \left(\frac{\Gamma(h \rightarrow f)_{\text{LHT}}}{\Gamma(h \rightarrow f)_{\text{SM}}} - 1 \right) + \text{BR}(h \rightarrow gg) (R_h - 1) \\ &\approx 1 - \frac{v_{\text{SM}}^2}{f^2} \cdot \begin{cases} 0.63, & \text{LHT}, \\ 0.51, & \text{LHTX}, \end{cases} \end{aligned} \quad (4.3.17)$$

and a similarly small reduction of the partial width of the decay into two photons

$$\begin{aligned} \frac{\Gamma(h \rightarrow \gamma\gamma)_{\text{LHT}}}{\Gamma(h \rightarrow \gamma\gamma)_{\text{SM}}} &= 1 - \frac{v_{\text{SM}}^2}{3f^2} \frac{|A_W^h(\tau_W)| + \frac{21}{4} + \frac{4f^2}{v^2} (C_1^{\text{LHT}} - 1)}{|A_W^h(\tau_W)| - \frac{4}{3}} \\ &\approx 1 - \frac{v_{\text{SM}}^2}{f^2} \cdot \begin{cases} 0.37, & \text{LHT}, \\ 0.58, & \text{LHTX}. \end{cases} \end{aligned} \quad (4.3.18)$$

The numerator in the v_{SM}^2/f^2 term in the first line contains the reduction of the W -boson amplitude, the contribution from the heavy charged vector W_H , and the combined top-modification and T_+ contribution. The total modification of the partial decay width into $\gamma\gamma$ is relatively small, since a large part of the contribution from W_H , which interferes destructively with the SM-like W -boson contribution, cancels against the reduction of the top and T_+ contribution²⁰. The rate of the combined process

$$R_{\gamma\gamma} \equiv \frac{R_h}{R_\Gamma} \frac{\Gamma(h \rightarrow \gamma\gamma)_{\text{LHT}}}{\Gamma(h \rightarrow \gamma\gamma)_{\text{SM}}} \approx 1 - \frac{v_{\text{SM}}^2}{f^2} \cdot \begin{cases} 2.99, & \text{LHT}, \\ 1.68, & \text{LHTX}, \end{cases} \quad (4.3.19)$$

²⁰Remind that the SM W and top amplitude interfere destructively.

thus follows very closely the modified production rate. The rate with preceding Higgs production from weak gauge boson fusion or associated Higgs production is almost unchanged. Assuming a bound of -20% maximal deviation from the SM one could derive the bounds $f \gtrsim 920$ GeV (LHT)²¹, and $f \gtrsim 690$ GeV (LHTX). In order to derive precise bounds from the recent experimental results one needs further knowledge about the experimental efficiencies. Unfortunately, a combination of CMS and ATLAS bounds on signal strengths does not yet exist. We will discuss this in more detail below for the RS model. Nevertheless, we conclude that the simplicity of the contributions and the strict reduction allows to set potentially strong Higgs physics bounds on models of compositeness in the near future. We will see below that this statement also holds true for the RS models we introduced in section 3.3. In principle, the LH model is related to deconstructed versions of specific extra-dimensional theories [428]. However, the detailed outcome of the modifications in Higgs processes has to be verified in each setup separately, and we will find qualitatively different, and quantitatively very different results for the standard RS setup compared to those presented above. We remark here that the authors of [429] used the technique of (4.3.12) to sum up the infinite-dimensional mass matrix in the weak eigenbasis of the RS model. In principle, this technique appears to be very convenient, since the exact diagonalization of this matrix is highly non-trivial [430]. We will comment below on the shortcomings of this approach. Here we only mention that working with a truncated mass matrix of the RS model and (4.3.12) would give a viable result for R_h of the same sign like in the LHT model and also potentially a large deviation from one.

We finally discuss one of the approximations made in (4.3.12), on which we did not explicitly comment yet. The Wilson coefficients $C_{1,5}^{\text{NP}}$, which adds to (4.3.5) and is obtained from integrating out heavy particles, must be evolved from the high scale of new physics to the Higgs-mass scale according to the renormalization-group equations. If the contributions are dominated by the corrections of the lightest particle of the new physics model, it is practical to integrate out all particles at a common scale M_{NP} . The evolution from this scale down to the Higgs-mass scale is described by the renormalization-group equations of the SM only. For the QCD evolution of the Wilson coefficient $C_1^{\text{NP}}(\mu)$, the result is given by [390, 431]

$$\frac{C_1^{\text{NP}}(\mu)}{C_1^{\text{NP}}(M_{\text{NP}})} = \frac{\beta(\alpha_s(\mu))/\alpha_s^2(\mu)}{\beta(\alpha_s(M_{\text{NP}}))/\alpha_s^2(M_{\text{NP}})} = 1 + \frac{13}{4} \frac{\alpha_s(\mu) - \alpha_s(M_{\text{NP}})}{\pi} + \mathcal{O}(\alpha_s^2). \quad (4.3.20)$$

In practice, the evolution from a new physics scale of several TeV down to $\mu \approx M_h$ has only a small effect of about 1% on the value of C_1^{NP} , since no leading logarithms appear in this result. The operator multiplying the coefficient C_5^{NP} in (4.3.5) is connected by the Adler-Bell-Jackiw anomaly to current operators with vanishing QCD anomalous dimension, it follows that this coefficient is scale independent in QCD, *i.e.* $C_5^{\text{NP}}(\mu) = C_5^{\text{NP}}(M_{\text{NP}})$.

4.3.3 Analytic Derivations in the Randall-Sundrum Model

In the following, we discuss warped extra dimensional models as specific realizations of new physics, where extra fermions contribute to loop mediated processes in Higgs production via gluon-gluon fusion. Along with those, also new gauge bosons contribute in the subsequent decays to $\gamma\gamma$ and γZ . Furthermore, there are also shifts in tree-level couplings that modify the

²¹During the completion of this thesis, a numerically detailed analysis of the bounds from Higgs physics and a comparison to EWPO bounds has appeared in [427]. The authors extract the maximal information presently available from [22, 23, 25–27] and [30–35] to obtain the bound $f > 410$ GeV (LHT) at 95% CL, while EWPOs still imply a stronger bound of $f > 550$ GeV (minimal bound reached for $x_L = 0.64$).

amplitudes with SM-like particles. The diagrams of all relevant loop and tree contributions are shown in figure 4.21.

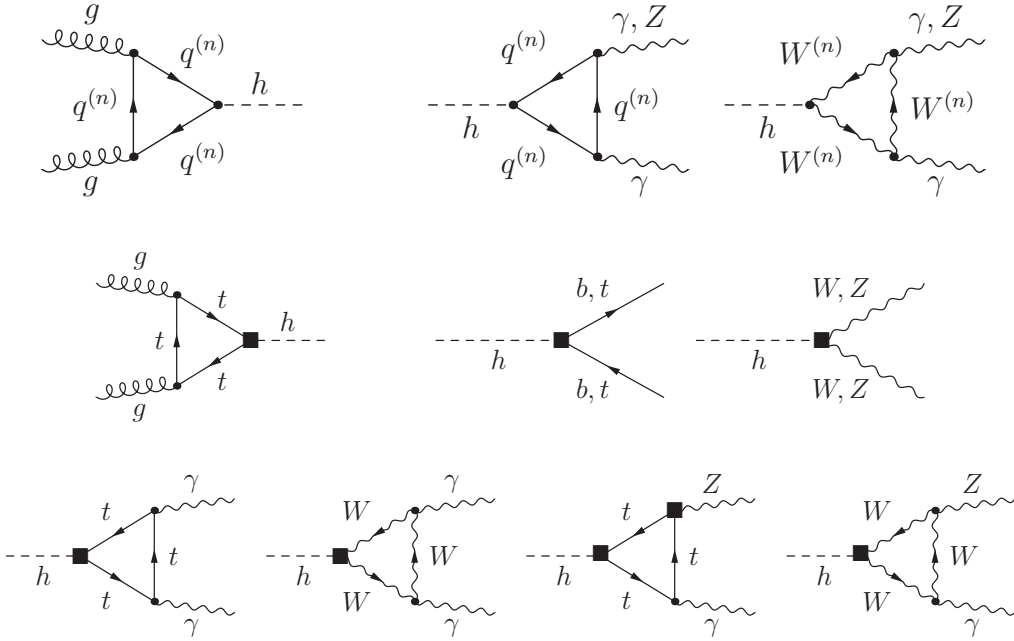


Figure 4.21: Feynman diagrams at one-loop involving KK excitations (upper row) and Feynman diagrams involving couplings to zero-mode fields that are modified compared to the SM. The couplings modified at $\mathcal{O}(v^2/M_{\text{KK}}^2)$ are indicated by a black square.

In general, we expect large effects on Higgs physics in the RS model. The reason is that the Higgs sector is localized on the IR brane, where also the KK profiles of fermions and heavy SM-like quarks are peaked, and where gauge boson zero modes are non-constant.

Before quantifying modifications, we will first clarify the subtle questions of convergence of the infinitely many KK-fermion-triangle diagrams. We choose Higgs production via gluon–gluon fusion to lay out the general strategy of how to obtain the physically correct result. To this end, we have to illuminate the relation between brane Higgs regularization and UV regularization of the theory. This is based on our discussion in [2], where we resolved a disagreement existing in the previous literature: While we found a significant suppression of the gluon–gluon fusion cross section relative to the SM by summing contributions from the first few KK modes [4], the authors of [429] found a significant enhancement by resumming the full tower of KK modes using completeness relations. Indeed, when applied to the same model, the two results for the ggh amplitude were of approximately equal strength but opposite sign. We will clarify that Higgs processes are not plagued by UV sensitivity and derive results for both the minimal and the custodial fermion embedding, which were introduced in section 3.3. Beyond that, we also give a recipe how to generalize the result to arbitrary fermion embeddings within the class of IR-brane-Higgs models.

After this conceptual discussion, we will show numerical results to quantify the constraining power on RS models that Higgs physics presently has and can further unfold in the future.

4.3.3.1 General Strategy for Loop Mediated Processes

The general form of the effective low-energy Lagrangian for ggh couplings was given in (4.3.5). In the following, we integrate out all KK quarks at the energy scale M_{KK} . The corresponding triangle diagram is depicted in figure 4.22 and the LO results are analogous to the top- and bottom-quark contribution of the SM discussed in section 4.3.1. Finally we also parametrize the shifts in the top- and bottom-quark contribution.

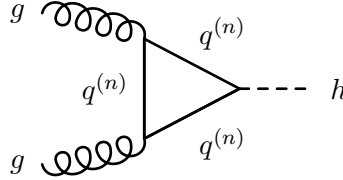


Figure 4.22: Virtual KK-quark contribution to the effective ggh couplings.

The unbroken $SU(3)_c$ implies gluon couplings to fermions that are diagonal in the mass basis. Thus, in any case a single KK-quark state $q^{(n)}$ runs in the loop. We gave the relevant couplings in (3.3.130) and (3.3.131). In the following, we abbreviate $g_{nn}^q \equiv g_{h\bar{q}_n q_n}^R$ and need the diagonal couplings only

$$\mathcal{L}_{hqq}^{\text{diag}} = - \sum_{q=u,d} \sum_n \left[\text{Re}(g_{nn}^q) h \bar{q}^{(n)} q^{(n)} + \text{Im}(g_{nn}^q) h \bar{q}^{(n)} i\gamma_5 q^{(n)} \right]. \quad (4.3.21)$$

The couplings are in general complex numbers, such that pseudo-scalar currents appear in the Lagrangian. In principle, these could have interesting implications for phenomenology [432]. However, the imaginary parts of the Yukawa couplings for SM-like fermions are very strongly suppressed in the RS model, as we have shown in section 3.3.8.1.

At the matching scale $\mu = M_{\text{KK}}$, the Wilson coefficients entering (4.3.5) have the simple one-loop results

$$\begin{aligned} C_1^{\text{KK}}(M_{\text{KK}}) &= \sum_q \sum'_n \frac{v \text{Re}(g_{nn}^q)}{m_n^q} A_q^h(\tau_{q_n}), \\ C_5^{\text{KK}}(M_{\text{KK}}) &= \sum_q \sum'_n \frac{v \text{Im}(g_{nn}^q)}{m_n^q} B_q^h(\tau_{q_n}), \end{aligned} \quad (4.3.22)$$

where $\tau_{q_n} = 4(m_n^q)^2/m_h^2 - i\varepsilon$. The prime on the summation symbol indicates that they extend over all KK-fermion states but exclude the zero modes, *i.e.* SM fermions $n = 1, 2, 3$ for $q = u, d$.

Since the KK quarks are much heavier than the Higgs boson, it is sufficient to use the asymptotic values $A_q^h(\infty) = B_q^h(\infty) = 1$ of the form factors. Even for quark masses as light as 1 TeV, the error of this approximation is sub per-mil. This implies that the relevant quantity we need to compute is given by

$$C_1^{\text{KK}}(M_{\text{KK}}) + i C_5^{\text{KK}}(M_{\text{KK}}) = \sum_q \sum'_n \frac{v g_{nn}^q}{m_n^q}. \quad (4.3.23)$$

The real part of the sum (4.3.23) determines C_1^{KK} , while the imaginary part gives C_5^{KK} .

We recall at this stage that both the Yukawa couplings and the mass eigenvalues depend on the regulator η used to smear out the Higgs profile. In addition, one needs to worry about the convergence of the infinite sum over KK modes. Indeed, since the Yukawa couplings g_{nn}^q are of $\mathcal{O}(1)$ and the masses of the KK modes are approximately evenly spaced multiples of the KK scale, naively one expects the sum in (4.3.23) to diverge logarithmically. Power counting for an infinite extra dimension would of course also suggest this. Taking into account 4d-gauge invariance²², we would have in D infinite space-time dimensions, with $E_{\text{bos}} = 3$ external bosons, and mass dimension $[g_V]$ of the vertices V , a superficial degree of divergence

$$\begin{aligned}\omega_D(\text{“triangle”}) &= D - \frac{D-2}{2}E_{\text{bos}} - \sum_V [g_V] - 2 \\ &= D - \frac{D-2}{2} \times 3 - 3 \times \frac{4-D}{2} - 2 = D - 5.\end{aligned}\tag{4.3.24}$$

Of course this is not the final answer. The additional momentum integral of an infinite extra dimension reduces to an infinite sum over the KK resonances, which have a specific structure. For the given non-trivial background metric, power-counting arguments lose their power to assess the renormalization structure intuitively. An example of a careful power counting for the process $\mu \rightarrow e\gamma$ has been performed in [230], however without taking into account regularization issues of the brane-Higgs profile. It shows the necessity to account for many peculiarities of the practical loop calculation. For this reason, we will not dwell on such arguments, since the additional insight is little, and instead discuss the physics by using the explicit calculation.

In order to define the sum in (4.3.23) properly, we regularize it by considering the partial sum up to a given highest KK level

$$\Sigma_q(N, \eta) = \sum_{n=1}^{n_f + Nn_F} \frac{vg_{nn}^q}{m_n^q}.\tag{4.3.25}$$

This sum now includes the n_f SM-like quarks plus the first N KK levels, where n_F is the number of KK modes per KK level. The notation is kept general like in section 3.3.118 in order to apply it to any fermion embedding. It will turn out that the sum over modes is finite despite naive expectation, because non-trivial cancellations happen among the modes contained in each KK level. Nevertheless, yet another, third regularization is present in the calculation, associated with the UV behavior of the theory. We discussed the reasons to generally regulate the 4d fermion-triangle calculation gauge invariantly in section 4.3.1. We also discussed in section 3.3.7 that in order to account for the gauge-hierarchy problem in RS, we must limit the range of validity of the model as an EFT. These two aspects become important in the following.

Concerning $\Sigma_q(N, \eta)$, practically we are left with a choice of the order of limits $\eta \rightarrow 0$ and $N \rightarrow \infty$. We will see that the limits do not commute. In most of the literature the Yukawa couplings are evaluated mode by mode, taking the regulator η to zero after computing the relevant overlap integrals. In [4] we took this approach to discuss the Higgs phenomenology in the custodial RS model. Here, it corresponds to taking the limit $\eta \rightarrow 0$ first, and hence

$$\Sigma_q^{(\text{low})} \equiv \lim_{N \rightarrow \infty} \left[\lim_{\eta \rightarrow 0} \Sigma_q(N, \eta) \right] = \lim_{N \rightarrow \infty} \sum_{n=1}^{n_f + Nn_F} \left[\frac{vg_{nn}^q}{m_n^q} \right]_{\eta \rightarrow 0}.\tag{4.3.26}$$

²²5d gauge invariance is broken by BCs and not spontaneously.

The alternative approach taken *e.g.* in [429, 433], considers the infinite sum over modes from the very beginning. This is accomplished by means of completeness relations for the fermion profiles. The regularization of the Higgs profile is taken to zero at the end of the calculation, such that this approach corresponds to

$$\Sigma_q^{(\text{res})} \equiv \lim_{\eta \rightarrow 0} \left[\lim_{N \rightarrow \infty} \Sigma_q(N, \eta) \right] = \lim_{\eta \rightarrow 0} \sum_{n=1}^{\infty} \frac{v g_{nn}^q}{m_n^q}. \quad (4.3.27)$$

In the following sections, we will derive closed analytical expressions for the limiting values in both cases – (4.3.26) and (4.3.27) – and subsequently discuss the physical interpretation of the results. For the rest of this section, we denote with Σ_q any of the two limiting orders.

First we return to the Wilson coefficients in (4.3.23). Using the full sum over all KK levels Σ_q we have to subtract the contributions from in KK level $N = 0$, *i.e.* the SM quarks, each of which equals 1 up to higher-order corrections in v/M_{KK} . By writing

$$\lim_{\eta \rightarrow 0} \Sigma_q(0, \eta) = \sum_{n=1,2,3} \lim_{\eta \rightarrow 0} \frac{v g_{nn}^q}{m_n^q} = \Sigma_q^0 - \varepsilon_q, \quad (4.3.28)$$

we split the result into a bulk mass independent part Σ_q^0 , and dependent part ε_q . The latter is given by

$$\varepsilon_q = \text{Tr} [\Phi_Q + \Phi_q] + \mathcal{O}\left(\frac{v^4}{M_{\text{KK}}^4}\right) \approx (\Phi_Q)_{33} + (\Phi_q)_{33}. \quad (4.3.29)$$

In the minimal and custodial RS model of sections 3.3.4.2 and 3.3.5.2, we obtain

- minimal ($q = u, d$):

$$\Sigma_q^0 = \text{Tr} \left[\frac{2\mathbf{X}_q}{\sinh(2\mathbf{X}_q)} \right] = \text{Tr} \left[\text{atanh}(\tilde{\mathbf{X}}_q) (\tilde{\mathbf{X}}_q^{-1} - \tilde{\mathbf{X}}_q) \right], \quad (4.3.30)$$

- custodial ($q = u, d$):

$$\Sigma_q^0 = \text{Tr} \left[\frac{2\sqrt{2}\mathbf{X}_q}{\sinh(2\sqrt{2}\mathbf{X}_q)} \right] = \text{Tr} \left[\text{atanh}(\sqrt{2}\tilde{\mathbf{X}}_q) ((\sqrt{2}\tilde{\mathbf{X}}_q)^{-1} - \sqrt{2}\tilde{\mathbf{X}}_q) \right]. \quad (4.3.31)$$

For notational convenience we also set $\Sigma_\lambda^0 \equiv \varepsilon_\lambda \equiv 0$.

The matrices \mathbf{X}_q and $\tilde{\mathbf{X}}_q$ were defined in (3.3.41). They depend only on the order one fundamental Yukawa matrices and the ratio v/M_{KK} . For the bulk mass independent part, the difference in going from the minimal to the custodial model is given by the additional factor of $\sqrt{2}$ in front of \mathbf{X}_q . This is easily understood from the multiplicity of the enlarged fermion sector with twisted BCs. In fact (3.3.41) implies that the misalignment between the fundamental Yukawa matrices $\mathbf{Y}_{\tilde{q}}$ and the ones defining the spectrum $\tilde{\mathbf{Y}}_{\tilde{q}}$ results in $\sqrt{2}\tilde{\mathbf{X}}_q = \tanh(\sqrt{2}\mathbf{X}_q)$ for $q = u, d$. The bulk mass dependent part ε_q is a subleading correction in most of the parameter space. It receives its main contribution from the third-generation terms, since the quantities $(\Phi_{Q,q})_{nn}$ defined in (3.3.132) are chirally suppressed for all light quarks.

The Wilson coefficients for the sectors of common charge are finally obtained as

$$C_{q,1}^{\text{KK}}(M_{\text{KK}}) + i C_{q,5}^{\text{KK}}(M_{\text{KK}}) = \Sigma_q - \Sigma_q^0 + \varepsilon_q, \quad C_i^{\text{KK}}(M_{\text{KK}}) = \sum_{q=u,d,\lambda} C_{q,i}^{\text{KK}}(M_{\text{KK}}). \quad (4.3.32)$$

Note that, like Σ_q^0 , we will see below that the full sum Σ_q also turns out to be real. The pseudo-scalar Wilson coefficient is therefore given by $C_5^{\text{KK}}(M_{\text{KK}}) = \text{Im}(\varepsilon_u + \varepsilon_d)$ and receives only contributions of $\mathcal{O}(v^4/M_{\text{KK}}^4)$, which have been neglected in the expression for ε_q in (4.3.29). Nevertheless, we will keep the discussion general in the following and use exact results in the numerical evaluation of section 4.3.4.

The cross section for Higgs production in gluon–gluon fusion can be written as

$$R_h = \frac{\hat{\sigma}(gg \rightarrow h)_{\text{RS}}}{\hat{\sigma}(gg \rightarrow h)_{\text{SM}}} = \frac{|\kappa_g|^2 + |\kappa_{5g}|^2}{\kappa_v^2}. \quad (4.3.33)$$

The factors κ_g and κ_{5g} encode the LO ratio of the non-interfering CP -even and CP -odd RS amplitude, divided by the total SM amplitude

$$\begin{aligned} \kappa_g &= \frac{C_1^{\text{KK}}(M_h) + \sum_{i=t,b} \text{Re}(\kappa_i) A_q^h(\tau_i)}{\sum_{i=t,b} A_q^h(\tau_i)}, \\ \kappa_{5g} &= \frac{3}{2} \frac{C_5^{\text{KK}}(M_h) + \sum_{i=t,b} \text{Im}(\kappa_i) B_q^h(\tau_i)}{\sum_{i=t,b} A_q^h(\tau_i)}. \end{aligned} \quad (4.3.34)$$

Here, the factors $\kappa_q = vg_{33}^q/m_q$ introduce modifications of the Higgs-boson couplings to top and bottom quarks with respect to their SM values. In the SM cross section (4.3.4), the dependence on the Higgs VEV was factored out as $(v_{\text{SM}})^{-2}$, with the rest of the result depending on input masses only. We proceed similarly with the RS result, using the modified VEV v of the RS model as calculated in (4.2.19). The factor κ_v in the denominator of (4.3.33) accounts for this shift. Consequently, κ_g and κ_{5g} are linear in the VEV v , which has been used here for κ_q and (4.3.22), and no further factors of κ_v are involved in the corresponding expressions.

In order to obtain a simple formula for κ_q , we employ (3.3.131) and the ZMA result (3.3.139) and furthermore expand in the Cabibbo angle using a Froggatt-Nielsen expansion as explained in section 3.3.4.2. The result reads

$$\kappa_q \approx 1 - (\Phi_Q)_{33} - (\Phi_q)_{33} - \frac{v^2}{3M_{\text{KK}}^2} \frac{\left(\mathbf{Y}_q \mathbf{Y}_q^\dagger \mathbf{Y}_q\right)_{33}}{(\mathbf{Y}_q)_{33}} \cdot \begin{cases} 1, & \text{minimal RS} \\ 2, & \text{custodial RS} \end{cases}. \quad (4.3.35)$$

Remark that the bulk-mass dependence in (4.3.35) is the same that also dominates bulk-mass dependent part of the Wilson-coefficient of heavy KK contributions. As shown in (4.3.29), it enters the latter with a negative sign. Consequently, the dominant bulk mass dependent contributions from the top quark enter the final expression (4.3.34) only proportional to the difference $A_q^h(\tau_t) - 1 \approx 4\%$, *i.e.* they cancel to a large extent.

4.3.3.2 Evaluation of the Two Regulator Limits

We are now ready to evaluate the two alternative regulator limits leading to the full sums of (4.3.26) and (4.3.27). We begin with examining the sum in (4.3.27), in which the regulator of the Higgs profile is removed after the infinite sum over KK modes has been performed. The authors of [429] succeed to evaluate this sum with the completeness relations (3.3.30) for the fermion profiles. The analysis relies on a perturbative treatment of Yukawa couplings, which yields the first non-trivial contribution in the expansion in v^2/M_{KK}^2 . A subtlety in

this calculation, worth recalling, is that in the perturbative approach the odd fermion profiles $\mathbf{S}_n^{(A)}(t)$ vanish on the IR brane. As a result, the contribution of each individual mode, and hence of any truncated KK sum, vanishes in the limit where the width of the Higgs-boson profile is taken to zero. A non-zero result for the $\mathcal{O}(v^2/M_{\text{KK}}^2)$ correction to (4.3.27) is obtained only after summing over the infinite tower of KK states.

An elegant way to derive a closed expression for the sum (4.3.27), valid to all orders in v/M_{KK} , is to relate it to the 5d fermion propagator of the theory. We proceed similar to [236], where this method has been applied to a model of 5d gauge-Higgs unification. It follows from the second relation in (3.3.129) and (3.3.110) that the infinite sum in (4.3.27), for fixed, non-zero η is given by

$$\lim_{N \rightarrow \infty} \Sigma_q(N, \eta) = \int_{\epsilon}^1 dt \delta^\eta(t-1) T_{RL}^q(t, t), \quad (4.3.36)$$

where

$$T_{RL}^q(t, t') = \frac{v}{\sqrt{2}} \text{Tr} \left[\begin{pmatrix} \mathbf{0} & \mathbf{Y}_q \\ \mathbf{Y}_q^\dagger & \mathbf{0} \end{pmatrix} \Delta_{RL}^q(t, t') \right]. \quad (4.3.37)$$

Notice that only the off-diagonal blocks of the propagator for $1 - \eta < t, t' < 1$ enter in this result. We find for a general fermion embedding

$$T_{RL}^q(t, t') = \text{Tr} \left[\mathbf{y}_{\bar{q}} \mathbf{e}_q \cosh \left(\mathbf{X}_{\bar{q}} \int_{t <}^{t >} ds \delta^\eta(s-1) \right) - \mathbf{X}_{\bar{q}} \sinh \left(\mathbf{X}_{\bar{q}} \int_{t <}^{t >} ds \delta^\eta(s-1) \right) \right], \quad (4.3.38)$$

where the normalized Yukawa matrix $\mathbf{y}_{\bar{q}}$ and the matrix \mathbf{e}_q have been defined in (3.3.122) and (3.3.124).

Obviously, for the special case $t = t'$, the trace in (4.3.38) is independent of both t and η . Thus the t -integration in (4.3.36) reduces to the normalization of the Higgs profile, which is independent of its regularized shape and equal to 1. We conclude that the full sum in (4.3.36) is in fact already independent of η . Remarkably, the infinite sum of KK states converges to the very simple result

$$\Sigma_q^{(\text{res})} = \text{Tr} [\mathbf{y}_{\bar{q}} \mathbf{e}_q], \quad (4.3.39)$$

despite the fact that it is superficially divergent. This hints to the existence of intricate cancellations between different contributions to the sum. In the following, we subsequently evaluate (4.3.39) for the minimal and custodial case. After that, we discuss the structure of the result for a general fermion embedding in terms of an expansion in v/M_{KK} .

- minimal ($q = u, d$) :

$$\Sigma_q^{(\text{res})} = \text{Tr} [\mathbf{X}_q \coth(\mathbf{X}_q)] = n_f + \frac{1}{3} \text{Tr} [\mathbf{X}_q^2] + \mathcal{O}\left(\frac{v^4}{M_{\text{KK}}^4}\right). \quad (4.3.40)$$

The first non-trivial term in the Taylor expansion agrees with the result derived in [429]. Note that this result is real, and hence it only contributes to the Wilson coefficient C_1^{KK} . From (4.3.32) and (4.3.28), we now obtain

$$\begin{aligned} C_{1(\text{res})}^{\text{KK}}(M_{\text{KK}}) &= \sum_{q=u,d} \left(\text{Tr} [\mathbf{X}_q \tanh(\mathbf{X}_q)] + \text{Re}(\varepsilon_q) \right) \\ &= \sum_{q=u,d} \text{Tr} \left[\mathbf{X}_q^2 + \text{Re}(\Phi_Q + \Phi_q) \right] + \mathcal{O}\left(\frac{v^4}{M_{\text{KK}}^4}\right). \end{aligned} \quad (4.3.41)$$

The contribution to the coefficient C_1^{KK} is positive and hence yields an enhancement of the ggh amplitude compared to the SM.

- custodial :

$$\begin{aligned}\Sigma_d^{(\text{res})} &= \text{Tr} [\sqrt{2}\mathbf{X}_d \coth(\sqrt{2}\mathbf{X}_d)], \\ \Sigma_u^{(\text{res})} &= \text{Tr} [\sqrt{2}\mathbf{X}_u \coth(\sqrt{2}\mathbf{X}_u)] + \Sigma_\lambda^{(\text{res})}, \\ \Sigma_\lambda^{(\text{res})} &= \text{Tr} [\sqrt{2}\mathbf{X}_d \tanh(\sqrt{2}\mathbf{X}_d)] = 2 \text{Tr} [\mathbf{X}_d^2] + \mathcal{O}\left(\frac{v^4}{M_{\text{KK}}^4}\right).\end{aligned}\tag{4.3.42}$$

We observe that the factor $\sqrt{2}$ — which encompasses the extension of the left-handed doublet to a bidoublet for the up sector, and the right-handed singlet to triplet extension for the down sector — leads to a doubling of the new physics contribution compared to the minimal RS result at leading order in v^2/M_{KK}^2 . Remark that one would obtain the same result in the case of an extended fermion sector that is $SU(2)_L \times SU(2)_R$ symmetric simply by extending both the down and up-type singlets to doublets with additional fermions of twisted BCs; a setup studied in [429] that is however at odds with precision measurements of the $Zb_L\bar{b}_L$ -coupling. In the custodial setup, which we employ, there exist even more important new contributions from the exotic fermions of charge $5/3$ and from new up-type quarks contained in the triplets. Both contributions are equal and given by $\Sigma_\lambda^{(\text{res})}$, which involves the triplet Yukawa coupling \mathbf{Y}_d (see (3.3.69)). The total contribution proportional to \mathbf{Y}_d is then approximately six times larger than the down-type new physics contribution in the minimal RS model. This shows that the result massively depends on the choice of the fermion sector. As a general rule of thumb, new fermions with twisted BCs contribute not proportional to their multiplicity, but the stronger, the higher their multiplet representation is, due to simple combinatorics. The final Wilson coefficient is given by

$$\begin{aligned}C_{1(\text{res})}^{\text{KK}}(M_{\text{KK}}) &= \text{Tr} [\sqrt{2}\mathbf{X}_u \tanh(\sqrt{2}\mathbf{X}_u)] \\ &\quad + 3 \text{Tr} [\sqrt{2}\mathbf{X}_d \tanh(\sqrt{2}\mathbf{X}_d)] + \text{Re}(\varepsilon_u + \varepsilon_d) \\ &= \text{Tr} \left[2\mathbf{X}_u^2 + 6\mathbf{X}_d^2 + \text{Re}(\Phi_U + \Phi_u + \Phi_D + \Phi_d) \right] + \mathcal{O}\left(\frac{v^4}{M_{\text{KK}}^4}\right).\end{aligned}\tag{4.3.43}$$

- generic :

In order to understand the model dependence of the contributions in the custodial model we can also expand the generic result of (3.3.125) in v/M_{KK} . This provides a compact result for $\Sigma_q^{(\text{res})}$, which illustrates the various sources of the leading order contributions in terms of the sub blocks of the generalized Yukawa matrix

$$\mathbf{Y}_{\vec{q}} = \begin{pmatrix} \mathbf{Y}_q^{(++)} & \mathbf{Y}_q^{(+-)} \\ \mathbf{Y}_q^{(-+)} & \mathbf{Y}_q^{(--) } \end{pmatrix}.\tag{4.3.44}$$

Here, the two superscripts indicate the UV BCs of the two fermions that enter the corresponding Yukawa coupling in the notation of (3.3.23). We obtain

$$\begin{aligned}\Sigma_q^{(\text{res})} &= n_f + \frac{v^2}{2M_{\text{KK}}^2} \left\{ \frac{1}{3} \left(\text{Tr} [\mathbf{Y}_q^{(++)} \mathbf{Y}_q^{(++)\dagger}] + \text{Tr} [\mathbf{Y}_q^{(+-)} \mathbf{Y}_q^{(+-)\dagger}] + \text{Tr} [\mathbf{Y}_q^{(-+)} \mathbf{Y}_q^{(-+)\dagger}] \right) \right. \\ &\quad \left. + \text{Tr} \left[\left(\mathbf{Y}_q^{(--) } - \frac{2}{3} \mathbf{Y}_q^{(-+)} \mathbf{Y}_q^{(++)^{-1}} \mathbf{Y}_q^{(+-)} \right) \mathbf{Y}_q^{(--) \dagger} \right] \right\} + \mathcal{O}\left(\frac{v^4}{M_{\text{KK}}^4}\right).\end{aligned}\tag{4.3.45}$$

The enhanced contribution from Yukawa couplings $\mathbf{Y}_q^{(-)}$ between two fermions with twisted BCs is a generic feature. The relative sign in the last line suggests that it could be compensated by mixing between all sectors like present in the up-sector of the custodial model above. However, for a general triplet-bidoublet coupling like in (3.3.68) the relation $\mathbf{Y}_q^{(+\pm)} = \pm \mathbf{Y}_q^{(-\pm)}$ holds, such that the two contributions in the last line both add constructively to the total result.

Now, we switch to the alternative order of regulator limits (4.3.26), for which the limits $N \rightarrow \infty$ and $\eta \rightarrow 0$ are taken in the opposite order compared to (4.3.27). In this case one first considers a finite sum over KK modes and derives the relevant Yukawa coupling for each mode by regularizing the Higgs profile, computing the overlap integral in (3.3.129), and then taking the limit $\eta \rightarrow 0$. The relevant Yukawa couplings in that limit have been given in (3.3.130).

Since the sum in (4.3.26) extends over a finite number of KK levels, it is not possible to use the elegant method of 5d propagators described in the previous section. In order to obtain a closed expression nonetheless, we adopt the strategy of first finding a solution in the special case of one generation and vanishing bulk masses. In this case the bulk EOMs and the eigenvalue equation that determines the masses of the KK modes can be solved analytically. The relevant spectrum and couplings for this toy model are summarized in appendix A.3. We will then generalize the result to n_f generations and argue that, as in the case (4.3.40), the general solution is independent of the bulk-mass parameters, too.

Equations (A.3.8) and (A.3.9) imply that in the simplified case we have

$$\lim_{\eta \rightarrow 0} \Sigma_q(N, \eta) \Big|_{\text{toy}} = \sum_{n=0}^{2N} \frac{v g_{nn}^q}{m_n^q} \Big|_{\eta \rightarrow 0} = \frac{X_q}{\cosh(2X_q)} \left[\frac{1}{x_0} + \sum_{k=1}^N \left(\frac{1}{k\pi + x_0} - \frac{1}{k\pi - x_0} \right) \right]. \quad (4.3.46)$$

In the one-generation case, we refer to the zero mode as $n = 0$, while $n \geq 1$ labels the KK modes. The first term in the bracket on the right-hand side of (4.3.46) arises from the SM-like quark, while the remaining sum is over pairs of KK modes belonging to the k^{th} KK level. Note that, for large k the individual terms in the sum fall off like $1/k$ only, but each pair combines to a contribution decreasing like $1/k^2$. Hence, the sum over KK modes is alternating and convergent, and it is possible to take the limit $N \rightarrow \infty$. We obtain for (4.3.26) in the case of a single fermion generation with vanishing bulk masses

$$\Sigma_q^{(\text{low})} \Big|_{\text{toy}} = \frac{X_q \coth(X_q)}{\cosh(2X_q)} = 1 - \frac{5}{3} X_q^2 + \mathcal{O}\left(\frac{v^4}{M_{\text{KK}}^4}\right). \quad (4.3.47)$$

This result differs from the finite sum in (4.3.46) only by terms of $\mathcal{O}(1/N)$, *i.e.* it shows proper decoupling behavior as it is expected for usual vector-like fermions. We have explicitly confirmed that the result (4.3.47) is stable under variations of the bulk masses. The calculation is summarized in appendix A.3. We also checked independence of the bulk masses numerically to very high precision.

Before we generalize the last result to n_f generations, we want to illuminate the discrepancy between the results (4.3.40) and (4.3.47). Obviously, the limits $\eta \rightarrow 0$ and $N \rightarrow \infty$ in (4.3.26) and (4.3.27) are non-commutative and will lead to a large difference for the effective ggh couplings, as we can easily observe in the expansion in v/M_{KK} . We will illuminate the physical origin of this difference in the following. This will later guide our search for a selection criterion of the physically correct result.

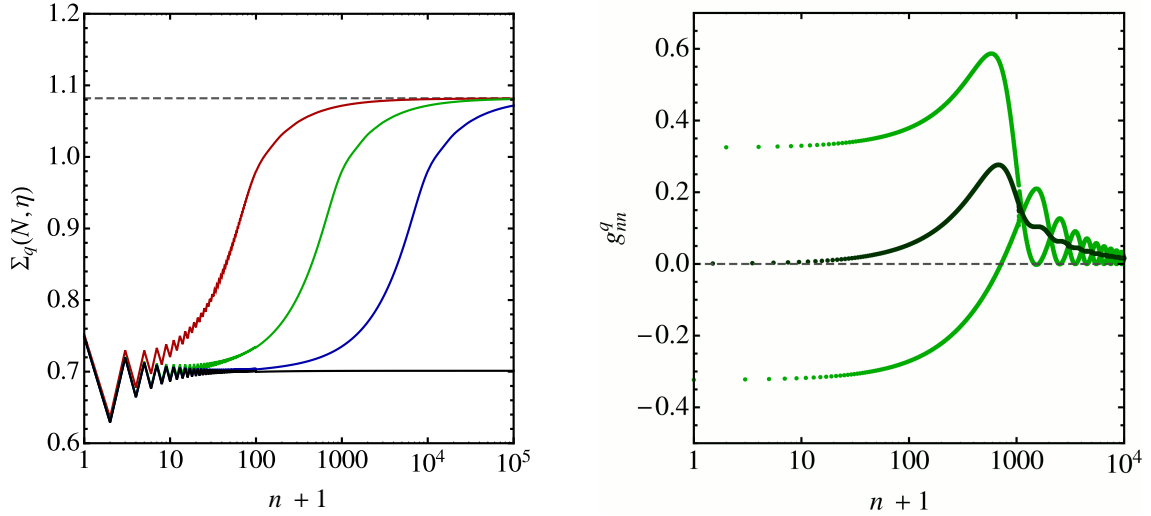


Figure 4.23: The left panel shows the partial sums $\Sigma_q(N, \eta)$ for different values of $n = 2N$ and η in the toy model with one generation and vanishing bulk-mass parameters. The curves refer to $\eta = 10^{-2}$ (red), 10^{-3} (green), 10^{-4} (blue), and 0 (black). We denote $n+1$ on the logarithmic abscissa in order to include the zero mode. The right panel shows Yukawa couplings g_{mn}^q of the KK-fermion states in the toy model for $\eta = 10^{-3}$. The dark points are the Yukawa couplings averaged over a single KK level.

In appendix A.3 we derive the explicit forms of the bulk profiles, masses, and Higgs couplings for the toy model with one generation, vanishing bulk masses, and a box shaped Higgs profile with finite $\eta > 0$. It turns out that the nature of the solution differs strongly, depending on the relative size of the KK fermion’s mass in comparison with a new scale. More precisely, the solution changes significantly if $m_n^q \approx vY_q/(\sqrt{2}\eta) = M_{\text{weak}}/\eta$. Here we assume, as usual, that $Y_q = \mathcal{O}(1)$ are anarchic and light fermion masses are generated by the zero mode localization. Recall that we can choose Y_q real and positive in the case of one generation. The appearance of the scale M_{weak}/η , which for very small η lies far above the TeV scale, is of crucial importance to physically interpret the discrepancy.

Here we demonstrate the emergence of the new scale in the toy model numerically. To this end, we obtain the masses and Higgs–fermion couplings from the formulas (A.3.4) and (A.3.6). In the left plot in figure 4.23, we show the numerical results for the regulated sum $\Sigma_q(n/2, \eta)$ as a function of the number of included KK states n , for four different values of η , *i.e.* we do not carry out any of the two limits in question. For the purpose of illustration we take $X_q = 0.5$, and depict also the intermediate steps where only one of the KK states of a KK level is added to the sum. We observe that for low values of n the sum receives alternating contributions, but quickly converges towards a value close to the result (4.3.47), which equals 0.701 in the present case. Yet, for higher n , there follows an intermediate region, roughly given by the range $0.1/\eta < 2n < 10/\eta$, in which the value of the sum changes by an $\mathcal{O}(1)$ amount. After this transition region, the sum converges to the value corresponding to the result (4.3.40), which equals 1.082 for our choice of X_q . In order to understand the origin of the three regions — in particular the appearance of the intermediate region, in which the sum grows by an $\mathcal{O}(1)$ amount despite the fact that the corresponding KK masses are extremely heavy — we show in the right plot of figure 4.23 the values of the Yukawa couplings g_{mn}^q in

our toy model for the choice $\eta = 10^{-3}$. For low values of n we derive in (A.3.9) that the Higgs couplings for each pair of KK-fermion states in the same KK level are of equal magnitude but opposite sign. In this case, we have seen in (4.3.46), that the contribution from the k^{th} KK level is

$$\frac{X_q}{\cosh 2X_q} \left(\frac{1}{k\pi + x_0} - \frac{1}{k\pi - x_0} \right) = -\frac{X_q}{\cosh 2X_q} \frac{2x_0}{k^2\pi^2 - x_0^2}, \quad (4.3.48)$$

forming a quadratically convergent instead of the naively expected harmonic series. The situation changes drastically in the intermediate region. We show in (A.3.11) that the couplings with odd n vanish, and those with even n reach a maximum, coincidentally both at $m_n^q \approx \sqrt{2}vY_q/\eta = 2M_{\text{weak}}/\eta$ for the given choice of parameters. Thus, there exists a range of logarithmic growth of the sum, over which its contribution can be qualitatively estimated as

$$\sum_{k=N_1}^{N_2} \frac{g_{\text{avg}}(k)}{k\pi} \approx \frac{\langle g_{\text{avg}} \rangle}{\pi} \ln \frac{N_2}{N_1}, \quad (4.3.49)$$

where $\langle g_{\text{avg}} \rangle$ denotes the mean value of $g_{\text{avg}}(k)$ in the interval $k \in [N_1, N_2]$, in which the average coupling in each KK level departs from zero. Physically, this intermediate region arises because, for fixed η , there exists a minimum KK mass $m_n^q \sim M_{\text{weak}}/\eta$ beyond which the KK-profile functions begin to significantly penetrate the box modeling the Higgs-boson profile. When this happens, the cancellation of the Yukawa couplings of KK modes within a KK level is no longer operative. Consequently, the generic logarithmic growth arises, which we expected from naive dimensional analysis. Only for yet much higher KK levels, when the profiles exhibit a large number of oscillations within the box, the couplings decrease sufficiently fast with k , such that the sum converges to the aforementioned upper limiting value.

In light of the fact that $\Sigma_q^{(\text{res})}$ contains order one contribution from very heavy modes and is therefore sensitive to UV physics, it is worthwhile to investigate the general result (4.3.47) for $\Sigma_q^{(\text{low})}$, which excludes this collective, UV resonance effect. In the next section, we will show that any UV regularization will render the following result for $\Sigma_q^{(\text{low})}$ as being physically correct.

Given the similarity of the result (4.3.47) with equation (4.3.40), we can still profit from the derivation of $\Sigma_q^{(\text{res})}$. We conjecture that in the case of three generations a general recipe to obtain $\Sigma_q^{(\text{low})}$ is to extend $\Sigma_q^{(\text{res})}$ with additional inverse matrices of $\cosh(2\mathbf{X}_q)$ inside the trace.

- minimal ($q = u, d$) :

$$\Sigma_q^{(\text{low})} = \text{Tr} \left[\frac{\mathbf{X}_q \coth(\mathbf{X}_q)}{\cosh(2\mathbf{X}_q)} \right] = n_f - \frac{5}{3} \text{Tr} \mathbf{X}_q^2 + \mathcal{O}\left(\frac{v^4}{M_{\text{KK}}^4}\right). \quad (4.3.50)$$

Like in (4.3.40) the result is real, such that only C_1^{KK} receives a contribution. Combining (4.3.32), (4.3.28), and (4.3.50), we find

$$\begin{aligned} C_{1(\text{low})}^{\text{KK}}(M_{\text{KK}}) &= \sum_{q=u,d} \left(-\text{Tr} \left[\frac{\mathbf{X}_q \tanh(\mathbf{X}_q)}{\cosh(2\mathbf{X}_q)} \right] + \text{Re}(\varepsilon_q) \right) \\ &= \sum_{q=u,d} \text{Tr} \left[-\mathbf{X}_q^2 + \text{Re}(\Phi_Q + \Phi_q) \right] + \mathcal{O}\left(\frac{v^4}{M_{\text{KK}}^4}\right). \end{aligned} \quad (4.3.51)$$

This time the contribution to C_1^{KK} is negative and thus yields a suppression of the $gg \rightarrow h$ amplitude compared with the SM. Incidentally, the first term in the expansion in powers of \mathbf{X}_q^2 has the opposite sign from the result (4.3.41). For the purpose of the numerical evaluation we want to express the result also with the Yukawa matrices $\tilde{\mathbf{Y}}_q$, which determine the spectrum

$$C_{1(\text{low})}^{\text{KK}}(M_{\text{KK}}) = \sum_{q=u,d} \left(-f(\tilde{\mathbf{X}}_q) + \text{Re}(\varepsilon_q) \right), \quad (4.3.52)$$

$$f(x) \equiv x \operatorname{atanh}(x) \frac{1-x^2}{1+x^2}. \quad (4.3.53)$$

• custodial :

$$\Sigma_d^{(\text{low})} = \text{Tr} \left[\sqrt{2} \mathbf{X}_d \frac{\coth(\sqrt{2} \mathbf{X}_d)}{\cosh(2\sqrt{2} \mathbf{X}_d)} \right],$$

$$\Sigma_u^{(\text{low})} = \text{Tr} \left[\sqrt{2} \mathbf{X}_u \frac{\coth(\sqrt{2} \mathbf{X}_u)}{\cosh(2\sqrt{2} \mathbf{X}_u)} \right] + \Sigma_\lambda^{(\text{low})}, \quad (4.3.54)$$

$$\Sigma_\lambda^{(\text{low})} = -\text{Tr} \left[\sqrt{2} \mathbf{X}_d \frac{\tanh(\sqrt{2} \mathbf{X}_d)}{\cosh(2\sqrt{2} \mathbf{X}_d)} \right] = -2 \text{Tr} [\mathbf{X}_d^2] + \mathcal{O}\left(\frac{v^4}{M_{\text{KK}}^4}\right).$$

Observe that also the sector of exotic fermions contributes negatively to C_1^{KK} this time. We summarize the contributions to the Wilson coefficients in terms of the function f introduced in (4.3.53)

$$\begin{aligned} C_{d,1(\text{low})}^{\text{KK}}(M_{\text{KK}}) &= \text{Tr} \left[-f(\sqrt{2} \tilde{\mathbf{X}}_d) + \text{Re}(\varepsilon_q) \right], \\ C_{u,1(\text{low})}^{\text{KK}}(M_{\text{KK}}) &= \text{Tr} \left[-f(\sqrt{2} \tilde{\mathbf{X}}_u) - f(\sqrt{2} \tilde{\mathbf{X}}_d) + \text{Re}(\varepsilon_q) \right], \\ C_{\lambda,1(\text{low})}^{\text{KK}}(M_{\text{KK}}) &= \text{Tr} \left[-f(\sqrt{2} \tilde{\mathbf{X}}_d) \right]. \end{aligned} \quad (4.3.55)$$

In total this leads to the very short final result

$$\begin{aligned} C_{1(\text{low})}^{\text{KK}}(M_{\text{KK}}) &= \text{Tr} \left[-f(\sqrt{2} \tilde{\mathbf{X}}_u) - 3f(\sqrt{2} \tilde{\mathbf{X}}_d) + \text{Re}(\varepsilon_u + \varepsilon_d) \right] \\ &= -2 \text{Tr} [\mathbf{X}_u^2] - 6 \text{Tr} [\mathbf{X}_d^2] + \mathcal{O}\left(\frac{v^4}{M_{\text{KK}}^4}\right). \end{aligned} \quad (4.3.56)$$

We compare this again to the alternative $SU(2)_L \times SU(2)_R$ symmetric quark embedding, which only promotes down- and up-type singlets to doublets, and leads to disfavored contributions to the $Z b_L \bar{b}_L$ coupling. In that case, the contribution proportional to the down-type-Yukawa matrices in (4.3.56) would not be enhanced by a factor 3. Thus, the alternative embedding would again give approximately twice the result of the minimal non-custodial embedding.

The formulas given here reproduce the numerical results obtained in [4]. We checked this with the large sample of more than 10^4 valid parameter points for 3 fermion generations, which we generated for the numerical analysis of the minimal and separately also for the custodial RS model. The numerical data is described in more detail below. We remark here

that for each parameter point, we calculated the zero modes plus the complete set of the first 4 KK levels and extrapolated the remaining contribution to $C_{1,q}^{(\text{low})}$ by assuming equidistant KK-mass spacing at higher levels. We found that the resulting contributions to all three sectors of common charge agree with the analytic result (4.3.56) within 1 per-mil.

We did not give a formal proof of (4.3.50) and (4.3.54) for more than one generation, which would be interesting beyond the numerical verification. Symmetry arguments help us to constrain at least the form of the answer. The result for the sum (4.3.26), expressed as a function of the fundamental parameters of the underlying 5d theory is given by $\Sigma_q^{(\text{low})} = \Sigma(\mathbf{Y}_q, \mathbf{c}_Q, \mathbf{c}_q)$. The EOMs (3.3.32) and boundary conditions (3.3.35) are valid in an arbitrary basis, in which the bulk-mass matrices \mathbf{c}_A are not necessarily diagonal. These relations are invariant under a set of three global symmetries. The first one is a symmetry under the exchange of $SU(2)$ doublets and singlets along with $\mathbf{Y}_q \leftrightarrow \mathbf{Y}_q^\dagger$. In addition, there are two symmetries related to unitary transformations of the Yukawa and bulk-mass matrices. When combined with the fact that in the one-generation case the result is found to be independent of the bulk-mass parameters, these symmetries imply that the quadratic term in \mathbf{X}_q must indeed be of the simple form shown in (4.3.50).

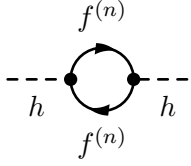
4.3.3.3 UV Regulation as a Decision Criterion

We have seen in the last section that KK fermions with masses far above the TeV scale seemingly change the result of Higgs production via gluon–gluon fusion by an $\mathcal{O}(1)$ amount. If this was the final answer, the theory would be plagued by a UV dependence even though the specific loop processes in question give finite results. Consequently, we would lose predictability for the given process. In the following, we clarify that this is fortunately not the case. We recall the importance of using a consistent UV regularization scheme when evaluating the gluon–gluon fusion amplitude. This is true in the SM, as we explained in section 4.3, and even more so in its 5d extensions. Here, we will study two different regularization schemes: dimensional regularization and the use of a hard momentum cutoff. While a dimensional regulator is particularly convenient in that it preserves gauge and Lorentz invariance, the second option is also a natural choice in the present case, since the theory presents only an effective theory below the Planck scale. Incorporating the effects of quantum gravity requires a UV completion. In section 3.3.7, we have already touched a peculiar feature of warped extra-dimensional models: Their effective UV cutoff depends on where the theory is probed along the extra dimension [103], more precisely, where the involved particles are localized. The physical reason is that due to warping the fundamental length and energy scales change along the extra dimension. More specifically, the effective cutoff scale at the position t in the extra dimension is of the order of the warped Planck scale

$$\Lambda_{\text{UV}}(t) \sim M_{\text{Pl}} e^{-\sigma(\phi)} = M_{\text{Pl}} \frac{\epsilon}{t} \equiv \frac{\Lambda_{\text{TeV}}}{t}. \quad (4.3.57)$$

To preserve predictivity, the cutoff should be sufficiently high, so that at least a small number of KK modes have masses below Λ_{TeV} , and hence $\Lambda_{\text{TeV}}/M_{\text{KK}} = \mathcal{O}(10)$. Otherwise incalculable threshold corrections of order $M_{\text{KK}}^n/\Lambda_{\text{TeV}}^n$ become important and call for a non-perturbative treatment of the unspecified UV-completing theory. We stress that imposing a UV cutoff is crucial in order for the RS model to provide a viable solution to the hierarchy problem. Self-energy contributions of fermions to the Higgs boson’s mass are estimated by naive dimension

analysis to be of the order

$$\delta m_h^2 \sim \sum_{m_{f^{(n)}} < \Lambda_{\text{TeV}}} \text{---} \overset{f^{(n)}}{\circ} \text{---} \sim \sum_{m_{f^{(n)}} < \Lambda_{\text{TeV}}} \frac{|Y_{f^{(n)}}|^2 m_{f^{(n)}}^2}{32\pi^2 M_{\text{KK}}^2}. \quad (4.3.58)$$


Since the Higgs–fermion couplings enter quadratically in this case, there are no possible cancellations between different chiralities, like we saw in the ggh -loop diagrams of the last section. Consequently, the divergent behavior is even worse than generically expected by new physics, due to the multiplicity of the KK spectrum with equidistant masses. Consequently, it is a necessity to localize the Higgs sector at least very near to the IR brane (in the vicinity of $t = 1$) and to choose an effective cutoff $\Lambda_{\text{UV}}(t)$ of the order of only several TeV for values of t that are on the Higgs profile’s support.

The question of how to introduce such a cutoff in practical one-loop calculations is far from being trivial and no rigorous scheme exists for how to distribute the cutoffs on the various momenta at a given vertex [231]²³. However, at loop momenta several times larger than M_{KK} , external momenta can be neglected and hence there remains a single 4d (euclidean) loop momentum $p_E^2 \equiv -p^2$ on which the cutoff should be imposed. Employing a t -dependent cutoff associated with every vertex of a Feynman diagram can be thought of as modeling the effect of a form factor, which accounts for the impact of quantum gravity on energy scales above the effective Planck scale at that point. In general, the t_i coordinates of the vertices are integrated over the entire bulk ($\epsilon \leq t_i \leq 1$), and hence the cutoff values vary between the TeV scale and the fundamental Planck scale. It was shown that this prescription allows for gauge-coupling unification in warped extra-dimensional models [103, 434–437]. The situation simplifies considerably for one-loop diagrams that contain vertices with Higgs bosons, such as the relevant diagram in figure 4.22. Denoting the coordinate of the two gluons by t_1 and t_2 and that of the Higgs boson by t_3 , the fact that $t_3 \approx 1$ ensures that the momentum cutoff on the 4d loop integral is

$$p_E \leq \min\{\Lambda_{\text{UV}}(t_1), \Lambda_{\text{UV}}(t_2), \Lambda_{\text{UV}}(t_3)\} = \Lambda_{\text{TeV}}. \quad (4.3.59)$$

The same mechanism applied to the 5d calculation of the radiative Higgs mass correction (4.3.58) guarantees that the hierarchy problem is solved in RS models.

In order to UV regularize the loop integral, our first ansatz is to use standard dimensional regularization of the four-momentum integration $d^{4-2\epsilon}p$, with $\epsilon > 0$. We then find that the sum in (4.3.25) gets modified to

$$\sum_{n=1}^{n_f + N n_F} \frac{v g_{nn}^q}{m_n^q} \left(\frac{\mu^2}{(m_n^q)^2} \right)^\epsilon, \quad (4.3.60)$$

where $\mu \sim \Lambda_{\text{TeV}}$ is the regularization scale. For very large masses $m_n^q \gg \mu$, the dimensional regulator gives rise to a suppression, which renders the sum over KK modes convergent even for arbitrary $\mathcal{O}(1)$ Yukawa couplings. The limits $N \rightarrow \infty$ and $\eta \rightarrow 0$ can therefore be taken without encountering any ambiguities. The contribution from the region of very heavy KK modes with $m_n^q \sim M_{\text{weak}}/\eta$, which we illustrated in figure 4.23, and which previously gave rise to an unsuppressed contribution of the form (4.3.49), now receives an extra suppression

²³We enlisted three non-equivalent examples in footnote 17 of section 3.3.7

factor $\eta^{2\varepsilon}$, and vanishes when one takes the limit $\eta \rightarrow 0$ (at fixed ε). The infinite sum then coincides with the result (4.3.26) up to harmless $\mathcal{O}(\varepsilon)$ corrections.

In the dimensional regularization scheme, gauge invariance is manifest in the 4d theory. Since the dimensional regulator also regularizes the infinite KK sum, we are guaranteed that the 5d theory remains gauge invariant, too. On the other hand, dimensional regularization is perhaps not the most intuitive way in which to introduce a UV cutoff. As an alternative, we will therefore rephrase the discussion in a regularization scheme based on using the hard momentum cutoff given in (4.3.59). In order to ensure 4d gauge invariance in this case, we first extract two powers of the external gluon momenta by taking appropriate derivatives, after which the remaining loop integral is superficially convergent. Introducing the UV cutoff on this integral, and neglecting the Higgs mass compared with m_n^q , we obtain

$$\sum_{n=1}^{n_f+Nn_F} 2vg_{nn}^q \int_0^{\Lambda_{\text{TeV}}^2} dp_E^2 p_E^2 \frac{m_n^q}{(p_E^2 + (m_n^q)^2)^3} = \sum_{n=1}^{n_f+Nn_F} \frac{vg_{nn}^q}{m_n^q} \left(\frac{\Lambda_{\text{TeV}}^2}{\Lambda_{\text{TeV}}^2 + (m_n^q)^2} \right)^2. \quad (4.3.61)$$

For small masses $m_n^q \ll \Lambda_{\text{TeV}}$ this reduces to the simple expression vg_{nn}^q/m_n^q used in the sum (4.3.25). For very large masses $m_n^q \gg \Lambda_{\text{TeV}}$, on the other hand, the UV cutoff gives rise to a strong suppression proportional to $\Lambda_{\text{TeV}}^4/(m_n^q)^4$, implying that such heavy KK modes decouple rapidly. It follows that, due to physical reasons, the sum over KK modes in (4.3.25) is effectively truncated once the KK masses exceed the scale Λ_{TeV} . In the RS model with a Higgs sector that is sufficiently brane-localized, *e.g.* for the IR-brane Higgs discussed here, the scale M_{weak}/η at which the very heavy KK modes start to contribute logarithmically to $\Sigma_q(N, \eta)$ is parametrically much larger than the effective cutoff scale Λ_{TeV} . It is then appropriate to truncate the sum at a value $N_{\text{KK}}^{\text{max}} \sim \Lambda_{\text{TeV}}/M_{\text{KK}}$ corresponding to KK masses much smaller than M_{weak}/η . It follows that

$$\lim_{\eta \rightarrow 0} \Sigma_q(N_{\text{KK}}^{\text{max}}, \eta) = \Sigma_q^{(\text{low})} + \mathcal{O}\left(\frac{N_{\text{KK}}^{\text{max}} v^2}{\Lambda_{\text{TeV}}^2}\right), \quad (4.3.62)$$

where the truncation error has the form of a threshold correction, which is always present in effective-theory calculations. Even in the case that only a single KK level is perturbative, the error remains below 2%.

We can summarize the above discussion by emphasizing the subtle fact that, in order to obtain the correct answer for the gluon–gluon fusion cross section in the RS model, it is essential to employ a consistent UV regularization scheme when evaluating the loop integral, despite the fact that the integral is convergent. When this is done, the convergence of the partial sum in (4.3.25) is improved in such a way that the order in which the two limits $N \rightarrow \infty$ and $\eta \rightarrow 0$ are taken becomes irrelevant. Specifically, in the two regularization schemes we have considered in our analysis, we find

$$\lim_{\substack{N \rightarrow \infty \\ \eta \rightarrow 0}} \sum_{n=1}^{n_f+Nn_F} \frac{vg_{nn}^q}{m_n^q} \rightarrow \begin{cases} \left. \sum_{n=1}^{\infty} \frac{vg_{nn}^q}{m_n^q} \left(\frac{\mu^2}{(m_n^q)^2} \right)^\epsilon \right|_{\eta=0} & = \Sigma_q^{(\text{low})} + \mathcal{O}(\epsilon), & \text{dim.reg.}, \\ \left. \sum_{n=1}^{\infty} \frac{vg_{nn}^q}{m_n^q} \left(\frac{\Lambda_{\text{TeV}}^2}{\Lambda_{\text{TeV}}^2 + (m_n^q)^2} \right)^2 \right|_{\eta=0} & = \Sigma_q^{(\text{low})} + \mathcal{O}\left(\frac{N_{\text{KK}}^{\text{max}} v^2}{\Lambda_{\text{TeV}}^2}\right), & \text{cutoff.} \end{cases} \quad (4.3.63)$$

In both schemes the infinite sums are superficially convergent.

The terms suppressed by a power of the UV cutoff, which appear on the right-hand side of (4.3.62), parametrize the difference between the asymptotic value $\Sigma_q^{(\text{low})}$ of the infinite sum and the sum over a finite number of KK modes. More generally, such threshold terms may also arise from the yet unknown effects of the UV completion of the RS model. From a low-energy perspective, the only requirement on such a completion that is relevant to us is that it must cure the hierarchy problem by taming loop momenta that exceed the fundamental scale of quantum gravity. As long as this is the case, the gluon–gluon fusion amplitude will also be regularized in the way discussed above. In the context of a specific UV completion, the threshold effects could be modeled at low energies by means of a brane-localized effective $h G_{\mu\nu}^a G^{\mu\nu,a}$ operator, suppressed by v/Λ_{TeV}^2 . The additional factor $N_{\text{KK}}^{\text{max}}$ reflects the high multiplicity of degrees of freedom in the low-energy EFT. For quite generic reasons, the coefficient of this operator must contain the loop factor $\alpha_s(\mu)/(4\pi)$ factored out in (4.3.5), even in cases where the UV completion of the RS model is strongly coupled. The reason is that the on-shell external gluons couple proportional to their QCD charges, and that any new heavy state that couples to the Higgs boson must be color neutral, so it cannot have a tree-level coupling to gluons. Hence, a generic UV completion will indeed give rise to a threshold correction of the form shown in (4.3.62). However, the difference between the two sums $\Sigma_q^{(\text{low})}$ (4.3.26) and $\Sigma_q^{(\text{res})}$ (4.3.27) cannot be attributed to such a brane-localized threshold term. As we have shown, it is instead determined by the absence or presence of a physical UV regulator and a sensible UV completion.

4.3.4 Phenomenology of the Randall-Sundrum Model

In the following, we shall quantify the implications of the RS model for the main channels of Higgs production and decays at Hadron colliders. To this end, we study the expected deviations from the SM amplitudes. They are already constrained by the experimental results on signal strengths as discussed in section 4.3.1. Again, we use a fixed reference mass of $M_h = 126 \text{ GeV}$ for the Higgs boson.

4.3.4.1 Production Channels

In the last section, we already laid out the relevant results to study the most important Higgs boson production channel via gluon–gluon fusion. We gave the relevant formula for the shift in the production cross section R_h in (4.3.33). For the Wilson coefficient C_1^{KK} , we use and verify numerically the analytic result (4.3.52), which we have shown to be physically viable, and for which the RS contributions decouple with the scale of new physics M_{KK} . We neglect the sub-percent threshold effects appearing in (4.3.62). This is to be understood implicitly for the remaining discussion.

We observed two important aspects for the dominant CP -even part of the RS amplitude parametrized by κ_g relative to the SM amplitude. First of all, we have seen that the dependence on fermion-bulk masses cancels to a large extent. Neglecting b -quark corrections, setting the top-form factor to one (approximately 5%, and 3% error respectively), using the approximation (4.3.29), and the Froggatt-Nielsen approximation (4.3.35) (both less than 1% error), we obtain

$$\kappa_g \approx 1 - \frac{v^2}{3M_{\text{KK}}^2} \frac{\left(\mathbf{Y}_q \mathbf{Y}_q^\dagger \mathbf{Y}_q\right)_{33}}{\left(Y_q\right)_{33}} \begin{Bmatrix} 1 \\ 2 \end{Bmatrix} - \text{Tr} \left[\begin{Bmatrix} f(\tilde{\mathbf{X}}_u) + f(\tilde{\mathbf{X}}_d) \\ f(\sqrt{2}\tilde{\mathbf{X}}_u) + 3f(\sqrt{2}\tilde{\mathbf{X}}_d) \end{Bmatrix} \right], \quad (4.3.64)$$

where the upper and lower constants in the curly brackets hold for the minimal and the custodial RS model. In the following, we will always use the full expression for deriving numerical results, while making as few approximations as possible. The general behavior and the suppression of κ_g can however be well understood from (4.3.64). The second important insight was that all KK-fermion-triangle contributions can be expressed by the trace of the analytic function $f(\tilde{\mathbf{X}}_q)$ defined in (4.3.53), with $\tilde{\mathbf{X}}_q$ defined in (3.3.41). This is also true for KK-fermion contributions to the decay into two gluons and two photons. The trace is determined by the non-negative, real square roots y_q^i of the eigenvalues of the hermitian matrices $\tilde{\mathbf{Y}}_q \tilde{\mathbf{Y}}_q^\dagger$ as

$$\text{Tr } f(\tilde{\mathbf{X}}_q) = \sum_i f\left(\frac{v \tilde{y}_q^i}{\sqrt{2} M_{\text{KK}}}\right), \quad \text{where } \mathbf{u} \tilde{\mathbf{Y}}_q \tilde{\mathbf{Y}}_q^\dagger \mathbf{u}^\dagger = \text{diag}(\tilde{y}_q^i)^2. \quad (4.3.65)$$

An additional factor $\sqrt{2}$ enters the arguments in the custodial model. Since the RS model is able to explain flavor hierarchies by localization in 5d, it is a feature of the model that the fundamental Yukawa matrices are structureless and of order one. Thus, the above result is roughly proportional to the rank of the Yukawa matrices, which is equal to the number of fermion generations. In other words, the KK towers of all six quarks in the minimal RS model give comparable contributions to the effective ggh vertex, irrespective of the mass of the corresponding SM fermion. In the custodial model, the sectors of different fermion charges get the relative weight factors included in (4.3.64), which are constant integers and still independent of the SM-fermion masses. This property is different from several other extra-dimensional extensions of the SM. For instance, in models based on universal extra dimensions, the 5d Yukawa couplings are hierarchical like in the SM, and hence the Higgs boson couplings to light fermions and their KK excitations are strongly suppressed [438]. Models of gauge–Higgs unification have the peculiar property that their contribution from KK excitations cancels the dominant effect from corrections to the Yukawa couplings of the SM quarks in the ggh amplitude. This leaves only chirally suppressed corrections, which are very small for all quarks except the top quark [236]. Hence, in these new-physics scenarios only the top quark and its heavy partners contribute to the effective ggh couplings, while Higgs boson production is independent of the masses and couplings of the KK excitations of light SM quarks. In this sense, such models are similar to four-dimensional models where the Higgs boson is realized as a pseudo-Nambu-Goldstone boson. We discussed examples in section 4.3.2.

We generated large sets of valid parameter points for the two RS variants discussed here. We have seen above that a strong dependence on the general size of the fundamental Yukawa elements is to be expected. Thus we generated parameters sets for multiple discrete values of y_{max} , where the elements of the Yukawa matrices are constrained by the condition $y_{\text{max}} > (Y_q)_{ij} > y_{\text{max}}/10$ and follow a uniform random distribution in this range. The lower bounds are irrelevant in practice, but included here for definiteness. Further details on the parameter sets, as well as intermediate results for the various values of y_{max} are included in appendix B.4.

As a first check of the data sets and the results entering (4.3.65), we fit a polynomial of second order to the median of the distribution for $\kappa_t + \epsilon_u$ in dependence on the scale M_{KK} . We expect from (4.3.35) roughly a quadratic scaling with y_{max} . Indeed, we find that the parametrization $1 + c v^2 y_{\text{max}}^2 / (2 M_{\text{KK}}^2)$ reproduces the behavior very well for $M_{\text{KK}} > 1.5 \text{ TeV}$ and for all relevant values of y_{max} . In the minimal and custodial model the coefficient c is of the expected size, 1.15 and 2.10 respectively, as obtained from a fit for $y_{\text{max}} = 3$. The

deviation from the quadratic scaling can be significant for low values of M_{KK} . The fourth order term induces a relative contribution of approximately +10% for $M_{\text{KK}} = 1$ TeV, when included in the fit. The Higgs–top coupling is thus somewhat less suppressed than naively expected for large values of $y_{\text{max}}/M_{\text{KK}}$. Deviations from quadratic scaling are even more pronounced for the resummed KK-tower contribution. To see this, we also fit the medians of $f(\tilde{\mathbf{X}}_{u,d})$ with the fit-model function

$$\text{med}(f(\tilde{\mathbf{X}}_q)) = 3 \left(1 - \frac{b v^2}{2M_{\text{KK}}^2} \right) f(a \bar{x}), \quad (4.3.66)$$

where $\bar{x} = v y_{\text{max}}/(\sqrt{2}M_{\text{KK}})$ in the minimal, and $\bar{x} = v y_{\text{max}}/M_{\text{KK}}$ in the custodial model. Again, this reproduces the numerical results well for $M_{\text{KK}} > 1.5$ TeV. Leaving a and b in (4.3.66) as a free fit parameter, we obtain for the custodial and minimal model, values of $y_{\text{max}} = 0.5 \dots 3$, and for $q = u, d$, indeed in every possible combination a value between $a = 0.97\text{--}1.03$. However, the higher order correction b becomes quite important for low values of M_{KK} . For instance, for the custodial model, $M_{\text{KK}} = 1.5$ TeV, and $y_{\text{max}} = 3$, we get a relative correction of approximately -30% from the non-vanishing value of the coefficient b . The parametrization (4.3.66) even fails completely for values of M_{KK} below 1.5 TeV. The function $f(x)$ in fact saturates as x grows and has a maximum at $x \approx 0.7$. This behavior distorts the naively expected parametrization in a very significant way. In the following, we rather calculate all cross sections and branching ratios separately for each parameter point, using the full expressions and derive typical values only for the final distribution. This has the additional advantage that we can access the deviations from the typical values, *i.e.* quantify the spread due to the new physics input parameters.

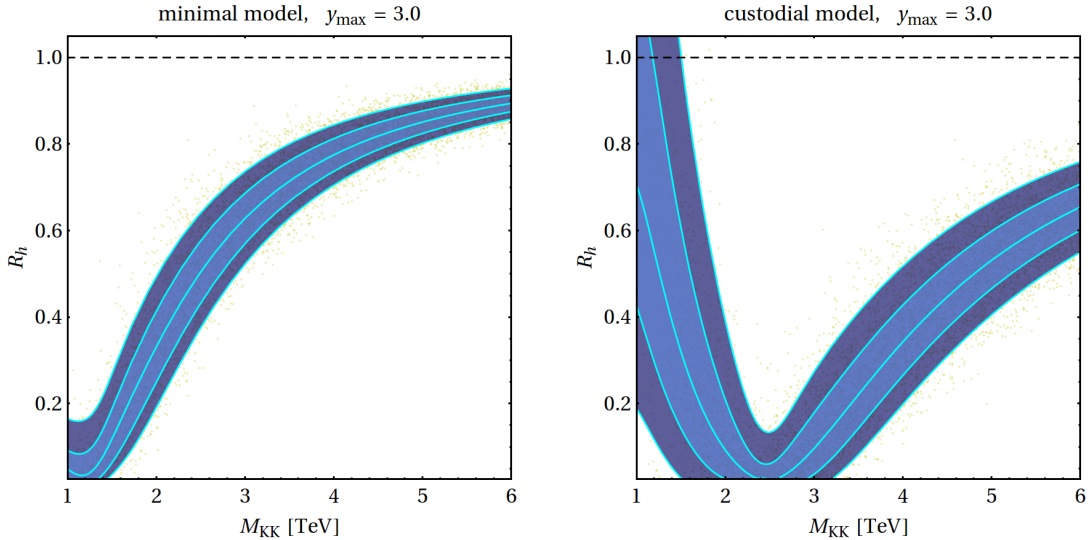


Figure 4.24: Fitted modification factor of the Higgs production rate via gluon–gluon fusion in the RS model with $y_{\text{max}} = 3$ compared to the SM. The left plot shows the minimal RS model, while the right plot shows the custodially protected model. The cyan lines are the 5%, 20%, 50%, 80%, and 95% quantiles. The points of the numerical scan are underlaid in faint yellow and only visible in regions where many points cluster, in order to qualitatively check the inclusiveness of the bands.

We show in figure 4.24 the distributions obtained for R_h in the minimal and custodial

model in the left and right panel for the most natural range, which is restricted by $y_{\max} = 3$. The maximal value corresponds to the perturbativity bound derived in [211] by means of naive dimensional analysis. The plots show the median value and the two-sided 60%, and 90% quantile of the parameter distribution, after imposing constraints on viable fermion masses and mixing angles, as a function of the scale M_{KK} . Recall that often also the lightest KK gluon mass $M_{G(1)} \approx 2.45 M_{\text{KK}}$ is used as a reference, as its value is a model-independent prediction for all RS scenarios with common warp factor ϵ . We observe a suppression of Higgs production via gluon–gluon fusion that is large and decouples slowly with M_{KK} . It is predominantly due the large contribution from KK loops, which can even completely compensate the SM amplitude for very low values of M_{KK} . This is possible in a broad region around 1.3 TeV in the minimal model. Since the multiplicity of KK states is higher in the custodial model, full compensation of the amplitude is already reached in a region around 2.5 TeV. For even lower values of M_{KK} the RS contribution can overcompensate the SM amplitude by more than twice its amount, leading to an effective enhancement of R_h for 5% of the parameter space below $M_{\text{KK}} = 1.5$ TeV and 20% below $M_{\text{KK}} = 1.2$ TeV. Remark that in order to calculate these numbers reliably, we had to use the exact expressions for the Higgs–fermion couplings and the resummed expression for the KK-loop contributions, since $v y_{\max}/M_{\text{KK}} \approx 0.5 (y_{\max}/3) (1.5 \text{ TeV}/M_{\text{KK}})$ is not a suitable expansion parameter anymore. A perturbative ansatz with mass insertions up to order v^2 would effectively lead to $f(\bar{x}) \approx \bar{x}^2$ and massively overestimate the KK-loop contributions in the low M_{KK} region.

We shortly comment on the quality of the approximation (4.3.64) for R_h , which allows to easily understand the main contributions of the modified top coupling and includes the analytic result for the KK loops. We applied the fits in the same way as we did for the exact expressions used for figure 4.24. As expected, the result agrees well, having a deviation at $M_{\text{KK}} = 1.5$ TeV of 1% in the minimal, and 3% in the custodial model for the largest quantile and even much less deviation for the median. This provides an explicit numerical check for the analytic results of the Wilson-coefficients from KK-loops (4.3.52) and (4.3.56), since we calculate the exact distribution of R_h by an explicit summation of the loop contributions of a few KK levels, and extrapolate the resummed result (see appendix B.4).

We also reconstruct the exact behavior for lower values of y_{\max} (see appendix B.4). We reduce y_{\max} down to 0.5, where the mean entry of a random Yukawa element is 0.1, *i.e.* one order of magnitude below the natural size. In the left panels of figure 4.25, we show the resulting two-dimensional dependence of the median. The right panels quantify the spread of the parameter distribution by illustrating the distance of the two-sided 90% quantile from the SM result. Supposing a constraint on R_h of maximally 50% deviation, a SM-like central value, and $y_{\max} = 3$, we could read off a constraint of $M_{\text{KK}} > 2$ TeV in the minimal and $M_{\text{KK}} \notin [1.8, 4]$ TeV in the custodial model. For $y_{\max} = 1.5$ the numbers would change to $M_{\text{KK}} > 1.1$ TeV and $M_{\text{KK}} > 2$ TeV. However, inferring such a constraint will be challenging, even after the full LHC program. This is due to the large theoretical uncertainty affecting the cross section normalization and the inability to access the partial decay width into gluons²⁴. In [376], a strategy to consider ratios of processes from gluon and vector boson fusion with the same final Higgs decay was proposed as an intermediate step. The normalization of $gg \rightarrow h \rightarrow VV$ to the analogous process from weak gauge boson fusion appears interesting, but has limited prospect, if the cuts applied for selecting weak gauge boson fusion are permeable to a significant amount of $gg \rightarrow h + 2j$ events (approximately 30% [376]). The main importance

²⁴ R_h is also equal to the partial decay width into gluons relative to the SM $\Gamma(h \rightarrow gg)_{\text{RS}}/\Gamma(h \rightarrow gg)|_{\text{SM}}$.

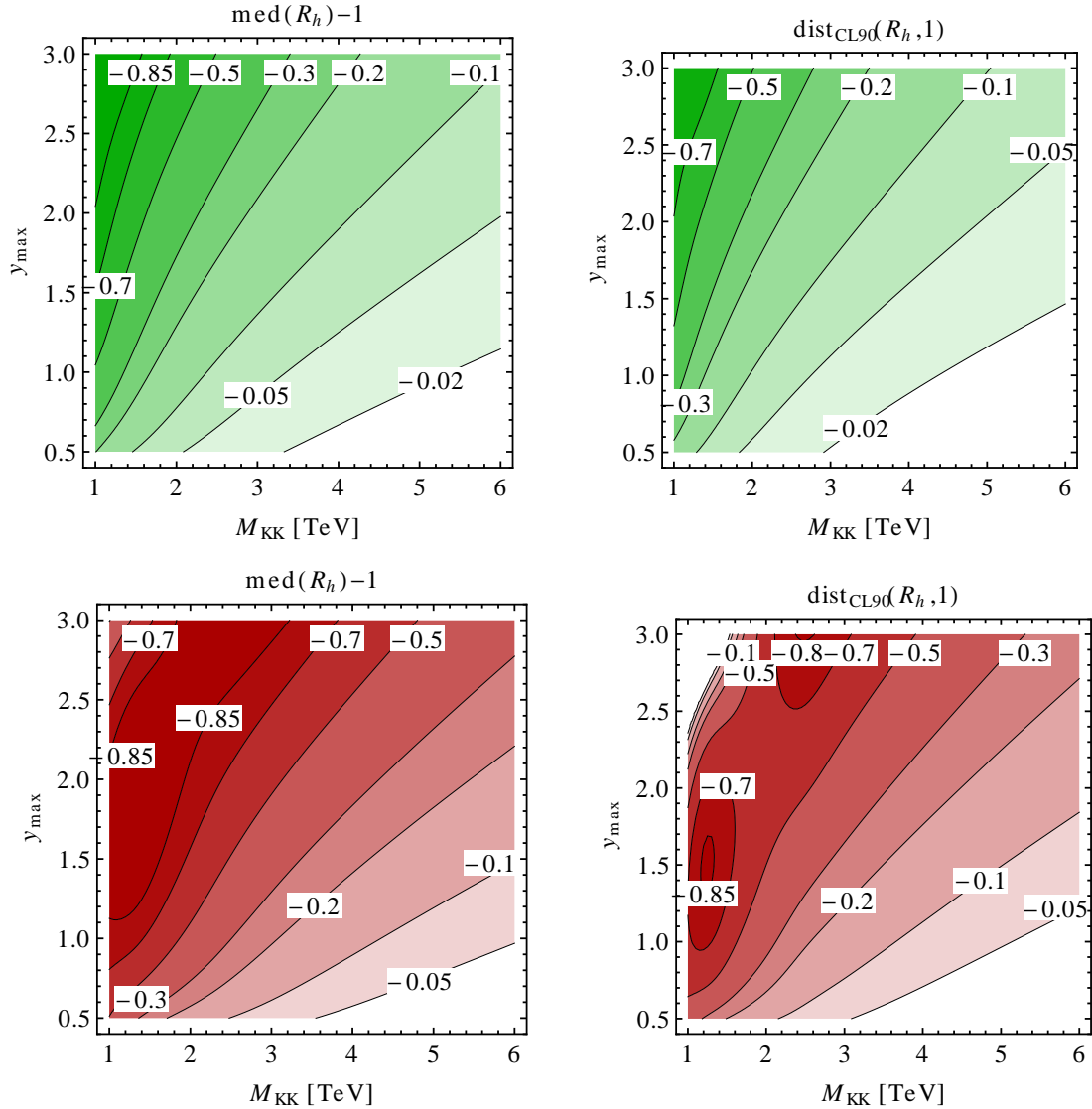


Figure 4.25: Enhancement of the Higgs production rate via gluon–gluon fusion in the RS model compared to the SM. The upper row (green shading) shows the results for the minimal model and the lower (red shading) for the custodially protected model. In the left panels we show the distance of the typical, *i.e.* median, value from the SM result. In the right panels we give the distance of the 90% two sided quantile of the RS parameter distribution from the SM result. The distance is defined to be negative if the quantile band is below one and to be zero if the band overlaps with one.

of the result given here is the general insight that KK-loops can lead to drastic changes in the overall production rate, and that this feature is in many cases not compensated by enhancements of the successive Higgs decays, as we will see below.

In order to better understand the parametric behavior of figure 4.25, we derive a rough two-parametric estimate for the median value in the region where $v y_{\text{max}}/M_{\text{KK}}$ is a suitable

expansion parameter. We obtain

minimal RS:

$$R_h \approx 1 - \frac{v^2}{2M_{\text{KK}}^2} (14.3 y_{\text{max}}^2 + 3.6) + \frac{v^4}{4M_{\text{KK}}^4} (62.6 y_{\text{max}}^4 + 47.1 y_{\text{max}}^2 + 4.4),$$

custodial RS:

$$R_h \approx 1 - \frac{v^2}{2M_{\text{KK}}^2} (51.8 y_{\text{max}}^2 + 7.3) + \frac{v^4}{4M_{\text{KK}}^4} (555.1 y_{\text{max}}^4 + 930.7 y_{\text{max}}^2 - 109.4). \quad (4.3.67)$$

The relative error of this parametrization compared to the exact median result is below 10% for $M_{\text{KK}} > 0.55 y_{\text{max}}$ in the minimal, and $M_{\text{KK}} > 1.42 y_{\text{max}}$ in the custodial model. The constant term in parenthesis of the second order coefficient is due to the shifted Higgs VEV κ_v . The second order y_{max} dependent coefficient and the fourth order coefficients are estimated from the exact numerical data. We see that the fourth order coefficients are large and partly counteract the large suppression of the second order coefficients. Nevertheless, the sensitivity of R_h to the overall size of the 5d Yukawa couplings is even more pronounced than the one arising from dipole-operator transitions such as $B \rightarrow X_s \gamma$ [255]. While the latter contributions also scale with y_{max}^2 , unlike R_h , they are (at the one-loop level) insensitive to the multiplicity of states in the KK-fermion sector. The main difference is that overlap integrals with profiles of the light external fermions are involved. This feature underscores that precision measurements of the Higgs boson properties provide an extraordinary tool for illuminating the quantum structure of electroweak interactions in RS scenarios.

Particularly, in the minimal RS model, the constraints from EWPOs related to the $Zb\bar{b}$ coupling restrict the size of the $\mathcal{O}(1)$ Yukawa couplings from below, as shown in figure 4.16. Oblique corrections to EWPOs constrain the KK excitations of SM particles to have masses in the 10 TeV range, *i.e.* $M_{\text{KK}} \gtrsim 4 \text{ TeV}$, what puts them outside of the reach for direct production at the LHC. Figure 4.25 shows that even for such a high KK-scale there can be significant virtual effects of KK particles in the Higgs-production cross section, provided that the 5d Yukawa couplings are not too small. We also discussed that the bounds from oblique correction can be relaxed either by one-loop contributions or by modifications of the model. An example is the LRS model, in which the size L of the extra dimension is reduced [192]. For R_h , this would only affect the subleading constant term in (4.3.67) and induce a shift of +4% at $M_{\text{KK}} = 1.5 \text{ TeV}$.

Suppression effects in $gg \rightarrow h$ were also reported in [207, 236, 439]. A direct numerical comparison with our findings is however not possible, since [207] only included zero-mode corrections, while [236, 439] studied RS variants that differ from the specific set-up considered here. In [440] the authors studied corrections to gluon–gluon fusion arising from virtual exchange of one light fermionic KK mode without considering the large multiplicity of KK fermions, which we found to be important. There, it is claimed that for a heavy bottom-quark partner with a mass $m_{b'}$ of a few hundred GeV, the Higgs-production cross section via $gg \rightarrow h$ can be significantly enhanced. We would like to point out that in order to achieve $m_{b'} \ll M_{\text{KK}}$ with the embedding of quarks as chosen in section 3.3.5.2, the P_{LR} symmetry has to be broken strongly via the bulk-mass parameters of the \mathcal{T}_1 multiplets by choosing $c_{\mathcal{T}_1 i}$ rather far away from $c_{\mathcal{T}_2 i}$. First of all, such choices of parameters need to be fine-tuned to reproduce the measured mass spectrum of the SM quarks for anarchic Yukawa couplings. Secondly, we found that, the bulk mass dependent terms of the top coupling modification cancel to a large

extent against the bulk mass dependent terms of the resummed KK-loop contribution. This result depends only on the approximation of a unit form factor for all KK quarks, which is applicable even for the light KK-quark masses considered in [440]. We furthermore add that choices of $c\tau_{1i}$ corresponding to a strong breaking of the P_{LR} symmetry lead, barring an accidental cancellation, to a sizable negative shift in the $Zb_L\bar{b}_L$ coupling, which is problematic in view of the stringent constraints arising from the $Z \rightarrow b\bar{b}$ pseudo observables discussed in section 4.2.2. As discussed in the previous section, also the authors of [429] attempt to resum all KK-loop contributions. However, their result for the Wilson coefficient is of approximately opposite sign, since they take into account the unphysical contribution from infinitely heavy KK resonances, which we have shown to be absent in a properly UV-regulated theory.

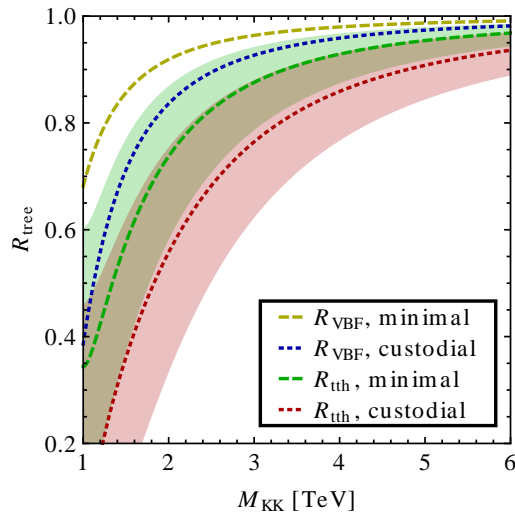


Figure 4.26: Ratios for the subleading Higgs production cross sections in RS over the SM result. The dashed lines show the result in the minimal, while the dotted lines correspond to the custodial RS model. The ratio for the vector-boson-fusion mode also applies to associated production with a W boson. For the associated production with top quarks, the result for the median value and the two-sided 90% quantile band are shown for $y_{\max} = 3$.

Compared to gluon–gluon fusion, Higgs boson production through weak gauge-boson fusion, $qq^{(\prime)} \rightarrow qq^{(\prime)}V^*V^* \rightarrow qq^{(\prime)}h$ with $V = W, Z$, receives moderate corrections of around -8% in the minimal and -16% in the custodial model for $M_{\text{KK}} = 2 \text{ TeV}$, due to a fast decoupling behavior. However, the corrections become very relevant for a lower KK-scale, namely -14% and -29% or $M_{\text{KK}} = 1.5 \text{ TeV}$. The same reduction also affects associated W -boson production²⁵, $q\bar{q}' \rightarrow W^* \rightarrow Wh$. We calculate the modification factors of the cross section in RS compared to the SM $R_{\text{VBF}} = R_{Wh} = \kappa_v^2 |\kappa_W|^2$ by the ratio of the leading tree-level results. Remark that the shifted Higgs VEV slightly reduces this modification. We show the general result in figure 4.26. There, we also show the modification of the cross section of associated top-quark-pair production, $q\bar{q} \rightarrow t\bar{t}^* \rightarrow t\bar{t}h$, which experiences a reduction, as well. It is given by $R_{tth} = \text{Re}(\kappa_t)^2 / \kappa_v^2$. For values of the KK scale in the ballpark of 2 TeV, this suppression typically amounts to -20% and -40% .

²⁵The modifications of Z - and W -boson fusion are in principle different in the minimal model, but the total weak gauge boson fusion rate is dominated by the W due to its larger coupling to quarks.

4.3.4.2 Decays Channels: General Aspects, ZZ , $b\bar{b}$

In the following, we quantitatively discuss the modifications of all decay channels that are relevant and can be observed at the LHC. We have already seen that all production channels and the tree-level couplings for decays into weak gauge bosons and b -quark pairs are suppressed in most of the parameter space. We will show that the most important decay channel into $\gamma\gamma$ is on the contrary enhanced. We will investigate the interesting interplay between the modifications in production and decay. Finally, we will discuss the decay into the γZ final state, which could in principle become phenomenologically interesting in the future, but turns out to be less useful for constraining the RS model.

We start with a general overview of how our intermediate quantities for the Higgs VEV shift and coupling modifications have to be combined in order to form modification ratios for the partial decay widths

$$\begin{aligned} \frac{\Gamma(h \rightarrow VV)_{\text{RS}}}{\Gamma(h \rightarrow VV)_{\text{SM}}} &= \kappa_v^2 |\kappa_V|^2, \quad V = WW, ZZ, \\ \frac{\Gamma(h \rightarrow A)_{\text{RS}}}{\Gamma(h \rightarrow A)_{\text{SM}}} &= \frac{|\kappa_A|^2}{\kappa_v^2}, \quad A = \gamma\gamma, \gamma Z, \\ \frac{\Gamma(h \rightarrow f\bar{f})_{\text{RS}}}{\Gamma(h \rightarrow f\bar{f})_{\text{SM}}} &= \frac{\text{Re}(\kappa_f)^2}{\kappa_v^2}, \quad f = b, t, \end{aligned} \quad (4.3.68)$$

and the total width of the Higgs

$$R_\Gamma \equiv \frac{\Gamma(h)_{\text{RS}}}{\Gamma(h)_{\text{SM}}} = 1 + \sum_{f=b\bar{b}, WW, ZZ} \text{BR}(h \rightarrow f) \left(\frac{\Gamma(h \rightarrow f)_{\text{RS}}}{\Gamma(h \rightarrow f)_{\text{SM}}} - 1 \right) + \text{BR}(h \rightarrow gg) (R_h - 1), \quad (4.3.69)$$

where we neglect the modification of branching ratios smaller than $\text{BR}(h \rightarrow ZZ)$ and the modification of $\text{BR}(h \rightarrow \tau^+\tau^-)$. Due to the UV localization of leptons, the latter is expected to be changed much less than the decay into $b\bar{b}$, which we discuss below. Finally, we also consider the combined process of production and decay for the restricted case of pure production from gluon–gluon fusion.

$$R_f \equiv \frac{[\sigma(gg \rightarrow h)\text{BR}(h \rightarrow f)]_{\text{RS}}}{[\sigma(gg \rightarrow h)\text{BR}(h \rightarrow f)]_{\text{SM}}} = \frac{R_h}{R_\Gamma} \frac{\Gamma(h \rightarrow f)_{\text{RS}}}{\Gamma(h \rightarrow f)_{\text{SM}}}. \quad (4.3.70)$$

We consider this quantity to be a guideline for the decays into the ZZ and $\gamma\gamma$ final state at the LHC. For a more precise analysis one should sum all production cross sections

$$\epsilon_{\text{ggF}}^f \sigma(gg \rightarrow h) + \epsilon_{\text{VBF}} \sigma(qq^{(\prime)} \rightarrow qq^{(\prime)} V^* V^* \rightarrow qq^{(\prime)} h) + \epsilon_{\text{Vh}} \sigma(q\bar{q}' \rightarrow W^* \rightarrow Wh), \quad (4.3.71)$$

with appropriate weight factors ϵ_X^f accounting for experimental efficiencies and cuts. The necessary data for such an analysis is not publicly available at present. A first step was made by the experimental collaborations, to break the data into two production categories, one including production from weak gauge boson fusion and the other associated W/Z production only [24, 36], but the resulting errors on the signal strengths are in most cases roughly $\pm 100\%$. Meanwhile, for all channels where gluon–gluon fusion dominates, we get a first estimate of potential constraints from R_f . Moreover, it has been discussed in [376] that a good intermediate solution is to consider ratios $R_f/R_{f'}$ for different final states f, f' . If both

final states have similar efficiencies, a large part of the uncertainties from the production processes and also from the total width drops out. The result with our simple definition of R_f is the same. For $f = b\bar{b}$, our definition of R_f is of little interest, since the observation of this state has to proceed almost exclusively from associated production with a W boson, in order to suppress the large background.

We begin the numerical discussion with the two largest branching ratios into $b\bar{b}$ and WW , in order to understand the behavior of the main modifications of the total Higgs width. Equivalently to the WW channel, we consider ZZ here, as it is more important for later purposes. Both channels receive the exact same modification in the custodial model and are 100% correlated (at tree level) in the minimal model, where the modifications in the WW channel are suppressed with c_w^2 compared to the ZZ channel.

The full numerical results for the total width are displayed in figure 4.27, where we also account for the subleading modifications included in (4.3.69). For natural values of the Yukawa

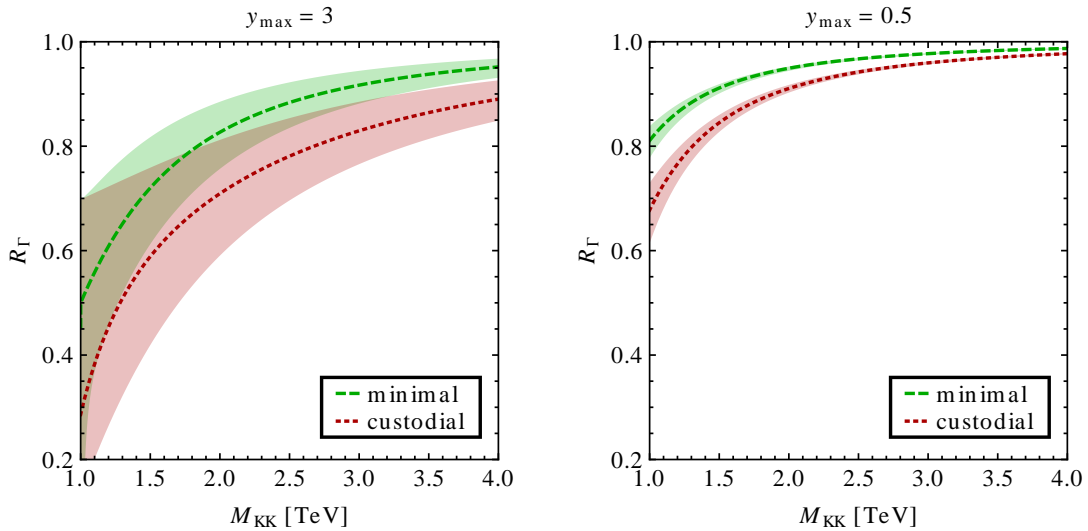


Figure 4.27: Modifications of the total Higgs width for a natural value of y_{\max} (left column) and an order of magnitude lower value (right column). The dashed lines show the median result in the minimal, while the dotted lines correspond to the custodial RS model. The shaded regions indicate the two-sided 90% quantile bands corresponding to the median line of the same color. Detailed views of the single bands are given in figure B.6.

entries, the depletion in R_Γ stems mainly from the reduced width into $b\bar{b}$. For $M_{\text{KK}} = 1.5$ TeV, it reaches -28% and -41% in the minimal and custodial model, respectively. We observe that part of this reduction in R_Γ does not decouple with y_{\max} . This is obvious for the WW contribution, due to the suppressed $WW h$ coupling, but also applies partly for the $b\bar{b}$ contribution, which is affected by the modified Higgs VEV. Even in the limit of vanishing Yukawa elements (or heavily fine tuned cancellations) a depletion of -7% and -13% remains in the given example. This has an interesting effect on the branching ratios into the ZZ compared to the $b\bar{b}$ state, which we present in figure 4.28. For natural values of the Yukawa entries, a large part of the reduction in the partial and total width cancels in all cases. Nevertheless, the reduction in the $b\bar{b}$ channel is typically larger such that the branching ratio into $b\bar{b}$ is typically reduced — and quite severely in the custodial model — while the branching ratio in ZZ is mostly enhanced. The spread due to the new physics parameter

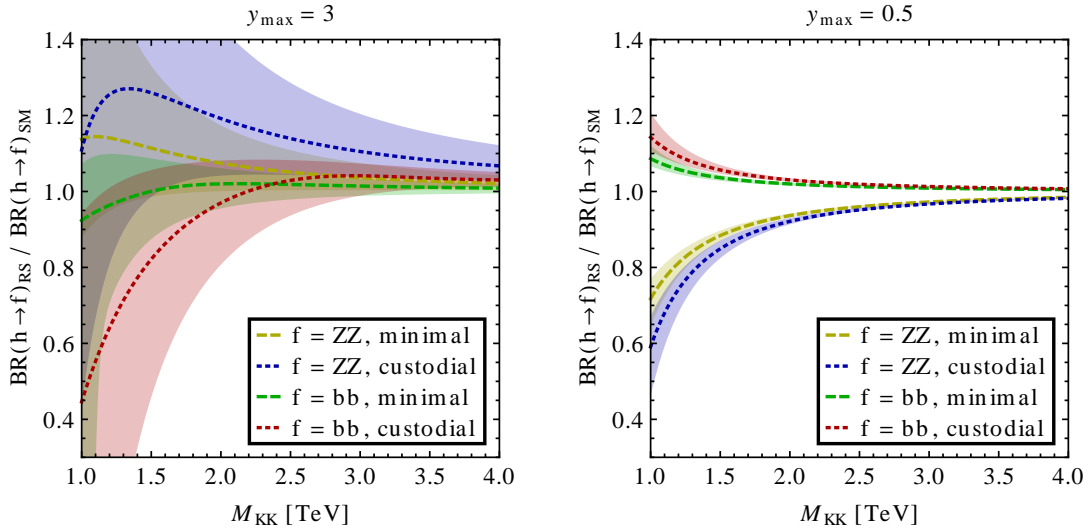


Figure 4.28: Modifications of the branching ratios for decays into ZZ and $b\bar{b}$. The interpretation of the displayed curves and bands is analogous to figure B.6. Detailed views of the single bands are given in figures B.3 and B.4.

space is of course large in this region such that no definite claims can be made, except that large enhancements in the $b\bar{b}$ channel are excluded. The behavior is totally reversed in the case of an order of magnitude lower Yukawa entries, where the modifications are typically smaller but less outspread. This is remarkable, since it allows to constrain the RS setup even in the case of tuned Yukawa matrices.

We illuminate the possible constraint from the gauge structure in figure 4.29, where we show the combined modification of production and subsequent decay into ZZ . The general dependence on y_{\max} and M_{KK} follows closely the dependence of R_h , as shown in figure 4.25. For natural values of y_{\max} above one, the suppression is slightly less than in R_h . For values of y_{\max} below one, the modification shrinks visibly slower than in R_h , since the rising total width and the suppressed ZZh coupling sets in. We assume a bound of at most 52% suppression, *i.e.* $R_{ZZ} > 0.48$. This value was found in an unfolding of the recent data attempted in [416] at a CL of 95%. We then derive from the 95% quantile of our parameter distribution of the custodial model a bound of $M_{\text{KK}} > 1.1$ TeV (first KK-gluon mass $M_{G^{(1)}} > 2.8$ TeV) for the case that the Yukawa is an order of magnitude lower than expected, *i.e.* $y_{\max} = 0.5$. The bound becomes higher for natural values of the Yukawa entries, but then one cannot exclude a region with low KK-scale: we obtain $M_{\text{KK}} \notin [2.0, 3.7]$ TeV ($M_{G^{(1)}} \notin [4.8, 9.1]$ TeV). In the minimal model, we derive in the same way a bound below 1 TeV for the order of magnitude reduced, and $M_{\text{KK}} > 1.9$ TeV ($M_{G^{(1)}} > 4.7$ TeV) for natural Yukawa entries.

We add that for the given Higgs mass, also the decay into a bottom and a strange quark is in principle possible, since the Higgs couplings have non-vanishing off-diagonal entries in the RS model. We find even for the custodial model, a KK-scale $M_{\text{KK}} = 1$ TeV and $y_{\max} = 3$, that 95% of the parameter space give a result for the branching ratio below $8 \cdot 10^{-3}$, which is way below the observable levels.

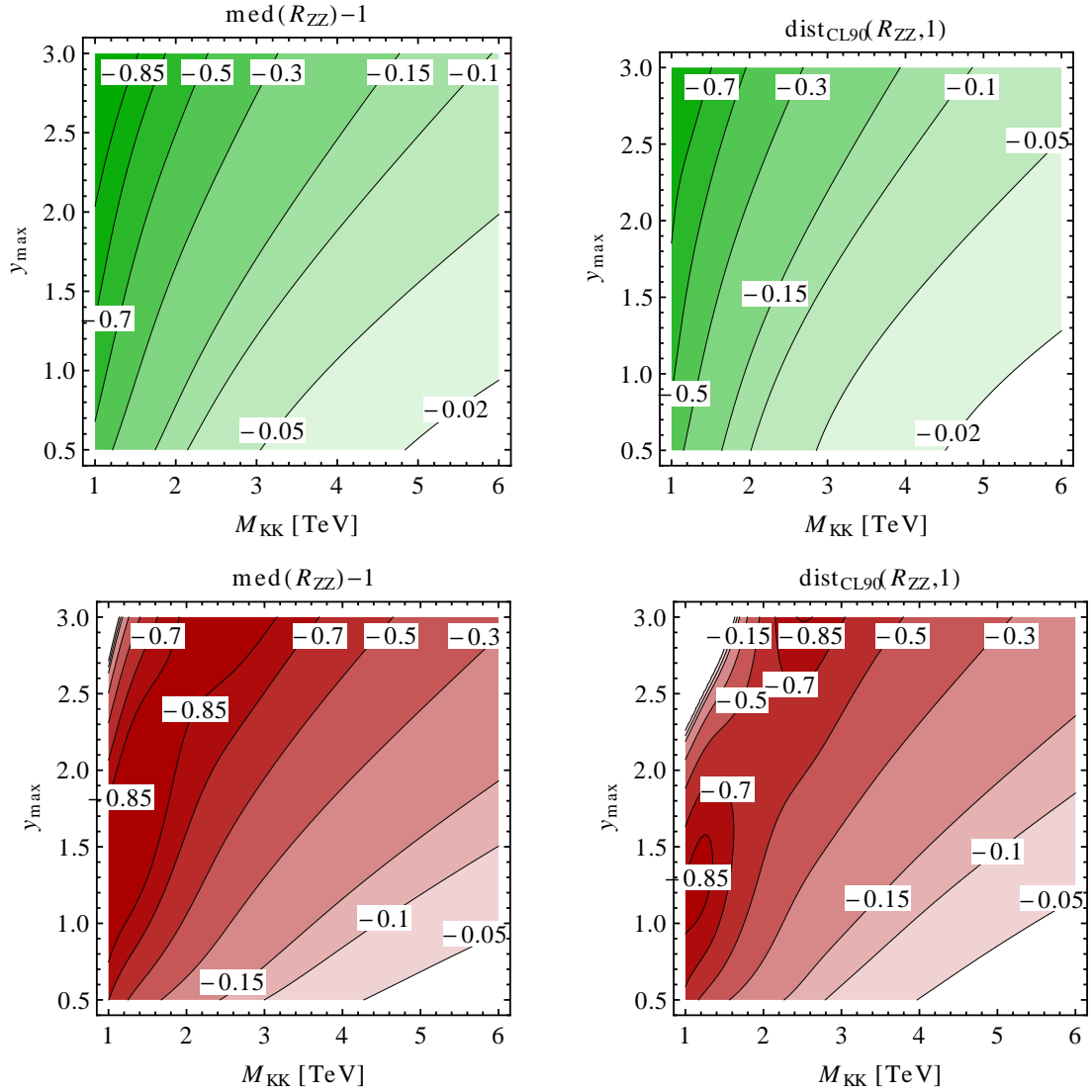


Figure 4.29: Modification factors R_{ZZ} for Higgs production and subsequent decay into two ZZ bosons. The upper row (green shading) shows the results for the minimal model and the lower (red shading) for the custodially protected model. In the left panels we show the distance of the typical, *i.e.* median, value from the SM result. In the right panels we give the distance of the two-sided 90% two sided quantile of the RS parameter distribution from the SM result. The distance is defined to be negative if the quantile band is below one and to be zero if the band overlaps with one.

4.3.4.3 The Decay into $\gamma\gamma$

We come to the most relevant decay channel into $\gamma\gamma$. Similar to (4.3.34) we write the ratio of leading order one-loop diagrams of the RS model relative to the SM as

$$\kappa_\gamma = \frac{\kappa_W A_W^h(\tau_W) + C_W^{\text{KK}} + \sum_{i=t,b} N_c Q_i^2 \text{Re}(\kappa_i) A_q^h(\tau_i) + \sum_{q=u,d,\lambda} N_c Q_q^2 C_{q,1}^{\text{KK}} + Q_l^2 C_{l,1}^{\text{KK}}}{A_W^h(\tau_W) + \sum_{i=t,b} N_c Q_i^2 A_q^h(\tau_i)}. \quad (4.3.72)$$

All Wilson coefficients are understood to be evaluated at the scale M_h . We neglect $\kappa_{\gamma 5}$ here, since its relative contribution to κ_γ is expected to be even smaller than $\kappa_{g 5}$ was for R_h , because of the dominant SM W -boson contribution for a light Higgs mass.

The Wilson coefficient $C_{l,1}^{\text{KK}}$ in (4.3.72) encodes effects from KK-leptons. However, we do not examine the different possibilities to realize the lepton sector, and the ways to generate right-handed neutrino masses [186, 199, 258, 441]. Here, we only assume a minimal realization, *i.e.* SM-representations in the minimal model and two $SU(2)_R$ doublets that replace the singlets in the custodial model. Since all KK-fermion contributions add constructively, this is a conservative way to estimate the minimal effect. Under this assumptions the details of the precise lepton spectrum can be entirely omitted to a very good approximation with the following trick [442]. We rewrite the KK-fermion contributions to (4.3.72) by reusing the ggh Wilson coefficient C_1^{KK} as

$$\sum_{q=u,d,\lambda} N_c Q_q^2 C_{q,1}^{\text{KK}} + Q_l^2 C_{l,1}^{\text{KK}} = \frac{4N_c}{9} C_1^{\text{KK}} + \frac{7N_c}{3} C_{\lambda,1}^{\text{KK}} + \left[C_{l,1}^{\text{KK}} - \frac{N_c}{3} C_{d,1}^{\text{KK}} \right], \quad (4.3.73)$$

where $C_{\lambda,1}^{\text{KK}}$ is only non-zero in the custodial model, but obviously has a large impact in the custodial model, due to the enhancement with the squared charge. We now use that — by construction of the model — the fundamental Yukawa matrices are random matrices with elements of similar magnitude. The last two terms in square brackets therefore tend to cancel each other, especially since (4.3.65) shows that the function f is mostly determined by the largest eigenvalue of $\tilde{\mathbf{Y}}_q \tilde{\mathbf{Y}}_q^\dagger$. For the scan over the parameter space, which we present below, a full inclusion of KK-lepton effects would not change average values and only marginally increase the spread, which is dominated by the dependence on the total width as we shall see. We can therefore safely neglect the terms in square brackets in (4.3.73). We emphasize that (4.3.73) relates the most important fermion contribution to κ_γ , which stems from all fermions with non-exotic charge $Q_{d,u}$, to the shift in the ggh amplitude κ_g . This is an interesting correlation, which enhances the constraining power of bounds on the $\gamma\gamma$ signal strength.

For the evaluation of (4.3.72), it is furthermore necessary to take into account all modifications of the triangle diagram with a weak gauge boson. By working in unitary gauge, it is also sufficient. Firstly, the WW^h -coupling is modified by the factor κ_W , which was defined in (3.3.152). Furthermore, we also have to include KK- W -boson loops. We resum them by using the 5d gauge boson propagator for vanishing momentum, which we derived in section 3.3.7. Observe, that in the case of gauge bosons, each term in the KK-sum over the 4d diagrams carries a mass squared in the denominator. Thus, the sum shows absolute convergence and there arise no subtleties of the kind we encountered for triangle diagrams with very heavy KK-fermions. In the calculation of the Wilson coefficient C_W^{KK} , we can safely use the decoupling limit for the form factors. Since $m_1^W \approx 2.5 M_{\text{KK}} \gg M_h$, corrections in the relevant mass

ratio $\tau_n^W \equiv 4(m_n^W)^2/M_h^2$ of order $\mathcal{O}(\tau_{W^{(1)}}^{-1})$ are sub per-mil. Setting $\vec{d}_W \equiv (c_W, -s_W)^T$, we obtain for both, the general custodial, and the minimal RS model ($c_W = 1$) the result

$$\begin{aligned} C_W^{\text{KK}} &= \frac{2\pi M_W^2}{c_W^2 M_{\text{KK}}^2} \sum_{n=1}^{\infty} \frac{\vec{d}_W^T \vec{\chi}_n^W(1) \vec{\chi}_n^W(1)^T \vec{d}_W}{(x_n^W)^2} A_W^h(\tau_{W^{(n)}}) \\ &= \frac{2\pi M_W^2}{c_W^2 M_{\text{KK}}^2} \vec{d}_W^T [\Sigma_W^{(1)}(1, 1) - \Pi_W^{(1)}(1, 1)] \vec{d}_W \left(-\frac{21}{4} + \mathcal{O}(\tau_{W^{(1)}}^{-1}) \right) \\ &= -\frac{21}{8} (1 - \kappa_W) \left(1 + \mathcal{O}(\tau_{W^{(1)}}^{-1}) \right). \end{aligned} \quad (4.3.74)$$

We observe that the KK- W contribution is related to the modification of the W contribution.

All aspects discussed above are conveniently summarized in a simplified expression for κ_γ :

$$\begin{aligned} \kappa_\gamma &= 1 + \frac{1}{|A_W^h(\tau_W)| - \frac{4}{3}A_q^h(\tau_t) - \frac{1}{3}A_q^h(\tau_b)} \left[- (1 - \kappa_W) \left(|A_W^h(\tau_W)| - \frac{21}{8} \right) \right. \\ &\quad \left. + (1 - \kappa_g) \frac{4}{3} \left(A_q^h(\tau_t) + A_q^h(\tau_b) \right) - (1 - \text{Re}(\kappa_b)) A_q^h(\tau_b) + 7(-C_{\lambda,1}^{\text{KK}}) \right]. \end{aligned} \quad (4.3.75)$$

This simplified result neither relies on any specific quark embedding, nor on the requirement of P_{LR} symmetry. We observe several cancellations between the various RS contributions. We already used the information on signs in the relevant Higgs mass range to make the cancellations more obvious in (4.3.75). The first term in square brackets comprises the negative contribution from the reduction of the $WW h$ -coupling, which is in turn canceled to approximately 42% by the contribution from higher KK modes of the W boson. The fermionic RS contribution comes with a positive sign, *i.e.* it interferes constructively with the SM amplitude. It is proportional to the modification in the ggh amplitude up to a very small negative correction factor for the b -quark and, in the custodial model, on additional large positive contribution from the exotic quarks.

We find an enhancement in the branching ratio $\text{BR}(h \rightarrow \gamma\gamma)$, which reaches large values for natural Yukawa entries and low values of M_{KK} . The combined fermionic contributions dominate over the reduction from the combined W contribution. In the minimal model, a large part of the total enhancement of the branching is due to the reduced total width. Together with the contributions from the exotic quarks, this leads to a massive total enhancement, in the custodial model. In this case, one can also nicely observe the saturation of the function f for high argument values, which we already mentioned in the discussion of R_h . We show this in the left panel of figure 4.30 for $y_{\text{max}} = 3$. In this case, the spread due to the total width becomes very large. We observe that the minimal modification, as inferred from the 5% quantile, has a maximum of $\text{BR}(h \rightarrow \gamma\gamma) = 3.2$ at $M_{\text{KK}} = 1.5 \text{ TeV}$. Somewhat unexpectedly, it decreases for lower values of M_{KK} . This comes from the exact treatment of Yukawa couplings and the resummation of KK loops. As we see from (4.3.65), the function f reaches a maximum for an eigenvalue of $\tilde{y}_q^i = 3.4 (M_{\text{KK}}/\text{TeV})$ and decreases for even higher values. The decrease in $\text{BR}(h \rightarrow \gamma\gamma)$ can thus be ascribed to the part of the parameter space with large eigenvalues of the squared Yukawa matrices. In combination with the deviations in the production cross section from gluon–gluon fusion, this typically leads to strong suppression for $M_{\text{KK}} \gtrsim 2 \text{ TeV}$ and strong enhancement for $M_{\text{KK}} \lesssim 2 \text{ TeV}$. However, the huge spread due to the choice of Yukawa matrices allows for no definite prediction in the latter region. For a lowered value $y_{\text{max}} = 1.5$, the region of possible enhancement is already shifted to $M_{\text{KK}} \lesssim 1.1 \text{ TeV}$ and it is

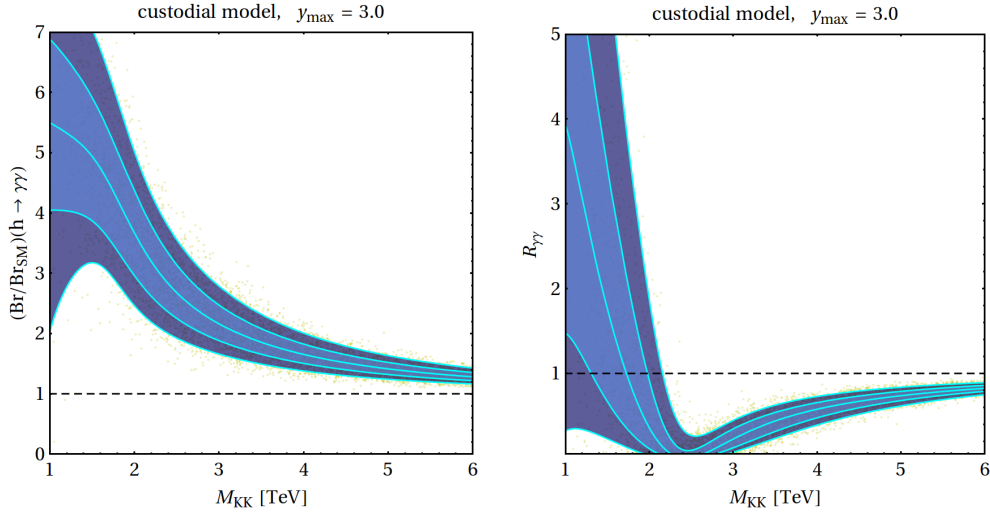


Figure 4.30: Fitted modification factor of the branching ratio (left panel), and preceding production from gluon–gluon fusion (right panel), for a decay into two photons in the custodial RS model with $y_{\max} = 3$, compared to the SM. See figure 4.24 for further descriptions.

effectively non-existent, when we go to even lower values of y_{\max} , as well as in the minimal model. Further details on the parametric behavior are deferred to appendix B.4 (figures B.7 and B.8).

A strong suppression of $R_{\gamma\gamma}$ prevails even for a low value of $y_{\max} = 0.5$. We find this region to be of interest, since for a low value of y_{\max} all relevant production channels are reduced by approximately the same amount, if we consider the lower tail of the deviations from the SM. The fact that the central values for the signal strength $\mu_{\gamma\gamma}$ of the recent data from both CMS and ATLAS are above one already allows us to derive a robust bound on the KK-scale. Weighting the main production mechanisms with the appropriate efficiencies like in (4.3.71), we obtain

$$\mu_{\gamma\gamma}|_{\text{RS}} = \left(1 + \frac{\epsilon_{\text{VBF}}^{\gamma\gamma} \sigma_{\text{VBF}} + \epsilon_{\text{Vh}}^{\gamma\gamma} \sigma_{\text{Vh}}}{\epsilon_{\text{ggF}}^{\gamma\gamma} \sigma_{\text{ggF}} + \epsilon_{\text{VBF}}^{\gamma\gamma} \sigma_{\text{VBF}} + \epsilon_{\text{Vh}}^{\gamma\gamma} \sigma_{\text{Vh}}} \left[\frac{R_{\text{VBF}}}{R_h} - 1 \right] \right) R_{\gamma\gamma}|_{\text{RS}}. \quad (4.3.76)$$

As long as the factor in square brackets is negative, or at least small, we can derive a bound from the comparison of a minimal expected RS suppression factors, with the minimally allowed experimental value at a given CL q^e :

$$\max_{\text{CL}=q^t}(\mu_{\gamma\gamma})_{\text{RS}} < \max_{\text{CL}=q^t}(R_{\gamma\gamma})_{\text{RS}} < \min_{\text{CL}=q^e}(\mu_{\gamma\gamma}). \quad (4.3.77)$$

Here, the maximum denotes the largest value of the theory’s q^t -quantile, *i.e.* a fraction q^t of the parameter space has stronger suppression. We choose $q = q^e = q^t = 95\%$ and 98% and use the bounds of the CMS measurement on the signal strength [29]. The resulting bounds are given in table 4.2 and are already of an interesting size in the custodial model, comparable to the bounds that remain from EWPOs (see (4.2.23)). We remark that the bound is of course not expected to increase strongly in the near future if additional analyzed data would point towards a more SM-like value of $\mu_{\gamma\gamma}$.

We end the discussion of the $\gamma\gamma$ -decay channel with a derived observable that could potentially be interesting in the near future. Using the ratio $R_{\gamma\gamma}/R_{ZZ}$, in the narrow width

RS model	q	$M_{\text{KK}} _{\text{min}}$	$M_{G^{(1)}} _{\text{min}}$	$R_{\text{VBF}}/R_h - 1$
custodial	95%	1.6	4.0	-0.09
custodial	98%	1.3	3.1	-0.21
minimal	95%	1.1	2.6	-0.16
minimal	98%	0.8	2.0	-0.30

Table 4.2: Lower bounds on the KK-scale inferred from the signal strength $\mu_{\gamma\gamma}$ measured by CMS [29], for small RS Yukawa matrices $0.05 < |(Y_q)_{ij}| < 0.5$.

approximation all reference to the production mechanism and total width drops out. Since they present the main source of spread in the factors $R_{\gamma\gamma}$ and R_{ZZ} due to the new physics parameter freedom, we obtain a more definite prediction than for the ratios $R_{\gamma\gamma}$ and R_{ZZ} alone. On the experimental side, a similar cancellation also occurs in the full ratio $\mu_{\gamma\gamma}/\mu_{ZZ}$ with properly weighted production cross sections, as long as one production channel is dominant or if the experimental efficiencies for both final states are similar. The former could be enforced by adding a 0-jet veto to the production mechanisms, which however reintroduces significant theoretical uncertainties [389, 443] that may not vanish in the ratio.

In the RS model, the ratio is in general enhanced as we show in figure 4.31. The enhancement is very strong in the custodial model and implies that the ratio has a good potential to bound the model. With the recent experimental data however, an enhancement rather accommodates the central values obtained by both experiments. Naively performing a weighted average of the ATLAS and CMS results given in table 4.1 without taking into account any correlations, we obtain $\mu_{\gamma\gamma}/\mu_{ZZ} = 1.9(6)$. Such enhancements can be achieved in the custodial model with low KK scale. Conversely hypothesizing a future measurement with 25% accuracy — according to [376] this should be possible with the final data set of the 2012 LHC run — and a central value of $\mu_{\gamma\gamma}/\mu_{ZZ} = 1$, we can see from the lower right panel in figure 4.31 that $R_{\gamma\gamma}/R_{ZZ}$ could indeed constrain the region with natural $y_{\text{max}} = 3$ to have $M_{\text{KK}} > 4.5$ TeV ($M_{G^{(1)}} > 10.9$ TeV), as inferred from the $q(=q^e=q^t) = 95\%$ CL. Presently however, the region of a KK scale $M_{\text{KK}} \lesssim 2$ TeV with natural Yukawa matrices is well suited to explain the central values of Higgs decays into bosons given by the CMS experiment.

4.3.4.4 The Decay into γZ

In order to compute also the second most interesting loop-induced decay channel, $h \rightarrow \gamma Z$, we use the ratio of RS to SM amplitude

$$\kappa_{\gamma Z} = \frac{1}{A_W^h(\tau_W, \lambda_W) + \sum_{i=t,b} N_c \frac{2Q_i \hat{v}_i}{c_w} A_q^h(\tau_i, \lambda_i)} \left[\kappa_W A_W^h(\tau_W, \lambda_W) + C_W^{\gamma Z, \text{KK}} \right. \quad (4.3.78)$$

$$\left. + \sum_{i=t,b} N_c \frac{2Q_i \hat{v}_i}{c_w} \text{Re}(\kappa_i \kappa_{Z,i}^V) A_q^h(\tau_i, \lambda_i) + \sum_{q=u,d,\lambda} N_c \frac{2Q_q \hat{v}_q}{c_w} C_{q,1}^{\gamma Z, \text{KK}} + \frac{2Q_l \hat{v}_l}{c_w} C_{l,1}^{\gamma Z, \text{KK}} \right].$$

We inserted the vectorial Z -fermion coupling \hat{v}_f as defined in (4.3.10). The first term in the numerator of (4.3.78) encodes the contribution to the $h \rightarrow \gamma Z$ transition arising from the W -boson-triangle graph. In principle, this also contains modifications of the triple gauge-boson coupling of the zero modes $g_{W^+W^-Z}$. As we discussed in section 3.3.8.3, they are suppressed by $\mathcal{O}(v^4/M_{\text{KK}}^4)$. We set them to their SM values in the evaluation of Higgs boson branching

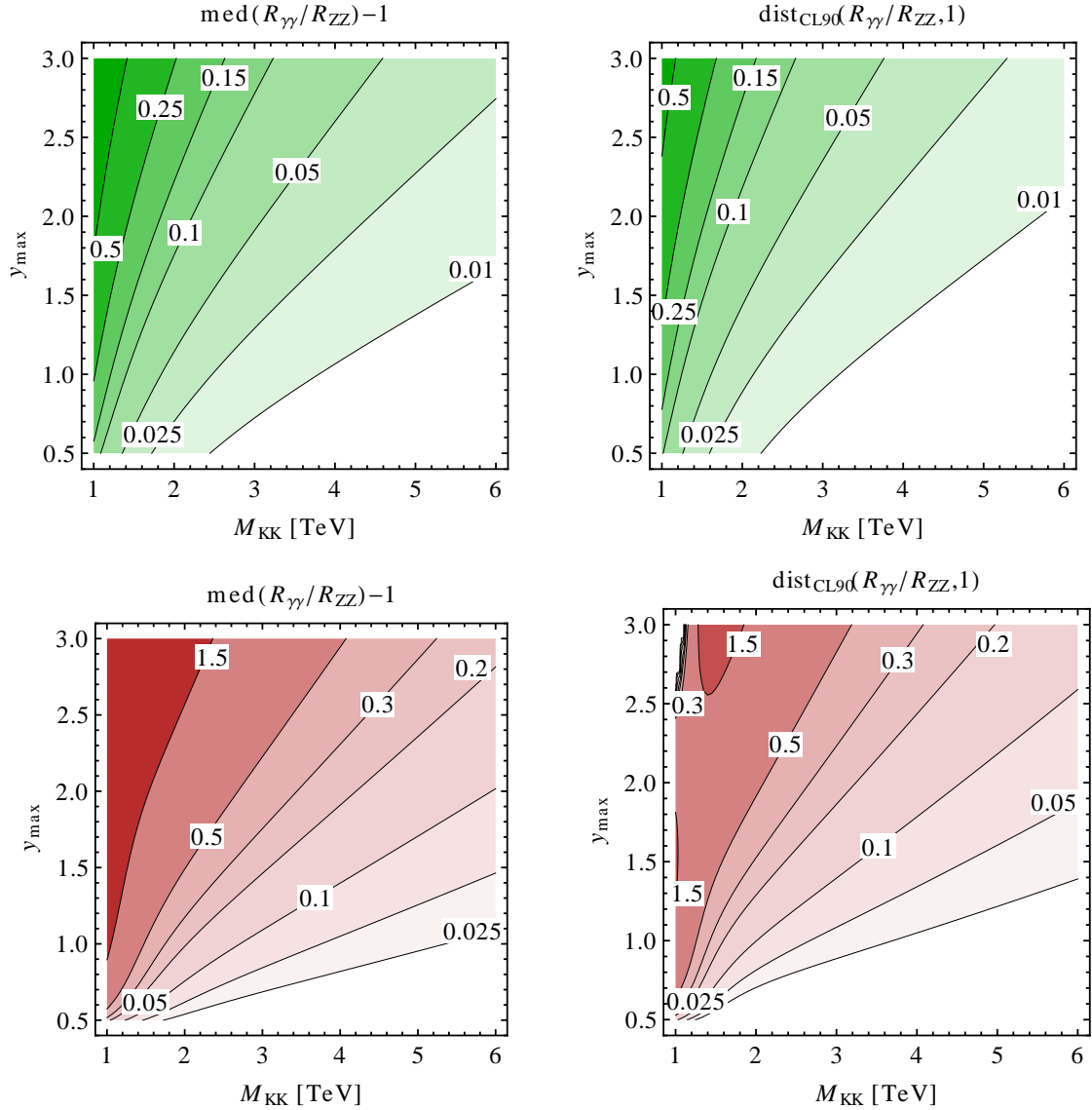


Figure 4.31: Ratio of the modification factors $R_{\gamma\gamma}/R_{ZZ}$. The upper row (green shading) shows the results for the minimal model and the lower (red shading) for the custodially protected model. In the left panels we show the distance of the typical, *i.e.* median, value from the SM result. In the right panels we give the distance of the two-sided 90% quantile of the RS parameter distribution from the SM result. The distance is defined to be negative if the quantile band is below one and to be zero if the band overlaps with one.

fractions. In this approximation the effect of virtual W -boson exchange is equivalent to the effect in the decay to $\gamma\gamma$.

The Wilson coefficient $C_W^{\gamma Z, \text{KK}}$ in (4.3.78) incorporates triangle diagrams with charged KK-boson excitations in the loop, displayed in the upper right corner of figure 4.21. This contribution can be written as

$$C_W^{\gamma Z, \text{KK}} = \frac{2\pi x_W^2}{c_W^2} \sum_{n=1}^{\infty} \frac{\vec{d}_W^T \vec{\chi}_n^W(1) \vec{\chi}_n^W(1)^T \vec{d}_W}{(x_n^W)^2} \mathcal{I}_{nn0}^{WWZ} A_W^h(\tau_{W^{(n)}}, \lambda_{W^{(n)}}). \quad (4.3.79)$$

It is again an excellent approximation to evaluate the loop function $A_W^h(\tau_n^W, \lambda_n^W)$ in the infinite mass limit $\tau_n^W, \lambda_n^W \rightarrow \infty$. The form factor then becomes $7c_w - 11/(6c_w) \approx 4.0$. In (4.3.79) we denoted the overlap integral of KK- W bosons and the Z -boson zero mode by \mathcal{I}_{nn0}^{WWZ} . We find

$$\begin{aligned} \mathcal{I}_{nn0}^{WWZ} &= \frac{(2\pi)^{3/2}}{L} \int_{\epsilon}^1 \frac{dt}{t} \left[(\vec{\chi}_0^Z(t))_1 (\vec{\chi}_n^W(t))_1^2 + \left(-\frac{t_w^2}{c_w c_W} \right)^T \vec{\chi}_0^Z(t) (\vec{\chi}_n^W(t))_2^2 \right] \\ &= \frac{2\pi}{L} \int_{\epsilon}^1 \frac{dt}{t} \vec{\chi}_n^W(t)^T \text{diag} (1, t_w^2) \vec{\chi}_n^W(t) + \mathcal{O}\left(\frac{v^2}{M_{\text{KK}}^2}\right) \\ &= \left\{ \begin{array}{l} t_w^2, \quad \text{custodial RS} \wedge n \text{ odd} \\ 1, \quad \text{else} \end{array} \right\} + \mathcal{O}\left(\frac{v^2}{M_{\text{KK}}^2}\right). \end{aligned} \quad (4.3.80)$$

Since the first term in the sum of (4.3.79) is already suppressed by a factor of v^2/M_{KK}^2 , the computation of $C_W^{\gamma Z, \text{KK}}$ to this order in principle requires only the knowledge of the overlap integral to zeroth order. This leads to the very simple result (4.3.80), at which we have arrived in two steps. In the second line we neglected the modification of the even and odd zero-mode profile of the Z boson. We then used the fact that also W - W' mixing of the two KK-modes of any given KK-level only starts at $\mathcal{O}(v^2/M_{\text{KK}}^2)$. We find that this approximation is in fact reasonable in the minimal model, where the universality of \mathcal{I}_{nn0}^{WWZ} implies that the expression (4.3.79) can be solved with the same calculation like for C_W^{KK} for the $\gamma\gamma$ final state in (4.3.74)

$$\text{minimal RS: } C_W^{\gamma Z, \text{KK}} = \frac{1}{2} \left(7c_w - \frac{11}{6c_w} \right) (1 - \kappa_W), \quad (4.3.81)$$

which equals approximately -77% of C_W^{KK} given in (4.3.74). The modification of the SM-like W^+W^-h -vertex κ_W was given in (3.3.152).

We perform the sum in (4.3.79) numerically and without further approximations, including four KK-levels of bosons and extrapolate the higher KK-level contribution from the factor (B.4.3). The extrapolation has the practical effect that it makes the numerical value suitable for comparison with the approximation (4.3.81), which uses the analytic resummation with the 5d propagator. We compare values for the exact numerics with the analytic approximation for selected values of M_{KK} in table 4.3. The absolute values in this table are to be compared with the SM amplitude of $A_W^h(\tau_W, \lambda_W) = 5.796$. The zero mode RS contribution dominates in all cases and is canceled to approximately one third by the contribution of KK modes. Both contributions are approximately doubled in the custodial model with P_{LR} symmetry compared to the minimal model. We observe a fast decoupling with the KK-scale, but

	M_{KK} [TeV]	1	2	3	4	5	6
minimal	$C_W^{\gamma Z, \text{KK}}$ numerically	0.366	0.105	0.048	0.027	0.017	0.012
	rel. dev. to (4.3.81)	19.9%	4.4%	1.9%	1.0%	0.6%	0.4%
	$(\kappa_W - 1) A_W^h(\tau_W, \lambda_W)$	-1.257	-0.314	-0.140	-0.079	-0.050	-0.035
custodial	$C_W^{\gamma Z, \text{KK}}$ numerically	0.671	0.234	0.102	0.055	0.034	0.023
	rel. dev. to (4.3.80)	42.3%	9.1%	2.2%	0.8%	0.5%	0.3%
	$(\kappa_W - 1) A_W^h(\tau_W, \lambda_W)$	-2.550	-0.638	-0.283	-0.159	-0.102	-0.071

Table 4.3: Numerical results for the KK-W-boson Wilson coefficient obtained from a fit to a large set of valid parameter points in the minimal and the custodial RS model with P_{LR} symmetry. The third row shows the relative error of the approximate analytic result in (4.3.81) for the minimal RS model compared to the numerical evaluation. For the custodial RS model we calculate the deviation of the full result compared to the result when the overlap integral is approximated by (4.3.80). For comparison we give the RS contribution to the W zero-mode amplitude.

relevant modifications for low values of M_{KK} . Especially in the range $M_{\text{KK}} < 2 \text{ TeV}$ it is more appropriate not to use the approximation (4.3.80) of the bosonic overlap integral. The deviations listed in table 4.3 show that the higher order term neglected in (4.3.80) has a large coefficient, which we find to be of $\mathcal{O}(L)^{26}$. For this reason, we use a fit to the full numerical data of $C_W^{\gamma Z, \text{KK}}$ with a sufficiently high polynomial and use the result in the following evaluations.

The terms in the second row of (4.3.78) are due to the modification of the zero-mode-fermion triangle and such diagrams with KK fermions in the loop. This is summarized in the Wilson coefficients

$$C_{q,1}^{\gamma Z, \text{KK}} = \sum_{n=n_f+1}^{\infty} \frac{v}{m_n^q} \text{Re} (g_{nn}^q \kappa_{Z,q_n}^V) A_q^h(\tau_{q_n}, \lambda_{q_n}). \quad (4.3.82)$$

Compared to $C_{q,1}^{\text{KK}}$, we must also account for the modified Z -fermion couplings by the factor κ_{Z,q_n}^V . Analogous factors for the top and bottom quark enter the zero-mode-fermion triangle. They are generically given by the ratio of the vectorial couplings as

$$\kappa_{Z,q_n}^V = \left[1 + \frac{M_Z^2}{4M_{\text{KK}}^2} \left(1 - \frac{1}{L} \right) \right] \frac{(g_{Z,L}^q)_{nn} + (g_{Z,R}^q)_{nn}}{\hat{v}_q}, \quad (4.3.83)$$

where we use the modification factors $g_{Z,\sigma}^q$ defined in (3.3.142) and the universal shift of (3.3.141). Numerically the top coupling is typically moderately reduced compared to the SM. The bottom coupling is strictly reduced, but the shift is irrelevant due to the subleading form factor, and the coupling is even protected in the case of the custodial model.

Due to the modification factors κ_{Z,q_n}^V , an analytic calculation of the KK sum (4.3.82) turns out to be impractical. Below, we resort to a completely numerical evaluation of the sum along the same lines described for the previous processes. However, it is instructive to examine the

²⁶This is to be expected from the expansion of the bosonic zero-mode profile one order higher than in (3.3.80): we find the coefficient of $(M_W/M_{\text{KK}})^4$ to be of $\mathcal{O}(L)$.

structure of (4.3.82) more closely, in order to approximate the KK-lepton contributions, like we did for the calculation of the $\gamma\gamma$ final state. To estimate the typical size of $C_{l,1}^{\gamma Z, \text{KK}}$, we need an analytic formula for the relative strength of the vector coupling between the Z boson and fermionic KK modes in (4.3.82). We find

$$\kappa_{Z, f_n}^V = 1 - \frac{(\delta_F)_{nn} - (\delta_f)_{nn}}{\hat{v}_f} + \mathcal{O}\left(\frac{m_Z^2}{M_{\text{KK}}^2}\right), \quad (4.3.84)$$

where the elements of the matrices $\delta_{F,f}$ are of $\mathcal{O}(1)$, since fermion mixing is large in KK-levels above the zero-modes. In the fermion embedding of the custodial model with active P_{LR} symmetry, it turns out that for down- and λ -type KK quarks κ_{Z, f_n}^V depends solely on the electric charge and the third component of the weak isospin of the involved fermions. We obtain to excellent approximation

$$\kappa_{Z, f_n}^V = 1 + \frac{T_L^{3fL}}{\hat{v}_f}, \quad (f = d, \lambda), \quad (4.3.85)$$

in the custodial model, while no such formula can be derived for up-type quark KK modes or the fermion embedding of the minimal model. Employing the decoupling limit, $\tau_n^f, \lambda_n^f \rightarrow \infty$, *i.e.* $A_q^h(\tau_n^f, \lambda_n^f) \rightarrow -1/3$, we first derive the expected ratios of

$$\text{custodial RS: } C_{d,1}^{\gamma Z, \text{KK}} \approx -0.82 C_{d,1}^{\text{KK}}, \quad C_{\lambda,1}^{\gamma Z, \text{KK}} \approx -0.28 C_{\lambda,1}^{\text{KK}}, \quad (4.3.86)$$

and secondly, that a good conservative estimate for the leptonic contribution is given by

$$\frac{Q_l \hat{v}_l C_{l,1}^{\gamma Z, \text{KK}}}{N_c Q_d \hat{v}_d C_{d,1}^{\gamma Z, \text{KK}}} \approx \frac{Q_l (\hat{v}_l + T_L^{3l})}{Q_d (\hat{v}_d + T_L^{3d})} = \frac{3 - 6s_w^2}{3 - 2s_w^2} \approx 0.64. \quad (4.3.87)$$

Here, we have again assumed a minimal realization of the leptonic embedding in the custodial model as described above (4.3.73). We employ the estimate (4.3.87) in the numerical evaluation. Admittedly, we cannot resort to such an elegant argument for the minimal RS model. However, in that case we expect the leptonic KK contribution to be negligible. This is due to the fact that no exotic fermions contribute to fermion mixing in the minimal embedding. Pure fermion singlet–doublet mixing renders the diagonal elements of δ_F and δ_f to be of similar numerical size (close to 0.5) in the down sector, where — in contrast to the up sector — none of the mass splittings is generated by a very strong IR localization of a zero mode fermion. Therefore, we expect the splitting $(\delta_F)_{nn} - (\delta_f)_{nn}$ that enters (4.3.84) to be similarly small for leptons. The modified Z –fermion couplings affect (4.3.82) only little; thus, the size of the Wilson coefficients (4.3.82) becomes similar for down-quarks and leptons. The small ratio of $\hat{v}_l/\hat{v}_d \approx 0.11$ finally renders the lepton contribution subleading compared to the down-, and completely negligible compared to the up-quark contributions.

We show the numerical results for the branching ratio in figure 4.32. There, the EWPO constraints on the $Zb\bar{b}$ couplings at 3σ CL are imposed on top of the usual constraints on fermion masses and mixing angles, since the couplings enter one of the contributing diagrams. They EWPO bounds reduce the possible enhancement in the minimal model significantly, from 30% without to 18% after the constraints at $M_{\text{KK}} = 2.3\text{TeV}$. In order to obtain a reliable fit result, we exclude the region $M_{\text{KK}} < 2.3\text{TeV}$ where less than 10% of the parameter points survive the EWPO bounds on the $Zb\bar{b}$ -couplings. The typical enhancement is 11% at the

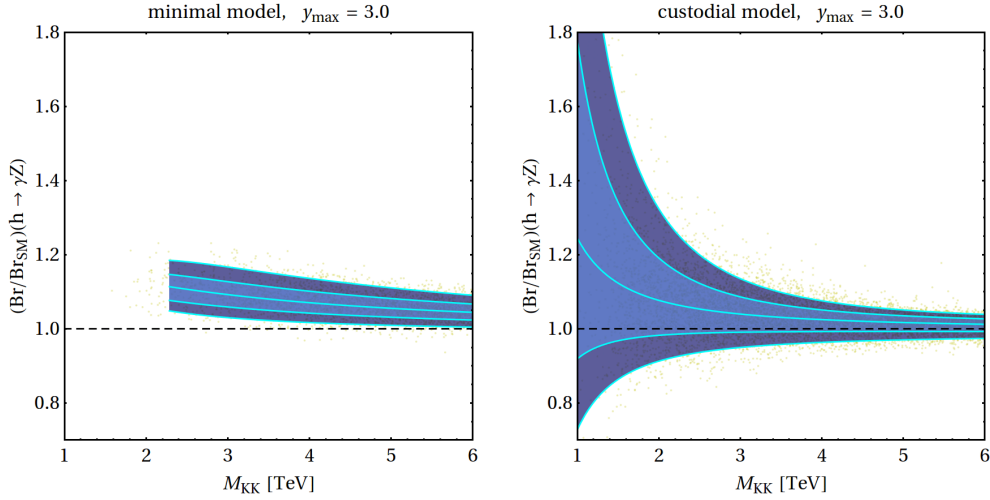


Figure 4.32: Fitted modification factor of the branching ratio compared to the SM for the decay $h \rightarrow \gamma Z$ in the minimal and custodial RS model with $y_{\max} = 3$. The EWPO bounds on the $Zb\bar{b}$ couplings are imposed and curves in the minimal model are only shown for the region where more than 10% of the parameter space are available. See figure 4.24 for further descriptions.

aforementioned scale. For the custodial model, we observe that both, moderate suppression, and up to large enhancement is possible. However, the typical enhancement is lower than in the minimal model (only 6% at the aforementioned KK-scale), *i.e.* typically the contributions from coupling modifications, KK-contributions and the reduction of the total width cancel to a large extent in the final combination. Large modifications are possible for lower values of the KK-scale, *e.g.* up to 60% for $M_{\text{KK}} = 1.5$ TeV. For lower values of y_{\max} the typical branching ratios decrease and follow more closely the reduction of the total contribution from bosonic loops. Detailed plots for this case are deferred to the appendix, see figure B.10. We conclude that a measurement of this decay channel at later stages of the LHC program could add valuable information if a pattern of large deviations from the SM should emerge from the decay channels that we discussed before. Having said that, we must add that we do not expect a significant impact on bounds on the KK-scale and the size of the Yukawa matrix elements from a measurement of $\text{BR}(h \rightarrow \gamma Z)$.

We summarize our extensive discussion on Higgs decay channels with the central insight. The very efficient method to circumvent bounds on the KK-scale from oblique electroweak corrections by the imposition of a custodial symmetry on the gauge sector also leads to larger quark multiplicities, which add constructively to the new physics contribution from the minimal RS model. Either one realizes fermions in the enlarged gauge symmetry without protecting the b -quark related EWPOs, in which case also a lower bound on y_{\max} and M_{KK} is active, or one chooses the specific custodial quark embedding presented in section 3.3.5.2, which has an even higher multiplicity due to the exotic quarks with charge $5/3$. We found that both ways of bypassing EWPO bounds via custodial protection increase the potential bounds from Higgs physics.

Chapter 5

Conclusion

A new scientific truth does not triumph by convincing its opponents and making them see the light, but rather because its opponents eventually die, and a new generation grows up that is familiar with it.

MAX PLANCK

We conclude this thesis with a summary of its main aspects and results. The common line of thought was the attempt to improve falsifiability of theories beyond the SM. This is achieved by using dynamical aspects of the models in order to constrain virtual contributions to precisely measured collider observables. One derives constraints on the models, most favorably on a common mass scale that determines the predicted resonances. The indirect processes we discussed here are known to be usually complementary to astrophysical observations and to collider searches for direct production, due to their inherent dependence on additional model parameters. This is subject to the given model dynamics. The dynamics can either be specified completely in a precise model or restricted by a general principle such as gauge invariance.

We started out with a brief recapitulation of the SM, its symmetry breaking aspects in particular, and the deficits and open questions it leaves. During the advent of the SM, theory was following experimental discoveries relatively close. Today, a plethora of models of new physics has been conceived. Many are motivated by solving some of the theoretical shortcomings of the SM; some are just possibilities which are not excluded yet. We showed that it is worthwhile to practically use the general principle of gauge invariance — or equivalently perturbative unitary — as a first classification step. We introduced a generic template Lagrangian for this purpose and summarized the constraints from Slavnov-Taylor identities on the level of Feynman rules. This allows to automatically include unphysical degrees of freedom in a general renormalizable gauge and implies further sum rules between the couplings. As a proof of concept, we solved the repeatedly emerging task of calculating the flavor changing one-loop penguin amplitude. An example is the FCNC $s \rightarrow dZ$ transition that leads to processes like the rare $K \rightarrow \pi\nu\bar{\nu}$ decays. We performed the renormalization and simplifications of the penguin amplitude by using Slavnov-Taylor identities and gave the full template result also for box-type diagrams. We verified the result with the SM and the LHT model. It is an interesting aspect that the Z -penguin amplitude in the LHT model is UV-insensitive due to the partly gauged symmetry structure, apart from chirally suppressed contributions. As a

byproduct, we simplified results as compared to the literature by introducing a proper vertex definition of the CKM matrix.

After this more conceptual part, we presented a full numerical analysis of bounds and correlations from flavor observables, electroweak precision observables, and Higgs processes in a specific example, the RS model. This model does not fall into the class of perturbatively unitary theories. Yet, it shows interesting structure in its couplings that stems from unique but few assumptions. It provides a theoretically appealing explanation of the gauge-hierarchy problem and quark hierarchies and thus received great interest in the past decade. For our purpose, we found the model to be of interest, since it presently is subject to relevant bounds from observables of all three aforementioned types. Furthermore, there remain unsolved conceptual questions about a proper regularization scheme for the calculation of virtual corrections in the five-dimensional warped background. We showed that in the calculation of Higgs processes, subtle questions of limiting procedures in combination with UV regularization are important in order to obtain correct results. After a careful treatment of these issues, we found that we are not limited by the unsolved questions or remnant UV dependence.

Before performing those calculations, we introduced and discussed in detail the RS model in a minimal setup with SM-like gauge structure and a setup with custodially protected gauge symmetry and fermion sector. We did this in a common notation that is extensible to even more general setups. This was followed by a comprehensive discussion of the KK decomposition within the mass basis. Paying special attention to Yukawa couplings with non-standard chirality, the direct treatment in the mass basis allowed to properly account for the influence of the δ -function regularization of the IR-localized Higgs boson on the 5d propagator of fermions. Our approach also has the merit that we were able to summarize the complete relevant coupling structure for three-point vertices and four-fermion operators in a very compact notation. This facilitates the interpretation of the various sources and size of contributions when compared to the approach of a 4d decomposition in the electroweak eigenstate basis followed by a re-diagonalization of large mass matrices. Already at the coupling level, we were able to summarize the differences between the minimal and custodial model in terms of a few universal constant factors. We found that, for instance, the left-handed $Zd_i\bar{d}_j$ couplings are suppressed by approximately the inverse volume of the extra dimension L^{-1} , and the right-handed couplings enhanced by a factor of $3c_w^2s_w^{-2}$ in the custodial compared to the minimal model. We gave the analogous factors for four fermion couplings, too. The KK-gluon couplings are the same in both versions of the model and are most important in kaon mixing.

We then began the numerical analyses of the RS model with a discussion of CP violation in kaon mixing. It provides the strongest flavor constraints on the mass scale of the model. Our first main finding was the significant spread in the distribution of the RS predictions, which stems mainly from the dependence on the Yukawa sector. We quantified this and derived new bounds from the lower edge of the resulting distribution by carrying out detailed numerical parameter scans. We found for the first KK-gluon mass — viz. 2.45 times the KK scale — $M_{G(1)} > 4.4 \text{ TeV}$, if we request 3% of allowed and non-fine-tuned parameter space at the 99% CL region. This bound, derived in a rigorous sense, is much weaker than what could be expected from the generic order of magnitude enhancement in ϵ_K , which is often quoted in the literature. It would lead to $M_{G(1)} \approx 20 \text{ TeV}$, if we request the median to agree with experiment at the same CL. We found that the aligned case with an $SU(3)_d$ flavor-symmetry helps to lower the bound, but conversely we found a much stronger limit for the little RS model due to effects in the UV-region of the bulk. We also considered direct CP violation in

$K \rightarrow \pi\pi$, *i.e.* ϵ'_K/ϵ_K , which gives an interesting constraint but a much weaker bound on $M_{G(1)}$ due to large theoretical uncertainties. We noticed that even major theoretical progress will not allow to make this observable a precision constraint on the KK scale. However, ϵ'_K/ϵ_K carries interesting complementary information, as it enforces the branching ratio of $K_L \rightarrow \pi^0 \nu \bar{\nu}$ to be not larger than twice the SM prediction. We also studied further correlations between rare (semi-)leptonic kaon decays that carry information on the chiral structure of the model and took into account the bounds imposed from ϵ_K and ϵ'_K/ϵ_K . Additional aspects of our discussion were an outlook for a promising future constraint from $B_s \rightarrow \mu \bar{\mu}$ and a discourse of non-standard CKM effects. For the latter, we gave analytical approximate formulas and showed that effects remain below observable levels. Here, it was necessary to use the four-fermion definition of the CKM and properly take into account the modification of G_F . We also found a cancellation of contributions in the custodial model, which countervails a possible enhancement at a lower accessible KK scale. In total, we observed that the severity of the “flavor problem” in the $\Delta S = 2$ sector of warped extra dimensions depends highly on the required amount of viable parameter space. The KK-scale bounds we gave are now well comparable to electroweak precision constraints.

Concerning the EWPOs, we then reviewed up-to-date analyses of the most important observables that significantly impact the constraints on models of new physics. We discussed the choice of input, effective parameters, and $Z \rightarrow b\bar{b}$ observables. For the RS model, we reviewed the mechanism of custodial protection in our formalism, which allows to clearly identify subleading non-protected contributions. In order to compare the different kinds of bounds in this thesis, we then re-derived the bounds from oblique corrections with the updated input. We found in the minimal RS model $M_{G(1)} > 11.3 \text{ TeV}$, the custodial RS model $M_{G(1)} > 4.1 \text{ TeV}$, and the LRS model $M_{G(1)} > 4.7 \text{ TeV}$ at the 3σ CL. Compare this to the strongest bound obtained from direct searches, which is $M_{G(1)} > 1.8 \text{ TeV}$ at the 2σ CL (see section 4.1.2.1). We also assessed the parameter dependence of the constraints from $Z \rightarrow b\bar{b}$ on the 5d bulk masses of the b quark.

The final part was then committed to Higgs production and decay modes. After a review of the SM results, the experimental status, and contributions from additional fermions in the simple example of the LHT model, our main focus was then to determine the analytical and numerical structure of the effects in the RS model. Our aim was to discuss the subtle issue of convergence of loop integrals, and the potential on constraining the parameter space.

We derived the RS one-loop contributions to Higgs-boson production via gluon-gluon fusion by a resummation of all KK-fermion-triangle diagrams. The calculation had a convergent result. We traced the origin of this non-trivial convergence and observed a cancellation between contributions of different chiralities for the vector-like KK fermions. We obtained analytic results for the minimal and custodial RS model and showed how to extend it to more general fermion embeddings. As an important aspect, we observed the cancellation of almost all bulk-mass dependence in the result, leading to a simpler prediction. However, we also recognized that the limits of the δ -function localization of the IR-brane Higgs boson and the infinite KK summation do not commute. They lead to $\mathcal{O}(1)$ different results depending on the order of limits. We were able to ascribe this behavior to contributions from ultra-heavy KK modes with masses in a broad region around a new scale M_{weak}/η . $\eta \ll 1$ determines the small localization of the regularized Higgs boson near the IR brane, and is eventually taken to zero at the end of the calculation. At the scale M_{weak}/η , the cancellation between different chiralities is suspended. We detected logarithmic growth of the ggh amplitude in the summation of many KK-modes around this scale. We demonstrated this explicitly for

the case of a single generation. A solution to this issue was given by the third regularization that is present in the problem. Any UV regulator, *e.g.* cut-off, or dimensional regularization, implies that the ultra-heavy fermion contributions are absent in a full calculation of the 5d amplitude.

With the finite UV-insensitive result, we were then able to discuss all leading Higgs-boson-production and decay modes. Besides the KK scale, the most important parameter is given by the maximal possible values of the 5d Yukawa matrix elements, which are naturally of $\mathcal{O}(1)$. We also considered reduced values of y_{\max} , and showed important results in the plane $M_{\text{KK}} - y_{\max}$. Concerning the production modes, we found a very strong suppression of gluon-gluon fusion. A suppression is also present in weak boson fusion, and the associated W , Z , and $t\bar{t}$ production modes. Concerning the subsequent decays, a strong reduction and spread of the total width was found to be due to the corrections in $h \rightarrow b\bar{b}$, if y_{\max} is of natural size.

We found an interesting interplay of modifications for lower than natural Yukawa values in the final branching ratios of $h \rightarrow ZZ$ and $h \rightarrow b\bar{b}$, which maintains a certain constraining potential in this region of parameter space. For $gg \rightarrow h \rightarrow ZZ$, we were able to derive a relevant bound at 95% CL. In the custodial model we found $M_{G^{(1)}} \notin [4.8, 9.1]$ TeV for natural Yukawa values, while for one order of magnitude reduced values we obtained $M_{G^{(1)}} > 2.8$ TeV. In the minimal model we derived $M_{G^{(1)}} > 4.7$ TeV for natural Yukawa entries.

The modifications in $h \rightarrow \gamma\gamma$ follow from an interplay of a reduced $WW h$ coupling, which is partially neutralized by positive KK- W contributions, and moreover exceeded by positive contributions from the top-Yukawa modification and from KK-fermions. In spite of the cancellations, we found a large possible enhancement for natural Yukawa values, particularly for the custodial model as it features exotic fermions of charge $5/3$. Conversely, we found a reduction for the case of Yukawa entries that are reduced one order of magnitude below their natural size. In combination with the reduced production channels, we derived the bound $M_{G^{(1)}} > 2.6$ TeV in the minimal and $M_{G^{(1)}} > 4.0$ TeV in the custodial model at 95% CL. We argued that no unfolding is necessary due to similar reductions in the relevant production channels. In total, we saw that the custodial model with $M_{G^{(1)}} \lesssim 4.8$ TeV and natural Yukawa values can be compatible even with present central values of the signal strengths.

We then emphasized that the spread of production and width drops in the ratio of signal strengths of the decay to ZZ and $\gamma\gamma$. This ratio could unfold its full constraining potential of around 11 TeV on $M_{G^{(1)}}$ in the case that the measurements would settle at SM values.

Finally, we also investigated all modifications of the decay into γZ . We derived expressions that properly take into account the modified Z couplings, as compared to the decay to $\gamma\gamma$. We found that up to 50% enhancement is possible in the custodial model, but less than 20% in the minimal model. This observable could be useful after the LHC upgrade and at high integrated luminosity.

We close this thesis with re-emphasizing that Higgs physics has reached the turning point in making the transition from discovery to precision physics in an astonishingly short amount of time. Already now, it provides additional bounds on new physics and the RS model in particular. We found that bypassing the strong EWPO bounds on the KK scale of the minimal RS model via custodial protection increases the potential bounds from Higgs physics. A small window of $M_{G^{(1)}} \in [4.4, 4.8]$ TeV remains open for natural versions of the custodial setup after taking into account all the bounds described above. We hope that Higgs physics will soon be able to close this window.

Appendix A

Collection of Formal Developments and Vertices

A.1 Collection of STIs for Feynman Rules

In the following, we summarize remaining STIs from the discussion in section 3.1.2. They are derived from the STIs

$$\begin{aligned}
0 &= \langle C_{v_1} C_{v_2} C_{v_3} C_{v_4} \rangle_{1\text{PI}} = \langle C_{v_1} C_{v_2} (V_{v_3} V_{v_4})_{\text{ph}} \rangle_{1\text{PI}} = \langle C_{v_1} C_{v_2} C_{v_3} (S_s)_{\text{ph}} \rangle_{1\text{PI}} \\
&= \langle C_{v_1} (V_{v_2} V_{v_2} S_s)_{\text{ph}} \rangle_{1\text{PI}} = \langle C_{v_1} C_{v_2} (S_{s_1} S_{s_2})_{\text{ph}} \rangle_{1\text{PI}} = \langle C_v (S_{s_1} S_{s_2} S_{s_3})_{\text{ph}} \rangle_{1\text{PI}}.
\end{aligned} \tag{A.1.1}$$

In the given order they read

$$\begin{aligned}
g_{\varphi_1 \varphi_2 \varphi_3 \varphi_4} &= \frac{-\sigma_{v_1} \sigma_{v_2} \sigma_{v_3} \sigma_{v_4}}{4m_{v_1} m_{v_2} m_{v_3} m_{v_4}} \sum_{s'} m_{s'}^2 \left(g_{v_1 v_4 s'} g_{v_2 v_3 \bar{s}'} + \text{symm}(v_2, v_3, v_4) \right), \\
g_{v_1 v_2 \varphi_3 \varphi_4} &= \frac{\sigma_{v_3} \sigma_{v_4}}{2m_{v_3} m_{v_4}} \left\{ \sum_{s'} g_{v_1 v_2 s'} g_{v_3 v_4 \bar{s}'} \right. \\
&\quad \left. + \sum_{v'} \left((m_{v_1}^2 + m_{v_2}^2 - 2m_{v'}^2) (g_{v_1 v_4 v'} g_{v_2 v_3 \bar{v}'} + g_{v_1 v_3 v'} g_{v_2 v_4 \bar{v}'}) \right. \right. \\
&\quad \left. \left. - \frac{(m_{v_1}^2 - m_{v_2}^2)(m_{v_3}^2 - m_{v_4}^2)}{m_{v'}^2} g_{v_1 v_2 v'} g_{v_3 v_4 \bar{v}'} \right) \right\}, \\
g_{\varphi_1 \varphi_2 \varphi_3 s} &= \frac{i \sigma_{v_1} \sigma_{v_2} \sigma_{v_3}}{6m_{v_1} m_{v_2} m_{v_3}} \left\{ \sum_{s'} (2m_s^2 - 3m_{s'}^2) g_{v_1 s s'} g_{v_2 v_3 \bar{s}'} \right. \\
&\quad \left. + m_s^2 \sum_{v'} \frac{m_{v_2}^2 - m_{v_3}^2}{m_{v'}^2} g_{v_1 v' s} g_{v_2 v_3 \bar{v}'} + \text{symm}(v_1, v_2, v_3) \right\}, \\
g_{v_1 v_2 \varphi_3 s} &= \frac{i \sigma_{v_3}}{m_{v_3}} \left\{ \sum_{v'} \left(-g_{v_1 v' s} g_{v_2 v_3 \bar{v}'} - g_{v_2 v' s} g_{v_1 v_3 \bar{v}'} \right. \right. \\
&\quad \left. \left. + g_{v_3 v' s} g_{v_1 v_2 \bar{v}'} \frac{m_{v_1}^2 - m_{v_2}^2}{2m_{v'}^2} \right) + \sum_{s'} g_{v_3 s s'} g_{v_1 v_2 \bar{s}'} \right\},
\end{aligned} \tag{A.1.2}$$

$$\begin{aligned}
g_{\varphi_1\varphi_2s_1s_2} &= \frac{\sigma_{v_1}\sigma_{v_2}}{2m_{v_1}m_{v_2}} \left\{ \sum_{s'} \left(g_{s_1s_2s'} g_{v_1v_2\bar{s}'} \right. \right. \\
&\quad \left. \left. + \left[g_{v_1s_1s'} g_{v_2s_2\bar{s}'} (2m_{s'}^2 - m_{s_1}^2 - m_{s_2}^2) + \text{symm}(s_1, s_2) \right] \right) \right. \\
&\quad \left. + \sum_{v'} \left(g_{v's_1s_1} g_{v_1v_2\bar{v}'} (m_{s_1}^2 - m_{s_2}^2) \frac{m_{v_1}^2 - m_{v_2}^2}{m_{v'}^2} \right. \right. \\
&\quad \left. \left. + \left[g_{v_1v's_2} g_{v_2\bar{v}'s_1} (m_{s_1}^2 + m_{s_2}^2) \frac{1}{4m_{v'}^2} + \text{symm}(v_1, v_2) \right] \right) \right\}, \\
g_{\varphi s_1s_2s_3} &= \frac{i\sigma_v}{m_v} \left\{ \sum_{s'} g_{s_1s_2s'} g_{vs_3\bar{s}'} - \sum_{v'} g_{v's_1s_2} g_{v\bar{v}'s_3} \frac{m_{s_1}^2 - m_{s_2}^2}{2m_{v'}^2} + \text{symm}(s_1, s_2, s_3) \right\}.
\end{aligned}$$

All rules given here and in section 3.1.2 hold in the limiting case of any of the particles being massless. The couplings of photons or gluons of course simplify considerably and can be expressed by using the $U(1)$ and $SU(3)$ charges defined in (3.1.1). Moreover, they can be separated into two classes: Couplings that involve another massive gauge boson and those without. Couplings of the latter class are either directly included in the covariant kinetic Lagrangian or zero. This includes¹

$$\begin{aligned}
g_{A\varphi_1\varphi_2} &= g_{AA\varphi_1\varphi_2} = g_{A\varphi_1s_1} = g_{AA\varphi_1s_1} = 0, \\
g_{AA\varphi_1\varphi_2} &= -2i(g_{Av_1\bar{v}_1})^2 \delta_{v_1\bar{v}_2}.
\end{aligned} \tag{A.1.3}$$

The equations also hold with G instead of A . The class of couplings with another massive gauge boson has to be derived from the STIs. They are given by

$$\begin{aligned}
g_{Av_1\varphi_2} &= ie m_{v_1} \delta_{v_1\bar{v}_2}, \\
g_{Av_1\varphi_2\varphi_3} &= e \sigma_{v_2}\sigma_{v_3} (Q_{v_2} - Q_{v_3}) \frac{m_{v_2}^2 + m_{v_3}^2 - m_{v_1}^2}{2m_{v_2}m_{v_3}} g_{v_1v_2v_3}, \\
g_{Av_1\varphi_2s} &= -ie \sigma_{v_2} (Q_{v_2} - Q_s) \frac{1}{2m_{v_2}} g_{v_1v_2s}, \\
g_{Av_1v_2v_3} &= -e (Q_{v_2} - Q_{v_3}) g_{v_1v_2v_3}, \\
g_{Avs_1s_2} &= e (Q_{s_1} - Q_{s_2}) g_{vs_1s_2}.
\end{aligned} \tag{A.1.4}$$

We used charge conservation to simplify the right-hand side for the quartic couplings. The corresponding equations with a gluon are

$$\begin{aligned}
g_{Gv_1\varphi_2}^{abc} &= i\sigma_{v_2} (T_{v_2}^a)_{bc} m_{v_1} \delta_{v_1\bar{v}_2}, \\
g_{Gv_1\varphi_2\varphi_3}^{abcd} &= \sigma_{v_2}\sigma_{v_3} \frac{m_{v_2}^2 + m_{v_3}^2 - m_{v_1}^2}{2m_{v_2}m_{v_3}} \sum_{c'} \left((T_{v_2}^a)_{cc'} g_{v_1v_2v_3}^{bc'd} - (T_{V_{a_3}}^a)_{dc'} g_{v_1v_2v_3}^{bcc'} \right), \\
g_{Gv_1\varphi_2s}^{abcd} &= -i\sigma_{v_2} \frac{1}{2m_{v_2}} \sum_{c'} \left((T_{v_2}^a)_{cc'} g_{v_1v_2s}^{bc'd} - (T_s^a)_{dc'} g_{v_1v_2s}^{bcc'} \right), \\
g_{Gv_1v_2v_3}^{abcd} &= -\sum_{c'} \left((T_{v_2}^a)_{cc'} g_{v_1v_2v_3}^{bc'd} - (T_{v_3}^a)_{dc'} g_{v_1v_2v_3}^{bcc'} \right), \\
g_{Gvs_1s_2}^{abcd} &= \sum_{c'} \left((T_{s_1}^a)_{cc'} g_{vs_1s_2}^{bc'd} - (T_{s_2}^a)_{dc'} g_{vs_1s_2}^{bcc'} \right).
\end{aligned} \tag{A.1.5}$$

¹To derive the vanishing couplings with physical scalars, one has to note that $g_{Av_1s_2} = 0$. This coupling has to come from the kinetic term of a multiplet Φ under the full gauge group. Thus, it is proportional to $\epsilon Q_\Phi A_\mu V_a^\mu (\Phi^\dagger T_{V_a} \Phi)$. The Goldstone directions are given by $T_{V_a} \langle \Phi \rangle$, so they cannot contain physical scalars.

For completeness, we remark that the ghost couplings can be derived by inserting another off-shell gauge boson in the derivation of (3.1.11). Following the derivations in [132, 133] one uses the BRST variation $sV_{v_1}^\mu(x) = \partial^\mu V_{v_1}(x) + i(gf)_{v_1 v_2 v_3} V_{v_2}^\mu(x) u_{v_3}(x)$, where $(gf)_{v_1 v_2 v_3}$ are the structure constants times corresponding couplings, rotated into the mass basis. Since the latter are per se unknown in our generic Lagrangian (3.1.2), which is already given in the mass basis, one removes the contact term again by considering connected Green's functions only. In this way, one can derive $g_{s\bar{u}_1 v_2} = -\frac{1}{2} g_{v_1 v_2 s}$ and $g_{v_3 \bar{u}_1 u_2} = g_{v_1 v_2 v_3}$. The index set for ghosts agrees with the one for gauge bosons, analogous to the indices for Goldstone bosons. The latter relation for gauge-boson couplings to ghost currents is already clear, since the same rotations are applied to gauge bosons and ghosts when going to the mass basis. Hence, we have reconstructed all unphysical couplings that are necessary for one-loop calculations in a general R_ξ gauge.

A.2 Formulas and Vertices of the Littlest Higgs Model

In this appendix we summarize some of the remaining relations for the LH model and the Feynman rules for the vertices in the model with T -parity.

In the Lagrangian, the kinetic terms for gauge bosons take the standard form. We rewrite them in terms of the SM-like gauge eigenstates. Using with charge eigenstates and $\epsilon^{+-3} = 1$ we obtain

$$\begin{aligned} \mathcal{L}_V &= -\frac{1}{4} \sum_{j=1,2} \left(\sum_{a=1,2,3} W_{j\mu\nu}^a W_j^{a\mu\nu} + B_{j\mu\nu} B_j^{\mu\nu} \right) \\ &= -\frac{1}{4} \left(\sum_{a=+,-,3} |\partial_\mu W_\nu^a - \partial_\nu W_\mu^a + ig\epsilon^{ab\bar{c}}(W_\mu^b W_\nu^c + W_\mu^{\bar{b}} W_\nu^{\bar{c}})|^2 \right. \\ &\quad + \sum_{a=+,-,3} |\partial_\mu W_\nu^{a'} - \partial_\nu W_\mu^{a'} + ig\epsilon^{ab\bar{c}}(W_\mu^b W_\nu^c - W_\nu^{\bar{b}} W_\mu^{\bar{c}} + \frac{\delta_g}{c_s} W_\mu^{\bar{b}} W_\nu^{\bar{c}})|^2 \\ &\quad \left. + |\partial_\mu B_\nu - \partial_\nu B_\mu|^2 + |\partial_\mu B'_\nu - \partial_\nu B'_\mu|^2 \right). \end{aligned} \tag{A.2.1}$$

The full redefinition of scalars, necessary to bring (3.2.16) and (3.2.17) into canonical form as discussed in the main text, is given by

$$\begin{aligned} \begin{pmatrix} h_m \\ \phi_m^0 \end{pmatrix} &= \begin{pmatrix} 1 - \frac{v^2 x_\lambda^2}{f^2} & \frac{v x_\lambda}{f \sqrt{2}} \\ -\frac{v x_\lambda}{f \sqrt{2}} & 1 - \frac{v^2}{12f^2} (1 + 3x_\lambda^2) \end{pmatrix} \begin{pmatrix} h \\ \phi^0 \end{pmatrix}, \\ \begin{pmatrix} \phi_m^P \\ \pi_m^0 \\ \eta_m \\ \omega_m^0 \end{pmatrix} &= \begin{pmatrix} 1 - \frac{v^2}{12f^2} (1 + 3x_\lambda^2) & -\frac{v}{\sqrt{2}f} x_\lambda & -\frac{\sqrt{5}v^2}{6\sqrt{2}f^2} & -\frac{v^2}{6\sqrt{2}f^2} \\ \frac{v}{\sqrt{2}f} x_\lambda & 1 - \frac{v^2}{12f^2} r_{22} & \frac{\sqrt{5}v}{2f} \delta_{g'} & \frac{v}{2f} \delta_g \\ \frac{\sqrt{5}v^2}{3\sqrt{2}f^2} \left(1 - \frac{3}{2} \delta_{g'} x_\lambda \right) & -\frac{\sqrt{5}v}{2f} \delta_{g'} & 1 - \frac{5v^2}{24f^2} (1 + 3\delta_{g'}^2) & -\frac{\sqrt{5}v^2}{6f^2} \left(1 - \frac{6x_H c' s'}{t_w c s} \right) \\ \frac{v^2}{3\sqrt{2}f^2} \left(1 - \frac{3}{2} \delta_g x_\lambda \right) & -\frac{v}{2f} \delta_g & -\frac{\sqrt{5}v^2}{6f^2} r_{42} & 1 - \frac{v^2}{24f^2} (1 + 3\delta_g^2) \end{pmatrix} \begin{pmatrix} \phi^P \\ \pi^0 \\ \eta \\ \omega^0 \end{pmatrix}, \\ r_{22} &= \left(1 + \frac{3}{2} (\delta_g^2 + 5\delta_{g'}^2) + 3x_\lambda^2 \right), \quad r_{42} = \left(1 + \frac{3t_w x_H (1 - \delta_g^2)}{10c c' s s'} \right), \end{aligned}$$

$$\begin{pmatrix} \phi_m^\pm \\ \pi_m^\pm \\ \omega_m^\pm \end{pmatrix} = \begin{pmatrix} 1 - \frac{1}{24} \frac{v^2}{f^2} (1+3x_\lambda^2) & -\frac{1}{2} \frac{v}{f} x_\lambda & -\frac{1}{12} \frac{v^2}{f^2} \\ \frac{1}{2} \frac{v}{f} x_\lambda & 1 - \frac{1}{12} \frac{v^2}{f^2} (1 + \frac{3}{2} (\delta_g^2 + x_\lambda^2)) & \frac{1}{2} \delta_g \frac{v}{f} \\ \frac{1}{6} \frac{v^2}{f^2} (1 - \frac{3}{2} \delta_g x_\lambda) & -\frac{1}{2} \frac{v}{f} \delta_g & 1 - \frac{1}{24} \frac{v^2}{f^2} (1+3\delta_g^2) \end{pmatrix} \begin{pmatrix} \phi^\pm \\ \pi^\pm \\ \omega^\pm \end{pmatrix}. \quad (\text{A.2.2})$$

In the following, we summarize all non-zero three-point couplings of physical particles in the model with T -parity. We derived them by implementing the full Lagrangian in a computer algebra system, with which we applied the functional derivatives and the necessary Taylor expansions in v/f . The triple vector couplings, including v^4/f^4 corrections, are given by

$$g_{W^+W^-} \left(\frac{A}{Z} \right) = g_{W_H^+W_H^-} \left(\frac{A}{Z} \right) = g \left(\frac{-s_w}{c_w} \right), \quad (\text{A.2.3})$$

$$g_{W^+W_H^-} \left(\frac{A_H}{Z_H} \right) = g \begin{pmatrix} \frac{v^2}{f^2} x_H \left(1 + \frac{v^2}{f^2} \left(\frac{1}{4} + \frac{2x_H}{3c_w s_w} \right) \right) \\ 1 - \frac{v^4}{f^4} \frac{x_H^2}{2} \end{pmatrix}. \quad (\text{A.2.4})$$

For the couplings of two vectors and one scalar we omit corrections of order v^3/f^3 , if a scalar rotation beyond the order included in (A.2.2) would contribute. We always keep track of the maximal reliable order in all vertices we derived. The resulting v^2/f^2 , and parts of the v^3/f^3 corrections are given by

$$\begin{aligned} \begin{pmatrix} g_{ZZh} \\ g_{W^+W^-h} \end{pmatrix} &= \frac{g^2 v}{2} \left(1 - \frac{v^2}{3f^2} \right) \begin{pmatrix} c_w^{-2} \\ 1 \end{pmatrix}, \\ \begin{pmatrix} g_{A_H A_H h} \\ g_{A_H Z_H h} \\ g_{Z_H Z_H h} \\ g_{W_H^+ W_H^- h} \end{pmatrix} &= -\frac{g^2 v}{2} \begin{pmatrix} t_w^2 \left(1 - \frac{v^2}{f^2} \left(\frac{4}{3} - \frac{2}{t_w} x_H \right) \right) \\ t_w \left(1 - \frac{v^2}{f^2} \left(\frac{4}{3} + \left(t_w - \frac{1}{t_w} \right) x_H \right) \right) \\ 1 - \frac{v^2}{f^2} \left(\frac{4}{3} + 2t_w x_H \right) \\ 1 - \frac{v^2}{f^2} \frac{1}{3} \end{pmatrix} + \mathcal{O}\left(\frac{v^3}{f^3}\right), \\ g_Z \left(\frac{A_H}{Z_H} \right) \phi^0 &= -\frac{g^2 v}{2\sqrt{2} c_w} \frac{v}{f} \left(1 - \frac{v^2}{f^2} \left(\frac{5}{12} - \frac{x_H}{t_w} \right) \right) \begin{pmatrix} t_w \\ 1 \end{pmatrix}, \\ \begin{pmatrix} g_{ZW_H^+ \phi^-} \\ g_{W^+ A_H \phi^-} \\ g_{W^+ Z_H \phi^-} \end{pmatrix} &= \frac{g^2 v}{4} \frac{v}{f} \begin{pmatrix} \frac{1}{c_w} \\ t_w \\ 1 \end{pmatrix} + \mathcal{O}\left(\frac{v^3}{f^3}\right), \quad g_{AW_H^+ \phi^-} = \mathcal{O}\left(\frac{v^3}{f^3}\right), \\ g_{W^+ W_H^+ \phi^{--}} &= -\frac{g^2 v}{2} \frac{v}{f} \left(1 - \frac{v^2}{6f^2} \right), \quad g_{W^+ W_H^- \phi^P} = i \frac{g^2 v}{45\sqrt{2}} \frac{v^3}{f^3}. \end{aligned} \quad (\text{A.2.5})$$

For the scalar–scalar–vector couplings there exists a second Lorentz-structure with Feynman rules proportional to the sum of the scalar momenta $p_2 + p_3$ instead of the difference $p_2 - p_3$,

whose coupling we denote by g^+ . The complete set of couplings is given by

$$\begin{aligned}
 g_{A\phi^+\phi^-} &= g_{A\phi^{++}\phi^{--}}/2 = -g s_w, \\
 \begin{pmatrix} g_{Z\phi^0\phi^P} \\ g_{Z\phi^+\phi^-} \\ g_{Z\phi^{++}\phi^{--}} \end{pmatrix} &= \frac{g}{c_w} \begin{pmatrix} i\left(1 - \frac{v^2}{4f^2}\right) \\ -\left(s_w^2 - \frac{v^2}{8f^2}\right) \\ 1 - 2s_w^2 \end{pmatrix}, \\
 \begin{pmatrix} g_{W^+\phi^0\phi^-} & g_{W^+\phi^0\phi^-}^+ \\ g_{W^+\phi^P\phi^-} & g_{W^+\phi^P\phi^-}^+ \\ g_{W^+\phi^+\phi^{--}} & g_{W^+\phi^+\phi^{--}}^+ \end{pmatrix} &= g \begin{pmatrix} 1/\sqrt{2} \\ i/\sqrt{2} \\ 1 \end{pmatrix} \left(1 - \frac{v^2}{8f^2}, -\frac{v^2}{12f^2}\right), \\
 \begin{pmatrix} g_{A_H h\phi^P}/t_w & g_{A_H h\phi^P}^+/t_w \\ g_{Z_H h\phi^P} & g_{Z_H h\phi^P}^+ \end{pmatrix} &= -\frac{ig}{2\sqrt{2}f} \left(1 + \frac{v^2}{f^2} \left(\frac{5}{12} \pm \frac{x_H}{t_w}\right), -\frac{1}{3} \left[1 - \frac{v^2}{f^2} \left(\frac{7}{60} \mp \frac{x_H}{t_w}\right)\right]\right), \\
 \left(g_{W_H^+ h\phi^-} & g_{W_H^+ h\phi^-}^+\right) &= -\frac{g}{4f} \left(1 + \frac{v^2}{24f^2}, -\frac{1}{3} \left[1 - \frac{11}{120} \frac{v^2}{f^2}\right]\right).
 \end{aligned} \tag{A.2.6}$$

To denote the couplings of fermions, we use $T_{3,u_H} \equiv T_{3,u} = 1/2$ and $T_{3,d_H} \equiv T_{3,d} = -1/2$. For the heavy fermions, these are not to be interpreted as charges, but only defined for notational convenience. The vertex definition of the CKM matrix V_{ij} in terms of the unitary matrix \hat{V}_{ij} , which is part of the diagonalization of the fundamental mass matrix, was given in (3.2.29). We also abbreviate $\bar{x}_L \equiv x_L/\hat{V}_{33}$. The couplings of vectors to fermion currents are given by

$$\begin{aligned}
 g_{A\bar{f}f}^{(L)} &= -g s_w Q_f, \\
 g_{Z\bar{f}f}^{(L)} &= \frac{g}{c_w} \left(\begin{pmatrix} T_{3f} - Q_f s_w^2 \\ -Q_f s_w^2 \end{pmatrix} - \frac{v^2}{8f^2} \begin{pmatrix} 4\bar{x}_L^2 (\delta_{f,t} - \delta_{f,T_+}) \\ \delta_{f,u_H} + \delta_{f,\nu_H} \end{pmatrix} \right), \\
 g_{Z\bar{t}T_+}^L &= \frac{v}{f} \frac{g}{2c_w} \bar{x}_L \left(1 + \frac{v^2}{2f^2} (2d_2 - \bar{x}_L^2)\right), \\
 g_{W^+\bar{u}_i d_j}^L &= \frac{g}{\sqrt{2}} V_{ij}, \quad g_{W^+\bar{\nu}_i e_j}^L = \frac{g}{\sqrt{2}} (V_{\text{PMNS}})_{ij}, \\
 g_{W^+\bar{T}_+ d_j}^L &= \frac{v}{f} \frac{g}{\sqrt{2}} \bar{x}_L \left(1 + \frac{v^2}{2f^2} (2d_2 + \bar{x}_L^2)\right) V_{3j}, \\
 g_{W^+\bar{u}_H, i d_{H,i}}^{(L)} &= g_{W^+\bar{\nu}_H, i e_{H,i}} = \frac{g}{\sqrt{2}} \begin{pmatrix} 1 \\ 1 - \frac{v^2}{8f^2} \end{pmatrix}, \\
 g_{\left(\begin{smallmatrix} A_H \\ Z_H \end{smallmatrix}\right) \bar{f}_{H,i} f_j}^L &= \frac{g}{2} \left(\begin{pmatrix} t_w/5 \\ 2T_{3,f} \end{pmatrix} + \begin{pmatrix} 2T_{3,f} \\ -t_w/5 \end{pmatrix} \frac{v^2}{f^2} x_H \right) (V_H f)_{ij}, \\
 g_{\left(\begin{smallmatrix} A_H \\ Z_H \end{smallmatrix}\right) \bar{u}_{H,i} T_+}^L &= \frac{v}{f} \frac{g}{2} \bar{x}_L \left(\begin{pmatrix} t_w/5 \\ 1 \end{pmatrix} \left(1 + \frac{v^2}{2f^2} (2d_2 + \bar{x}_L^2)\right) + \begin{pmatrix} 1 \\ -t_w/5 \end{pmatrix} \frac{v^2}{f^2} x_H \right) (V_H u)_{i3}, \\
 g_{A_H \bar{T}_-(t, T_+)}^{(L)} &= \frac{2}{5} g t_w \begin{pmatrix} \frac{v}{f} \bar{x}_L \left(1 + \frac{v^2}{f^2} d_2\right) & -\left(1 - \frac{v^2}{2f^2} \bar{x}_L^2\right) \\ \sqrt{x_L} \left(1 - \frac{v^2}{2f^2} (1-x_L) (1-2\bar{x}_L^2)\right) & -\sqrt{1-x_L} \left(1 + \frac{v^2}{2f^2} x_L (1-2\bar{x}_L^2)\right) \end{pmatrix}, \\
 g_{Z_H \bar{T}_-(t, T_+)}^{(L)} &= \frac{2}{5} g t_w x_H \begin{pmatrix} -\frac{v^3}{f^3} \bar{x}_L & \frac{v^2}{f^2} \\ -\frac{v^2}{f^2} \sqrt{x_L} & \frac{v^2}{f^2} \sqrt{1-x_L} \end{pmatrix},
 \end{aligned} \tag{A.2.7}$$

$$\begin{pmatrix} g_{W_H^+ \bar{u}_{H,i} d_j}^L \\ g_{W_H^- \bar{d}_{H,i} u_j}^L \\ g_{W_H^+ \bar{\nu}_{H,i} e_j}^L \\ g_{W_H^- \bar{e}_{H,i} \nu_j}^L \end{pmatrix} = \frac{g}{\sqrt{2}} \begin{pmatrix} (V_{Hd})_{ij} \\ (V_{Hu})_{ij} \\ (V_{He})_{ij} \\ (V_{H\nu})_{ij} \end{pmatrix}, \quad g_{W_H^- \bar{d}_{H,i} T_+}^L = \frac{v}{f} \frac{g}{\sqrt{2}} \bar{x}_L \left(1 + \frac{v^2}{2f^2} (2d_2 + \bar{x}_L^2) \right) (V_{Hu})_{ij}.$$

The couplings of scalars to fermion currents are given by

$$\begin{aligned} g_{h \bar{f}_i f_j}^{L/R} &= -\frac{m_{f,i}}{v} \left(1 - \frac{v^2}{6f^2} \right), \quad (f = d, e), \quad g_{h \bar{f}_{H,i} f_{H,i}}^{L/R} = \frac{m_{H,i}^f v}{f} \frac{v}{4f}, \quad (f = u, \nu), \\ g_{h \bar{u}_i u_i}^{L/R} &= -\frac{m_{u,i}}{v} \left(1 - \frac{v^2}{f^2} \left(\frac{2}{3} - \delta_{i3} (x_L - \bar{x}_L^2) \right) \right), \\ g_{h \bar{T}_+ T_+}^{L/R} &= \frac{m_{T_+}}{f} \frac{v}{f} \bar{x}_L \left(V_{33} - \bar{x}_L + \frac{v^2}{f^2} \left(\frac{\bar{x}_L^2}{V_{33}} (2 - x_L) - \bar{x}_L \left(\frac{10}{3} - 5x_L + \frac{3}{2} x_L^2 \right) + \left(\frac{1}{2} - x_L - \frac{1}{2} x_L^2 \right) V_{33} \right) \right), \\ g_{h \bar{t} T_+}^{(L)} &= \begin{pmatrix} \frac{m_{t,i}}{v} \frac{v}{f} \left(V_{33} - \bar{x}_L + \frac{v^2}{2f^2} \bar{x}_L (3 - (3+2/V_{33}^2) x_L + 5\bar{x}_L^2) \right) \\ -\frac{m_{T_+}}{f} \bar{x}_L \left(1 - \frac{v^2}{2f^2} (3 - (4+2/V_{33}^2) x_L + 5\bar{x}_L^2) \right) \end{pmatrix}, \\ g_{\phi^0 \bar{f}_{H,i} f_j}^R &= \frac{m_{f,j} v}{\sqrt{2} v f} \left(1 + \frac{1}{4} \frac{v^2}{f^2} \right) (V_{Hf})_{ij}, \quad (f = u, d, e), \quad g_{\phi^0 \bar{u}_{H,i} T_+}^R = \frac{m_{T_+}}{\sqrt{2} f} \frac{v}{f} \bar{x}_L (V_{Hu})_{i3}, \end{aligned}$$

$$\begin{aligned} g_{\phi^P \bar{\nu}_{H,i} \nu_j}^L &= -\frac{i}{4} \frac{m_{H,i}^\nu v^2}{\sqrt{2} f f^2} (V_{H\nu})_{ij}, \quad g_{\phi^P \bar{f}_{H,i} f_j}^R = i \frac{m_{f,j} v}{\sqrt{2} v f} \left(1 + \frac{1}{12} \frac{v^2}{f^2} \right) (V_{Hf})_{ij}, \quad (f = d, e), \\ g_{\phi^P \bar{u}_{H,i} (u_j, T_+)}^{(L)} &= -\frac{i}{\sqrt{2}} \begin{pmatrix} \frac{m_{H,i}^u v^2}{4f f^2} (V_{Hu})_{ij} & \frac{m_{H,i}^u v^3 \bar{x}_L}{3f f^3} (V_{Hu})_{i3} \\ \frac{m_{u,j} v}{v f} \left(1 - \frac{v^2}{4f^2} \right) (V_{Hu})_{ij} & \frac{m_{T_+}}{f} \frac{v}{f} \bar{x}_L (V_{Hu})_{i3} \end{pmatrix}, \\ g_{\phi^+ \bar{\nu}_{H,i} e_j}^{L/R} &= \frac{1}{\sqrt{2}} (V_{He})_{ij} \left(\frac{m_{H,i}^e v^2}{f} \frac{v^2}{8f^2}, \frac{m_{e,j} v}{v f} \left(1 - \frac{v^2}{8f^2} \right) \right), \quad g_{\phi^- \bar{e}_{H,i} \nu_j}^L = -\frac{1}{\sqrt{2}} (V_{H\nu})_{ij} \frac{m_{H,i}^\nu v^2}{f} \frac{v^2}{8f^2}, \\ g_{\phi^+ \bar{u}_{H,i} d_j}^{L/R} &= \frac{1}{\sqrt{2}} (V_{Hd})_{ij} \left(\frac{m_{H,i}^d v^2}{f} \frac{v^2}{8f^2}, \frac{m_{d,j} v}{v f} \left(1 - \frac{v^2}{8f^2} \right) \right), \\ g_{\phi^+ \bar{d}_{H,i} (u_j, T_+)}^{(L)} &= -\frac{1}{\sqrt{2}} \begin{pmatrix} \frac{m_{H,i}^u v^2}{8f f^2} (V_{Hu})_{ij} & \frac{m_{H,i}^u v^3 \bar{x}_L}{6f f^3} (V_{Hu})_{i3} \\ \frac{m_{u,j} v}{v f} \left(1 - \frac{v^2}{8f^2} \right) (V_{Hu})_{ij} & \frac{m_{T_+}}{f} \frac{v}{f} \bar{x}_L (V_{Hu})_{i3} \end{pmatrix}. \end{aligned} \tag{A.2.8}$$

We have calculated all the couplings of the Goldstone bosons from the local symmetry π^0 , π^\pm , η , ω^0 , ω^\pm of adjacency three and checked that they fulfill the STIs (3.1.14) to leading order in v/f . In table A.1 we list whether higher orders also fulfill the STIs.

A.2. FORMULAS AND VERTICES OF THE LITTLEST HIGGS MODEL

	$\frac{f}{v}$	1	$\frac{v}{f}$	$\frac{v^2}{f^2}$	$\frac{v^3}{f^3}$
$g(A,Z)W^+\pi^-$		+		+	
$g(A,Z)W_H^+\omega^-, g_{ZH}W^+\omega^-$	+		+		u
$g_{AH}W^+\omega^-, g_{ZH,W_H^+}\pi^-$			+		u
$g_{W^+W_H^-}\omega^0$	+		+		x
$g_{AH}W_H^+\pi^-$		+		x	
$g_{W^+W_H^-}\eta$			+		x
$g(A,Z)\pi^+\pi^-, g_{W^+\pi^0}\pi^-$		+			
$g_{Z\omega^+\omega^-}, g_{W^+\omega^0}\omega^-$		+		+	
$g_{W^+\eta}\omega^-$				+	
$g_{ZH}\pi^+\omega^-, g_{W_H^+\pi^0}\omega^-, g_{W_H^+,\pi^-,\omega^0}$			+		+
$g_{AH}\pi^+\omega^-, g_{W_H^+}\pi^-\eta$			+		x
$g_{Z\pi^0}h, g_{W^+\pi^-}h$		+		+	
$g_{Z(\eta,\omega^0)\phi^0}, g_{Z\omega^+\phi^-}, g_{W^+(\eta,\omega^0)\phi^-}, g_{W^+\omega^+\phi^{--}}$				+	
$g(A_H,Z_H)\pi^0\phi^0, g(A_H,Z_H)\pi^+\phi^-, g(A_H,Z_H)(\eta,\omega^0)h, \dots$ $\dots g_{W_H^+\pi^0}\phi^-, g_{W_H^+\pi^+}\phi^{--}, g_{W_H^+}\omega^-h$			+		+
$g_{W_H^+}\pi^-\phi^P$					x
$g_{\pi^0\bar{f}_i f_i}^{L,R} (f = u, d, e), g_{\pi^+\bar{u}_i d_j}^{L,R}, g_{\pi^+\bar{\nu}_i e_j}^{L,R}, g_{\pi^0\bar{T}_+ t}^L, g_{\pi^+\bar{T}_+ d_j}^L$		+		+	
$g_{\pi^0\bar{T}_+ t}^R, g_{\pi^+\bar{T}_+ d_j}^R$			+		+
$g_{\pi^0\bar{T}_+ T_+}^{L,R}$			+		x
$g_{\pi^0\bar{u}_{H,i} u_{H,i}}, g_{\pi^0\bar{\nu}_{H,i} \nu_{H,i}}, g_{\pi^+\bar{u}_{H,i} d_{H,i}}, g_{\pi^+\bar{\nu}_{H,i} e_{H,i}} \text{ (all = 0)}$				x	
$g_{(\eta,\omega^0)\bar{f}_{H,i} f_j}^L, (f = d, e)$		+		+	
$g_{(\eta,\omega^0)\bar{f}_{H,i} f_j}^R, (f = d, e)$			+		x
$g_{(\eta,\omega^0)\bar{f}_{H,i} f_j}^L, (f = u, \nu)$		+		x	
$g_{(\eta,\omega^0)\bar{u}_{H,i} u_j}^R, g_{(\eta,\omega^0)\bar{u}_{H,i} T_+}^L$			+		+
$g_{(\eta,\omega^0)\bar{u}_{H,i} T_+}^R$			+		x
$g_{\eta(\bar{u}_i, \bar{T}_+) T_-}^L$		+		+	
$g_{\omega^0(\bar{u}_i, \bar{T}_+) T_-}^L$				+	
$g_{\omega^-\bar{u}_{H,i} d_j}^L, g_{\omega^-, -\nu_{H,i} e_j}^L$		+		+	
$g_{\omega^-\bar{u}_{H,i} d_j}^R, g_{\omega^-, -\nu_{H,i} e_j}^R$			+		+
$g_{\omega^+\bar{d}_{H,i} u_j}^L, g_{\omega^+, -e_{H,i} \nu_j}^L$		+		x	
$g_{\omega^+\bar{d}_{H,i} u_j}^R, g_{\omega^+\bar{d}_{H,i} T_+}^L$			+		+
$g_{\omega^+\bar{d}_{H,i} T_+}^R$			+		x

Table A.1: Check of STIs (3.1.14) for the LHT model and linear gauge fixing. Entries are only given at the orders that are present in the couplings. A “+” indicates the coupling fulfills the STI at the given order, an “x” if otherwise, and a “u” if we cannot derive it, *e.g.* because of missing scalar rotations at the given order.

A.3 Analytic Solutions for the RS Model with One Generation

A Toy Model with Vanishing Bulk Masses

In this appendix we consider a toy RS model, which is used for illustrative purposes in the discussion of Higgs physics in the main text. This simplified setup provides a nice test case for our general results and conclusions. We use a single fermion generation with BCs that reproduce a light zero mode and vanishing bulk-mass parameters $c_Q = c_u = c_d = 0$. Furthermore, the EOMs (3.3.32) can be solved exactly if we adopt a sufficiently simple, regularized Higgs profile, so we simply use a box of width η , *i.e.* $\delta^\eta(t-1) = \eta^{-1}$ for $1-\eta < t < 1$ and zero otherwise.

Without loss of generality, we employ a real and positive Yukawa coupling Y_q , and set $\epsilon = 0$. The latter simplification is possible in the case of vanishing bulk masses, since the wave functions are non-singular near the UV brane. The solutions resemble the case of a flat extra dimension, where the profiles are given by simple trigonometric functions. We have

$$\mathcal{Q}_L^{(n)}(t) = N_n \begin{pmatrix} \cos(x_n t) \\ \mp \sin(x_n t) \end{pmatrix}, \quad \mathcal{Q}_R^{(n)}(t) = N_n \begin{pmatrix} \sin(x_n t) \\ \pm \cos(x_n t) \end{pmatrix}; \quad t \leq 1 - \eta, \quad (\text{A.3.1})$$

where the upper signs hold for even values of n , including the light zero mode $n = 0$, and the lower signs holds for odd values. Also in the relevant case for Higgs couplings $t > 1 - \eta$, we obtain simple profiles involving hyperbolic function. The generalized mass matrix of (3.3.33) is given by

$$\mathcal{M}_q(t) = z \begin{pmatrix} 0 & 1 \\ 1 & 0 \end{pmatrix}, \quad z = \frac{vY_q}{\sqrt{2}M_{\text{KK}}} \frac{1}{\eta}; \quad t \geq 1 - \eta, \quad (\text{A.3.2})$$

and the solution the EOMs reads

$$\begin{pmatrix} \mathcal{Q}_L^{(n)}(t) \\ \mathcal{Q}_R^{(n)}(t) \end{pmatrix} = N_n \begin{pmatrix} r_1 \cosh \left[\sqrt{z^2 - x_n^2} (1-t) \right] \\ \mp r_2 \sinh \left[\sqrt{z^2 - x_n^2} (1-t) \right] \\ r_2 \sinh \left[\sqrt{z^2 - x_n^2} (1-t) \right] \\ \pm r_1 \cosh \left[\sqrt{z^2 - x_n^2} (1-t) \right] \end{pmatrix}; \quad t \geq 1 - \eta, \quad (\text{A.3.3})$$

$$r_1 = \frac{\cos [x_n(1-\eta)]}{\cosh \left[\sqrt{z^2 - x_n^2} \eta \right]}, \quad r_2 = \frac{\sin [x_n(1-\eta)]}{\sinh \left[\sqrt{z^2 - x_n^2} \eta \right]}.$$

Remark that this solution immediately shows a certain relevance of the quantity z , which we defined in (A.3.2). For $x_n > z$, the square-roots develop an imaginary part and the profile functions change their shape, now being trigonometric again. More explicitly, we can cancel the resulting imaginary factors, such that the form of (A.3.3) holds with the replacements $\sqrt{z^2 - x_n^2} \rightarrow \sqrt{x_n^2 - z^2}$ and $\cosh \rightarrow \cos$, $\sinh \rightarrow \sin$.

We emphasize that this will also imply a different form of the derived couplings for masses $m_{q_n} > vY_q/(\sqrt{2}\eta) \approx M_{\text{weak}}/\eta$ above a new scale² M_{weak}/η . For very small η , this scale lies far above the TeV scale and is eventually pushed even beyond the Planck scale in the limit of IR-brane localization.

²Recall that in the anarchic RS model the fundamental Yukawa elements are of order one.

The mass eigenvalues x_n are determined by matching the profile functions at $t = 1 - \eta$

$$\tan [x_n(1 - \eta)] = \begin{cases} \pm \sqrt{\frac{z \mp x_n}{z \pm x_n}} \tanh [\sqrt{z^2 - x_n^2} \eta], & x_n < z, \\ -\sqrt{\frac{x_n \mp z}{x_n \pm z}} \tan [\sqrt{x_n^2 - z^2} \eta], & x_n > z. \end{cases} \quad (\text{A.3.4})$$

These equations can easily be solved numerically. For the normalization factors we obtain

$$N_n^{-2} = 1 + \frac{z}{z^2 - x_n^2} \left[\pm \frac{1}{2} \sin [2x_n(1 - \eta)] - \eta \left(z \mp x_n \cos [2x_n(1 - \eta)] \right) \right]. \quad (\text{A.3.5})$$

Using these results, it is not difficult to calculate the relevant overlap integrals with the Higgs profile. After a series of elementary simplifications we arrive at

$$\begin{aligned} g_{h\bar{q}_n q_n}^R &= \frac{m_n}{v} N_n^2 \frac{z}{z^2 - x_n^2} \left[\pm \frac{1}{2} \sin [2x_n(1 - \eta)] - \eta \left(z \mp \frac{z^2}{x_n} \cos [2x_n(1 - \eta)] \right) \right] \\ &= \frac{m_n}{v} \left[1 - N_n^2 \left(1 \mp \frac{\eta z}{x_n} \cos [2x_n(1 - \eta)] \right) \right], \end{aligned} \quad (\text{A.3.6})$$

for the coupling of two fermions of equal KK level to the Higgs boson. Again the upper and lower signs correspond to odd and even KK level. The expression is valid for all regions, both $x_n < z$ and $x_n > z$. To demonstrate how the different form of the profiles is reflected in the value of the couplings, we approximate the result in three regions, always neglecting the corresponding small mass ratio and relative $\mathcal{O}(\eta)$ corrections.

1) $x_n \ll z$: We observe the typical equidistant spacing of masses given by the solutions to

$$\tan^2(x_n) = \tanh^2(y_q); \quad y_q = \frac{vY_q}{\sqrt{2}M_{\text{KK}}}, \quad (\text{A.3.7})$$

The zero mode has mass $x_0 = \arctan(\tanh(y_q))$ and the following masses are given by

$$x_n = \begin{cases} \frac{n}{2} \pi + x_0 & , n \text{ even} \\ \frac{n+1}{2} \pi - x_0 & , n \text{ odd} \end{cases}. \quad (\text{A.3.8})$$

The couplings of the two KK modes in a given KK level are of opposite sign

$$g_{h\bar{q}_n q_n}^R = \pm \frac{Y_q}{\sqrt{2}} \frac{1}{\cosh(2X_q)}. \quad (\text{A.3.9})$$

2) $x_n \approx z$: In this region we set $x_n = z(1 + \zeta_n)$ and use ζ_n as an expansion parameter. We observe from the characteristic equation

$$\tan(x_n(1 - \eta)) = -y_q \begin{cases} \mathcal{O}(\zeta_n) & , n \text{ even} \\ 2 + \mathcal{O}(\zeta_n) & , n \text{ odd} \end{cases}, \quad (\text{A.3.10})$$

that the spacing between KK levels is approximately equidistant. However, there are relevant changes in the Higgs–fermion couplings. Over a broad range around $x_n \approx z$

they grow with increasing KK level for fermions of both even and odd BCs, *i.e.* even and odd n . They both eventually reach individual maxima, where also the odd couplings have turned positive. We expand the characteristic equation and the odd couplings linearly in ζ_n , in order to verify the zero crossing analytically and found that

$$g_{h\bar{q}_n q_n}^R|_{n \text{ odd}} \approx 0, \quad \text{at} \quad \zeta_n = \frac{1}{4y_q^2} + \mathcal{O}(y_q^0). \quad (\text{A.3.11})$$

Similarly, by expanding to third order in ζ_n , we found the maximal value for the even coupling

$$g_{h\bar{q}_n q_n}^R|_{n \text{ even}} \approx y_q \left(1 + \frac{2}{3} y_q^2 + \mathcal{O}(y_q^4) \right), \quad \text{at} \quad \zeta_n = 1 + \mathcal{O}(y_q^2). \quad (\text{A.3.12})$$

Remark that the power series in ζ_n gives good results even for $\zeta_n > 1$, since higher orders in ζ_n also come with additional powers of y_q . The results (A.3.11) and (A.3.12) thus reproduce the numerical results with a good quality.

3) $x_n \gg z$: Approximately equidistant spacing is still preserved by the characteristic equation

$$\tan^2(x_n(1 - \eta)) = \tan^2(x_n \eta). \quad (\text{A.3.13})$$

The couplings of both chirality types stay positive, but undergo a damped oscillation with increasing KK level. We verify this numerically in section 4.3.3 of the main text.

Stability under Variations of the Bulk Masses

The states with $x_n \ll z$, called case 1) in the last section, are of physical interest. We argue in the main text, that the heavy resonances — cases 2) and 3) — will be decoupled automatically by a proper UV regulation of the theory. Therefore we consider a small variation of the bulk mass parameters $\delta c_{Q,q}$ under this condition. It is straightforward to derive the characteristic equation for $\eta \rightarrow 0$ and to first order in $\delta c_{Q,q}$. It reads

$$\tan^2(x_n) = \tilde{y}_q^2 + \delta c \frac{\tan(x_n)}{\cos^2(x_n)} \text{Si}(2x_n); \quad \tilde{y}_q = \tanh(y_q). \quad (\text{A.3.14})$$

Here, we were allowed to neglect UV brane effects, so again we took the limit $\epsilon \rightarrow 0$. Since the characteristic equation is symmetric in c_Q and c_q , both variables have the same coefficient in the linearization, and we set $\delta c \equiv \delta c_Q + \delta c_q$. The sine integral in (A.3.14) is defined as $\text{Si}(z) = \int_0^z dt \sin(t)/t$. Denoting the solutions (A.3.8) of the case with vanishing bulk masses as $x_n^{(0)}$ and using (A.3.6) we obtain

$$x_n = x_n^{(0)} + \frac{\delta c}{2} \text{Si}(2x_n),$$

$$\frac{\partial}{\partial c} \frac{v g_{h\bar{q}_n q_n}^R}{m_n} \Big|_{\eta \rightarrow 0} = -\frac{y_q}{1 + \tilde{y}_q^2} \text{Si}(2x_n^{(0)}) \left[\pm (1 - \tilde{y}_q^2) (x_n^{(0)})^{-2} + 2\tilde{y}_q (x_n^{(0)})^{-1} \right]. \quad (\text{A.3.15})$$

The variation of the total sum of the last line is indeed zero as we show now. We set $\xi \equiv x_0^{(0)}/\pi$ and obtain

$$\frac{\partial}{\partial c} \sum_{n=0}^{\infty} \frac{v g_{h\bar{q}_n q_n}^R}{m_n} = -\frac{y_q}{1 + \tilde{y}_q^2} \left\{ (1 - \tilde{y}_q^2) \left[\sum_{k=1}^{\infty} \left(\frac{\text{Si}(2\pi(k + \xi))}{\pi^2(k + \xi)^2} - \frac{\text{Si}(2\pi(k - \xi))}{\pi^2(k - \xi)^2} \right) + \frac{\text{Si}(2\pi\xi)}{(\pi\xi)^2} \right] \right.$$

$$\left. + 2\tilde{y}_q \left[\sum_{k=1}^{\infty} \left(\frac{\text{Si}(2\pi(k + \xi))}{\pi(k + \xi)} + \frac{\text{Si}(2\pi(k - \xi))}{\pi(k - \xi)} \right) + \frac{\text{Si}(2\pi\xi)}{\pi\xi} \right] \right\}, \quad (\text{A.3.16})$$

where we summed over KK levels k and separated the zero mode contribution that appears as the last term in each of the square brackets. The expressions inside each square bracket can be shown to cancel using relations for special functions that can be found *e.g.* in [444]. We use the series expansion of the sine integral, the Hurwitz zeta function ζ , and the following relations for the Bernoulli polynomials B_n

$$\text{Si}(z) = \sum_{m=0}^{\infty} s_m z^{2m+1}, \quad s_m = \frac{(-1)^m}{(2m+1)(2m+1)!}, \quad (\text{A.3.17})$$

$$\zeta(n, z) = \sum_{m=0}^{\infty} (m+z)^{-n}, \quad \zeta(-n, z) = -\frac{B_{n+1}(z)}{n+1}, \quad n \in \mathbb{N}_+^0, \quad (\text{A.3.18})$$

$$B_n(1-z) = (-1)^n B_n(z), \quad B_n(1+z) = B_n(z) + n z^{n-1}. \quad (\text{A.3.19})$$

The sum in the first square bracket in (A.3.16) becomes

$$\begin{aligned} \sum_{k=1}^{\infty} \left(\frac{\text{Si}(2\pi(k+\xi))}{(k+\xi)^2} - \frac{\text{Si}(2\pi(k-\xi))}{(k-\xi)^2} \right) &= \sum_{m=0}^{\infty} s_m \sum_{k=1}^{\infty} ((k+\xi)^{2m-1} - (k-\xi)^{2m-1}) \\ &= - \sum_{m=0}^{\infty} s_m \xi^{2m-1} = -\frac{1}{\xi^2} \text{Si}(2\pi\xi), \end{aligned} \quad (\text{A.3.20})$$

and the other sum is treated analogously. Consequently, the total variation in (A.3.16) vanishes. In summary we have shown that the total sum $\sum_n (v g_{h\bar{q}_n q_n}^R / m_n |_{\eta \rightarrow 0})$ is stable under small variations of any of the two bulk-mass parameters. One can in principle continue along the same lines for all higher derivatives, where one needs complicated derivatives of the series expansion of the Bessel function with respect to the order parameter, instead of the simple relations (A.3.17). Since the total sum has no poles and is built of products and quotients of Bessel functions that are entire functions in the order parameter, such a calculation would prove rigorously that the total sum indeed vanishes for all bulk-mass parameters.

Appendix B

Collection of Numerical and Technical Details

B.1 Loop Functions

We summarize the loop functions used in section 4.1. Following reference [250] they are defined with $\varepsilon = (4 - D)/2$ as

$$\begin{aligned} \frac{i}{(4\pi)^2} B_0(m_1, m_2) \left(\frac{4\pi}{\mu^2} e^{-\gamma_E} \right)^\varepsilon &= \int \frac{d^D q}{(2\pi)^D} \frac{1}{q^2 - m_1^2} \frac{1}{q^2 - m_2^2}, \\ \frac{i}{(4\pi)^2} C_0(m_1, m_2, m_3) \left(\frac{4\pi}{\mu^2} e^{-\gamma_E} \right)^\varepsilon &= \int \frac{d^D q}{(2\pi)^D} \frac{1}{q^2 - m_1^2} \frac{1}{q^2 - m_2^2} \frac{1}{q^2 - m_3^2}, \\ \frac{i}{(4\pi)^2} D_0(m_1, m_2, m_3, m_4) \left(\frac{4\pi}{\mu^2} e^{-\gamma_E} \right)^\varepsilon &= \int \frac{d^D q}{(2\pi)^D} \frac{1}{q^2 - m_1^2} \frac{1}{q^2 - m_2^2} \frac{1}{q^2 - m_3^2} \frac{1}{q^2 - m_4^2}. \end{aligned} \quad (\text{B.1.1})$$

These functions read

$$\begin{aligned} B_0(m_1, m_2) &= \frac{1}{\varepsilon} + 1 + \left\{ \frac{m_1^2 \ln \left(\frac{\mu^2}{m_1^2} \right)}{m_1^2 - m_2^2} + \text{symm}(m_1, m_2) \right\}, \\ C_0(m_1, m_2, m_3) &= \frac{m_1^2 m_2^2 \ln \left(\frac{m_2^2}{m_1^2} \right)}{(m_1^2 - m_2^2)(m_1^2 - m_3^2)(m_2^2 - m_3^2)} + \text{symm}(m_1, m_2, m_3), \\ D_0(m_1, m_2, m_3, m_4) &= \frac{m_1^2 \ln m_1^2}{(m_1^2 - m_2^2)(m_1^2 - m_3^2)(m_4^2 - m_1^2)} + \text{symm}(m_1, m_2, m_3, m_4), \end{aligned} \quad (\text{B.1.2})$$

where the symbol $\text{symm}(\dots)$ indicates that one has to sum the preceding terms over all cyclic permutations of the masses without multiplication of a symmetry factor. We furthermore define the combinations of loop functions

$$\begin{aligned} \tilde{C}_0(m_1, m_2, m_3) &= B_0(m_2, m_3) + m_1^2 C_0(m_1, m_2, m_3), \\ \tilde{D}_0(m_1, m_2, m_3, m_4) &= C_0(m_2, m_3, m_4) + m_1^2 D_0(m_1, m_2, m_3, m_4), \end{aligned} \quad (\text{B.1.3})$$

which arise from the loop integrals (B.1.1) with an additional q^2 in the numerator.

The functions that describe the effects of quark and boson loops in the production and decay of the Higgs boson are proportional to the so called form factors as introduced in chapter 4.3. The analytic expressions are summarized *e.g.* in [142]. In our conventions they are given by

$$\begin{aligned}
 A_q^h(\tau) &= \frac{3\tau}{2} [1 + (1 - \tau) f(\tau)], & B_q^h(\tau) &= \tau f(\tau), \\
 A_W^h(\tau) &= -\frac{3}{4} [2 + 3\tau + 3\tau(2 - \tau) f(\tau)], \\
 A_q^h(\tau, \lambda) &= -I(\tau, \lambda) + J(\tau, \lambda), \\
 A_W^h(\tau, \lambda) &= c_w \left\{ 4 \left(3 - \frac{s_w^2}{c_w^2} \right) I(\tau, \lambda) + \left[\left(1 + \frac{2}{\tau} \right) \frac{s_w^2}{c_w^2} - \left(5 + \frac{2}{\tau} \right) \right] J(\tau, \lambda) \right\}.
 \end{aligned} \tag{B.1.4}$$

The function B_q^h for the CP -violating part can be found in [445]. The functions $I(\tau, \lambda)$ and $J(\tau, \lambda)$, relevant for final states of two different gauge bosons ($Z\gamma$), take the form

$$\begin{aligned}
 I(\tau, \lambda) &= -\frac{\tau\lambda}{2(\tau - \lambda)} [f(\tau) - f(\lambda)], \\
 J(\tau, \lambda) &= \frac{\tau\lambda}{2(\tau - \lambda)} + \frac{\tau^2\lambda^2}{2(\tau - \lambda)^2} [f(\tau) - f(\lambda)] + \frac{\tau^2\lambda}{(\tau - \lambda)^2} [g(\tau) - g(\lambda)],
 \end{aligned} \tag{B.1.5}$$

while the functions $f(\tau)$ and $g(\tau)$ [446] read

$$f(\tau) = \arctan^2 \left(\frac{1}{\sqrt{\tau - 1}} \right) = \begin{cases} -\frac{1}{4} \left[\ln \left(\frac{1 + \sqrt{1 - \tau}}{1 - \sqrt{1 - \tau}} \right) - i\pi \right]^2, & \tau \leq 1, \\ \arcsin^2 \left(\frac{1}{\sqrt{\tau}} \right), & \tau > 1, \end{cases} \tag{B.1.6}$$

$$g(\tau) = \sqrt{\tau - 1} \arctan \left(\frac{1}{\sqrt{\tau - 1}} \right) = \begin{cases} \frac{1}{2} \sqrt{1 - \tau} \left[\ln \left(\frac{1 + \sqrt{1 - \tau}}{1 - \sqrt{1 - \tau}} \right) - i\pi \right], & \tau \leq 1, \\ \sqrt{\tau - 1} \arcsin \left(\frac{1}{\sqrt{\tau}} \right), & \tau > 1. \end{cases} \tag{B.1.7}$$

B.2 Numerical Input Parameters

Here we collect the numerical values of input parameters used throughout the numerical discussion of the RS model. We order them thematically in the following.

Concerning the parameters entering the discussion of EWPOs in section 4.2, we follow essentially [344]. We use [69] for the strong coupling constant and the most recent Tevatron average of the top-quark mass [447]

$$\begin{aligned}
 G_F &= 1.1663787(6) \cdot 10^{-5} \text{ GeV}^{-2}, & s_w^2 &= 0.23116(12), \\
 \alpha_s(M_Z) &= 0.1184(7), & \Delta\alpha_{\text{had}}^{(5)}(M_Z) &= 0.02757(10), \\
 M_W &= 80.385(15) \text{ GeV}, & M_Z &= 91.1875(21) \text{ GeV}, & m_t &= 173.18(94) \text{ GeV}.
 \end{aligned} \tag{B.2.1}$$

The numerical value of the fine structure constant at M_Z is parametrized by the on-shell value $\alpha(M_Z) = \alpha/(1 - \Delta\alpha(M_Z))$, with the value in the Thomson limit $Q^2 = 0$ being $\alpha^{-1} = 137.035999074(44)$ [69]. The hadronic contribution to $\Delta\alpha(M_Z)$ is taken from [448]. Unless noted otherwise, the reference value for the Higgs-boson mass is $M_h = 126$ GeV.

In the flavor analyses of section 4.1 we employ the following numerical values:

Parameter	Value \pm Error	Reference	Parameter	Value \pm Error	Reference
M_K	497.614(24) MeV	[69]	$(\epsilon'_K/\epsilon_K)_{\text{exp}}$	$16.6(23) \cdot 10^{-4}$	[69]
f_K	156.1(11) MeV	[449]	$B_6^{(1/2)}$	[0.8, 2.0]	[291]
B_1^{sd}	0.52(2)	[274]	$B_8^{(3/2)}$	[0.8, 1.2]	[291]
B_2^{sd}	0.54(3)	[274]	κ_L	$2.247(13) \cdot 10^{-10}$	[302]
B_3^{sd}	0.94(8)	[274]	κ_+	$0.5210(25) \cdot 10^{-10}$	[302]
B_4^{sd}	0.82(5)	[274]	Δ_{EM}	-0.003	[302]
B_5^{sd}	0.63(7)	[274]	X_t	1.469(17)	[305]
$m_s(2 \text{ GeV})$	93.4(11) MeV	[449]	$P_{c,u}$	0.41(4)	[306–309]
$m_d(2 \text{ GeV})$	3.41(5) MeV	[449]	y_c	-0.20(3)	[311]
φ_ϵ	$43.52(5)^\circ$	[69]	$y_{\gamma\gamma}$	0.4(5)	[312]
κ_ϵ	0.94(2)	[275]	y_A	-0.68(3)	[314]
$(\Delta M_K)_{\text{exp}}$	$3.484(6) \cdot \text{meV}$	[69]	$ a_S $	1.20(20)	[315, 316]
$ \epsilon_K _{\text{exp}}$	$2.228(11) \cdot 10^{-3}$	[69]	y_V	0.73(4)	[314]
$m_t(m_t)$	163.6(11) GeV	[447]	M_{B_d}	5.2796(2) GeV	[69]
$m_c(m_c)$	1.279(1) GeV	[450]	M_{B_s}	5.3668(2) GeV	[69]
η_{tt}	0.5765(65)	[327]	m_μ	105.66 MeV	[69]
η_{cc}	1.87(76)	[279]	f_{B_d}	190.6(47) MeV	[449]
η_{ct}	0.496(47)	[451]	f_{B_s}	227.6(50) MeV	[449]
$ V_{us} $	0.2252(9)	[69]	τ_{B_d}	1.525(9) ps	[452]
$ V_{cb} $	0.0409(11)	[69]	τ_{B_s}	$(1.472_{-0.026}^{+0.024})$ ps	[452]
			c_A	0.96 ± 0.02	[303, 304]

In the numerical analysis of the RS model we generated parameter points and checked their validity by requiring the fermionic spectrum to comply with the following values of $\overline{\text{MS}}$ quark masses evaluated at the scale $M_{\text{KK}} = 1$ TeV

$$\begin{aligned}
 m_u &= (1.5 \pm 1.0) \text{ MeV}, & m_c &= (560 \pm 40) \text{ MeV}, & m_t &= (144 \pm 5) \text{ GeV}, \\
 m_d &= (3.0 \pm 2.0) \text{ MeV}, & m_s &= (50 \pm 15) \text{ MeV}, & m_b &= (2.3 \pm 0.1) \text{ GeV}.
 \end{aligned}
 \tag{B.2.2}$$

They correspond to the low-energy values as compiled in [453]. The central values and errors of the Wolfenstein parameters are taken from [454] and read

$$\lambda = 0.2255 \pm 0.0009, \quad A = 0.807 \pm 0.018, \quad \bar{\rho} = 0.147_{-0.017}^{+0.029}, \quad \bar{\eta} = 0.343 \pm 0.016.
 \tag{B.2.3}$$

The requirements on the data sets of RS points are the same as used in [3] and were not updated here. Small variations (within error ranges) of the values in (B.2.2) and (B.2.3) are irrelevant, as they affect only the RS contributions and not the leading SM values.

B.3 Description of the Parameter Scans in RS Models

Here we describe in detail the procedure used for scanning the parameter space of the RS model. The discussion is mainly aimed at the scan of the parameter space of the minimal RS model, as used in the discussion of flavor physics in section 4.1.2. The general technique for the analysis of Higgs physics in section 4.3.3 is essentially the same; the small differences are summarized in appendix B.4. First, we describe a set of standard parameter ranges, which we call the standard scenario (labeled *std*). Below, we introduce variations of the standard choice and investigate in detail to which extent the different scenarios allow us to relax the strong constraints arising from EWPOs and quark-flavor physics. We set the volume of the extra dimension to the maximal value $L = \ln(10^{16}) \approx 37$ as a standard choice. The parameter points are generated in a three-step process. First, we determine sets of Yukawa matrices $\tilde{Y}_{u,d}$ that allow to reproduce the observed values of the Wolfenstein parameters $\bar{\rho}$ and $\bar{\eta}$. Since the latter two quantities are to leading order in hierarchies independent of the values $F(c_{A_i})$ [1], it turns out to be computationally expensive to find suitable pairs of Yukawa matrices $\tilde{Y}_{u,d}$ by a simple random sampling. To generate proper sets we proceed in the following way. We randomly pick one element of the Yukawa matrices, keeping its phase ϕ and modulus y arbitrary. The remaining elements are then generated from a uniform distribution in the ranges $\arg(\tilde{Y}_{u,d})_{ij} \in [0, 2\pi)$ and $|(\tilde{Y}_{u,d})_{ij}| \in [0.1, y_{\max}]$. The lower limit enforces Yukawa entries of natural size. For the upper limit we use a standard value of $y_{\max} = 3$, which was derived in [211] as a perturbativity bound by means of naive dimensional analysis. It is the standard choice for y_{\max} employed in several articles on flavor effects in warped extra-dimension models [211, 212, 229, 254, 255, 261, 455]. We calculate the Wolfenstein parameters $\bar{\rho}$ and $\bar{\eta}$ by means of the ZMA formula [1]

$$\bar{\rho} - i\bar{\eta} = \frac{(\tilde{Y}_d)_{33}(M_u)_{31} - (\tilde{Y}_d)_{23}(M_u)_{21} + (\tilde{Y}_d)_{13}(M_u)_{11}}{(\tilde{Y}_d)_{33}(M_u)_{11} \left[\frac{(\tilde{Y}_d)_{23}}{(\tilde{Y}_d)_{33}} - \frac{(\tilde{Y}_u)_{23}}{(\tilde{Y}_u)_{33}} \right] \left[\frac{(M_d)_{21}}{(M_d)_{11}} - \frac{(M_u)_{21}}{(M_u)_{11}} \right]}, \quad (\text{B.3.1})$$

where M_q is the matrix of minors of \tilde{Y}_q . Using the randomly picked Yukawa element, we minimize the function

$$\chi^2(x) = \sum_n \left(\frac{x_n^{\text{exp}} - x_n^{\text{theo}}}{\sigma_n^{\text{exp}}} \right)^2, \quad x = \{\bar{\rho}, \bar{\eta}\}, \quad (\text{B.3.2})$$

with respect to ϕ and y , again requiring $0.1 \leq y \leq y_{\max}$. Here x_n^{exp} and x_n^{theo} denote the experimental and theoretical value of the n^{th} observable and σ_n^{exp} is the standard deviation of the corresponding measurement. We compile the used values of the observables in appendix B.2.

After the elements of the Yukawa matrices $\tilde{Y}_{u,d}$ have been fixed, we choose a random value from a uniform distribution for the bulk-mass parameter $c_{u_3} \in (-1/2, c_{u_3}^{\max}]$, with $c_{u_3}^{\max} = 2$ being the standard choice¹. Then, we calculate the complete set of observables $x = \{m_u, m_d, m_s, m_c, m_b, m_t, A, \lambda, \bar{\rho}, \bar{\eta}\}$ in terms of the zero-mode profiles of the remaining

¹The choice of c_{u_3} as a prior is motivated by the fact that this bulk-mass parameter determines the degree of compositeness of the top quark. While the lower limit of the allowed range of c_{u_3} is motivated by the fact that the right-handed top quark should be localized near the IR brane, the upper limit is chosen in a somewhat *ad hoc* way. Allowing for $c_{u_3}^{\max} \gg 1$ would however take away an attractive feature of the RS model, namely that it explains the quark hierarchies in terms of fundamental parameters of $\mathcal{O}(1)$.

c_{A_i} . To this end we use the Froggatt-Nielsen relations to leading order in the Cabibbo angle $\lambda \approx 0.23$

$$\begin{aligned}
 m_u &= \frac{v}{\sqrt{2}} \frac{|\det(\mathbf{Y}_u)|}{|(M_u)_{11}|} |F(c_{Q_1})F(c_{u_1})|, & m_d &= \frac{v}{\sqrt{2}} \frac{|\det(\mathbf{Y}_d)|}{|(M_d)_{11}|} |F(c_{Q_1})F(c_{d_1})|, \\
 m_c &= \frac{v}{\sqrt{2}} \frac{|(M_u)_{11}|}{|(Y_u)_{33}|} |F(c_{Q_2})F(c_{u_2})|, & m_s &= \frac{v}{\sqrt{2}} \frac{|(M_d)_{11}|}{|(Y_d)_{33}|} |F(c_{Q_2})F(c_{d_2})|, \\
 m_t &= \frac{v}{\sqrt{2}} |(Y_u)_{33}| |F(c_{Q_3})F(c_{u_3})|, & m_b &= \frac{v}{\sqrt{2}} |(Y_d)_{33}| |F(c_{Q_3})F(c_{d_3})|,
 \end{aligned} \tag{B.3.3}$$

$$\lambda = \frac{|F(c_{Q_1})|}{|F(c_{Q_2})|} \left| \frac{(M_d)_{21}}{(M_d)_{11}} - \frac{(M_u)_{21}}{(M_u)_{11}} \right|, \quad A = \frac{|F(c_{Q_2})|^3}{|F(c_{Q_1})|^2 |F(c_{Q_3})|} \left| \frac{\frac{(Y_d)_{23}}{(Y_d)_{33}} - \frac{(Y_u)_{23}}{(Y_u)_{33}}}{\left[\frac{(M_d)_{21}}{(M_d)_{11}} - \frac{(M_u)_{21}}{(M_u)_{11}} \right]^2} \right|.$$

The values of the zero-mode profiles $F(c_{A_i})$ are then determined from the best fit to the $\chi^2(x)$ function, supplemented by the constraints $F(c_{A_i}) \leq F(c_{u_3}^{\max})$. Points with $\chi^2(x)/\text{dof} > 11.5/10$, corresponding to a combined 68% CL, are rejected. As a last step, we recompute $\chi^2(x)$ for points that pass the test, now using the exact formulas for the quark masses and Wolfenstein parameters and remove all points that show a deviation of more than 3σ in at least one observable.

In order to assure that our algorithm populates the whole parameter space without introducing spurious correlations, we have inspected the final distributions of parameters. While the magnitudes and phases of the elements of the Yukawa matrices are all nearly flatly distributed, the shapes of the distributions of the quark masses and Wolfenstein parameters are nearly Gaussian with a width of at most twice the corresponding experimental uncertainty. We consider this as a strong indication that we achieve full coverage of the parameter space in an unbiased way. These features are basic prerequisites guaranteeing that the spread of achievable values for observables, and correlations between different observables indeed have a physical origin and are not artifacts of an imperfect Monte Carlo sampling.

In order to assess the robustness of our predictions for flavor observables, we also investigate how sensitively they depend on the values of the most relevant parameters of the model. We therefore study three different benchmark scenarios that differ by the allowed maximal magnitude of the Yukawa couplings, the structure of the bulk-masses matrices, and the value of the logarithm of the warp factor. The benchmark scenarios are designed specifically to suppress harmful contributions to electroweak precision and quark flavor observables without the necessity of a custodial protection of the gauge group and therefore present particular cases of viable minimal models of warped extra dimensions with improved prospects for discovery at the LHC. Our benchmark scenarios are defined as follows:

- “standard” scenario (std)

This scenario uses the standard parameters, which we introduced above.

- “aligned” scenario (SU3d):

In this scenario we impose common bulk masses c_{d_i} in the sector of right-handed down-type quarks. This is feasible, since the mass splittings in the down-type quark sector can be naturally accommodated by $\mathcal{O}(1)$ variations of the Yukawa couplings. The universal bulk-mass parameters can be achieved by imposing a $U(3)$ flavor symmetry, under which

	standard	aligned	LRS
c_{Q_1}	-0.63 ± 0.03	-0.66 ± 0.02	-1.34 ± 0.16
c_{Q_2}	-0.57 ± 0.05	-0.59 ± 0.03	-1.04 ± 0.18
c_{Q_3}	-0.34 ± 0.32	-0.24 ± 0.43	-0.49 ± 0.34
c_{u_1}	-0.68 ± 0.04	-0.65 ± 0.03	-1.58 ± 0.18
c_{u_2}	-0.51 ± 0.12	-0.50 ± 0.12	-0.79 ± 0.26
c_{u_3}	$] - 1/2, 2]$	$] - 1/2, 2]$	$] - 1/2, 5/2]$
c_{d_1}	-0.65 ± 0.03	-0.60 ± 0.02	-1.44 ± 0.17
c_{d_2}	-0.62 ± 0.03	-0.60 ± 0.02	-1.28 ± 0.17
c_{d_3}	-0.58 ± 0.03	-0.60 ± 0.02	-1.05 ± 0.13

Table B.1: Central values and statistical uncertainties of the bulk-mass parameters in the three benchmark scenarios. The shown errors correspond to 1σ ranges when fitting the distributions to a Gaussian function, except for c_{u_3} for which a flat prior is chosen in the given range. See text for details.

the fields that give rise to the right-handed down-type quark zero modes transform as triplets, and all other fields as singlets [254]. Besides the natural suppression of corrections to ϵ_K [254], this scenario has the appealing feature that it leads to a unique pattern of deviations in the $K \rightarrow \pi\nu\bar{\nu}$ sector.

- little RS scenario (LRS):

From a purely phenomenological point of view, it is possible to lower the UV cutoff from the Planck scale to a value only few orders of magnitude above the TeV scale, even though in this case a true solution to the hierarchy problem is postponed to higher energy. Since many amplitudes in the RS model are enhanced by L , it is worthwhile to address the question to what extent certain experimental constraints can be avoided by such a choice [192]. Thus, we consider a “volume-truncated” variant of our first scenario characterized by $L = \ln(10^3) \approx 7$. This affects the amount of splitting between the bulk-mass parameters, which is necessary to achieve the fermion hierarchies. In order to cover the full shape of the distributions for the bulk-mass parameters, we allow for $c_{u_3}^{\max} = 5/2$. In this “little” RS scenario [192] the bound from oblique EWPOs is lowered to a size that is comparable to the custodial model (see figure 4.12). However, no improvement concerning ϵ_K is achieved compared to the standard benchmark scenario [229].

The statistical approach outlined in the last section provides us with distributions of bulk-mass parameters rather than with their precise values. The obtained results are different in the individual benchmark scenarios, and in order to make this work self-contained, we summarize the central values and standard deviations of the parameters c_{A_i} for the three cases in table B.1. We also illustrate the distribution in the standard scenario in figure B.1. All distributions are nearly Gaussian, apart from those of c_{Q_3} , which feature a small tail to higher values, and those of c_{u_3} , which are chosen as flat priors. Notice that while the central values of the bulk-mass parameters in the standard and aligned benchmark scenarios are very similar, the splitting between the individual c_{A_i} parameters is on average much bigger in the

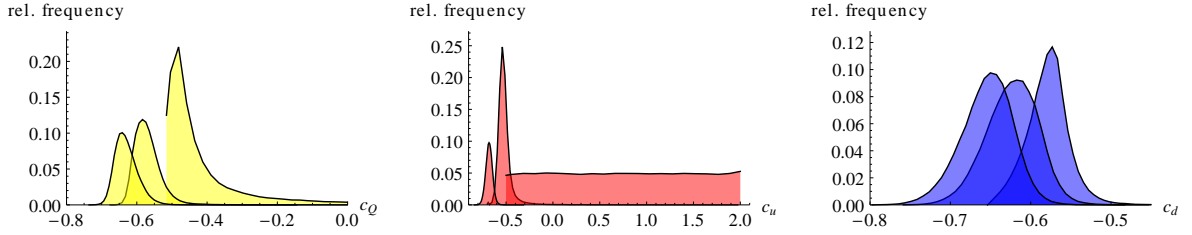


Figure B.1: Bulk-mass parameter distribution resulting from the Monte Carlo sampling with standard parameter choices (std).

LRS scenario due to the smaller “volume factor” L . We have verified that the precise form of the distributions is essentially independent of the details of the algorithm used to scan the parameter space. Besides inspecting the coverage of our Monte-Carlo sampling, we also assess the numerical and perturbative stability of each single parameter point. For this purpose we use the quantitative measure for fine-tuning

$$\Delta_{\text{BG}}(\mathcal{O}) = \max_{p \in \mathcal{P}} \left| \partial_{\ln(p)} \ln(\mathcal{O}) \right|, \quad (\text{B.3.4})$$

introduced by Barbieri and Giudice [326]. In our case, the set of model parameters \mathcal{P} includes the Yukawa couplings, their complex conjugates, and the bulk masses.

We identify two different situations, where $\Delta_{\text{BG}}(\mathcal{O})$ can become large, rendering the results unstable under small variations of the input parameters. The first case corresponds to large values of the observable \mathcal{O} , where the variation is dominated by a single contribution. In this case it is sufficient to apply the fine-tuning measure to the matrices $\Delta_A^{(l)}$ and δ_A , defined in (3.3.145) and (3.3.148), which constitute the new-physics contributions to all the relevant couplings (KK photons and gluons, Z boson and its KK excitations) in our analysis. In practice, we use the analytic form of those matrices from [1], obtained from a Froggatt-Nielsen analysis to leading order in λ . The contributions to $\Delta_{\text{BG}}(\Delta_A^{(l)}, \delta_A)$ stemming from variations of the bulk-mass parameters c_{A_i} scale either as L or 1 if $c_{A_i} < -1/2$ or $c_{A_i} > -1/2$. Similarly, variations with respect to the Yukawa entries typically lead to contributions of $\mathcal{O}(1)$, but can also become larger if individual elements $(Y_{u,d})_{ij}$ appearing in the denominators of the expressions for $\Delta_A^{(l)}$ and δ_A cancel each other. However, even in such a case the resulting contribution to $\Delta_{\text{BG}}(\Delta_A^{(l)}, \delta_A)$ never exceeds 100 for points consistent with the observed quark masses and mixing, implying no severe fine-tuning.

The situation is different for untypically small values of \mathcal{O} . As we show explicitly in section 4.1.2.4, this situation occurs in the case of $|\epsilon_K|$, where the experimental constraint forces the new-physics contribution to be small compared to the typical values that arise in the model at hand. In this case we calculate $\Delta_{\text{BG}}(|\epsilon_K|)$ taking into account the full expression for $|\epsilon_K|$ with all interferences and RG effects, and reject parameter points that show an excessive fine-tuning stronger than one per mil, *i.e.* $\Delta_{\text{BG}}(|\epsilon_K|) > 1000$. The resulting data sets consist of more than 60,000 valid parameter points in each scenario. We have verified that (reasonable) variations of the chosen cut on $\Delta_{\text{BG}}(|\epsilon_K|)$ neither change the shape of the distribution of allowed scatter points nor affect any of our conclusions. In contrast, restricting the amount of allowed fine-tuning to values of around 10 would result in distributions that show a sharp cutoff of values below the lower end of the experimental allowed region of $|\epsilon_K|$.

B.4 Numerical Scans of Higgs Processes in RS Models

In the following, we summarize the full numerical results for Higgs processes obtained from the parameter scans in the RS model. To this end we generated one large set of valid parameter points in the ZMA like described in appendix B.3. Then we adapted the parameters to several allowed ranges of the fundamental $\mathcal{O}(1)$ Yukawa matrices, which are taken to be uniformly distributed in $|(\tilde{Y}_{u,d})_{ij}| \in [y_{\max}/10, y_{\max}]$, by using the reparametrization invariance [1], which is valid in the ZMA

$$F(c_{Q_i}) \rightarrow \eta F(c_{Q_i}), \quad F(c_{Q_i}) \rightarrow \eta F(c_{Q_i}), \quad \tilde{Y}_q \rightarrow 1/\eta^2 \tilde{Y}_q. \quad (\text{B.4.1})$$

We choose three discrete values $y_{\max} = 3, 1.5, \text{ and } 0.5$ and investigate the minimal and the custodially protected setup of the RS model, as defined and discussed in sections 3.3.4 and 3.3.5, with a warp factor of $\epsilon = 10^{-15}$. For each of the six approximate ZMA parameter sets, we separately check each parameter point with exact expressions and require it to fulfill the observed zero-mode fermion spectrum and mixing angles. Thereafter, approximately 14,000 valid points remain in each set. Additionally, we impose the constraint on the $Zb\bar{b}$ couplings in the case of $h \rightarrow \gamma Z$ where this coupling in fact enters. We checked that all other observables are uncorrelated with this coupling and with other constraints from flavor-physics, such as CP violation in $K-\bar{K}$ mixing. This is in fact expected and obvious from the analytic results of section 4.3.3. Imposing the constraints would only thin out the parameter sets for low values of M_{KK} and impair the statistical quality of our conclusions in this interesting region of parameter space. The constraints from oblique corrections to EWPOs, as discussed in section 4.2.2, are of a different quality, since they restrict mainly the KK scale (see (4.2.23)). However, we mentioned that loop-effect can potentially lower these bounds. In order to compare the constraining potential of Higgs processes with EWPO bounds, we show the results down to a low scale of $M_{\text{KK}} = 1 \text{ TeV}$.

We calculate the KK-loop contributions by explicitly summing up the contributions of the first four KK levels of heavy quarks. These are in total $4 \times (6 + 6)$ KK quarks in the minimal and $4 \times (15 + 9 + 9)$ in the custodial model, where the numbers in brackets are the multiplicities of up, down and exotic quarks in each KK level.² In order to determine this spectrum exactly, one first has to find the solutions to the eigenvalue equation (3.3.43). This is done by the same method like the determination of the exact zero-mode spectrum, which we used to select valid parameter points. However, we have to improve the method when applying it to the KK spectrum. The bracketing of the zeros of (3.3.43) is non-trivial for the KK modes. In the case of the up-type quark sector in the custodial model we must determine 15 roots of a 9×6 determinant, which in practice turns out to be intricate, because one needs to find suitable starting points to search for the roots. We obtain these starting values by diagonalizing a truncated mass matrix obtained in the perturbative approach [200, 430, 456] to the Yukawa matrices. Then we feed this into an adapted version of a bracketed secant zero algorithm, using also the information from alternating signs of the determinant between the zeros which have multiplicity one. Furthermore, we implemented a bisection fallback method for those cases where a very non-linear behavior of the determinant is detected, in order to approach

²In the absence of soft P_{LR} breaking, $c_{\mathcal{T}_{1i}} = c_{\mathcal{T}_{2i}}$, three out of the 15 (9) states in each up-type (λ -type) quark-KK level will have masses that resemble the ones found in the spectrum for $(Y_{u,d})_{ij} = 0$. This feature is easy to understand, because a unitary transformation \mathcal{U} acting on the quarks $(U, U')^T \rightarrow \mathcal{U}(U, U')^T$ reshuffles only the Yukawa interactions, but leaves all other bilinear terms in the action as well as the BCs invariant. The combinations $(U - U')/\sqrt{2}$ and $(\Lambda - \Lambda')/\sqrt{2}$ are thus unaffected by the Higgs mechanism.

the zero faster. We implemented this in the computational software program *Mathematica* with optimized and parallelized code. This allows to generate the large data sets in roughly one week of single-core CPU time on modern machines.

Having the numerical result at hand, we can verify the analytic results of section 4.3.3 as an additional check. To achieve a high precision for the numerical results we extrapolate the sum entering $\Sigma_q^{(\text{low})}$ from the first four KK levels to the resummed result, by using

$$\sum_{n=1}^{\infty} \frac{v g_{nn}^q}{m_n^q} = \frac{v}{M_{\text{KK}}} \left(\sum_{n=1}^{n_f+n_F} \frac{g_{nn}^q}{x_n^q} + \rho_{2,4} \sum_{n=n_f+n_F+1}^{n_f+4n_F} \frac{g_{nn}^q}{x_n^q} \right). \quad (\text{B.4.2})$$

The factor $\rho_{m,n}$ summarizes the extrapolation of the contribution from all higher KK levels, starting from the $(n+1)^{\text{th}}$, based on the numerical result for the m^{th} up to the n^{th} level, which have to be found numerically. We choose to exclude the 1st KK level from the extrapolation. Above that a very regular pattern emerges, such that the factor $\rho_{m,n}$ can be derived analytically. We make use of the knowledge that the summed contributions from the k^{th} KK level scale approximately with $\sim (((k-1)\pi - \bar{x}_1^q)^2 - (\bar{x}_0^q)^2)^{-1}$, where we set $\bar{x}_{0,1}^q$ to the average value of the zero mode and first KK-level masses. Numerically this turns out to be very accurate for approximating the unknown higher KK-level contributions. The resummed correction factor is analytically given by

$$\begin{aligned} \rho_{m,n} &= \left(1 - \frac{\psi_0(n + (\bar{x}_1^q + \bar{x}_0^q)/\pi) - \psi_0(n + (\bar{x}_1^q - \bar{x}_0^q)/\pi)}{\psi_0(m-1 + (\bar{x}_1^q + \bar{x}_0^q)/\pi) - \psi_0(m-1 + (\bar{x}_1^q - \bar{x}_0^q)/\pi)} \right)^{-1} \\ &= \left(1 - \frac{\psi_0'(n + \bar{x}_1^q/\pi)}{\psi_0'(m-1 + \bar{x}_1^q/\pi)} \right)^{-1} + \mathcal{O}\left(\frac{(\bar{x}_0^q)^2}{6\pi^2}\right), \end{aligned} \quad (\text{B.4.3})$$

where ψ_0 denotes the digamma function. The extrapolation factor turns out to be independent of \bar{x}_0^q to very good precision, such that we neglect this dependence and use $\rho_{2,4} \approx 1.209 + 0.237(\bar{x}_1^q/2.5)$. Remark that this rescales the contributions starting from the second level and only has a minor impact compared to the contribution from the first KK level. However, it is reassuring for the check of the analytical result and verifying statements about their bulk mass independence.

In the figures B.2–B.10 we show all two-dimensional fits to the parameter distribution of the KK scale versus a given cross-section ratio, width ratio, or ratio of branching ratios, which we defined in section 4.3.4. The cyan curves correspond to the 5%, 20%, 50%, 80%, and 95% quantiles. Thus, at a given scale M_{KK} , 60% / 90% of the parameter space is contained in the light / dark blue bands. The bands are underlaid with the parameter points in faint yellow. The fits to the quantiles are obtained by first applying a fine grained binning in x -direction, calculating the quantiles, and then fitting a global model to the resulting distributions. Since the observables involve absolute values and interfering amplitudes of different parametric behavior, we choose in each case a fit model that is adapted to the data and check for a high quality of the fit. By default we try to use a quadratic polynomial³ in $(\text{TeV}/M_{\text{KK}})^2$. In the case of the total Higgs width and $y_{\text{max}} = 3$, and also for $R_{\gamma\gamma}/R_{ZZ}$ and $y_{\text{max}} = 3$ in the custodial model, it is necessary and sufficient to extend the model to a Pade approximant, *i.e.* the ratio of two quadratic polynomials. In all other cases, where an extremum arises

³We use three fit parameters, one being the normalization. We check that the normalization turns out to be like expected, *i.e.* one in most cases.

due to the aforementioned reasons, we resort to a more sophisticated model. This involves the sum of Fermi-functions, each multiplied by a quadratic polynomial. The Fermi-functions smoothly connect two regions, where *e.g.* a sign shift in the amplitude implies a minimum for the absolute value of the amplitude. This is necessary since the quantile of the resulting distribution does not exhibit a kink but rather has a smooth minimum.

Remark that, in order to obtain a reliable fit result, we have to exclude the region where less than 10% of the parameter points survive the bound on the $Zb\bar{b}$ -couplings from the fit to $R_{\gamma Z}$. This bound is shown in the left panel of figure 4.16 and discussed in the corresponding section of the main text.

In the following, we enlist the pseudo-observables in the order in which they are discussed in the main text of section 4.3.4. A discussion of the results is given there.

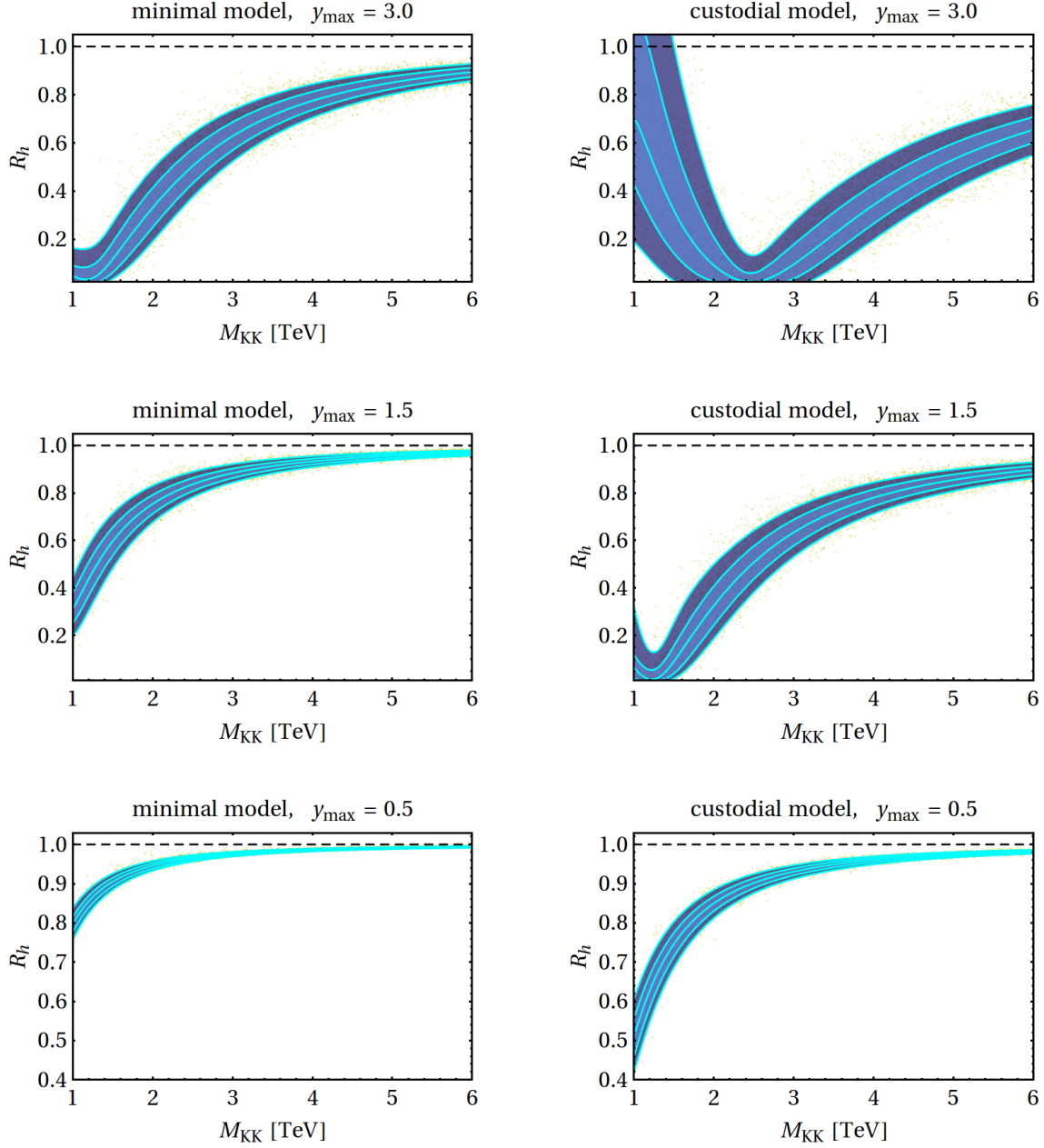


Figure B.2: Fits to the 90%, 60% CLs and median of the parameter distributions of R_h , the ratio of Higgs production via gluon–gluon fusion in RS divided by the SM result. The left column shows results in the minimal RS setup, while in the right column shows results for the custodially protected model. The SM result is marked by the dashed line. Further details are given in the main text.

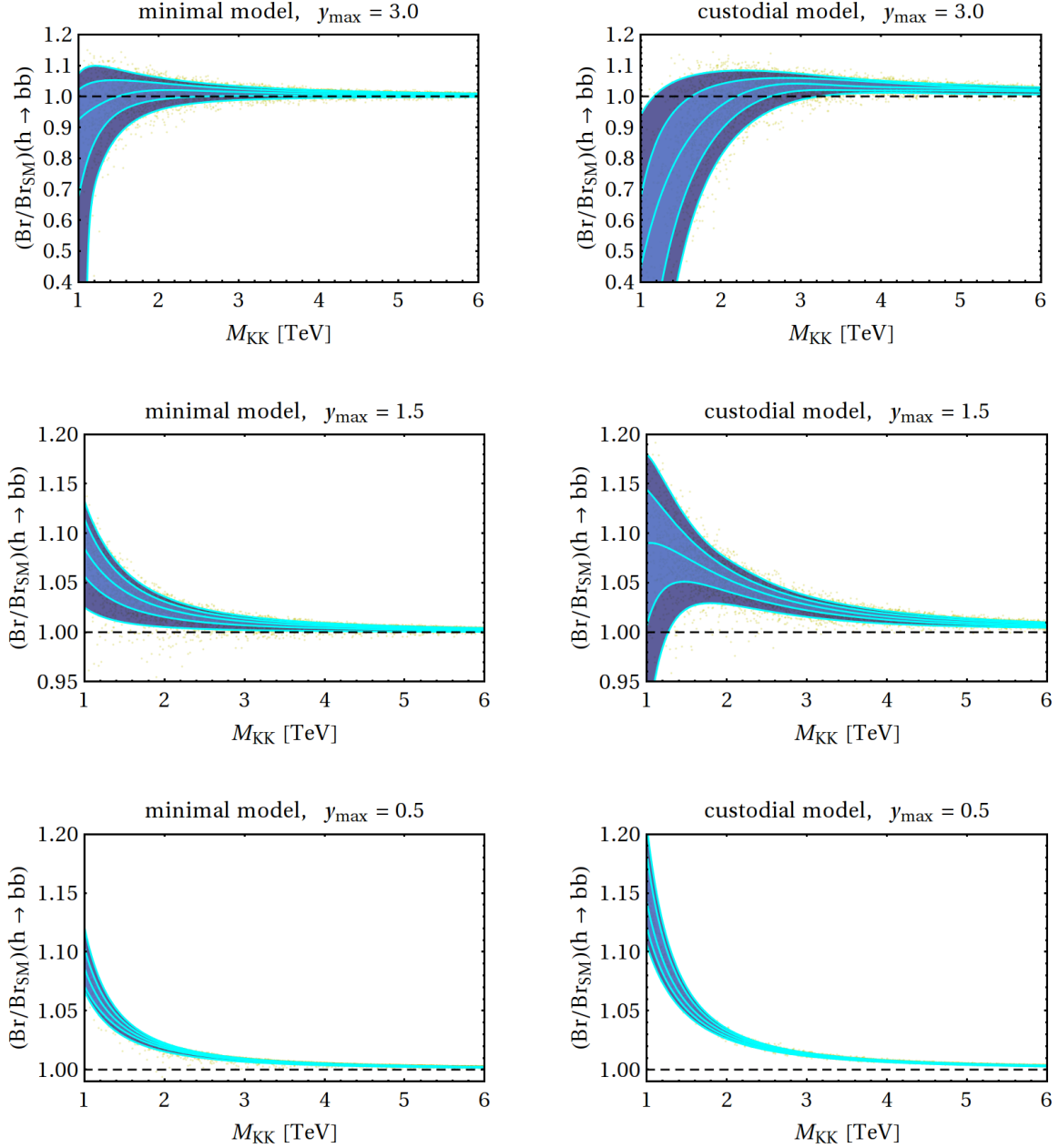


Figure B.3: Fits to the 90%, 60% CLs and median of the parameter distributions of the branching ratio for $h \rightarrow b\bar{b}$ in the RS model divided by the SM result. The left column shows results in the minimal RS setup, while in the right column shows results for the custodially protected model. The SM result is marked by the dashed line. Further details are given in the main text.

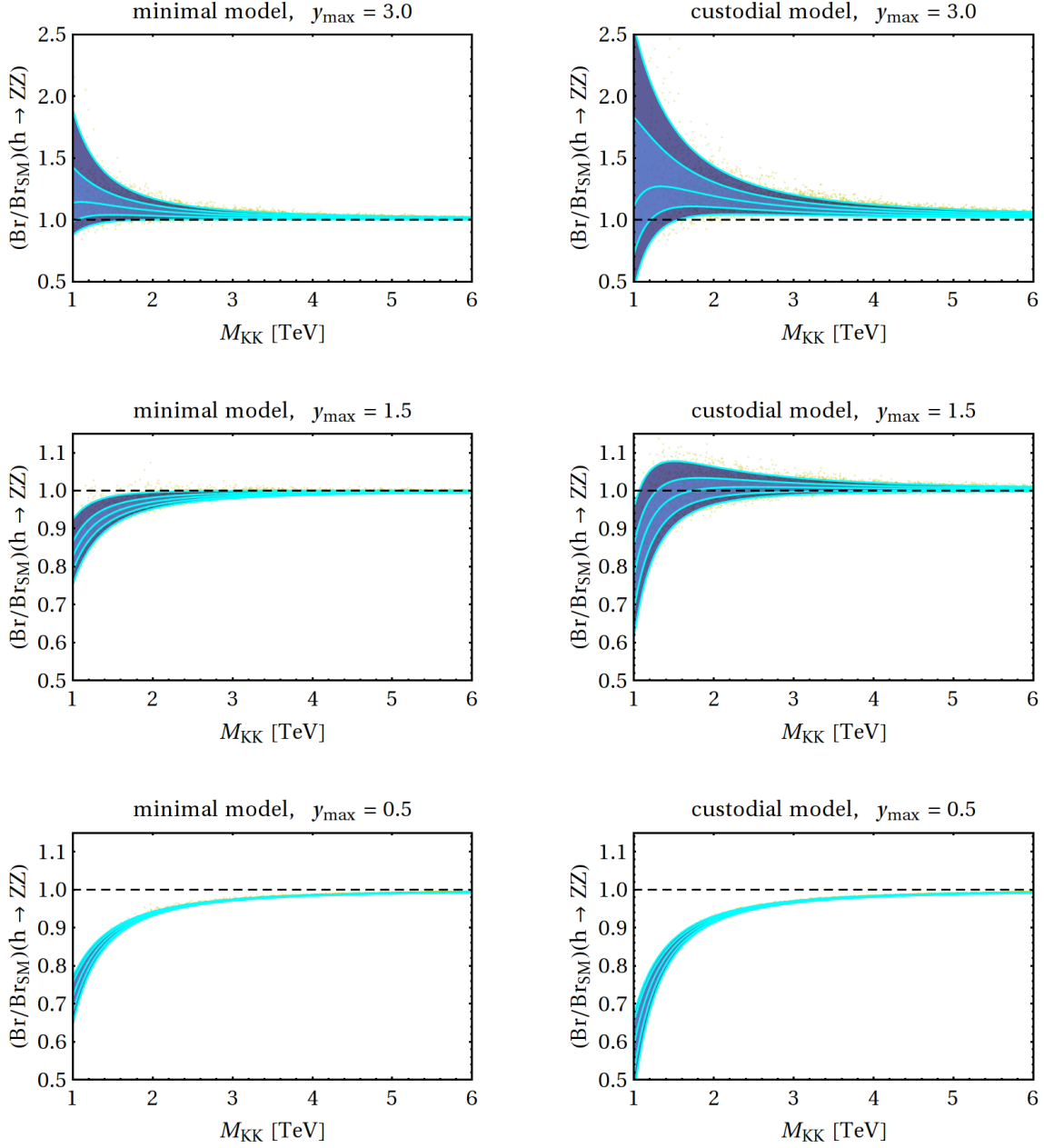


Figure B.4: Fits to the 90%, 60% CLs and median of the parameter distributions of the branching ratio for $h \rightarrow ZZ$ in the RS model divided by the SM result. The left column shows results in the minimal RS setup, while in the right column shows results for the custodially protected model. The SM result is marked by the dashed line. Further details are given in the main text.

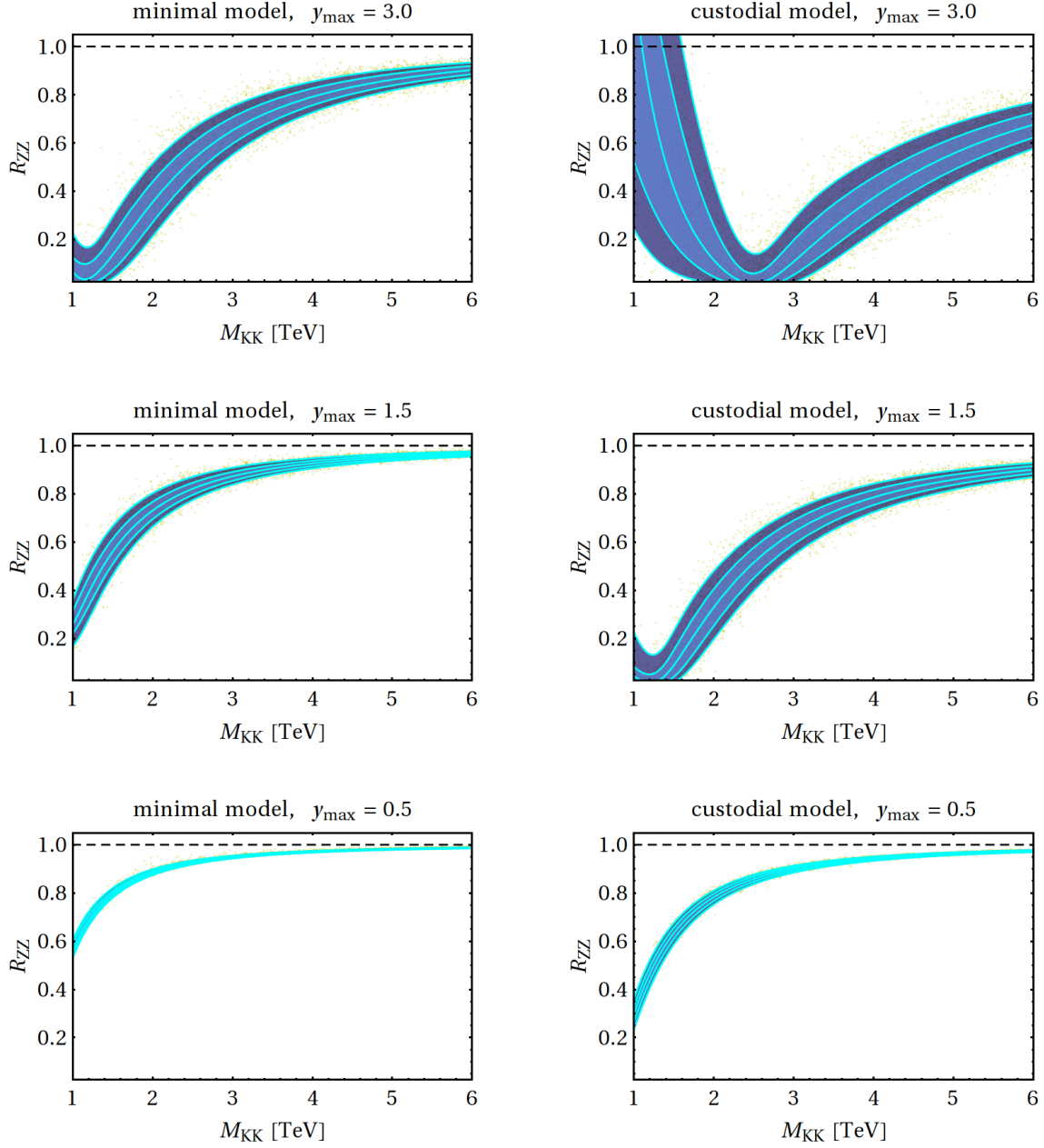


Figure B.5: Fits to the 90%, 60% CLs and median of the parameter distributions of R_{ZZ} , the predicted signal strength of the process $gg \rightarrow h \rightarrow ZZ$ in the RS model. The left column shows results in the minimal RS setup, while in the right column shows results for the custodially protected model. The SM result is marked by the dashed line. Further details are given in the main text.

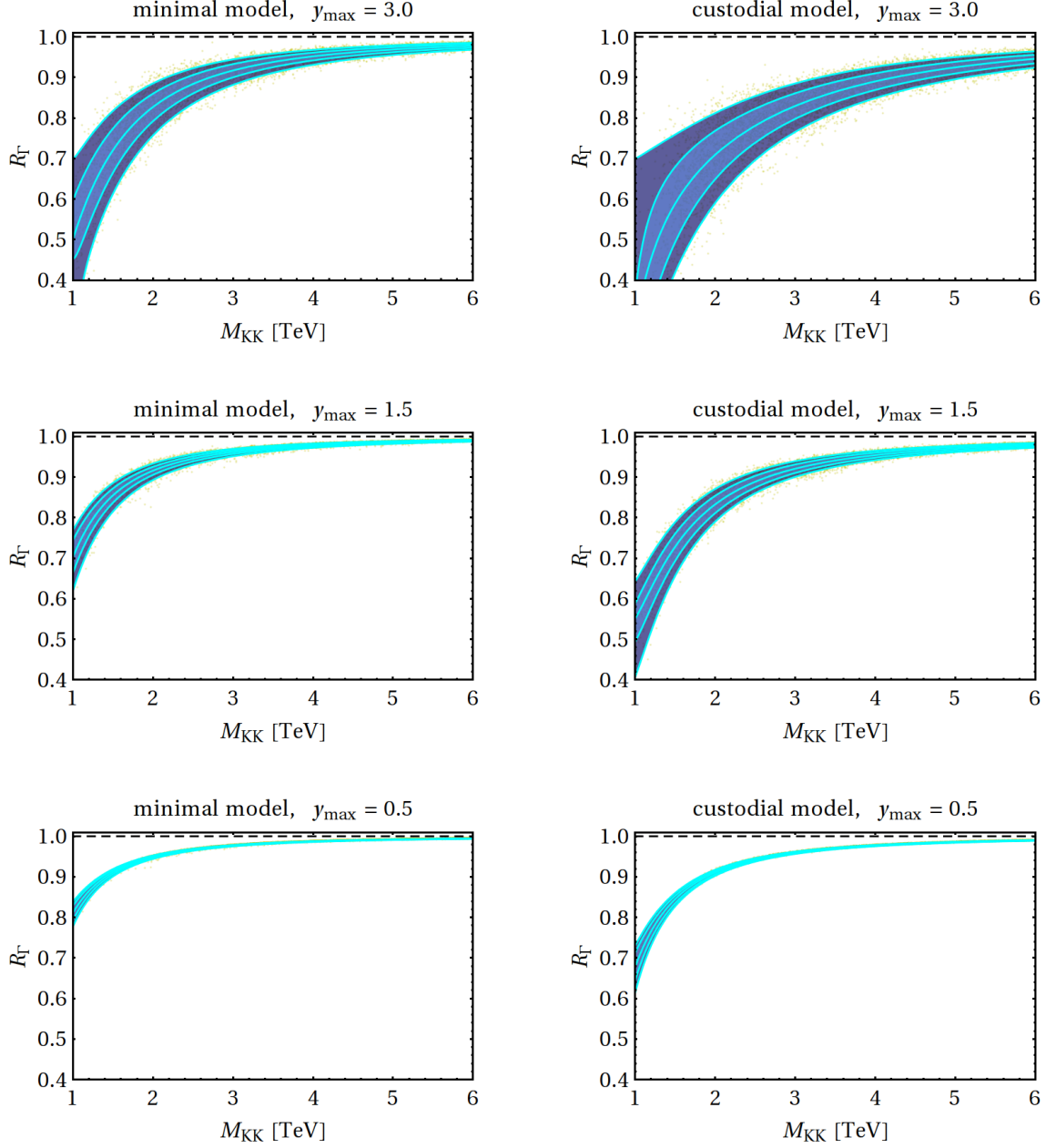


Figure B.6: Fits to the 90%, 60% CLs and median of the parameter distributions of R_Γ , the ratio of the total Higgs width in the RS model divided by the SM result. The left column shows results in the minimal RS setup, while in the right column shows results for the custodially protected model. The SM result is marked by the dashed line. Further details are given in the main text.

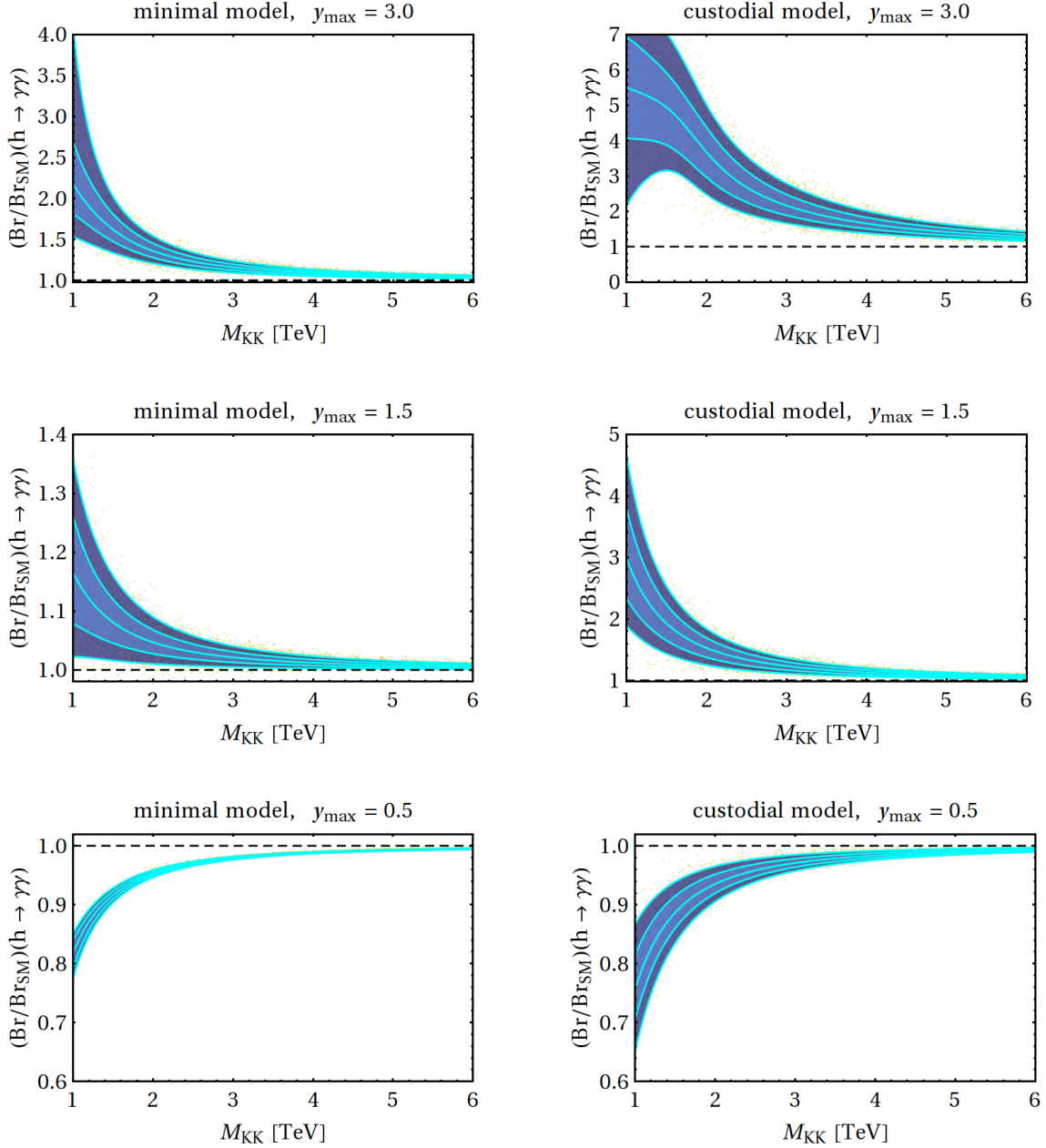


Figure B.7: Fits to the 90%, 60% CLs and median of the parameter distributions of the branching ratio for $h \rightarrow \gamma\gamma$ in the RS model divided by the SM result. The left column shows results in the minimal RS setup, while in the right column shows results for the custodially protected model. The SM result is marked by the dashed line. Further details are given in the main text.

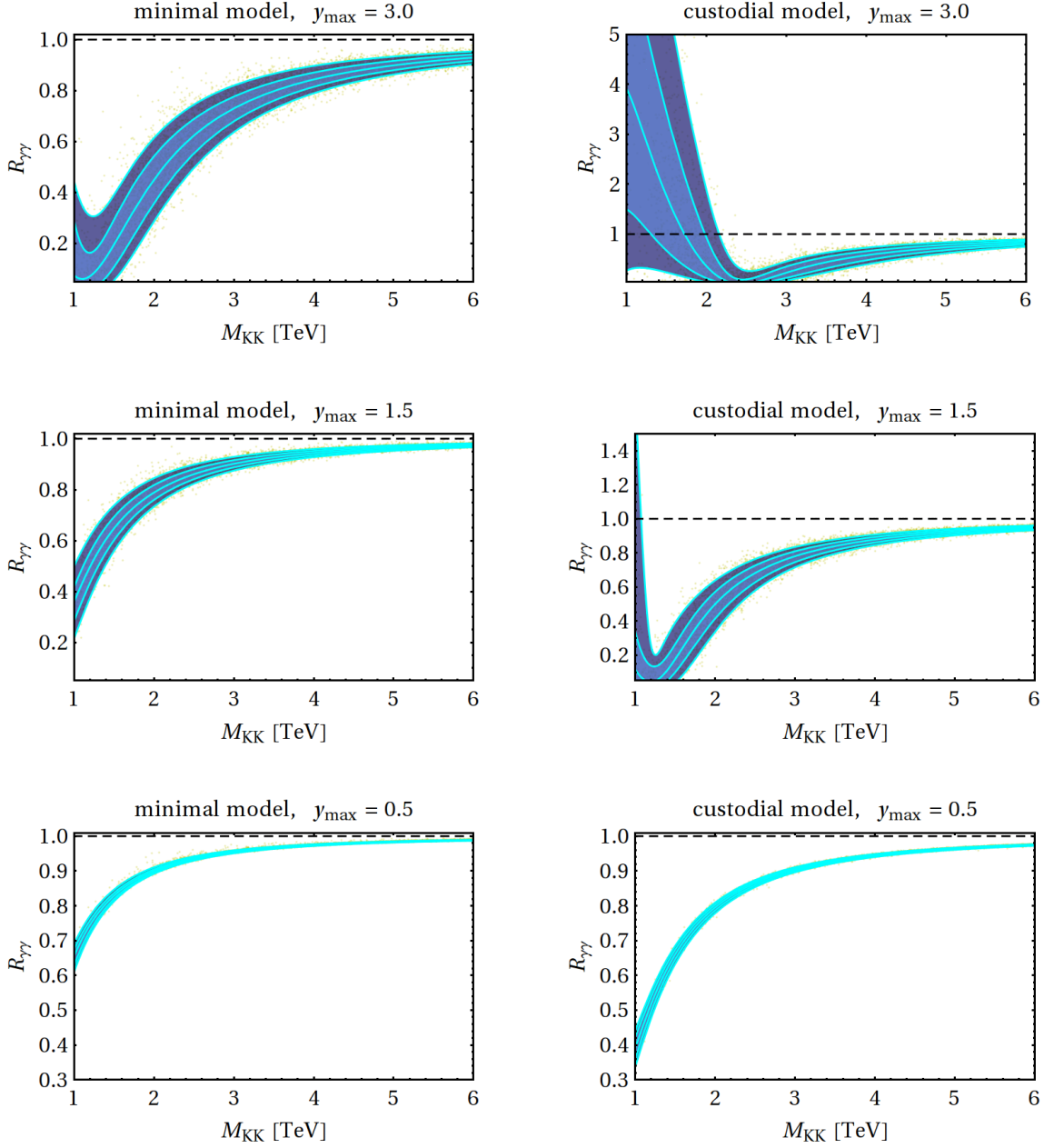


Figure B.8: Fits to the 90%, 60% CLs and median of the parameter distributions of $R_{\gamma\gamma}$, the predicted signal strength of the process $gg \rightarrow h \rightarrow \gamma\gamma$ in the RS model. The left column shows results in the minimal RS setup, while in the right column shows results for the custodially protected model. The SM result is marked by the dashed line. Further details are given in the main text.

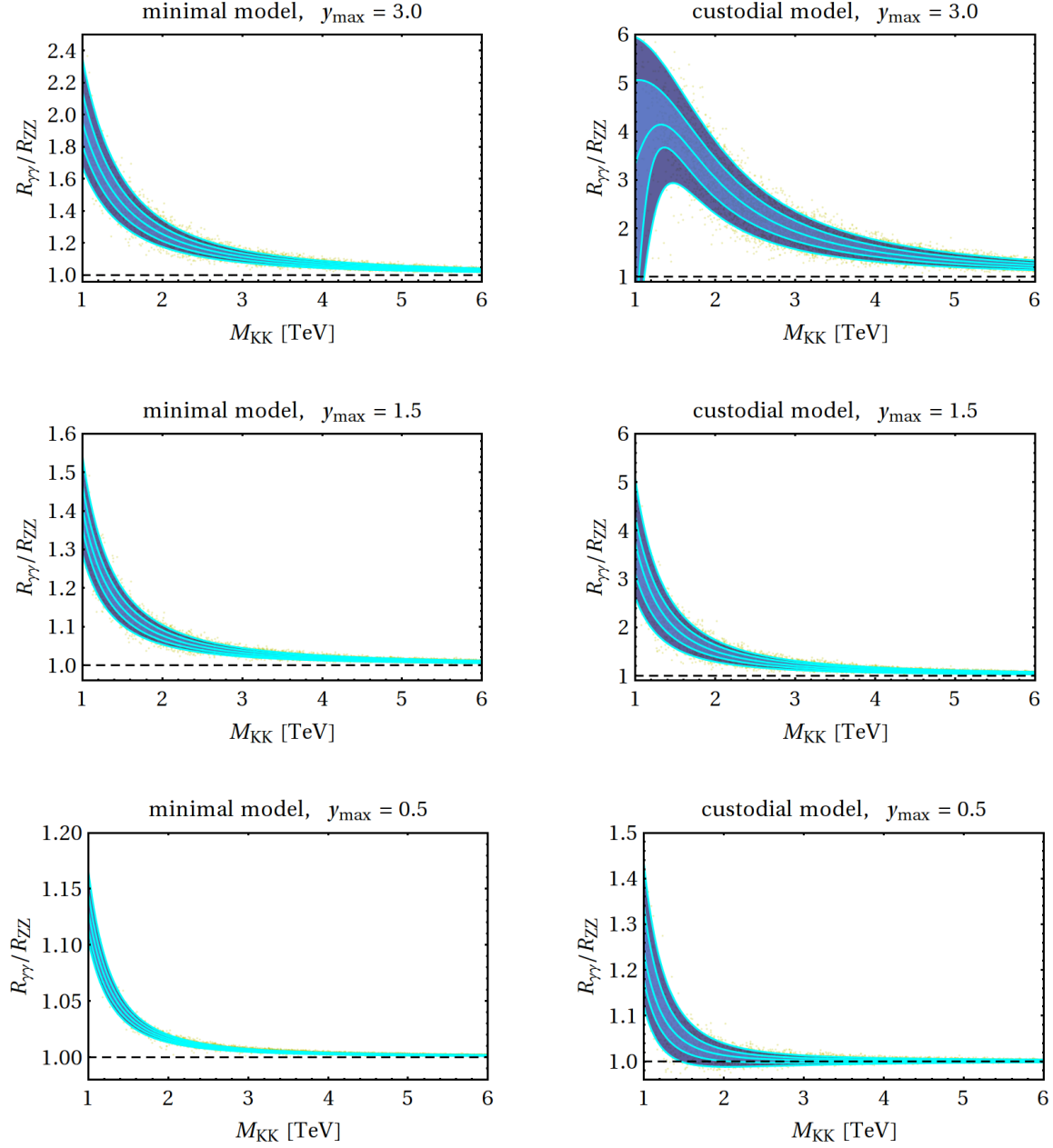


Figure B.9: Fits to the 90%, 60% CLs and median of the parameter distributions of $R_{\gamma\gamma}/R_{ZZ}$, the ratio of the two corresponding two predicted signal strength in the RS model. The left column shows results in the minimal RS setup, while in the right column shows results for the custodially protected model. The SM result is marked by the dashed line. Further details are given in the main text.

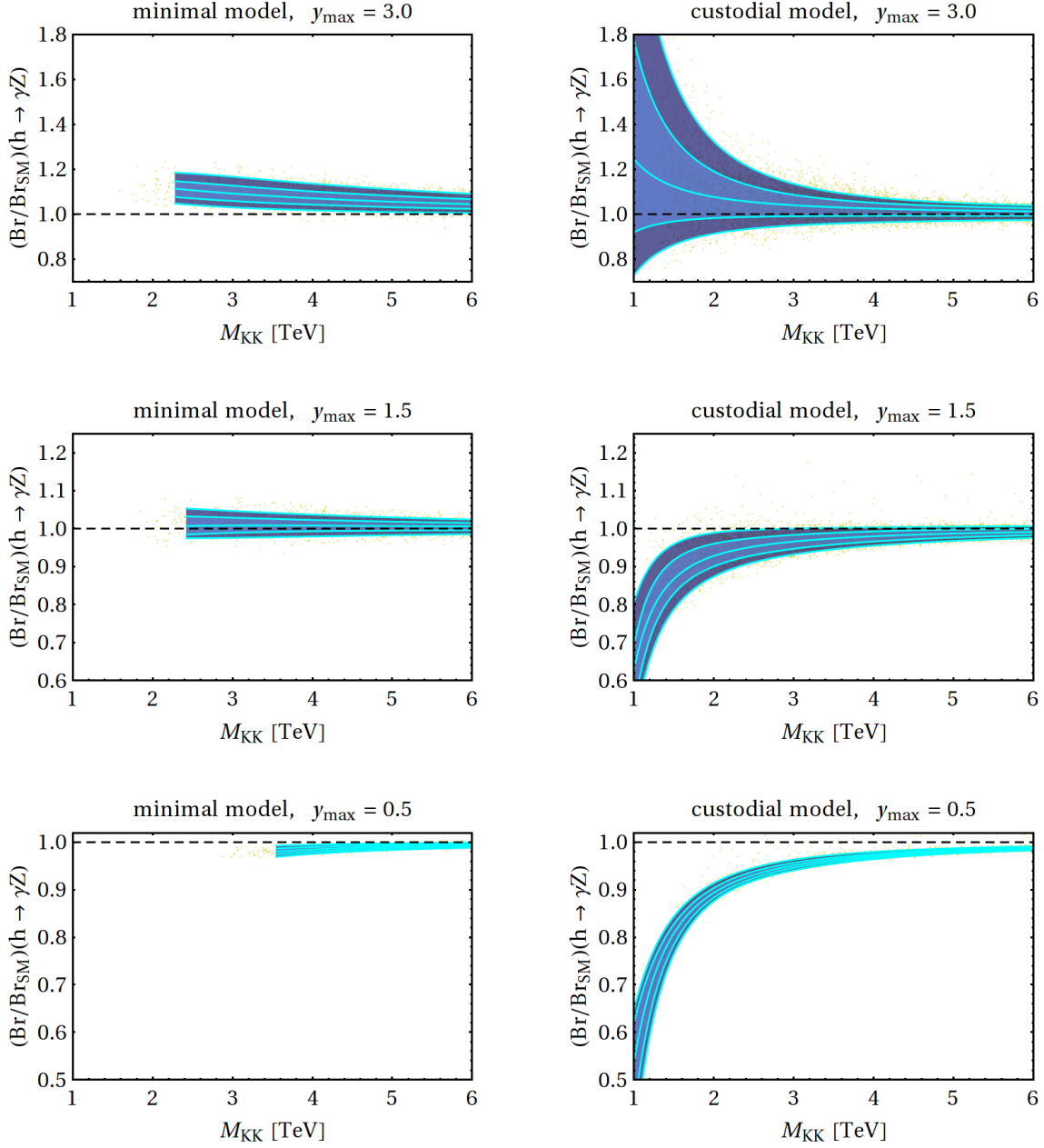


Figure B.10: Fits to the 90%, 60% CLs and median of the parameter distributions of the branching ratio for $h \rightarrow \gamma Z$ in the RS model divided by the SM result. The left column shows results in the minimal RS setup, while in the right column shows results for the custodially protected model. The SM result is marked by the dashed line. Further details are given in the main text.

Bibliography

- [1] S. Casagrande, F. Goertz, U. Haisch, M. Neubert, and T. Pfoh *JHEP* **0810** (2008) 094, [arXiv:0807.4937](#).
- [2] M. Carena, S. Casagrande, F. Goertz, U. Haisch, and M. Neubert *JHEP* **1208** (2012) 156, [arXiv:1204.0008](#).
- [3] M. Bauer, S. Casagrande, U. Haisch, and M. Neubert *JHEP* **1009** (2010) 017, [arXiv:0912.1625](#).
- [4] S. Casagrande, F. Goertz, U. Haisch, M. Neubert, and T. Pfoh *JHEP* **1009** (2010) 014, [arXiv:1005.4315](#).
- [5] S. Glashow *Nucl.Phys.* **22** (1961) 579–588.
- [6] S. Weinberg *Phys.Rev.Lett.* **19** (1967) 1264–1266.
- [7] A. Salam *Conf.Proc.* **C680519** (1968) 367–377. Originally printed in *Svartholm: Elementary Particle Theory, Proceedings Of The Nobel Symposium Held 1968 At Lerum, Sweden*, Stockholm 1968, 367-377.
- [8] D. Gross and F. Wilczek *Phys.Rev.Lett.* **30** (1973) 1343–1346.
- [9] H. D. Politzer *Phys.Rev.Lett.* **30** (1973) 1346–1349.
- [10] D. Gross and F. Wilczek *Phys.Rev.* **D8** (1973) 3633–3652.
- [11] M. Gell-Mann *Phys.Lett.* **8** (1964) 214–215.
- [12] G. Zweig. In *Lichtenberg, D. B. (Ed.), Rosen, S. P. (Ed.): Developments In The Quark Theory Of Hadrons, Vol. 1*, 22-101 and CERN-TH-401 & CERN-TH-412 (unpublished).
- [13] J. I. Friedman, H. W. Kendall, and R. E. Taylor *Rev. Mod. Phys.* **63** (Jul, 1991) 629–629. <http://link.aps.org/doi/10.1103/RevModPhys.63.629>.
- [14] **Gargamelle Neutrino Collaboration**, F. Hasert *et al.* *Phys.Lett.* **B46** (1973) 138–140.
- [15] **TASSO Collaboration**, R. Brandelik *et al.* *Phys.Lett.* **B86** (1979) 243.
- [16] S. Glashow, J. Iliopoulos, and L. Maiani *Phys.Rev.* **D2** (1970) 1285–1292.
- [17] **SLAC-SP-017 Collaboration**, J. Augustin *et al.* *Phys.Rev.Lett.* **33** (1974) 1406–1408.
- [18] **E598 Collaboration**, J. Aubert *et al.* *Phys.Rev.Lett.* **33** (1974) 1404–1406.
- [19] M. Kobayashi and T. Maskawa *Prog.Theor.Phys.* **49** (1973) 652–657.
- [20] **CDF Collaboration**, F. Abe *et al.* *Phys.Rev.Lett.* **74** (1995) 2626–2631, [arXiv:hep-ex/9503002](#).
- [21] **DO Collaboration**, S. Abachi *et al.* *Phys.Rev.Lett.* **74** (1995) 2422–2426, [arXiv:hep-ex/9411001](#).
- [22] **ATLAS Collaboration**, G. Aad *et al.* *Phys.Lett.B* (2012) , [arXiv:1207.7214](#).
- [23] **ATLAS Collaboration** Tech. Rep. ATLAS-CONF-2012-091, Jul, 2012.
- [24] **ATLAS Collaboration** Tech. Rep. ATLAS-CONF-2012-127, Sep, 2012.
- [25] **ATLAS Collaboration** Tech. Rep. ATLAS-CONF-2012-162, Nov, 2012.
- [26] **ATLAS Collaboration** Tech. Rep. ATLAS-CONF-2012-168, Dec, 2012.
- [27] **ATLAS Collaboration** Tech. Rep. ATLAS-CONF-2012-169, Dec, 2012.
- [28] **ATLAS Collaboration** Tech. Rep. ATLAS-CONF-2012-170, Dec, 2012.
- [29] **CMS Collaboration**, S. Chatrchyan *et al.* *Phys.Lett.B* (2012) , [arXiv:1207.7235](#).
- [30] **CMS Collaboration** Tech. Rep. CMS-PAS-HIG-12-015, Jul, 2012.
- [31] **CMS Collaboration** Tech. Rep. CMS-PAS-HIG-12-020, Jul, 2012.
- [32] **CMS Collaboration** Tech. Rep. CMS-PAS-HIG-12-041, Nov, 2012.

- [33] **CMS Collaboration** Tech. Rep. CMS-PAS-HIG-12-042, Nov, 2012.
- [34] **CMS Collaboration** Tech. Rep. CMS-PAS-HIG-12-043, Nov, 2012.
- [35] **CMS Collaboration** Tech. Rep. CMS-PAS-HIG-12-044, Nov, 2012.
- [36] **CMS Collaboration** Tech. Rep. CMS-PAS-HIG-12-045, Nov, 2012.
- [37] F. Englert and R. Brout *Phys.Rev.Lett.* **13** (1964) 321–323.
- [38] P. W. Higgs *Phys.Lett.* **12** (1964) 132–133.
- [39] P. W. Higgs *Phys.Rev.Lett.* **13** (1964) 508–509.
- [40] G. Guralnik, C. Hagen, and T. Kibble *Phys.Rev.Lett.* **13** (1964) 585–587.
- [41] **CDF Collaboration, D0 Collaboration**, T. Aaltonen *et al.* *Phys.Rev.Lett.* **109** (2012) 071804, [arXiv:1207.6436](#).
- [42] **CDF Collaboration, D0 Collaboration**, CDF, D. Collaborations, the Tevatron New Physics, and H. Working [arXiv:1207.0449](#).
- [43] S. Weinberg [arXiv:hep-th/9702027](#).
- [44] É. Cartan and P. Adam, *Sur la structure des groupes de transformations finis et continus*. Nony, 1894.
- [45] R. Jost *Helv.Phys.Acta* **30** (1957) 409–416.
- [46] G. 't Hooft and M. Veltman *Nucl.Phys.* **B44** (1972) 189–213.
- [47] K. G. Wilson *Phys.Rev.* **179** (1969) 1499–1512.
- [48] S. Weinberg, *The quantum theory of fields. Vol. 2: Modern applications*. Cambridge University Press, 1996.
- [49] J. C. Collins, *Renormalization: An Introduction to Renormalization, the Renormalization Group and the Operator-Product Expansion*. Cambridge monographs on mathematical physics. Cambridge University Press, 1984.
- [50] S. Weinberg, *The Quantum theory of fields. Vol. 1: Foundations*. Cambridge University Press, 1995.
- [51] S. Weinberg *Phys.Rev.Lett.* **43** (1979) 1566–1570.
- [52] W. Buchmuller and D. Wyler *Nucl.Phys.* **B268** (1986) 621.
- [53] B. Grzadkowski, M. Iskrzynski, M. Misiak, and J. Rosiek *JHEP* **1010** (2010) 085, [arXiv:1008.4884](#).
- [54] C. Burgess and H. J. Schnitzer *Nucl.Phys.* **B228** (1983) 464.
- [55] C. Burgess, S. Godfrey, H. Konig, D. London, and I. Maksymyk *Phys.Rev.* **D49** (1994) 6115–6147, [arXiv:hep-ph/9312291](#).
- [56] F. del Aguila, M. Perez-Victoria, and J. Santiago *Phys.Lett.* **B492** (2000) 98–106, [arXiv:hep-ph/0007160](#).
- [57] Z. Han and W. Skiba *Phys.Rev.* **D71** (2005) 075009, [arXiv:hep-ph/0412166](#).
- [58] V. Cirigliano, J. Jenkins, and M. Gonzalez-Alonso *Nucl.Phys.* **B830** (2010) 95–115, [arXiv:0908.1754](#).
- [59] J. Aguilar-Saavedra *Nucl.Phys.* **B843** (2011) 638–672, [arXiv:1008.3562](#).
- [60] C. Zhang and S. Willenbrock *Phys.Rev.* **D83** (2011) 034006, [arXiv:1008.3869](#).
- [61] M. Bohm, A. Denner, and H. Joos, *Gauge theories of the strong and electroweak interaction*. Vieweg+Teubner Verlag, 2001.
- [62] S. L. Adler and W. A. Bardeen *Phys.Rev.* **182** (1969) 1517–1536.
- [63] W. A. Bardeen *Phys.Rev.* **184** (1969) 1848–1857.
- [64] C. Bouchiat, J. Iliopoulos, and P. Meyer *Phys.Lett.* **B38** (1972) 519–523.
- [65] H. Georgi and S. L. Glashow *Phys.Rev.* **D6** (1972) 429.
- [66] D. J. Gross and R. Jackiw *Phys.Rev.* **D6** (1972) 477–493.
- [67] R. Mohapatra and A. Smirnov *Ann.Rev.Nucl.Part.Sci.* **56** (2006) 569–628, [arXiv:hep-ph/0603118](#).
- [68] N. Cabibbo *Phys.Rev.Lett.* **10** (1963) 531–533.
- [69] **Particle Data Group**, J. Beringer *et al.* *Phys.Rev.* **D86** (2012) 010001.
- [70] A. Belavin, A. M. Polyakov, A. Schwartz, and Y. Tyupkin *Phys.Lett.* **B59** (1975) 85–87.
- [71] G. 't Hooft *Phys.Rev.Lett.* **37** (1976) 8–11.
- [72] G. 't Hooft *Phys.Rev.* **D14** (1976) 3432–3450.

- [73] L. Wolfenstein *Phys.Rev.Lett.* **51** (1983) 1945.
- [74] B. Pontecorvo *Sov.Phys.JETP* **6** (1957) 429.
- [75] B. Pontecorvo *Sov.Phys.JETP* **26** (1968) 984–988.
- [76] Z. Maki, M. Nakagawa, and S. Sakata *Prog.Theor.Phys.* **28** (1962) 870–880.
- [77] **Daya Bay Collaboration**, D. M. Webber [arXiv:1211.1609](#).
- [78] G. Fogli, E. Lisi, A. Marrone, D. Montanino, A. Palazzo, *et al.* *Phys.Rev.* **D86** (2012) 013012, [arXiv:1205.5254](#).
- [79] S. N. Gupta *Proc.Phys.Soc.* **A63** (1950) 681–691.
- [80] K. Bleuler *Helv.Phys.Acta* **23** (1950) 567–586.
- [81] L. Faddeev and V. Popov *Phys.Lett.* **B25** (1967) 29–30.
- [82] C. Becchi, A. Rouet, and R. Stora *Phys.Lett.* **B52** (1974) 344.
- [83] C. Becchi, A. Rouet, and R. Stora *Annals Phys.* **98** (1976) 287–321.
- [84] I. Tyutin [arXiv:0812.0580](#).
- [85] N. Nakanishi *Prog. Theor. Phys.* **35** (1966) .
- [86] B. Lautrup *Mat. Fys. Medd. Dan. Vid. Selsk.* **35** (1967) .
- [87] C. Grosse-Knetter and R. Kogerler *Phys.Rev.* **D48** (1993) 2865–2876, [arXiv:hep-ph/9212268](#).
- [88] G. Degrassi, S. Di Vita, J. Elias-Miro, J. R. Espinosa, G. F. Giudice, *et al.* *JHEP* **1208** (2012) 098, [arXiv:1205.6497](#).
- [89] W. Grimus, L. Lavoura, and B. Radovic *Phys.Lett.* **B674** (2009) 117–121, [arXiv:0902.2325](#).
- [90] G. Hinshaw, D. Larson, E. Komatsu, D. Spergel, C. Bennett, *et al.* [arXiv:1212.5226](#).
- [91] G. Bertone, D. Hooper, and J. Silk *Phys.Rept.* **405** (2005) 279–390, [arXiv:hep-ph/0404175](#).
- [92] J. L. Feng *Ann.Rev.Astron.Astrophys.* **48** (2010) 495–545, [arXiv:1003.0904](#).
- [93] J. Bond, G. Efstathiou, and J. Silk *Phys.Rev.Lett.* **45** (1980) 1980–1984.
- [94] G. Jungman, M. Kamionkowski, and K. Griest *Phys.Rept.* **267** (1996) 195–373, [arXiv:hep-ph/9506380](#).
- [95] T. Appelquist, H.-C. Cheng, and B. A. Dobrescu *Phys.Rev.* **D64** (2001) 035002, [arXiv:hep-ph/0012100](#).
- [96] A. Sakharov *Pisma Zh.Eksp.Teor.Fiz.* **5** (1967) 32–35.
- [97] M. Gavela, P. Hernandez, J. Orloff, O. Pene, and C. Quimbay *Nucl.Phys.* **B430** (1994) 382–426, [arXiv:hep-ph/9406289](#).
- [98] A. Pilaftsis *J.Phys.Conf.Ser.* **171** (2009) 012017, [arXiv:0904.1182](#).
- [99] H. Georgi and S. Glashow *Phys.Rev.Lett.* **32** (1974) 438–441.
- [100] P. Langacker *Phys.Rept.* **72** (1981) 185.
- [101] S. Raby.
- [102] K. R. Dienes, E. Dudas, and T. Gherghetta *Phys.Lett.* **B436** (1998) 55–65, [arXiv:hep-ph/9803466](#).
- [103] L. Randall and M. D. Schwartz *JHEP* **0111** (2001) 003, [arXiv:hep-th/0108114](#).
- [104] M. Veltman *Acta Phys.Polon.* **B8** (1977) 475.
- [105] S. P. Martin [arXiv:hep-ph/9709356](#).
- [106] A. Djouadi *Phys.Rept.* **459** (2008) 1–241, [arXiv:hep-ph/0503173](#).
- [107] M. Veltman *Acta Phys.Polon.* **B12** (1981) 437.
- [108] S. Weinberg *Phys.Rev.* **D13** (1976) 974–996.
- [109] E. Gildener *Phys.Rev.* **D14** (1976) 1667.
- [110] S. Weinberg *Rev.Mod.Phys.* **61** (1989) 1–23.
- [111] C. Baker, D. Doyle, P. Geltenbort, K. Green, M. van der Grinten, *et al.* *Phys.Rev.Lett.* **97** (2006) 131801, [arXiv:hep-ex/0602020](#).
- [112] R. Jackiw and C. Rebbi *Phys.Rev.Lett.* **37** (1976) 172–175.
- [113] C. Llewellyn Smith *Phys.Lett.* **B46** (1973) 233–236.
- [114] J. M. Cornwall, D. N. Levin, and G. Tiktopoulos *Phys.Rev.Lett.* **30** (1973) 1268–1270.
- [115] J. M. Cornwall, D. N. Levin, and G. Tiktopoulos *Phys.Rev.* **D10** (1974) 1145.
- [116] B. W. Lee, C. Quigg, and H. Thacker *Phys.Rev.* **D16** (1977) 1519.
- [117] M. S. Chanowitz, M. Furman, and I. Hinchliffe *Phys.Lett.* **B78** (1978) 285.
- [118] M. S. Chanowitz, M. Furman, and I. Hinchliffe *Nucl.Phys.* **B153** (1979) 402.

- [119] H. A. Weldon *Phys.Rev.* **D30** (1984) 1547.
- [120] P. Langacker and H. A. Weldon *Phys.Rev.Lett.* **52** (1984) 1377.
- [121] J. Gunion, H. Haber, and J. Wudka *Phys.Rev.* **D43** (1991) 904–912.
- [122] K. Babu, J. Julio, and Y. Zhang *Nucl.Phys.* **B858** (2012) 468–487, [arXiv:1111.5021](#).
- [123] C. Bobeth, M. Misiak, and J. Urban *Nucl.Phys.* **B567** (2000) 153–185, [arXiv:hep-ph/9904413](#).
- [124] A. J. Buras and J. Girrbach *JHEP* **1203** (2012) 052, [arXiv:1201.1302](#).
- [125] M. S. Chanowitz and M. K. Gaillard *Nucl.Phys.* **B261** (1985) 379.
- [126] G. Gounaris, R. Kogerler, and H. Neufeld *Phys.Rev.* **D34** (1986) 3257.
- [127] T. Hahn *Comput.Phys.Commun.* **140** (2001) 418–431, [arXiv:hep-ph/0012260](#).
- [128] K. Fujikawa, B. Lee, and A. Sanda *Phys.Rev.* **D6** (1972) 2923–2943.
- [129] H.-J. He, Y.-P. Kuang, and C.-P. Yuan *Phys.Rev.* **D51** (1995) 6463–6473, [arXiv:hep-ph/9410400](#).
- [130] Y.-P. Yao and C. Yuan *Phys.Rev.* **D38** (1988) 2237.
- [131] A. J. Buras and J. Girrbach *JHEP* **1202** (2012) 143, [arXiv:1201.2563](#).
- [132] T. Ohl and C. Schwinn *Eur.Phys.J.* **C30** (2003) 567–582, [arXiv:hep-ph/0305334](#).
- [133] C. Schwinn [arXiv:hep-ph/0307057](#).
- [134] T. Hahn and M. Perez-Victoria *Comput.Phys.Commun.* **118** (1999) 153–165, [arXiv:hep-ph/9807565](#).
- [135] M. Jacob and G. Wick *Annals Phys.* **7** (1959) 404–428.
- [136] E. Wigner, *Gruppentheorie und ihre Anwendung auf die Quantenmechanik der Atomspektren*. Academic Press, 1959.
- [137] C. Itzykson and J. Zuber.
- [138] M. Luscher and P. Weisz *Phys.Lett.* **B212** (1988) 472.
- [139] W. J. Marciano, G. Valencia, and S. Willenbrock *Phys.Rev.* **D40** (1989) 1725.
- [140] L. Durand, P. N. Maher, and K. Riesselmann *Phys.Rev.* **D48** (1993) 1084–1096, [arXiv:hep-ph/9303234](#).
- [141] K. Riesselmann and S. Willenbrock *Phys.Rev.* **D55** (1997) 311–321, [arXiv:hep-ph/9608280](#).
- [142] A. Djouadi *Phys.Rept.* **457** (2008) 1–216, [arXiv:hep-ph/0503172](#).
- [143] N. Cabibbo, L. Maiani, G. Parisi, and R. Petronzio *Nucl.Phys.* **B158** (1979) 295–305.
- [144] N. Arkani-Hamed, A. G. Cohen, and H. Georgi *Phys.Lett.* **B513** (2001) 232–240, [arXiv:hep-ph/0105239](#).
- [145] N. Arkani-Hamed, A. Cohen, E. Katz, and A. Nelson *JHEP* **0207** (2002) 034, [arXiv:hep-ph/0206021](#).
- [146] D. B. Kaplan and H. Georgi *Phys.Lett.* **B136** (1984) 183.
- [147] D. B. Kaplan, H. Georgi, and S. Dimopoulos *Phys.Lett.* **B136** (1984) 187.
- [148] M. Schmaltz *JHEP* **0408** (2004) 056, [arXiv:hep-ph/0407143](#).
- [149] S. Chang *JHEP* **0312** (2003) 057, [arXiv:hep-ph/0306034](#).
- [150] R. Contino, L. Da Rold, and A. Pomarol *Phys.Rev.* **D75** (2007) 055014, [arXiv:hep-ph/0612048](#).
- [151] T. Han, H. E. Logan, B. McElrath, and L.-T. Wang *Phys.Rev.* **D67** (2003) 095004, [arXiv:hep-ph/0301040](#).
- [152] A. J. Buras, A. Poschenrieder, S. Uhlig, and W. A. Bardeen *JHEP* **0611** (2006) 062, [arXiv:hep-ph/0607189](#).
- [153] C. Csaki, J. Hubisz, G. D. Kribs, P. Meade, and J. Terning *Phys.Rev.* **D67** (2003) 115002, [arXiv:hep-ph/0211124](#).
- [154] J. L. Hewett, F. J. Petriello, and T. G. Rizzo *JHEP* **0310** (2003) 062, [arXiv:hep-ph/0211218](#).
- [155] M.-C. Chen and S. Dawson *Phys.Rev.* **D70** (2004) 015003, [arXiv:hep-ph/0311032](#).
- [156] H.-C. Cheng and I. Low *JHEP* **0309** (2003) 051, [arXiv:hep-ph/0308199](#).
- [157] J. Hubisz and P. Meade *Phys.Rev.* **D71** (2005) 035016, [arXiv:hep-ph/0411264](#).
- [158] I. Low *JHEP* **0410** (2004) 067, [arXiv:hep-ph/0409025](#).
- [159] H.-C. Cheng and I. Low *JHEP* **0408** (2004) 061, [arXiv:hep-ph/0405243](#).
- [160] T. Goto, Y. Okada, and Y. Yamamoto *Phys.Lett.* **B670** (2009) 378–382, [arXiv:0809.4753](#).

- [161] B. Grinstein, R. Kelley, and P. Uttayarat *JHEP* **0909** (2009) 040, arXiv:0904.1622.
- [162] B. Grinstein, R. Kelley, and P. Uttayarat *PoS ICHEP2010* (2010) 392, arXiv:1102.4010.
- [163] J. Hubisz, S. J. Lee, and G. Paz *JHEP* **0606** (2006) 041, arXiv:hep-ph/0512169.
- [164] A. Belyaev, C.-R. Chen, K. Tobe, and C.-P. Yuan *Phys.Rev.* **D74** (2006) 115020, arXiv:hep-ph/0609179.
- [165] M. Blanke, A. J. Buras, A. Poschenrieder, S. Recksiegel, C. Tarantino, *et al.* *JHEP* **0701** (2007) 066, arXiv:hep-ph/0610298.
- [166] I. Low and A. Vichi *Phys.Rev.* **D84** (2011) 045019, arXiv:1010.2753.
- [167] D. Pappadopulo and A. Vichi *JHEP* **1103** (2011) 072, arXiv:1007.4807.
- [168] A. Paul, I. I. Bigi, and S. Recksiegel *Phys.Rev.* **D83** (2011) 114006, arXiv:1101.6053.
- [169] J. Hubisz, P. Meade, A. Noble, and M. Perelstein *JHEP* **0601** (2006) 135, arXiv:hep-ph/0506042.
- [170] M. Antonelli, D. M. Asner, D. A. Bauer, T. G. Becher, M. Beneke, *et al.* *Phys.Rept.* **494** (2010) 197–414, arXiv:0907.5386.
- [171] F. del Aguila, J. Illana, and M. Jenkins *JHEP* **1009** (2010) 040, arXiv:1006.5914.
- [172] S. R. Coleman, J. Wess, and B. Zumino *Phys.Rev.* **177** (1969) 2239–2247.
- [173] J. Callan, Curtis G., S. R. Coleman, J. Wess, and B. Zumino *Phys.Rev.* **177** (1969) 2247–2250.
- [174] M. Blanke, A. J. Buras, A. Poschenrieder, S. Recksiegel, C. Tarantino, *et al.* *Phys.Lett.* **B646** (2007) 253–257, arXiv:hep-ph/0609284.
- [175] L. Randall and R. Sundrum *Phys.Rev.Lett.* **83** (1999) 3370–3373, arXiv:hep-ph/9905221.
- [176] N. Arkani-Hamed, S. Dimopoulos, and G. Dvali *Phys.Lett.* **B429** (1998) 263–272, arXiv:hep-ph/9803315.
- [177] D. Kapner, T. Cook, E. Adelberger, J. Gundlach, B. R. Heckel, *et al.* *Phys.Rev.Lett.* **98** (2007) 021101, arXiv:hep-ph/0611184.
- [178] S. Cullen and M. Perelstein *Phys.Rev.Lett.* **83** (1999) 268–271, arXiv:hep-ph/9903422.
- [179] V. Rubakov and M. Shaposhnikov *Phys.Lett.* **B125** (1983) 136–138.
- [180] N. Arkani-Hamed and M. Schmaltz *Phys.Rev.* **D61** (2000) 033005, arXiv:hep-ph/9903417.
- [181] I. R. Klebanov and M. J. Strassler *JHEP* **0008** (2000) 052, arXiv:hep-th/0007191.
- [182] S. B. Giddings, S. Kachru, and J. Polchinski *Phys.Rev.* **D66** (2002) 106006, arXiv:hep-th/0105097.
- [183] S. Kachru, R. Kallosh, A. D. Linde, and S. P. Trivedi *Phys.Rev.* **D68** (2003) 046005, arXiv:hep-th/0301240.
- [184] F. Brummer, A. Hebecker, and E. Trincherini *Nucl.Phys.* **B738** (2006) 283–305, arXiv:hep-th/0510113.
- [185] H. Davoudiasl, J. Hewett, and T. Rizzo *Phys.Lett.* **B473** (2000) 43–49, arXiv:hep-ph/9911262.
- [186] Y. Grossman and M. Neubert *Phys.Lett.* **B474** (2000) 361–371, arXiv:hep-ph/9912408.
- [187] C. Csaki, J. Erlich, and J. Terning *Phys.Rev.* **D66** (2002) 064021, arXiv:hep-ph/0203034.
- [188] W. D. Goldberger and M. B. Wise *Phys.Rev.Lett.* **83** (1999) 4922–4925, arXiv:hep-ph/9907447.
- [189] J. Hewett and T. Rizzo *JHEP* **0308** (2003) 028, arXiv:hep-ph/0202155.
- [190] C. Csaki, J. Hubisz, and S. J. Lee *Phys.Rev.* **D76** (2007) 125015, arXiv:0705.3844.
- [191] H. de Sandes and R. Rosenfeld *Phys.Rev.* **D85** (2012) 053003, arXiv:1111.2006.
- [192] H. Davoudiasl, G. Perez, and A. Soni *Phys.Lett.* **B665** (2008) 67–71, arXiv:0802.0203.
- [193] A. Pomarol *Phys.Lett.* **B486** (2000) 153–157, arXiv:hep-ph/9911294.
- [194] S. Chang, J. Hisano, H. Nakano, N. Okada, and M. Yamaguchi *Phys.Rev.* **D62** (2000) 084025, arXiv:hep-ph/9912498.
- [195] T. Gherghetta and A. Pomarol *Nucl.Phys.* **B586** (2000) 141–162, arXiv:hep-ph/0003129.
- [196] S. J. Huber and Q. Shafi *Phys.Rev.* **D63** (2001) 045010, arXiv:hep-ph/0005286.
- [197] H. Davoudiasl, J. Hewett, and T. Rizzo *Phys.Rev.* **D63** (2001) 075004, arXiv:hep-ph/0006041.
- [198] S. J. Huber, C.-A. Lee, and Q. Shafi *Phys.Lett.* **B531** (2002) 112–118, arXiv:hep-ph/0111465.
- [199] S. J. Huber and Q. Shafi *Phys.Lett.* **B498** (2001) 256–262, arXiv:hep-ph/0010195.

- [200] S. J. Huber *Nucl.Phys.* **B666** (2003) 269–288, arXiv:hep-ph/0303183.
- [201] K. Agashe, G. Perez, and A. Soni *Phys.Rev.Lett.* **93** (2004) 201804, arXiv:hep-ph/0406101.
- [202] K. Agashe, G. Perez, and A. Soni *Phys.Rev.* **D71** (2005) 016002, arXiv:hep-ph/0408134.
- [203] J. Scherk and J. H. Schwarz *Phys.Lett.* **B82** (1979) 60.
- [204] L. Nilse arXiv:hep-ph/0601015.
- [205] E. Stueckelberg *Helv.Phys.Acta* **11** (1938) 225–244.
- [206] A. Pais *Journal of Mathematical Physics* **3** no. 6, (1962) 1135–1139.
- [207] A. Azatov, M. Toharia, and L. Zhu *Phys.Rev.* **D80** (2009) 035016, arXiv:0906.1990.
- [208] R. Bertlmann, *Anomalies in quantum field theory*, vol. 91 of *International Series of Monographs on Physics*. Oxford University Press, 1996.
- [209] C. Csaki, J. Hubisz, and P. Meade arXiv:hep-ph/0510275.
- [210] F. Goertz arXiv:1112.6387.
- [211] C. Csaki, A. Falkowski, and A. Weiler *JHEP* **0809** (2008) 008, arXiv:0804.1954.
- [212] M. Blanke, A. J. Buras, B. Duling, S. Gori, and A. Weiler *JHEP* **0903** (2009) 001, arXiv:0809.1073.
- [213] J. A. Bagger, F. Feruglio, and F. Zwirner *Phys.Rev.Lett.* **88** (2002) 101601, arXiv:hep-th/0107128.
- [214] K. Agashe, A. Delgado, M. J. May, and R. Sundrum *JHEP* **0308** (2003) 050, arXiv:hep-ph/0308036.
- [215] C. Csaki, C. Grojean, L. Pilo, and J. Terning *Phys.Rev.Lett.* **92** (2004) 101802, arXiv:hep-ph/0308038.
- [216] K. Agashe, R. Contino, L. Da Rold, and A. Pomarol *Phys.Lett.* **B641** (2006) 62–66, arXiv:hep-ph/0605341.
- [217] H. Georgi, E. E. Jenkins, and E. H. Simmons *Phys.Rev.Lett.* **62** (1989) 2789. [Erratum-ibid. **63**, 1540 (1989)].
- [218] H. Georgi, E. E. Jenkins, and E. H. Simmons *Nucl.Phys.* **B331** (1990) 541.
- [219] V. D. Barger, E. Ma, and K. Whisnant *Phys.Rev.Lett.* **46** (1981) 1501.
- [220] X. Li and E. Ma *Phys.Rev.Lett.* **47** (1981) 1788.
- [221] E. Malkawi, T. M. Tait, and C. Yuan *Phys.Lett.* **B385** (1996) 304–310, arXiv:hep-ph/9603349.
- [222] G. Isidori *PoS* **CD09** (2009) 073, arXiv:0911.3219.
- [223] G. Burdman and L. Da Rold *JHEP* **0811** (2008) 025, arXiv:0809.4009.
- [224] M. S. Carena, E. Ponton, J. Santiago, and C. E. Wagner *Nucl.Phys.* **B759** (2006) 202–227, arXiv:hep-ph/0607106.
- [225] M. E. Albrecht, M. Blanke, A. J. Buras, B. Duling, and K. Gemmler *JHEP* **0909** (2009) 064, arXiv:0903.2415.
- [226] S. Casagrande diploma thesis, Johannes-Gutenberg Universität Mainz. <http://wwwthep.physik.uni-mainz.de/Publications/theses/dip-casagrande.pdf>.
- [227] C. Froggatt and H. B. Nielsen *Nucl.Phys.* **B147** (1979) 277.
- [228] T. Appelquist and J. Carazzone *Phys.Rev.* **D11** (1975) 2856.
- [229] M. Bauer, S. Casagrande, L. Grunder, U. Haisch, and M. Neubert *Phys.Rev.* **D79** (2009) 076001, arXiv:0811.3678.
- [230] C. Csaki, Y. Grossman, P. Tanedo, and Y. Tsai *Phys.Rev.* **D83** (2011) 073002, arXiv:1004.2037.
- [231] M. Beneke, P. Dey, and J. Rohrwild arXiv:1209.5897.
- [232] M. Blanke, B. Shakya, P. Tanedo, and Y. Tsai *JHEP* **1208** (2012) 038, arXiv:1203.6650.
- [233] M. S. Carena, A. Delgado, E. Ponton, T. M. Tait, and C. Wagner *Phys.Rev.* **D71** (2005) 015010, arXiv:hep-ph/0410344.
- [234] J. Hirn and V. Sanz *Phys.Rev.* **D76** (2007) 044022, arXiv:hep-ph/0702005.
- [235] M. Puchwein and Z. Kunszt *Annals Phys.* **311** (2004) 288–313, arXiv:hep-th/0309069.
- [236] A. Falkowski *Phys.Rev.* **D77** (2008) 055018, arXiv:0711.0828.
- [237] I. Low, R. Rattazzi, and A. Vichi *JHEP* **1004** (2010) 126, arXiv:0907.5413.
- [238] K. Agashe and R. Contino *Phys.Rev.* **D80** (2009) 075016, arXiv:0906.1542.

- [239] A. J. Buras, B. Duling, and S. Gori *JHEP* **0909** (2009) 076, [arXiv:0905.2318](#).
- [240] N. D. Christensen and C. Duhr *Comput.Phys.Commun.* **180** (2009) 1614–1641, [arXiv:0806.4194](#).
- [241] B. Grinstein, M. Redi, and G. Villadoro *JHEP* **1011** (2010) 067, [arXiv:1009.2049](#).
- [242] T. Feldmann *JHEP* **1104** (2011) 043, [arXiv:1010.2116](#).
- [243] F. del Aguila, M. Perez-Victoria, and J. Santiago *JHEP* **0009** (2000) 011, [arXiv:hep-ph/0007316](#).
- [244] A. J. Buras, C. Grojean, S. Pokorski, and R. Ziegler *JHEP* **1108** (2011) 028, [arXiv:1105.3725](#).
- [245] A. J. Buras, P. H. Chankowski, J. Rosiek, and L. Slawianowska *Nucl.Phys.* **B659** (2003) 3, [arXiv:hep-ph/0210145](#).
- [246] P. Gambino, P. Grassi, and F. Madricardo *Phys.Lett.* **B454** (1999) 98–104, [arXiv:hep-ph/9811470](#).
- [247] A. Denner and T. Sack *Nucl. Phys.* **B347** (1990) 203–216.
- [248] A. J. Buras [arXiv:hep-ph/9806471](#). To appear in 'Probing the Standard Model of Particle Interactions', F. David and R. Gupta, eds., 1998, Elsevier Science B.V.
- [249] C. Nishi *Am.J.Phys.* **73** (2005) 1160–1163, [arXiv:hep-ph/0412245](#).
- [250] M. Gorbahn, S. Jager, U. Nierste, and S. Trine *Phys.Rev.* **D84** (2011) 034030, [arXiv:0901.2065](#).
- [251] T. Inami and C. Lim *Prog.Theor.Phys.* **65** (1981) 297.
- [252] B. Yang, X. Wang, and J. Han *Nucl.Phys.* **B847** (2011) 1–16, [arXiv:1103.2506](#).
- [253] M. Blanke, A. J. Buras, A. Poschenrieder, C. Tarantino, S. Uhlig, *et al.* *JHEP* **0612** (2006) 003, [arXiv:hep-ph/0605214](#).
- [254] J. Santiago *JHEP* **0812** (2008) 046, [arXiv:0806.1230](#).
- [255] K. Agashe, A. Azatov, and L. Zhu *Phys.Rev.* **D79** (2009) 056006, [arXiv:0810.1016](#).
- [256] S. J. Huber and Q. Shafi *Phys.Lett.* **B544** (2002) 295–306, [arXiv:hep-ph/0205327](#).
- [257] S. J. Huber and Q. Shafi *Phys.Lett.* **B583** (2004) 293–303, [arXiv:hep-ph/0309252](#).
- [258] K. Agashe, T. Okui, and R. Sundrum *Phys.Rev.Lett.* **102** (2009) 101801, [arXiv:0810.1277](#).
- [259] M. Carena, A. D. Medina, N. R. Shah, and C. E. Wagner *Phys.Rev.* **D79** (2009) 096010, [arXiv:0901.0609](#).
- [260] **LHCb Collaboration**, R. Aaij *et al.* [arXiv:1211.2674](#).
- [261] M. Blanke, A. J. Buras, B. Duling, K. Gemmler, and S. Gori *JHEP* **0903** (2009) 108, [arXiv:0812.3803](#).
- [262] R. Kitano *Phys.Lett.* **B481** (2000) 39–44, [arXiv:hep-ph/0002279](#).
- [263] W.-F. Chang and J. N. Ng *Phys.Rev.* **D71** (2005) 053003, [arXiv:hep-ph/0501161](#).
- [264] K. Agashe, A. E. Blechman, and F. Petriello *Phys.Rev.* **D74** (2006) 053011, [arXiv:hep-ph/0606021](#).
- [265] G. Perez and L. Randall *JHEP* **0901** (2009) 077, [arXiv:0805.4652](#).
- [266] B. Lillie, L. Randall, and L.-T. Wang *JHEP* **0709** (2007) 074, [arXiv:hep-ph/0701166](#).
- [267] K. Agashe, A. Belyaev, T. Krupovnickas, G. Perez, and J. Virzi *Phys.Rev.* **D77** (2008) 015003, [arXiv:hep-ph/0612015](#).
- [268] **ATLAS Collaboration**, G. Aad *et al.* [arXiv:1211.2202](#).
- [269] **CMS Collaboration**, S. Chatrchyan *et al.* *JHEP* **1212** (2012) 015, [arXiv:1209.4397](#).
- [270] J. A. Bagger, K. T. Matchev, and R.-J. Zhang *Phys.Lett.* **B412** (1997) 77–85, [arXiv:hep-ph/9707225](#).
- [271] M. Ciuchini, V. Lubicz, L. Conti, A. Vladikas, A. Donini, *et al.* *JHEP* **9810** (1998) 008, [arXiv:hep-ph/9808328](#).
- [272] A. J. Buras, M. Misiak, and J. Urban *Nucl.Phys.* **B586** (2000) 397–426, [arXiv:hep-ph/0005183](#).
- [273] B. Duling *JHEP* **1005** (2010) 109, [arXiv:0912.4208](#).
- [274] V. Bertone, N. Carrasco, M. Ciuchini, P. Dimopoulos, R. Frezzotti, *et al.* [arXiv:1207.1287](#).
- [275] A. J. Buras, D. Guadagnoli, and G. Isidori *Phys.Lett.* **B688** (2010) 309–313, [arXiv:1002.3612](#).
- [276] K. Anikeev, D. Atwood, F. Azfar, S. Bailey, C. Bauer, *et al.* [arXiv:hep-ph/0201071](#).

- [277] E. Andriyash, G. Ovanesyan, and M. Vysotsky *Phys.Lett.* **B599** (2004) 253–259, [arXiv:hep-ph/0310314](#).
- [278] E. Andriyash, G. Ovanesyan, and M. Vysotsky *Phys.Atom.Nucl.* **69** (2006) 286–292, [arXiv:hep-ph/0502111](#).
- [279] J. Brod and M. Gorbahn *Phys.Rev.Lett.* **108** (2012) 121801, [arXiv:1108.2036](#).
- [280] G. Beall, M. Bander, and A. Soni *Phys.Rev.Lett.* **48** (1982) 848.
- [281] F. Gabbiani, E. Gabrielli, A. Masiero, and L. Silvestrini *Nucl.Phys.* **B477** (1996) 321–352, [arXiv:hep-ph/9604387](#).
- [282] G. Colangelo, J. Gasser, and H. Leutwyler *Nucl.Phys.* **B603** (2001) 125–179, [arXiv:hep-ph/0103088](#).
- [283] A. J. Buras, M. Jamin, and M. E. Lautenbacher *Nucl.Phys.* **B408** (1993) 209–285, [arXiv:hep-ph/9303284](#).
- [284] S. Bosch, A. Buras, M. Gorbahn, S. Jager, M. Jamin, *et al.* *Nucl.Phys.* **B565** (2000) 3–37, [arXiv:hep-ph/9904408](#).
- [285] A. J. Buras, M. Jamin, M. Lautenbacher, and P. H. Weisz *Nucl.Phys.* **B370** (1992) 69–104.
- [286] A. J. Buras, M. Jamin, M. E. Lautenbacher, and P. H. Weisz *Nucl.Phys.* **B400** (1993) 37–74, [arXiv:hep-ph/9211304](#).
- [287] A. J. Buras, M. Jamin, and M. E. Lautenbacher *Nucl.Phys.* **B400** (1993) 75–102, [arXiv:hep-ph/9211321](#).
- [288] M. Ciuchini, E. Franco, G. Martinelli, and L. Reina *Phys.Lett.* **B301** (1993) 263–271, [arXiv:hep-ph/9212203](#).
- [289] M. Ciuchini, E. Franco, G. Martinelli, and L. Reina *Nucl.Phys.* **B415** (1994) 403–462, [arXiv:hep-ph/9304257](#).
- [290] P. Gambino and U. Haisch *JHEP* **0009** (2000) 001, [arXiv:hep-ph/0007259](#).
- [291] A. J. Buras and M. Jamin *JHEP* **0401** (2004) 048, [arXiv:hep-ph/0306217](#).
- [292] J. Bijnens and J. Prades *Nucl.Phys.Proc.Suppl.* **96** (2001) 354–363, [arXiv:hep-ph/0010008](#).
- [293] J. Bijnens, E. Gamiz, and J. Prades *JHEP* **0110** (2001) 009, [arXiv:hep-ph/0108240](#).
- [294] M. Knecht, S. Peris, and E. de Rafael *Phys.Lett.* **B508** (2001) 117–126, [arXiv:hep-ph/0102017](#).
- [295] T. Hambye, S. Peris, and E. de Rafael *JHEP* **0305** (2003) 027, [arXiv:hep-ph/0305104](#).
- [296] **RBC Collaboration**, T. Blum *et al.* *Phys.Rev.* **D68** (2003) 114506, [arXiv:hep-lat/0110075](#).
- [297] P. Boucaud, V. Gimenez, C. D. Lin, V. Lubicz, G. Martinelli, *et al.* *Nucl.Phys.* **B721** (2005) 175–211, [arXiv:hep-lat/0412029](#).
- [298] T. Bhattacharya, N. Christ, G. T. Fleming, G. Kilcup, R. Gupta, *et al.* *Nucl.Phys.Proc.Suppl.* **106** (2002) 311–313, [arXiv:hep-lat/0111004](#).
- [299] T. Bhattacharya, G. T. Fleming, R. Gupta, G. Kilcup, W. Lee, *et al.* *Nucl.Phys.Proc.Suppl.* **140** (2005) 369–371, [arXiv:hep-lat/0409046](#).
- [300] P. Boyle, N. Christ, N. Garron, E. Goode, T. Janowski, *et al.* [arXiv:1212.1474](#).
- [301] E. Pallante, A. Pich, and I. Scimemi *Nucl.Phys.* **B617** (2001) 441–474, [arXiv:hep-ph/0105011](#).
- [302] F. Mescia and C. Smith *Phys.Rev.* **D76** (2007) 034017, [arXiv:0705.2025](#).
- [303] G. Buchalla and A. J. Buras *Nucl.Phys.* **B548** (1999) 309–327, [arXiv:hep-ph/9901288](#).
- [304] M. Misiak and J. Urban *Phys.Lett.* **B451** (1999) 161–169, [arXiv:hep-ph/9901278](#).
- [305] J. Brod, M. Gorbahn, and E. Stamou *Phys.Rev.* **D83** (2011) 034030, [arXiv:1009.0947](#).
- [306] G. Isidori, F. Mescia, and C. Smith *Nucl.Phys.* **B718** (2005) 319–338, [arXiv:hep-ph/0503107](#).
- [307] A. Buras, M. Gorbahn, U. Haisch, and U. Nierste *Phys.Rev.Lett.* **95** (2005) 261805, [arXiv:hep-ph/0508165](#).
- [308] A. J. Buras, M. Gorbahn, U. Haisch, and U. Nierste *JHEP* **0611** (2006) 002, [arXiv:hep-ph/0603079](#).
- [309] J. Brod and M. Gorbahn *Phys.Rev.* **D78** (2008) 034006, [arXiv:0805.4119](#).
- [310] F. Mescia, C. Smith, and S. Trine *JHEP* **0608** (2006) 088, [arXiv:hep-ph/0606081](#).
- [311] M. Gorbahn and U. Haisch *Phys.Rev.Lett.* **97** (2006) 122002, [arXiv:hep-ph/0605203](#).
- [312] G. Isidori and R. Unterdorfer *JHEP* **0401** (2004) 009, [arXiv:hep-ph/0311084](#).

- [313] J.-M. Gerard, C. Smith, and S. Trine *Nucl.Phys.* **B730** (2005) 1–36, [arXiv:hep-ph/0508189](#).
- [314] A. J. Buras, M. E. Lautenbacher, M. Misiak, and M. Munz *Nucl.Phys.* **B423** (1994) 349–383, [arXiv:hep-ph/9402347](#).
- [315] **NA48/1 Collaboration**, J. Batley *et al.* *Phys.Lett.* **B576** (2003) 43–54, [arXiv:hep-ex/0309075](#).
- [316] **NA48/1 Collaboration**, J. Batley *et al.* *Phys.Lett.* **B599** (2004) 197–211, [arXiv:hep-ex/0409011](#).
- [317] G. Buchalla, G. D’Ambrosio, and G. Isidori *Nucl.Phys.* **B672** (2003) 387–408, [arXiv:hep-ph/0308008](#).
- [318] S. Friot, D. Greynat, and E. De Rafael *Phys.Lett.* **B595** (2004) 301–308, [arXiv:hep-ph/0404136](#).
- [319] K. De Bruyn, R. Fleischer, R. Knegjens, P. Koppenburg, M. Merk, *et al.* *Phys.Rev.Lett.* **109** (2012) 041801, [arXiv:1204.1737](#).
- [320] S. Jager and J. M. Camalich [arXiv:1212.2263](#).
- [321] A. J. Buras, J. Girschbacher, D. Guadagnoli, and G. Isidori *Eur.Phys.J.* **C72** (2012) 2172, [arXiv:1208.0934](#).
- [322] C. Cheung, A. L. Fitzpatrick, and L. Randall *JHEP* **0801** (2008) 069, [arXiv:0711.4421](#).
- [323] **Heavy Flavor Averaging Group**, Y. Amhis *et al.* [arXiv:1207.1158](#).
- [324] **ATLAS Collaboration** tech. rep., 1999.
- [325] **CMS Collaboration**, G. Bayatian *et al.* *J.Phys.* **G34** (2007) 995–1579.
- [326] R. Barbieri and G. Giudice *Nucl.Phys.* **B306** (1988) 63.
- [327] A. J. Buras, M. Jamin, and P. H. Weisz *Nucl.Phys.* **B347** (1990) 491–536.
- [328] **E949 Collaboration**, A. Artamonov *et al.* *Phys.Rev.Lett.* **101** (2008) 191802, [arXiv:0808.2459](#).
- [329] **E391a Collaboration**, J. Ahn *et al.* *Phys.Rev.* **D81** (2010) 072004, [arXiv:0911.4789](#).
- [330] Y. Grossman and Y. Nir *Phys.Lett.* **B398** (1997) 163–168, [arXiv:hep-ph/9701313](#).
- [331] M. Blanke *Acta Phys.Polon.* **B41** (2010) 127, [arXiv:0904.2528](#).
- [332] A. J. Buras *Phys.Lett.* **B566** (2003) 115–119, [arXiv:hep-ph/0303060](#).
- [333] A. Buras, P. Gambino, M. Gorbahn, S. Jager, and L. Silvestrini *Phys.Lett.* **B500** (2001) 161–167, [arXiv:hep-ph/0007085](#).
- [334] S. Davidson, G. Isidori, and S. Uhlig *Phys.Lett.* **B663** (2008) 73–79, [arXiv:0711.3376](#).
- [335] O. Gedalia, G. Isidori, and G. Perez *Phys.Lett.* **B682** (2009) 200–206, [arXiv:0905.3264](#).
- [336] R. Bouchendir, P. Cladé, S. Guellati-Khélifa, F. Nez, and F. Biraben *Physical Review Letters* **106** no. 8, (Feb., 2011) 080801, [arXiv:1012.3627](#).
- [337] J. Erler and P. Langacker.
- [338] **ALEPH Collaboration, DELPHI Collaboration, L3 Collaboration, OPAL Collaboration, SLD Collaboration, LEP Electroweak Working Group, SLD Electroweak Group, SLD Heavy Flavour Group**, S. Schael *et al.* *Phys.Rept.* **427** (2006) 257–454, [arXiv:hep-ex/0509008](#).
- [339] **SLD Collaboration**, K. Abe *et al.* *Phys.Rev.Lett.* **84** (2000) 5945–5949, [arXiv:hep-ex/0004026](#).
- [340] **CMS Collaboration**, S. Chatrchyan *et al.* *Phys.Rev.* **D84** (2011) 112002, [arXiv:1110.2682](#).
- [341] D. Y. Bardin, P. Christova, M. Jack, L. Kalinovskaya, A. Olchevski, *et al.* *Comput.Phys.Commun.* **133** (2001) 229–395, [arXiv:hep-ph/9908433](#).
A. Arbuzov, M. Awramik, M. Czakon, A. Freitas, M. Grunewald, *et al.* *Comput.Phys.Commun.* **174** (2006) 728–758, [arXiv:hep-ph/0507146](#).
- [342] J. Erler [arXiv:hep-ph/0005084](#).
- [343] H. Flacher, M. Goebel, J. Haller, A. Hocker, K. Monig, *et al.* *Eur.Phys.J.* **C60** (2009) 543–583, [arXiv:0811.0009](#).
M. Baak, M. Goebel, J. Haller, A. Hoecker, D. Ludwig, *et al.* *Eur.Phys.J.* **C72** (2012) 2003, [arXiv:1107.0975](#).
- [344] M. Baak, M. Goebel, J. Haller, A. Hoecker, D. Kennedy, *et al.* [arXiv:1209.2716](#).
- [345] A. Freitas and Y.-C. Huang *JHEP* **1208** (2012) 050, [arXiv:1205.0299](#).

- [346] S. Heinemeyer, W. Hollik, and G. Weiglein *Phys.Rept.* **425** (2006) 265–368, [arXiv:hep-ph/0412214](#).
- [347] G. Altarelli and R. Barbieri *Phys.Lett.* **B253** (1991) 161–167.
- [348] M. E. Peskin and T. Takeuchi *Phys.Rev.Lett.* **65** (1990) 964–967.
- [349] M. E. Peskin and T. Takeuchi *Phys.Rev.* **D46** (1992) 381–409.
- [350] R. Barbieri, A. Pomarol, R. Rattazzi, and A. Strumia *Nucl.Phys.* **B703** (2004) 127–146, [arXiv:hep-ph/0405040](#).
- [351] **LEP Collaborations, ALEPH Collaboration, DELPHI Collaboration, L3 Collaboration, LEP Electroweak Working Group, SLD Electroweak Group, SLD Heavy Flavour Group, OPAL Collaboration**, t. S. Electroweak [arXiv:hep-ex/0412015](#).
- [352] R. S. Chivukula, E. H. Simmons, H.-J. He, M. Kurachi, and M. Tanabashi *Phys.Lett.* **B603** (2004) 210–218, [arXiv:hep-ph/0408262](#).
- [353] M. E. Peskin and J. D. Wells *Phys.Rev.* **D64** (2001) 093003, [arXiv:hep-ph/0101342](#).
- [354] J. Field *Mod.Phys.Lett.* **A13** (1998) 1937–1954, [arXiv:hep-ph/9801355](#).
- [355] B. Batell, S. Gori, and L.-T. Wang [arXiv:1209.6382](#).
- [356] C. Bouchart and G. Moreau *Phys.Rev.* **D80** (2009) 095022, [arXiv:0909.4812](#).
- [357] M. S. Carena, E. Ponton, T. M. Tait, and C. Wagner *Phys.Rev.* **D67** (2003) 096006, [arXiv:hep-ph/0212307](#).
- [358] A. Delgado and A. Falkowski *JHEP* **0705** (2007) 097, [arXiv:hep-ph/0702234](#).
- [359] H. Davoudiasl, S. Gopalakrishna, E. Ponton, and J. Santiago *New J.Phys.* **12** (2010) 075011, [arXiv:0908.1968](#).
- [360] M. S. Carena, E. Ponton, J. Santiago, and C. Wagner *Phys.Rev.* **D76** (2007) 035006, [arXiv:hep-ph/0701055](#).
- [361] H. Davoudiasl, J. Hewett, and T. Rizzo *Phys.Rev.* **D68** (2003) 045002, [arXiv:hep-ph/0212279](#).
- [362] M. S. Carena, A. Delgado, E. Ponton, T. M. Tait, and C. Wagner *Phys.Rev.* **D68** (2003) 035010, [arXiv:hep-ph/0305188](#).
- [363] H. Georgi, A. K. Grant, and G. Hailu *Phys.Lett.* **B506** (2001) 207–214, [arXiv:hep-ph/0012379](#).
- [364] H.-C. Cheng, K. T. Matchev, and M. Schmaltz *Phys.Rev.* **D66** (2002) 036005, [arXiv:hep-ph/0204342](#).
- [365] J. A. Cabrer, G. von Gersdorff, and M. Quiros *Phys.Lett.* **B697** (2011) 208–214, [arXiv:1011.2205](#).
- [366] A. Carmona, E. Ponton, and J. Santiago *JHEP* **1110** (2011) 137, [arXiv:1107.1500](#).
- [367] A. Djouadi, G. Moreau, and F. Richard *Nucl.Phys.* **B773** (2007) 43–64, [arXiv:hep-ph/0610173](#).
- [368] C. Bouchart and G. Moreau *Nucl.Phys.* **B810** (2009) 66–96, [arXiv:0807.4461](#).
- [369] J. F. Gunion, H. E. Haber, G. L. Kane, and S. Dawson *Front.Phys.* **80** (2000) 1–448.
- [370] J. F. Gunion [arXiv:hep-ph/0212150](#).
- [371] L. Landau *Dokl.Akad.Nauk Ser.Fiz.* **60** (1948) 207–209.
- [372] C.-N. Yang *Phys.Rev.* **77** (1950) 242–245.
- [373] A. Denner *Fortsch.Phys.* **41** (1993) 307–420, [arXiv:0709.1075](#).
- [374] G. Passarino and M. Veltman *Nucl.Phys.* **B160** (1979) 151.
- [375] H. Georgi, S. Glashow, M. Machacek, and D. V. Nanopoulos *Phys.Rev.Lett.* **40** (1978) 692.
- [376] A. Djouadi [arXiv:1208.3436](#).
- [377] T. Plehn *Lect.Notes Phys.* **844** (2012) 1–193, [arXiv:0910.4182](#).
- [378] J. R. Ellis, M. K. Gaillard, and D. V. Nanopoulos *Nucl.Phys.* **B106** (1976) 292.
- [379] M. A. Shifman, A. Vainshtein, M. Voloshin, and V. I. Zakharov *Sov.J.Nucl.Phys.* **30** (1979) 711–716.
- [380] B. A. Kniehl and M. Spira *Z.Phys.* **C69** (1995) 77–88, [arXiv:hep-ph/9505225](#).
- [381] R. V. Harlander, H. Mantler, S. Marzani, and K. J. Ozeren *Eur.Phys.J.* **C66** (2010) 359–372, [arXiv:0912.2104](#).
- [382] D. Graudenz, M. Spira, and P. Zerwas *Phys.Rev.Lett.* **70** (1993) 1372–1375.

- [383] M. Spira, A. Djouadi, D. Graudenz, and P. Zerwas *Nucl.Phys.* **B453** (1995) 17–82, [arXiv:hep-ph/9504378](#).
- [384] M. Spira [arXiv:hep-ph/9510347](#).
- [385] R. V. Harlander and W. B. Kilgore *Phys.Rev.Lett.* **88** (2002) 201801, [arXiv:hep-ph/0201206](#).
- [386] C. Anastasiou and K. Melnikov *Nucl.Phys.* **B646** (2002) 220–256, [arXiv:hep-ph/0207004](#).
- [387] V. Ravindran, J. Smith, and W. L. van Neerven *Nucl.Phys.* **B665** (2003) 325–366, [arXiv:hep-ph/0302135](#).
- [388] **LHC Higgs Cross Section Working Group**, S. Dittmaier *et al.* [arXiv:1101.0593](#).
- [389] S. Dittmaier, S. Dittmaier, C. Mariotti, G. Passarino, R. Tanaka, *et al.* [arXiv:1201.3084](#).
- [390] V. Ahrens, T. Becher, M. Neubert, and L. L. Yang *Eur.Phys.J.* **C62** (2009) 333–353, [arXiv:0809.4283](#).
- [391] S. Moch and A. Vogt *Phys.Lett.* **B631** (2005) 48–57, [arXiv:hep-ph/0508265](#).
- [392] E. Laenen and L. Magnea *Phys.Lett.* **B632** (2006) 270–276, [arXiv:hep-ph/0508284](#).
- [393] A. Idilbi, X.-d. Ji, J.-P. Ma, and F. Yuan *Phys.Rev.* **D73** (2006) 077501, [arXiv:hep-ph/0509294](#).
- [394] V. Ravindran *Nucl.Phys.* **B752** (2006) 173–196, [arXiv:hep-ph/0603041](#).
- [395] A. Idilbi, X.-d. Ji, and F. Yuan *Nucl.Phys.* **B753** (2006) 42–68, [arXiv:hep-ph/0605068](#).
- [396] V. Ahrens, T. Becher, M. Neubert, and L. L. Yang *Phys.Rev.* **D79** (2009) 033013, [arXiv:0808.3008](#).
- [397] A. Martin, W. Stirling, R. Thorne, and G. Watt *Phys.Lett.* **B652** (2007) 292–299, [arXiv:0706.0459](#).
- [398] S. Glashow, D. V. Nanopoulos, and A. Yildiz *Phys.Rev.* **D18** (1978) 1724–1727.
- [399] D. Jones and S. Petcov *Phys.Lett.* **B84** (1979) 440.
- [400] R. Cahn and S. Dawson *Phys.Lett.* **B136** (1984) 196.
- [401] U. Aglietti, A. Belyaev, S. Berge, A. Blum, R. Bonciani, *et al.* [arXiv:hep-ph/0612172](#).
TeV4LHC Higgs Working Group, <http://maltoni.home.cern.ch/maltoni/TeV4LHC/>.
- [402] R. N. Cahn, S. D. Ellis, R. Kleiss, and W. J. Stirling *Phys.Rev.* **D35** (1987) 1626.
- [403] R. Raitio and W. W. Wada *Phys.Rev.* **D19** (1979) 941.
- [404] Z. Kunszt *Nucl.Phys.* **B247** (1984) 339.
- [405] R. M. Barnett, H. E. Haber, and D. E. Soper *Nucl.Phys.* **B306** (1988) 697.
- [406] D. A. Dicus and S. Willenbrock *Phys.Rev.* **D39** (1989) 751.
- [407] **LEP Working Group for Higgs boson searches, ALEPH Collaboration, DELPHI Collaboration, L3 Collaboration, OPAL Collaboration**, R. Barate *et al.* *Phys.Lett.* **B565** (2003) 61–75, [arXiv:hep-ex/0306033](#).
- [408] **TEVNPH (Tevatron New Phenomina and Higgs Working Group), CDF and D0 Collaboration** [arXiv:1107.5518](#).
- [409] **ATLAS Collaboration**, G. Aad *et al.* *Phys.Rev.* **D86** (2012) 032003, [arXiv:1207.0319](#).
- [410] **CMS Collaboration**, S. Chatrchyan *et al.* *Phys.Lett.* **B710** (2012) 26–48, [arXiv:1202.1488](#).
- [411] J. M. Butterworth, A. R. Davison, M. Rubin, and G. P. Salam *Phys.Rev.Lett.* **100** (2008) 242001, [arXiv:0802.2470](#).
- [412] A. Djouadi, J. Kalinowski, and M. Spira *Comput.Phys.Commun.* **108** (1998) 56–74, [arXiv:hep-ph/9704448](#).
- [413] H.-Q. Zheng and D.-D. Wu *Phys.Rev.* **D42** (1990) 3760–3763.
- [414] S. Actis, G. Passarino, C. Sturm, and S. Uccirati *Phys.Lett.* **B670** (2008) 12–17, [arXiv:0809.1301](#).
- [415] J. Baglio and A. Djouadi *JHEP* **1103** (2011) 055, [arXiv:1012.0530](#).
- [416] G. Belanger, B. Dumont, U. Ellwanger, J. Gunion, and S. Kraml [arXiv:1212.5244](#).
- [417] Y. Grossman, Z. Surujon, and J. Zupan [arXiv:1301.0328](#).
- [418] **CMS Collaboration**, S. Chatrchyan *et al.* *JHEP* **1205** (2012) 123, [arXiv:1204.1088](#).
- [419] **ATLAS Collaboration**, G. Aad *et al.* [arXiv:1210.5468](#).
- [420] G. D. Kribs, T. Plehn, M. Spannowsky, and T. M. Tait *Phys.Rev.* **D76** (2007) 075016, [arXiv:0706.3718](#).
- [421] M. S. Chanowitz [arXiv:1212.3209](#).

- [422] O. Eberhardt, G. Herbert, H. Lacker, A. Lenz, A. Menzel, *et al.* [arXiv:1209.1101](#).
- [423] A. Denner, S. Dittmaier, A. Muck, G. Passarino, M. Spira, *et al.* *Eur.Phys.J.* **C72** (2012) 1992, [arXiv:1111.6395](#).
- [424] G. Giudice, C. Grojean, A. Pomarol, and R. Rattazzi *JHEP* **0706** (2007) 045, [arXiv:hep-ph/0703164](#).
- [425] C.-R. Chen, K. Tobe, and C.-P. Yuan *Phys.Lett.* **B640** (2006) 263–271, [arXiv:hep-ph/0602211](#).
- [426] K. Agashe, R. Contino, and A. Pomarol *Nucl.Phys.* **B719** (2005) 165–187, [arXiv:hep-ph/0412089](#).
- [427] J. Reuter and M. Tonini [arXiv:1212.5930](#).
- [428] N. Arkani-Hamed, A. Cohen, E. Katz, A. Nelson, T. Gregoire, *et al.* *JHEP* **0208** (2002) 021, [arXiv:hep-ph/0206020](#).
- [429] A. Azatov, M. Toharia, and L. Zhu *Phys.Rev.* **D82** (2010) 056004, [arXiv:1006.5939](#).
- [430] F. Goertz and T. Pfoh *JHEP* **0810** (2008) 035, [arXiv:0809.1378](#).
- [431] T. Inami, T. Kubota, and Y. Okada *Z.Phys.* **C18** (1983) 69.
- [432] A. V. Manohar and M. B. Wise *Phys.Lett.* **B636** (2006) 107–113, [arXiv:hep-ph/0601212](#).
- [433] C. Delaunay, J. F. Kamenik, G. Perez, and L. Randall [arXiv:1207.0474](#).
- [434] A. Pomarol *Phys.Rev.Lett.* **85** (2000) 4004–4007, [arXiv:hep-ph/0005293](#).
- [435] K.-w. Choi, H. D. Kim, and I.-W. Kim *JHEP* **0211** (2002) 033, [arXiv:hep-ph/0202257](#).
- [436] W. D. Goldberger and I. Z. Rothstein *Phys.Rev.Lett.* **89** (2002) 131601, [arXiv:hep-th/0204160](#).
- [437] K. Agashe, A. Delgado, and R. Sundrum *Nucl.Phys.* **B643** (2002) 172–186, [arXiv:hep-ph/0206099](#).
- [438] F. J. Petriello *JHEP* **0205** (2002) 003, [arXiv:hep-ph/0204067](#).
- [439] G. Cacciapaglia, A. Deandrea, and J. Llodra-Perez *JHEP* **0906** (2009) 054, [arXiv:0901.0927](#).
- [440] A. Djouadi and G. Moreau *Phys.Lett.* **B660** (2008) 67–71, [arXiv:0707.3800](#).
- [441] G. von Gersdorff, M. Quiros, and M. Wiechers [arXiv:1208.4300](#).
- [442] F. Goertz, U. Haisch, and M. Neubert *Phys.Lett.* **B713** (2012) 23–28, [arXiv:1112.5099](#).
- [443] C. F. Berger, C. Marcantonini, I. W. Stewart, F. J. Tackmann, and W. J. Waalewijn *JHEP* **1104** (2011) 092, [arXiv:1012.4480](#).
- [444] M. Abramowitz and I. A. Stegun, *Handbook of Mathematical Functions with Formulas, Graphs, and Mathematical Tables*. Dover, New York, ninth dover printing, tenth gpo printing ed., Jun, 1964. <http://www.math.sfu.ca/~cbm/aands/>.
- [445] M. Beneke and M. Neubert *Nucl.Phys.* **B651** (2003) 225–248, [arXiv:hep-ph/0210085](#).
- [446] L. Bergstrom and G. Hulth *Nucl.Phys.* **B259** (1985) 137.
- [447] **CDF Collaboration, D0 Collaboration**, T. Aaltonen *et al.* [arXiv:1207.1069](#).
- [448] M. Davier, A. Hoecker, B. Malaescu, and Z. Zhang *Eur.Phys.J.* **C71** (2011) 1515, [arXiv:1010.4180](#).
- [449] J. Laiho, E. Lunghi, and R. S. Van de Water *Phys.Rev.* **D81** (2010) 034503, [arXiv:0910.2928](#). Updates available on <http://latticeaverages.org/>.
- [450] K. Chetyrkin, J. Kuhn, A. Maier, P. Maierhofer, P. Marquard, *et al.* *Phys.Rev.* **D80** (2009) 074010, [arXiv:0907.2110](#).
- [451] J. Brod and M. Gorbahn *Phys.Rev.* **D82** (2010) 094026, [arXiv:1007.0684](#).
- [452] **Heavy Flavor Averaging Group**, E. Barberio *et al.* [arXiv:0808.1297](#).
- [453] **Particle Data Group**, C. Amsler *et al.* *Phys.Lett.* **B667** (2008) 1–1340.
- [454] **CKMfitter Group**, J. Charles *et al.* *Eur.Phys.J.* **C41** (2005) 1–131, [arXiv:hep-ph/0406184](#).
- [455] C. Csaki, A. Falkowski, and A. Weiler *Phys.Rev.* **D80** (2009) 016001, [arXiv:0806.3757](#).
- [456] F. del Aguila and J. Santiago *Phys.Lett.* **B493** (2000) 175–181, [arXiv:hep-ph/0008143](#).

Acknowledgments

And now for something completely different.

————— MONTY PYTHON

First and foremost I would like to thank my supervisor Martin Gorbahn for the possibility to work on a enthralling project, the very good collaboration, and for supporting my vague ideas and the help in turning them into a firm work. I would also like to thank him for comments and suggestions on a first version of this manuscript.

I highly acknowledge the support of Sebastian Jaeger and Matthias Neubert and I want to thank them for invitations to Sussex and Mainz. The great time in China with Matthias will stay lively in my mind.

I want to thank all my other collaborators during the last years Joachim Brod, Martin Bauer, Uli Haisch, Florian Goertz, and Torsten Pfoh for their great work and the many insights this provided for me.

Lots of small errors have crept into this manuscript in the course of its creation. Thanks to proof-reading from Christoph Bobeth, Joachim Brod, Emmanuel Stamou, Stefan Vickers, Daniel Bölinger, Julia Dietrichs, and Dan Greenwald, many, if not essentially all, were traced and removed. I like to thank them for straightening some of the most clumsy passages and improving the readability of the text. I also like to thank the former four of them for being great floor mates, for the many coffee breaks and an open ear for all sorts of things.

A lot of inspiration and knowledge about quantum field theory is thanks to Anna Brunnbauer and David Nolde, who showed great interest in my tutorial on advanced QFT and always had brilliant comments.

There are many more people, who have contributed to my work through discussions, questions, comments, and lectures. Please feel acknowledged, even you do not find your name in a list of many here.

I would like to express my gratitude to all the administration and coordination of the Excellence Cluster Universe, for creating excellent working condition, a pleasant atmosphere, and for the well-deserved success in the approval of the cluster continuation.

Many thanks also go to Christoph Promberger and Florian Kuchler for our organization of the fantastic PhD meeting 2010 Berchtesgaden, and to Thorsten Feldmann for the organization of the lively and interesting B-physics Workshop in Neckarzimmern.

Personally I profited most from my private environment, my parents, my brother, all of my friends, and I deeply thank them for their unconditional support of any kind, the interest in my work, and for keeping me grounded. Most deeply, I thank you Julia for you love and for your patience.

I gratefully acknowledge the support of the DFG Cluster of Excellence “Origin and Structure of the Universe”.